CIVIL ENGINEERING STUDIES
STRUCTURAL RESEARCH SERIES NO. 311

A YIELD CRITERION FOR REINFORCED CONCRETE UNDER BIAXIAL MOMENTS AND FORCES

by
ROLF J. LENSCHOW
and
METE A. SOZEN

A Report on a Research Project
Sponsored by
THE NATIONAL SCIENCE FOUNDATION
Research Grant GK-171

UNIVERSITY OF ILLINOIS
URBANA, ILLINOIS
JULY 1966

A YIELD CRITERION FOR REINFORCED CONCRETE UNDER BIAXIAL MOMENTS AND FORCES

by

ROLF J. LENSCHOW

and

METE A. SOZEN

UNIVERSITY OF ILLINOIS
URBANA, ILLINOIS
JULY 1966

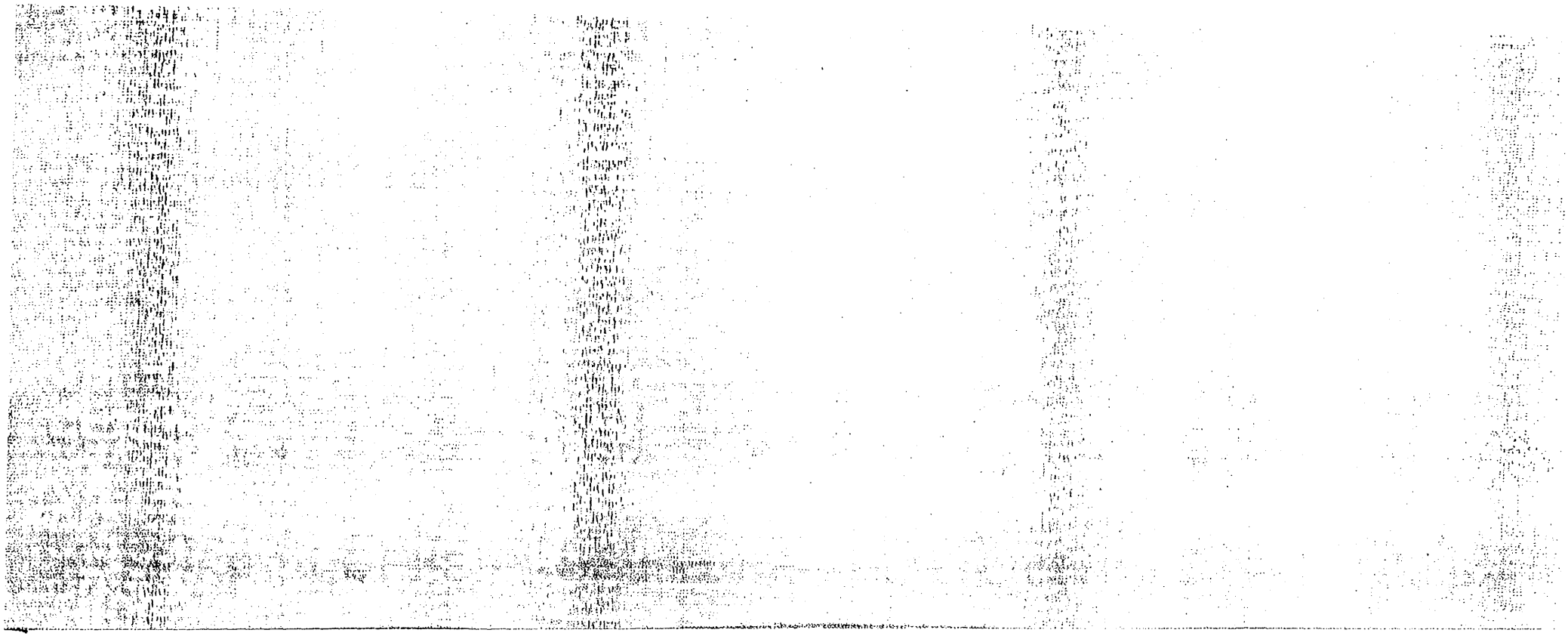

ACKNOWLEDGMENT

The investigation described in this report was carried out in the Structural Research Laboratory of the Department of Civil Engineering, University of Illinois, under Grant GK-171 from the National Science Foundation.

This report is based on a doctoral dissertation prepared by R. J. Lenschow, Research Assistant in Civil Engineering, under the direction of Dr. M. A. Sozen, Professor of Civil Engineering.

The invaluable assistance provided by A. Cardenas and M. Criswell is gratefully acknowledged.

TABLE OF CONTENTS

TABLE OF CONTENTS (Continued)

TABLE OF CONTENTS (Continued)

LIST OF TABLES

LIST OF FIGURES

LIST OF FIGURES (Continued)

LIST OF FIGURES (Continued)

LIST OF FIGURES (Continued)

LIST OF FIGURES (Continued)

LIST OF FIGURES (Continued)

LIST OF FIGURES (Continued)

LIST OF FIGURES (Continued)

LIST OF FIGURES (Continued)

LIST OF FIGURES (Continued)

LIST OF FIGURES (Continued)

LIST OF FIGURES (Continued)

LIST OF FIGURES (Continued)

LIST OF FIGURES (Continued)

LIST OF FIGURES (Continued)

LIST OF FIGURES (Continued)

LIST OF FIGURES (Continued)

1. INTRODUCTION

1.1. Object

The over-all objective of this study was to develop a general yield criterion for reinforced concrete plates subjected to combinations of bending and twisting moments. The work included tests on slab elements and theoretical studies leading to the definition of a general yield criterion.

In addition to the analysis of the conditions at yield, detailed studies were made of the load-deformation characteristics of reinforced concrete elements subjected to combinations of bending and twisting moments. The results of these studies are applicable to problems concerning reinforcement for membrane forces as well as bending moments.

The theoretical and experimental work confirmed the applicability of Johansen's criterion under practical conditions, provided the principal moments are of equal sign. The test results showed that the effect on flexural strength of the reorientation of reinforcing bars at the yield lines was negligible.

1.2. Outline of Tests

A study of earlier tests concerning the yield criterion for reinforced concrete slabs summarized in Chapter 2 indicated that the properties of the test specimens and the methods of applying the moments were critical. Two new types of test specimens were used in the investigation:

(1) The "circular" test specimen (Fig. 4.20) was used in the particular case of applied isostatic moment (equal moments in all directions).

(2) The rectangular specimen (Fig. 4.19) was used for uniaxial and torsional moments. The moments were applied at the ends so that the middle part, the test area, was subjected to constant moment. (The dead load moment was negligible.)

The reinforcement was mutually perpendicular in all specimens. The average slab thickness was 4.12 in. Concrete cover was 3/8 in.

The test setup was designed to minimize the parasitical restraints from the supporting and loading equipment.

The tests included 22 specimens in three different series relating to different loading conditions.

(1) Isostatic Moment

Three specimens, C1, C2 and C3, with isotropic reinforcement, one percent in each direction were subjected to isostatic moment. The concrete strength was the only variable.

(2) Uniaxial Moment

(a) Three specimens, B4, B10, and B13, were "standard" specimens used as reference for the other tests. The concrete strength was between 4000 and 5000 psi and the main layer of reinforcement was parallel to the span direction. The amount of steel was one percent in each layer.

(b) Two specimens, B5 and B6, were pilot specimens built to examine and overcome the edge problems with inclined reinforcement.

The only variable was the inclination of the reinforcement with respect to the span.

(c) Test specimens B7 and B8 had isotropic but inclined reinforcement, one percent in each layer. The inclination of the reinforcement to the direction of the span was 45° for B7, and 22.5° (or 67.5°) for B8.

(d) Three specimens, B9, B11, and B12, had nonisotropic reinforcement, with one percent reinforcement in the "main" direction and one half percent in the perpendicular direction. The inclination of the "main" reinforcement to the span direction was 45°, 22.5° and 67.5°.

(3) Torsional Moment

(a) The two first test specimens, B14 and B15, of this series were pilot specimens cast to study edge problems. The directions of the reinforcement were 0° and 45° to the longitudinal axis of the specimen.

(b) Specimens B16, B17, and B18 were all isotropically reinforced, top and bottom, with one percent reinforcement in each layer. The reinforcing bars made angles of 0, 22.5, and 45° with the axis of the specimen.

(c) Specimens B19 and B20 were also isotropically reinforced but with one half percent reinforcement in each layer. The inclinations of the reinforcement were 45° and 0° to the longitudinal axis.

(d) Test specimens B21 and B22 were nonisotropically reinforced. The reinforcement in the main direction was one percent and in the perpendicular direction one fourth percent. The reinforcement

was the same top and bottom. The direction of the main reinforcement was parallel to the transverse axis.

A detailed description of the test setup, procedure and results is given in Appendix A. A survey of measured and computed results is given in Table 3.1.

1.3. Outline of Analytical Studies

Unlike most analytical studies on plates, the studies in this investigation were not concerned with the analysis of reinforced concrete structures, but dealt with a reinforced concrete element under various external and internal conditions. The following studies have been carried out:

(1) Investigation of the reorientation of inclined reinforcing bars across the yield lines in a reinforced concrete element. Computations were made on various assumptions in order to obtain the range of the possible reorientation of the reinforcing bars.

(2) From a simple consideration of a small concrete element enclosing a reinforcing bar, an analytical method was developed for determining the stiffness of a concrete element and the effectiveness of the reinforcement.

(3) An analytical method was derived for determining the "balanced" amount of reinforcement, which denotes the condition for which the yield stress in the steel and the limiting strain in the concrete is reached simultaneously. The "balanced" amount of reinforcement depends on the same factors as that for a beam but, in addition,

is affected by the orientation of the reinforcement and the nature of the external moments.

(4) The direction of the yield line was determined by establishing the line of least resistance with respect to the external loading conditions.

(5) A yield criterion was developed and presented in a graphical form.

2. HISTORICAL REVIEW

2.1. Introductory Remarks

This chapter describes the background for the present investigation. The development of the yield line theory is briefly recorded. Experimental investigations of the yield criterion are reported in more detail.

The yield-line theory and the yield criterion are closely related. The yield criterion describes the role of the material in the yield-line theory and will remain as one of the pivotal assumptions in further development of the theory. The main goal of this chapter is to provide a perspective of the various existing assumptions for the yield criterion.

2.2. The Yield-Line Theory

The yield-line theory is the theory of plasticity modified to apply to reinforced concrete slabs. Ingerslev (1)* developed and used the yield-line theory in some analyses of the strength of reinforced concrete slabs in 1921. He introduced the concept of a yield line with constant bending moment over its entire length and assumed that no shear or twisting moments could exist along the yield line.

When Johansen (2) worked along the same lines, he found that the principal moment by itself could not take care of the elementary equilibrium conditions along the yield lines. To satisfy the equilibrium conditions, Johansen introduced the well known nodal forces, which

*Numbers in parentheses refer to entries in the References.

actually represent twisting moments and shear. Johansen was then able to develop the yield-line theory on mathematical grounds. His yield-line theory will usually give an upper bound solution, which has been shown to be the exact solution for a few cases. An upper-bound solution may overestimate the carrying capacity.

In the U.S.A., Prager (3) has carried out general studies in plasticity, some of which can be applied to reinforced concrete slabs; especially the derivation to determine whether an upper bound solution is an exact solution.

Hillerborg (4) has developed an "equilibrium theory" or the "strip method." He chooses two of the three unknowns in the plate equilibrium equation and lets the equilibrium condition determine the third unknown. This method gives lower-bound solutions, and may in some cases give a rather low estimate of the carrying capacity.

Nielsen (5) follows to a certain extent the same line as Prager and finds both upper-bound and lower-bound solutions. Where these two solutions coincide, the result is exact. If the solutions do not coincide the lower-bound solution may give a good idea how well the yield-line theory can estimate the carrying capacity in a specific case.

Although the conventional yield-line theory as developed by Johansen may be on the unsafe side, experiments show generally a higher carrying capacity than predicted by the theory. This has led Wood (6) to examine the effect of the membrane forces. He has further pointed out that reinforcement inclined to the yield-line may be bent across the crack in the concrete and consequently increase the yield moment.

Kwiencinski (7,8) adopted the idea that reinforcement inclined to the failure line is partly bent across the failure line and coupled this with Ingerslev's assumption of no twisting moment in the yield line. On these assumptions, he developed a new approach to the yield-line theory.

In spite of numerous papers on this subject, with critical remarks and new ideas, the yield-line theory in practical use is the one developed by Johansen. His theory has proved to be very useful for determining the ultimate carrying capacity of reinforced concrete slabs. But Johansen's assumptions of the underlying yield criterion has not been confirmed by experiments. In fact, the most recent test series (11,12) may have added more confusion than confidence to the assumed yield criterion.

2.3. The Yield Criterion for Reinforced Concrete Plates Used by Johansen

Johansen has based his theory implicitly on a yield criterion which can be interpreted as described below for the three practical conditions of reinforcing schemes:

(1) Isotropically reinforced plate

The yield criterion is shown graphically in Fig. 2.1a. The bold lines show the yield condition for the moments in the x- and y-directions.

Because of its shape, Johansen's yield criterion is often referred to as the "square" yield criterion, and it states: The ultimate moment in one direction is independent of the moment in the perpendicular direction. In the graphical presentation in 2.1a no

twisting moment is shown. Occasionally the "square" yield criterion is presented in three dimensions with respect to the M_x, M_y and M_{xy} axes. But this seems to result in an unnecessarily complicated yield surface. The M_x and M_y axes can always be rotated so that they coincide with the principal directions of the external moments, and the twisting moment becomes zero. According to Johansen, the internal (resisting) moments are equal in all directions and do not produce twisting moments along the yield line.

(2) Nonisotropically reinforced plate

In the case where the directions of the reinforcement and the principal moments coincide, the yield criterion can be represented graphically in two dimensions. Figure 2.1b shows a case with unequal amounts of reinforcement in the top and bottom of the plate but each level contains isotropic reinforcement. In Fig. 2c the reinforcement in top and bottom of the slab is identical but with different amounts in the two directions.

A general case is shown in Fig. 2.1d. It may be considered as a combination of the cases in Fig. 2.1b and 2.1c.

If the directions of the reinforcement and the principal moments deviate, the twisting moment is no longer zero. For a graphical presentation, a common practice is to let the twisting moment make the third axis in a three-dimensional coordinate system. The result is a conical yield surface. Because this graphical method may not give a very clear illustration of the yield conditions, and because it is not absolutely needed in this chapter, it will not be explained or discussed here. The relationship between the moments M_x, M_y and M_{xy} can be

determined from Mohr's circle, Fig. 2.2a, in the same way as for the stresses σ_x, σ_y and τ_{xy} respectively.

(3) Skew reinforcement or reinforcement in more than two directions

In this case Johansen considers the two principal directions of the moment resistances provided by the various directions of reinforcement. Referring to Fig. 2.2b, the principal moment capacities are

$$\left.\begin{matrix} M_1 \\ M_2 \end{matrix}\right\} = \frac{1}{2}\left(\Sigma M_i \pm \sqrt{(\Sigma M_i \cos 2\alpha_i)^2 + (\Sigma M_i \sin 2\alpha_i)^2}\right) \text{ for } i = 1,2,\ldots \tag{2.1}$$

and their directions are $\varphi_{1,2}$

$$\tan\varphi_{1,2} = \frac{\Sigma M_i \sin 2\alpha_i}{\Sigma M_i \cos 2\alpha_i}, \quad i = 1,2,\ldots \tag{2.2}$$

The case may be considered equivalent to an orthogonally but non-isotropically reinforced plate for which the moment capacities in the φ_1 and φ_2 directions are M_1 and M_2 respectively.

Johansen's yield criterion has the same characteristics as that used in the general theory of plasticity. The plastic strains are perpendicular to the yield surface (or the yield line). In the corners of the various yield criteria shown in Fig. 2.1 the strains are in an unstable position with respect to direction.

Johansen writes it is imperative that the yield-line theory should be consistent with test results if theory is to be used in practice. In order to examine his theory, he compares his theoretical

predictions with test results of slab tests obtained by Bach and Graf (9), and himself (2). Johansen finds that his theory is in reasonably good agreement with the test results; but the yield criterion is never tested explicitly. All that can be concluded is that the total or "average" effect of the assumed yield criterion for the specific test slabs is reasonably close to the predicted effect.

Direct investigations of the yield criterion for reinforced concrete plates have been reported in two cases, namely the investigations by Nielsen (10) at the Academy of Engineering, Copenhagen, and Baus and Tolaccia (11) at the University of Liege.

2.4. Tests by Nielsen (10)

Nielsen tested reinforced concrete plates subjected to pure torsion. For isotropic reinforcement, his loading condition would correspond to the corners of the yield criterion in quadrants 2 and 4 as shown in Fig. 2.1a, since $M_x = -M_y$, or $-M_x = M_y$.

The specimen is shown in Fig. 2.3. The upward and downward loads provide the torsional moment. The forces from the concentrated loads were transmitted to the plate by steel channels along the edges. The reinforcement was welded to the channels. Table 2.1 gives specifications of the test specimens and the results. Both isotropically and nonisotropically reinforced slabs were tested. The symbol μ denotes the ratio of the amount of reinforcement in one direction to that in the perpendicular direction such that μ is less than or equal to unity. In all test specimens the directions of the yield lines were observed to be inclined at 45 degrees to the reinforcing bars. Let M and μM be

the yield moments in the directions of the steel bars. According to Johansen, the yield moment across the observed yield line is

$$M_\alpha = M \cos^2\alpha + \mu M \sin^2\alpha = \frac{M}{2}(1 + \mu) \qquad (2.3)$$

because $\cos^2 45^\circ = \sin^2 45^\circ = 0.5$.

Nielsen assumes that the ratio between the concrete stresses in the direction of the reinforcing bars, is also μ. Furthermore, he assumes that the usual relations between stresses based on equilibrium and represented by Mohr's circle are valid. From Nielsen's assumptions it is derived for small percentages of steel

$$M_\alpha = M\sqrt{\mu} \qquad (2.4)$$

Thus, the ratio between M_α in Eq. 2.3 and 2.4 is $1/2(\mu + 1)/\sqrt{\mu}$. It may be noticed that only in specimens 3 and 4 in Table 3.1 will there be a marked difference between the predictions of Eq. 2.3 and 2.4. Consequently, the close correlation between measured and calculated values indicated in the last column of Table 2.1 supports Johansen as well as Nielsen, except for the results of specimens 3 and 4.

The use of steel channels welded to the reinforcing bars along the edges of the specimens gives rise to the following objections:

(1) When a reinforced concrete cross section is subjected to bending cracks, the neutral axis moves towards the compression zone. The plane at the mid-height of the section expands in the direction of the bending moment. In a plate with equal top and bottom reinforcement, the expansion at mid-height is independent of the sign of the bending

moment. Thus the torsional moment which can be represented by two perpendicular moments of opposite sign, results in an expansion of the plane at the mid-height in all directions. The edge channels resist an expansion of the plate and act like prestressing rods along the edges.

(2) The channels exclude the possibility of a "shear" failure that would occur along a line parallel to an edge.

(3) The channels force the yield lines to form along a line making an angle of 45 degrees with the edge. Although it may be argued that the yield lines should form at 45 degrees to the edges even in the case of nonisotropic reinforcement, the edge channel excludes any verification of this assertion.

2.5. Tests by Baus and Tolaccia (11)

Baus and Tolaccia, under the direction of Professor Louis and Professor Massonet, have carried out the first systematic experimental research to determine the yield criterion for reinforced concrete plates under uniaxial and biaxial moments. Their reinforced concrete test specimens were 1.30 by 1.30m with a thickness of 8 cm. Cylinder tests (15 by 30 cm) at 28 days gave a compressive strength of 280 kg/cm^2 (4000 psi). The reinforcement was 10 mm bars of flat top steel, yield stress was 2830 kg/cm^2(40,300 psi) and ultimate stress was 3830 kg/cm^2(54,500 psi). The loading system is shown in Fig. 2.4. The jacks are so connected that the leverarms can give a uniformly distributed moment along each edge. The reinforcement in two typical plates is shown in Fig. 2.5a and b. The investigators found it

necessary to provide the extra reinforcement along the edges to prevent the jaws or the forks of the leverarms from breaking the edges of the specimen. Some test results are shown in Fig. 2.6. The results shown in Fig. 2.6a refer to the specimen described in Fig. 2.5a and those in Fig. 2.6b refer to the specimen in Fig. 2.5b. The shape of this yield criterion is quite different from that of Johansen which is shown in Fig. 2.6 by broken lines. Baus and Tolaccia illustrate the difference of the two yield criteria applied to the yield lines in a practical case, Fig. 2.7. The investigators suggest several reasons for the increase of moment capacity in going from uniaxial to biaxial bending. Some of their suggestions are quoted below. For the case with the reinforcement parallel to the edges of the plate and for biaxial moments of equal signs: "The concrete on the compression side is subjected to biaxial compression. This causes an effect analogous to that of a precompression of the specimen. This effect is most important when the compressive stress and Poisson's Ratio of the concrete are high." For the case with reinforcement parallel to the edges and biaxial moments of opposite signs: "The tensioned concrete surrounding the steel is subjected to a transverse compression which squeezes it against the bars, thus augmenting its bond and hindering the cracking. If one assumes that cracking of the concrete in tension is not produced before the reinforcement reaches plastification, the moment required in order to obtain this plastification is also a function of the tensile strength of the concrete." For the reinforcement inclined 45 degrees to the edges of the plate: "The moment capacity of a test specimen or a plate element is dependent on the

crack formation in the concrete. It is differentiated between the general crack direction and the local crack direction and the local crack direction. The latter is a result of the former. The reinforcing bars are plastified perpendicularly to the local cracks and thus the plate gains strength in this direction."

What Baus and Tolaccia term "perpendicular plastification" has been referred to as "kinking" by Wood (6) who has demonstrated it with the sketch shown in Fig. 2.8. Initially the reinforcing bar is inclined to the crack. As the crack opens, the bar is bent or kinked across the crack.

Baus and Tolaccia's concept of the tendency of reinforcement to bend across the crack is more complex than the idea presented by Wood. Figure 2.9a shows the case of uniaxial moment with the reinforcement inclined at 45 degrees to the moment direction. In this case the investigators assume no local change of the direction of the reinforcement. Figure 2.9b shows the case with equal moments in all directions. According to Baus and Tolaccia, the reinforcing bars in one direction are bent, while the bars in the other direction remain straight.

The problem of "perpendicular plastification" or "kinking" is an important one and will be discussed in detail in Chapter 3 of this report. However, certain remarks are pertinent here.

If reorientation of the reinforcement is to be claimed at all, it is difficult to see how it can be ignored for the condition shown in Fig. 2.9a. The phenomenon claimed in Fig. 2.9a is kinematically inadmissible, as is the one shown in Fig. 2.9b. Furthermore,

if it is considered that Fig. 2.9b refers to a case of equal moments in all planer directions, it would appear that while the moment capacity in one direction is enhanced by the reorientation of the reinforcement, the capacity in another direction is reduced.

A crucial question is whether the test specimen used by Baus and Tolaccia represented an element of a concrete plate with the moments well controlled and known throughout the element. The moments from the levers used should provide a uniformly distributed moment within a short distance from the edge, according to St. Venant's principle. This is shown in Fig. 2.10 along cross section A-A. Noticing that the unit moment capacity of the edges which have additional reinforcement is approximately twice that of the center part of the specimen, the distribution of the yield moment is as shown for section B-B in Fig. 2.10.

The transition from the uniformly distributed moment to the stepwise uniformly distributed moment will bring in moments in the perpendicular direction and also twisting moments. Figure 2.11a shows approximately the paths of the stress trajectories of the tensile forces in the case of an applied uniaxial moment. The compatibility conditions force the trajectories of the stresses in the compression zone of the concrete to take much smoother paths, Fig. 2.11b) Figure 2.11 demonstrates that a moment in one direction may set up significant stresses in the perpendicular direction. By considering the components of the forces, the forces in the perpendicular direction can be estimated to be about 20 percent of the forces in the reinforcement in the direction of the moment.

The confinement of the interior part of the test specimen is further enhanced by the different position of the neutral axis in the middle and in the edge strips (see Fig. 2.12). If it is assumed that shear forces will keep the curvature approximately uniform across the specimen, the tendency for horizontal expansion at mid-height is considerably larger for the light reinforced middle part than for the heavier reinforced edge strip.

The over-all effect on the test area (the area with lighter reinforcement as shown in Fig. 2.5) is similar to the effect obtained by prestressing the plate.

Figure 2.13 shows the crack pattern for the plate in Fig. 2.5a subjected to uniaxial moment. The diagonal cracks in the corners support the hypothesis about uneven moment distribution. An isotropically reinforced element subjected to a uniaxial, uniform moment should not develop diagonal yield lines.

2.6. Tests by Kwiecinski (12)

Kwiecinski's investigation was closely related to his yield-line theory, which is based on the two principles:

1. Partial "kinking" of the reinforcement.
2. No twisting moment can exist along the yield-line.

Kwiecinski tested 16 specimens to check the first point. The specimen and loading conditions are shown in Fig. 2.14. The reinforcement net is the same for all specimens, but rotated 15, 30 and 45 degrees with respect to the span direction. Kwiecinski's interpretation of the test results is shown in Fig. 2.14b.

In Kwiecinski's theory the effect of kinking is assumed to be maximum when the reinforcement is inclined at 45 degrees to the moment direction (see Fig. 2.14) and the effects of kinking for other inclinations are related to the maximum value.

From the interpretation of the results of his tests, Kwiecinski concluded that the maximum enhancement of the moment capacity attributable to kinking was 18.8 percent, a quantity in reasonable agreement with a statement by Wood (6) who found the corresponding magnitude to be 16 percent. Wood has not, however, reported the tests leading to his conclusion.

Kwiecinski used small specimens (Fig. 2.14). Seven or eight bars crossed the yield line. No provision was made to provide anchorage of the end of the bars. The specimens with bars inclined to the edges, failed in bond. In evaluation of the moment capacity, the investigator considered a reduced number of bars. Considering that up to 50 percent of the bars may be subjected to bond failure, the modified test results are bound to depend on personal opinion and experience.

2.7. Tests by Houbolt (13)

This investigation was carried out in 1941-42, before the discussion of kinking had started. The object of the investigation was to examine the effectiveness of reinforcement in skew bridge slabs, where the layers of the reinforcement may make different angles with each other and with the directions of principal moments. Hence, this too was an investigation on the kinking phenomenon.

The test slabs were 5 ft 3 in. square in plan and had an over-all depth of 5.17 in. The span was 5 ft. The loads were applied at the third points of the span as shown in Fig. 2.15. The bars made angles of α_1 and α_2 with the direction of the span. The spacing of the 3/8-in. plain round bars and their orientation are given in Table 2.2 for the 15 test slabs. The bars were hooked at the ends. The yield stress was 50,200 psi. The effective depths of the bars and the concrete strength are listed in Table 2.2. The calculated values of the moment are based on an conventional interpretation of the effectiveness of the reinforcement with kinking completely ignored.

The comparison of the measured and calculated values does not indicate any significant kinking. To the contrary, the carrying capacity tends to decline somewhat when the direction of the reinforcement deviates from the span direction. The test specimen rested on kink-edge supports restrained from horizontal motion. Generally such supports will have the following effects: (1) the supports set up axial forces (membrane forces) that will tend to increase the carrying capacity, and (2) the supports partly hinder twisting of the slab that may be produced by nonisotropic reinforcement. A twisting moment caused by the reinforcement will influence the formation of the yield-lines so that the carrying capacity of the slab is minimized. Unless twisting does not exist or is completely prevented, it is not correct to assume the yield line to form perpendicular to the external principal moment, as done by Houbolt. In two particular cases, H7 and H15, Houbolt reported that the slab corner was lifted off the support which indicates that these two specimens had an angle of twist. These two

tests rank with the very lowest "effectiveness" in Table 2.2. Consequently, the scatter in the last column in the table is partly due to erroneous assumptions. The study of formation of yield-lines and moment capacities will be dealt with in detail later. It can be concluded the Houbolt test results are satisfactory with regard to kinking, but other important properties were obscured by the support conditions.

2.8. Tests by Silverj (14)

Silverj investigated reinforced concrete specimens subjected to uniaxial bending. His test setup has several similarities with that of Houbolt. By coincidence, Silverj's study has been in effect a continuation of Houbolt's work. Some details of Silverj's test setup are shown in Fig. 2.16. The load was applied by 24 equally spaced jacks in the test area. Silverj was primarily interested in non-isotropically reinforcement and tested specimens with reinforcing bars in one direction only, see Fig. 2.17. Nineteen tests were carried out, five tests with the reinforcement parallel to the span, three series of tests each comprising three specimens were carried out with the reinforcing bars inclined 15, 30 and 37.5 degrees to the span, and finally four tests were carried out with the bars at 45 degrees to the direction of the span. The amount of reinforcement varied from 0.49 to 1.00 percent. The bars were of "flat-top" steel with yield stress 3020 kg/cm^2 (43,000 psi). The concrete strength was 350 kg/cm^2 (5000 psi) after 6 hours of steam curing and eventually rose to about 450 kg/cm^2 (6400 psi) after 10 days. The concrete strengths refer to

7-cm cube tests. The resulting moment capacities at yield and ultimate are shown in Fig. 2.18. In order to compare the test results directly, the moments are divided by the respective number of bars, n, crossing the testing area and the distance, j, from the center of the reinforcement to the resultant compression force in the section.

According to Johansen, the effectiveness of a reinforcing bar declines as $\cos\alpha$, where α denotes the deviation from the direction of the span. If a normalizing of the reinforcement takes place in the direction of the span, the effectiveness of a reinforcing bar is not reduced by a deviation from the direction of the uniaxial moment. Silverj's test results indicate no significant effect of partly normalizing or kinking of the reinforcement. It is interesting to observe that in most test specimens the curvature is concentrated at one yield line, as would also be expected in the case of a live load. The mode of failure is similar to that in the investigations of Kwiecinski (12), but the conclusions of the two researchers do not agree.

Silverj's experiments do not give conclusive information about the formation of yield lines for two reasons:

1. The cracking moment was of the same magnitude as the yield moment, in some cases even greater than the yield moment.

2. The supports were not able to rotate about an axis in the direction of the span and resisted twisting moments along the yield line.

2.9. Tests by Peter (15)

Peter's object, as Houbolt's, was to examine any possible decrease in effectiveness of the reinforcement whose direction deviates from the external principal stresses. He investigated reinforced concrete plate elements subjected to tension. The test specimens were 160 by 160 by 8 cm. The bars made angles of α_1 and α_2 with the direction of the tensile force. The diameter, spacing and the orientation of the reinforcement are given in Table 2.3 for seven test specimens. The bars were hooked in the ends. The yield stress was about 4500 kg/cm^2 (64,000 psi). The tensile forces in column 8 of Table 2.3 were calculated ignoring any possible reorientation of the reinforcement at the cracks. Furthermore a reduction of 10 percent was used to account for "size effect," this effect being attributed to possible imperfections in the test specimen and setup. Peter considers the "kinking-phenomenon" to be a local distortion related entirely to the crack and the characteristics of the reinforcement, whatever causes the cracking. Peter's, Houbolt's, and Silverj's test results support this idea. Duplicate tests give an indication of the scatter of the test results. It can be concluded that kinking did not result in any significant change of the tension capacity in the test series carried out by Peter.

2.10. Concluding Remarks

The yield-line theory is generally recognized as a powerful method for determining the carrying capacity of slabs. The theory has not, however, had a corresponding progress as a design method--or more

correctly as a proportioning method outside the U.S.S.R. There is no doubt, however, that the yield-line theory has greatly influenced building codes in most countries.

Comité Europeen du Beton has made preparations to introduce the yield-line theory as a design method in the European countries, probably in a modified form which will guard against excessive deformations. This development has intensified the discussion of the yield-line theory. The discussion so far has not resulted in a clear crystallization of the theory. Since Johansen (2) introduced his nodal forces to satisfy the equilibrium conditions, the physical interpretation of these forces have been a topic of discussion. For example, Nielsen (16) introduces nodal forces of "type 1 and 2," while Wood (17) writes about "Reasons for the occasional breakdown of nodal force theory." The result is that the engineer avoids the whole problem by considering the virtual work equations instead of the equations for equilibrium. The total work done by the nodal forces is always zero and thus the nodal forces do not enter the work equations.

However the theory of virtual work has also got its problems. Prager (3) and later Nielsen (5), for instance, claim that the "exact" solution is known for a square plate, while Nylander (18) shows that he can arrange the yield-lines such that the carrying capacity of the plate is less than that given by the "exact" solution, as illustrated in Fig. 2.19.

It seems to be more and more realized by everyone that one of the major causes that contributes to the confusion is the absence of a generally accepted yield criterion.

The described research work at the University of Liege are the only investigations whose object was to determine the entire yield criterion experimentally. Several other investigators have been concerned by various facets of the question. Thus, the local normalizing of the reinforcing bars has been the subject of considerable attention. In chronological order, the conclusions with regard to this problem have been as follows. Houbolt (13) did not even consider the possibility of a significant effect from a normalizing of the reinforcement, neither did his test results indicate anything in that direction. Wood (6) wrote in his book that in tests carried out at the Building Research Station an increase of up to 16 percent in yield moment was recorded in the case of reinforcing bars crossing the yield line at an angle of 45°. Nielsen's experiments (10) where the reinforcing bars also were inclined 45° to the yield line, indicated no significant effect of normalizing of reinforcing bars. The investigators at the University of Liege let this effect play a major role in their explanation of the obtained increased moment capacity under biaxial bending. Kwiecinski found a significant kinking effect for specimens under uniaxial moment and with the bars deviating from the span direction. At Liege no similar effect was found in the corresponding cases.

It can certainly be concluded that many questions are still open within the yield-line theory. But the first requisite for progress is a solid foundation, a well confirmed yield criterion for reinforced concrete slabs.

3. EFFECTIVENESS OF REINFORCING BARS INCLINED TO THE PRINCIPAL STRESS AXES

3.1. Introductory Remarks

This chapter describes the studies carried out in the present investigation in relation to the problem of local normalizing of reinforcing bars to the yield lines. The object of the chapter is to arrive at a conclusion with regard to the significance of the effect of the normalizing of the reinforcing bars.

Before introducing the present investigation, it may be pertinent to offer a few critical remarks on the traditional presentation of the problem, illustrated by the sketch in Fig. 3.1a. A reinforcing bar is inclined to the local direction of the crack. As the crack opens, the bar becomes normal to the crack. This would be a complete normalizing or "full kinking." If the concrete crushes at the edge of the crack, the bar is bent less. This would be a partial normalizing or "partial kinking." It seems obvious from this sketch that some reorientation of the reinforcing bar must take place. In Fig. 3.1b, the same case is shown in more realistic proportions as it may appear in a slab with a deflection several times that at yielding of the reinforcement. In this case, it is unreasonable to expect significant effects from reorientation of the reinforcement.

The work presented in this chapter is based on analytical studies and experiments on reinforced concrete plate specimens.

3.2. Premises Used in the Analytical Solutions

With the help of idealized assumptions about the materials involved and the geometry, it is possible to make analytical studies of the possibilities of the normalizing of reinforcing bars to the yield lines. General premises on which these studies are based are discussed in this section.

First it should be mentioned that the possibility of a reduction in strength caused by bar reorientation will not be considered because no such effect has been measured or theorized. It is true that, if the reinforcing bars are not colinear with the principal stresses, the moment for a given elastic deformation may be less. However, the ultimate moment resistance is not known to be reduced.

Two assumptions are made with reference to the reinforcing bars:

(1) The reorientation of the reinforcing bars is considered to be a local phenomenon at the yield line, so that it is sufficient to consider a single bar that crosses the crack or yield line at an angle other than 90 degrees.

(2) The bending stiffness of the reinforcing bar is assumed to be negligible. The bending stiffness is effectively zero for a bar of "flat-top" steel which is already subjected to its axial yield force, if the axial force remains constant as the bar bends.

Three different solutions are developed for three different assumptions about the mechanical behavior of the materials:

(1) The stress-strain curve for the concrete is assumed to be linearly elastic.

(2) The stress-strain curve for the concrete is assumed to be rigid-plastic.

(3) An analysis of the bar reorientation phenomenon is made independently of the stress-strain curve for the concrete in compression by assuming that the increase in force perpendicular to the section made possible by bar reorientation is transferred from the steel to the concrete uniformly over a finite length.

3.3. Reorientation of Bars in "Elastic" Concrete

Consider Fig. 3.2. From geometry it can be concluded that the reinforcing bar is antisymmetric with respect to the intersection between the center lines of the crack and the bar. Therefore, this point of intersection will remain fixed independently of the width of the crack and the conditions on either side of the crack. Using the coordinate system shown in Fig. 3.2b, the equilibrium conditions require

$$F_s \frac{d^2y}{dx^2} = - q \qquad (3.1)$$

where F_s = force in the bar

q = pressure per unit length exerted on the concrete by the bar.

Since the concrete is assumed linearly elastic, the pressure, q, can be expressed as

$$q = - ky \qquad (3.2)$$

From Eq. 3.1 and 3.2

$$\frac{d^2y}{dx^2} - \frac{k}{F_s} y = 0, \qquad \text{for } x \geq 0 \tag{3.3}$$

Solution of this differential equation is

$$y = A \exp\left(\sqrt{\frac{k}{F_s}}\, x\right) + B \exp\left(-\sqrt{\frac{k}{F_s}}\, x\right) \tag{3.4}$$

where "exp" stands for the exponential function, for example, $\exp a = e^a$. A and B are constants determined by the boundary conditions

(1) $x \to \infty$, $\lim y = 0$, $A = 0$

(2) $x = 0$, $y - y'(0.5w \cos\alpha - y \tan\alpha) = -0.5w \sin\alpha$

where α is the inclination of the bar with respect to the perpendicular to the crack as shown in Fig. 3.2, and w is the width of the crack. The relation in the boundary condition (2) is derived from the geometry shown in Fig. 3.2, and the antisymmetry as explained in the beginning of this section.

Combining Eq. 3.4 and the boundary condition (2)

$$B = \frac{1 + \sqrt{\frac{k}{F_s}}\, \frac{w}{2} \cos\alpha}{2\sqrt{\frac{k}{F_s}}\, \tan\alpha} \left[1 - \sqrt{1 + \frac{2\sqrt{\frac{k}{F_s}}\, w \tan\alpha \sin\alpha}{\left(1 + \sqrt{\frac{k}{F_s}}\, \frac{w}{2} \cos\alpha\right)^2}} \right] \tag{3.5}$$

Because w is small compared with unity

$$B \approx -0.5w \sin\alpha \tag{3.6}$$

Substituting Eq. 3.6 into Eq. 3.4 (A = 0)

$$y \approx -0.5w \sin\alpha \exp\left(-\sqrt{\frac{k}{F_s}}\, x\right) \tag{3.7}$$

The slope is found by differentiation,

$$y' \approx 0.5w\sqrt{\frac{k}{F_s}}\,\sin\alpha\,\exp\left(-\frac{k}{F_s}x\right) \tag{3.8}$$

At the edge of the crack, x = 0,

$$y_o \approx -0.5w\,\sin\alpha \tag{3.9}$$

and

$$y'_o \approx +0.5w\sqrt{\frac{k}{F_s}}\,\sin\alpha \tag{3.10}$$

Equation 3.10 expresses the reorientation of the bar related to its original direction. In a specific case, F_s and α are known, w may be given, assumed or measured. The "spring" constant, k, can be estimated from the modulus of elasticity of the concrete and the geometry of the section. A numerical example will be given in Section 3.6.

3.4. Reorientation in "Rigid-Plastic" Concrete

The assumption implies that the pressure, q, exerted by the reinforcing bar on the concrete, is constant over a length, L_p, which is required for equilibrium. This is the only difference from the previous case. Hence

$$\frac{d^2y}{dx^2} + \frac{q}{F_s} = 0 \qquad 0 \le x \le L_p \tag{3.11}$$

Solution of Eq. 3.11

$$y = -\frac{q}{2F_s}x^2 + Cx + D \tag{3.12}$$

where C and D are constant determined by the boundary conditions

(1) $x = L_p$, $y = 0$ and $y' = 0$

(2) $x = 0$, $y - y'(0.5w \cos\alpha - y \tan\alpha) = -0.5w \sin\alpha$

Condition (2) was explained in Section 3.3.

Substituting Eq. 3.12 into the boundary conditons (1) and (2)

$$-0.5 \frac{q}{F_s} L_p^2 + C L_p + D = 0$$

$$- \frac{q}{F_s} L_p + C = 0 \qquad (3.13)$$

$$D - C (0.5w \cos\alpha - D \tan\alpha) = -0.5w \sin\alpha$$

Solution of Eq. 3.13

$$C = \frac{q}{F_s} L_p \qquad (3.14)$$

$$D = \frac{-q}{2F_s} L_p^2 \qquad (3.15)$$

where L_p can be determined by

$$\frac{q}{F_s} \tan\alpha \, L_p^3 + L_p^2 + w \cos\alpha \, L_p - \frac{F_s w}{q} \sin\alpha = 0 \qquad (3.16)$$

For small values of L_p the following approximation for L_p can be derived

$$L_p \approx \sqrt{\frac{w F_s \sin\alpha}{q}} \qquad (3.17)$$

The values of y and y' at the edge of the crack, x = 0, are found by substituting Eq. 3.17 into Eq. 3.14 and 3.15

$$y_o \approx -0.5w \sin\alpha \tag{3.18}$$

$$y'_o \approx \sqrt{\frac{w\ q\ \sin\alpha}{F_s}} \tag{3.19}$$

As in the previous section y'_o is the deviation of the bar from its original direction at the edge of the crack caused by the bar reorientation at the crack.

3.5. Reorientation of Bars Based on Constant Rate of Transfer

It is assumed that the enhancement in force perpendicular to the section due to reorientation of the reinforcing bars is uniformly distributed over the length, L, in Fig. 3.3. Indirectly, this may require some crushing of the concrete at the edge of the crack.

The assumed rate of force transfer is possible if the bar bends into the shape described by Eq. 3.20

$$y = A_1 x^2 + B_1 x + C_1 \tag{3.20}$$

where the coordinate system is as shown in Fig. 3.2b and A_1, B_1, and C_1 are constants which can be determined from the boundary conditions

(1) $x = L$, $y = A_1L^2 + B_1L + C_1 = 0$

and $y' = 2A_1L + B_1 = 0$

(2) $x = 0$, $y - y' (0.5w \cos\alpha - y \tan\alpha) = -0.5w \sin\alpha$

The derivation of (2) is explained for the corresponding case in Section 3.3.

Substituting Eq. 3.20 into the boundary condition (2)

$$C_1 - 0.5w \cos\alpha\, B_1 + B_1 C_1 \tan\alpha + 0.5w \sin\alpha = 0 \qquad (3.21)$$

Combining boundary conditions (1) with Eq. 3.21

$$B_1 = \frac{-(L + w\cos\alpha) + \sqrt{(L + w\cos\alpha)^2 + 4Lw \sin\alpha \tan\alpha}}{2L \tan\alpha} \qquad (3.22)$$

The other constants can be expressed in terms of B_1

$$A_1 = -\frac{B_1}{2L} \qquad (3.23)$$

$$C_1 = -\frac{B_1 L}{2} \qquad (3.24)$$

Because w is very small in relation to L, Eq. 3.22 can be simplified considerably without any significant loss in accuracy. Thus

$$A_1 \approx -0.5\,\frac{w}{L^2}\sin\alpha; \qquad B_1 \approx \frac{w}{L}\sin\alpha; \qquad C_1 \approx -0.5w\sin\alpha \qquad (3.25)$$

The values of y and y' at the edge of the crack, x = 0, are

$$y_o \approx -0.5w \sin\alpha \qquad (3.26)$$

$$y'_o \approx \frac{w}{L}\sin\alpha \qquad (3.27)$$

The slope, y'_o, represents the reorientation of the bar across the

crack. The distance, L, may be estimated on the basis of observation or empirical formulae.

It is also interesting to check whether Eq. 3.20 is consistent with the basic assumption used in this section: uniform rate of force transfer from the bar to the concrete.

The transferred force, F_x, at any point, x, is

$$F_x = [\cos(\alpha - \varphi_o) - \cos(\alpha - \varphi)]F_s \qquad (3.28)$$

where φ_o is the reorientation at x = 0 and φ is the reorientation at an arbitrary x. For the small angles that occur in this case φ_o may be approximated with y'_o and φ with y', and $\cos\varphi_o \approx \cos\varphi \approx 1.0$, $\sin\varphi_o \approx \varphi_o$ and $\sin\varphi = \varphi$. Introducing these approximations and the expressions for y'_o and y' into Eq. 3.28

$$F_x \approx \frac{wx}{L^2} \sin\alpha \, F_s \qquad (3.29)$$

Equation 3.29 expresses that the force is transmitted from the steel over to the concrete at a constant rate, which agrees with the original assumption.

3.6. Discussion of the Analytical Solutions

In order to demonstrate and discuss the results of the three analytical approaches, the following case is chosen:

(1) The reinforcement is isotropic and is made up of 0.5-in. bars spaced at 4 in. The yield stress of the steel is 40,000 psi.

(2) The concrete strength, f'_c, is 5000 psi. The modulus of elasticity, E_c, is assumed to be 3,000,000 psi. The "plastic" pressure

on the concrete is also assumed to be 5000 psi. A fairly high estimate of the "spring constant," k, of the concrete gives $k = 2E_c/3 = 2{,}000{,}000$ psi. The concrete cover is 0.5 in. α is 45°.

(3) The minimum crack spacing is expected to be about 1 in.

These numerical values are introduced in the previous three derivations.

Assuming concrete to be linearly elastic, from Eq. 3.10

$$y'_o = 4\sqrt{2}\, w \tag{3.30}$$

Assuming concrete to be rigid-plastic, from Eq. 3.19

$$y'_o = 0.48\sqrt{w} \tag{3.31}$$

Assuming uniform transfer of the increment force due to normalizing of the bar, from Eq. 3.27

$$y'_o = \sqrt{2}\, w \tag{3.32}$$

The following consideration results in an upper limit for all three of the analytical approaches. Consider a section of a reinforced concrete slab as shown in Fig. 3.3. If the bars are reoriented at the cracks, a section through a crack will develop an increased moment capacity. Such an increase of capacity can be effective only if the section between the cracks is able to resist the increased moment. The path of a reinforcing bar is antisymmetric with respect to the center line between the cracks. The direction of the bar is not changed at this point. Therefore, the concrete has to resist the additional moment due to the reorientation of the bar at the

crack. That is, an enhancement of the moment capacity due to bar reorientation cannot exceed a magnitude corresponding to the cracking moment of the section. This consideration is of little value if the conditions are such that the curvature is concentrated in single yield lines.

The results of the three analytical methods are illustrated in Fig. 3.4. At very small crack widths, say below 0.001 in., the assumption of concrete as a linearly elastic material is believed to be the most realistic. However, by increasing crack width this assumption results in a fast increase of the maximum stress and at a crack width of 0.003 in. the stress can be estimated to be 5000 psi. At this stress level local crushing of the concrete may take place and it would not be realistic to extend the curve beyond this point.

The assumption of concrete as a rigid-plastic material cannot necessarily apply at very small crack widths with the stress level in the elastic region. However, the curve gives a good idea about the conditions at large crack widths if it is assumed that no crushing at the very edge would take place. However, it is most likely that crushing will take place at a rather small crack width as indicated by the linearly elastic approach.

The assumption of a constant rate of transmitting the force to the concrete gives probably the most reliable picture at crack widths beyond 0.01 in. The curve in Fig. 3.4 demonstrates the effect of the crushing. It is not possible to analyze the crushing of the concrete and its effect, but it is believed that if the concrete is crushed so much that the force transfer can be practically uniform

through the uncracked section, no more crushing is likely to take place.

The above discussion may give an idea of the mechanism of response at the crack. A linearly elastic response of concrete should be expected at very small cracks. With increasing crack width and the resulting increasing concrete stresses the characteristics of the response will gradually change from that of an elastic material to that of a plastic one. However, the stresses cannot be raised very high before a crushing at the edge takes place. This causes an abrupt decrease in both the bar reorientation and the concrete stresses. As the crack continues to open, the stresses are built up until the next crushing of the concrete takes place as illustrated by the broken line in Fig. 3.4. The upper and lower limits are the curves based on the analysis presented in the previous sections.

The analysis has brought out two important points.

(1) If the reinforcing bar is inclined to the crack, some reorientation has to take place. The enhancement of moment capacity, however, is usually not sufficiently significant to play a role in the carrying capacity of a slab. At very large deflections of a slab structure the reorientation might contribute a palpable amount to the carrying capacity, but at this advanced stage the reorientation effect is usually overshadowed by such phenomena as strain hardening of the reinforcement and membrane forces. In the example illustrated in Fig. 3.4 the reorientation of the reinforcement at yielding is about 1.0 degree. The corresponding increase in moment capacity is about 1.7 percent. At a deformation corresponding to five times that at

yield, the increase in moment capacity should be between 2 and 5 percent.

(2) The small or negligible effect of the reorientation of the reinforcement can be explained by a simple analysis. Since Johansen (2) introduced the "staircase" crack pattern to explain the negligible effect of the reorientation of the reinforcement, the same idea has been adopted in several papers, but the idea has also been an object of criticism, not only considered as a minor point but as a major weakness in Johansen's yield-line theory. A local crack pattern like the one of a "staircase" has never been observed and this concept certainly weakens the impression of realism, which is the condition for the existence of the yield-line theory. Hence, by replacing the "staircase" or "stepwise" crack pattern with an analysis like the one demonstrated above, the yield-line theory would have a more realistic basis.

3.7. Tests to Study the Bar Reorientation Phenomenon

The following sections of this chapter present and discuss the test results of the present investigation pertinent to the problem of the local reorientation of reinforcing bars.

The theoretical analyses in the previous sections emphasized the need for experiments. The justification for the assumptions in the analyses can be given by tests only. However, the tests are arranged so that the test results can give direct information about the effect of the bar reorientation independent of theories or hypotheses.

An outline of the tests is given in Section 1.2. In four of the test specimens the directions of the reinforcement were chosen so that the reinforcing bars were perpendicular to the yield lines. Thus the results of these four tests without reorientation of the bars can be used as reference for the other tests where a reorientation may take place.

The properties of the test specimens and the test results are given in Table 3.1. A detailed description of the test specimens, the test rig, and data reduction is given in Appendix A.

3.8. Test Specimens Subjected to Uniaxial Moment

The results from the tests under uniaxial bending are presented and discussed in this section. The uniaxial-moment test is simple to carry out. The test is really a test of a beam. Hence, earlier experiences from beam tests contribute to the understanding of this test. If the effect of reorientation of the reinforcement is a local phenomenon depending on the crack but not on the cause of the crack, the uniaxial test should be fully satisfactory for a general investigation of the effect of bar reorientation. The results described in the following two sections support the assumption of the bar reorientation being a local phenomenon.

The moment-curvature relationships of four test specimens, B4, B7, B8 and B10, all isotropically reinforced, are shown in Fig. 3.5. The yield lines formed perpendicular to the direction of the span in all four specimens as shown in Fig. 3.6, such that the reinforcement crossed the yield line at an angle of 90 degrees in

test B4 and B10, at 45 degrees in test B7 and at 22.5 and 67.5 degrees in test B8. The results in Fig. 3.5 give no indication of an enhancement in moment capacity because of the inclined reinforcement in test B7 and B8. It may be noticed that this conclusion is valid all the way up to a deformation corresponding to 10 times that at yielding at specimen B4. The observed maximum crack width at ultimate moment was about 0.03 in.

Three test specimens, B9, B11 and B12, with nonisotropic reinforcement were also subjected to uniaxial moment. The direction of the main layer of reinforcement with respect to the span direction was 45 degrees in B9, 22.5 degrees in B11 and 67.5 degrees in B12. It will be shown in the next chapters that in the case of nonisotropic reinforcement the yield lines do not generally form perpendicular to the direction of the span. Therefore, a direct comparison as in the previous case is no longer practical. An indirect comparison is made in Table 3.1. In computing the values in the table, the effect of a bar reorientation, if any, is consistently neglected. Hence, the good agreement between computed and measured values in Table 3.1 indicates that the effect of the reorientation of the reinforcing bars has no significance.

3.9. Test Specimens Subjected to Isostatic Moment

The term "isostatic moment" is used in this paper to refer to a state of equal moments in all planar directions. This is a unique, extreme case which suits well the purpose of examining the

reorientation of the reinforcing bars under conditions different from external uniaxial moment.

As it is seen from the outline in Section 1.2, three specimens, C1, C2 and C3, were subjected to isostatic moment. The reinforcement was isotropic and directly comparable to the symmetric reinforcement in the specimens under uniaxial bending.

The measured moment-curvature relationships for specimens C1, C2, and C3 are compared with those for specimens B4 and B7 in Fig. 3.7.

There is no observed difference in strength between the case of isostatic bending and that of uniaxial bending. It can be concluded that a bar reorientation, if any, has no significant effect in the case of isostatic bending. This result is not surprising. By assuming the reorientation to be a local problem, concerning the crack and the reinforcing bar and their directions only, no reorientation should be expected. Consider a typical crack pattern for isostatic moment as shown in Fig. 3.8. The formation of cracks in the test area are nearly identical to the reinforcement scheme in the plate. The apparent reason for this is that when the concrete is stressed equally in all directions, a reinforcing bar will weaken a concrete section in the line of the bar. In fact, in Fig. 3.8 the reinforcing bars are usually found right in the cracks. Because the reinforcement is rectangular, the cracks and the bars also form right angles. Consequently, no reorientation should take place.

The unlikeliness of having an enhancement in moment capacity because of bar reorientation in the case of isostatic bending can be argued more generally as follows. Consider a yield line in an

arbitrary direction. The moment capacity across the yield line has to match the isostatic moment and so must the moment capacity along the yield line. If a reorientation should take place across the yield line the moment capacity would increase perpendicular to the yield line but would decrease parallel to the yield line. Hence, the capability of the plate to carry an isostatic moment is decreased. Should such a development take place, the plate would deform in the weaker direction until a sufficient "counter reorientation" takes place. Thus the original moment capacity is regained, but by no means enhanced.

The eventual collapse of the specimens for isostatic bending was characterized by the collapse of one "loading wing." The reinforcement of a circular test is shown in Fig. 3.9. The reinforcement in the test area enters four "loading wings" at angles of 60 and 30 degrees and the two remaining wings at zero degree with respect to the axes of the wings. In the three tests, C1, C2 and C3, one of the four wings with inclined reinforcement collapsed first. The failure lines were practically perpendicular to the axis of the wing but did not cross the extra reinforcement. Although it cannot be claimed that the inclined reinforcement weakens the capacity across the yield line, it can certainly be concluded that the effect of reorientation could not have had any significant effect in this case. If it had, failure would have occurred in the wings whose axes were parallel to reinforcement axes.

3.10. Test Specimens Subjected to Torsional Moment

Torsion tests may be considered to be another extreme condition under which the reorientation of the reinforcing bar may occur.

In the present investigation several torsion tests were carried out as indicated in Table 3.1 or in Section 1.2.

The test results of the specimens with isotropic reinforcement are shown in Fig. 3.10, while the rest of the torsion tests are compared indirectly in Table 3.1, where the effect of bar reorientation is completely ignored in the computed figures.

Measured curves of torsional moment vs. principal curvature for three specimens, B16, B17 and B18, are shown in Fig. 3.10. All the specimens formed yield lines at 45 degrees with respect to the direction of the span (Fig. 3.11) so that the reinforcement in specimen B16 was inclined 45 degrees to the yield lines; in specimen B17 the reinforcement was inclined 22.5 and 67.5 degrees to the yield lines, while the reinforcement in specimen B18 crossed the yield lines at 90 degrees.

It should be mentioned that the failure line at collapse did not always follow the direction of the yield lines that were dominant at an earlier stage.

The result from the uniaxial-moment test, B13, is shown in Fig. 3.10 for direct comparison with the results of the torsion tests. The greater capacity of specimen B18 can be explained by the higher yield stress of the reinforcement (see Table 3.1). Neither the

results in Fig. 3.10 nor those in Table 3.1 indicate any significant effect of a reorientation of the reinforcing bars.

All specimens were inspected during and after testing. The cracks were carefully observed. It was never possible to discover a systematic local crack pattern which deviated from the general direction of the yield line. A special attention was given to the local direction of the crack at the reinforcing bar, but no trend could be found that could support any hypothesis of a local yield line in the shape of a "staircase."

A reorientation of the reinforcing bar of more than 5 degrees can be directly observed, but no such reorientation was found in any specimen.

3.11. Concluding Remarks

The following remarks will refer to the results of the present investigation as well as the results of the investigations that were reviewed in the previous chapter.

If a reinforcing bar crosses a crack in the concrete at an inclined angle, a reorientation of the reinforcement has to take place according to the conditions for compatibility. The question is whether the reorientation has a significant effect upon the carrying capacity of a plate element. The matter of significance may be a subject for discussion, but will not be dealt with in this paper. An increase in moment capacity below 3 to 5 percent will not be considered significant in this investigation.

The reorientation of the reinforcing bars was estimated by analytical methods in this chapter. Other attempts to compute the bar orientation by analysis are not known. The reason may be that any analysis has to be based on uncertain assumptions and an exact answer cannot be expected. However, the analysis can show that the effect of reorientation is negligible in a practical case; and it is not necessary to demonstrate an unrealistic local crack pattern to explain this. Qualitatively, the analysis indicates that the bar reorientation increases with larger inclination, α, of the bar to the crack; higher concrete strength; smaller bar diameter; and lower yield stress in the reinforcement.

It is conceivable that an element can be proportioned so that a normalizing or full "kinking" will take place across the crack. But this element will have very little resemblance to an ordinary reinforced concrete element.

In fact, the test specimens in the present test series should give a more pronounced effect of the bar reorientation than should a practical structure. The unusually small dimension of the reinforcement in the 4-in. thick slab, the moderate yield stress and the high concrete quality in the test specimens are all factors that favor a large bar reorientation. Nevertheless, no enhancement of moment capacity attributable to bar reorientation was observed.

The results of the present investigation with respect to bar reorientation are directly supported by the results of tests carried out by Houbolt (13), Nielsen (10), Peter (15) and Silverj (14).

Opposing evidence is provided by Baus and Tolaccia (11) and Kwiecinski (12). In the former test series the results with respect to reorientation were not consistent as explained in Chapter 2. The latter test series encountered severe bond problems at the edge of the specimen. These bond problems were similar to those in the pilot tests B5 and B6 (see Table 3.1), where the bond failure overshadowed any effect of bar reorientation. Wood, in a later paper (19), seems to be inclined to ignore the "kinking" effect.

Experimental and analytical results indicate that the bar reorientation has no significant effect on the yield criterion for reinforced concrete slabs.

In the following chapters the effect of reorientation of the reinforcing bar will be ignored. The corresponding theoretical inaccuracies are believed to be far less than those attached to the yield-line theory itself, which is based on small deformation theory and not on the complex large deformation theory.

4. EFFECT OF REINFORCEMENT DIRECTION ON STIFFNESS OF PLATE ELEMENTS

4.1. Introductory Remarks

The force-deformation relationship of a reinforced concrete plate element is considered in this chapter. The object is to derive the stiffness of plate elements with the reinforcement in an arbitrary direction and subjected to axial forces or moments in order to cover the conditions that may appear in slabs, shells, folded plates, and walls.

The effect of the direction of the reinforcement on the stiffness of plate elements is rarely taken into account in computations of reinforced concrete structures. An isotropically reinforced slab is usually assumed to possess equal flexural stiffness in all directions. It is shown in this chapter that this assumption is incorrect. For example, the flexural stiffness can be increased more than twofold as the reinforcement rotates from 45° to 0° with respect to the principal bending moment.

Before the concrete cracks, an ordinary amount of reinforcement has a very small effect on the stiffness of the element. Beyond the yield-point of an elasto-plastic element the condition is unstable with reference to the deformations. Hence, the region considered in this chapter is the load-deformation curve between cracking and yielding.

Axial loading of an element is considered first in this chapter. Expressions are derived for the deformations with respect to

load and direction of the reinforcement. Instability is not considered.

In the next sections the derivations for axial loaded elements are extended to elements subjected to biaxial moments.

Tests are briefly described and test results are given for plate elements subjected to uniaxial moment, isostatic moment, and torsional moment.

The results from the derivations and the tests are compared and discussed.

The experiments are described in detail in Appendix A and the test results are summarized in Table 3.1.

The scope of this report is primarily related to the yield criterion for reinforced concrete plates. The scope is not, however, strictly limited to the region beyond yielding for the following reasons:

(1) To arrive at the yield condition, the element has to go through the uncracked state and the cracked "proportional" stage. The fact that a reinforced concrete structure has sufficient capacity at yield does not eliminate the possibility that the structure may break down before it reaches the yield point. This is one reason why the existing yield-line theory cannot serve as a design method.

(2) A structure reaches the yield stage in the instant the last yield line in the mechanism is formed. The last yield line can then be considered to be in the "proportional" range as well as in the plastic range. Therefore, the geometric conditions and the stiffness under service load in the direction perpendicular to the last yield

line determine the necessary rotations at the other yield lines. Knowing the stiffness is imperative to be able to check the rotation at the yield lines.

4.2. Load-Deformation Relationships for a Reinforced Concrete Element Subjected to In-Plane Stresses

In this section the effect of moments and curvatures are assumed to be negligible.

Consider an element in tension as shown in Fig. 4.1. The cracks are shown in full lines, while the reinforcement is shown with broken lines. The stress in the reinforcement in a cross section which coincides with a crack is

$$\sigma_{sc} = \frac{N_n}{A_s} \text{ (in the crack)} \tag{4.1}$$

where

σ_{sc} = stress in steel in the crack

A_s = area of steel per unit width

N_n = external force per unit width in the n-direction

The steel stress will not be constant between two cracks because the concrete is bonded to the steel and will carry a part of the tension force. The general expression for the steel stress is

$$\sigma_s = f(n) = \frac{1}{A_s}[N_n - (h - A_s)\sigma_{ct}] \tag{4.2}$$

where σ_{ct} = average concrete stress over the cross section and a function of n; and h = height of the specimen.

The unit average elongation over a length, L, is

$$\epsilon_{sa} = \frac{1}{A_s E_s}\left[N_n - \frac{1}{L}\int_0^L (h - A_s)\sigma_{ct}\,dn\right] \tag{4.3}$$

where E_s = modulus of elasticity of steel.

The integration term in Eq. 4.3 is of significance at small loads close to the cracking load. Figure 4.2 shows qualitatively the effect of bond on the load-deformation curve. As the load increases the contribution from the concrete becomes less, and may be ignored at loads close to the yield point in a moderately reinforced plate element. If the reinforcement is so light that the cracking load is of the same order as the yield load, the contribution of the concrete will be significant also at yielding.

The average stress in the reinforcing bar, σ_{sa}, can be defined as

$$\sigma_{sa} = \epsilon_{sa} E_s \tag{4.4}$$

Consider the conditions in Fig. 4.3. The original position of the bars is shown by broken lines while the deformed stage is shown by bold lines.

The relationship between the steel strain, ϵ_{sa}, and ϵ_n, ϵ_t and γ_{nt} which are the over-all or average strains for the element is expressed by

$$\begin{aligned}(1 + \epsilon_{sa})^2 = {} & [(1 + \epsilon_t)\sin\alpha + (1 + \epsilon_n)\cos\alpha \sin\gamma_{nt}]^2 \\ & + [(1 + \epsilon_n)\cos\alpha(\cos\gamma_{nt})]^2\end{aligned} \tag{4.5}$$

where ϵ_n, ϵ_t and γ_{nt} are as shown in Fig. 4.3. Neglecting small second order terms, the unit elongation perpendicular to the cracks

$$\epsilon_n = \epsilon_{sa} \sec^2\alpha - \epsilon_t \tan^2\alpha - \gamma_{nt} \tan \alpha \tag{4.6}$$

The relation between the unit force, N_n, and the stress in the bar with reference to the state at the crack is

$$N_n = \sigma_s A_s \cos^2\alpha \tag{4.7}$$

and

$$N_{nt} = \sigma_s A_s \sin\alpha \cos\alpha \tag{4.8}$$

when N_{nt} = shear force per unit width in a cross section perpendicular to the n-direction.

Combining Eq. 4.4, 4.6 and 4.7

$$\epsilon_n = \frac{\sigma_{sa} N_n}{\sigma_s E_s A_s} \sec^4\alpha - \epsilon_t \tan^2\alpha - \gamma_{nt} \tan\alpha \tag{4.9}$$

For a layer of reinforcement in the perpendicular direction ($\alpha + 90^\circ$) with the area of reinforcement per unit width equal to μA_s as shown in Fig. 4.4

$$\epsilon_n = \frac{\sigma'_{sa} N_n}{\mu\sigma'_s E_s A_s} \frac{1}{\sin^4\alpha} - \epsilon_t \cot\text{an}^2\alpha + \gamma_{nt} \tan\alpha \tag{4.10}$$

The symbol μ is the ratio between the amounts of reinforcement in the two directions and is usually connected to the direction with the least reinforcement so that $\mu \leq 1.0$.

For both layers combined

$$N_n = A_s(\sigma_s \cos^2\alpha + \mu\sigma'_s \sin^2\alpha) \tag{4.11}$$

$$N_{nt} = A_s(\sigma_s - \mu\sigma'_s)\sin\alpha \cos\alpha$$

Let

$$\sigma_{sa}/\sigma_s = \kappa \text{ and } \sigma'_{sa}/(\sigma'_s\mu) = \kappa' \tag{4.12}$$

where the primes refer to the reinforcement with steel area μA_s.

From 4.9, 4.10 and 4.12

$$\epsilon_n = \frac{N_n\kappa\kappa' - \epsilon''_t(\kappa' + \kappa)\cos^2\alpha \sin^2\alpha E_s A_s}{(\kappa' \cos^4\alpha + \sin^4\alpha)E_s A_s} \tag{4.13}$$

where $\epsilon''_t = \epsilon_t + \gamma_{nt}(\kappa' \cot\alpha - \tan\alpha)/(\kappa' + \kappa)$ (4.14)

and N_n represent the total external force in the n-direction.

In the remaining part of this section following approximations are made

$$\begin{aligned} \kappa &= 1 \\ \kappa' &= \frac{1}{\mu} \end{aligned} \tag{4.15}$$

Equation 4.15 indicates that a load-deformation curve represented by a straight line like the line A-C in Fig. 4.2 will be considered.

From Eq. 4.13, 4.14 and 4.15

$$\epsilon_n = \left[\frac{N_n}{E_s A_s} - \epsilon'_t(1 + \mu)\cos^2\alpha \sin^2\alpha\right] \frac{1}{\cos^4\alpha + \mu \sin^4\alpha} \tag{4.16}$$

where $$\epsilon_t' = \epsilon_t + \gamma_{nt}(\text{cotan}\alpha - \mu\ \text{tan}\alpha)/(1 + \mu) \qquad (4.14a)$$

For isotropic reinforcement

$$\epsilon_n = \left\{\frac{N_n}{E_s A_s} - 0.5\epsilon_t' \sin^2 2\alpha\right\} \frac{2}{1 + \cos^2 2\alpha} \qquad (4.17)$$

Equations 4.16 and 4.17 do not refer to any particular direction of the cracks. The formation and direction of cracks are discussed in Chapter 6.

Equation 4.17 is illustrated in Fig. 4.5. The direction of the reinforcement with respect to the n-axis is defined by the angle α as shown in Fig. 4.4. The directions of the strains are shown in Fig. 4.3. In Fig. 4.5, the angle α varies as expressed by the abscissa while the planar forces are held constant. The ratio between the strains ϵ_n and ϵ_{no}, which is the strain for $\alpha = 0^o$, is plotted as the ordinate. The curves in the figure indicate that strain in one direction is highly dependent on the strain in the other direction. For a uniaxial state of stress, where $N_t = 0$ and the transverse faulting is restrained ($\gamma_{nt} \approx 0$), the strain ϵ_t is small compared with ϵ_n after the stress, N_n, has caused cracking of the concrete. In this case, the elongation of the element is doubled by letting the reinforcement rotate from $\alpha = 0$ to $\alpha = 45^o$. It is further seen from Fig. 4.5 that a negative transverse strain (compression) will increase the elongation in the n-direction if $0^o < \alpha < 90^o$, while a positive strain (tension) will decrease the elongation in the n-direction. In the case of equal principal strains in both directions, $\epsilon_n = \epsilon_t$,

the elongation becomes independent of the inclination of the reinforcement, α.

Figures 4.6 and 4.7 illustrate the case for nonisotropic reinforcement expressed by Eq. 4.16. As it should be suspected, the orientation of the reinforcement plays an increasingly significant role as μ approaches zero, while the influence of transverse strain remains approximately constant.

It is interesting to compare the information provided in Fig. 4.5 and 4.7 in order to study the effectiveness of different reinforcing schemes. If the curves for $\epsilon_t' = 0$ in the two figures are compared, it is seen that up to $\alpha = 30^\circ$, the "transverse" reinforcement in the isotropic slab has little effect on the flexibility. Consequently, in the same range of α, the case for $\mu = 0$ is practically as efficient as the case for $\mu = 1.0$. This implies the wherever additional reinforcement is needed in isotropically reinforced plates, such reinforcement can be added in only one direction provided $\alpha \leq 30^\circ$, where α refers to the final crack pattern for the element with the additional reinforcement.

The relationship between σ_s and σ_s' can be derived from Eq. 4.6 assuming steel to be linearly elastic

$$\frac{\sigma_s'}{\sigma_s} = \frac{\epsilon_n \sin^2\alpha + \epsilon_t \cos^2\alpha - \gamma_{nt} \sin\alpha \cos\alpha}{\epsilon_n \cos^2\alpha + \epsilon_t \sin^2\alpha + \gamma_{nt} \sin\alpha \cos\alpha} \tag{4.18}$$

Combining Eq. 4.11 and 4.18

$$N_n = A_s \sigma_s \left[\cos^2\alpha + \mu \frac{\epsilon_n \sin^4\alpha + \epsilon_t \cos^2\alpha \sin^2\alpha - \gamma_{nt} \sin^3\alpha \cos\alpha}{\epsilon_n \cos^2\alpha + \epsilon_t \sin^2\alpha + \gamma_{nt} \sin\alpha \cos\alpha}\right] \tag{4.19}$$

$$N_{nt} = A_s \sigma_s \left[1 - \mu \frac{\epsilon_n \sin^2\alpha + \epsilon_t \cos^2\alpha - \gamma_{nt} \sin\alpha \cos\alpha}{\epsilon_n \cos^2\alpha + \epsilon_t \sin^2\alpha + \gamma_{nt} \sin\alpha \cos\alpha} \right] \qquad (4.20)$$

Equation 4.20 shows that $N_{nt} = 0$ in a few special cases only, except for $\alpha = 0^\circ$ and 90°.

4.3. Moment-Curvature Relationships Under Uniaxial Moment

A general solution for combinations of moments can be derived with reference to the case for uniaxial moment. Hence, a reinforced concrete plate under uniaxial moment will be considered first.

Figure 4.8 shows a section perpendicular to the cracks. For the case where the reinforcing bars are parallel and perpendicular to the cracks, this element can be considered to be a beam element. In the analysis of a reinforced concrete beam the following approximations are usually made, and will also be made in this report.

(1) Contribution from the tensile stresses perpendicular to the cracks in a cracked concrete section is ignored.

(2) Reduction of strain in the reinforcement because of bond in the concrete sections between the cracks is also ignored.

Although neither approximation is very good at the cracking load, the approximations are usually reasonably good closer to the yield point.

With the above approximations and the assumption that the strain distribution over the depth of the section is linear, the strain and stress can be represented as in Fig. 4.9. The n-axis is chosen perpendicular to the cracks in the following expressions: The curvature

in the n-direction

$$\Phi_n = \epsilon_{cn}/c_n \tag{4.21}$$

The curvature in the t-direction

$$\Phi_t = \epsilon_{ct}/c_t \tag{4.22}$$

From equilibrium in the n-direction

$$\sum_{i=1}^{4} N_{ni} + \sum_{i=1}^{2} F_{ni} = 0 \text{ (No external axial forces)} \tag{4.23}$$

For equilibrium in the t-direction

$$\sum_{i=1}^{4} N_{ti} + \sum_{i=1}^{2} F_{ti} = 0 \text{ (No external axial forces)} \tag{4.24}$$

Moment in the n-direction

$$M_n = \sum_{i=1}^{4} d_i N_{ni} + \sum_{i=1}^{2} a_i F_{ni} \tag{4.25}$$

Moment in the t-direction

$$M_t = \sum_{i=1}^{4} d_i N_{ti} + \sum_{i=1}^{2} b_i F_{ti} \tag{4.26}$$

$$M_{nt} = \sum_{i=1}^{4} d_i N_{nti} + \sum_{i=1}^{2} \lambda_i F_{nti} \tag{4.27}$$

$$M_{tn} = \sum_{i=1}^{4} d_i N_{nti} + \sum_{i=1}^{2} \lambda_i F_{tni} \qquad (4.28)$$

h and d_i are given, c_n, c_t, a_i, b_i λ_i and λ_i' have to be determined.

The relationships between the forces in the reinforcement, N_n, N_t, N_{nt}, and the strains are given in the previous section 4.2. The integrated stresses in the concrete, F_{ni}, F_{ti}, and F_{tni} have to be determined.

An exact computation of the stresses in the concrete is practically impossible. The model shown in Fig. 4.10 is used to estimate the strain and stresses in the concrete.

In a region of constant moment and reinforcement no resultant forces are transferred from the steel to the concrete.

The derivations for the resisting moment and the flexural stiffness are made with respect to the unit slice shown in Fig. 4.10. This slice represents a portion of a reinforced concrete specimen bounded by two flexural cracks. The reinforcement runs in both directions and top and bottom. The figure is drawn for the case where there is a compressive force on the top.

The derivations are continued with the following additional premises:

(1) No stress is transmitted across a crack except by reinforcement.

(2) A strip of concrete bounded by cracks (Fig. 4.10) resists stresses only along its axis.

(3) Compressed concrete is in a state of plane stress.

(4) The bending and shearing stiffnesses of the reinforcing bars are not significant.

It should also be noted that, with the reinforcement totally yielded, the direction of one of the principal curvatures is perpendicular to a yield line in isotropically reinforced plates. Consequently, faulting along the yield line is zero, and

$$\epsilon_t' = \epsilon_t \qquad (\gamma_{nt} = 0) \qquad (4.29)$$

For nonisotropically reinforced plates, the directions of the yield line, principle curvature, and principal moment may not coincide.

Consistent with the general assumptions above, the following simplifications can be introduced in the equations for equilibrium and moments given by Eq. 4.23 through 4.28 and Fig. 4.10

$$F_{nti} = F_{tni} \qquad (4.30)$$

or specifically

$$F_{nt2} = F_{tn2} \qquad (4.31)$$

$$F_{nt1} = 0 \qquad (4.32)$$

and Eq. 4.27 and 4.28 become

$$M_{nt} = M_{tn} = \sum_{i=1}^{4} d_i N_{nti} + \lambda_2 F_{nt2} \qquad (4.33)$$

The stress in concrete is determined by the stress-strain relationship of the concrete, the equilibrium conditions and the curvature of the section.

The formulae for moments and curvatures can be stated in a more convenient form by considering layer 1 and 2 in Fig. 4.10 as a reinforcing net in one level. The same assumption is made for layers 3 and 4.

The distance from the top face to the resultant force of the reinforcing bars at the bottom in Fig. 4.10 is determined as follows. The reinforcing bars with area A_s per unit width in layer 1 are inclined by an angle α to the n-axis, and the reinforcing bars in layer 2 are perpendicular to those in layer 1 and have a steel area μA_s per unit width.

The distance from the top face to the resultant force of the reinforcing bars in the n-direction d_{nb} is found as follows:

From Eq. 4.16 and Fig. 4.9

$$N_n = E_s A_s \left[\epsilon_n(\cos^4\alpha + K\mu \sin^4\alpha) + \epsilon_t'(1 + K\mu)\cos^2\alpha \sin^2\alpha\right] \tag{4.34}$$

where $K = (d_2 - c_n)/(d_1 - c_n)$.

The moment of layer 1 and 2 with respect to the top face

$$N_n d_{nb} = E_s A_s\left[\epsilon_n(d_1 \cos^4\alpha + d_2 K\mu \sin^4\alpha) + \epsilon_t'(d_1 + d_2 K\mu)\cos^2\alpha \sin^2\alpha\right] \tag{4.35}$$

For all practical purposes the ratio K can be set equally to unity in Eq. 4.35, hence

$$d_{nb} = \frac{\epsilon_n(d_1\cos^4\alpha + d_2\mu \sin^4\alpha) + \epsilon_t'(d_1 + d_2\mu)\cos^2\alpha \sin^2\alpha}{\epsilon_n(\cos^4\alpha + \mu \sin^4\alpha) + \epsilon_t'(1 + \mu)\cos^2\alpha \sin^2\alpha} \qquad (4.36)$$

In the t-direction: By interchanging ϵ_n and ϵ_t, cosα and sinα

$$d_{tb} = \frac{\epsilon_t(d_1 \sin^4\alpha + d_2\mu \cos^4\alpha) + \epsilon_n'(d_1 + d_2\mu)\cos^2\alpha \sin^2\alpha}{\epsilon_t(\sin^4\alpha + \mu \cos^4\alpha) + \epsilon_n'(1 + \mu)\cos^2\alpha \sin^2\alpha} \qquad (4.37)$$

where d_{tb} is the distance from the top face to the resultant force in the t-direction.

and $$\epsilon_n' = \epsilon_n + \gamma_{nt}(\mu \cot\alpha - \tan\alpha)/(1 + \mu) \qquad (4.37a)$$

From Eq. 4.6 and 4.8

$$d_{ntb} = \frac{\epsilon_n(d_1\cos^2\alpha - d_2\mu \sin^2\alpha) + \epsilon_t(d_1\sin^2\alpha - d_2\mu \cos^2\alpha) + \gamma_{nt}(d_1+\mu d_2)\sin\alpha\cos\alpha}{\epsilon_n(\cos^2\alpha - \mu \sin^2\alpha) + \epsilon_t(\sin^2\alpha - \mu \cos^2\alpha) + \gamma_{nt}(1 + \mu)\sin\alpha \cos\alpha} \qquad (4.38)$$

It may be observed that all three quantities, d_{nb}, d_{tb} and d_{ntb} are all a magnitude between d_1 and d_2. An estimate of the three quantities by inspection would usually result in an error of less than 5 percent in the moment capacity. The maximum possible error is in most cases not more than 10 to 15 percent.

The distances from the top face to the resultant forces in layers 3 and 4 in Fig. 4.9 can be found in the same way. Equations 4.36, 4.37 and 4.38 give the distances from the top surface to the resultant forces in the n-, t-, and nt-direction, d_{nu}, d_{tu}, and d_{ntu}, respectively

by replacing ϵ_n, ϵ_t, d_1, d_2, μ and α with ϵ_n^o, ϵ_t^o, d_3, d_4, μ^o and α^o. The superscript ^{o} refers to the conditions at the top face.

Consider a slab element subjected to uniaxial moment. The element has isotropic reinforcement in the tension zone and no reinforcement in the compression zone. The n-direction is perpendicular to cracks and parallel to the span. There is no cracking in a transverse cross section of the element. Therefore ϵ_t' is small relative to ϵ_n and can be ignored. The concrete is considered linearly elastic in the compression zone. From the equilibrium condition, Eq. 4.23, the height of the compression zone, c_n, can be found to be

$$c_n = d_{nb}\left[\sqrt{r_1^2 + 2r_1} - r_1\right] \tag{4.39}$$

where

$$r_1 = A_s E_s \frac{\cos^4\alpha + \sin^4\alpha}{d_{nb} E_c} \tag{4.40}$$

From Eq. 4.36 and 4.40

$$r_1 = A_s \frac{E_s}{E_c} \frac{(\cos^4\alpha + \sin^4\alpha)^2}{d_1 \cos^4\alpha + d_2 \sin^4\alpha} \tag{4.41}$$

From Eq. 4.25

$$M_n = N_n\left(d_{nb} - \tfrac{1}{3} c_n\right) \tag{4.42}$$

The curvature, Φ_n, in the n-direction

$$\Phi_n = \frac{\epsilon_n}{d_{nb} - c_n} \tag{4.43}$$

The ratio Φ_n/M_n expresses the flexibility of the element in the n-direction while the inverse ratio M_n/Φ_n is usually denoted the flexural stiffness. The flexibility is significantly influenced by the orientation of the reinforcement.

Figure 4.11 shows how the flexibility is related to the amount and direction of the reinforcement in an isotropically reinforced concrete element. In the example, d_1 and d_2 are assumed to be equal, that is, the reinforcement is considered to be in one plane. The flexibility is expressed by the ordinate and the deviation of the reinforcement from the direction of the span, α, is marked along the abscissa. The increase in flexibility by having the reinforcement rotated from zero to 45 degrees to the span direction is 80 percent for $A_s/d_1 = 0.005$ and 63 percent for $A_s/d_1 = 0.020$. A_s is the cross-sectional area of reinforcement in one direction. Thus, A_s/d_1 is the reinforcement ratio in that direction. The relative influence of the direction of the reinforcement on the flexibility is greater for a lightly reinforced slab than for an element with heavier reinforcement. As the amount of reinforcement goes down, the increase in flexibility approaches 100 percent by having the reinforcement rotated from zero to 45° with respect to the span direction.

The stresses and strains are also affected by the direction of the reinforcement as illustrated in Fig. 4.12. The ordinate indicates what may be considered the inverse of the "section modulus" of the element. Thus, for the uncracked section, the section modulus is $h^2/6.0 = d_1^2/4.3$ if $d_1/h = 0.85$. Figure 4.12 shows that the direction of the isotropic reinforcement has a significant effect on the "section modulus."

Since concrete is considered linearly elastic in this example, Fig. 4.12 represents the maximum concrete strain if the ordinate scale is divided by the modulus of elasticity of concrete, E_c.

In order to secure satisfactory ductility, most building codes have limitations on the amount of reinforcement so that the concrete shall not crush before the reinforcement yields. This consideration is, however, transferred from the beam theory where different directions of reinforcement are not encountered and an increase in maximum stress in concrete like that shown in Fig. 4.12 is not considered.

The stresses in the reinforcement can be obtained by Eq. 4.19 and 4.42 which in the above example reduces to

$$\frac{\sigma_s}{M_n} = \frac{1}{(\cos^2\alpha + \sin^2\alpha\tan^2\alpha)(d_1 - c_n/3)\, A_s} \qquad (4.44)$$

where c_n is given by Eq. 4.39. The stress, σ_s, refers to the reinforcing bars at an angle α from the n-direction. Equation 4.44 is illustrated in Fig. 4.13. The maximum stress in the reinforcement occurs when the reinforcement is inclined about 30° to the n-direction, while the "effective stress," that is the stress component in the n-direction, is fairly constant for $0^\circ < \alpha < 30^\circ$ but decreases rapidly for an increasing angle, α, in excess of 30°.

4.4. Moment-Curvature Relationships Under Biaxial Moments

In the case of reinforced concrete element under biaxial bending the transverse strain can no longer be considered to be negligible compared with the strain in the longitudinal direction.

Poisson's ratio has negligible effect in the cracked zone of the element, and is of little significance in the compression zone with regard to the moment-curvature relationship. The Poisson's ratio will be assumed to be zero in this section

(a) Isotropically Reinforced Plate

Consider first the case of an isotropically reinforced element. The n-t directions are assumed to coincide with the direction of the principal curvatures, Φ_n and Φ_t. The directions of the reinforcement is denoted x and y and the x-y coordinate system is rotated counterclockwise an angle α with respect to the n-t coordinate system. The strains in the bars in the x- and y-directions are denoted ϵ_{sx}, ϵ_{sy} for the bottom and ϵ_{sx}^{o}, ϵ_{sy}^{o} for the top reinforcement (Fig. 4.9). The strains in the n-t directions at the level of the reinforcement are correspondingly denoted ϵ_n and ϵ_t, and ϵ_n^o and ϵ_t^o. From Eq. 4.6 ($\gamma_{nt} = 0$)

$$\begin{aligned}
\epsilon_{sx} &= \epsilon_n \cos^2\alpha + \epsilon_t \sin^2\alpha \\
\epsilon_{sy} &= \epsilon_n \sin^2\alpha + \epsilon_t \cos^2\alpha \\
\epsilon_{sx}^{o} &= \epsilon_n^{o} \cos^2\alpha^{o} + \epsilon_t^{o} \sin^2\alpha^{o} \\
\epsilon_{sy}^{o} &= \epsilon_n^{o} \sin^2\alpha^{o} + \epsilon_t^{o} \cos^2\alpha^{o}
\end{aligned} \tag{4.45}$$

The strains ϵ_n and ϵ_n^o are found by considering the moment acting on a section perpendicular to the n-direction. Similarly, ϵ_t and ϵ_t^o are obtained from the strains on a section perpendicular to the t-direction.

Two extreme cases of biaxial moments are of special interest, isostatic moment and torsion.

(1) Isostatic moment, expressed by

$$M_n = M_t \tag{4.46}$$

Equation 4.46 implies that

$$\epsilon_n = \epsilon_t \text{ and } \epsilon_n^o = \epsilon_t^o \, . \tag{4.47}$$

such that Eq. 4.45 becomes

$$\begin{aligned}
\epsilon_{sx} &= \epsilon_n(\cos^2\alpha + \sin^2\alpha) = \epsilon_n = \epsilon_t \\
\epsilon_{sy} &= \epsilon_t(\cos^2\alpha + \sin^2\alpha) = \epsilon_t = \epsilon_n \\
\epsilon_{sx}^o &= \epsilon_n^o(\cos^2\alpha^o + \sin^2\alpha^o) = \epsilon_n^o = \epsilon_t^o \\
\epsilon_{sy}^o &= \epsilon_y^o(\cos^2\alpha^o + \sin^2\alpha^o) = \epsilon_n^o = \epsilon_t^o
\end{aligned} \tag{4.48}$$

Equations 4.48 indicate that the plate has the same moment-curvature characteristics as an element with reinforcement parallel to the span and subjected to a uniaxial moment.

(2) Pure torsion, expressed by

$$M_n = -M_t \tag{4.49}$$

In the case of isotropic reinforcement equal at top and bottom of the element, Eq. 4.49 implies

$$\epsilon_n = \epsilon_t^o \text{ and } \epsilon_t = \epsilon_n^o \tag{4.50}$$

Such that Eq. 4.45 becomes

$$\begin{aligned} \epsilon_{sx} &= \epsilon_n \cos^2\alpha + \epsilon_t \sin^2\alpha \\ \epsilon_{sy} &= \epsilon_n \sin^2\alpha + \epsilon_t \cos^2\alpha \\ \epsilon^o_{sx} &= \epsilon_t \cos^2\alpha^o + \epsilon_n \sin^2\alpha^o \\ \epsilon^o_{sy} &= \epsilon_t \sin^2\alpha^o + \epsilon_n \cos^2\alpha^o \end{aligned} \tag{4.51}$$

Assuming the case with the reinforcing bars parallel in top and bottom ($\alpha = \alpha^o$), Eq. 4.51 gives

$$\begin{aligned} \epsilon_{sx} &= \epsilon^o_{sy} \\ \epsilon_{sy} &= \epsilon^o_{sx} \end{aligned} \tag{4.52}$$

and further from Eq. 4.51

$$\begin{aligned} \epsilon^o_{sx} + \epsilon_{sx} &= \epsilon_n(\sin^2\alpha + \cos^2\alpha) + \epsilon_t(\cos^2\alpha + \sin^2\alpha) = \epsilon_n + \epsilon_t \\ \epsilon^o_{sy} + \epsilon_{sy} &= \epsilon_n(\cos^2\alpha + \sin^2\alpha) + \epsilon_t(\sin^2\alpha + \cos^2\alpha) = \epsilon_n + \epsilon_t \end{aligned} \tag{4.53}$$

From Eqs. 4.52 and 4.53

$$\epsilon_{sx} + \epsilon_{sy} = \epsilon^o_{sx} + \epsilon^o_{sy} = \epsilon_n + \epsilon_t = \epsilon^o_n + \epsilon^o_t \tag{4.54}$$

By using Eq. 4.54, the equilibrium conditions are considerably simplified. Force in the bottom reinforcement in the n-direction

$$N_n = A_s E_s(\epsilon_{sx} \cos^2\alpha + \epsilon_{sy} \sin^2\alpha) \tag{4.55}$$

can be derived from Eq. 4.59

$$\frac{A_s E_s \Phi_n}{M_n} = \frac{1}{(d_{nb}\cos^2\alpha + d_{nu}\sin^2\alpha)^2 + (d_{nb}\sin^2\alpha + d_{nu}\cos^2\alpha)^2 - 4c_n h/3 + 2c_n^2/3} \tag{4.63}$$

Equation 4.63 is illustrated in Fig. 4.14 with the flexibility plotted along the ordinate axis and the angle between the reinforcement and the n-direction plotted along the abscissa axis.

Figure 4.14 shows that it is possible to double or even triple the curvature of a reinforced concrete slab by having the reinforcement rotated through 45°.

The compressive strains and stresses in concrete are very sensitive to the orientation of the reinforcement. Figure 4.15 shows the maximum compressive stress along the ordinate axis and the orientation of the reinforcement, α, along the abscissa axis. The conditions at $\alpha = 0^\circ$ represent the conventional concept of the slab behavior. It can be readily concluded that the code limitations do by no means leave out the possibility of a heavily overreinforced concrete slab.

(b) Nonisotropically Reinforced Plate

Consider the case with a nonisotropically reinforced concrete plate element. The yield lines no longer generally coincide with the principal external moment and the principal curvatures generally coincide with neither the yield lines nor the principal moments.

In accordance with the above statement, the "shear strain" or the "faulting," γ_{nt}, cannot be considered equal to zero for the n-direction perpendicular to the direction of the yield line.

Force in the top reinforcement in the n-direction

$$N_n^o = A_s E_s (\epsilon_{sx}^o \cos^2\alpha + \epsilon_{sy}^o \sin^2\alpha) \tag{4.56}$$

From Eq. 4.54, 4.55 and 4.56

$$N_n + N_n^o = A_s E_s (\epsilon_n + \epsilon_t) \tag{4.57}$$

Assuming concrete to be linearly elastic

$$N_n + N_n^o - 0.5\, c_n \sigma_c = 0 \tag{4.58}$$

$$N_n d_{nb} + N_n^o d_{nu} - (N_n + N_n^o)\, c_n/3 = M_n \tag{4.59}$$

The curvature is

$$\Phi_n = \frac{\sigma_c}{E_c c_n} = \frac{\epsilon_n - \epsilon_t}{d_{nb} - d_{nu}} = \frac{\epsilon_n}{d_{nb} - c_n} \tag{4.60}$$

The symbol σ_c refers here to the concrete stress at the surface at the compression side.

From Eq. 4.57, 4.58 and 4.60

$$\frac{c_n}{h} = \sqrt{4r_2^2 + 2r_2} - 2r_2 \tag{4.61}$$

where

$$r_2 = \frac{A_s E_s}{E_c h} \tag{4.62}$$

The moment-curvature relationship expressed by the flexibility Φ_n/M_n

Because the moment is equal in all directions, the failure line appears parallel to the main reinforcement. The solution is trivial. The moment-curvature relationship in one direction does not interfere significantly with that in the perpendicular direction (Poisson's ration ≈ 0).

(2) Pure torsion, expressed by

$$M_1 = -M_2 \tag{4.49}$$

where M_1 and M_2 are the principal moments. The area per unit width of the reinforcing bars placed in the x-direction is A_s and A_s^o and in the y-direction μA_s and $\mu^o A_s^o$. The superscript (^{o}) indicates that the position of the reinforcement is at the top surface. With regard to moment-curvature relationship, the extreme orientations of the reinforcement are (a) parallel to the principal moments and (b) at 45^o to the principal moments.

The case where the reinforcement is parallel to the principal moments is trivial and the flexibility in either direction is the same as for an element with the reinforcement parallel to the span, subjected to uniaxial bending.

Consider the case with the reinforcement at 45^o to the principal moment, and $A_s^o = A_s$, $\mu^o = \mu$. Because of the symmetry of the reinforcement and the external moments with respect to a line parallel to the reinforcing bars, the principal curvatures have to be parallel to the principal moments. The line of the least resistance, which is assumed to be the direction of the yield line, does not coincide with the principal curvature if the ratio of the reinforcement in the two

From Eq. 4.6 and 4.45, assuming the same directions of the reinforcement in top and bottom of the element

$$\begin{aligned}
\epsilon_{sx} &= \epsilon_n \cos^2\alpha + \epsilon_t \sin^2\alpha + \gamma_{nt} \sin\alpha \cos\alpha \\
\epsilon_{sy} &= \epsilon_n \sin^2\alpha + \epsilon_t \cos^2\alpha - \gamma_{nt} \sin\alpha \cos\alpha \\
\epsilon^o_{sx} &= \epsilon^o_n \cos^2\alpha + \epsilon^o_t \sin^2\alpha + \gamma^o_{nt} \sin\alpha \cos\alpha \\
\epsilon^o_{sy} &= \epsilon^o_n \sin^2\alpha + \epsilon^{t^o}_t \cos^2\alpha - \gamma^o_{nt} \sin\alpha \cos\alpha
\end{aligned} \tag{4.64}$$

Equation 4.64 expresses that in order to determine ϵ_{sx} and ϵ_{sy} (or ϵ^o_{sx} and ϵ^o_{sy}) it is necessary to know the strains in three directions or the strains in two directions and the direction of a principal strain. The simplest way to find the strains is to let the direction of the n-axis be perpendicular to the cracks and consider a section through a crack. Knowing the moment M_n, the strain, ϵ_n, can be found by the equilibrium conditions and strain-stress relationships for concrete and steel. The computation of the strain, ϵ_t, may be found similarly. The shear strain γ_{nt} may be more difficult to determine, but if the directions at the principal curvatures can be determined, an indirect computation of γ_{nt} becomes simple. Then all the strains in Eq. 4.64 can be derived provided the directions of the yield lines are known. The directions of the principal curvature depend on geometric conditions, and the orientation of the yield lines will be derived in Chapter 6.

The two extreme cases of biaxial moments are again considered, this time with nonisotropically reinforced concrete plate elements.

(1) Isostatic moment, expressed by

$$M_n = M_t \tag{4.46}$$

where σ_{ca} is the average compressive stress in concrete.

From Eq. 4.69

$$\frac{\epsilon_{sx}}{\mu\epsilon_{sy}} = \frac{1 - \sin 2\gamma}{1 + \sin 2\gamma} \tag{4.70}$$

Substituting Eq. 4.65 into 4.70,

$$\epsilon_{sx} = \sqrt{\mu}\ \epsilon_{sy} \tag{4.71}$$

From equilibrium and assuming concrete in compression to be linearly elastic

$$\frac{c_n}{h} = \sqrt{4r_3^2 + 2r_3} - 2r_3 \tag{4.72}$$

where

$$r_3 = A_s E_s \frac{\mu \sin^2(45-\gamma) + \sqrt{\mu}\ \cos^2(45-\gamma)}{E_c h} \tag{4.73}$$

Equation 4.73 can be simplified by introducing Eq. 4.65

$$r_3 = \frac{2A_s E_s\ \mu}{E_c h(1 + \sqrt{\mu})} \tag{4.74}$$

The flexibility of the element is

$$\frac{\Phi_u}{M_1} = \frac{\Phi_n}{M_n} = \frac{12}{E_c c_n^{\,2}(3h - 2c_n)} \tag{4.75}$$

In Fig. 4.17 the flexibility is shown as a function of μ. Consistently with the previous curves the ratio, E_s/E_c, is chosen to be

perpendicular directions, μ, is different from unity. The direction of a yield line at the first yield is derived in Chapter 5, Eq. 5.75. For a lightly reinforced concrete, Eq. 5.74 gives a good approximation

$$-\sin 2\gamma \approx \frac{1 - \sqrt{\mu}}{1 + \sqrt{\mu}} \tag{4.65}$$

where γ is the angle between the direction of the perpendicular to the considered principal moment and the direction of the respective yield line.

After setting $\alpha_1 = (45^\circ - \gamma)$ for the perpendicular to the first yield line (see Fig. 4.16), Eq. 4.64 becomes

$$\begin{aligned} 2\epsilon_{sx} &= \epsilon_n + \epsilon_n \sin 2\gamma + \epsilon_t - \epsilon_t \sin 2\gamma + \gamma_{nt} \cos 2\gamma \\ 2\epsilon_{sy} &= \epsilon_n - \epsilon_n \sin 2\gamma + \epsilon_t + \epsilon_t \sin 2\gamma - \gamma_{nt} \cos 2\gamma \end{aligned} \tag{4.66}$$

and $\alpha_2 = (135^\circ + \gamma)$ for the direction perpendicular to the second yield line

$$\begin{aligned} 2\epsilon_{sx} &= \epsilon_n^o + \epsilon_n^o \sin 2\gamma + \epsilon_t^o - \epsilon_t^o \sin 2\gamma - \gamma_{nt}^o \cos 2\gamma \\ 2\epsilon_{sy} &= \epsilon_n^o - \epsilon_n^o \sin 2\gamma + \epsilon_t^o + \epsilon_t^o \sin 2\gamma + \gamma_{nt}^o \cos 2\gamma \end{aligned} \tag{4.67}$$

Considering symmetry and antisymmetry

$$\epsilon_{sx} = \epsilon_{sx}^o \,, \quad \epsilon_{sy} = \epsilon_{sy}^o \tag{4.68}$$

From equilibrium in the x- and y-direction

$$\begin{aligned} 2A_s E_s \, \epsilon_{sx} &= \sigma_{ca} c_n (1 - \sin 2\gamma) \\ \mu 2A_s E_s \, \epsilon_{sy} &= \sigma_{ca} c_n (1 + \sin 2\gamma) \end{aligned} \tag{4.69}$$

reinforcement has nearly the same effect as long as the ratio $\mu \geq 0.5$, provided the reinforcement is repeated in top and bottom of the slab.

Once the directions of the principal curvatures and the yield lines are determined, the moment-curvature relationship for a nonisotropically reinforced concrete element subjected to an arbitrary combination of moments is not more difficult to estimate than that for an isotropically reinforced concrete element. The main problem for nonisotropically reinforced elements is to determine the directions of the yield lines. This question is considered in Chapter 6.

(c) Nonproportional Loading

It should be emphasized that all previous considerations in this chapter refer to proportional loading. It is well known from the theory of inelasticity that the load-deformation relationship depends on the path or the history of the loading. The properties of a reinforced concrete section may be even more removed from the conditions for a linear elastic medium.

The difference between a proportional and a nonproportional loading of a reinforced concrete element is shown qualitatively for a specific case in Fig. 4.18. The element is isotropically reinforced with the directions of the bars inclined at 45° to the directions of the principal moments, M_1 and M_2.

The case with proportional loading where $M_1 = M_2$ also with respect to time, is the regular case which is dealt with earlier in this section. The corresponding moment-curvature relationship is shown by broken lines.

8.0 so that Eq. 4.75 can be rewritten as

$$\frac{\Phi_u}{M_1} = \frac{96}{E_s c_n^2 (3h - 2c_n)} \tag{4.76}$$

The curve in Fig. 4.17 represents a case where the total amount of reinforcement is kept constant, but the ratio of the reinforcing bars in one direction to those in the perpendicular direction is equal to μ. Hence the amount of reinforcement in the main direction, A_{sk}, has to be

$$2(1 + \mu) A_{sk} = 4A_s \tag{4.77}$$

where A_s represents the isotropic case. Ordinarily the ratio μ is chosen so that $0 \leq \mu \leq 1$. Equation 4.76 plotted in Fig. 4.17 indicates that the flexibility increases as μ decreases, that is, the moment-curvature relationship is affected as if some reinforcement were removed in the isotropically reinforced element. The equivalent amount of isotropic reinforcement, A_{seq}, with respect to the moment-curvature relationship can be found by Eq. 4.78

$$\frac{A_{seq}}{A_s} = \frac{4\mu}{(1 + \mu)(1 + \sqrt{\mu})} \tag{4.78}$$

It can be observed from Eq. 4.78 and Fig. 4.17 that the flexibility is little influenced by the nonisotropically distribution of the reinforcement as long as $\mu \geq 0.5$. It will also be shown later on that the moment capacity of the element is practically constant in this range of the ratio μ. Hence, it can be concluded that any distribution of the

The test setup provided a test area with constant moments and no external vertical shear. The external moment conditions were

(1) uniaxial moment

(2) isostatic moment

(3) pure torsion.

The test setup, the test, procedure and measurement technique are described briefly in this section because a detailed description is given in Appendix A. Table 3.1 gives a survey of the test specimens, their properties and the loading conditions.

All the test specimens were moderately reinforced with "flat-top" steel. During the loading the test specimens usually passed through the following characteristic points:

(1) cracking of the concrete in tension

(2) yielding of the reinforcement in tension (sometimes in stages)

(3) ultimate moment capacity

(4) failure characterized by a crushing of the concrete

(a) Cracking of the Concrete

During the loading, the cracking of the concrete was usually first registered by the strain gages that were cemented on the tension surface of the specimen. Thereafter, the strain rate in the tension steel showed a significant increase. The deflection measurements did not show a significant rate of increase before more load was applied. At this moment the first hair cracks could be traced by a magnifying glass. Figure 4.22 shows how the observed first cracking is related to moment and the compressive cylinder strength, f'_c, while Fig. 4.23

In the case with nonproportional loading the moment, M_1, may be applied first. The moment-curvature curve is shown by bold lines, and the positions after the full M_1 is applied are marked by A. Then, the perpendicular moment, M_2, is applied. At the time M_2 is applied, M_1 has already prestressed the element in the direction of M_2, and M_2 may not be able to crack the concrete. The curvatures caused by the moment, M_2, are shown by the arrows going from A to B in Fig. 4.18.

The fact that the moment-curvature relationship of a reinforced concrete slab generally depends on the load path or the load history, rules out the possibility of superimposing the effect of one load combination onto the effect of another. At certain combinations of load history and orientation of the reinforcement, the stiffness of the slab may be increased several hundred percent for an additional loading of the slab.

4.5. Experimental Results

The results and observations of the experimental work which are related to the behavior of reinforced concrete plate elements below the yield load are described in this section.

The dimensions of the two types of test specimens which were used for the experiments are shown in Fig. 4.19 and 4.20. The directions and the amount of reinforcement were varied as shown in Fig. 4.21. The strength of the concrete was intentionally varied in some series.

The spacing of the cracks varied between 1.0 in. and 3.0 in. The reinforcement affected the spacing of the initial cracks to some degree. In the case with reinforcing bars parallel to the crack direction, the spacing of the cracks had a tendency to be close to that of the reinforcing bars.

(b) Moment-Curvature Relationships

The obtained moment-curvature relationship is shown qualitatively in Fig. 4.24. The nearly horizontal portion B-B' was observed only in a few cases. The loading was carried out by incremental loads between points A and P, and by incremental deflections from point P to failure. This loading procedure excludes the observation of some points on the "real" curve from A to P, such as point B". A point such as B' may or may not be observed.

It was observed, however, that the distance B-B' was always small compared with B-D. That is, the tensile stresses in the concrete may increase the over-all flexural stiffness even after cracking. The effect of the tensile stresses in concrete decreased as the element approached the yield point. Naturally, these observations are consistent with what is ordinarily observed in beam tests.

In this section the term "stiffness" is used for the slope of the line A-P, or the ratio M_p/Φ_p in Fig. 4.24. The inverse value of the stiffness is termed the "flexibility."

The present investigation showed that the stiffness of the element was dependent on both the amount of steel and the directions of the reinforcing bars with respect to the principal moments. In the following presentation of the stiffnesses or flexibilities measured in

shows how the first cracking is related to moment and tensile split cylinder strength, f'_t.

It cannot be expected that the types of the measurements mentioned above are able to indicate when the first local cracks occur on the surface. Whether the first cracks are registered by strain gages depends entirely on the position of the gage relative to the cracks. The results in Fig. 4.22 and 4.23 show that the measured moment-curvature relationship does not provide a good indication of the first local crack.

Figures 4.22 and 4.23 indicate that the tensile strength of concrete measured by split cylinder test (6 by 6-in.) is more closely related to the cracking phenomenon than the compressive strength of concrete.

Assuming the concrete to be linearly elastic, the moment at cracking can be easily computed on basis of the tensile strength of the concrete. As suspected, the computed moment is considerably below the cracking moment obtained from the measured moment-curvature relationship. On the other hand, the occurrence of the first local hairline cracks may be predicted fairly well on the basis of the tensile strength from split cylinder tests.

In the following, the term "cracking moment" refers to the moment at cracking as it is reflected by the moment-curvature relationship.

The initial cracking was perpendicular to the maximum principal moment in all specimens.

in specimens B6 and B8 was 22.5° (or 67.5°). Another difference between these specimens was that specimens B5 and B6 had no special arrangement for securing the anchorage in the bars that were cut at the edges of the specimen, while the reinforcing bars in specimens B7 and B8 had double hooks at the ends. The moment-curvature relationships for the specimens, B5, B6, B7 and B8, are shown in Fig. 4.27 and compared with the specimens B4 and B10. The results show that the anchorage of the ends has little effect on the stiffness below the yield point, but is vital in obtaining the ductility of the slab.

The results in Fig. 4.27 indicate the flexibility of a slab with the reinforcement at an angle of 22.5° with respect to the direction of the applied moment was about 30 percent greater than with the reinforcement parallel to the applied moment. The corresponding increase in flexibility of an element with the reinforcement at 45° to the direction of the applied moment was about 70 percent.

A state of pure torsion was obtained by twisting the specimen shown in Fig. 4.19 so that the direction of the external principal moments were at an angle of 45° to the edges of the specimen. Because the principal moments were of opposite signs, it was necessary to reinforce the torsion specimens both at the top and the bottom.

In order to be able to compare with the uniaxial state of moment, specimen B13 was isotropically reinforced in the top and the bottom as was the specimen B10 on one side. The resulting moment-curvature relationship is shown in Fig. 4.28, and compared with the data from tests B4 and B10. As expected there was no significant difference in the stiffnesses of test specimens B13 and B10.

tests, two isotropically reinforced specimens subjected to uniaxial moment are chosen as reference. The moment-curvature relationships of these two specimens B4 and B10 are shown in Fig. 4.25. In specimen B4 the deeper layer of reinforcement is parallel to the applied moment, while the shallower layer of reinforcement is parallel to the applied moment in specimen B10. The amount of reinforcement in the second shallower layer is 9 percent higher than in the first layer in order to compensate approximately for the loss in effective depth. It is seen in Fig. 4.25 that the increase of reinforcement made the strengths equal, but did not quite equalize the stiffnesses in the two directions.

Figure 4.26 shows the moment-curvature relationships for three specimens, C1, C2 and C3, subjected to isostatic moment and with the same isotropic reinforcement as in B4 and B10, but with the concrete strengths f'_c equal to 6610, 4580 and 2700 psi. The results indicate that the large variation of concrete strength was reflected by the cracking moment, but not by the stiffness and the strength of the element. The stiffnesses in the two directions of the reinforcing bars were little different and the results in Fig. 4.26 represent the averages of the curvatures in two directions. The stiffnesses of specimens C1, C2 and C3 are practically the same as those of specimens B4 and B10.

In the next series the direction of the isotropic reinforcement was varied with respect to the applied uniaxial moment. In specimens B5 and B7 the angle between the reinforcing bars and the direction of the applied moment was 45°, while the corresponding angle

As the direction of the reinforcing bars was changed from 0° to 22.5 (and 67.5°), and 45° with respect to a principal moment, the flexibility increased correspondingly at a ratio of approximately 1.0:1.5:2.5.

Two specimens, B19 and B20, were isotropically reinforced with half the amount of steel used in the previous specimens (approximately 0.5 percent in each layer). Specimen B19 had the reinforcement parallel to the principal moments, while specimen B20 had the reinforcement inclined at 45° to the principal moments. The moment-curvature relationships are shown in Fig. 4.30. The yield point is not very distinct for either of the specimens. The flexibility may be estimated to be between 2.0 and 2.5 greater for the specimen B20 with the reinforcement inclined 45° to the principal moment than for the specimen B19 with the reinforcement parallel to the principal moment.

Test B20 was one of the few tests that exhibited a distinct horizontal plateau in the moment-curvature curve at cracking.

Five specimens had nonisotropic reinforcement. Three of the specimens, B9, B11 and B12, were subjected to uniaxial moment and two specimens, B21 and B22, were subjected to pure torsion.

The specimens B9, B11 and B12 had the reinforcement inclined to the direction of the external uniaxial moment. The case with the nonisotropic reinforcement parallel to the direction of the moment was not expected to give any additional information and was not tested.

The moment-curvature relationships of specimens B9, B11 and B12 are shown in Fig. 4.31. The reinforcement in one direction was twice the reinforcement in the other direction. The former is called

Five torsion tests were carried out with the same isotropic reinforcement as used in specimen B13. In specimens B15 and B18 the reinforcing bars were parallel or perpendicular to the external principal moments. In specimens B14 and B16 the reinforcing bars were inclined 45° to the principal moments, while in specimen B17 the reinforcing bars were inclined 22.5° or 67.5° to the principal moments. The difference between specimens B15 and B18, and also between specimens B14 and B16, was that the former had no extra shear reinforcement along the edges while the latter had extra reinforcement along the edges with the flexural reinforcement remaining unchanged. As long as the edges did not fail in shear, the behavior of the element did not seem to be influenced by the extra shear reinforcement at the edge. Hence, the extra edge reinforcement had no significant effect on the stiffness in the range of a "service" load but was necessary to secure the ductility of the slab element.

The results from five specimens, B14, B15, B16, B17 and B18, are compared in Fig. 4.29 with those from the reference specimens B4 and B13. The results show that for the case where the reinforcement was parallel to the principal moments (B15 and B18), the elements had the same stiffness under torsional moment as under uniaxial moment.

The other specimens with the reinforcement inclined to the principal moments did not have a sharp yield point, which leaves the determination of the stiffness values more to judgment than in the previous cases. Specimen B17, with the reinforcing bars inclined 22.5° and 67.5°, had two yield points whereof the first one was fairly distinct. Specimens B14 and B16 behaved like an overreinforced slab with no pronounced yield point and with little ductility.

reinforcement was provided to resist the deadload and the applied moment was set equal to the applied twisting moment. The results in Fig. 4.32 show that the moment-curvature relationships for specimens B21 and B22 are nearly the same as that of specimen B20 which had equal reinforcement in both directions that corresponded to half the main reinforcement in the specimens B21 or B22.

(c) Moment-Strain Relationships

Strains in the concrete were measured by electric strain gages cemented to the surfaces of the specimen. After cracking, the strain gages on the cracked surfaces became unreliable, and an attempt was made to obtain additional readings of the strains by photogrammetry (ref. Appendix B).

Figure 4.33 shows strain readings on the compression side of the three specimens, B4, B10 and B13, which had the reinforcing bars parallel to direction of the applied uniaxial moment. Specimens B4 and B10 had reinforcement at one side only, while B13 had reinforcement at both sides.

It can be observed from Fig. 4.33 that the moment-strain relationships were approximately the same for all specimens both in the longitudinal and the transverse direction. It is interesting to note that Poisson's ratio seems to play a minor role and may be estimated to be between 5 and 10 percent. The shape of the curves in Fig. 4.33 from the cracking moment to yield indicates that the slab element behaved approximately "elastically."

Figure 4.34 shows the moment-strain relationships of two specimens in which the reinforcement was not parallel to the direction

the "main" direction and the latter the "transverse" direction. The respective main directions for specimens B9, B11 and B12 were 45°, 22.5° and 67.5° to the direction of the external principal moment. Tests B4 and B19 should be equivalent to nonisotropic reinforcement with the main direction at 0° and 90° to the direction of the applied moment. The results in Fig. 3.31 show that specimen B4 was the stiffest one, but both specimens B9 and B12 with 45° and 67.5° inclination of the main reinforcement were a little less stiffer than the other reference specimen B19. The stiffness of specimen B11 with 22.5° inclination of the main reinforcement was closer to the stiffness of specimen B4 than that of B19.

In each of the three specimens B9, B11 and B12, the direction of the cracks and the direction of the principal curvatures were changing from the time of cracking almost all the way up to failure. Therefore the angle between the direction of the reinforcement and the direction of the principal moment was different from that between the reinforcement and the principal curvatures. However, the change in the direction of the principal curvature below the yield point was only on the order of 2° - 7° and had little effect on the stiffness of the element.

In the torsion specimens B21 and B22 (Fig. 4.32), the ratio between the main and transverse reinforcement was 4:1, or $\mu = 0.25$. Both specimens had the reinforcement inclined at 45° to the external principal moments. The difference between specimen B21 and B22 is that in B21 the deadload moment was vectorially added to the twisting moment in computing the applied moment; in the second case, B22, extra

The results show that there was no significant difference in the compressive strains in specimens under uniaxial moments and under pure torsion as long as the reinforcement was parallel to the principal moments. This is illustrated in Fig. 4.37 which shows the results from specimen B18 under pure torsion compared with those from B4 and B13 under uniaxial bending. The torsion specimens B16, B17 and B18 were isotropically reinforced with the reinforcing bars inclined to the principal moments at 45°, 22.5° (or 67.5°) and 0° respectively. The test results show an increase of concrete strain of about 35 percent for specimen B17 with the reinforcement at 22.5° and an increase of strain of about 140 percent for specimen B16 with the reinforcement at 45° to the direction of the principal moment. In the latter case the concrete stress probably reached its peak value at the time the reinforcement reached its yield point. This may explain the limited ductility of this specimen, B16, as indicated in the moment-curvature relationship in Fig. 3.10. In other words, the specimen behaved nearly as if it was overreinforced.

The torsion specimens B19 and B20 were isotropically reinforced with half the amount of reinforcement that was used in the previous series (B13 to B18). Specimen B19 had the reinforcement in the directions of the principal moments. A significant decrease in compressive concrete strains at the yield point was observed compared with the corresponding specimens B15 and B18 with twice the amount of reinforcement. But specimen B20 with the reinforcement at 45° to the principal moments had little or no significant decrease in compressive concrete strain at yield point compared with the corresponding

of the uniaxial moment. The specimens B7 and B8 were isotropically reinforced. The direction of the bars was at 45° to the span direction in specimen B7 and at 22.5° and 67.5° to the span direction in specimen B8. The results in Fig. 4.34 show that the rotation of the reinforcement had a significant effect on the strain in the concrete both in the longitudinal and transverse direction with respect to the span. The increase in transverse positive strain is greater than what corresponds to the Poisson's ratio estimated from the results in Fig. 4.33. The reason for this is the considerable transverse compression on the tension side caused by the inclined reinforcement.

The transverse strains on the tension and the compression surface are compared in Fig. 4.35. There were large negative strains on the tension side of specimens B7 and B8, while B10, representing an element with reinforcement parallel to the span, showed no significant strain in the transverse direction on the tension side. It should be mentioned that the strains measured on the cracked surfaces were quite scattered and some personal judgment was used in drawing the curves for tensile concrete strains.

In the case of isostatic moment the strains on the compression side were less than the corresponding strains for a specimen under uniaxial moment. This is illustrated by the results in Fig. 4.36. Specimens C1 and C2 were subjected to isostatic moment and B4 and B10 to uniaxial moment. It is interesting to notice that if the Poisson's ratio effect, represented by the positive strains in Fig. 4.36, is subtracted from the results of specimens C1 and C2, the sums will nearly coincide with the results of specimens B4 and B10.

in each direction corresponding to half the amount of the main reinforcement in specimen B21 or B22.

The measurement of the reinforcement strains was more reliable than those of the concrete strains. The steel strains were in the order of 0.0001 before cracking. The strain readings indicated usually a linear moment-strain relationship from cracking to the yield point.

A closer look at the steel strains is most interesting in connection with the yield and ultimate moment and the formation of the yield lines which are discussed in the next chapters. Hence, more detailed explanations of the observed steel strains are given in the next chapters.

4.6. Comparison and Discussion of Analytical and Experimental Results

The theory presented in Sections 4.2 through 4.4 and the test results reported in Section 4.5 are compared in this section.

No direct experimental study was carried out with regard to load-deformation relationships for a reinforced concrete element subjected to axial stresses. But the derivations made for an element loaded in its own plane were extended and applied to an element subjected to moments. Therefore, if test results support the theory for elements subjected to moments, they should also confirm the theory for elements subjected to in-plane stresses.

(a) Concrete Element Subjected to In-Plane Stresses

A direct comparison of the results of the theory in Section 4.2 with test results can be made by the results obtained by

specimen B16. The moment-strain relations are shown in Fig. 4.38. The readings indicate that the compressive strain in concrete at yield for B20 was about 0.17 percent.

Concrete strains on the surfaces of nonisotropically reinforced specimens subjected to uniaxial moment are shown in Fig. 4.39 and 4.40. The moment capacity in the main direction was twice that in the perpendicular direction. Specimen B11 had the main reinforcing bars at 22.5° to the span direction, B9 at 45° to the span, and B12 at 67.5° to the span. The cases with the inclination of 0° and 90° are represented by results from specimens B4 and B19. The longitudinal compressive concrete strains are shown in Fig. 4.39. As the main reinforcing bars were rotated from 0° to 90° to the span direction, the reinforcement became less effective and also more flexible so that the compressive strains at yield increased for all three specimens with inclined reinforcement.

The measurements of transverse concrete strains showed that the reinforcement produced considerable transverse compression at the surface in the longitudinal compression as illustrated in Fig. 4.40.

In the torsion specimens with nonisotropic reinforcement, the ratio between main reinforcement and transverse reinforcement was 4:1 ($\mu = 0.25$). Specimens B21 and B22 both had the reinforcing bars at an angle of 45° to the external principal moments. It is interesting to note in Fig. 4.41 that the compressive strains in the concrete in specimens B21 and B22 were similar to those in B20, an isotropically reinforced specimen with the amount of reinforcing bars

element subjected to biaxial stresses. His theoretical results do not seem to agree with the theoretical or experimental results presented in this chapter.

The question of effectiveness of reinforcing bars inclined to the direction of the maximum principal stress may be encountered when providing additional reinforcement in a heavily stressed section.

Assuming that an isotropically reinforced element behaves satisfactorily with regard to deformations, the effectiveness of additional reinforcing steel making an angle α with the perpendicular to the crack direction can be defined as the ratio N_{nf}/N_{na}, where N_{nf} is the component of the steel force for the added reinforcement in the direction perpendicular to the cracks (the n-direction) per unit width in the crack direction at a given deformation and N_{na} is the force component per unit width in the n-direction for isotropic reinforcement placed at the same angle α and with the amount of steel in each direction equal to that of the additional steel. This effectiveness may be determined from Eq. 4.16 and 4.17, assuming ϵ'_t to be small compared with ϵ_n

$$\frac{N_{nf}}{N_{na}} = \frac{2 \cos^4 \alpha}{1 + \cos^2 2\alpha} \tag{4.79}$$

The magnitude of the ratio N_{nf}/N_{na} is 1.0 for $\alpha = 0^\circ$, 0.90 for $\alpha = 30^\circ$, 0.50 for $\alpha = 45^\circ$ and 0.10 for $\alpha = 60^\circ$.

It should be noticed that Eq. 4.79 relates the effectiveness of the reinforcement in one direction to the effectiveness of isotropic reinforcement, which itself is a function of the angle α and

Peter (15). Peter applied uniaxial tension to a concrete element, 1.60m by 1.60m by 0.08m, with the reinforcement, No. 2 and No. 3 high strength deformed bars, at the mid-height. The direction of the reinforcement was varied by 10°, from 0° to 40°. Most of the elements in the investigation were isotropically reinforced.

Figure 4.42 shows test results obtained by Peter for isotropically reinforced elements. The ratio ϵ_n/ϵ_{no} is plotted along the y-axis. The strain ϵ_{no} is the strain in the direction of the load with the reinforcement in the same direction. The strain ϵ_n is the strain in the load direction, but with the direction of the reinforcement deviating from the load direction by the angle α plotted along the x-axis. The numerals in the plot refer to the loading stages. The numeral 3 indicates a load close to the ultimate while the numerals 2 and 1 roughly correspond to 85 and 70 percent of the ultimate load. Thus, the results along one ordinate axis represents the same specimen. The scatter was unfortunately high, and the results are not likely to give strong support to any theoretical derivation. The trend may be said to favor the theory in Section 4.2.

It is also interesting to note the curve that Peter assumed to be a reasonable curve on the basis at his experience. His estimate is indicated by the broken curve in Fig. 4.42 and it may be observed that this line is almost identical with the theoretical curve (solid line) based on Section 4.2.

The tests by Peter were performed with uniaxial tensile loading. The test results refer only to one curve for $\epsilon_t \approx 0$ in Fig. 4.5. Peter also proposed a theory for a reinforced concrete

Modulus of elasticity for concrete, $E_c = 4.15 \times 10^6$ psi;
for steel, $E_s = 29 \times 10^6$ psi.

In Fig. 4.43 the flexibility is plotted along the ordinate axis and the angle β between the reinforcement and the span direction is plotted along the abscissa axis.

Figure 4.43 shows results from six test specimens and the theory derived in Section 4.3. The agreement between the results from tests and theory is good. The assumption that the concrete in compression is linearly elastic on this stress level is reasonably good for prediction of flexibility.

An indication of the nonlinearity of the stress-strain curve of concrete is expressed by Fig. 4.44, which shows the corresponding strains along the ordinate axis. The differences between predicted and measured strains are about 10 percent and the test results support the theory. The nonisotropic case is presented in Fig. 4.45 and 4.46. The test results and the computed values showed the same nonsymmetric trend. The differences between theoretical and observed flexibility are less than 10 percent for all points. The measured strains were higher than those computed by about the same amount as for the isotropic case.

In the case of uniaxial moment and inclined reinforcement, the reinforcing bars caused significant concrete stresses and strains in the transverse direction which were compressive at the level of the reinforcement and tensile at the opposite side. This was observed in all test specimens with inclined reinforcement. But neither the electric strain gages nor photogrammetry gave reliable measurements of the magnitude of the strains on the cracked surface. The transverse

has maximum flexibility at $\alpha = 45^{\circ}$. The relation results in a sharp drop in the ratio N_{nf}/N_{na} after the angle α has passed 45°. Thus, Eq. 4.79 gives small effectivenesses for additional one-direction reinforcement whose angle α is greater than 45°.

If an equal amount of reinforcement were added in the perpendicular direction to the one-direction reinforcement, Eq. 4.79 would state that the reinforcement would again be isotropic.

It may be pertinent to emphasize that Eq. 4.79 refers to the resultant crack direction. An inclined "extra" reinforcement will influence the crack pattern such that this additional reinforcement will be less efficient than if the crack pattern had remained unchanged. This "principle of the least resistance" is discussed in Chapters 6 and 7.

(b) Concrete Element Subjected to Uniaxial Moment

The results of theoretical computations and test observations are summarized in Table 3.1.

Figure 4.43 illustrates the measured and computed flexibility of an isotropically reinforced element subjected to a uniaxial moment. The reinforcement was approximately 1.0 percent in each layer. The thickness, the concrete quality and the yield stress of the reinforcement varied some during the testing. As "standard" values for the theoretical computations, the following were chosen:

Thickness, $h = 4.12$ in.

Concrete quality, $f'_c = 5000$ psi

Steel yield stress, $f_y = 50{,}000$ psi

decreasing modulus of elasticity. Therefore, in order to keep the derivations in Section 4.4 in its general form, it was thought that the most convenient approach would be to use a fictitious ratio of E_s/E_c that corresponds to the effect of the "softening" at the concrete under high strains.

By inspection of the formulas for the strains as a function of the orientation of the reinforcement and the stress-strain relationship for concrete, a reasonable equivalent ratio between the moduli of elasticity for steel and concrete which was found to be valid for the torsion specimens in this investigation is

$$\frac{E_s}{E_c} = 7 + 3 \sin^4 2\alpha \qquad (4.78)$$

Figure 4.47 shows the flexibility of isotropically reinforced elements with about 1.0 percent steel in each layer, subjected to torsion. The abscissa represents the angle, β, between the reinforcement and the direction of the principal moments. As the angle, β, was rotated from 0° to 45°, the measured flexibility of the element increased to 2.0 - 2.5 times the flexibility at $\beta = 0^\circ$. The theoretical computations predict the test results within 10 percent.

Figure 4.48 indicates a drastic change in concrete strain, which may triple as the reinforcement is rotated from 0° to 45° with respect to the principal moment. The specimen with the reinforcement under 45° to the principal moment may no longer possess the ductile behavior that is imperative for the yield-line theory.

stresses in specimen B7, for example, with the reinforcement at 45° to the span were computed to be -1200 psi (comp.) at the surface on the reinforcement side of the element, and +370 psi (tension) on the opposite or "compression" side. The high tensile stress led eventually to longitudinal cracks in the "compression" side of some of the specimens.

There are many similarities between the test specimens subjected to in-plane uniaxial stresses and those subjected to a uniaxial moment. Thus, the theoretical curves in Fig. 4.42 and 4.43 have almost identical form. It appears that it would be easier to get consistent results using a test specimen subjected to bending than by a specimen subjected to tension. In the bent specimen, the compression zone has a stabilizing effect and provides an excellent anchorage zone for the inclined reinforcement. In the case of a pure tension specimen, all concrete is cracked in tension and the inclined reinforcement has to be anchored in the cracked zones.

(c) Concrete Elements Subjected to Torsion

Torsion is the loading condition for which the orientation of the reinforcement has the greatest influence on the flexibility and the deformations of a reinforced concrete element.

The experimental and computed results show that the maximum concrete strains were far beyond the point where the concrete may be considered to be a linearly elastic material.

The effect of the inelastic behavior of concrete on the moment-curvature relationship of an element with increasing strains is similar to the effect of a linearly elastic material with a

The specimens with 0.5 percent reinforcement in each layer showed the same general behavior as those with 1.0 percent, but the increase in flexibility and compressive strains with inclined reinforcement was a little less pronounced in the case with a smaller amount of reinforcement, as it can be seen from the results plotted in Fig. 4.49 and 4.50. It is interesting to note that reducing the reinforcement by 50 percent will reduce the corresponding compressive strains only by approximately 20 to 30 percent (Fig. 4.48 and 4.50).

The results of two nonisotropically reinforced specimens are also plotted in Fig. 4.49 and 4.50. The main reinforcement was about 1.0 percent in each layer and the transverse reinforcement was 0.25 percent in each layer. Theoretically, this arrangement of the reinforcement and an inclination 45° with respect to the principal moment should result in approximately 5 to 10 percent higher magnitude of the flexibility and the strain in relation to the case with 0.5 percent reinforcement in each direction (see Eq. 4.78).

It is evident from the above studies that the conventional computations on an "elastic" and isotropic basis are not applicable in predicting the stress distribution in a plate or slab structure. More load may go in the direction of the reinforcing bars than an "elastic" consideration indicates and less load may be taken by the resisting twisting moment than computed according to "elastic" theory of plates.

The ultimate load is much less sensitive to the orientation of the reinforcement than the flexibility. This will be considered in the next chapter.

5. YIELD MOMENT OF A REINFORCED CONCRETE SECTION

5.1. Introductory Remarks

The primary object of this chapter is to study the flexural yield capacity of reinforced concrete plate sections. Deformations of the section are ignored except in cases where the yield deformation may be so large as to constitute a limitation to the development of the yield moment.

It should also be noted that the definition of the yield moment for plates is not as simple as it is in the case of beams. Since the slab is reinforced in more than one direction, the yield stress may be reached at different moments in different layers of reinforcement.

In general, a section at a yield line will have two different yield points. A single yield point will be observed when only one layer of reinforcement crosses the yield line or if both layers (in the case of two-way reinforcement) cross the yield line at specific angles depending on the relations between the resisting and applied moments. The stress-strain characteristics of the reinforcing bars will be taken to be elasto-plastic. It is assumed that reinforcement is provided in two mutually perpendicular directions. In the following derivations, the "main" direction of reinforcement will refer to the direction in which the bars yield first, the other direction being called the "transverse" direction.

5.2. Conditions at the Yielding of the Reinforcement

The conditions at the first and second yielding will be considered in this section.

(a) Conditions at First Yielding

The main reinforcing bars have to satisfy Eq. 5.1, derived from Eq. 4.18 in order to reach yield at the first yield point. Thus, the main reinforcing bars will coincide with the x-direction if

$$\frac{\epsilon_n \sin^2\alpha + \epsilon_t \cos^2\alpha - \gamma_{nt} \sin\alpha\cos\alpha}{\epsilon_n \cos^2\alpha + \epsilon_t \sin^2\alpha + \gamma_{nt} \sin\alpha\cos\alpha} \leq 1.0 \qquad (5.1)$$

The notation is the same as in Chapter 4. If Eq. 5.1 is not satisfied, the main direction will coincide with the y-direction. For convenience, the coordinate system in this section will be arranged such that the main direction and the x-direction of the reinforcement coincide, and the ratio between the reinforcement in the y-direction and the x-direction is μ. Hence, the ratio μ, as it is defined for this section, may be greater or less than unity.

The force per unit width, N_{nl}, exerted perpendicular to the yield line at the first yield is found from Eq. 4.19

$$N_{nl} = A_s f_y \left[\cos^2\alpha + \mu \frac{\epsilon_n \sin^4\alpha + \epsilon_t \sin^2\alpha\cos^2\alpha - \gamma_{nt}\sin^3\alpha\cos\alpha}{\epsilon_n \cos^2\alpha + \epsilon_t \sin^2\alpha + \gamma_{nt} \sin\alpha \cos\alpha}\right] \qquad (5.2)$$

The shear force of the reinforcement, N_{ntl}, at the same load is

$$N_{ntl} = A_s f_y \left[1 - \mu \frac{\epsilon_n \sin^2\alpha + \epsilon_t \cos^2\alpha - \gamma_{nt} \sin\alpha\cos\alpha}{\epsilon_n \cos^2\alpha + \epsilon_t \sin^2\alpha + \gamma_{nt} \sin\alpha\cos\alpha} \right] \sin\alpha\cos\alpha \qquad (5.3)$$

It is interesting to note that the unit forces N_{nl} and N_{ntl} at the first yield do not depend only on the inclination of the reinforcement expressed by the angle α, but also on the combinations of the applied moments, which affect the ratios ϵ_t/ϵ_n and γ_{nt}/ϵ_n.

(b) Conditions at Second Yielding

The conditions for the reinforcement at second yield are simple. Both layers of reinforcement have reached the yield stress and the force per unit width perpendicular to the yield line, N_{n2}, is

$$N_{n2} = A_s f_y (\cos^2\alpha + \mu \sin^2\alpha) \qquad (5.4)$$

and the shear force N_{nt2} is

$$N_{nt2} = A_s f_y (1 - \mu) \sin\alpha\cos\alpha \qquad (5.5)$$

To obtain the second yield, however, excessive concrete deformations may be necessary. Since such deformations may not be tolerable, the second yield may not be reached even if the slab is "under-reinforced" for uniaxial bending.

If both layers of reinforcement cross the yield line, the first and second yield points coincide when

$$\epsilon_n(\sin^2\alpha - \cos^2\alpha) = \epsilon_t(\sin^2\alpha - \cos^2\alpha) + \gamma_{nt} \sin 2\alpha \qquad (5.6)$$

If ϵ_n and ϵ_t are principal strains ($\gamma_{nt} = 0$), there is one common yield point for the two layers of reinforcement if $\epsilon_n = \epsilon_t$ or if $\alpha = \pi/4$.

The ratio between the deformations at second yield and the deformations at first yield, R_{21}, is

$$R_{21} = \frac{\epsilon_n \cos^2\alpha + \epsilon_t \sin^2\alpha + \gamma_{nt} \sin\alpha\cos\alpha}{\epsilon_n \sin^2\alpha + \epsilon_t \cos^2\alpha - \gamma_{nt} \sin\alpha\cos\alpha} \tag{5.7}$$

For example, for $\alpha = 22.5^\circ$ and $\epsilon_t = \gamma_{nt} = 0$, the second yield will occur at a deformation which is six times that at first yield.

Because the strength contribution of reinforcing bars which form a small angle with the yield line is negligible, the importance of reaching the second yield point may have little practical significance for the strength of the section. The effectiveness of the reinforcing bars as a function of the angle α is shown in Fig. 4.13 for the case of an element subjected to uniaxial moment with the strains ϵ_t and γ_{nt} assumed to be small. It can be concluded that the effect of the reinforcing bars at an angle greater than $\alpha = 70^\circ$ is negligible.

5.3. Yield Moment of a Section With Bottom Reinforcement Only

In the following the "yield moment" of a reinforced concrete section will not be related to either one of the yield points of the reinforcement. All the reinforcement will be assumed to have reached yield and the concrete will be assumed to be in the inelastic

range as indicated in Fig. 5.1. The average compressive concrete stress in Fig. 5.1 is assumed to be a known quantity.

The two layers of reinforcement crossing each other at one side of the slab element are assumed to have the same height. The procedure to convert a practical case into this idealized condition was shown in Chapter 4.

(a) Variation of the Yield Moment With the Direction of the Yield Line

An isotropically reinforced concrete slab element has the same yield moment capacity for any direction of the yield line. The resisting moment across a yield line in a nonisotropically reinforced concrete element is generally accompanied by a twisting moment as a result of the nonisotropy of the reinforcement. The shear forces produced by the reinforcement must be counteracted by shear forces in the concrete as shown in Fig. 5.2. These generate the twisting moment.

Whether the shear forces change the capacity of the compression zone of concrete to resist perpendicular stresses is a question concerning the failure criterion for concrete. In this section it will be assumed, as it is in the beam theory, that moderate shear stresses do not significantly change the capacity of the uncracked zone to resist compressive stresses.

The force per unit width of the reinforcement perpendicular to the yield line is

$$N_n = A_s f_y(\cos^2\alpha + \mu \sin^2\alpha) \qquad (5.8)$$

The shear force per unit width is

$$N_{nt} = A_s f_y (1 - \mu) \cos\alpha \sin\alpha \tag{5.9}$$

The resisting moment per unit width perpendicular to the reinforcement in the x-direction is

$$M_x = A_s f_y d\left(1 - k_1 \frac{A_s f_y}{\sigma_{ca}}\right) \tag{5.10}$$

Correspondingly, in the y-direction

$$M_y = \mu A_s f_y d\left(1 - k_1 \frac{\mu A_s f_y}{\sigma_{ca}}\right) \tag{5.11}$$

where σ_{ca} is the average compressive stress in the uncracked zone and k_1 expresses the position at the centroid of the compression stress block (Fig. 5.1). In Eq. 5.10 and 5.11, and in the following computations, the usual sign conventions for concrete design is used; tensile stress and strain in the reinforcement and compressive stress and strain in concrete are all considered positive.

The resisting twisting moment is zero if the yield-line is perpendicular or parallel to the direction of the reinforcement

$$M_{xy} = M_{yx} = 0 \tag{5.12}$$

The resisting moment across a yield line perpendicular to an arbitrary direction n can be derived from Eq. 5.8, 5.10 and 5.11

$$M_n = M_x \cos^2\alpha + M_y \sin^2\alpha + \left(\frac{1}{\mu} M_y - M_x\right)(1 - \mu)\sin^2\alpha\cos^2\alpha \tag{5.13}$$

The twisting moment can be derived from Eq. 5.9, 5.10 and 5.11

$$M_{nt} = (M_x - M_y)\sin\alpha\cos\alpha + (\frac{1}{\mu} M_y - M_x)(\sin^2\alpha + \mu\cos^2\alpha)\sin\alpha\cos\alpha \tag{5.14}$$

The last product on the right-hand side of Eq. 5.13 and 5.14 reflects the fact that the depth of the neutral axis varies as the yield line is rotated. The distribution of shear stresses over the compressive stress block at a yield line is assumed to be similar to that of the compressive forces (Fig. 5.1).

It is interesting to note that the resisting moment does not vary during the rotation of the yield line according to the equilibrium conditions. Hence, while the external moments may be expressed by Mohr's circle, the resisting moments cannot accurately be expressed in the same way. According to Eq. 5.13 and 5.14 the resisting moment can be accurately expressed by equilibrium conditions (Mohr's circle) in the case

$$\mu = 1.0 \tag{5.15}$$

The resisting moment in various directions can be determined from M_x and M_y using equilibrium conditions if the resisting moment arm in the section perpendicular to the x-axis does not significantly differ from the resisting moment arm in the section perpendicular to the y-axis. Figures 5.3 and 5.4 show the resisting moments in bold lines computed by Eq. 5.13 and 5.14. The moments are presented in polar coordinates where the radial direction expresses the magnitude of the moment and the angle α is the angle between the perpendicular to the yield line and the x-axis. In the example the following values were used

$$f_y = 20\sigma_{ca},\ \mu = 0.25,\ k_1 = 0.4 \text{ and } A_{sx}/d = 0.02,\ A_{sy} = \mu A_{sx}$$

The notations are given in the list of notations.

The broken lines refer to the approximate equations

$$M_n = M_x \cos^2\alpha + M_y \sin^2\alpha \tag{5.16}$$

$$M_{nt} = (M_x - M_y) \sin\alpha\cos\alpha \tag{5.17}$$

Thus, the approximate Eq. 5.16 and 5.17 for the resisting moments coincide with the equilibrium conditions.

As illustrated in Fig. 5.3 and 5.4 the errors involved in the approximate Eq. 5.16 are less than five percent in an ordinary slab, while the errors in Eq. 5.17 are usually less than ten percent.

The equations in this section refer to a state of moments that does not result in cracking of the top face in any direction; that is, the moment perpendicular to the yield line has to be positive or less than the cracking moment if it is negative.

5.4. Yield Moment of a Section With Top and Bottom Reinforcement

In the previous section the simplifying assumption was made that all reinforcement crossing the yield line in the tension side of the section has reached the yield stress. A similar assumption cannot be made for the reinforcement in the compression zone of a section at the yield line. The reinforcement in the compression zone may yield in compression. It may also yield in tension as it has already been observed in the case of torsion (Chapter 4).

It is also possible that the reinforcement on either side may not reach the yield point even with moderate amounts of reinforcement. This will be demonstrated in the following.

(a) General Derivations

Consider the yield line section perpendicular to the n-direction, Fig. 5.5a. The strain in the n-direction is

$$\epsilon_n = a_n + b_n z \tag{5.18}$$

From Fig. 5.5b, the strain in the t-direction is

$$\epsilon_t = a_t + b_t z \tag{5.19}$$

If the yield line does not coincide with the principal curvature, the shear strain is finite

$$\gamma_{nt} = a_{nt} + b_{nt} z \tag{5.20}$$

The following simplifying assumptions are made:

(1) The reinforcing bars at either side of the element are assumed to be at the same level.

(2) The concrete cover thickness is the same at the top and at the bottom so that the value of z at the level of the top reinforcement is

$$z_n^o = z_t^o = -(d - 0.5h) \tag{5.21}$$

and at level of the bottom reinforcement

$$z_n = z_t = +(d - 0.5h) \tag{5.22}$$

The strain in the reinforcement in the x-direction is derived from Eq. 4.6.

$$\epsilon_{sax} = \epsilon_n \cos^2\alpha + \epsilon_t \sin^2\alpha + \gamma_{nt} \sin\alpha \cos\alpha \tag{5.23}$$

For the top reinforcement in the same direction

$$\epsilon^o_{sax} = \epsilon^o_n \cos^2\alpha + \epsilon^o_t \sin^2\alpha + \gamma^o_{nt} \sin\alpha \cos\alpha \tag{5.24}$$

The strains in the reinforcement in the y-direction are found the same way

$$\epsilon_{say} = \epsilon_n \sin^2\alpha + \epsilon_t \cos^2\alpha - \gamma_{nt} \sin\alpha \cos\alpha \tag{5.25}$$

$$\epsilon^o_{say} = \epsilon^o_n \sin^2\alpha + \epsilon^o_t \cos^2\alpha - \gamma^o_{nt} \sin\alpha \cos\alpha \tag{5.26}$$

Combining Eq. 5.18 - 5.26

$$\epsilon_{sax} = a_n \cos^2\alpha + a_t \sin^2\alpha + a_{nt} \sin\alpha \cos\alpha + z_n(b_n \cos^2\alpha + b_t \sin^2\alpha + b_{nt} \sin\alpha \cos\alpha) \tag{5.27}$$

$$\epsilon^o_{sax} = a_n \cos^2\alpha + a_t \sin^2\alpha + a_{nt} \sin\alpha \cos\alpha - z_n(b_n \cos^2\alpha + b_t \sin^2\alpha + b_{nt} \sin\alpha \cos\alpha) \tag{5.28}$$

$$\epsilon_{say} = a_n \sin^2\alpha + a_t \cos^2\alpha - a_{nt} \sin\alpha \cos\alpha + z_n(b_n \sin^2\alpha + b_t \cos^2\alpha - b_{nt} \sin\alpha \cos\alpha) \tag{5.29}$$

$$\epsilon^{o}_{say} = a_n \sin^2\alpha + a_t \cos^2\alpha - a_{nt} \sin\alpha \cos\alpha$$
$$- z_n(b_n \sin^2\alpha + b_t \cos^2\alpha - b_{nt} \sin\alpha \cos\alpha) \qquad (5.30)$$

Assuming the n-direction perpendicular to a yield line, the resisting moment can be found by considering Fig. 5.6

$$M_n = A_M(d - 0.5h) + A_A(0.5h - k_1 A_A/\sigma_{ca}) \qquad (5.31)$$

where

$$A_M = E_s \left[e_1(A_s - A_s^o)\cos^2\alpha + z_n g_1(A_s + A_s^o) \cos^2\alpha + e_2(\mu A_s - \mu^o A_s^o)\sin^2\alpha \right.$$
$$\left. + z_n g_2(\mu A_s + \mu^o A_s^o)\sin^2\alpha\right] \qquad (5.32)$$

and

$$A_A = E_s \left[e_1(A_s + A_s^o)\cos^2\alpha + z_n g_1(A_s - A_s^o) \cos^2\alpha + e_2(\mu A_s + \mu^o A_s^o)\sin^2\alpha \right.$$
$$\left. + z_n g_2(\mu A_s - \mu^o A_s^o)\sin^2\alpha\right] \qquad (5.33)$$

where

$$\begin{aligned} e_1 &= a_n \cos^2\alpha + a_t \sin^2\alpha + a_{nt} \sin\alpha \cos\alpha \\ e_2 &= a_n \sin^2\alpha + a_t \cos^2\alpha - a_{nt} \sin\alpha \cos\alpha \\ g_1 &= b_n \cos^2\alpha + b_t \sin^2\alpha + b_{nt} \sin\alpha \cos\alpha \\ g_2 &= b_n \sin^2\alpha + b_t \cos^2\alpha - b_{nt} \sin\alpha \cos\alpha \end{aligned} \qquad (5.34)$$

and

σ_{ca} is the average concrete stress in the compression zone.

To determine the yield moment, σ_{ca} should be chosen so that the section possesses some ductility after "yielding." The symbols h and k_1 are shown in Fig. 5.6.

The twisting moment is

$$M_{nt} = A_T(d - 0.5h) + A_R(0.5h - k_1 A_A/\sigma_{ca}) \tag{5.35}$$

where

$$A_T = E_s \Big[e_1(A_s - A_s^o) + z_n g_1(A_s + A_s^o) - e_2(\mu A_s - \mu^o A_s^o) - z_n g_2(\mu A_s + \mu^o A_s^o)\Big] \sin\alpha \cos\alpha \tag{5.36}$$

and

$$A_R = E_s \Big[e_1(A_s + A_s^o) + z_n g_1(A_s - A_s^o) - e_2(\mu A_s + \mu^o A_s^o) - z_n g_2(\mu A_s - \mu^o A_s^o)\Big] \sin\alpha \cos\alpha \tag{5.37}$$

In Eq. 5.35 the distribution of shear stresses over the compression zone is assumed to have the same form as the compressive stresses.

Equations 5.31 through 5.37 present the general expressions for the normal moment and the torsional moment at the yield line if the yield point of the reinforcing bars is not reached.

If the strain in the reinforcement in one direction is beyond the yield strain, the term $E_s \epsilon_{sax}$ has to be replaced by f_y, etc. Hence, from Eq. 5.27 through 5.30 and 5.34

$$\left.\begin{aligned} E_s \epsilon_{sax} &= E_s(e_1 + z_n g_n) \leq f_y \\ E_s \epsilon^o_{sax} &= E_s(e_1 - z_n g_1) \leq f_y \end{aligned}\right\} \tag{5.38}$$

$$\left.\begin{aligned} E_s \epsilon_{say} &= E_s(e_2 + z_n g_2) \leq f_y \\ E_s \epsilon^o_{say} &= E_s(e_2 - z_n g_2) \leq f_y \end{aligned}\right\}$$

If the cracks or yield lines form only on one side of a moderately reinforced element, the quantities a_t, b_t, a_{nt} and b_{nt} are positive or have such small negative values that all the tensile reinforcement that can contribute significantly to the yield moment is brought up to or beyond the yield point before the concrete is excessively strained.

In the case with cracking on only one side of the element, there may be no need for reinforcement on the compression side, and if there are reinforcing bars in the uncracked zone of concrete, their contribution to the yield moment is so small that the resisting moment is practically the same as described in Section 5.3.

(b) Isotropically Reinforced Concrete Element Subjected to Torsion

In order to get a clear understanding of what Eq. 5.31 - 5.37 imply, the reinforcement shall be assumed to be repeated top and bottom, so that

$$\begin{aligned} A_s &= A^o_s \\ \mu &= \mu^o \end{aligned} \tag{5.39}$$

Hence Eq. 5.32, 5.33, 5.36 and 5.37 are simplified to

$$A_M = 2E_s A_s z_n [g_1 \cos^2\alpha + \mu g_2 \sin^2\alpha] \tag{5.40}$$

$$A_A = 2E_s A_s [e_1 \cos^2\alpha + \mu e_2 \sin^2\alpha] \tag{5.41}$$

$$A_T = 2E_s A_s z_n [g_1 - \mu g_2] \sin\alpha \cos\alpha \tag{5.42}$$

$$A_R = 2E_s A_s [e_1 - \mu e_2] \sin\alpha \cos\alpha \tag{5.43}$$

Furthermore, the case of isotropic reinforcement ($\mu = 1.0$) and pure twisting shall be considered so that

$$\begin{aligned} a_n &= a_t = a_u = a_v \\ a_{nt} &= 0 \\ b_n &= -b_t = b_u \cos 2\theta \\ b_{nt} &= b_u \sin 2\theta \end{aligned} \tag{5.44}$$

Substituting Eq. 5.44 into Eq. 5.34

$$\begin{aligned} e_1 &= a_n \\ e_2 &= a_n \\ g_1 &= b_u(\cos 2\theta \cos 2\alpha + \sin 2\theta \sin\alpha \cos\alpha) \\ g_2 &= b_u(-\cos 2\theta \cos 2\alpha - \sin 2\theta \sin\alpha \cos\alpha) \end{aligned} \tag{5.45}$$

where the subscript u and v refer to the directions of the principal curvatures, and θ is the angle between the direction of the principal curvature and the perpendicular to the yield line as shown in Fig. 4.16. Substituting Eq. 5.45 into 5.40 - 5.43

$$\begin{aligned} A_M &= 2E_s A_s z_n b_u(\cos 2\theta \cos 2\alpha + \sin 2\theta \sin\alpha \cos\alpha)(\cos^2\alpha - \sin^2\alpha) \\ A_A &= 2E_s A_s a_n \\ A_T &= 2E_s A_s z_n b_u(\cos 2\theta \cos 2\alpha + \sin 2\theta \sin\alpha \cos\alpha)(\sin 2\alpha) \\ A_R &= 0 \end{aligned} \tag{5.46}$$

Isotropic Reinforcement, $\alpha = 45^{\circ}$

Consider first an isotropically reinforcement element with $\alpha = 45^{\circ}$ for which $\theta = 0$ and Eq. 5.45 becomes

$$\begin{aligned} A_M &= 0 \\ A_A &= 2E_s A_s a_n \\ A_T &= 0 \\ A_R &= 0 \end{aligned} \tag{5.47}$$

Substituting Eq. 5.47 into Eq. 5.31 and 5.35

$$M_n = 2E_s A_s a_n (0.5h - k_1 2E_s A_s a_n / \sigma_{ca}) \tag{5.48}$$

$$M_{nt} = 0 \tag{5.49}$$

It should be noticed that M_n is the resisting moment across the yield line, while M_{nt} would not be the capacity of twisting resistance, but the twisting moment produced by M_n. Equation 5.48 expresses the moment capacity of the plate if $\sigma_s \leq f_y$.

From Fig. 5.5 and 5.6, the following relationships are obtained

$$2a_n E_s A_s = c_n \sigma_{ca} \tag{5.50}$$

and

$$\epsilon_c (0.5h - c_n) = c_n a_n \tag{5.51}$$

Combining Eq. 5.48, 5.50 and 5.51

$$\frac{M_n}{h^2 \sigma_{ca}} = (0.5 + 2k_1 B_p)\sqrt{B_p^2 + B_p} - (0.5 + k_1 + 2k_1 B_p)B_p \tag{5.52}$$

where $B_p = E_s A_s \epsilon_c/(\sigma_{ca} h)$.

For the considered isotropically reinforced plate element, the yield lines will have the same directions as the principal moments. If the reinforcement crosses the yield lines at 45^o and the yield point can be reached, all the reinforcement is brought to yield at the same time. The yield moment is

$$M_n' = 2A_s f_y(\frac{h}{2} - 2k_1 A_s f_y/\sigma_{ca}) \tag{5.53}$$

In order to compare Eq. 5.52 and 5.53, Eq. 5.43 is rewritten in the form

$$\frac{M_n'}{h^2\sigma_{ca}} = B_p(1.0 - 4k_1 B_p \epsilon_y/\epsilon_c)\epsilon_y/\epsilon_c \tag{5.54}$$

The results of Eq. 5.52 and 5.54 are shown in Fig. 5.7. In effect, this plot shows the variation of the resisting moment with the amount of reinforcement. The ratio ϵ_y/ϵ_c is chosen equal to 1.0 and k_1 equal to 0.4. It should be emphasized that the yield stress can be reached only if the element has light reinforcement. With heavier reinforcement the effectiveness of the steel is reduced because the stresses drop off almost at the same rate the reinforcement is increased.

Figure 5.7 may also represent a beam with longitudinal and transverse reinforcement. The "yielding" mechanism for a plate or beam element will be described in the following.

If the slab element is isotropically reinforced, the directions of the yield lines are perpendicular to the directions of

the principal moments, which make 45° angles with the longitudinal axes. The strain distributions over the depth of the section in the directions of the yield lines are equal but inverted with respect to each other. Thus, they combine to give no curvature in the longitudinal direction. Consequently, the steel strain is equal to the strain at mid-height. It follows that if the neutral axes in the directions of the yield lines should occur at mid-height, the steel strain is zero.

The above indicates that the neutral axis cannot be at the mid-height in a cracked torsion specimen. As the amount of reinforcement is increased in an element, the neutral axis will tend to approach the mid-hight, and this will reduce the strain in the steel for a given concrete strain. By increasing the amount of reinforcement the strains are brought below that of the steel yield stress. From this point on, the increase of reinforcement has little effect on the moment capacity because the limiting concrete strain requires a reduction in the steel strain such that the relative increase in quantity of reinforcement is practically equal to the relative loss in effective steel stress.

It seems natural to consider the reinforcement at point C in Fig. 5.7 as the "balanced" amount of reinforcement. Below point C the capacity of the reinforcement is the critical factor, while the concrete strength is the critical factor beyond point C.

The "balance point" can be found from Eq. 5.52 and 5.54 by trial and error

$$(0.5 + 2k_1B_p)(\sqrt{1 + 1/B_p}) + 2k_1B_p\left(2\left[\frac{\epsilon_y}{\epsilon_c}\right]^2 - 1\right) - 0.5 - \frac{\epsilon_y}{\epsilon_c} - k_1 = 0 \qquad (5.55)$$

Equation 5.55 can be converted into an explicit form for B_p, but such an expression is more complex than Eq. 5.55. From Eq. 5.55 the reinforcement at the balance point is approximately

$$A_s f_y \approx 0.125\ \sigma_{ca} h \tag{5.56}$$

If more accuracy is desired Eq. 5.56 may serve as a first estimate in using Eq. 5.55.

Isotropic Reinforcement, Any Specified Value of α

Consider the previous case, but with an arbitrary rotation of the reinforcement, α, with respect to the principal moment. The assumed conditions are

$$A_s = A_s^o, \quad \mu = \mu^o = 1, \quad \theta = 0^o \tag{5.57}$$

Substituting these values into Eq. 5.46

$$\begin{aligned} A_M &= E_s A_s z_n b_u \cos^2 2\alpha \\ A_A &= 2E_s A_s a_n \\ A_T &= 2E_s A_s b_u \cos 2\alpha \sin 2\alpha \\ A_R &= 0 \end{aligned} \tag{5.58}$$

Substituting Eq. 5.58 into 5.31

$$\frac{M_n}{h^2 \sigma_{ca}} = B_p z_n^2 \cos^2 2\alpha / (h^2 \sqrt{B_p^2 + B_p} - h^2 B_p) + (0.5 + 2k_1 B_p)\sqrt{B_p^2 + B_p}$$
$$- (0.5 + k_1 + 2k_1 B_p) B_p \tag{5.59}$$

where $B_p = A_s E_s \epsilon_c / (\sigma_{ca} h)$

Equation 5.59 is illustrated in Fig. 5.8 in relation to the deviation in which the reinforcement is assumed to yield. The general trend is similar to that for uniaxial bending. The steel yield stress is the governing factor for specimens with small amounts of reinforcement and the concrete strain is the governing factor for specimens with large amounts of reinforcement. For the case with the reinforcement in the direction of the principal moment ($\alpha = 0$), the yielding of the reinforcement is the governing factor also for large amounts of reinforcement if $\epsilon_c/\epsilon_y \geq 1.0$.

Figure 5.8 shows that for small amounts of reinforcement the torsion capacity is nearly independent of the direction of the isotropic reinforcement. However, the stiffness is very sensitive to the direction of the reinforcement even for small amounts of steel as shown in Chapter 4.

(c) Nonisotropically Reinforced Concrete Element Subjected to Torsion

The case where the directions of the principal moments coincide with the directions of the reinforcing bars is equivalent to an element with reinforcement parallel to an applied uniaxial moment.

In the following, an element with the reinforcement inclined at 45° to the principal moments is considered. The reinforcement is assumed to be the same top and bottom. Hence, the case corresponds also to the general case of a beam with longitudinal reinforcing bars and stirrups. The reinforcement may be stressed so that (1) all reinforcement is at yield, (2) the reinforcement is at yield in one direction only, and (3) the reinforcement does not reach the yield stress because of limiting concrete deformations.

Assume All Reinforcement at Yield

The yield line pattern in an element is shown in Fig. 5.9. The reinforcing bars are in the x- and y-directions and the principal moments in the u- and v-directions. The yield lines which form in the top face deviate an angle γ from the u-direction, and those at the bottom face deviate γ' from the v-direction. The magnitudes of γ and γ' have to be equal because of symmetry.

According to the premises in this report, the concrete compressive principal stress occurs parallel to the yield lines. The second principal stress is assumed to be negligible. From equilibrium of the cross section perpendicular to the x-direction

$$2A_s f_y = \sigma_{ca} c_n (1 - \sin 2\gamma) \tag{5.60}$$

and correspondingly in the perpendicular direction

$$\mu 2A_s f_y = \sigma_{ca} c_n (1 + \sin 2\gamma) \tag{5.61}$$

where the angle γ is as shown in Fig. 5.9. Equations 5.60 and 5.61 relate the forces in the reinforcement to the forces in the concrete. The torsional moment capacity may be determined conveniently by considering a section perpendicular to the x- or y-axis

$$M_{yx} = 0.5\sigma_{ca} c_n \cos 2\gamma (h - 2k_1 c_n) \tag{5.62}$$

Combining Eq. 5.60, 5.61 and 5.62

$$M_{yx} = A_s f_y \sqrt{\mu}\, (h - 2k_1 (1 + \mu) A_s f_y / \sigma_{ca}) \tag{5.63}$$

The appearance of the term $\sqrt{\mu}$ in Eq. 5.63 reflects the rotation of the

yield line. Without a rotation of the yield line, the corresponding factor would be $(1/2 + 1/2\ \mu)$. It can be concluded that the ratio $\sqrt{\mu}/(1/2 + 1/2\mu)$ does not deviate significantly from unity for $\mu > 0.5$, if the ratio μ is chosen so that $\mu \leq 1.0$. The direction of the yield line is found from Eq. 5.60 and 5.61

$$-\sin 2\gamma = \frac{1 - \mu}{1 + \mu} \tag{5.64}$$

The derivations show that isotropic reinforcement is the most efficient in resisting torsion.

Assume Reinforcement at Yield in One Direction Only

The reinforcement in the layer with the smaller reinforcement is strained more. Hence, this is the reinforcement that is assumed to be yielding. Assuming $0 < \mu \leq 1.0$, the reinforcement in the y-direction will yield first and is the "main" reinforcement according to the definition in Section 5.1. The equilibrium equations are derived as for Eq. 5.60 and 5.61

$$2A_s E_s \epsilon_{ax} = \sigma_{ca} c_n (1 - \sin 2\gamma) \tag{5.65}$$

$$\mu 2A_s f_y = \sigma_{ca} c_n (1 + \sin 2\gamma) \tag{5.61}$$

In Eq. 5.65 it was necessary to introduce the steel strain ϵ_{ax}, and Eq. 5.61 and 5.65 can be solved only if this strain is known. The following strain compatibility equations are available

$$-\epsilon_c = 0.5(\epsilon_{ax} + \epsilon_{ay}) - 0.5(\epsilon_{ax} - \epsilon_{ay}) \sin 2\gamma - 0.5 h b_u \cos 2\gamma \tag{5.66}$$

$$-0.5(\epsilon_{ax} - \epsilon_{ay})\cos 2\gamma + 0.5hb_u \sin 2\gamma = 0 \qquad (5.67)$$

$$\epsilon_c/c_n = b_u \cos 2\gamma \qquad (5.68)$$

where ϵ_c is the limiting strain of the concrete in the direction of the principal compression stress, which coincides with the direction of the yield line; and b_u is the curvature in the direction of the applied principal moments. Equation 5.66 is based on the fact that ϵ_{ax} and ϵ_{ay}, which are the strains in the reinforcement, are also principal strains at the midheight of the plate specimens. Equation 5.67 takes into account that the principal compressive stress in the concrete is a maximum value. Equation 5.68 expresses that the principal curvature coincides with the principal moment because of symmetry.

Combining Eq. 5.62 and 5.61, the moment capacity can be expressed as

$$M_{yx} = \mu A_s f_y \sqrt{\frac{1 - \sin 2\gamma}{1 + \sin 2\gamma}} \left[h - k_1 4\, \mu A_s f_y/(\sigma_{ca}(1 + \sin 2\gamma))\right] \qquad (5.69)$$

The angle γ is the only unknown in Eq. 5.69, and this angle can be determined from Eq. 5.61, 5.65, 5.66, 5.67 and 5.68 which result in the implicit equation for γ

$$4\mu^2 A_s f_y (1 + \sin^2 2\gamma)^2/(E_s \epsilon_c h\, \sigma_{ca}) + 0.5(1 + \sin 2\gamma)^3 - \mu 2 A_s f_y \cos^2 2\gamma = 0 \qquad (5.70)$$

Solutions of Eq. 5.70 are shown graphically in Fig. 5.10. The magnitude of the limiting strain in the concrete, ϵ_c, is set equal to the yield strain for the reinforcing steel, ϵ_y, in order to have some

rotational capacity left. The angle in the form of "sin2γ" is marked on the horizontal axis, and the vertical axis is the solution of the equation. This demonstration indicates clearly that the angle γ approaches zero as the amount of reinforcement increases and as the ratio μ approaches unity.

The resulting moment capacity by this approach will be shown in comparison with the other two approaches at the end of this section.

(3) Assume All Reinforcement Below the Yield Stress

The problem to solve is similar to that for partial yielding and the following set of equations are available for the solution of the problem

$$2A_s E_s \epsilon_{ax} = \sigma_{ca} c_n (1 - \sin 2\gamma) \tag{5.65}$$

$$\mu 2A_s E_s \epsilon_{ay} = \sigma_{ca} c_n (1 + \sin 2\gamma) \tag{5.71}$$

$$-\epsilon_c = 0.5(\epsilon_{ax} + \epsilon_{ay}) - 0.5(\epsilon_{ax} - \epsilon_{ay}) \sin 2\gamma - 0.5 b_u \cos 2\gamma \tag{5.66}$$

$$-0.5(\epsilon_{ax} - \epsilon_{ay}) \cos 2\gamma + 0.5h\, b_u \sin 2\gamma = 0 \tag{5.67}$$

$$\epsilon_c / c_n = b_u \cos 2\gamma \tag{5.68}$$

The moment capacity can be derived from Eq. 5.62, 5.71, 5.65, 5.66, 5.67 and 5.68.

$$\frac{M_{yx}}{\sigma_{ca} h^2} = \frac{-2\mu B_p \cos 2\gamma \sin 2\gamma}{(1 + \sin 2\gamma)^2 - \mu(1 - \sin 2\gamma)^2} \left[1 + \frac{4k_1 B_p \sin 2\gamma}{(1 + \sin 2\gamma)^2 - \mu(1 - \sin 2\gamma)^2} \right] \tag{5.72}$$

where $B_p = A_s E_s \epsilon_c / (\sigma_{ca} h)$.

The geometric expressions in Eq. 5.72 can be rewritten in a simpler manner, but it would complicate the solution of the equation. The angle γ is determined by

$$-8B_p\mu[(1+\sin 2\gamma)-\mu(1-\sin 2\gamma)]\sin 2\gamma\cos^2 2\gamma = [(1+\sin 2\gamma)^2-\mu(1-\sin 2\gamma)^2]^2 \tag{5.73}$$

A graphical solution of Eq. 5.73, which is presented in Fig. 5.11 indicates that the angle γ decreases in magnitude with increasing amount of reinforcement and with the ratio μ approaching unity.

The graphical solution in Fig. 5.11 is not accurate enough to yield a satisfactory result for the moment capacity in Eq. 5.72. It is seen from Eq. 5.73 that as the amount of reinforcement represented by B_p approaches zero, the angle γ will approach a value corresponding to

$$-\sin 2\gamma = \frac{1-\sqrt{\mu}}{1+\sqrt{\mu}} \tag{5.74}$$

The angle expressed in Eq. 5.74 may be considered as a singular point, and by expanding Eq. 5.73 from this point the angle γ can be found with accuracy by

$$-\sin 2\gamma = [a - a\sqrt{\mu} - 0.5b - 0.5\sqrt{b^2+4ac}\,]/[a(1+\sqrt{\mu})] \tag{5.75}$$

where $a = (1+\sqrt{\mu})^2/B_p + 3\mu\sqrt{\mu} + 5\sqrt{\mu} - 3\mu - 1)$

$b = 8\mu\sqrt{\mu} + 4\sqrt{\mu} - 10\mu - 2\mu^2$

$c = 4(\mu - \sqrt{\mu})^2$

Substituting Eq. 5.75 into 5.72 gives the moment capacity. For any specific value of μ, the computation is simplified by first determining a, b and c in Eq. 5.75.

For small amounts of reinforcement, all the reinforcing bars are brought to yield before failure. As the amount of reinforcement is increased, a stage is reached where reinforcing bars in one direction yield while the bars in the other direction are still in the elastic range. If the reinforcement is increased beyond this stage, the specimens will fail before any reinforcement reaches the yield stress. Figures 5.12 and 5.13 illustrate the moment capacity with increasing amounts of reinforcement. The moment capacity is shown along the vertical axis, and the amount of reinforcement along the horizontal axis such that the symbol A_s' represents one fourth of the total reinforcement per unit width in the whole section. For example, if $\mu = 0.25$ and if the larger reinforcement ratio is 1.0, A_s' refers to a reinforcement ratio of 0.625.

It should be noted that to assume that the reinforcement has reached the yield stress may give results considerably in error even for amounts of reinforcement as low as one percent reinforcement in each layer.

The stage where partial yielding governs is very limited. The error by ignoring this stage appears to be insignificant.

The governing curve in Fig. 5.12 and 5.13 is the one indicating the least capacity or the lower steel stress. The capacity will not approach zero for x-axis values over 0.5 as implied by the

curve for "full yielding" because finite moment capacities can be achieved at lower steel stresses.

The results of the computed moment capacities are put together in Fig. 5.14. The illustration emphasizes that the efficiency of the reinforcement is largely dependent on the percentage of reinforcement in the specimen.

Equation 5.75 may also be applied in the "proportional" region of the moment-curvature relationship. Consider the term $B_p = A_s E_s \epsilon_c / (\sigma_{ca} h)$. Assuming concrete to be linearly elastic, $\epsilon_c / \sigma_{ca} = 2\epsilon_c / (E_c \epsilon_c) = 2/E_c$; hence

$$B'_p = 2A_s E_s / (E_c h) \tag{5.76}$$

Thus, B_p in Eq. 5.75 should be replaced by B'_p if the "proportional" part of the moment-curvature curve is considered. This procedure was used to find the crack direction in Chapter 4 (Eq. 4.65).

5.5. Test Results and Discussion

The measured yield and ultimate moments of 18 specimens are compared with computed values in Table 3.1. The agreement between the measured and computed moments is good. The computed values for ultimate moments average three percent lower than the measured ones, if the cases with strain hardening of the reinforcement are excluded.

For computation of the yield moment the concrete was considered to be linearly elastic with a modulus of elasticity

$$E_c = 63500 \sqrt{f'_c} \tag{5.77}$$

as given in ACI 318-63(20). For computation of the ultimate moment, the average stress in the concrete was assumed to be

$$\sigma_{ca} = 10000/(1 + 8000/f'_c) \qquad (5.78)$$

which had been found to be an adequate value for beams (21). The ultimate moment was computed by the formulae derived in this section by assuming the constant, k_1, to be 0.4.

As it can be seen from Table 3.1, a significant difference in measured and computed moment was always accompanied by a large curvature, which indicates strain hardening in the steel.

The forces in the reinforcement at ultimate load are directly related to the moment capacity, and the critical question is whether the yield stress can be reached. In the following, the steel strain will be considered for various external and internal conditions.

(a) Strains in Reinforcing Bars Placed in the Direction of an Applied Principal Moment

Figure 5.15 shows the curvature-strain relationship for specimens C2, B4 and B18 which were subjected to isostatic, uniaxial and torsional moment. The conclusion is trivial as would be expected; the moment-strain relationships are practically identical.

(b) Strains in Reinforcing Bars Inclined 22.5° and 67.5° to the Direction of Principal Moments

Figure 5.16 shows the measured steel strain in the case of uniaxial bending, B8, and pure twisting, B17. The curves demonstrate distinctly a first yield point. According to Eq. 5.7, the strain in the reinforcing bars inclined 22.5° and 67.5° to a line perpendicular

to the cracks should be strained in the ratio 6.0:1.0, provided the transverse strains are negligible as in specimen B8. The ratio measured at first yield was about 3.5:1.0. This might have been difficult to explain if a change in the direction of the cracks had not been observed during the test. Because of the less effective layer of reinforcing bars at 22.5° to the crack, the line of the least resistance will not be perpendicular to the applied uniaxial moment. The observed change in the crack direction was approximately 10°. If this 10° change is taken into account, Eq. 5.7 gives a theoretical strain ratio of 3.7:1.0.

The strain ratios in the torsion specimen are more complex (Fig. 5.16) because the transverse strain ϵ_t plays an important role. At cracking and immediately afterwards, the reinforcing bars at 67.5° to the line perpendicular to the crack are strained in compression. They pick up tensile strains only after a curvature of 35×10^{-5} in.$^{-1}$ has been exceeded. This trend is in good agreement with Eq. 5.7. At cracking, the strains across and parallel to the crack direction are equal in magnitude but opposite in sign, which results in a negative strain ratio between the reinforcing bars according to Eq. 5.7. As the curvature increases, the strain perpendicular to the crack direction increases at a greater rate than the strain parallel to the cracks. Consequently, the strain ratio changes from a negative to a positive value.

(c) Strains in Reinforcing Bars Inclined 45° to the Direction of the Principal Moments

Figure 5.17 shows the curvature-strain relationship for three specimens with isotropic reinforcement. Specimen B7 is subjected to

uniaxial moment, and specimens B16 and B20 are subjected to torsion. Specimens B7 and B16 have one percent steel in each layer, while B20 has one-half percent.

The strain readings indicate that specimen B16 had nearly the balanced amount of reinforcement. The steel stress reached yield just before the concrete crushed. This is in agreement with Eq. 5.56 which predicts specimen B16 to be a nearly balanced reinforced element. Figure 5.18 may indicate more clearly that B16 did not possess the ductility that is characteristic for an underreinforced element.

The rectangular specimen used in this investigation may well be considered as a slender deep beam. Test results from the other extreme, a beam with square cross section, are shown in Fig. 5.19. The results are taken from an investigation by Hsu (22). Six beam specimens had a cross section 10.0 in. by 10.0 in., and were isotropically reinforced. The average reinforcement yield stress was 48,000 psi, and the compressive cylinder strength of concrete was about 3900 psi. For comparison with the analytical approach in this section, the average compressive stress in the concrete at failure was taken as 2700 psi ($0.7f'_c$) and the limiting concrete strain was assumed to be 0.003. It should be noticed that the lowest measured capacity was reported to be identical with the carrying capacity at cracking, which explains the difference between the measured and predicted results because the analysis ignores the contribution from tensile stresses in the concrete. The agreement between the experimental and analytical results is good.

6.2. The Minimum Resistance and Equilibrium

The principle applied to determine the formation of the yield line is as follows: yielding of the element will occur at a location in the plate where the ratio of the external moment to the resisting moment is maximum regardless of the absolute value of the external moment.

According to energy principles, the orientation of the yield line corresponding to a true minimum resistance should satisfy the equilibrium conditions. Moreover, where it is more convenient, the equilibrium conditions may be used directly to find the orientation of the yield lines.

Consider the slab in Fig. 6.1. The directions of the reinforcing bars are the x- and y-directions and the corresponding unit resisting moments are M_x and M_y (positive), and M_x^o and M_y^o (negative). For convenience, positive and negative moments are defined such that M_x and M_y are the governing resisting moments when the element is subjected to the applied moments M_1 and M_2 as shown in Fig. 6.1. The moments M_1 and M_2 are principal moments in the u- and v-directions.

The resisting moments at the yield line are (Fig. 6.1b)

$$M_n = M_y \cos^2(\beta + \gamma) + M_x \sin^2(\beta + \gamma) \tag{6.1}$$

$$M_t = M_y \sin^2(\beta + \gamma) + M_x \cos^2(\beta + \gamma) \tag{6.2}$$

$$M_{nt} = (M_x - M_y) \sin(\beta + \gamma) \cos(\beta + \gamma) \tag{6.3}$$

The components of the applied moments at the yield line are

6. FORMATION OF YIELD LINES

6.1. Introductory Remarks

In the application of the yield line theory it may be more important and also more difficult to determine or to estimate the location of the yield lines than to determine the capacity of a cross section. This chapter will deal with the formation of the yield lines in an element where the forces at the boundaries are known. It will be demonstrated that the yield line is not necessarily perpendicular to the direction of the maximum principal moment. As a corollary, it will be shown that twisting moments along the yield line, the existence of which sometimes has been claimed to be untenable, play a most important role.

For a slab element with equal moment capacity in all directions, the formation of the yield line will coincide with the direction of the applied principal moment, in which case the solution is trivial. In this chapter a nonisotropically reinforced concrete slab element will be considered. It will be assumed that the relationship between the resisting moments can be described by the equilibrium conditions (Mohr's circle). As it was shown in Chapter 5, this is an approximation, but even with a high degree of nonisotropy, the error involved is within a few percent. The above assumptions imply that the elements considered are underreinforced.

$$ME_n = M_2 \cos^2\gamma + M_1 \sin^2\gamma \tag{6.4}$$

$$ME_t = M_2 \sin^2\gamma + M_1 \cos^2\gamma \tag{6.5}$$

$$ME_{nt} = (M_2 - M_1) \sin\gamma \cos\gamma \tag{6.6}$$

The applied moment will not exceed the capacity of the element if

$$/ME_n/ < /M_n/ \tag{6.7}$$

and

$$/ME_t/ < /M_t/ \tag{6.8}$$

and

$$/ME_{nt}/ < /M_{nt}/ \tag{6.9}$$

The applied moments are equal to the carrying capacity when any of the above three inequalities becomes an equality. Along a yield line of minimum capacity expressions 6.7 and 6.8 become equalities simultaneously. Let expression 6.7 become an equality

$$ME_n = M_n \tag{6.10}$$

For convenience let

$$\nu M_x = M_y \tag{6.11}$$

and

$$\omega M_1 = M_2 \tag{6.12}$$

The "principle of the least resistance" may be expressed by

$$\frac{d}{d\gamma} \frac{ME_n}{M_n} = 0 \tag{6.12}$$

Combining Eq. 6.1, 6.2, 6.4, 6.5 and 6.12

$$M_{nt} ME_n + ME_{nt} M_n = 0 \tag{6.13}$$

Therefore, if $ME_n = M_n$, then $M_{nt} = -ME_{nt}$. That is, at the yield line, which is the line with minimum resistance, the component of external normal moments at the yield line is equal to the moment capacity across the yield line, and the internal twisting moment is in equilibrium with the external twisting moment at the yield line.

Next, the resisting moment, M_t, and the component of the applied moment, ME_t, (the moments parallel to the yield line) will be compared. From Eq. 6.1, 6.2, 6.4 and 6.5

$$M_n + M_t = M_x + M_y \tag{6.14}$$

$$ME_n + ME_t = M_1 + M_2$$

From 6.10 and 6.14

$$\frac{M_t}{ME_t} = \frac{M_x + M_y - M_n}{M_1 + M_2 - M_n} \tag{6.15}$$

Equation 6.15 shows that

$$M_t \geq ME_t \text{ because } M_x + M_y \geq M_1 + M_2$$

Only in particular cases are the moments M_t and ME_t equal

(1) $M_x = M_y$ and $M_1 = M_2$

(2) $M_x = -M_y$ and $M_1 = -M_2$

(3) $M_1 = M_x$ and $M_2 = M_y$ and $\beta = 0$

In the usual case with $M_t > ME_t$, the equilibrium is provided by the concrete in the cross section, that is, the difference $(M_t - ME_t)$ is compensated by an eccentric "prestressing force" in the t-direction. This phenomenon was described in Chapter 4 where several strain measurements confirmed the above statement.

6.3. The Orientation of the Yield Lines in a Slab Element

It is indicated in the previous section that the orientation of a yield line can be determined from the "principle of least resistance" or the equilibrium condition.

The direction of the yield line is determined by the angle γ. (Fig. 6.1) From Eq. 6.1, 6.3, 6.4, 6.6, 6.11 and 6.13, it can be derived as shown in Appendix D that

$$- \tan^2\gamma - \omega c_1 \tan\gamma + \omega = 0 \tag{6.16}$$

where

$$\omega c_1 = [(\nu - \omega) \cot\!\text{an}^2\beta + 1 - \nu\omega]/[(1 - \nu) \cot\!\text{an}\beta] \tag{6.17}$$

From Eq. 6.16

if $\omega \neq 0$

$$\tan\gamma = -0.5\omega c_1 + 0.5\sqrt{c_1^2\omega^2 + 4\omega} \tag{6.18}$$

if $\omega = 0$ ($M_2 = 0$, $M_1 \neq 0$)

$$\tan\gamma = -(1 + \nu \cot\text{an}^2\beta)/[(1 - \nu) \cot\text{an}\beta] \tag{6.19}$$

if $M_1 = 0$ and $M_2 \neq 0$

$$\tan\gamma = (M_y - M_x) \cot\text{an}\beta/[M_y + M_x \cot\text{an}^2\beta] \tag{6.20}$$

Example 1: A nonisotropically reinforced element subjected to uniaxial moment.

The direction β of the reinforcement is chosen 45° (see Fig. 6.1) and the $M_x/M_y = 0.5$. The uniaxial moment acts in the v-direction. From Eq. 6.20

$$\gamma = 18.4^\circ \tag{6.21}$$

The capacity of the element with respect to the uniaxial moment in the v-direction is

$$M_v = M_2 = [M_y \cos^2(\beta + \gamma) + M_x \sin^2(\beta + \gamma)]/\cos^2\gamma \tag{6.22}$$

Introducing the quantities in the example into Eq. 6.22

$$M_v = 0.67 M_y \tag{6.23}$$

It may be noted that for a yield line perpendicular to the direction of the maximum principal external moment, the capacity of the element would have been $M_v = 0.75\ M_y$ which is a significant overestimation of the carrying capacity.

Example 2: A nonisotropically reinforced element subjected to pure torsion.

The state of pure torsion can be represented by $M_2 = -M_1$ or $\omega = -1$. The angle β, representing the direction of the reinforcement as shown in Fig. 6.1, is chosen to be 45°. Introducing the above quantities into Eq. 6.16, 6.17 and 6.18

$$\tan\gamma = -(1 + \nu - 2\sqrt{\nu})/(1 - \nu) \tag{6.24}$$

Equation 6.24 can be rewritten to read

$$-\sin 2\gamma = (1 - \nu)/(1 + \nu) \tag{6.25}$$

In the case of pure torsion $\mu = \nu$. Thus, Eq. 6.25 is identical with Eq. 5.64 in the previous chapter which was derived from equilibrium considerations.

6.4. The Orientation of the Yield Lines in Plate Elements Subjected to In-Plane Forces

The results obtained in the previous section can be applied to reinforced concrete elements subjected to in-plane forces. Equations 6.16 through 6.19 are valid for in-plane forces if

$$\begin{aligned} \nu\, N_x &= N_y \\ \omega\, N_1 &= N_2 \end{aligned} \tag{6.26}$$

where N_x, N_y are the resisting principal forces in the x- and y-directions, and N_1 and N_2 are the applied principal forces in the u- and v-directions. If only one significant principal force N_2 is

applied ($N_1 \approx 0$, see Eq. 6.20)

$$\tan\gamma = (N_y - N_x) \cot\beta / [N_y + N_x \cot^2\beta] \tag{6.27}$$

where the angles are as shown in Fig. 6.1.

The above considerations assume that the loading conditions are such that tensile yield lines occur. The tension is assumed to be resisted by the reinforcement only. Hence

$$\nu = \mu \tag{6.28}$$

The direction of the cracks before yielding may not be parallel to the yield lines. In the proportional range of the stress-strain relationship the direction of the cracks is a factor in determining the effectiveness of the reinforcement, as was mentioned in Chapter 4.

The relationship between N_y and N_x is (see Eq. 4.18)

$$N_y/N_x = \mu(\epsilon_n \sin^2\alpha + \epsilon_t \cos^2\alpha - \gamma_{nt} \sin\alpha\cos\alpha)/(\epsilon_n \cos^2\alpha + \epsilon_t \sin^2\alpha + \gamma_{nt} \sin\alpha\cos\alpha) \tag{6.29}$$

Equation 4.79 expresses the effectiveness of "extra" reinforcement by the term N_{nt}/N_{na}, which is a function of the angle α. A simplified expression for α will be derived in order to obtain an approximate and safe estimate of the ratio N_{nt}/N_{na} in Eq. 4.79.

It is desirable to eliminate the term ϵ_t in Eq. 6.29. If ϵ_t is positive, ignoring it is conservative since, for a given value of ϵ_n, a positive value of ϵ_t would cause higher stresses in the reinforcement. If ϵ_t is negative, it is considerably small in comparison to ϵ_n

in a cracked section because a negative ϵ_t indicates and is limited to compressive strains in the concrete; hence, it can be ignored. Therefore

$$N_y/N_x = \mu(\epsilon_n \sin^2\alpha - \gamma_{nt} \sin\alpha\cos\alpha)/(\epsilon_n \cos^2\alpha + \gamma_{nt} \sin\alpha\cos\alpha) \tag{6.29a}$$

The same reasoning as for ϵ_t holds for the smaller of the external forces. A negative transverse force would compress the concrete and the deformations would be small, while a positive transverse force would increase the effectiveness of the reinforcing bars.

Let $N_2 \neq 0$ and $N_1 = 0$, for which Eq. 6.27 applies. The ratio N_y/N_x depends on whether the faulting or the shear strain, γ_{nt}, is restrained. The faulting before yielding is assumed to be small compared with ϵ_n. Hence from Eq. 6.29a

$$N_y/N_x = \mu \sin^2\alpha/\cos^2\alpha = \mu \cotan^2(\beta + \gamma) \tag{6.30}$$

Combining Eq. 6.30 and 6.27

$$\tan\gamma = \frac{\sqrt[3]{\mu \tan\beta} - \tan\beta}{1 + \tan\beta \sqrt[3]{\mu \tan\beta}} \tag{6.31}$$

where, from Fig. 6.1

$$\alpha = 90^\circ - \beta - \gamma \tag{6.32}$$

Introducing Eq. 6.32 into 4.79 gives an approximate, safe estimate of the effectiveness of the "extra" reinforcement.

Example 1. Let $\beta = 45^{\circ}$ and $\mu = 0.5$

From Eq. 6.31

$$\tan\gamma = -0.115$$

$$\gamma = -6.6^{\circ}, \quad \alpha = 51.6^{\circ}$$

From Eq. 4.79

$$N_{nt}/N_{na} = 0.283$$

The rotation of the crack by -6.6° reduces the ratio N_{nt}/N_{na} from 0.500 to 0.283.

Example 2. Let $\mu = 0$, $\beta \neq 90^{\circ}$

From Eq. 6.31

$$\tan\gamma = -\tan\beta$$

$$\gamma = -\beta$$

For reinforcement provided in one direction only, the cracks would coincide with the direction of the reinforcement if the tensile strength of the concrete is negligible.

It can be concluded that the effectiveness of extra reinforcement in one direction depends on the ratio between "extra" and "base" reinforcement as well as the direction of the extra reinforcement.

6.5. Test Results

Observations related to the formation of yield lines are reported in this section.

In all test specimens, regardless of the reinforcement, the initial cracks appeared perpendicular to the maximum principal external

moment. Further development of these cracks depended on the direction and distribution of the reinforcement.

The development of cracks in specimen B8 (Fig. 6.2) is a typical illustration of the nature of the crack development. Specimen B8 was a rectangular element subjected to uniaxial moment, with one percent reinforcement in both layers which were at 22.5° and 67.5° to the span direction.

The initial cracks appeared perpendicular to the span direction as shown in Fig. 6.2a. Further cracking was apparently influenced by the reinforcement and rotated in a direction that would even out some of the strain differences in the two layers (Fig. 6.2b). After yielding of the reinforcement the yield lines "readjusted" to be perpendicular to the span direction as shown in Fig. 6.2c.

In the case of nonisotropic reinforcement in specimens subjected to uniaxial bending (specimens B9, B11 and B12), the yield lines were not perpendicular to the span or the external principal moment.

Specimen B9 had reinforcement at 45° to the span direction, one percent reinforcement in one direction and one-half percent in the perpendicular direction. During the test, the yield line rotated to avoid the stronger layer of reinforcement. The photographs in Fig. 6.3 show the yield lines at failure. Figure 6.3a shows the tension side. Cracks in several directions relate the history of the development of the crack pattern during the test. The initial cracks were vertical (with respect to the orientation of the photograph in the page). As the load increased the cracks rotated by stepwise "leaps" from one vertical crack to another. Although it is not possible to pinpoint

exactly the orientation of the yield lines in the photograph, the over-all direction in the yielding zone seems to be very close to the chalk lines, the direction of which is based on the analytical results given in this chapter. The photograph in Fig. 6.3b, which shows the failure in the compression zone, eliminates any doubt about a significant inclination of the yield lines with respect to the "vertical" direction. Some of the concrete cover is removed in Fig. 6.3a to demonstrate how the yield lines try to avoid the heaviest layer of reinforcement.

Specimen B11 (Fig. 6.4) had one percent reinforcement at 22.5° to the span direction and one-half percent reinforcement at 67.5° to the span. The reinforcement is uncovered in the upper left corner in the photograph (Fig. 6.4a). The development of the yield-line pattern was similar to that for specimen B9. The chalk lines in Fig. 6.4a indicate about 2° greater deviation from the vertical than the analytical prediction. Figure 6.4b shows the direction of the final yield lines more clearly.

In specimen B12 the ratio of the reinforcement in the two directions was again 0.5. The one-percent layer deviated 67.5° from the span direction, and the one-half percent layer was at 22.5° to the span direction. As it can be seen in Fig. 6.5, the rotation of the yield lines is considerably less in specimen B12 than in the two previous specimens (B9 and B11). The chalk lines indicate the computed directions of the yield lines. Figure 6.5b shows the compression side after failure.

Two nonisotropically reinforced specimens subjected to torsion were tested. The amount of reinforcement in the longitudinal direction was one quarter of a percent in each layer in top and bottom, while the amount of reinforcement in the transverse direction was one percent in each layer. The initial cracking appeared at 45° to the longitudinal axis, and the orientation remained unchanged till after yielding. In the loading period between yield and ultimate load, the direction of the apparent governing yield lines changed. The yield line patterns for specimen B21 and B22 are shown in Fig. 6.6. The final orientation of the yield lines was approximately the same for the two specimens. From Fig. 6.6b, it can be seen that the deviation of the yield lines from one of the principal moments is about 15° for specimen B22.

6.6. Concluding Remarks

The observed reorientation of the yield lines was made possible by the special test setup in this investigation, where the support and loading system did not introduce undue forces under the deformations of the specimens.

It may be interesting to note that in the case of tests with uniaxial moment, the supports in former investigations have usually allowed the specimen to rotate about their transverse axes at the supports, but not about the longitudinal axes (13,14). If the conditions were such that twisting moments were produced at the yield lines, the supports would take the major part of the twisting moment and the yield lines would then appear perpendicular to the principal moment.

"Transversely rigid" supports may also significantly increase the moment capacity in the longitudinal direction, as it was shown by the first example in the previous section.

A survey of the computed and observed orientation of the yield lines in the specimens of this investigation with nonisotropic reinforcement is given below.

Specimen	Load	β	μ	Measured γ	Computed γ
B9	U	45°	0.5	$16\text{-}18^\circ$	18.4°
B11	U	22.5°	0.5	$17\text{-}20^\circ$	17.1°
B12	U	67.5°	0.5	$9\text{-}11^\circ$	10.8°
B21	T	45°	0.25	$15\text{-}18^\circ$	18.5°
B22	T	45°	0.25	$14\text{-}17^\circ$	18.5°

The symbols U and T refer to uniaxial and torsional bending; β is the angle between the heavier reinforcement layer and the direction of the maximum moment; γ is the deviation of the yield lines from the perpendicular line to the maximum moment direction. The symbol μ is the ratio between the reinforcement in the lighter layer and that in the heavier layer.

The experimental results leave no doubt that under given conditions the twisting moments at the yield lines represent an important factor for the orientation of the yield lines and the capacity of the nonisotropically reinforced concrete elements.

7. THE YIELD CRITERION

7.1. Introductory Remarks

The yield criterion considered in this chapter refers to the flexural yield condition of a reinforced concrete slab element. A general application of the yield criterion and any analysis based on the theory of plasticity presumes a theoretically indefinite ductility after the yield condition is reached at a cross section. For practical solutions, the required ductility is dependent on the boundary conditions, loading conditions and the geometry of the structure. Another important factor in connection with the ductility or the rotational capacity is whether the total rotation is developed in a zone comprising several yield lines or whether the conditions are such that the rotation has to be produced in a narrow strip. Consequently, it is not possible to state an exact requirement for the rotational capacity. However, for most practical cases, a structural element which can deform three to five times the deformation at yield should have sufficient rotational capacity.

If plain concrete can be considered as one material, a reinforced concrete element consists of two materials, concrete and steel. The concrete has limited ductility while the reinforcing steel is required to be ductile. Consequently, if the limiting strain in the concrete is the critical factor for the load carrying capacity, the yield-line theory should not be applied without a special examination

of the problem, and then only with great caution. If the steel is the governing factor, the section should possess an adequate margin of ductility.

For reinforced concrete beams, the two conditions described above are designated "overreinforced" and "underreinforced" sections, while the "balanced" section is one in which both conditions are supposed to be realized simultaneously. For a beam subjected to uniaxial bending, the balanced reinforcement can be expressed solely in terms of material properties and geometry of the critical section.

As shown in Chapter 5, the "balanced" amount of reinforcement in a reinforced concrete element is not only dependent on the conditions stated for the beam but also on the relation between the external principal moments and on their directions relative to the directions of the reinforcing bars. In order to simplify the presentation, reinforced concrete elements will be grouped into three categories:

Category 1 comprises all elements in which the yield stresses in the reinforcement are the governing factor for the carrying capacity under all external loading conditions.

Category 2 comprises the elements which are underreinforced under some external loading conditions but overreinforced under different external conditions.

Category 3 comprises the cases in which the concrete elements are overreinforced regardless of the combination and the direction of the external moments.

7.2. The Yield Criterion, Category 1

The upper limit for the amount of steel in one layer is given by Eq. 5.55, which is approximated by Eq. 5.56

$$A_s f_y \approx 0.125\ \sigma_{ca} h \tag{7.1}$$

where A_s = area of steel per unit width in one layer

f_y = yield stress of the reinforcement

σ_{ca} = average concrete stress in the compression zone

h = height of the section

In Chapter 6 it was assumed that the steel stress was the governing factor and thus Chapter 6 deals with Category 1. The yield criterion in this case was determined by Eq. 6.22, 6.16 and 6.17, which are repeated here for convenience

$$M_2 = \omega M_1 = [M_y \cos^2(\beta + \gamma) + M_x \sin^2(\beta + \gamma)]/\cos^2\gamma \tag{7.2}$$

where γ is determined by

$$-\tan^2\gamma - \omega c_1 \tan\gamma + \omega = 0$$

with

$$\omega c_1 = [(\nu - \omega)\ \mathrm{cotan}^2\beta + 1 - \nu\ \omega]/[(1 - \nu)\ \mathrm{cotan}\beta]$$

The coordinate system and the angles are shown in Fig. 6.1.

A graphical presentation of the yield criterion stated by Eq. 7.2 is given in Fig. 7.1 through 7.4. The moments and their directions are presented in a polar coordinate system.

Figure 7.1 shows the directions of the applied principal moments u and v. The magnitude of the moment is the radial distance

from origin to the considered point on the curve. The direction of the moment at the considered point is the radial direction related to the u or v axis. In Fig. 7.1 the element is assumed to be isotropically reinforced so that the resisting positive moment is equal in all directions ($M_x = M_y$). Thus, the resisting moment is represented by the circle. The applied load is assumed to be a positive uniaxial moment. The shape of the curve results directly from equilibrium conditions (or Mohr's circle). As the applied moment is increased, the curve representing the applied moment will expand maintaining its original shape. When the curve touches the line or circle of resistance, the yield capacity is reached. The common point of the two curves represents the moment and the direction, γ, of the yield line. As can be seen, the angle γ is zero in this case. Because of the symmetry with respect to the horizontal line, the lower part is not needed and will be reserved for negative moments.

The case in Fig. 7.2 is more interesting. The element is nonisotropically reinforced ($M_x \neq M_y$) on one side (top or bottom). The applied moments M_1 and M_2 are positive and different in magnitude. The principal directions of the applied moments are different from those of the resisting moments (Fig. 6.1). The location of the point of intersection of the applied and resisting moment curves in Fig. 7.2 demonstrates that the yield-line direction, γ, does not coincide with either the direction of an applied moment or with the direction of the resisting moments M_x or M_y. It is seen that the applied moment in the v-direction cannot reach the resisting moment in that direction. The same phenomenon was shown analytically in Example 1 of Section 6.3.

Figure 7.3 shows the case of pure torsion, or equal applied moments of opposite sign. The element is assumed to be isotropically reinforced with equal amounts of reinforcement in the top and bottom. Therefore, the resistance is represented by a full circle. The figure demonstrates how the positive and negative yield lines are developed simultaneously. The yield lines are perpendicular to each other.

The case in Fig. 7.4 also refers to pure torsion, but the element is nonisotropically reinforced with the reinforcement repeated top and bottom. The directions of the reinforcement are set at 45° to the directions of the applied principal moments. The graphical presentation shows that the negative and positive yield lines caused by negative and positive moments are no longer perpendicular to each other and that the applied moment does not quite reach the resisting moment in the u- and v-directions. This phenomenon was discussed in Chapter 5 (Eq. 5.63). The ratio of the resisting to the applied moment in the u-direction is $0.5(1 + \nu)/\sqrt{\nu}$, where ν denotes the ratio between the resisting moments.

The graphical procedure is simple to use. Given the ratio between--and the direction of--the applied principal moments, and the resisting moments and their directions, the curves can be obtained from equilibrium conditions (Mohr's circle) for any desired case. Having obtained the shape of the applied moment curve, it is merely a question of enlarging it until the yield condition appears.

The yield criterion can be presented in a very simple manner in two particular cases: (1) for isotropically reinforced elements and (2) for the case where the directions of the applied principal moments

coincide with the directions of the reinforcement. In these cases the derivations in this report agree with Johansen's yield criteria, which were discussed in Chapter 2 and shown in Fig. 2.1.

7.3. The Yield Criterion, Category 2

The fact that Eq. 7.1 is based on a limiting concrete strain, ϵ_c, equal to the yield stress in the steel, ϵ_y, insures that all cases included in Category 1 are at least 15 percent underreinforced.

For a slab in Category 2 it is possible that an assumed yield line may pass through regions which are definitely underreinforced, and also through overreinforced regions, although the slab may be evenly reinforced throughout its area. In such a case, it would be too conservative to declare categorically that the yield line theory should not be used. If the yield lines in the overreinforced regions are about the last ones to be formed, the required rotational capacity is a minimum that may not exceed the rotational capacity of a overreinforced section. On the other hand, if excessive rotation of the overreinforced sections is required, a yield line in the overreinforced region may lose its capacity before the last yield lines are formed. In such a case, the yield-line theory cannot be applied to determine the capacity of the slabs.

Consider the specific case for an element with equal, isotropic reinforcement top and bottom. The directions of the reinforcement make 45° with the directions of the principal applied moments. As long as the relative amount of reinforcement, A_s/h, is under the limit

given by Eq. 7.1, the yield criterion has the well known square shape as shown in Fig. 7.5a.

If the amount of reinforcement is twice that given by Eq. 7.1, the yield criterion will be as shown in Fig. 7.5b. The bold lines in Fig. 7.5b indicate the regions of the yield criterion where the reinforcement is still the governing factor and the element has considerable ductility beyond yielding. Hence, if the load combinations are such that the bold lines of the yield criterion determine the capacity, the yield line theory can be applied as in Category 1. The broken lines in Fig. 7.5b indicate the region of the "yield criterion" where the limiting concrete strain governs, and the element has little ductility. If the load combinations are such that a broken line is reached, the application of the yield-line theory has to be restricted to the particular case for which the required rotation of the considered yield line is little. Therefore, the broken line may be used if the considered yield line is the last to occur.

The modified shape of the criterion is based on the derivations in Chapter 5. Figure 7.6 shows the relation between moment capacity and the amount of reinforcement under the same conditions as in Fig. 7.5. Where the steel stresses govern ($f_s = f_y$) and where the concrete strains govern ($f_s < f_y$) is indicated in Fig. 7.6. Three representative cases are examined: (1) isostatic moment, (2) uniaxial moment, and (3) torsional moment.

Figures 7.5c and 7.5d show the further development of the yield criterion as the amount of steel increases. It may be noted that the "bold-line" region, for which the yield-line theory applies,

appears to be constant in absolute magnitude as the reinforcement increases. However, the ductile region covers a relatively small part of the yield criterion when the amount of reinforcement is increased above that shown in Fig. 7.5c.

It should be mentioned that if the directions of the isotropic reinforcement had been parallel to the directions of the principal moments, the yield criterion would have kept its square shape also for a large amount of reinforcement.

The yield criterion for the general case with nonisotropic reinforcement in an arbitrary direction does not deviate in principle from the special case with isotropic reinforcement, but the deviation of the yield line from the directions of the principal moments makes a general analytical or graphical presentation more complex. The most practical method is probably to use the procedure in Section 7.2 and check the obtained values by the derived expressions in Chapter 5 and see if the section is overreinforced.

It may also be noted that in the case of nonisotropic reinforcement in top and bottom parallel to the principal moments, the shape of the yield criterion will remain rectangular for large amounts of reinforcement.

7.4. "Yield Criterion," Category 3

This category, which includes sections which are overreinforced under any condition, has very little to do with a general yield criterion or with the yield-line theory. However, if it can be shown in a particular case that the yield line in the overreinforced

region is the very last to appear, the yield line theory should still be applicable.

7.5. Concluding Remarks

It should immediately be emphasized that Category 1 covers nearly all the cases which are encountered in ordinary design. A designer would very seldom work with slabs in Category 2, and if so, the conditions are not likely to be in the "broken line" region of the yield criterion. Hence, the principles presented in Section 7.2 can be used in this case.

It may be said that the resisting moment capacities which are graphically shown by curved lines in Section 7.2, actually are sections of a three-dimensional yield surface, as are Tresca's and von Mieses' yield criteria. The concept of the yield criterion presented as a surface may be useful for the general understanding, but for solution of problems the graphical presentation in Section 7.2 is more powerful and illustrative.

The application of the yield criterion expressed analytically and graphically in this chapter should serve as a general basis for the yield-line theory.

8. SUMMARY

8.1. Outline of Investigation

The primary objective of this investigation was to establish a flexural yield criterion for reinforced concrete plates and to determine the conditions for which a yield criterion exists. The secondary objective was to obtain a better understanding of the behavior of reinforced concrete plates in the whole spectrum of response from initial loading to failure. These two objectives were closely interrelated.

The investigation was carried out by parallel theoretical and experimental studies. Tests of 22 specimens are described in this report. The test results are compared and discussed in the text, while a detailed description is given in Appendix A. The properties of the test specimens and results are summarized in Table 3.1 and Fig. 4.19 and 4.20. Three of the test specimens were subjected to isostatic moment, ten specimens were subjected to uniaxial moment, and nine specimens to pure torsion. The main variables in the test specimens were the direction and the distribution of the reinforcement. Seventeen specimens were isotropically reinforced and five specimens had nonisotropic reinforcement. The amount of reinforcement in each layer was 1.0, 0.5 or 0.25 percent, and the nonisotropy ratio μ was 0.5 or 0.25. The directions of the reinforcement were 0°, 22.5°, 45° or 67.5° with respect to the applied principal moment.

The analytical expressions for deformation and strength were derived on the basis of equilibrium and compatibility of a cracked section. The experimental and analytical results were in good agreement. The results indicated that the effect of the reorientation of inclined reforcing across cracks was negligible. The flexibility of a reinforced plate element was found to be more complex than conventionally assumed. The yield criterion was presented in a simple manner both analytically and graphically.

8.2. The Yield Criterion

A general application of the yield criterion requires ductility of the considered section beyond the deformations at yielding. The investigation showed that the general ductility requirement limited the amount of reinforcement in plate elements far below the amount which is conventionally considered to result in ductile behavior as implied by building codes. A simplified, approximate expression was derived for the balanced amount of reinforcement

$$A_s f_y = 0.125 \sigma_{ca} h \qquad (8.1)$$

The notation is given in Appendix C.

The analytical expression for the yield criterion was derived to be

$$\omega M_1 = M_2 = [M_x \sin^2(\beta + \gamma) + M_y \cos^2(\beta + \gamma)]/\cos^2\gamma \qquad (8.2)$$

where β is the angle between the directions of M_1 and M_x, and γ is determined by

$$-\tan^2\gamma - \omega c_1 \tan\gamma + \omega = 0$$

where

$$\omega c_1 = [(\nu - \omega)\ \mathrm{cotan}^2\beta + 1 - \nu\omega]/[(1 - \nu)\ \mathrm{cotan}\beta]$$

The coordinate system and the angles are shown in Fig. 6.1. A graphical presentation of the yield criterion stated by Eq. 8.2 is given in Fig. 7.1 through 7.4.

The yield criterion recognizes that twisting moments may exist along the yield line, which affects both the direction of the yield line and the moment capacity of the element.

The yield criterion is generally applicable to reinforced concrete members. It is in good agreement with the test results obtained in this investigation. Other reported test results for a plate subjected to axial forces and for a beam subjected to torsion were studied quantitatively. The results of this study demonstrated the wide applicability of the yield criterion given by Eq. 8.2, where the notation M may designate a general force such that M stands for moment in computations for slabs and beams and for axial force in computations for plates subjected to in-plane forces.

8.3. Reorientation of the Reinforcing Bars

No evidence was found of a significant effect with regard to the reorientation of reinforcing bars inclined to the cracks either from experimental results or analytical studies. No "stepwise" or "staircase" crack pattern was observed. Neither could a direct

observation of the reinforcing bars reveal any significant reorientation or "kinking."

8.4. Flexibility of Slab Elements

The test results showed that the flexibility of an isotropically reinforced concrete element is directly related to the direction of the reinforcement and the combination of the applied moments. The flexibility of an element may double or triple by rotating the reinforcement with respect to the direction of the applied moments. For the nonisotropically reinforced elements this phenomenon might be even more pronounced. The test results were in agreement with the analytical computations which were based on strain relations.

The investigation did not support the conventional plate theory which is based on linear elasticity and isotropy or simple anisotropy of the plate element. On the contrary, the basic assumptions in the conventional plate theory appear to have very little resemblance to the behavior of the reinforced concrete slab element. Therefore, no matter how intricate the method of solution, any approach based on conventional plate theory may not predict the moment distribution more accurately than a reasonably good estimate based on simple equilibrium considerations.

8.5. Yield Moment

The investigation brought out clearly that the stress conditions at the yield line can be understood only if the general strain pattern is known. For example, the reinforcement in the concrete

compression zone at a yield line may be yielding in tension.

Whether a cross section was underreinforced was found to be not only dependent on the geometric and material properties of the section but also on the combination of the applied loads. A section which appeared to be extremely ductile under one load combination could show the characteristic load-deformation curve of an over-reinforced element under another load combination.

8.6. Orientation of Yield Lines

The orientation of the yield lines in an isotropically reinforced element was always perpendicular to the applied principal moment.

For nonisotropically reinforced element the orientation of the yield line was governed by the "principle of the least resistance." For all five nonisotropically reinforced test specimens the rotation of the yield line could be predicted by the principle of the least resistance described in Chapter 6.

8.7. Proportional and Nonproportional Loading

All test specimens were subjected to proportional loading. However, it can be concluded from the test observations that the final deformations could have been entirely different for nonproportional loading. An illustrative example is given in Chapter 4.

REFERENCES

1. Aa. Ingerslev, "Om en elementär Beregningsmaade av krydsarmerede Plader," Ingeniøren 27, Aug. 1921, pp. 507.

2. K. W. Johansen, "Yield Line Theory," Cement and Concrete Association, (London), 1962, 181 pp.

3. W. Prager, "An Introduction to Plasticity," Addison-Wesley Publishing Co., Reading, U.S.A., pp. 57-68.

4. A. Hillerborg, "Strimlemetoden foer Platton paa Pelare, Vinkelplattor, m.m.," Svenska Riksbyggen, 1959.

5. M. P. Nielsen, "Exact Solutions in the Plastic Plate Theory," Bygningsstatiske Meddelelsen, Vol. 34, Copenhagen, 1963, 28 pp.

6. R. H. Wood, "Plastic and Elastic Design of Slabs and Plates," The Ronald Press Co., New York, 1961. 344 pp., pp. 12-14.

7. M. W. Kwiecinski, "Yield Criterion for Initially Isotropic Reinforced Slab," Magazine of Concrete Research, Vol. 17, No. 51, June 1965, pp. 97-100.

8. M. W. Kwiecinski, "Yield Condition for Orthotropically Reinforced Slab," University of Wales, Swansea, 1965, Research Report No. CR 1965.

9. C. Bach and O. Graf, "Deutscher Ausschuss fur Eisenbeton," Vol. 30, 1915. 309 pp.

10. M. P. Nielsen, "Vridningsgforsøg med Jernbetonplader," Academy of Engineering, Copenhagen, 1965. 157 pp.

11. R. Baus and S. Tolaccia, "Calcul à la Rupture des Dalles en Beton Armé et Etude Experimental du Critère de Rupture en Flexion Pure," Annales de l'Institute Technique du Batiment et des Travaux Publics No. 189, Sept. 1963. pp. 871-894.

12. M. W. Kwiecinski, "Some Tests on the Yield Criterion for a Reinforced Concrete Slab," Magazine of Concrete Research: Vol. 17, No. 52, Sept. 1965. pp. 135-138.

13. J. H. Houbolt, "The Effectiveness of Various Arrangements of Reinforcement in Concrete Slabs," M.S. Thesis in Civil Engineering at University of Illinois, 1942. 57 pp.

14. D. G. Silverj, "Contriuto Teorico Sperimentale al Calcolo a Rottura Delte Piastre in Cemento Armato," Universita Degli Studi di Roma, Istituto di Scienza Delle Construzioni, Pubblicazione No. 11-44, 1965. 28 pp.

15. J. Peter, "Zur Bewehrung von Scheiben und Schalen für Hauptspannungen Schiefwinklig zur Bewehrungsrichtung," Dr.Ing. Thesis at Technishe Hochschule Stuttgart, 1964. 181 pp.

16. M. P. Nielsen, "Plasticitetsteorien for Jernbetonplader," Academy of Engineering, Copenhagen, 1962. 173 pp.

17. R. H. Wood, "Plastic Design of Slabs Using Equilibrium Methods," Proc. of the International Symposium, FLA./Nov. 10-12, 1964. pp. 319-336.

18. H. Nylander, "Knutkrafter vid brottlinjeteorien," Nordisk Betong 7, 1963, No. 1. pp. 45-48.

19. R. H. Wood, "Recent Advances in Nodal-Force Theory for Slabs and the Use of the Theory With Electronic Computers," Comité-Européen du Beton 10e Session Pleniere Dalles, Structures Planes London, Oct. 1966. pp. 6.

20. "ACI Standard Building Code Requirements for Reinforced Concrete," (ACI 318-63) American Concrete Institute, June 1963. pp. 318-51.

21. T. Warwaruk, M. A. Sozen and C. P. Siess, "Strength and Behavior in Flexure of Prestressed Concrete Beams," University of Illinois Engineering Experiment Station Bulletin No. 464, pp. 85.

22. T. T. C. Hsu, "Torsion of Structural Concrete - Behavior of Reinforced Concrete Rectangular Members," Unpublished report from Portland Cement Association, Illinois, Feb. 1966. pp. 12.

23. B. Hallert, "Photogrammetry," McGraw-Hill Series, New York, 1950. pp. 79-95.

TABLE 2.1

TESTS UNDER PURE TORSION (NIELSEN)
Properties of Specimens and Test Results

Specimen	Reinforcement in the x-direction top and bottom	Reinforcement in the y-direction top and bottom	$F_{jx}^{ou}\sigma_F$ kg	μ	σ_c kg/cm^2	V_F Calculated kg	V_F Measured kg	V_F Measured / Calculated
1	R7 per 10	R7 per 10	105	1	335	1200	1280	1.07
2	R7 per 10	R7 per 10	136	1	325	1520	1450	0.95
3	R10 per 10	R5 per 10	235	0.24	315	1280	1310	1.02
4	R8 per 10	R5 per 10	239	0.24	308	1290	1280	0.99
5	R8 per 10	R7 per 10	162	0.75	240	1520	1580	1.04
6	R8 per 10	R7 per 10	166	0.73	282	1550	1580	1.02
7	R8 per 10	R6 per 10	189	0.59	323	1610	1630	1.01
8	R8 per 10	R6 per 10	187	0.60	310	1590	1630	1.03

R7 per 10 denotes "round steel" with diameter 7 mm spaced 10 cm.

F_{jx}^{ou} = area per cm of the reinforcement in the x-direction equal in top and bottom

σ_F = yield stress in reinforcement

σ_c = compressive strength of concrete

$\mu = F_{jy}/F_{jx}$

$V_F \approx \sqrt{\mu}\, M_F$, where M_F is the yield moment referring to the reinforcement F_j

TABLE 2.2

TESTS UNDER UNIAXIAL BENDING (HOUBOLT)
Properties of Specimens and Test Results

Mark	Concrete Strength f'_c psi (kg/cm^2)	Orientation and Spacing of Reinforcement				Unit Ultimate Moment		
		α_1 deg.	s_1 in. (cm)	α_2 deg.	s_2 in. (cm)	Calculated kip (t)	Measured kip (t)	Measured / Calculated
H1	5130 (361)	0	3 (7.6)	90	6 (15.2)	8.3 (3.8)	8.6 (3.9)	1.04
H2	4910 (345)	45	3 (7.6)	45	3 (7.6)	7.9 (3.6)	8.0 (3.6)	1.01
H3	3800 (367)	30	3 (7.6)	30	3 (7.6)	11.5 (5.2)	11.3 (5.1)	0.98
H4	3980 (280)	60	3 (7.6)	60	3 (7.6)	4.0 (1.8)	4.2 (1.9)	1.05
H5	4020 (283)	30	3 (7.6)	60	3 (7.6)	8.0 (3.6)	8.6 (3.9)	1.07
H6	3830 (269)	0	3 (7.6)	45	3 (7.6)	11.6 (5.3)	11.4 (5.2)	0.98
H7	3780 (266)	45	3 (7.6)	90	6 (15.2)	4.2 (1.9)	3.8 (1.7)	0.91
H8	3760 (264)	0	3 (7.6)	90	6 (15.2)	8.2 (3.7)	8.8 (4.0)	1.07
H9	3820 (269)	45	3 (7.6)	45	6 (15.2)	6.1 (2.8)	6.3 (2.9)	1.03

TABLE 2.2 (Continued)

TESTS UNDER UNIAXIAL BENDING (HOUBOLT)
Properties of Specimens and Test Results

Mark	Concrete Strength f'_c psi (kg/cm^2)	Orientation and Spacing of Reinforcement				Unit Ultimate Moment		
		α_1 deg.	s_1 in. (cm)	α_2 deg.	s_2 in. (cm)	Calculated kip (t)	Measured kip (t)	Measured / Calculated
H10	3450 (243)	30	3 (7.6)	30	6 (15.2)	8.9 (4.0)	9.1 (4.1)	1.02
H11	4210 (296)	60	3 (7.6)	60	6 (15.2)	3.1 (1.4)	3.1 (1.4)	1.00
H12	4040 (284)	60	3 (7.6)	30	6 (15.2)	5.0 (2.3)	5.0 (2.3)	1.00
H13	3880 (273)	30	3 (7.6)	60	6 (15.2)	7.1 (3.2)	7.3 (3.3)	1.03
H14	3540 (214)	45	3 (7.6)	0	6 (15.2)	7.8 (3.5)	8.3 (3.8)	1.06
H15	4380 (308)	45	6 (15.2)	90	6 (15.2)	2.1 (1.0)	2.0 (0.9)	0.96

d_1 = 4.67 in. (11.8cm), d_2 = 4.3 in. (10.9cm)

TABLE 2.3

TESTS UNDER UNIAXIAL TENSION (PETER)

Properties of Specimen and Test Results

Mark	Orientation, Diameter and Spacing of the Reinforcement						Calculated -10% for "size effect"	Tensile Force Measured	Measured / Calculated
	α_1 deg	D_1 mm	S_1 cm	α_2 deg	D_2 mm	S_1 cm	t	t	
S2r0	0	8	10	90	8	10	40.0	40.0	1.00
S2r10	10	8	10	80	8	10	34.7	35.1	1.01
S2r10W	10	8	10	80	8	10	45.0	44.1	0.98
S2r20	20	8	10	70	8	10	42.2	39.4	0.93
S2r20W	20	8	10	70	8	10	43.9	43.3	0.99
S2r30	30	8	10	60	8	10	38.0	38.8	1.02
S2r40	40	8	10	50	8	10	37.7	40.8	1.08

W denotes a duplicated test.

TABLE 3.1

PROPERTIES OF SPECIMENS AND TEST RESULTS

Mark	Concrete Strength 6x12 in. cylinder	Yield Stress of Reinforcement	Thickness	Direction and Spacing of Reinforcement: α_1	$\frac{s_1}{s_1}$ (top / bottom)	α_2	$\frac{s_2}{s_2}$	Measured: Yield Moment	Yield Curvature	Ultimate Moment	Ultimate Curvature	Orientation of Yield Line	Computed: Yield Moment	Yield Curvature	Ult. Moment	Orientation of Yield Line	Measured / Computed: Yield Moment	Measured / Computed: Ult. Moment	Load: B = Biaxial Mom., U = Uniaxial Mom., T = Torsion	Comments
	psi	psi	in.	deg.	in.	deg.	in.	k-in./in.	10^{-5} in.	k-in./in.	10^{-5} in.	deg.	k-in./in.	10^{-5} in.	k-in./in.	deg.				
C1	6610	50,000	4.12	0	1.50 / --	90	1.375 / --	5.60	80	5.75	350	0 / 90	5.39 / 5.43	67 / 73	5.69 / 5.73	Any	1.03	1.01	B	
C2	4580	50,000	4.12	0	1.50 / --	90	1.375 / --	5.60	80	6.10*	800	0 / 90	5.35 / 5.38	69 / 76	5.63 / 5.66	"	1.04	1.08*	B	*Strain hardening
C3	2700	50,000	4.12	0	1.50 / --	90	1.375 / --	5.50	75	5.80	300	0 / 90	5.28 / 5.31	72 / 80	5.50 / 5.50	"	1.04	1.05	B	
B4	4740	50,000	4.15	0	1.50 / --	90	1.375 / --	5.60	75	5.85	500	90	5.39	68	5.68	90	1.04	1.03	U	
B5	4850	50,000	4.12	-45	1.50 / --	45	1.375 / --	5.32	131	(5.32)	(131)	90	5.54	134	5.65	90	0.96*	-*	U	*Bond failure
B6	4890	50,000	4.12	67.5	1.50 / --	-22.5	1.375 / --	5.20 (5.40)	100 / 160	5.57	245	90	4.81 / 5.75	84 / 63	5.73	90	1.04	0.97*	U	*Partial bond failure
B7	5150	50,000	4.14	-45	1.50 / --	45	1.375 / --	5.60	140	5.85	600	90	5.62	170	5.76	90	1.00	1.02	U	
B8	3700	50,000	4.18	-22.5	1.50 / --	67.5	1.375 / --	5.00	90	6.08	650	90	4.76	79	5.75	90	1.05	1.08*	U	*Strain hardening
B9	3820	50,000	4.23	-45	3.00 / --	45	1.375 / --	3.90	140	4.45*	800	73	3.90	120	4.00	71.6	1.00	1.11*	U	*Strain hardening
B10	4920	50,000	4.14	90	1.50 / --	0	1.375 / --	5.55	90	6.10	760	90	5.48	78	5.77	90	1.01	1.06*	U	*Strain hardening
B11	4800	50,000	4.12	-22.5	1.50 / --	67.5	2.75 / --	4.50	100	5.35	650	-71	4.65	83	5.08	-72.9	0.97	1.05	U	
B12	5170	47,600	4.12	-22.5	3.00 / --	67.5	1.375 / --	2.80	72	3.82	790	80	2.80	65	3.75	79.2	1.00	1.02	U	
B13	4240	47,900	4.01	90	1.50 / 1.375	0	1.375 / 1.50	5.20	80	5.96*	1444	90	4.93	74	5.42	90	1.05	1.10*	U	*Strain hardening
B14	6040*	47,900	4.09	90	1.50 / 1.375	0	1.375 / 1.50	No definite yield point		**	325	45	--	--	(5.80)	45	--	--	T	**Bond failure *10 days strength
B15	5260	47,900	4.09	-45	1.50 / 1.375	45	1.375 / 1.50	5.20	76	(5.33)	242	45	4.95	74	5.78	45	1.05	--	T	(Bond failure)
B16	4730	48,300	4.04	90	1.375 / 1.375	0	1.50 / 1.50	No definite yield point		5.43	269	45	--	--	5.58	45	--	0.97	T	
B17	5530	50,800	4.03	-22.5	1.50 / 1.50	67.5	1.375 / 1.375	No definite yield point		5.88	412	45	5.51	102	5.98	45	--	0.98	T	
B18	5040	56,100	4.08	-45	1.50 / 1.50	45	1.375 / 1.375	5.90	75	6.61	360	45	6.06	77	6.41	45	0.97	1.03	T	
B19	5345	53,100	4.06	-45	3.00 / 3.00	45	2.75 / 2.75	2.80	65	3.35	797	45	2.87	55	3.23	45	0.98	1.04	T	
B20	5490	51,750	4.04	90	3.00 / 3.00	0	2.75 / 2.75	3.02	139	3.42	333	45	2.96	115	3.34	45	1.02	1.05	T	
B21	5180	47,800	4.03	90	1.50 / 1.50	0	5.50 / 5.50	2.88	165	3.00	430	28	2.80	170	3.00	26.5	1.03	1.00	T	
B22	5460	53,750	4.06	90	1.50 / 1.50	0	5.50 / 5.50	3.39	195	3.51	292	29	3.30	195	3.40	26.5	1.03	1.03	T	

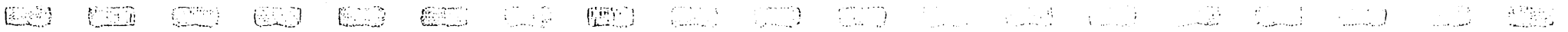

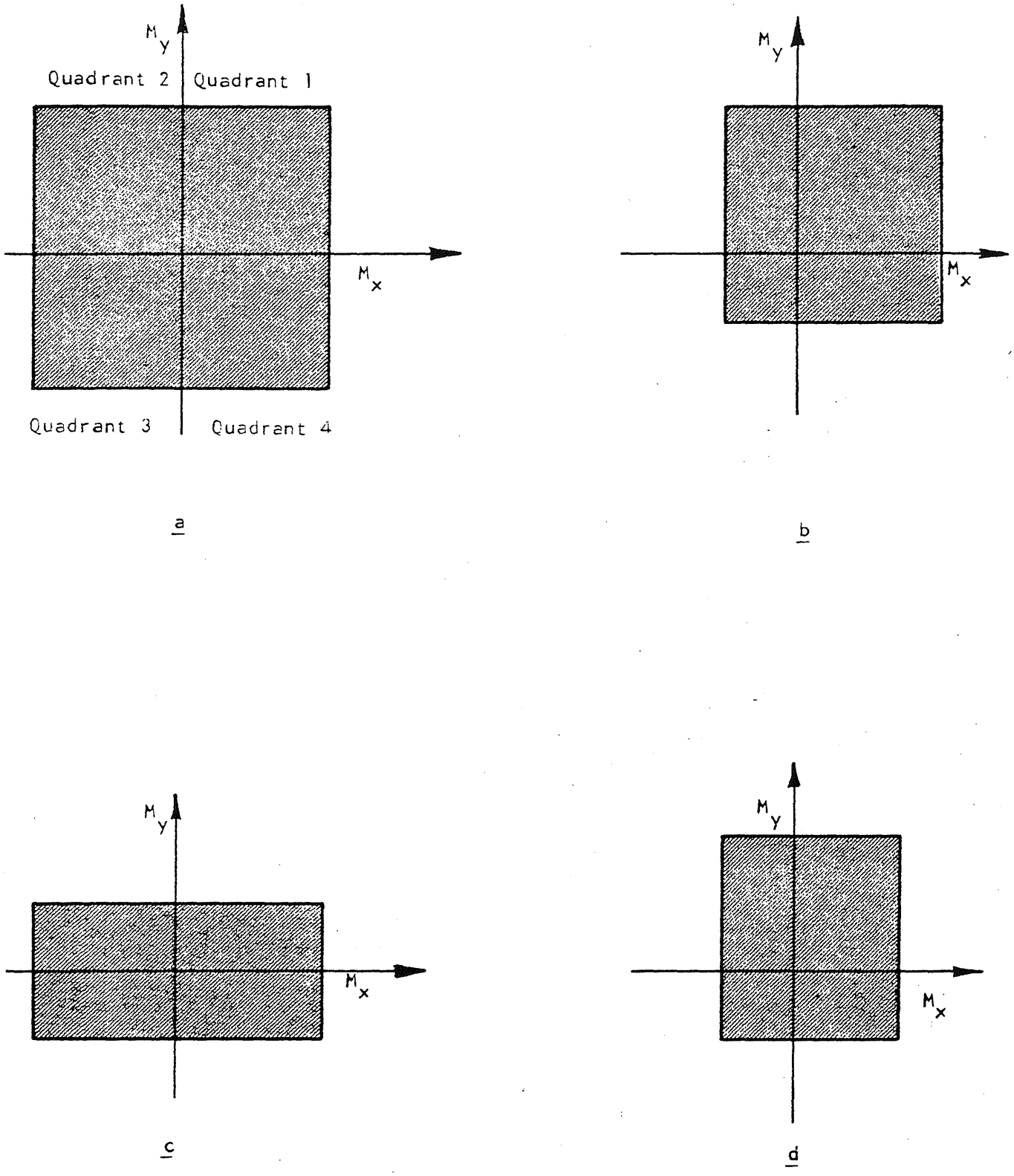

FIG. 2.1 YIELD CRITERIA (JOHANSEN)

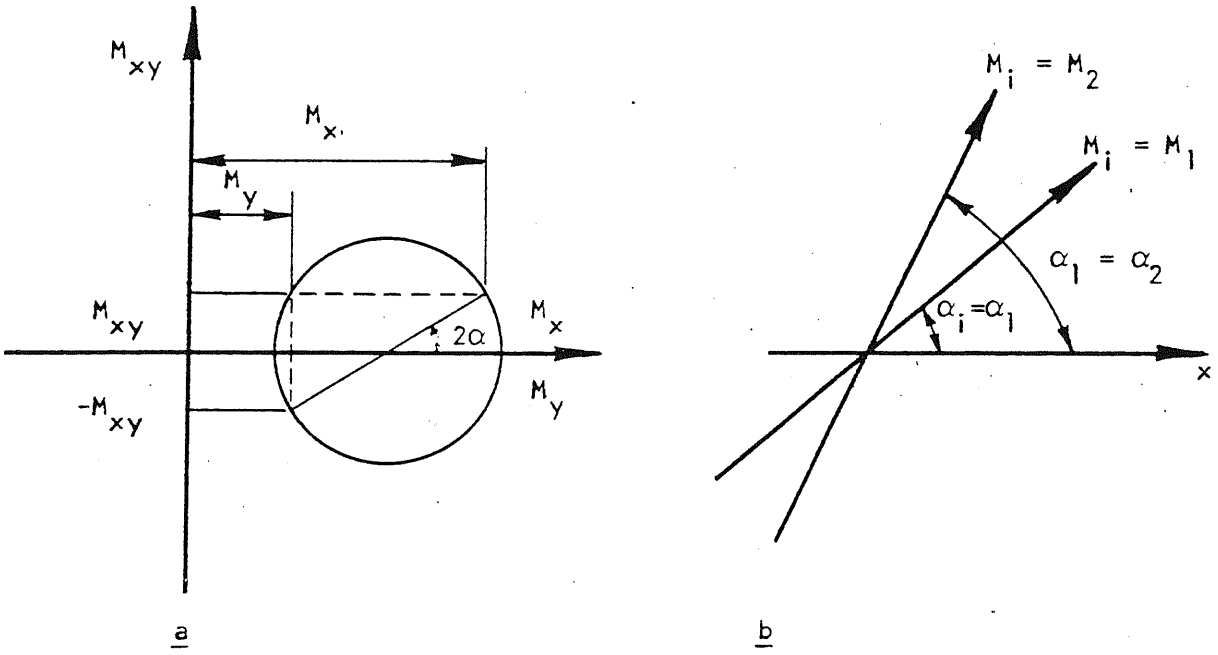

FIG. 2.2 MOHR'S CIRCLE FOR MOMENTS

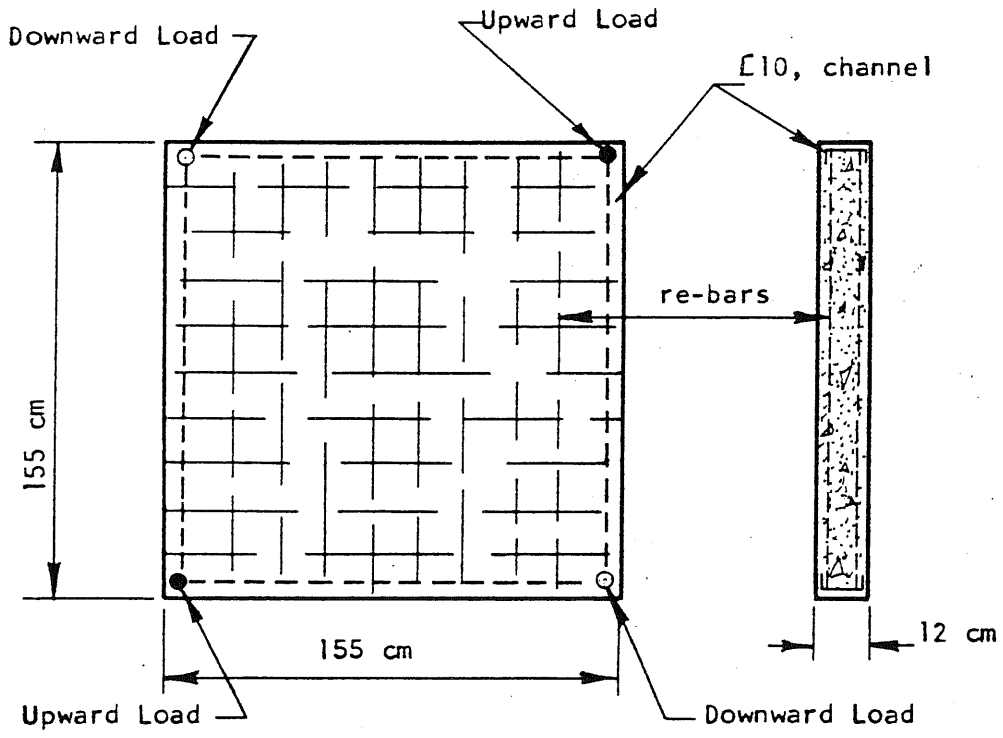

FIG. 2.3 TEST SPECIMEN FOR TORSION (NIELSEN)

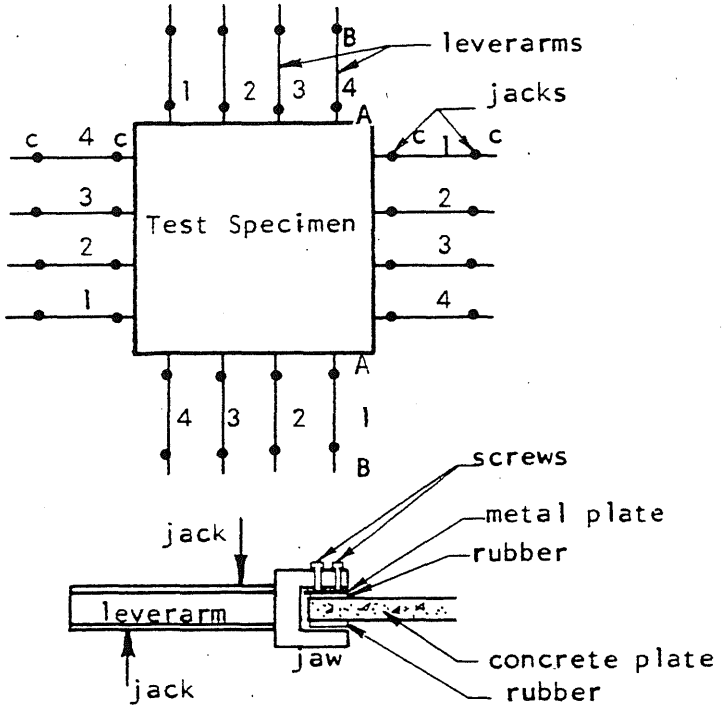

FIG. 2.4 LOADING SYSTEM (LIÉGE)

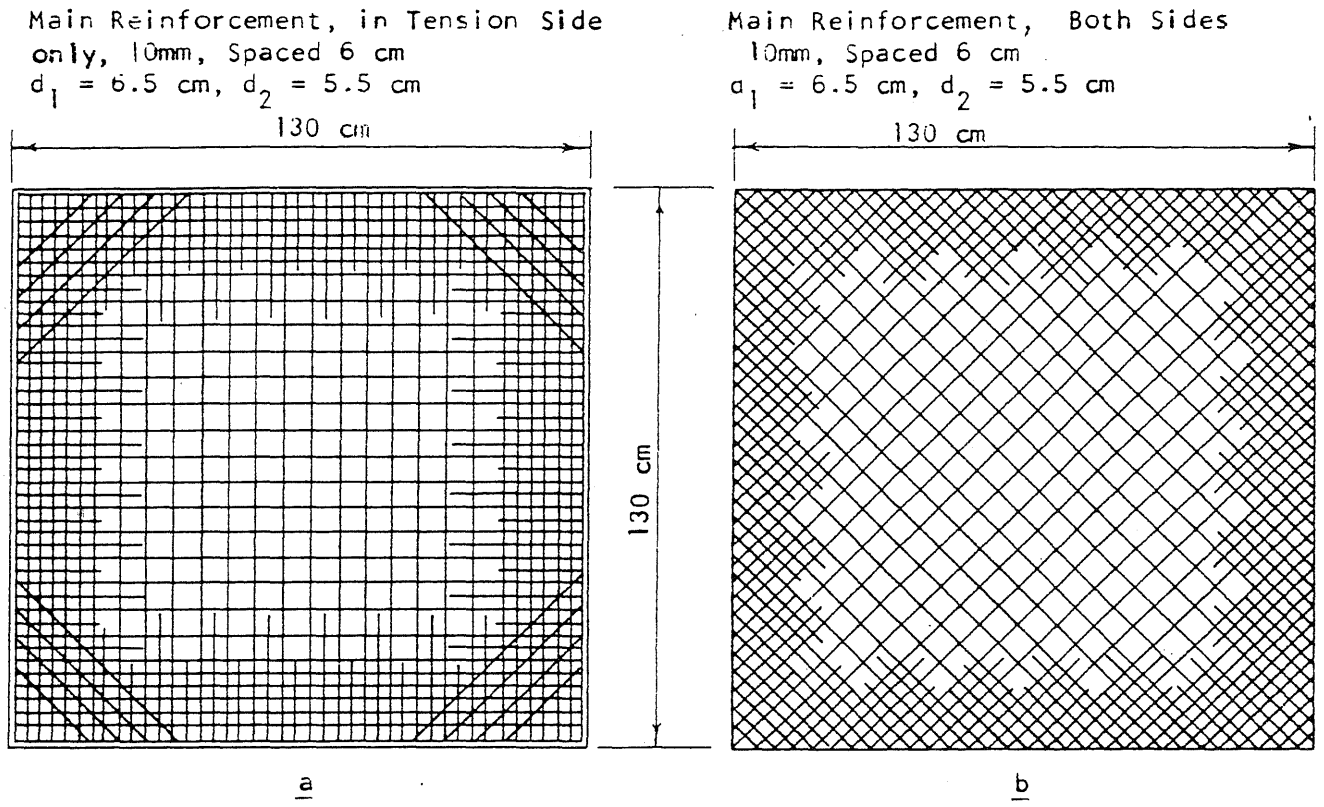

FIG. 2.5 REINFORCEMENT (LIÉGE)

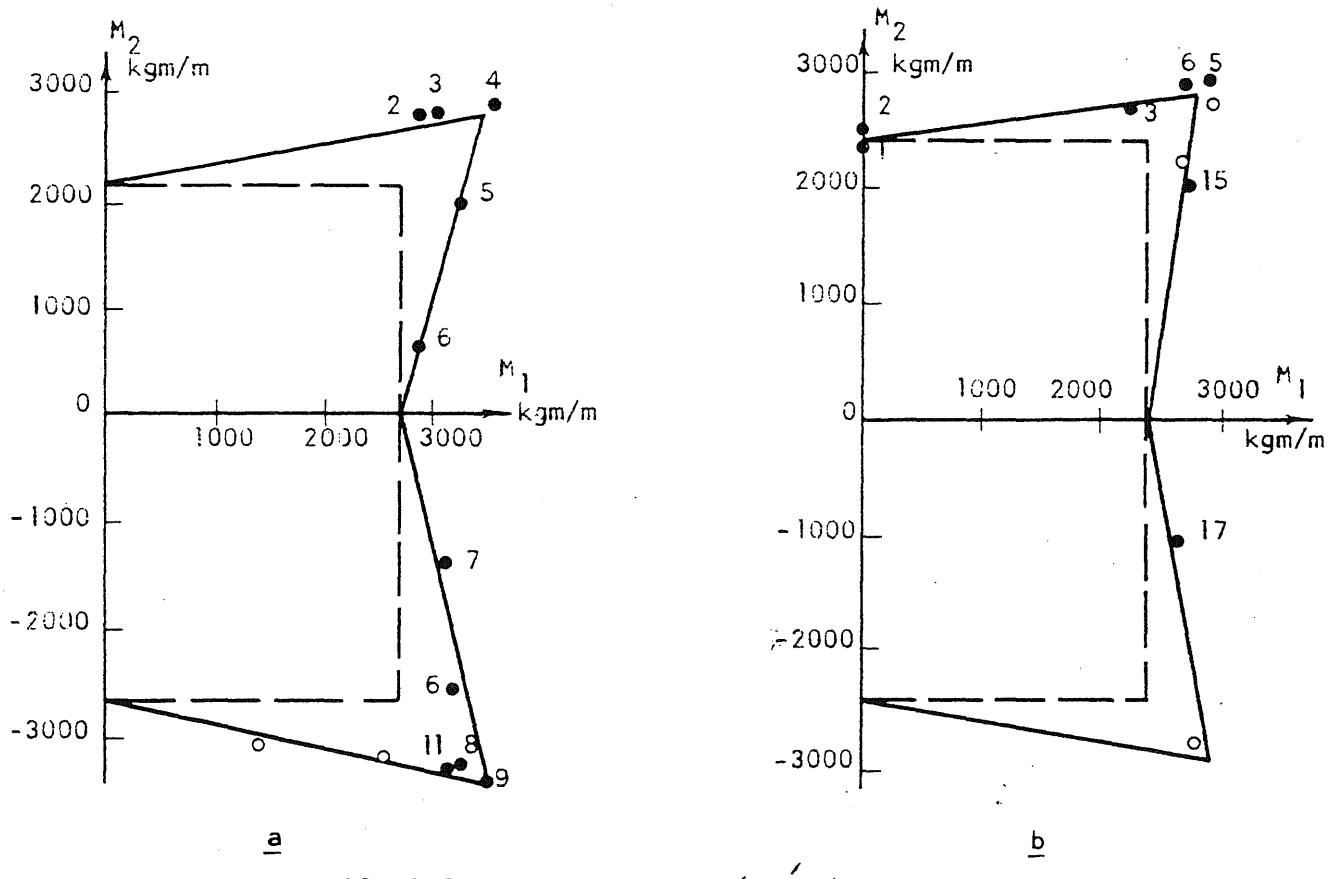

FIG. 2.6 YIELD CRITERIA (LIÉGE)

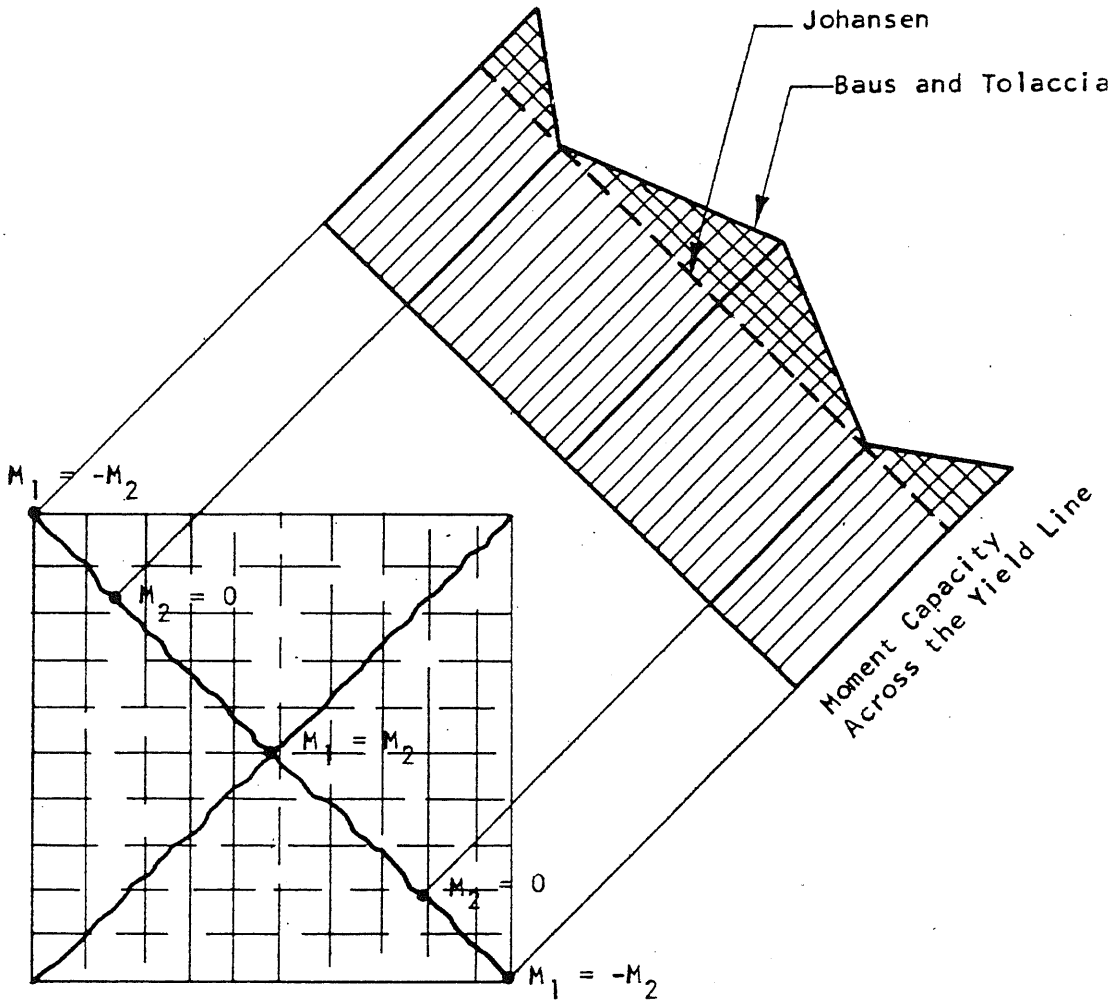

FIG. 2.7 APPLICATION OF YIELD CRITERIA

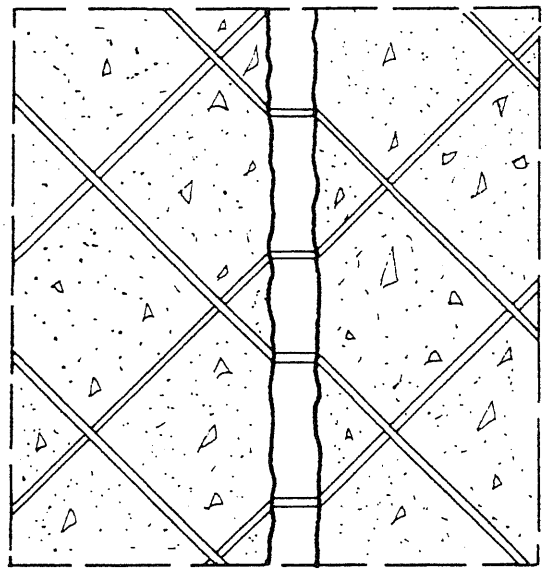

FIG. 2.8 "KINKING" OF THE REINFORCEMENT

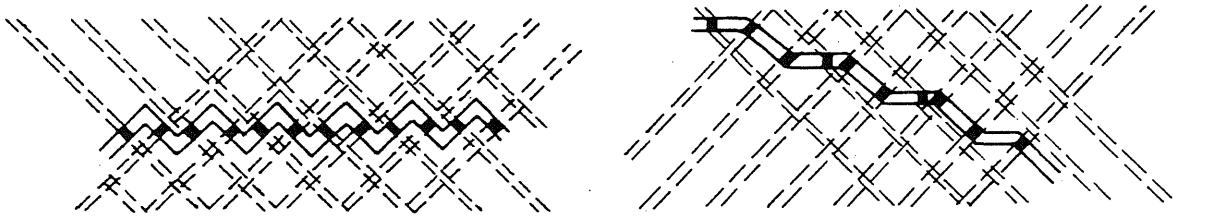

Uniaxial Moment

a

Equal Moments in All Planar Directions

b

FIG. 2.9 "PERPENDICULAR PLASTIFICATION" OF THE REINFORCEMENT AS PRESENTED BY BAUS AND TOLACCIA

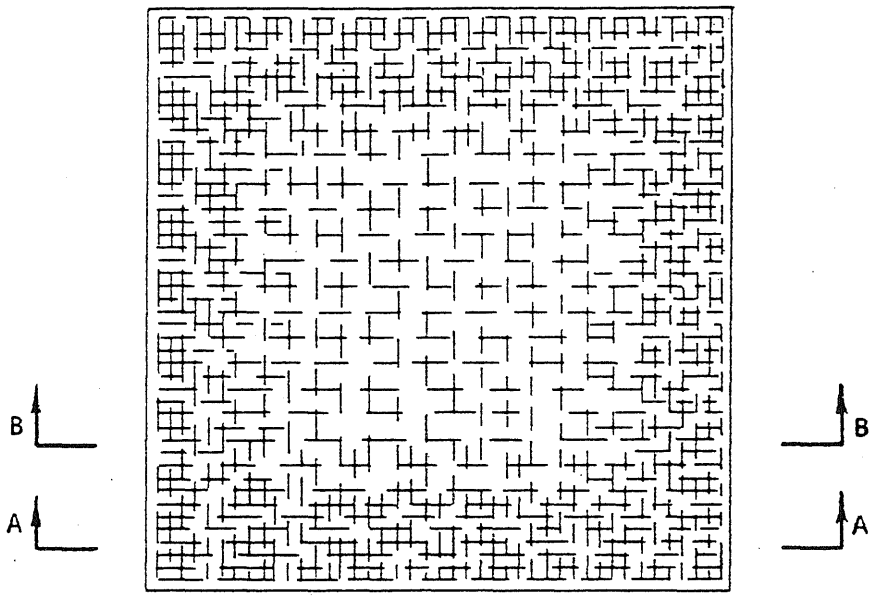

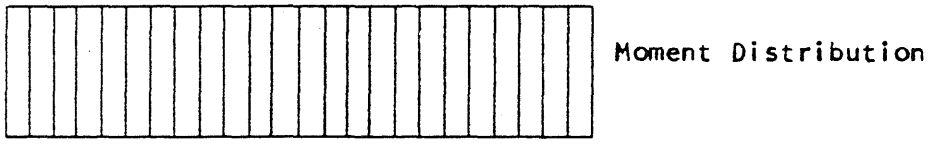

Section A-A

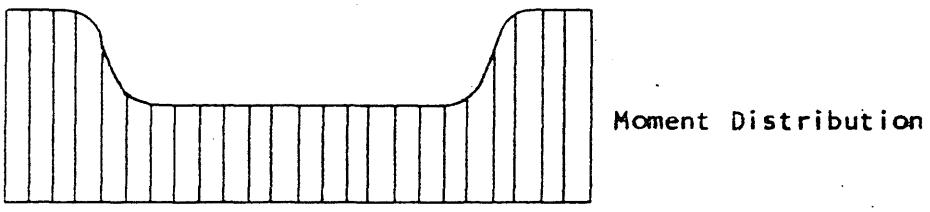

Section B-B

FIG. 2.10 DISTRIBUTION OF ULTIMATE MOMENT IN TEST SPECIMENS AT THE UNIVERSITY OF LIEGE

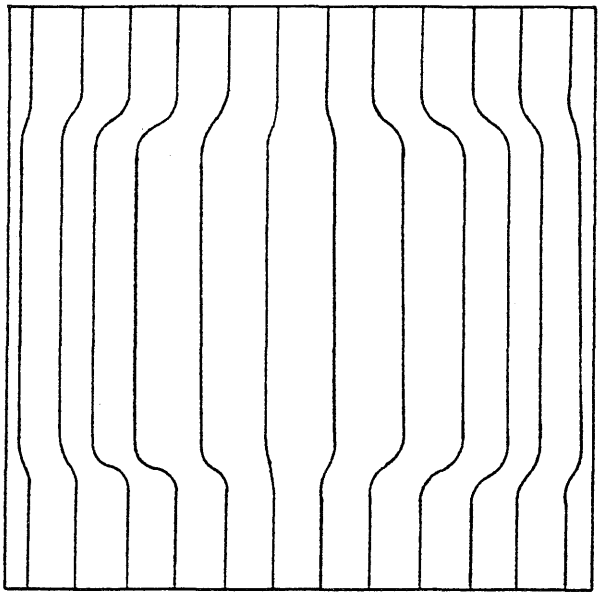

Trajectories for Tensile Forces in The Reinforcement

a

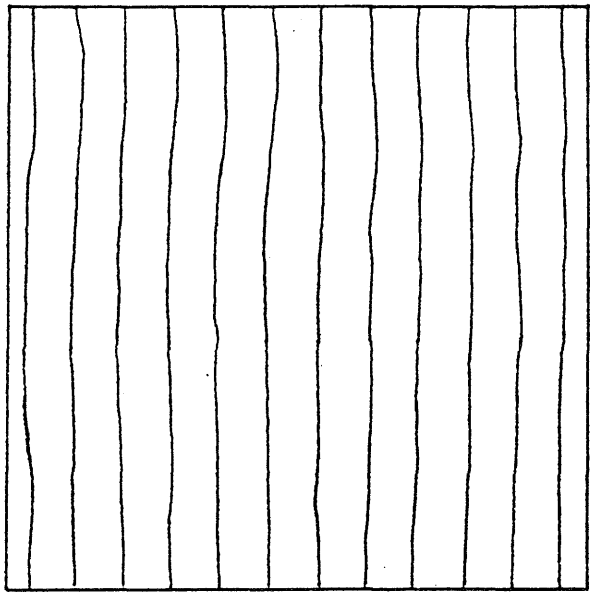

Trajectories For Principal Compressive Forces in Concrete

b

FIG. 2.11 STRESS TRAJECTORIES FOR UNIAXIAL MOMENT (LIÉGE)

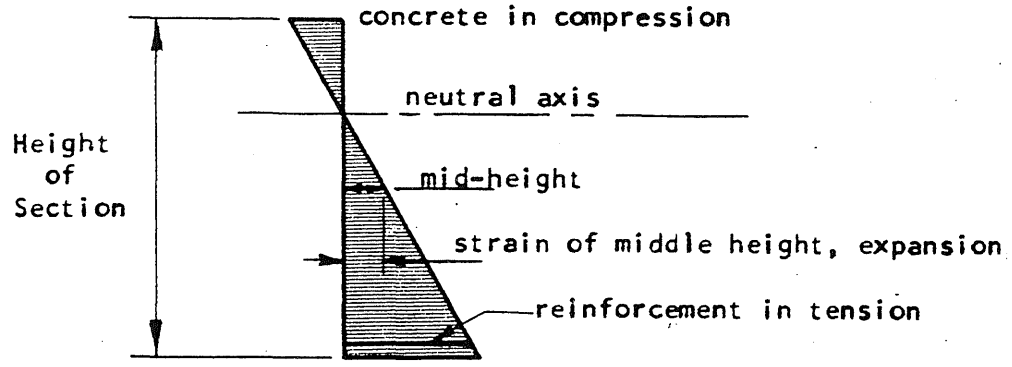

FIG. 2.12 STRAIN IN AN UNDERREINFORCED SECTION

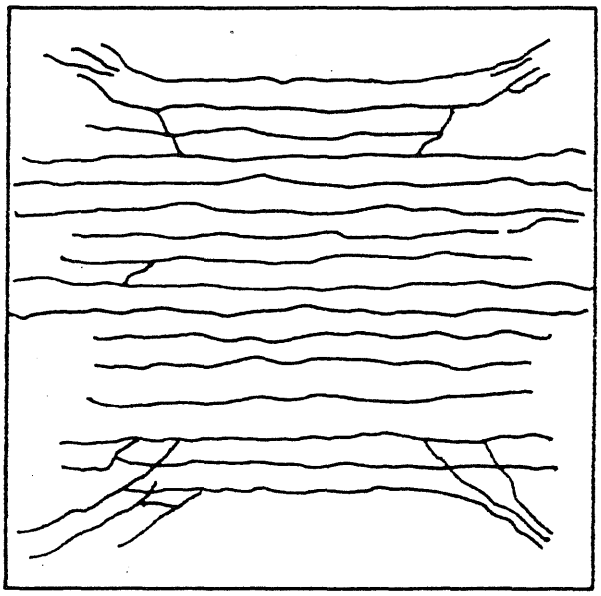

FIG. 2.13 CRACK FORMATION UNDER UNIAXIAL BENDING (LIÉGE)

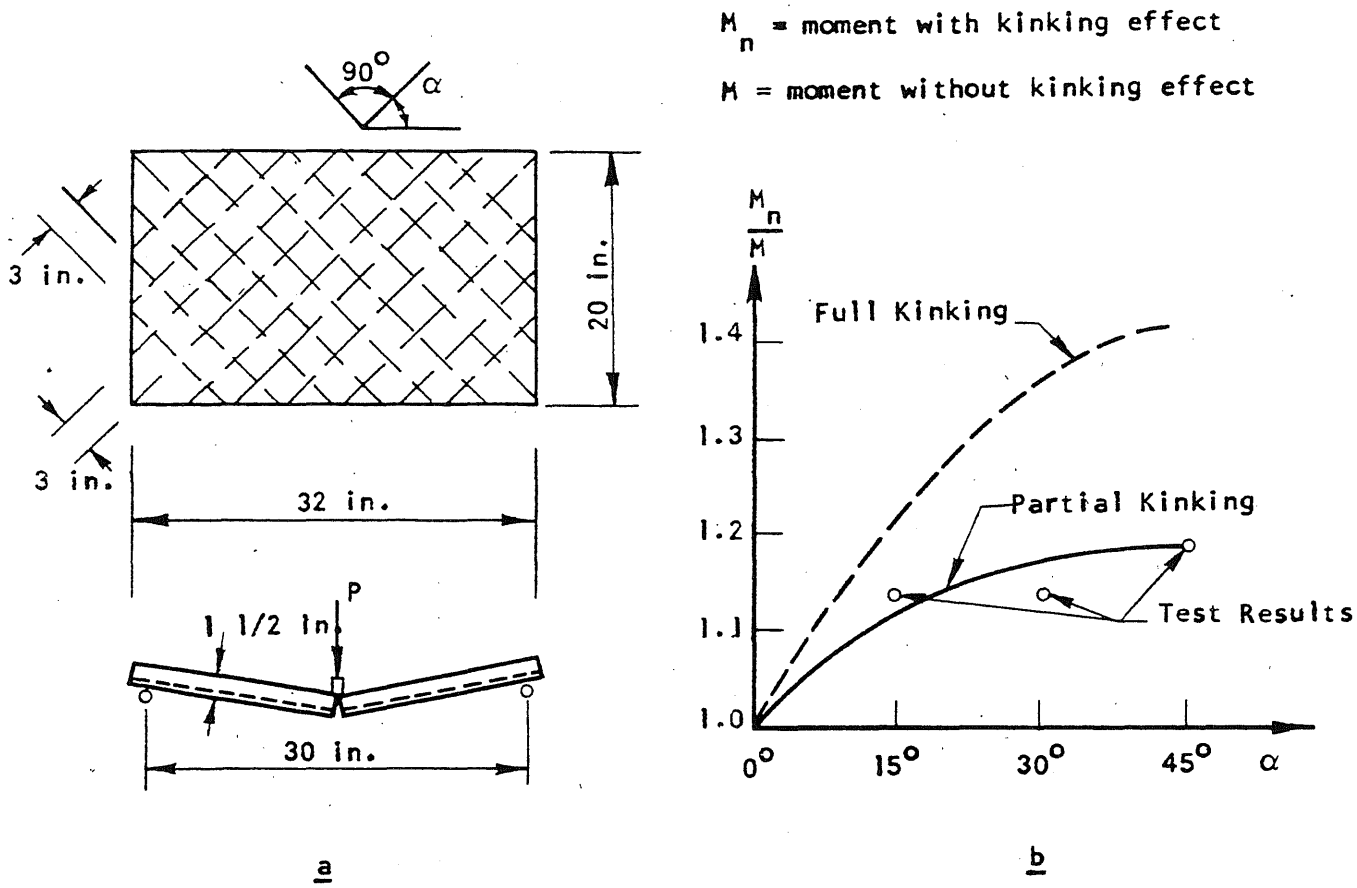

FIG. 2.14 TEST SPECIMEN AND RESULTS (KWIECINSKI)

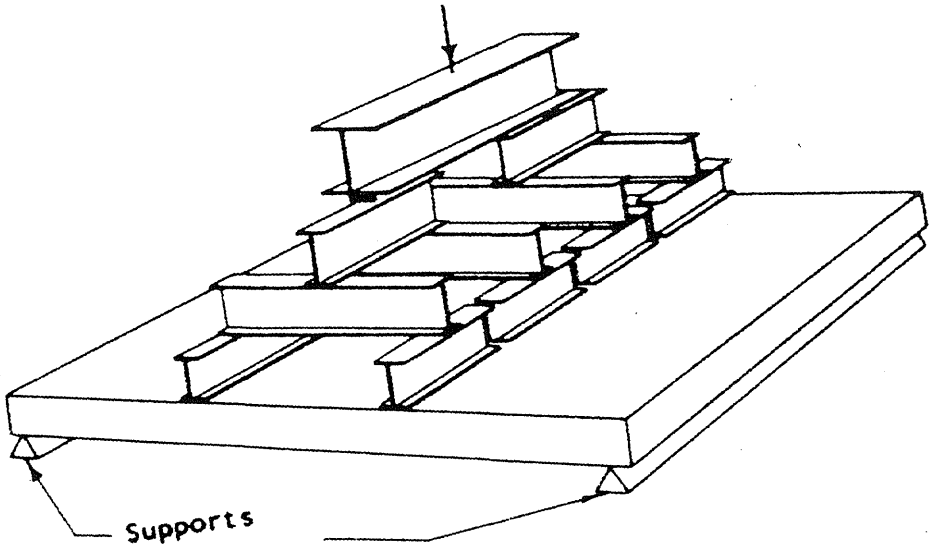

FIG. 2.15 TEST SETUP USED BY HOUBOLT

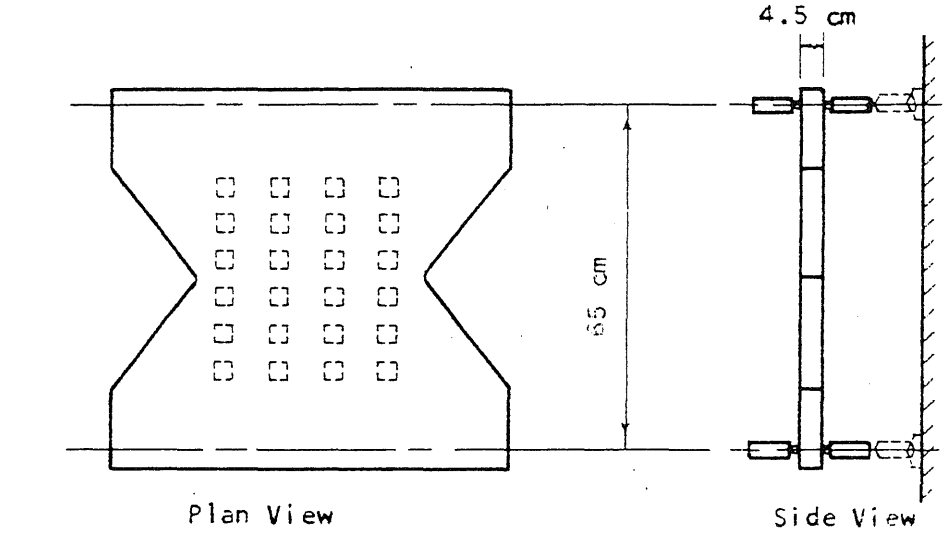

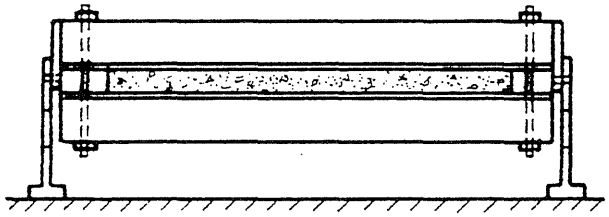

FIG. 2.16 TEST SETUP USED BY SILVERJ

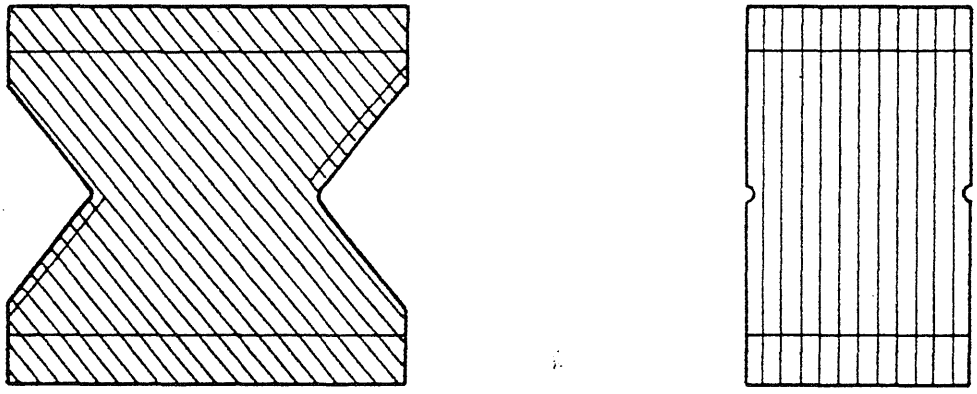

FIG. 2.17 TEST SPECIMENS (SILVERJ)

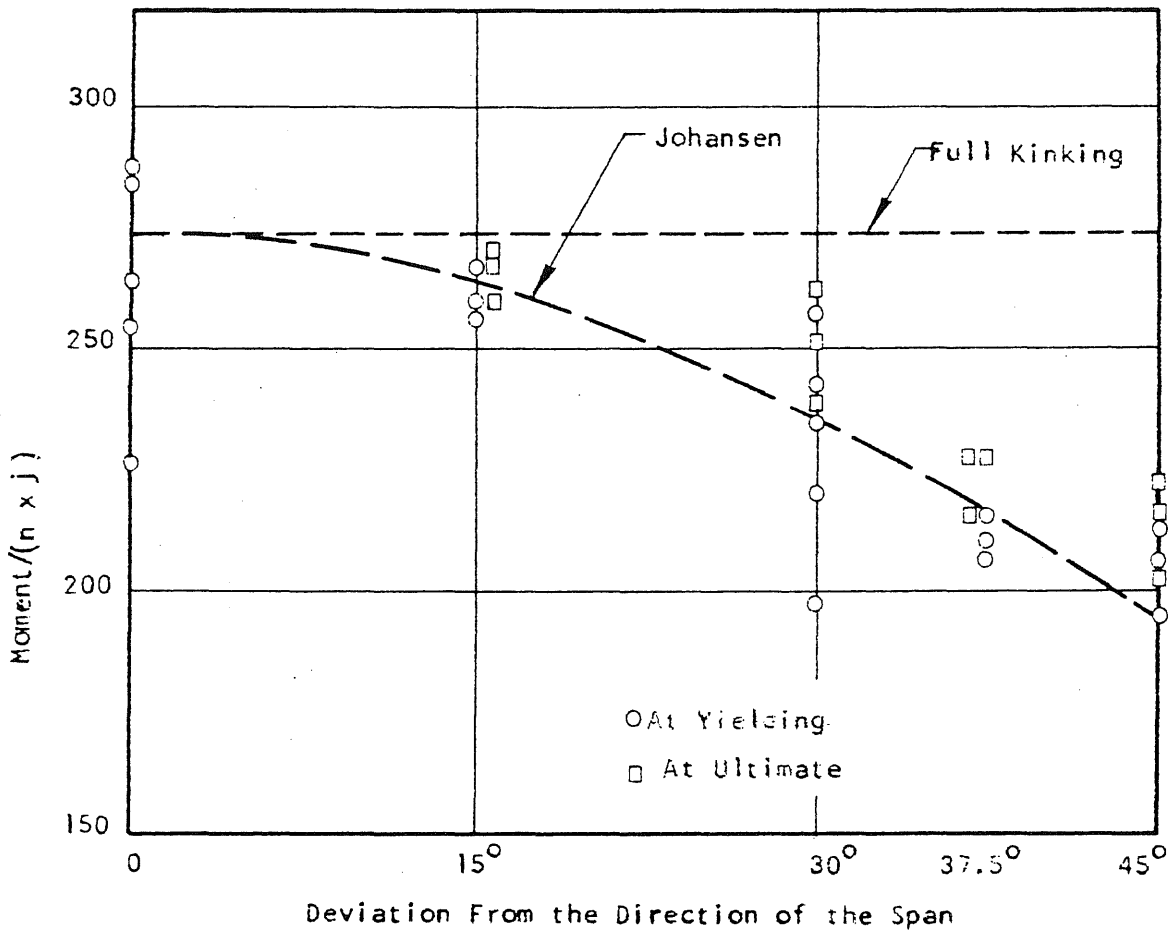

FIG. 2.18 TEST RESULTS (SILVERJ)

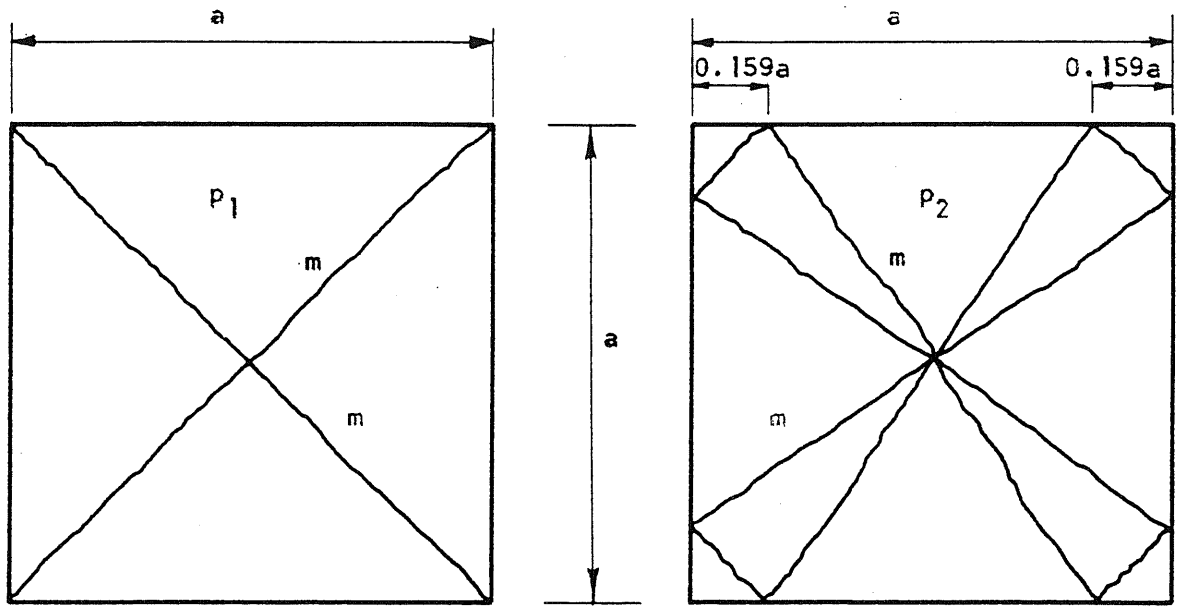

$$p_1 = 24 \frac{m}{a^2}$$

"Exact" solution

a

$$p_2 = 22 \frac{m}{a^2}$$

Nylander's solution

b

FIG. 2.19 SOLUTIONS FOR THE LOAD CARRYING CAPACITY

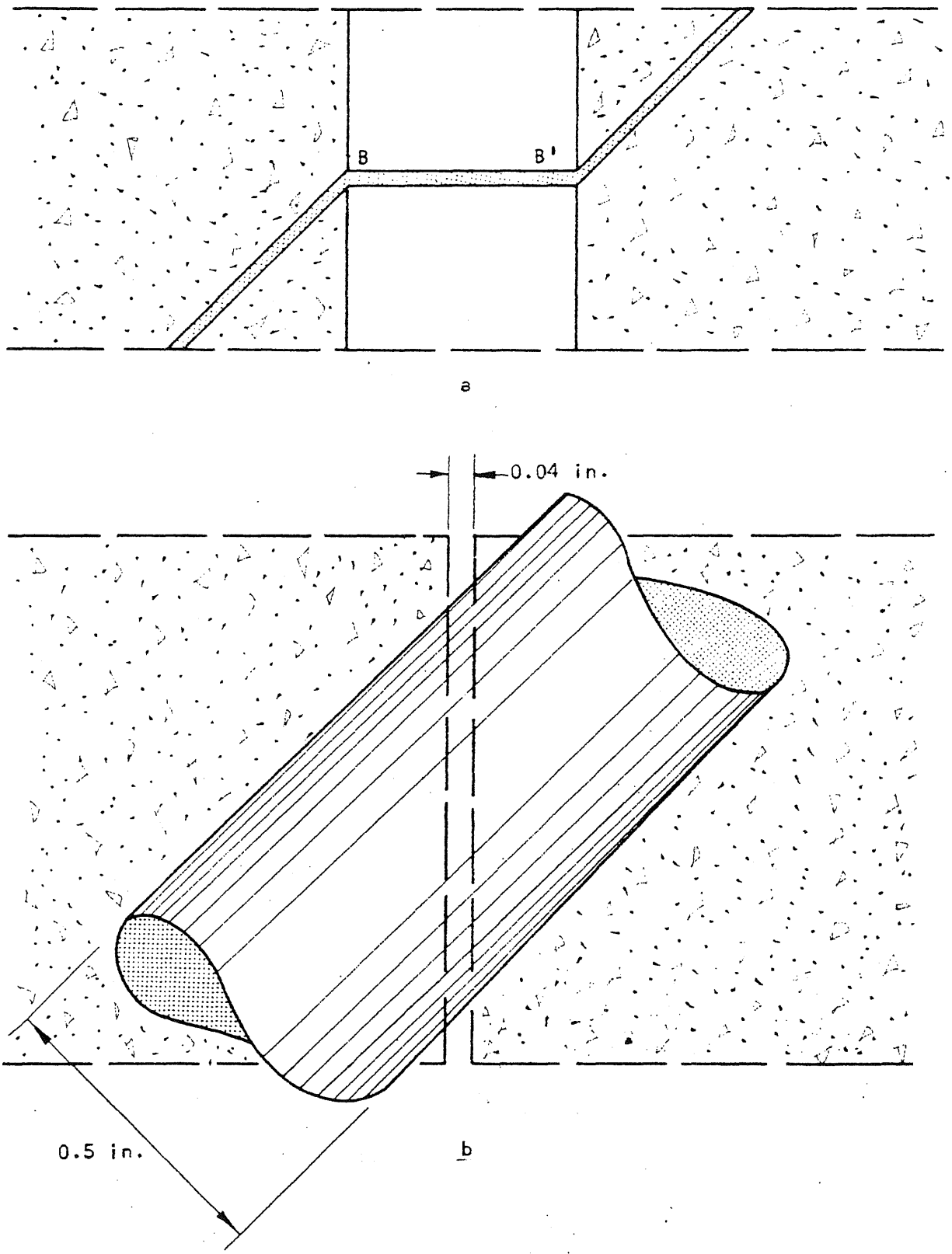

FIG. 3.1 REORIENTATION OF THE REINFORCING BAR

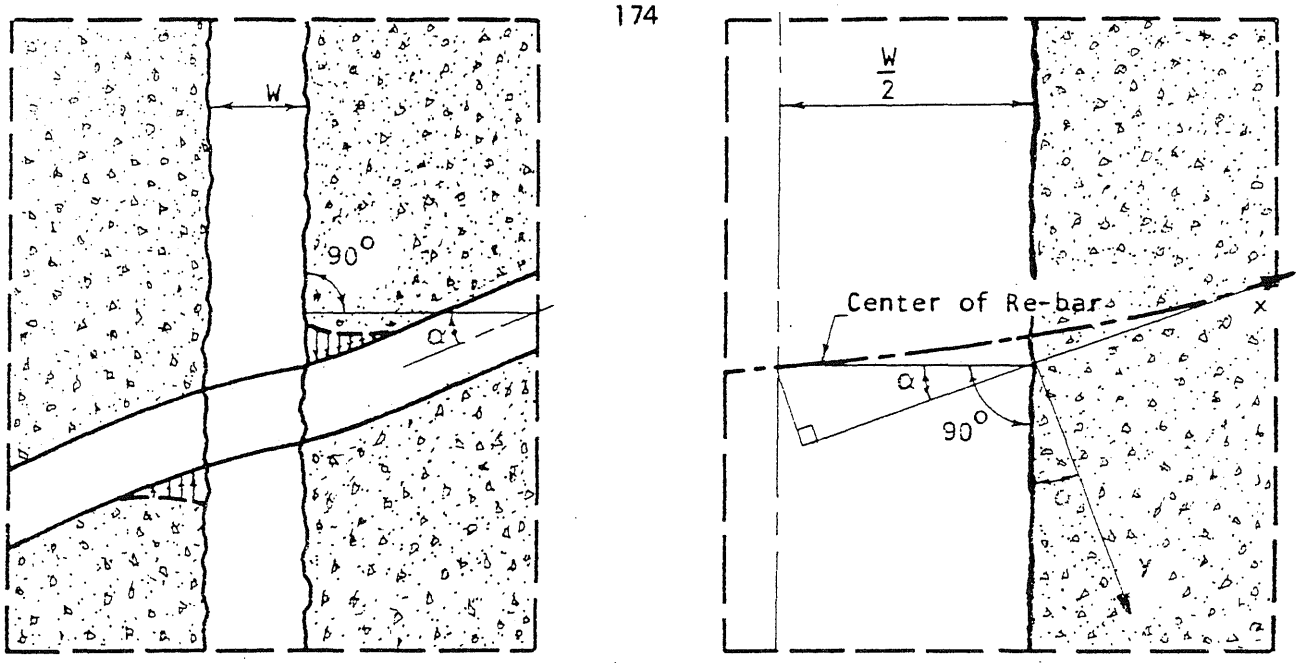

a

Transverse Stresses at Crack Edge

b

Geometry at the Crack

FIG. 3.2 DETAILS OF THE CRACK

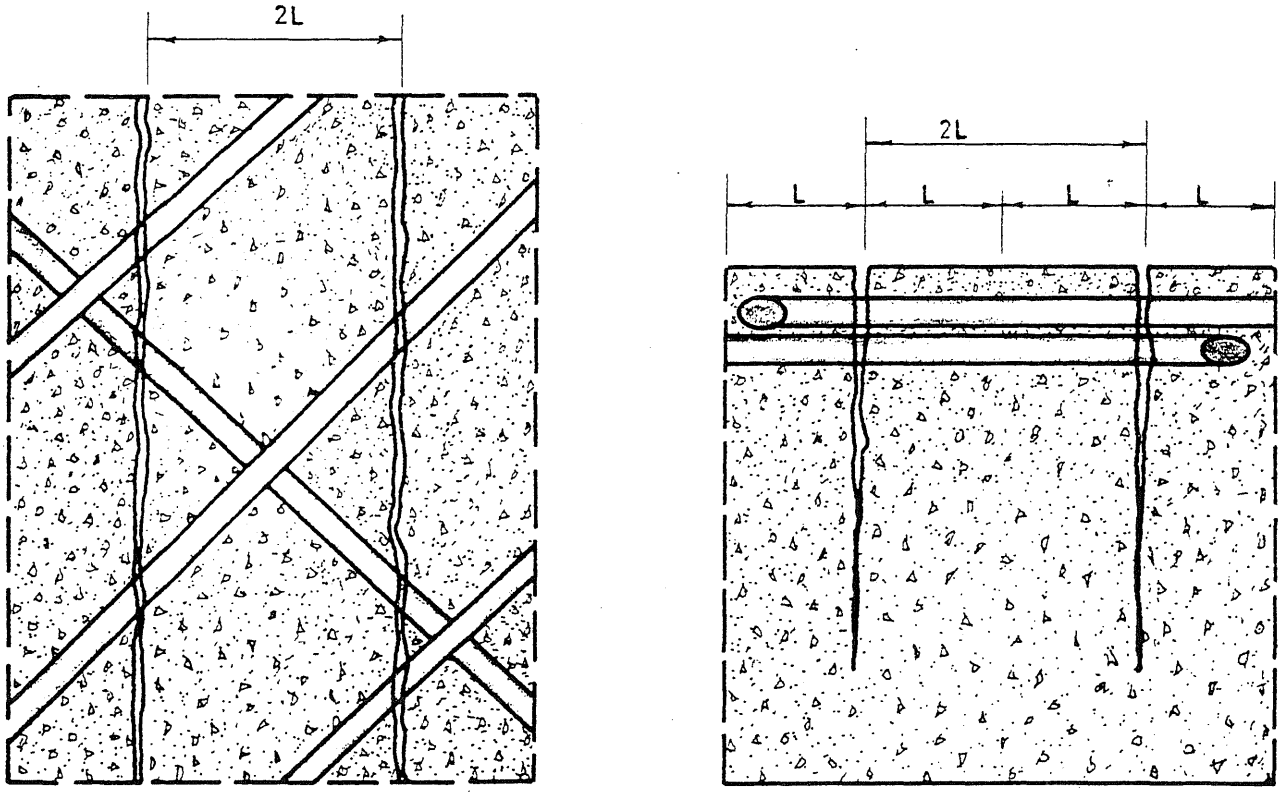

a

b

FIG. 3.3 REINFORCEMENT IN A CRACKED CONCRETE SECTION

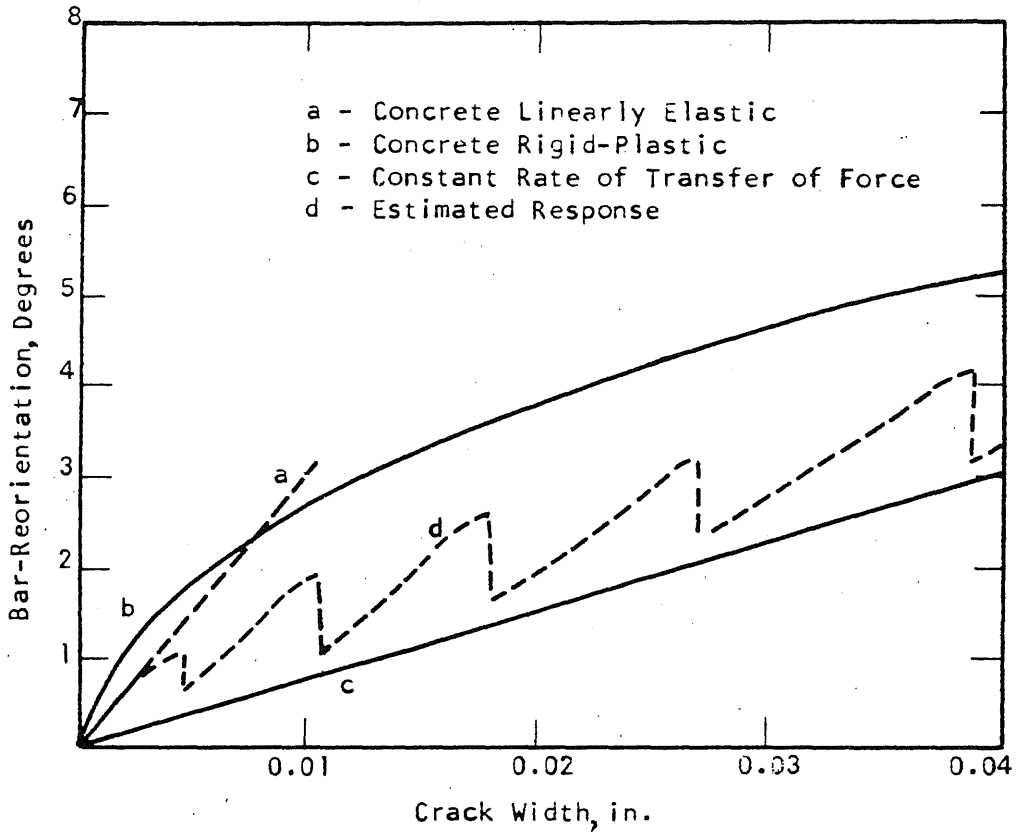

FIG. 3.4 COMPUTED REORIENTATION OF A NO. 4 REINFORCING BAR INCLINED 45 DEGREES TO THE CRACK

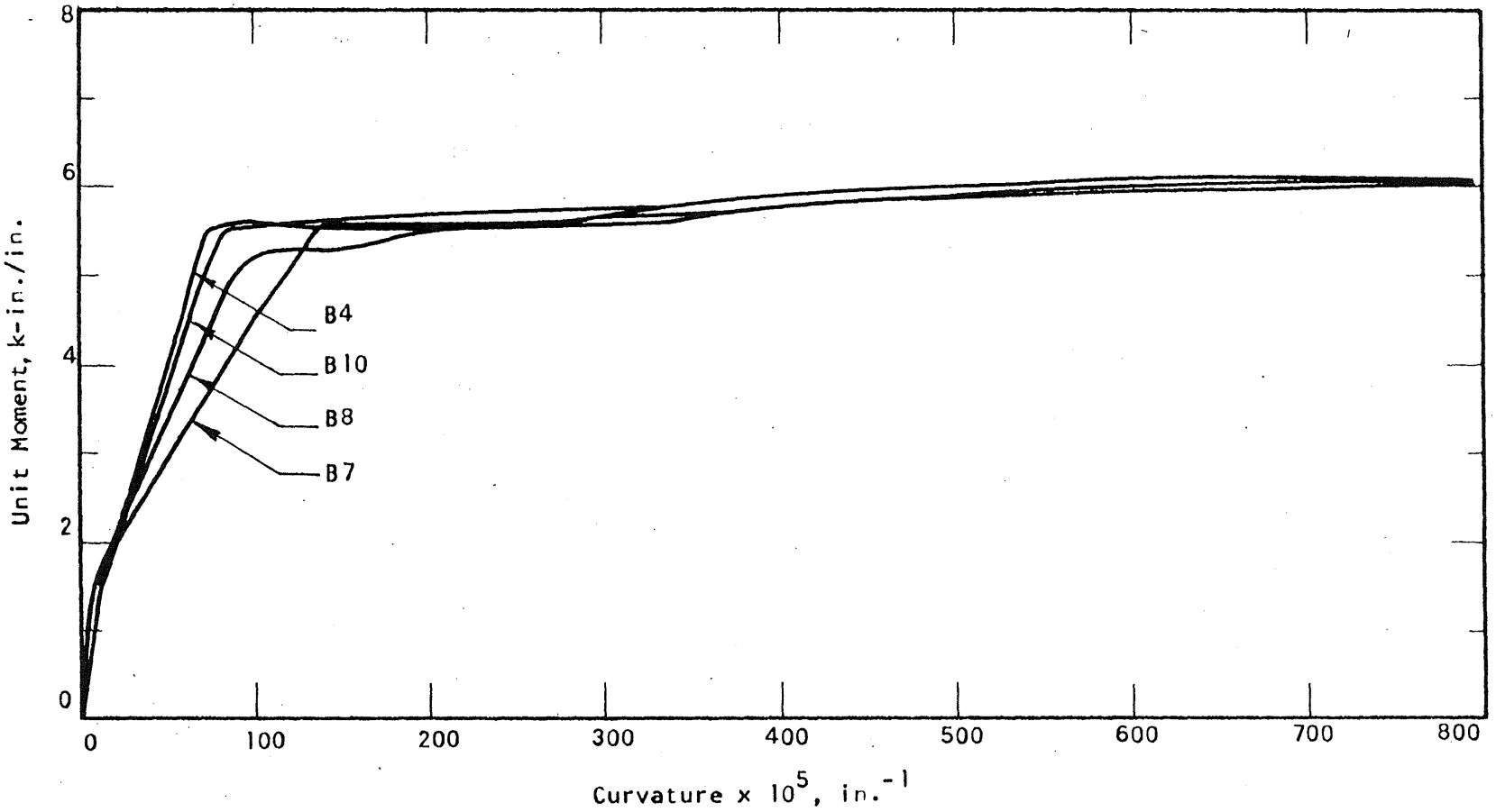

FIG. 3.5 COMPARISON OF TESTS B4, B7, B8 AND B10

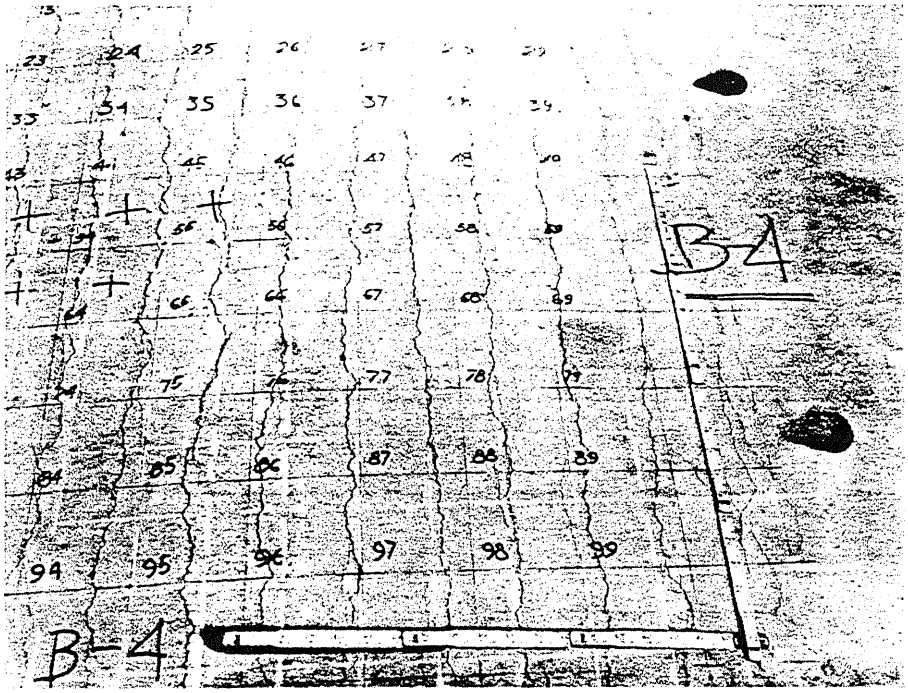

a Test Specimen B4

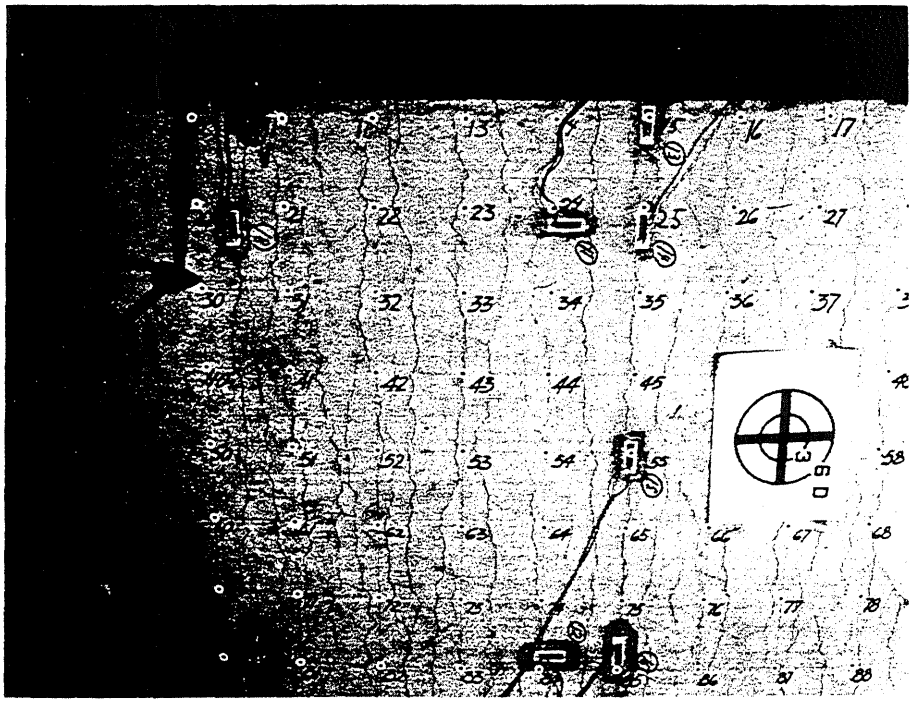

b Test Specimen B7

FIG. 3.6 CRACK PATTERN UNDER UNIAXIAL BENDING

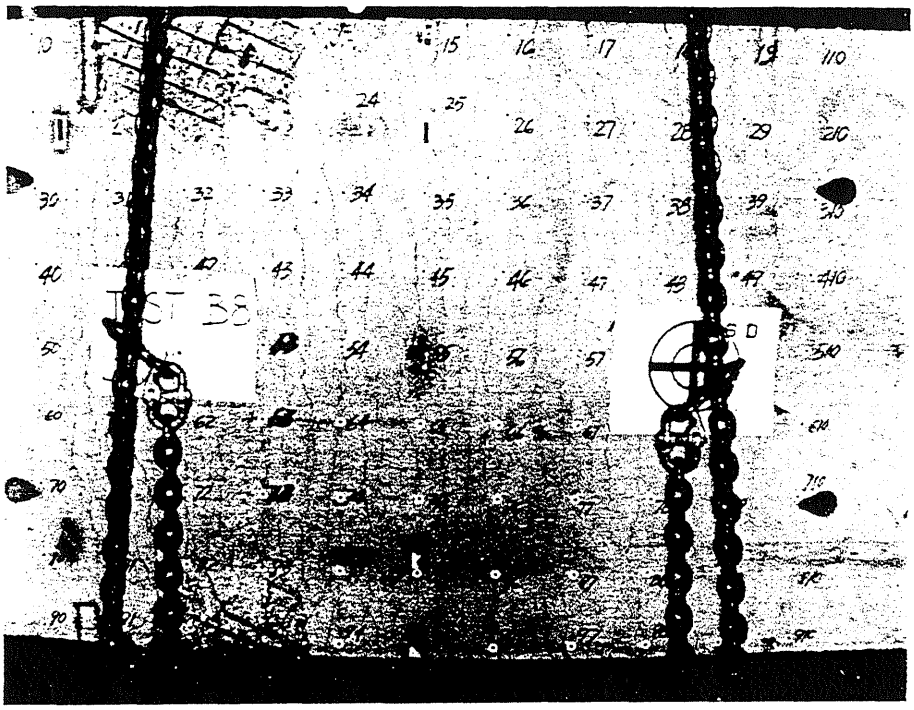

c Test Specimen 8

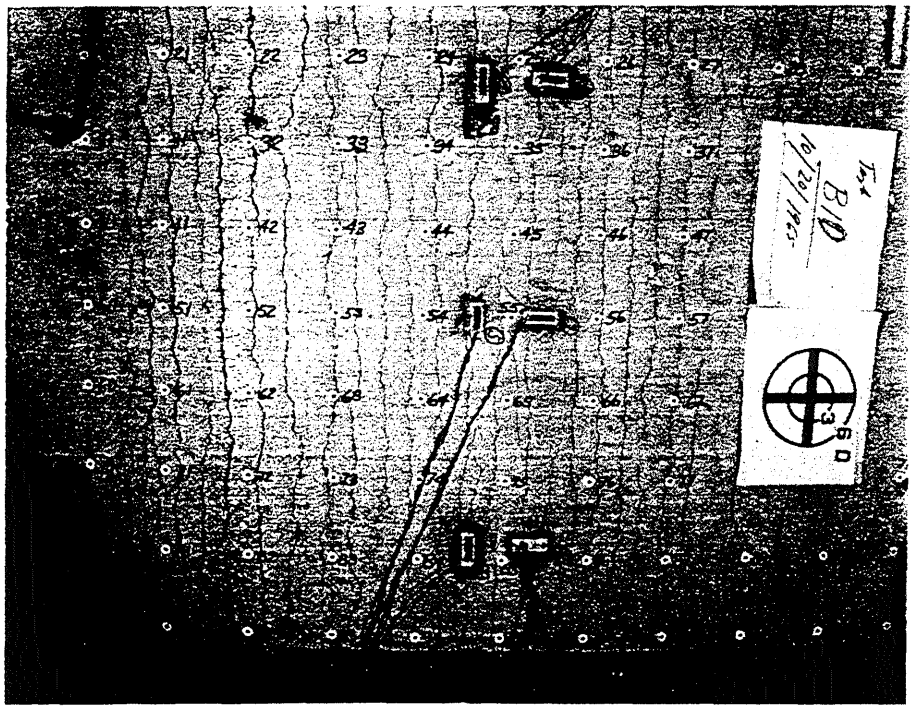

d Test Specimen 10

FIG 3.6 (Cont.) CRACK PATTERN UNDER UNIAXIAL BENDING

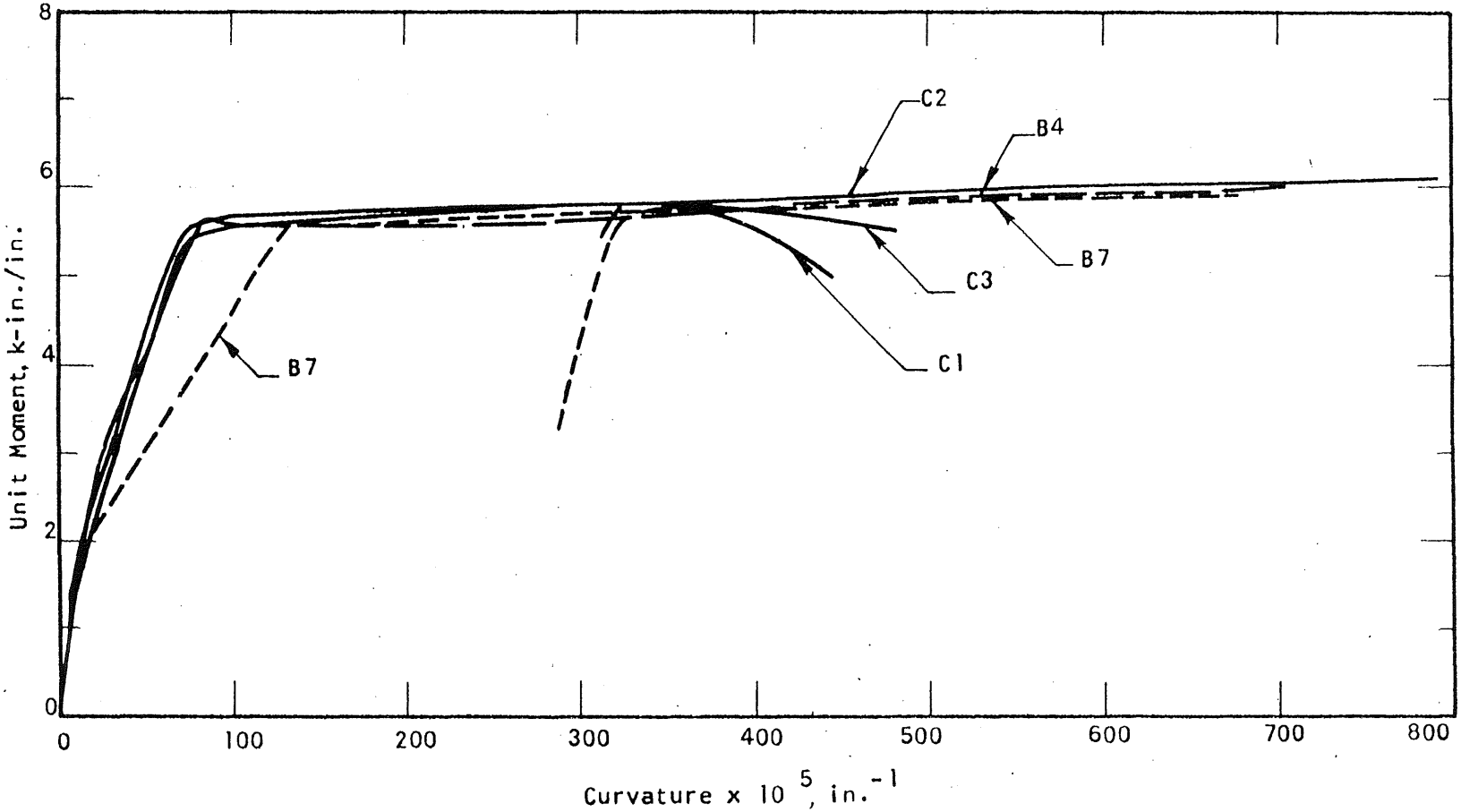

FIG. 3.7 COMPARISON OF TESTS C1, C2, C3, B4 AND B7

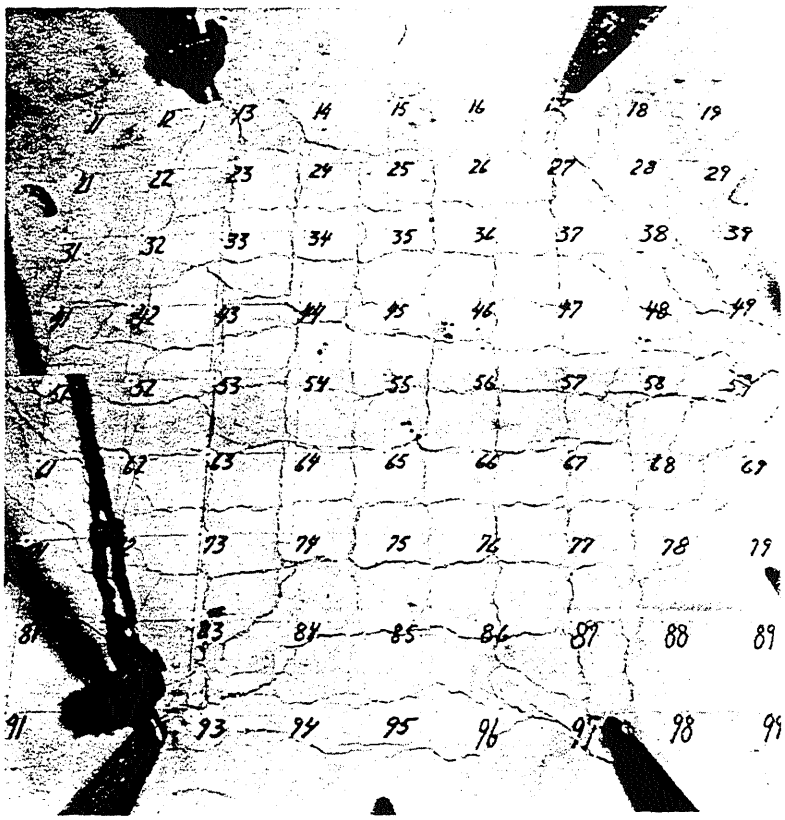

FIG. 3.8 CRACK PATTERN UNDER ISOSTATIC BENDING

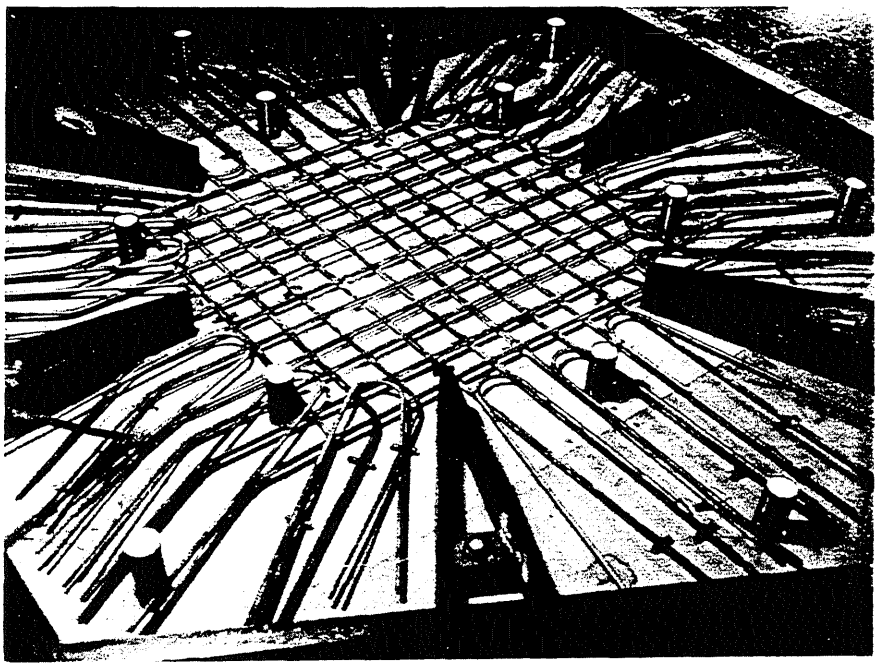

FIG. 3.9 REINFORCEMENT IN A "CIRCULAR" SPECIMEN

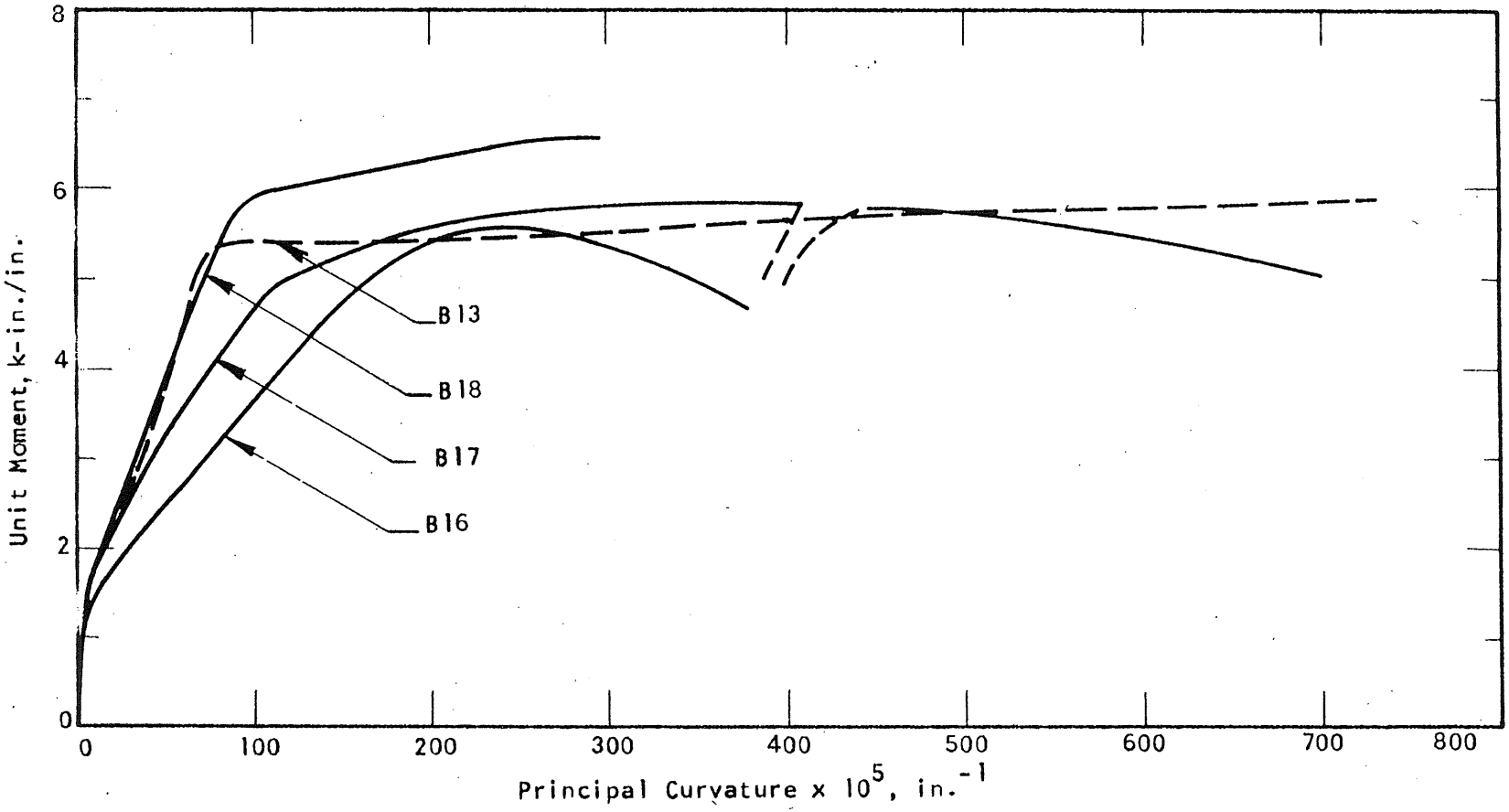

FIG. 3.10 COMPARISON OF TESTS B13, B16, B17 AND B18

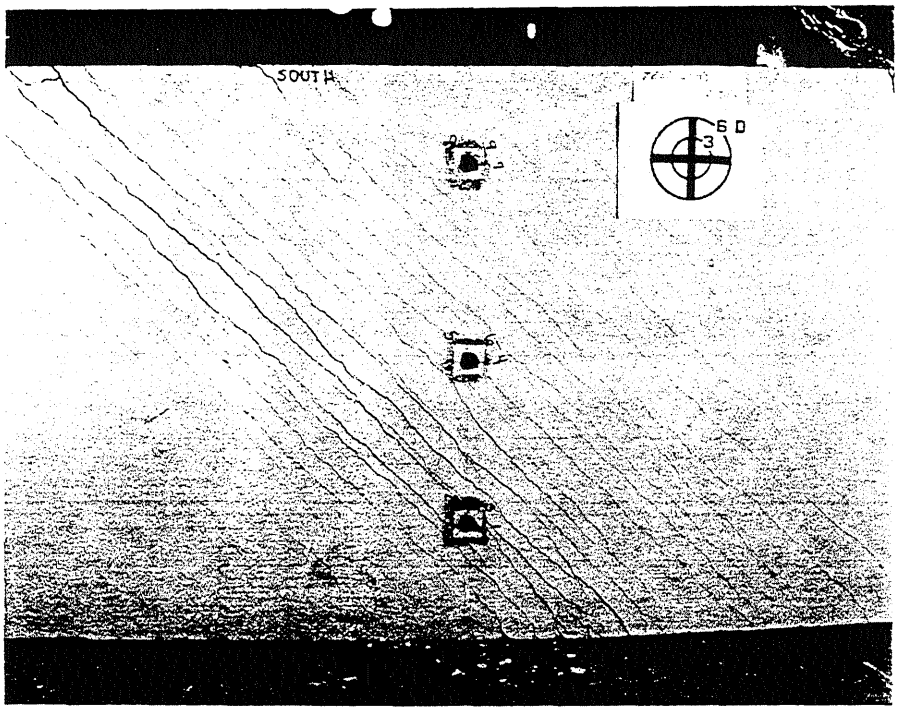

Test Specimen B18

FIG. 3.11 CRACK PATTERN UNDER TORSION

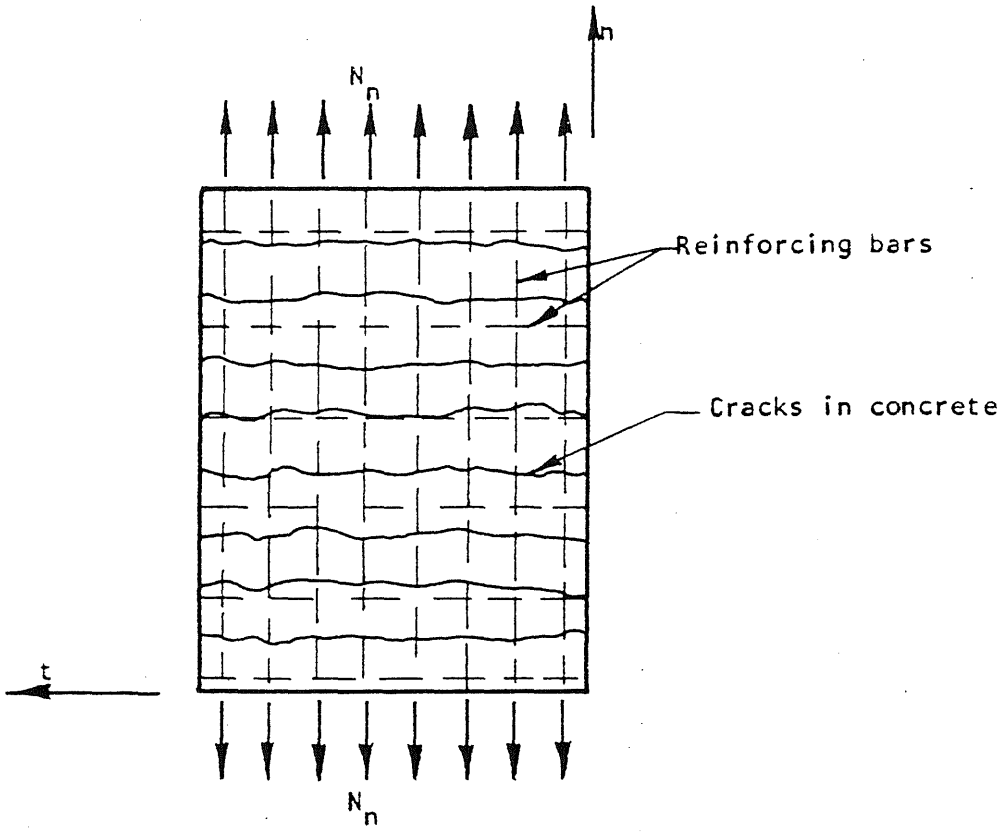

FIG. 4.1 REINFORCED CONCRETE PLATE ELEMENT IN TENSION

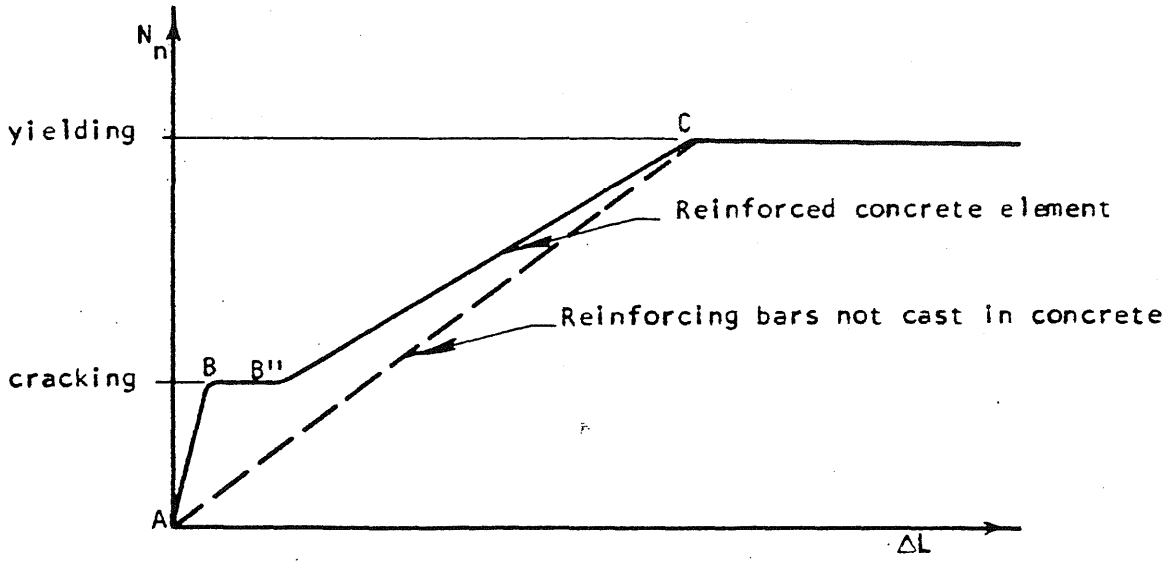

FIG. 4.2 ELONGATION-LOAD CURVE FOR A REINFORCED CONCRETE PLATE ELEMENT

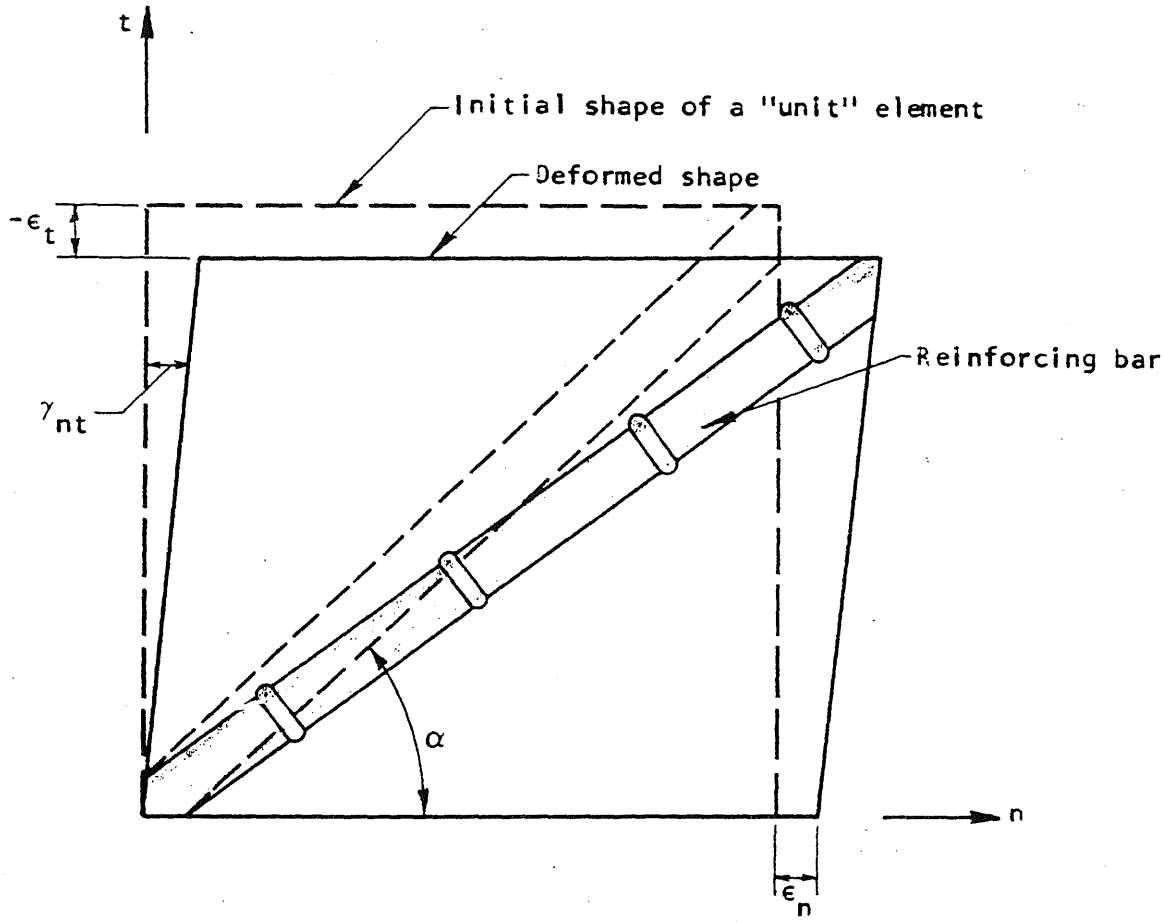

FIG. 4.3 DEFORMED SHAPE OF A UNIT ELEMENT OF A REINFORCED CONCRETE PLATE

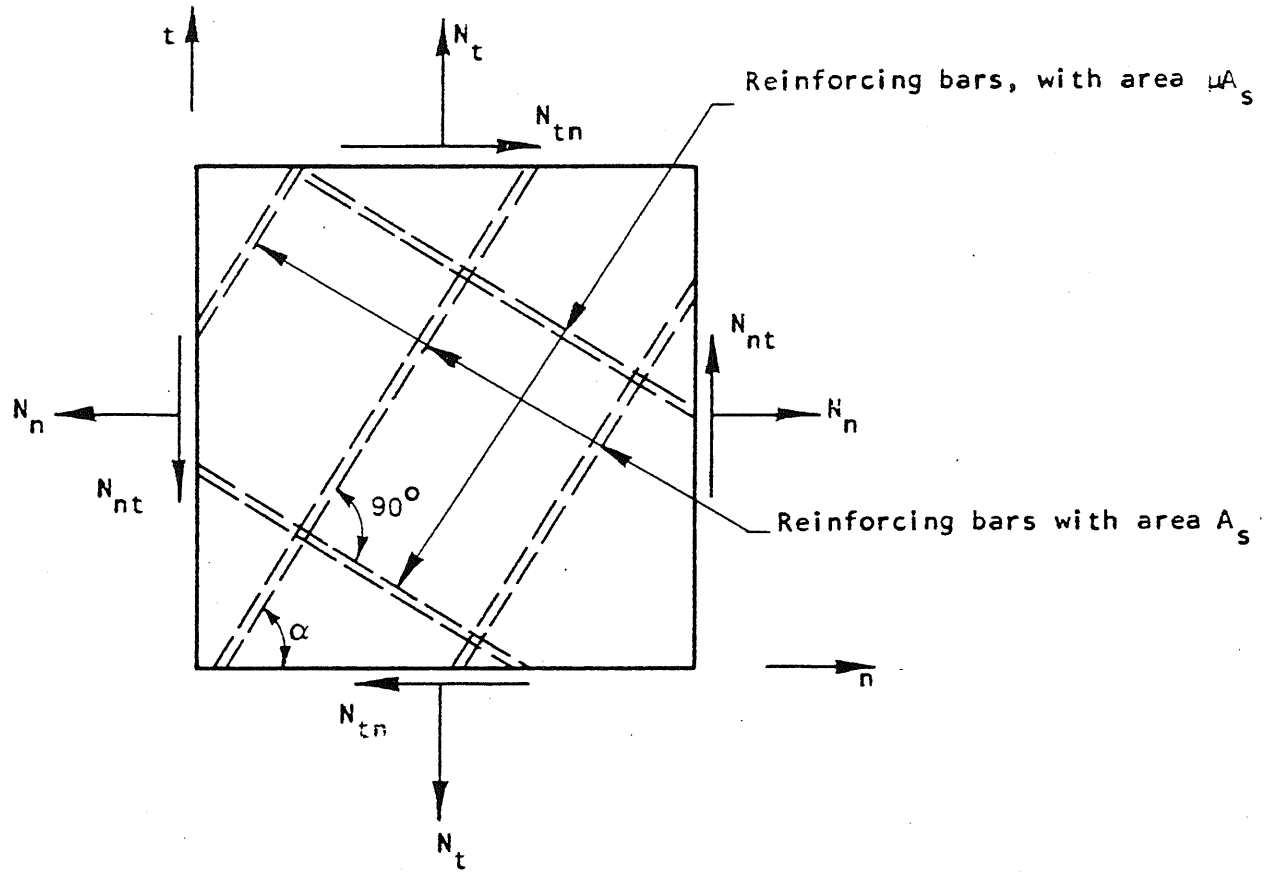

FIG. 4.4 REINFORCEMENT IN A UNIT ELEMENT OF A REINFORCED CONCRETE PLATE

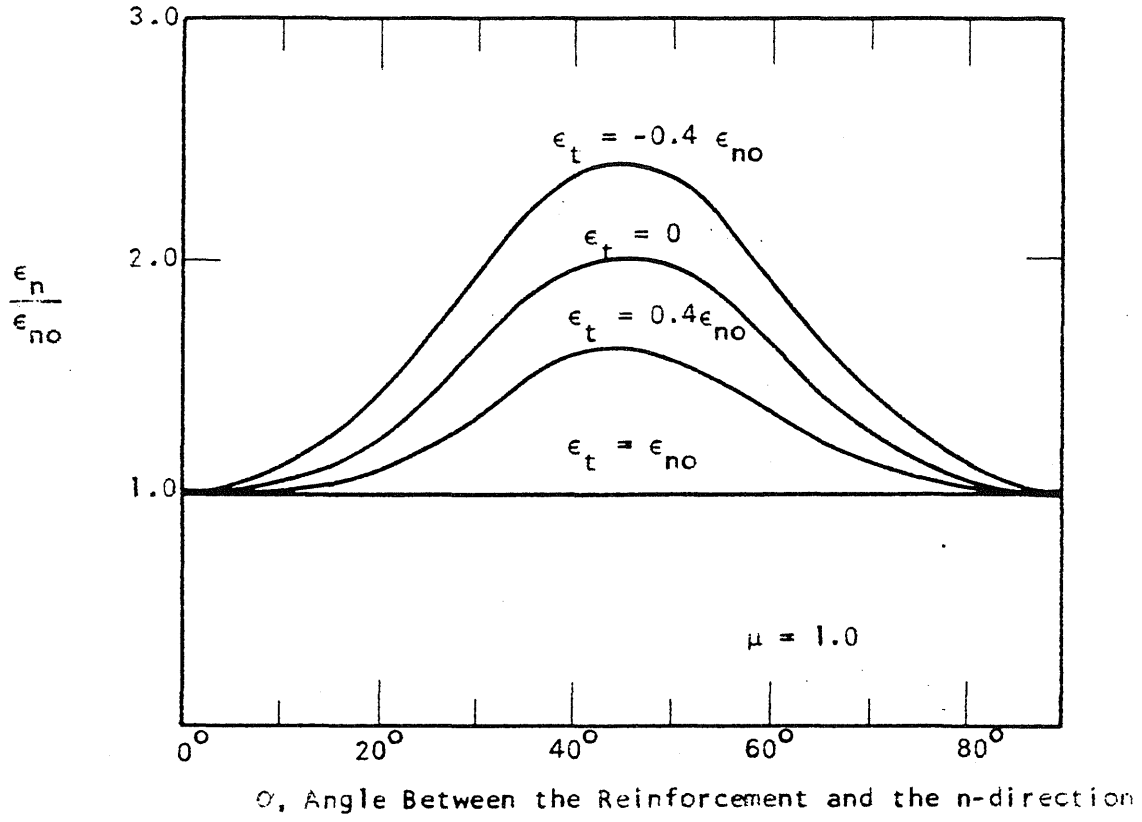

FIG. 4.5 ELONGATION OF AN ISOTROPICALLY REINFORCED ELEMENT SUBJECTED TO IN-PLANE FORCES

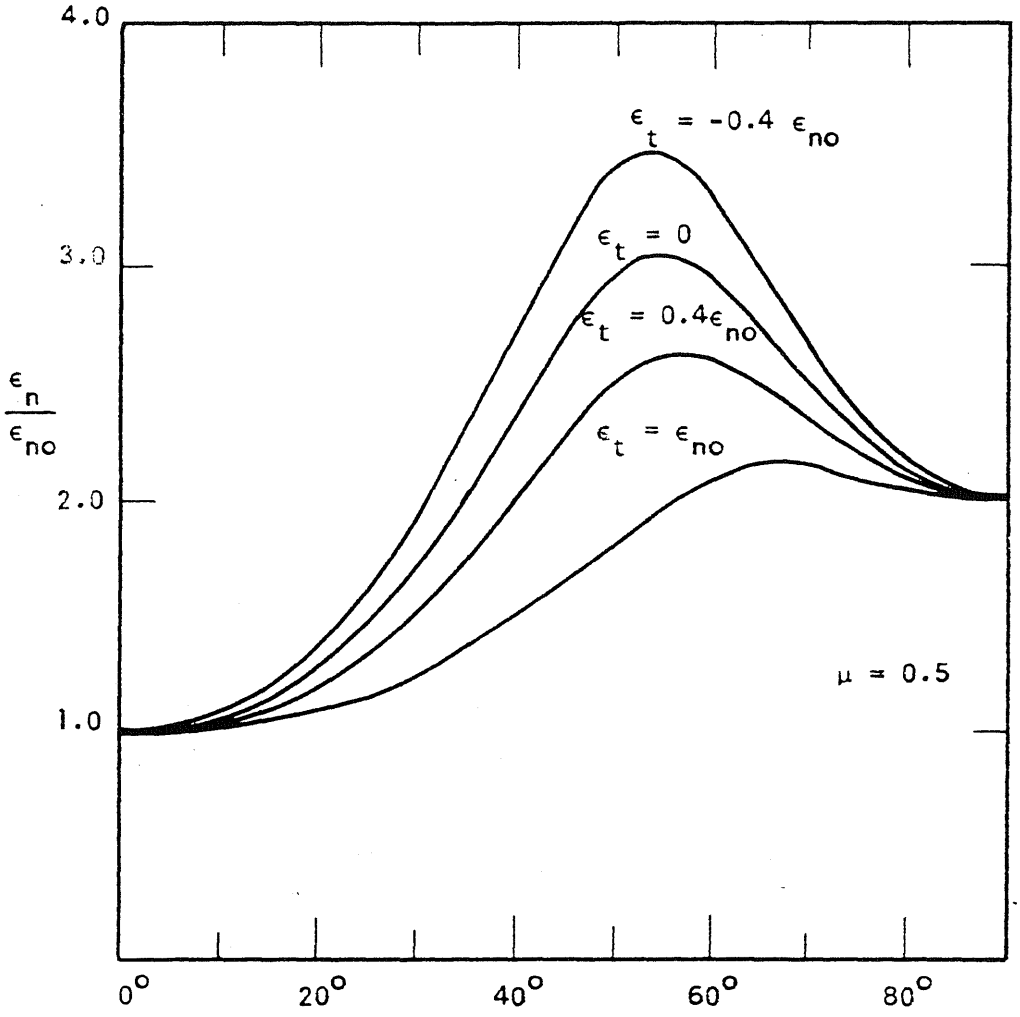

FIG. 4.6 ELONGATION OF A NONISOTROPICALLY REINFORCED ELEMENT SUBJECTED TO IN-PLANE FORCES

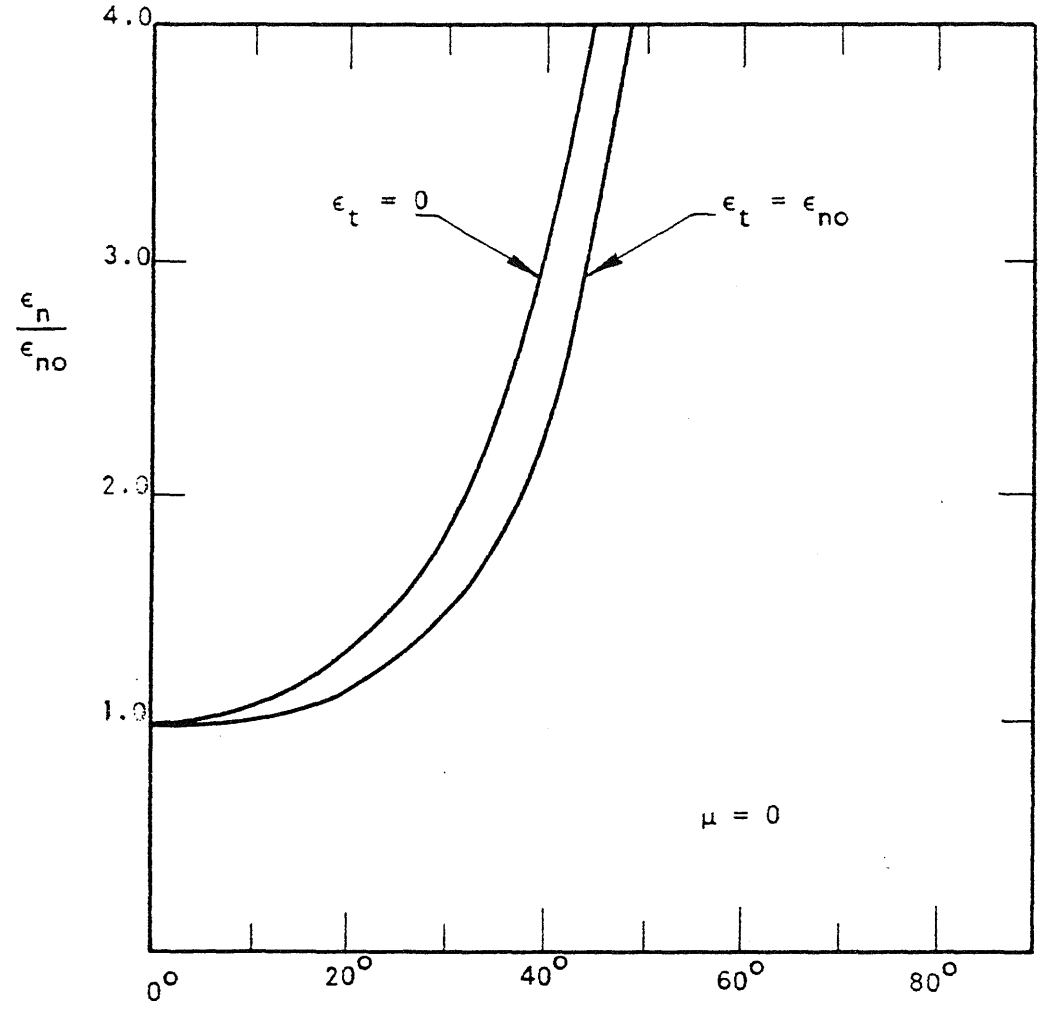

FIG. 4.7 ELONGATION OF A NONISOTROPICALLY REINFORCED ELEMENT SUBJECTED TO IN-PLANE FORCES

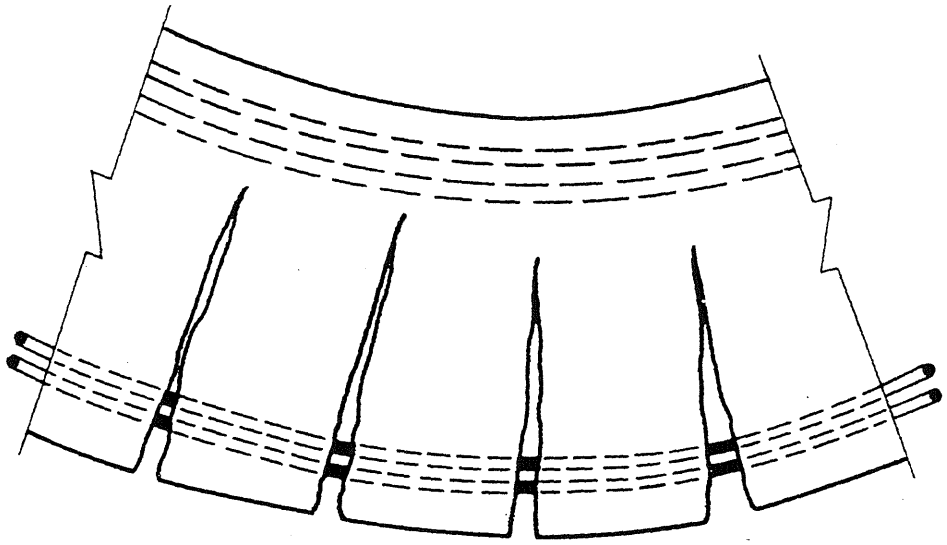

FIG. 4.8 FLEXURAL CRACKING

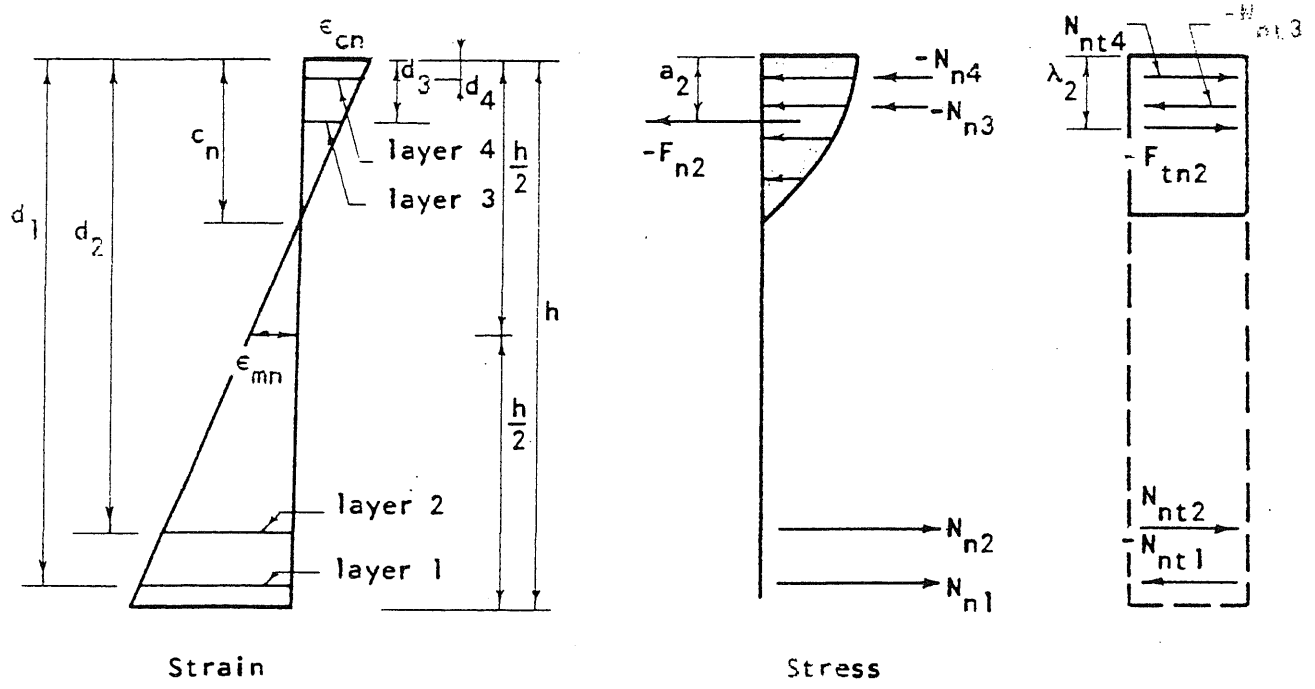

Section in the n-direction

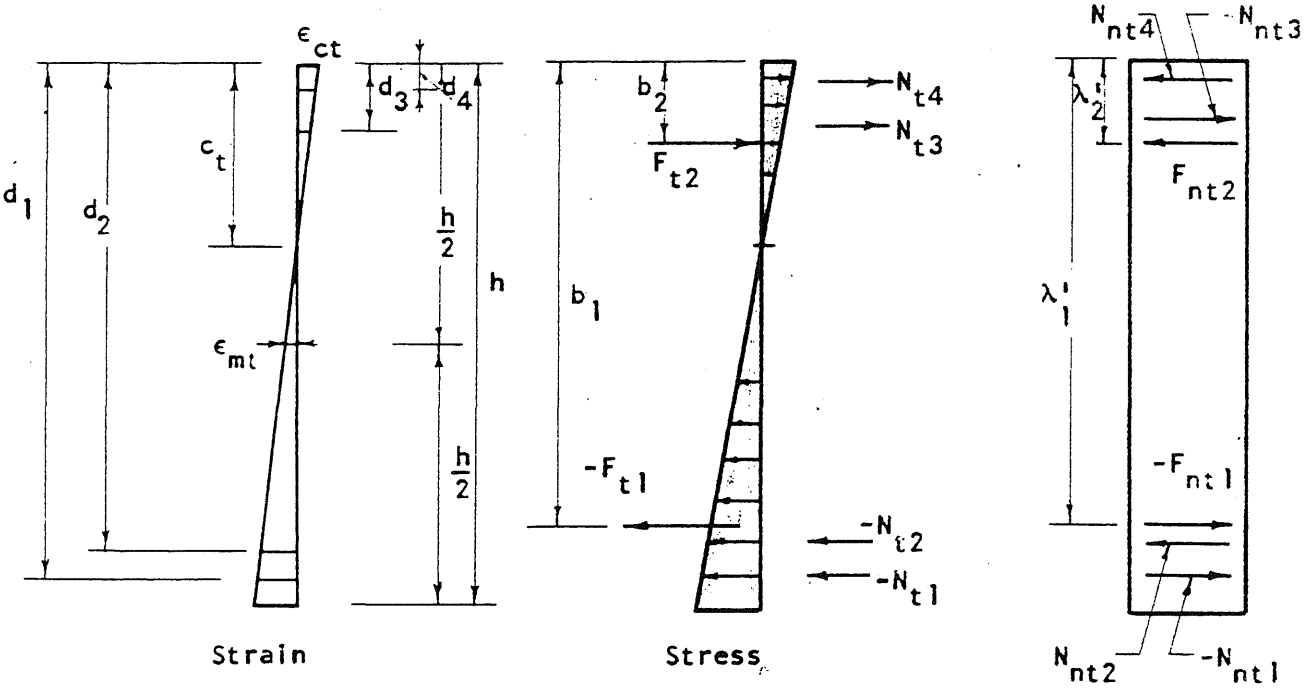

Section in the t-direction

FIG. 4.9 ELEMENT UNDER UNIAXIAL MOMENT

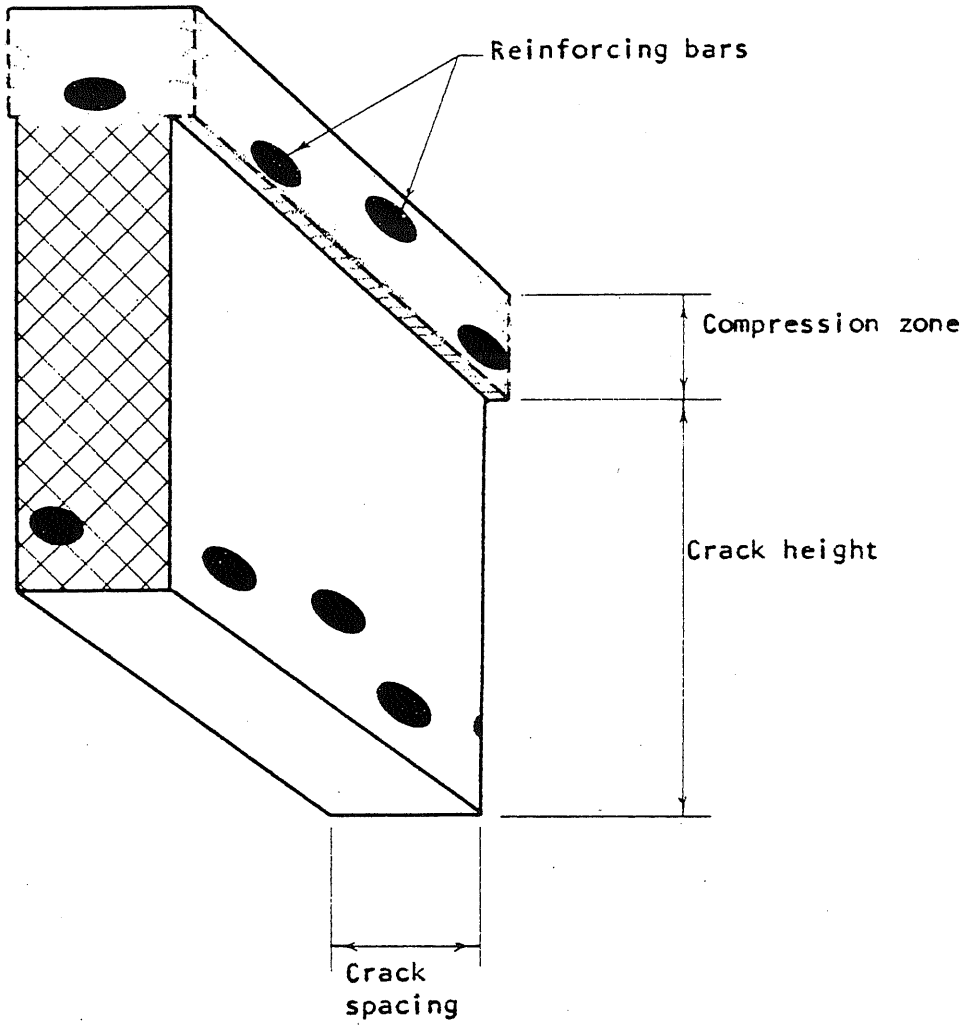

FIG. 4.10 A CUT-OUT SECTION OF A REINFORCED CONCRETE SLAB ELEMENT

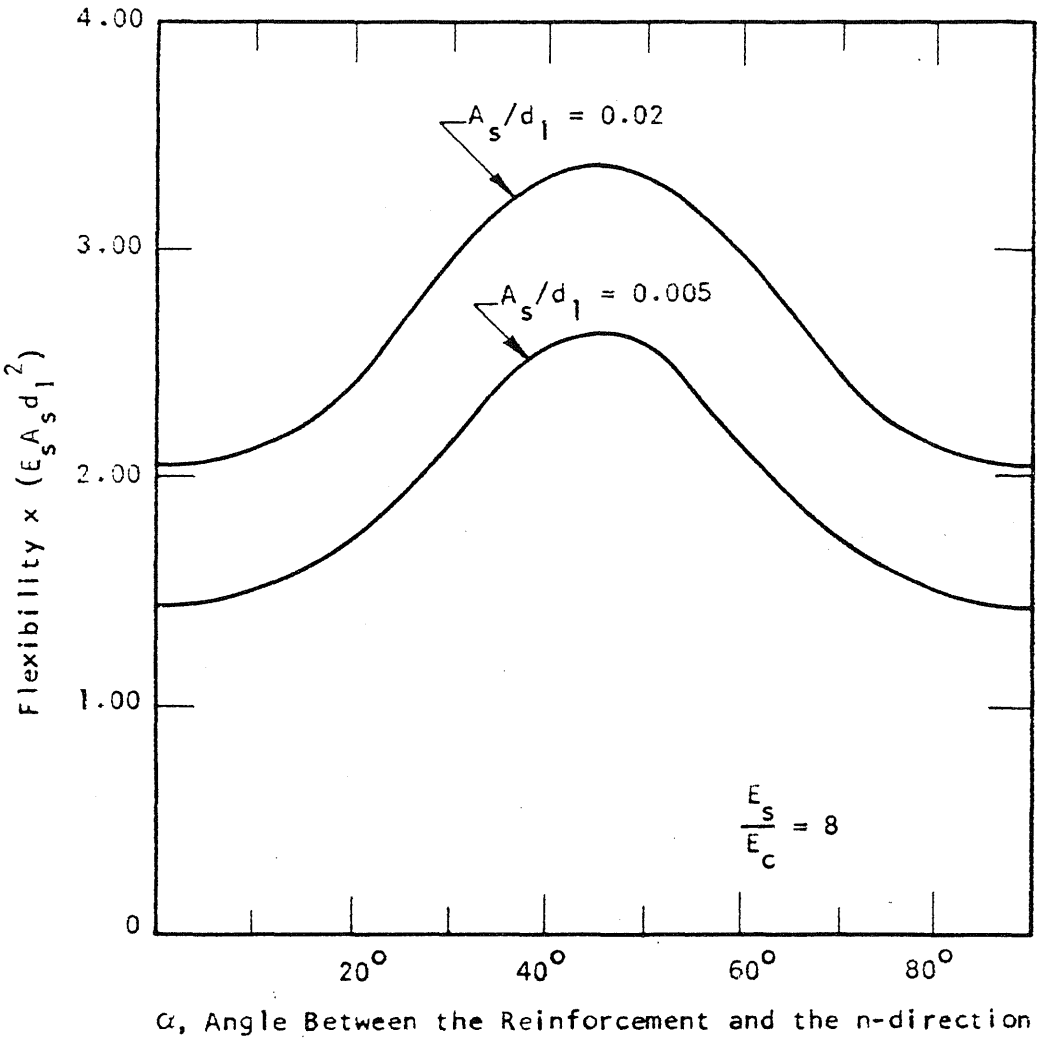

FIG. 4.11 FLEXIBILITY OF AN ISOTROPICALLY REINFORCED ELEMENT SUBJECTED TO UNIAXIAL MOMENT

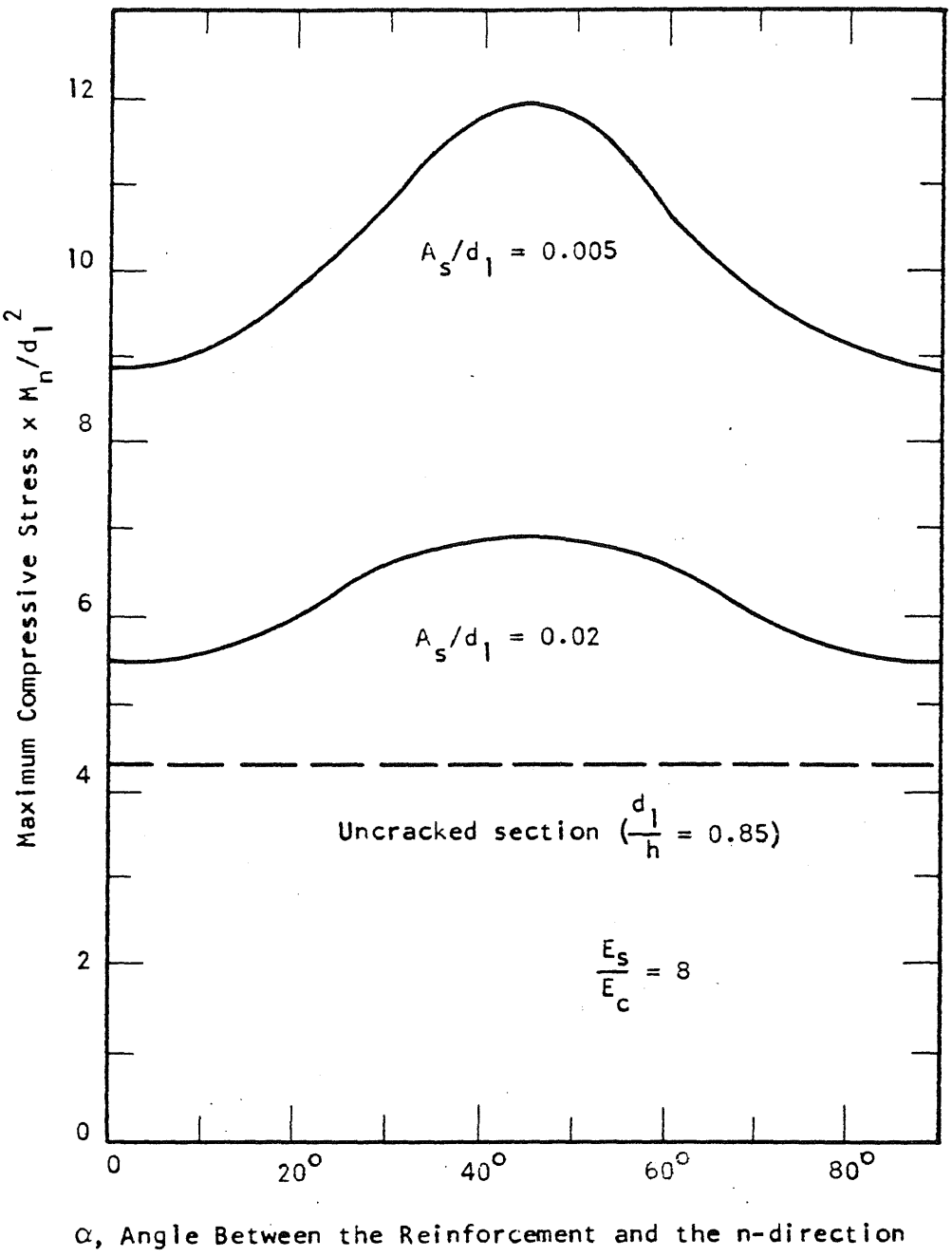

FIG. 4.12 MAXIMUM COMPRESSIVE STRESSES IN AN ISOTROPICALLY REINFORCED ELEMENT SUBJECTED TO UNIAXIAL MOMENT

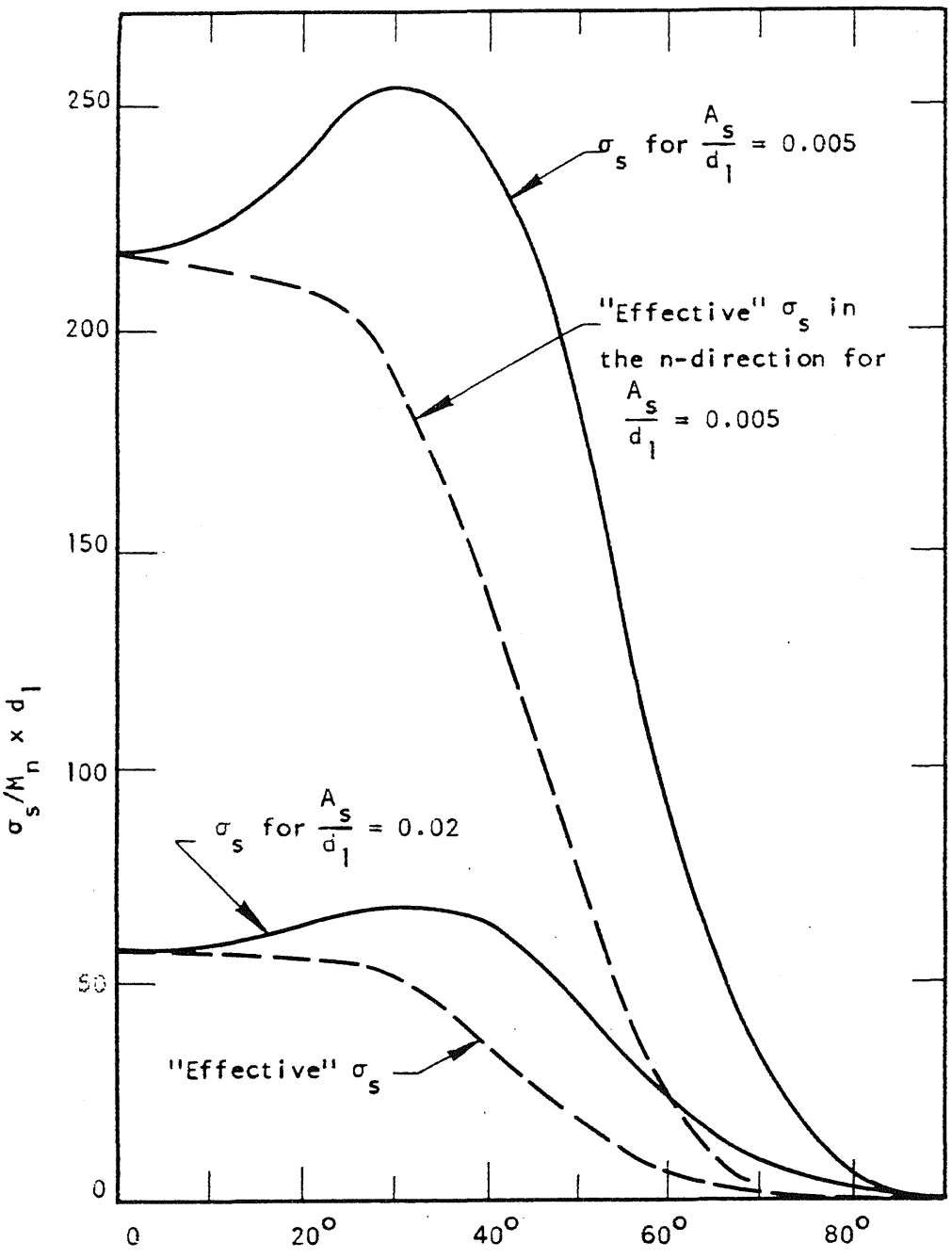

FIG. 4.13 STRESSES IN ONE DIRECTION OF THE REINFORCEMENT IN AN ISOTROPICALLY REINFORCED ELEMENT SUBJECTED TO UNIAXIAL MOMENT

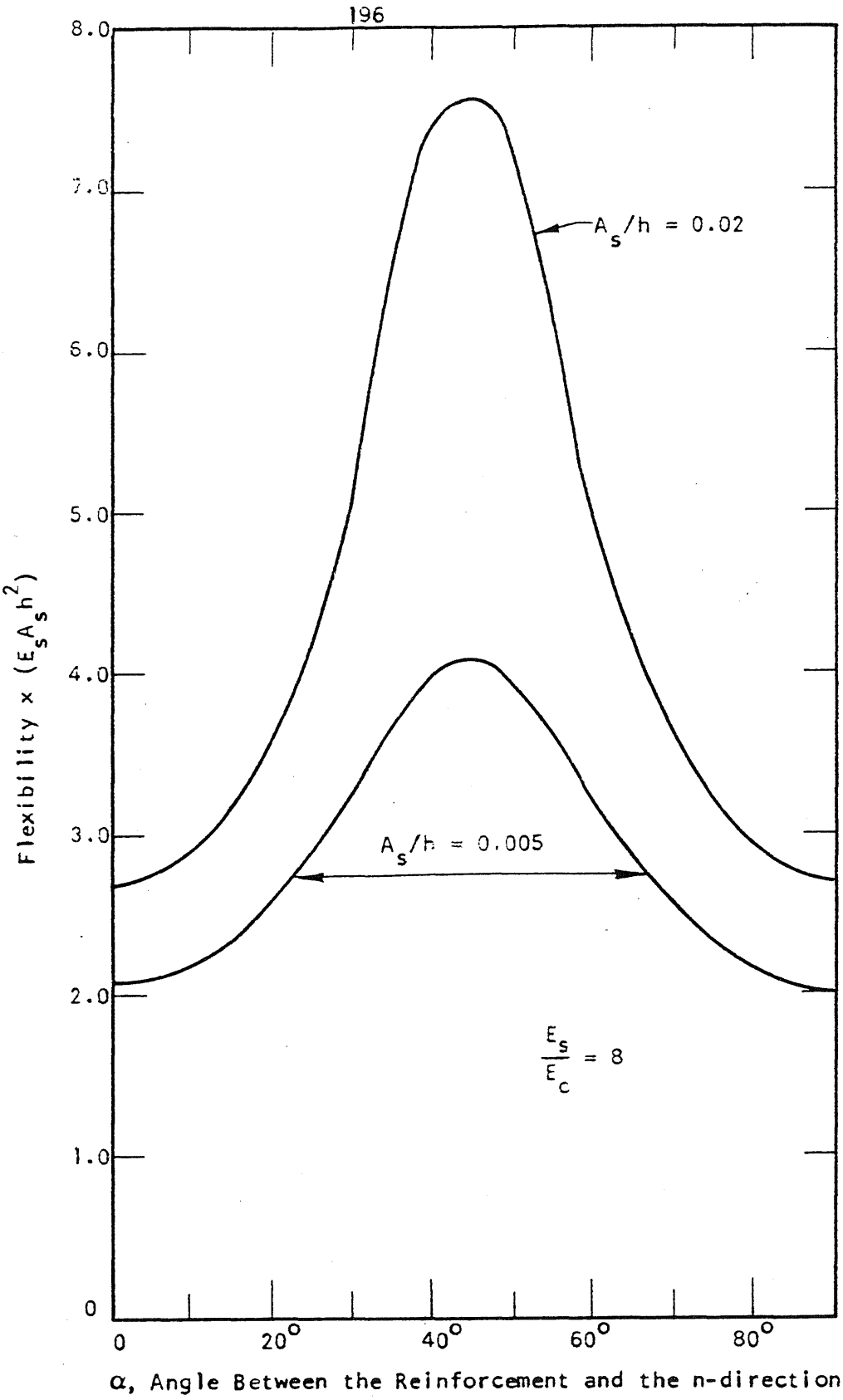

FIG. 4.14 FLEXIBILITY OF AN ISOTROPICALLY REINFORCED ELEMENT SUBJECTED TO PURE TORSION

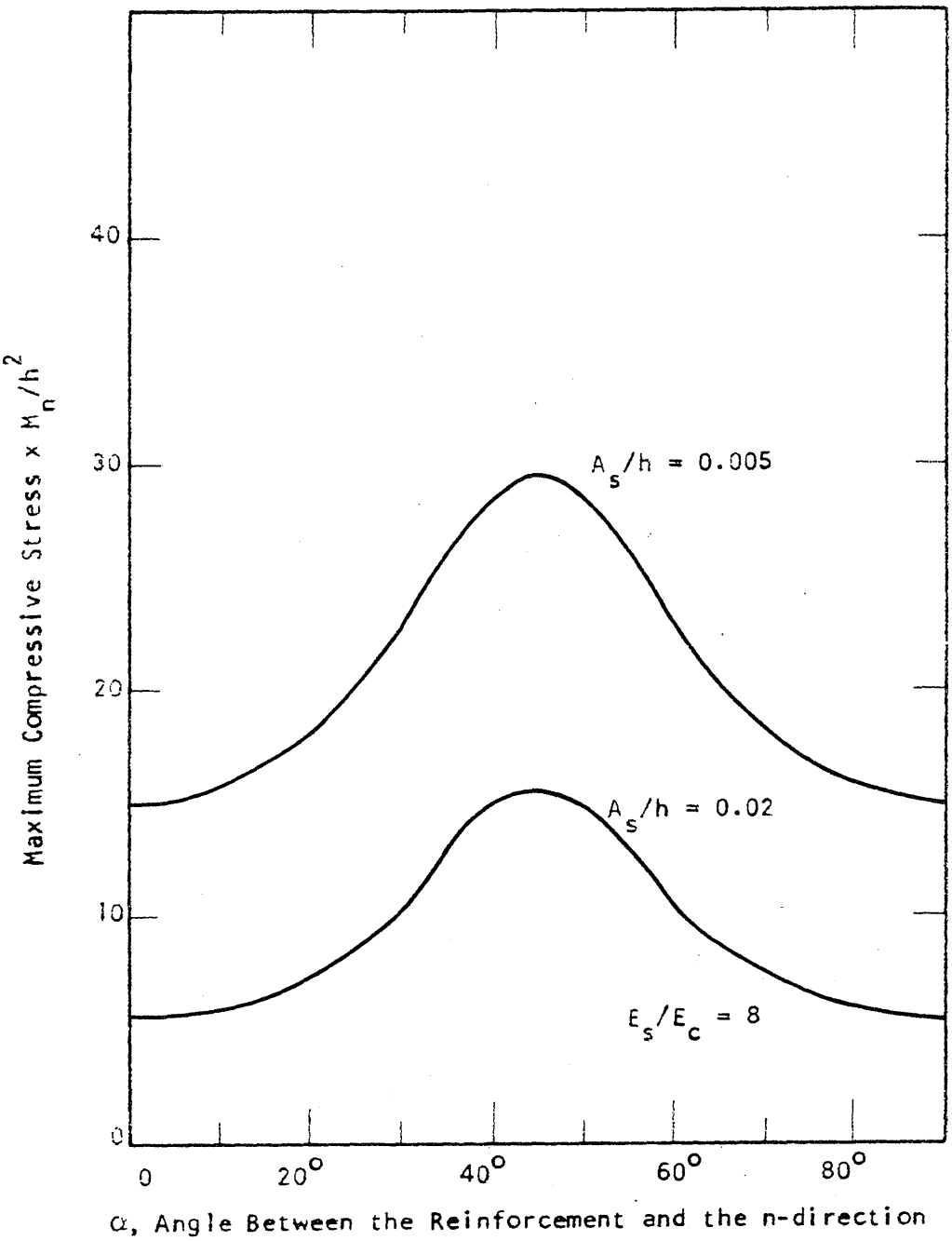

FIG. 4.15 MAXIMUM COMPRESSIVE STRESS IN AN ISOTROPICALLY REINFORCED ELEMENT SUBJECTED TO PURE TORSION

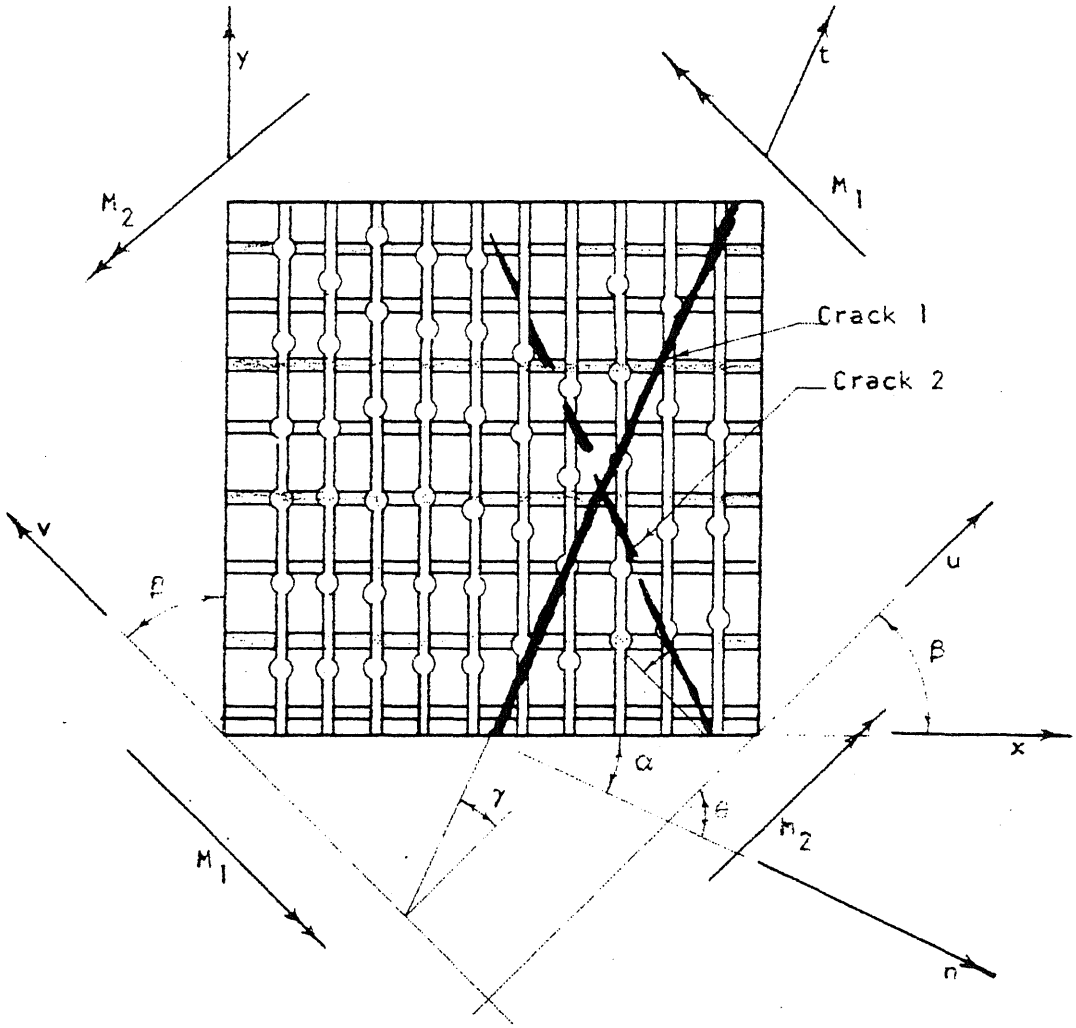

FIG. 4.16 COORDINATE SYSTEMS

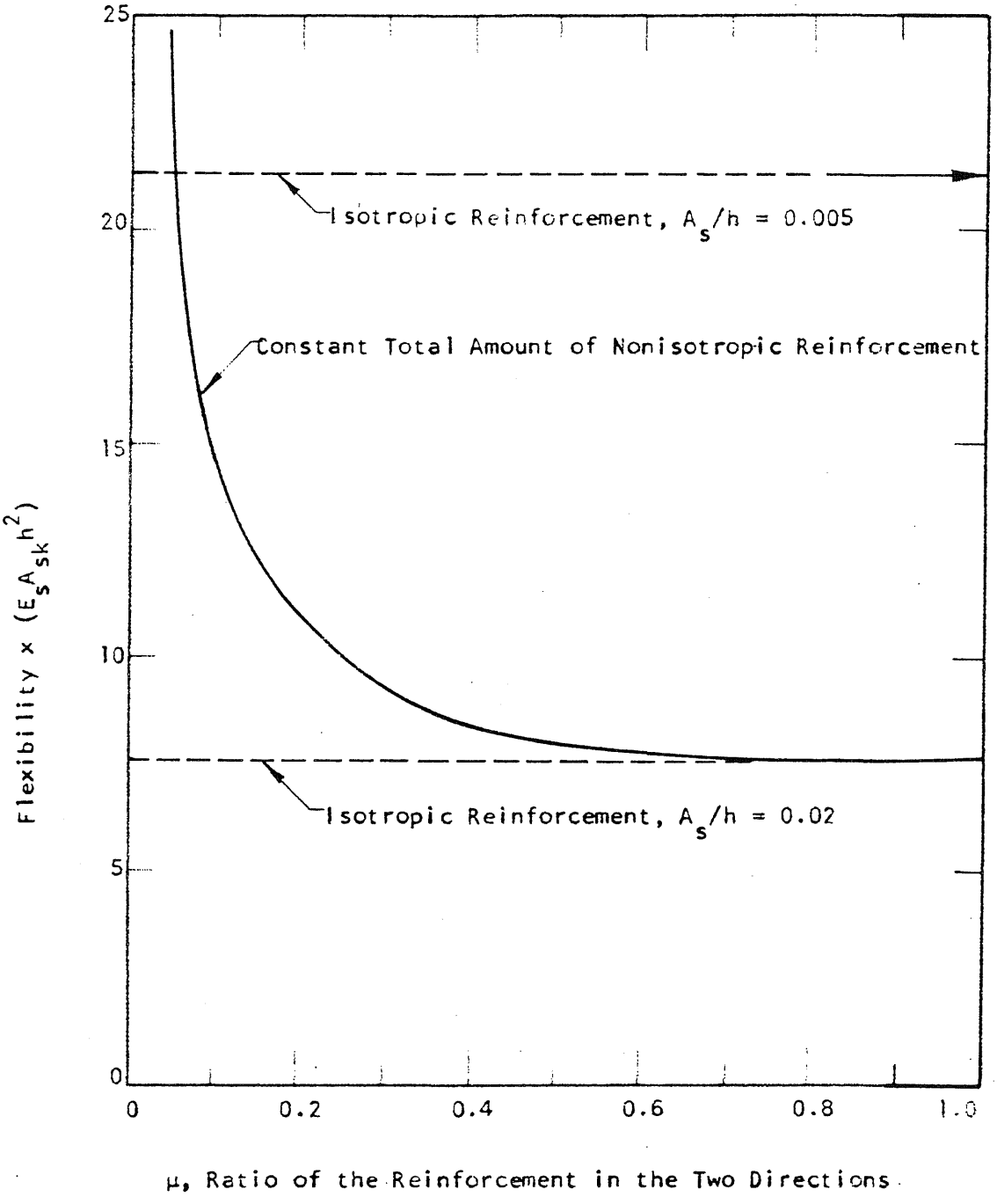

FIG. 4.17 FLEXIBILITY OF A NONISOTROPICALLY REINFORCED ELEMENT SUBJECTED TO PURE TORSION

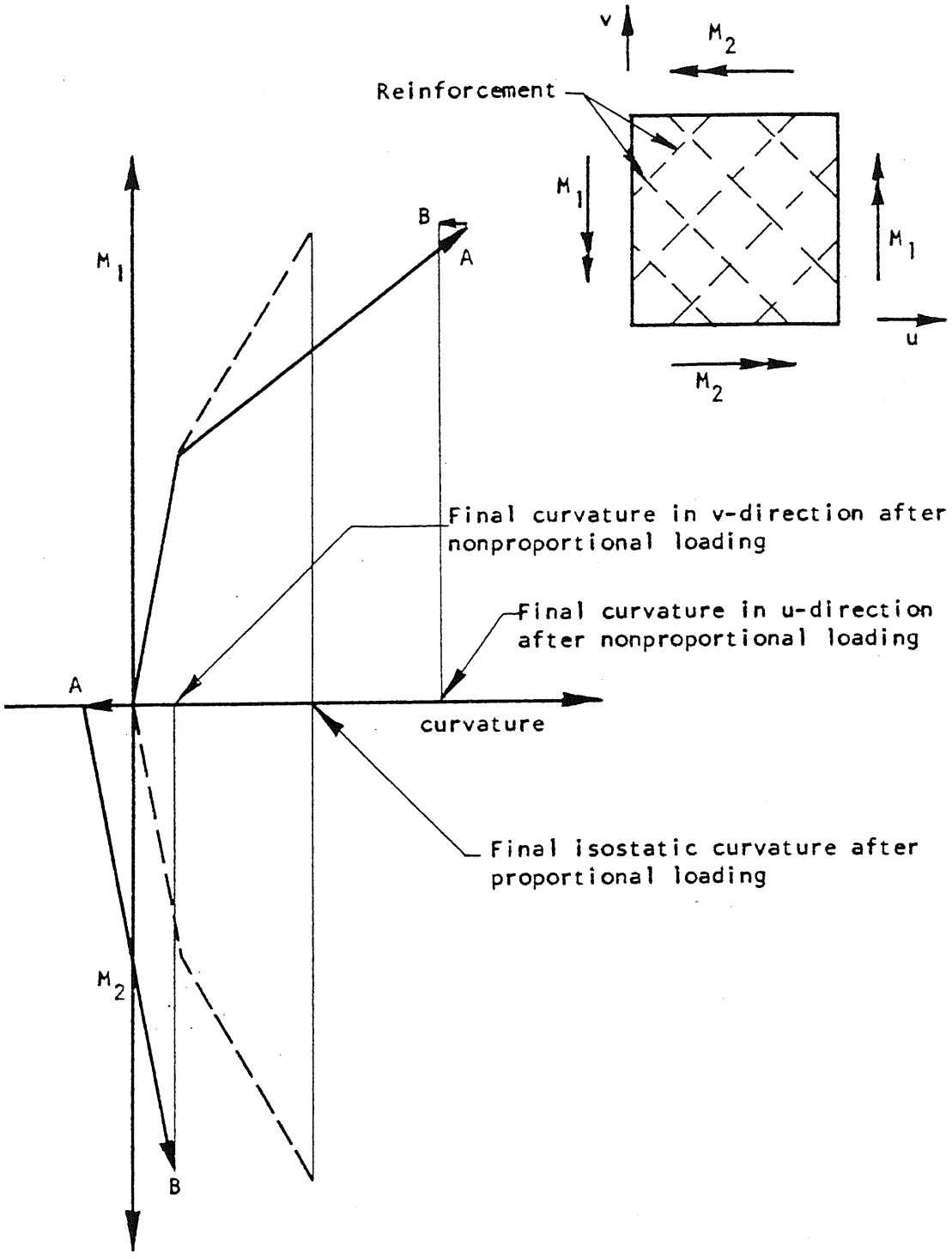

FIG. 4.18 PROPORTIONAL AND NON-PROPORTIONAL LOADING OF A REINFORCED CONCRETE ELEMENT

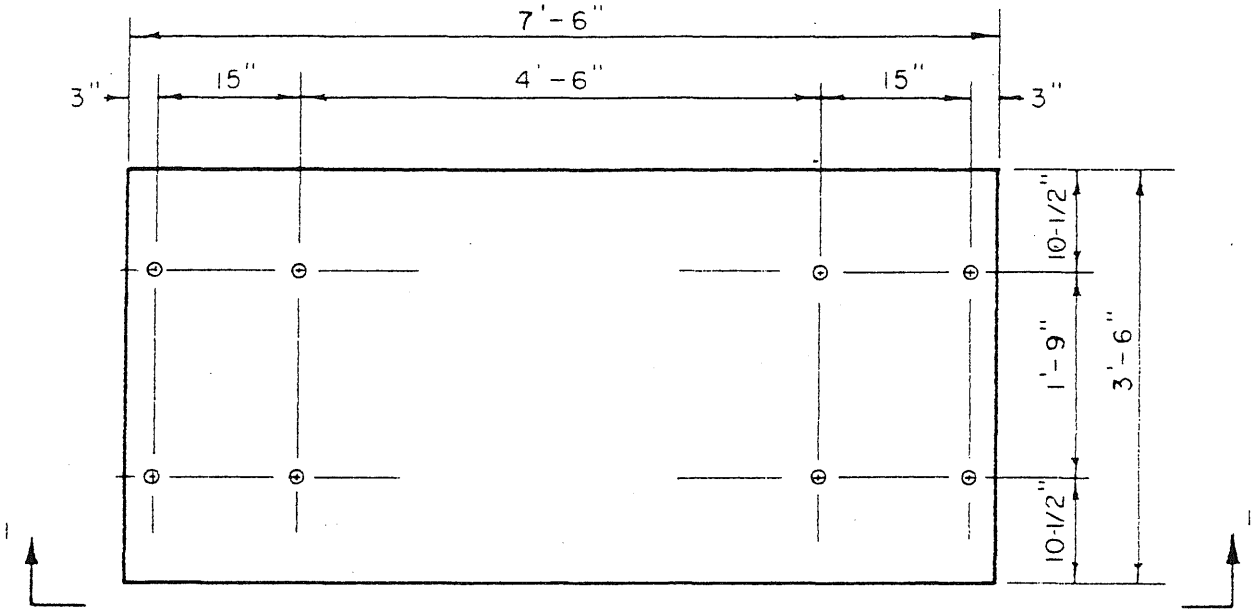

Planview of Concrete Slab

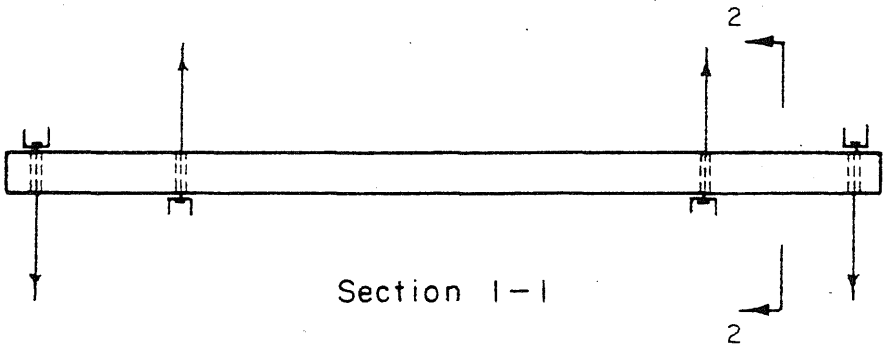

Section 1-1

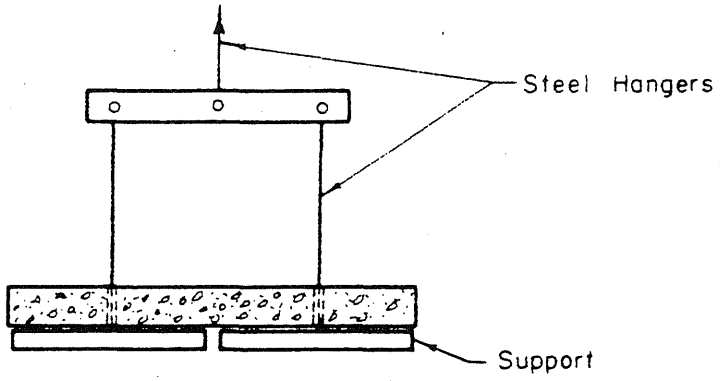

Section 2-2

Loading Arrangement

FIG. 4.19 TEST SPECIMEN "B"

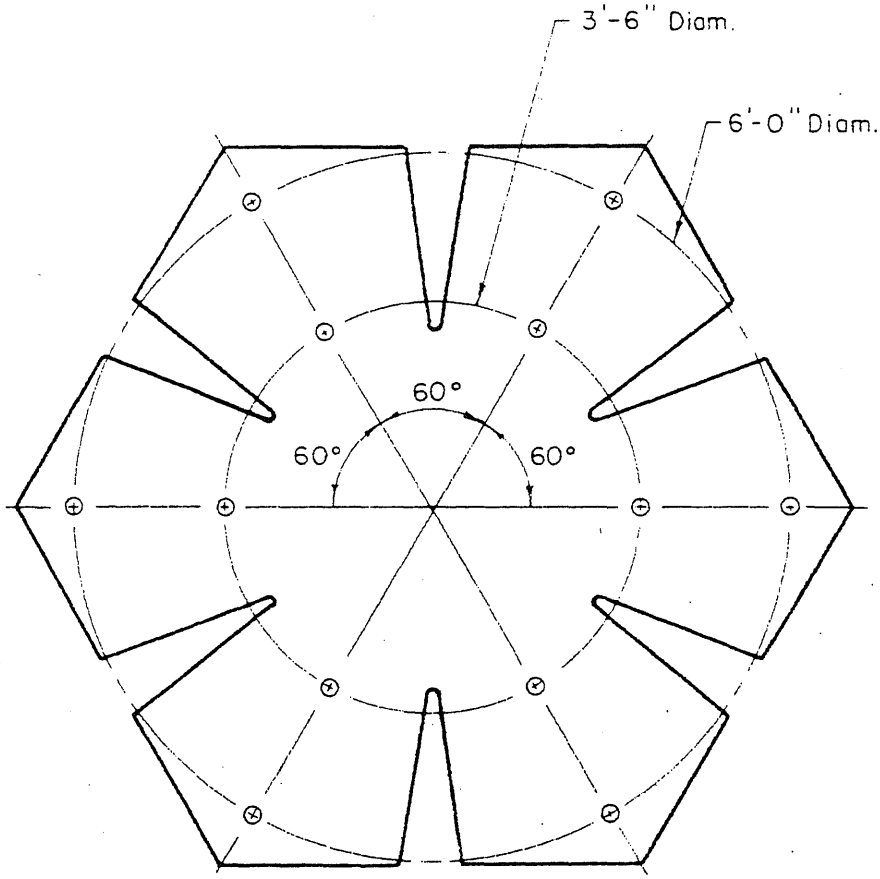

FIG. 4.20 TEST SPECIMEN "C"

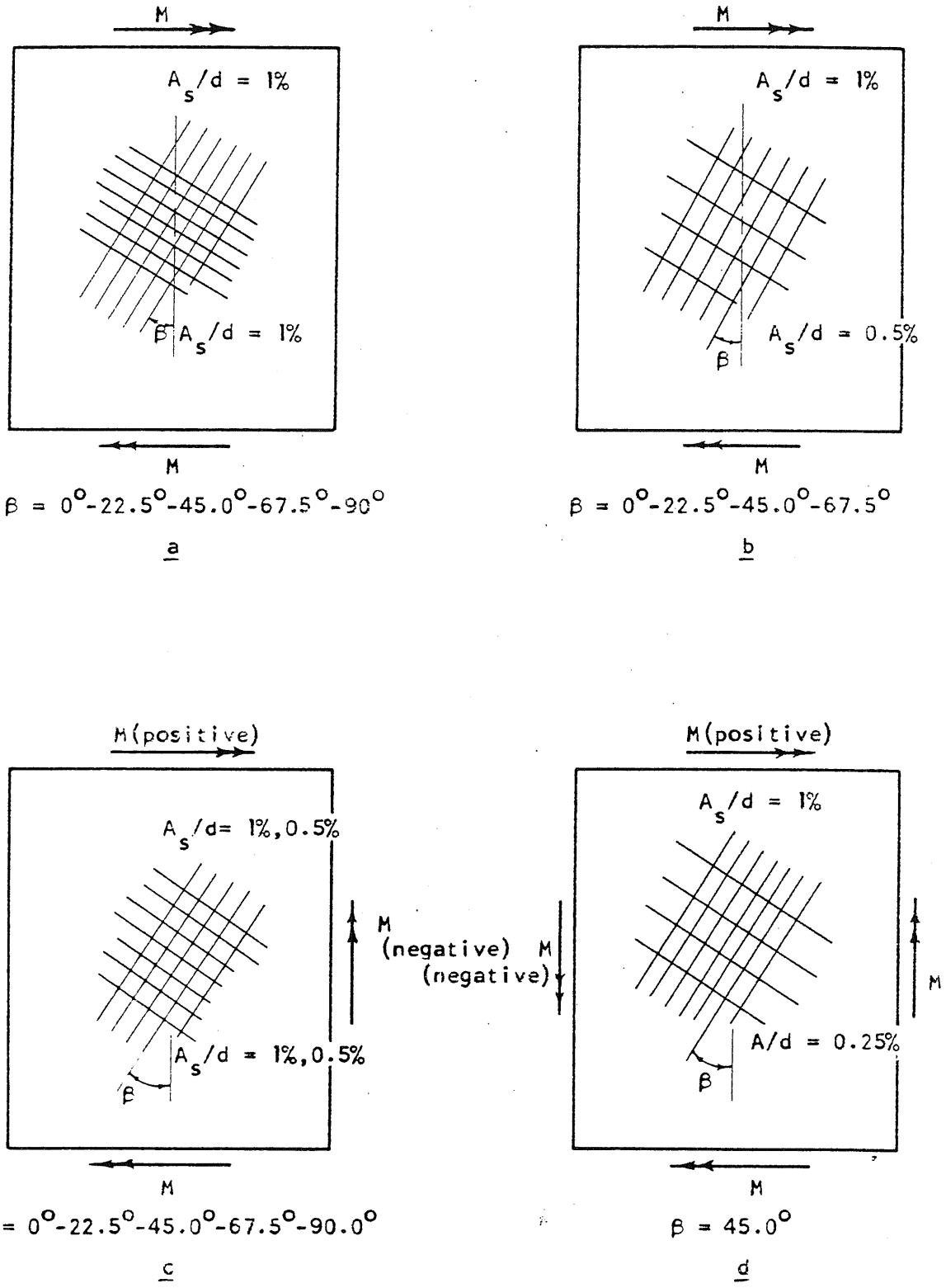

FIG. 4.21 ORIENTATION OF THE REINFORCEMENT

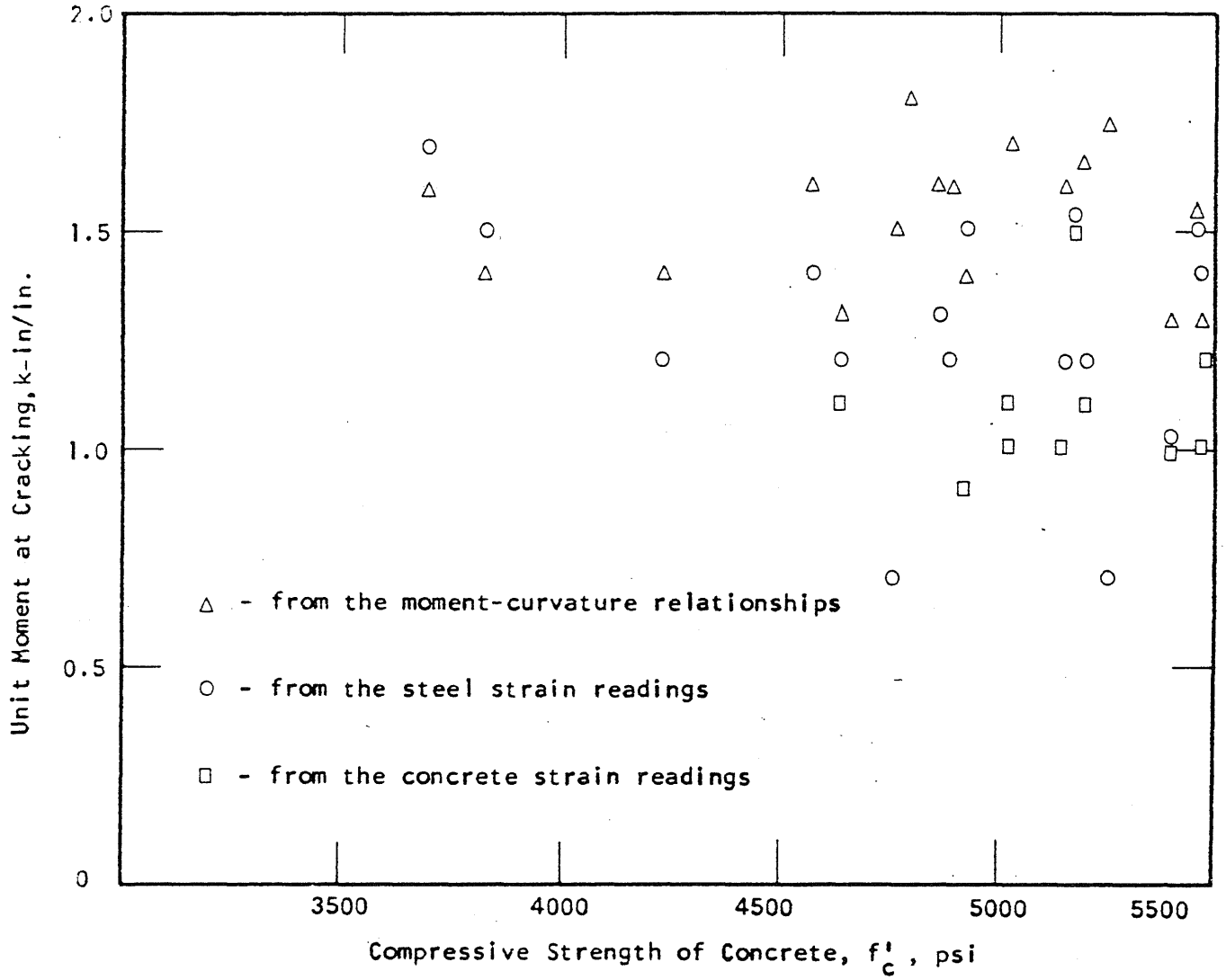

FIG. 4.22 MOMENT AT CRACKING

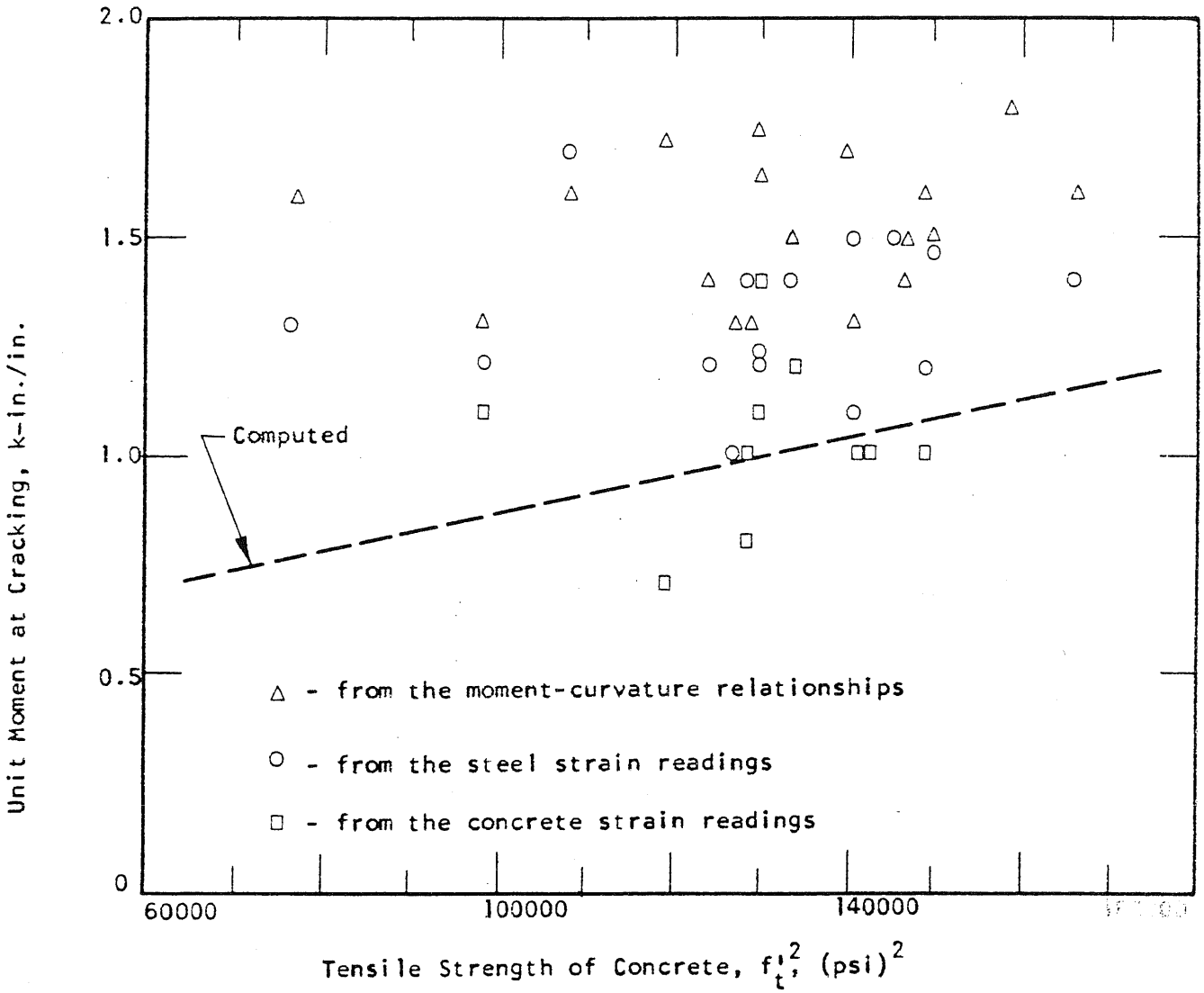

FIG. 4.23 MOMENT AT CRACKING

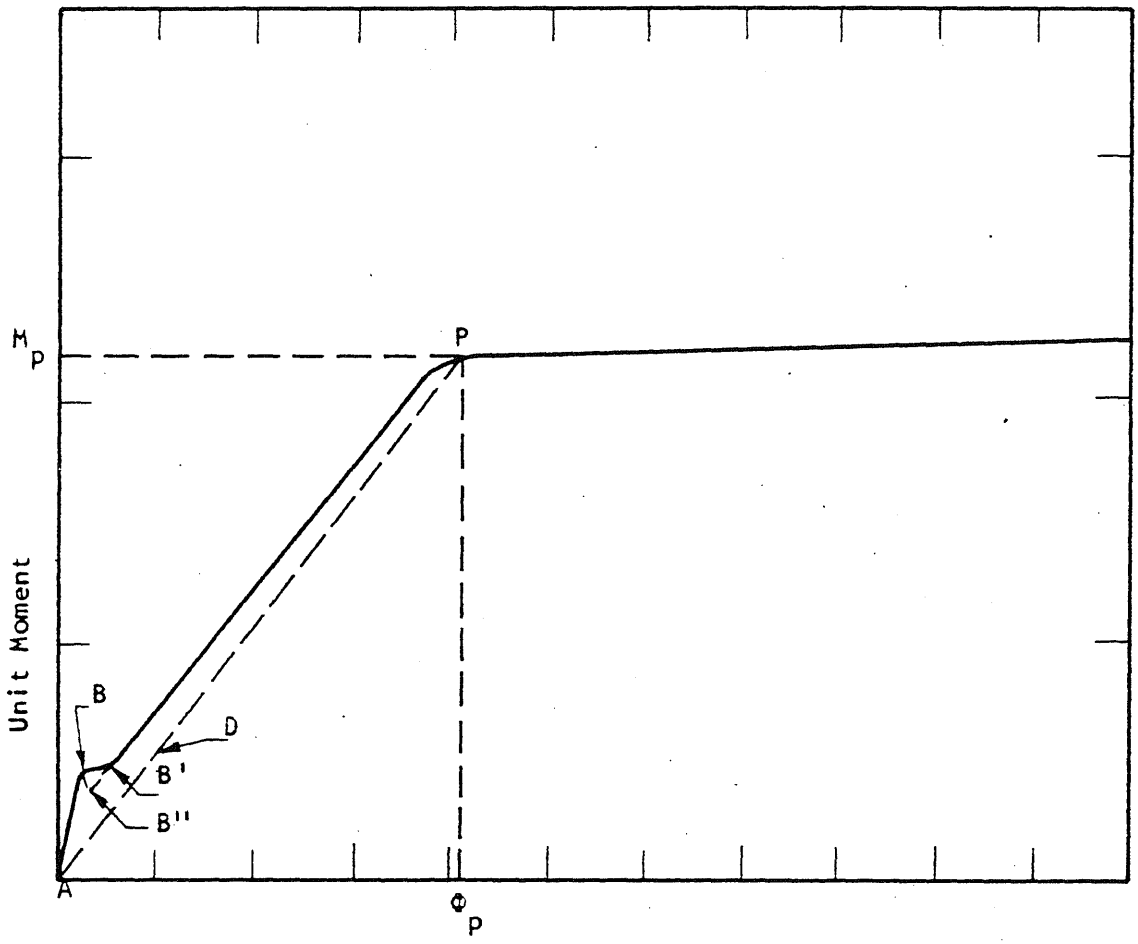

FIG. 4.24 MOMENT-CURVATURE RELATIONSHIP

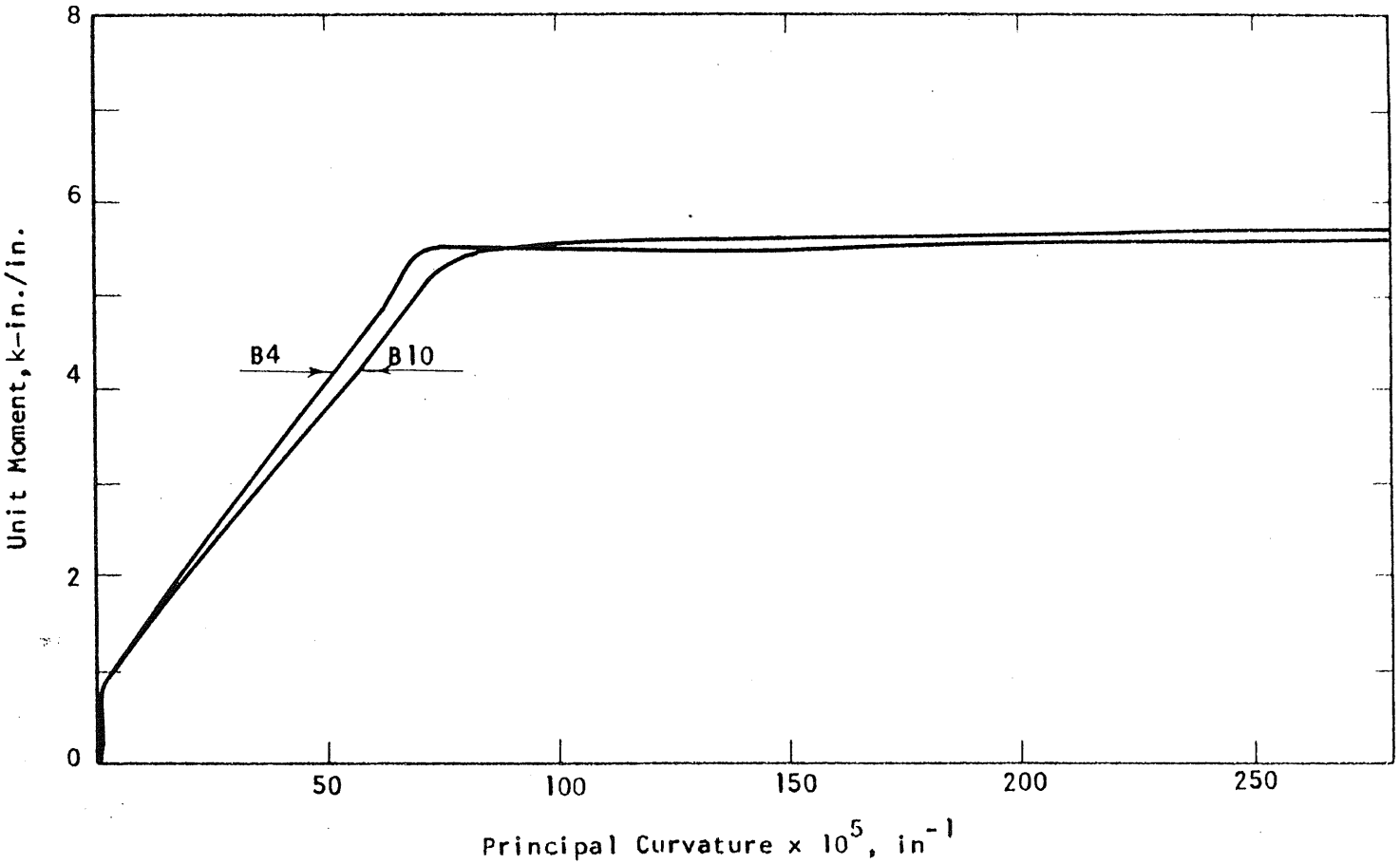

FIG. 4.25 MOMENT-CURVATURE RELATIONSHIPS FOR TEST SPECIMENS B4 AND B10

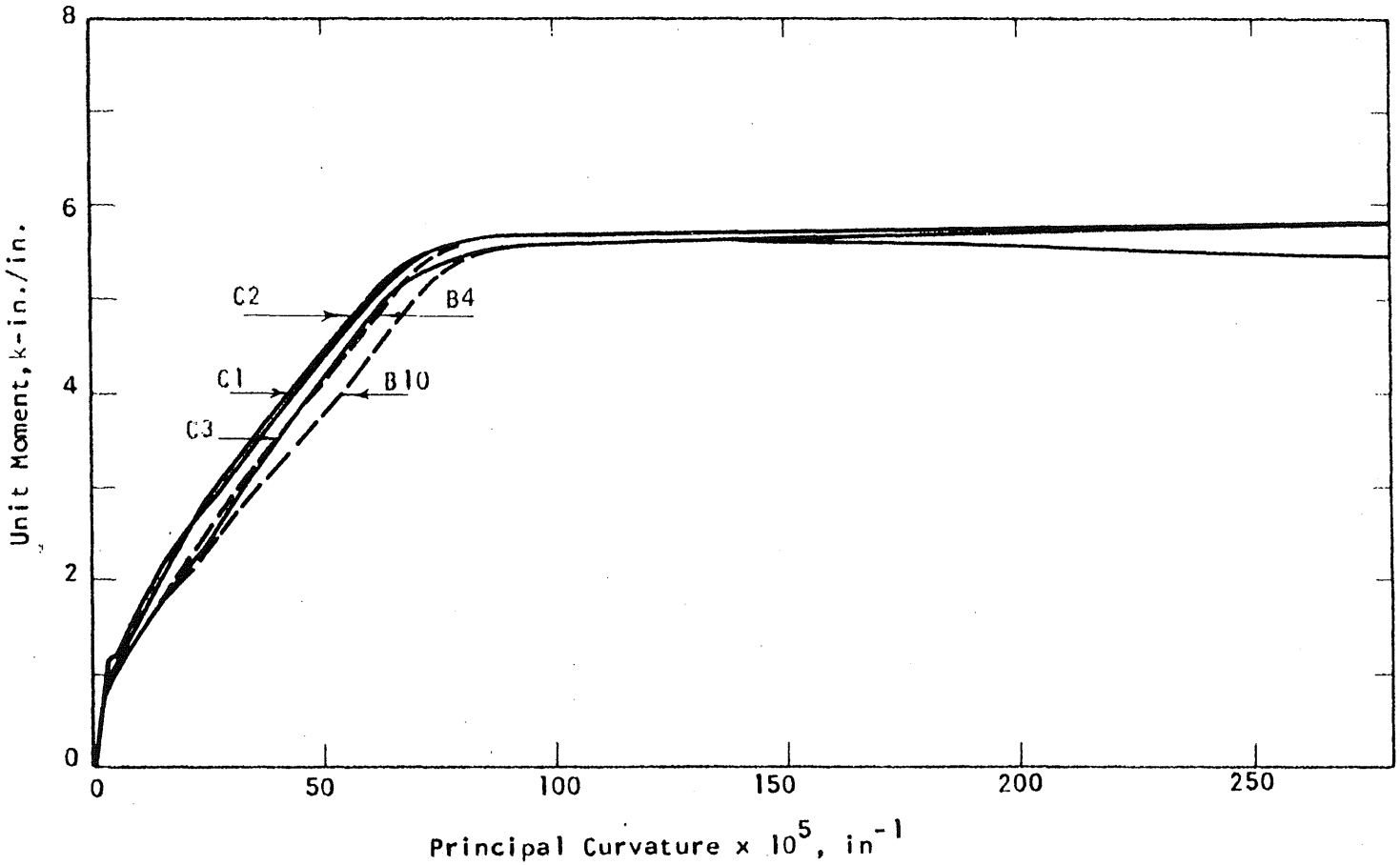

FIG. 4.26 MOMENT-CURVATURE RELATIONSHIPS FOR TEST SPECIMENS UNDER ISOSTATIC MOMENT

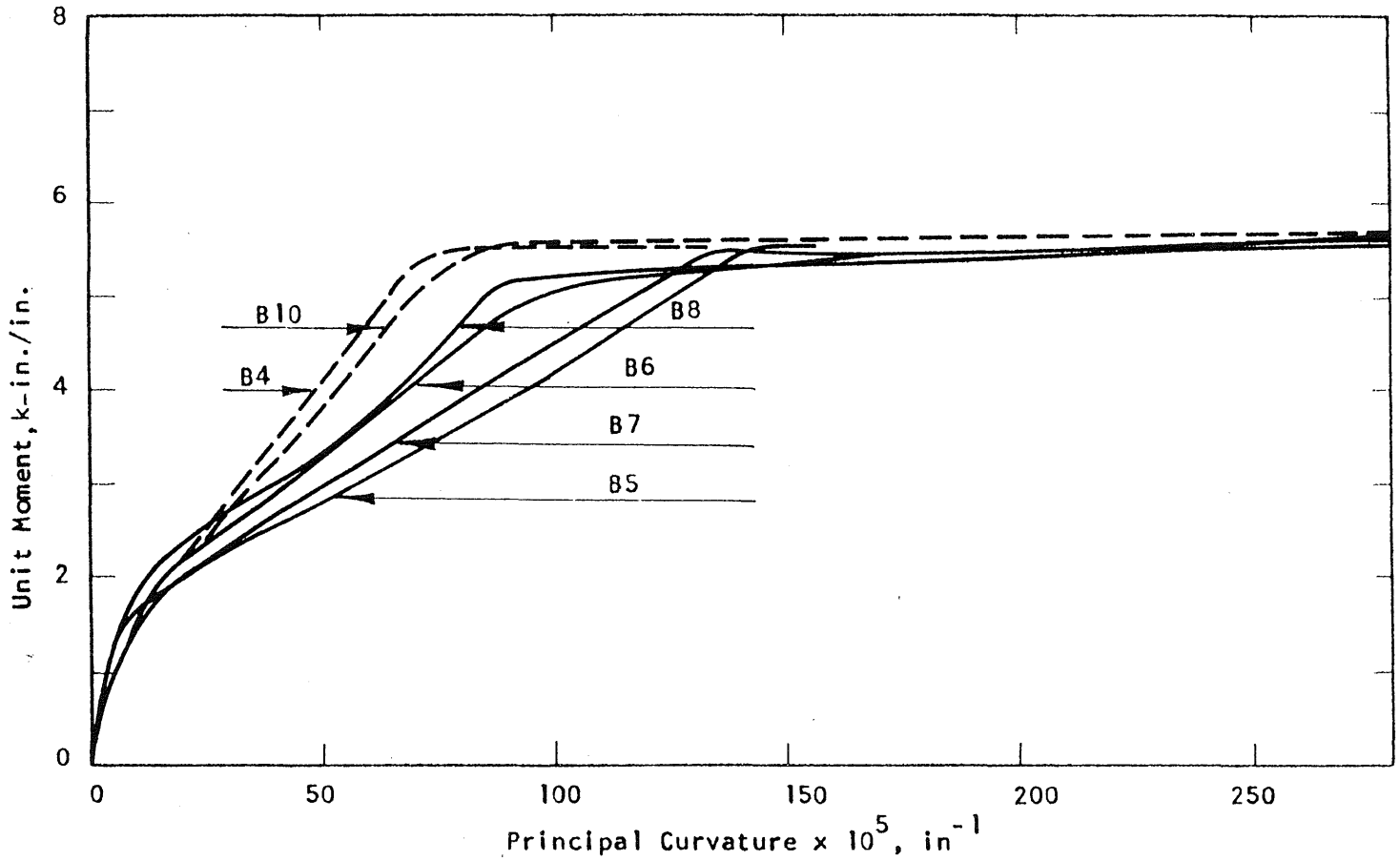

FIG. 4.27 MOMENT-CURVATURE RELATIONSHIPS FOR TEST SPECIMENS UNDER UNIAXIAL MOMENT

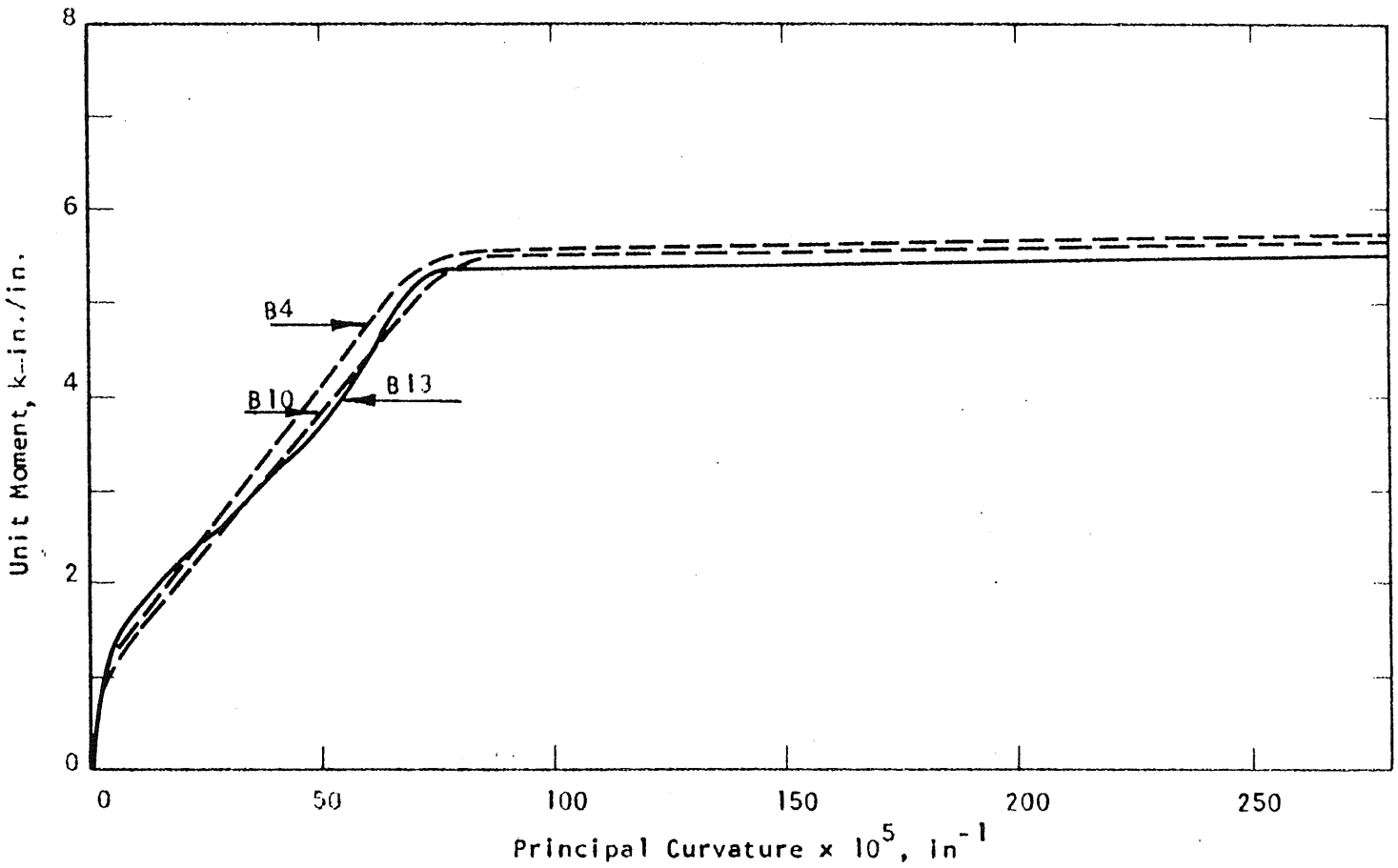

FIG. 4.28 MOMENT-CURVATURE RELATIONSHIP FOR TEST SPECIMEN B13

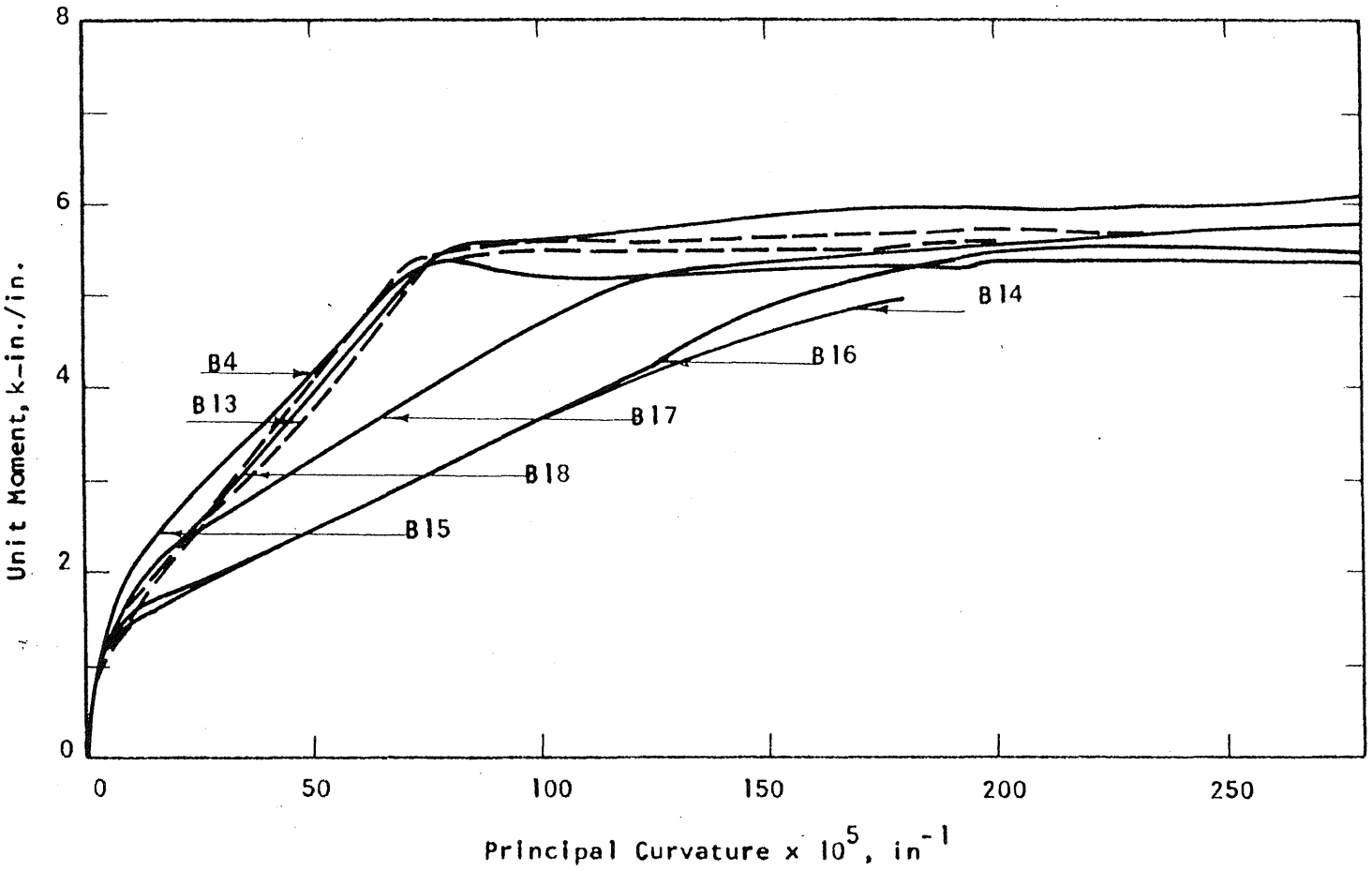

FIG. 4.29 MOMENT-CURVATURE RELATIONSHIPS FOR SPECIMENS SUBJECTED TO PURE TORSION

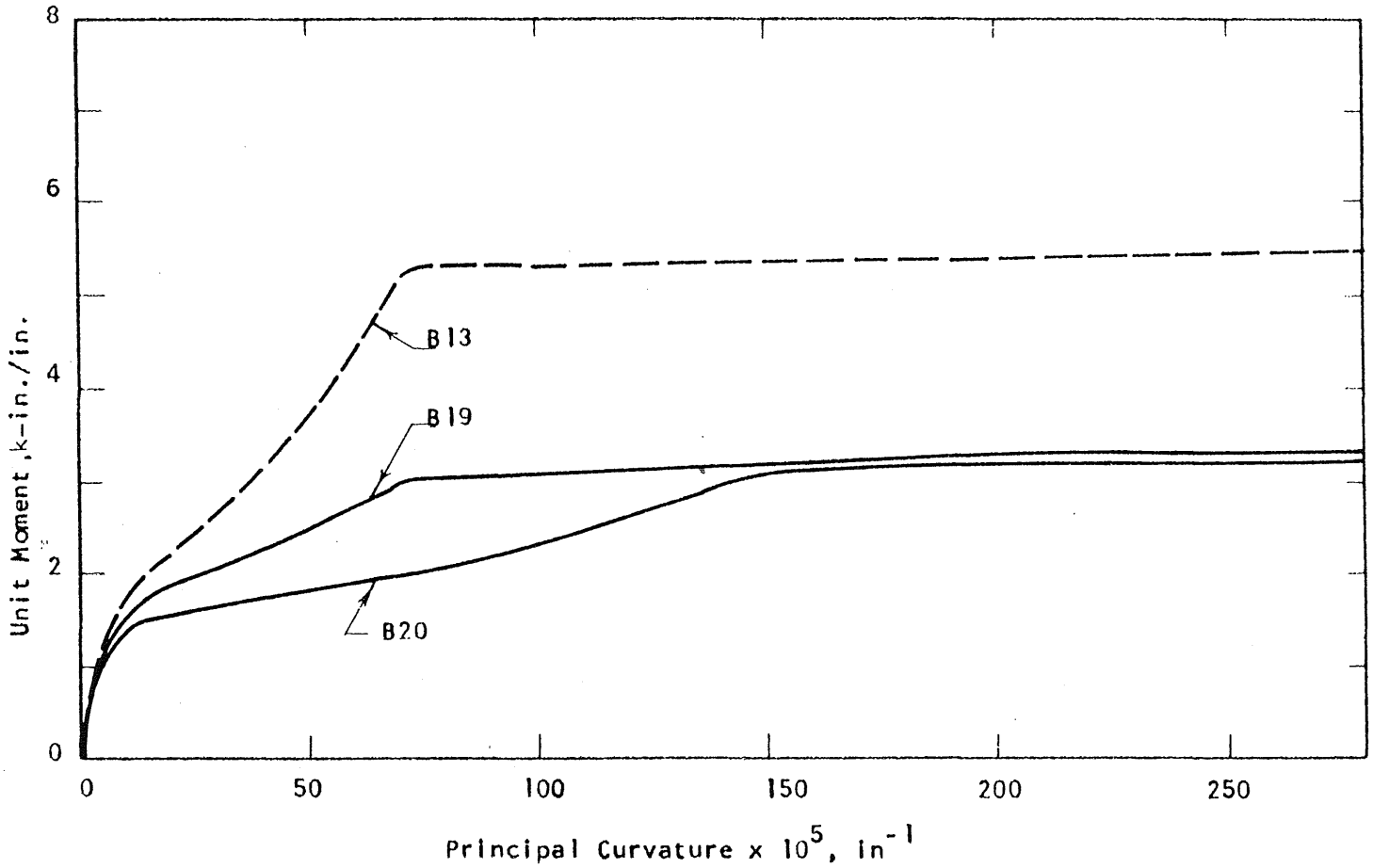

FIG. 4.30 MOMENT-CURVATURE RELATIONSHIP FOR SPECIMENS SUBJECTED TO PURE TORSION

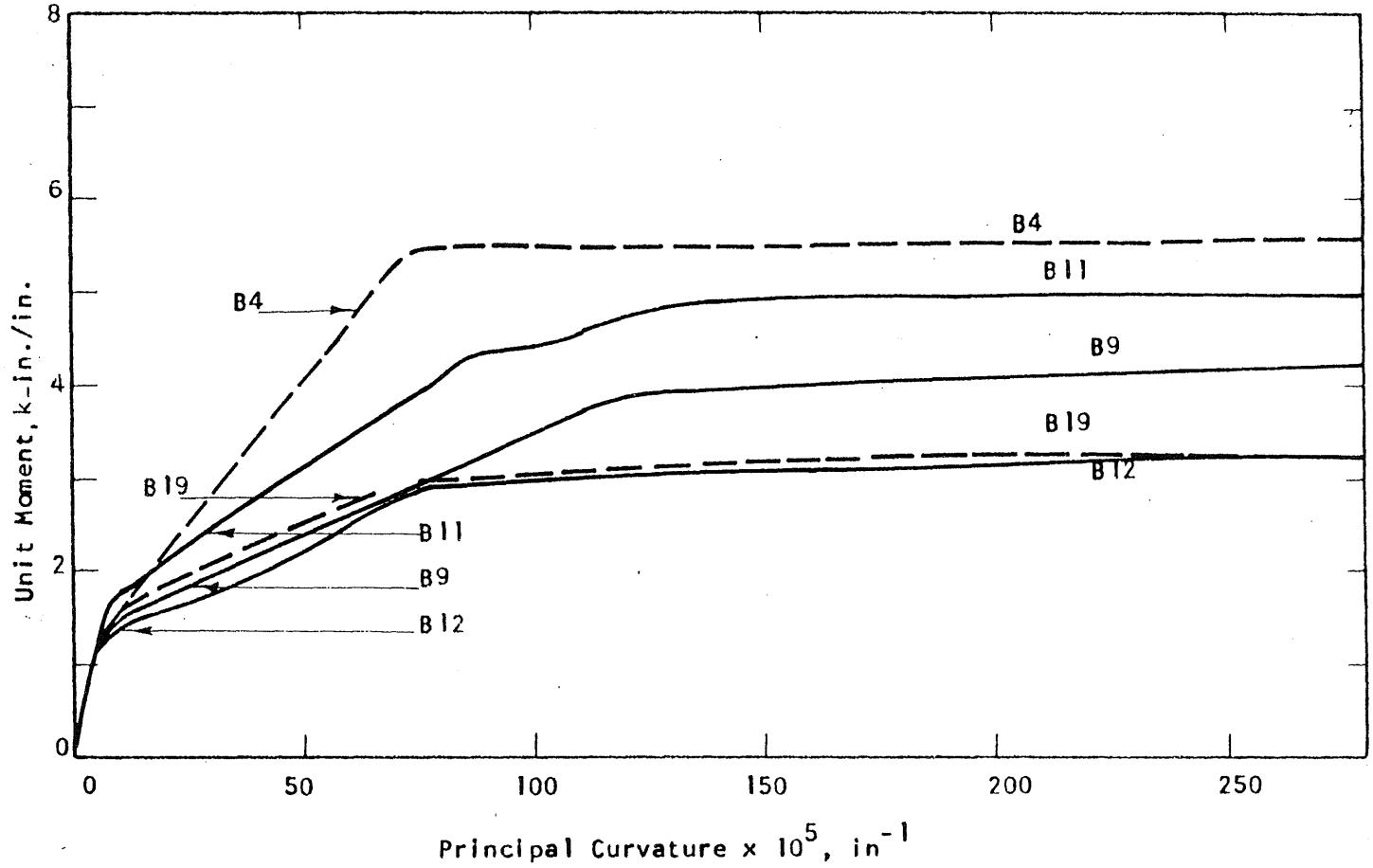

FIG. 4.31 MOMENT-CURVATURE RELATIONSHIPS FOR SPECIMENS SUBJECTED TO UNIAXIAL MOMENT

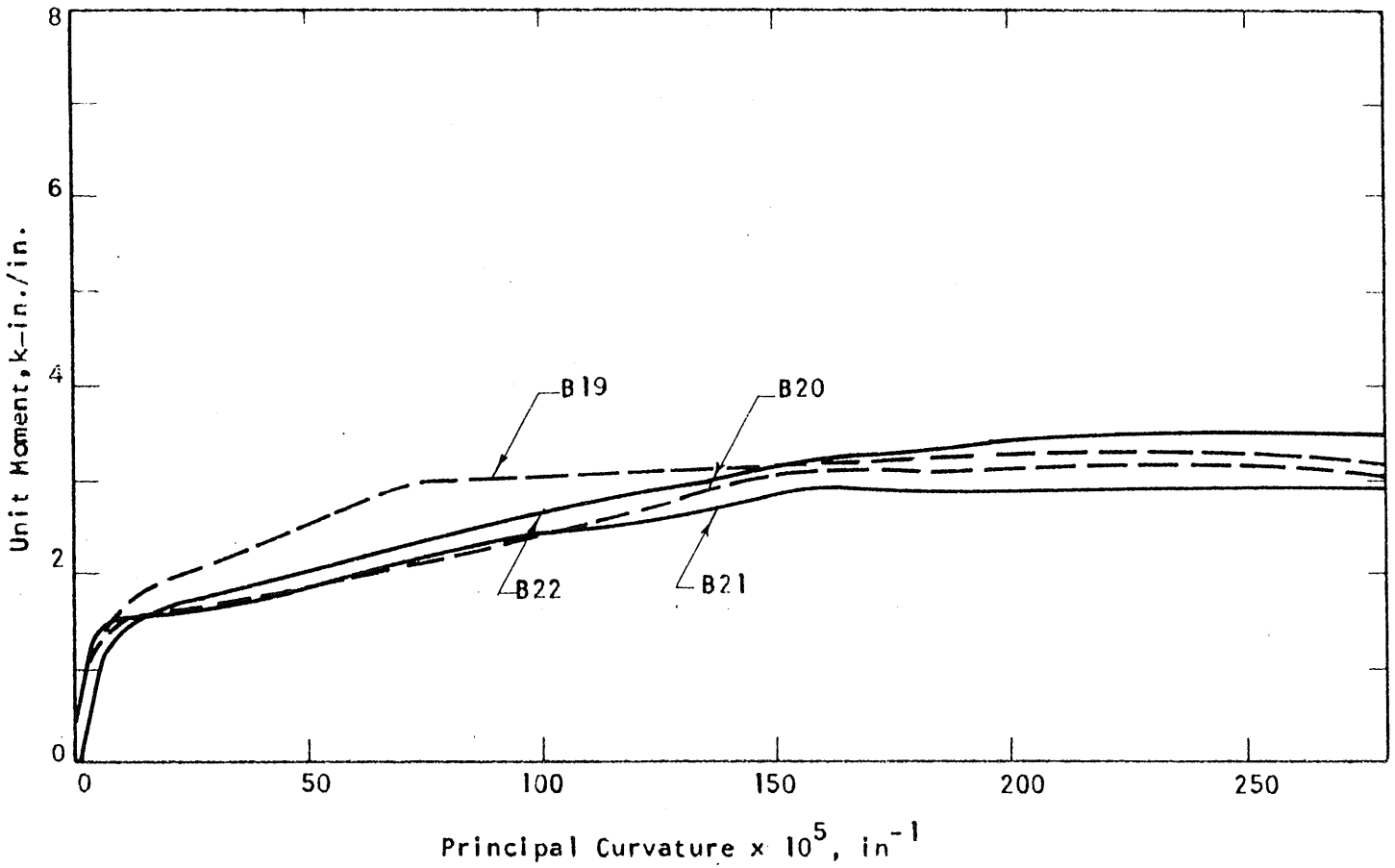

FIG. 4.32 MOMENT-CURVATURE RELATIONSHIPS FOR SPECIMENS SUBJECTED TO PURE TORSION

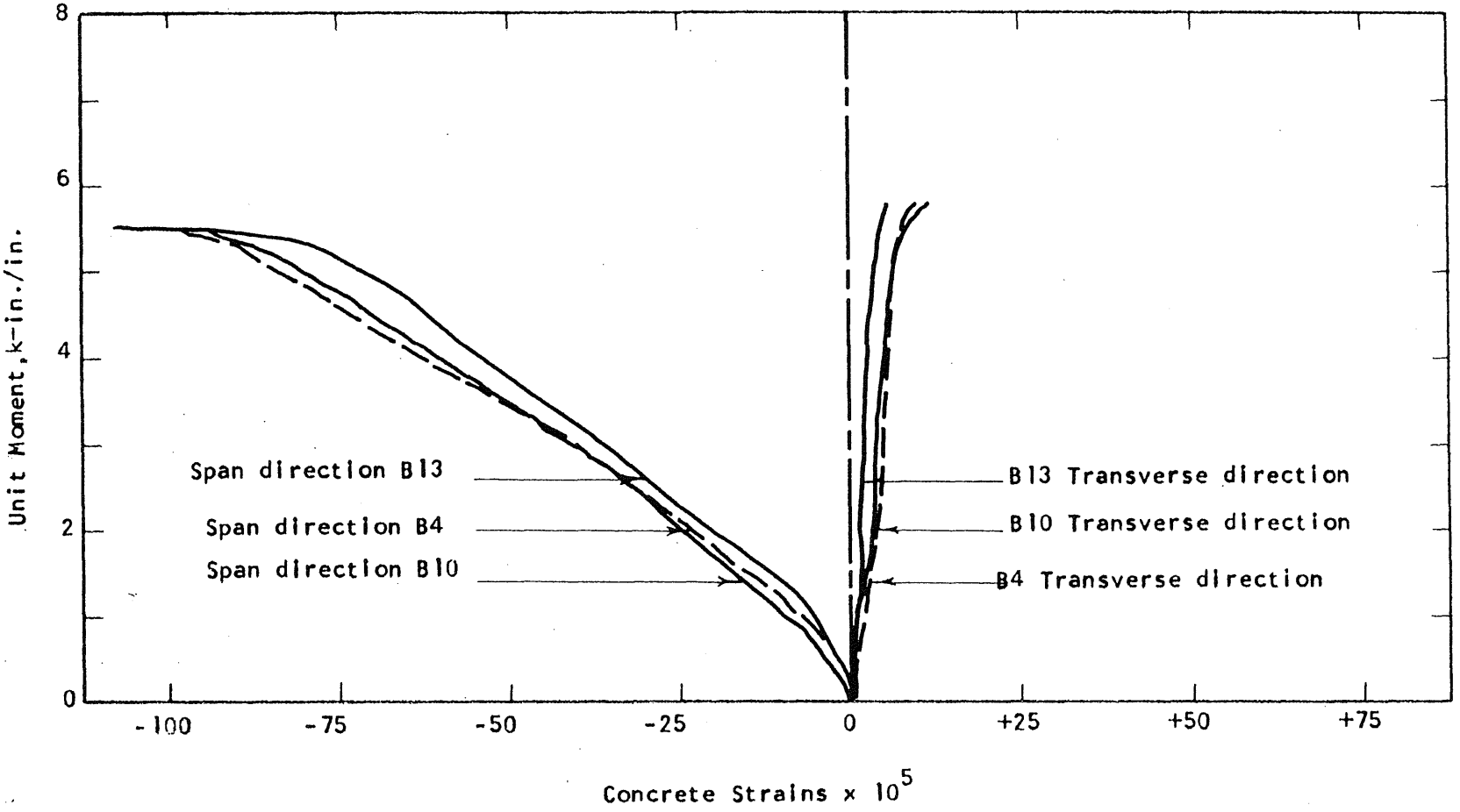

FIG. 4.33 STRAINS ON THE COMPRESSION SIDE OF SPECIMENS SUBJECTED TO UNIAXIAL BENDING

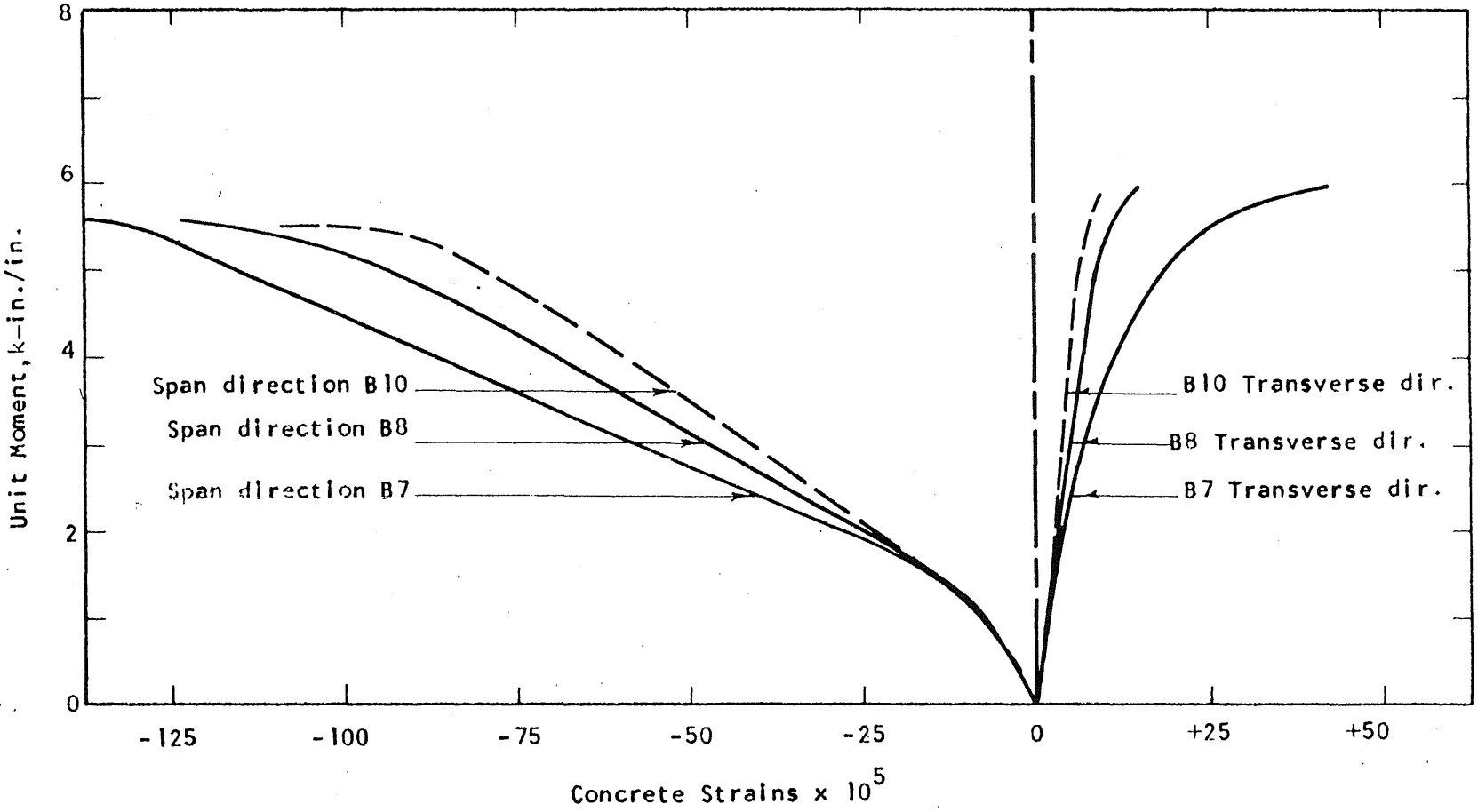

FIG. 4.34 STRAINS ON THE COMPRESSION SIDE OF SPECIMENS SUBJECTED TO UNIAXIAL BENDING

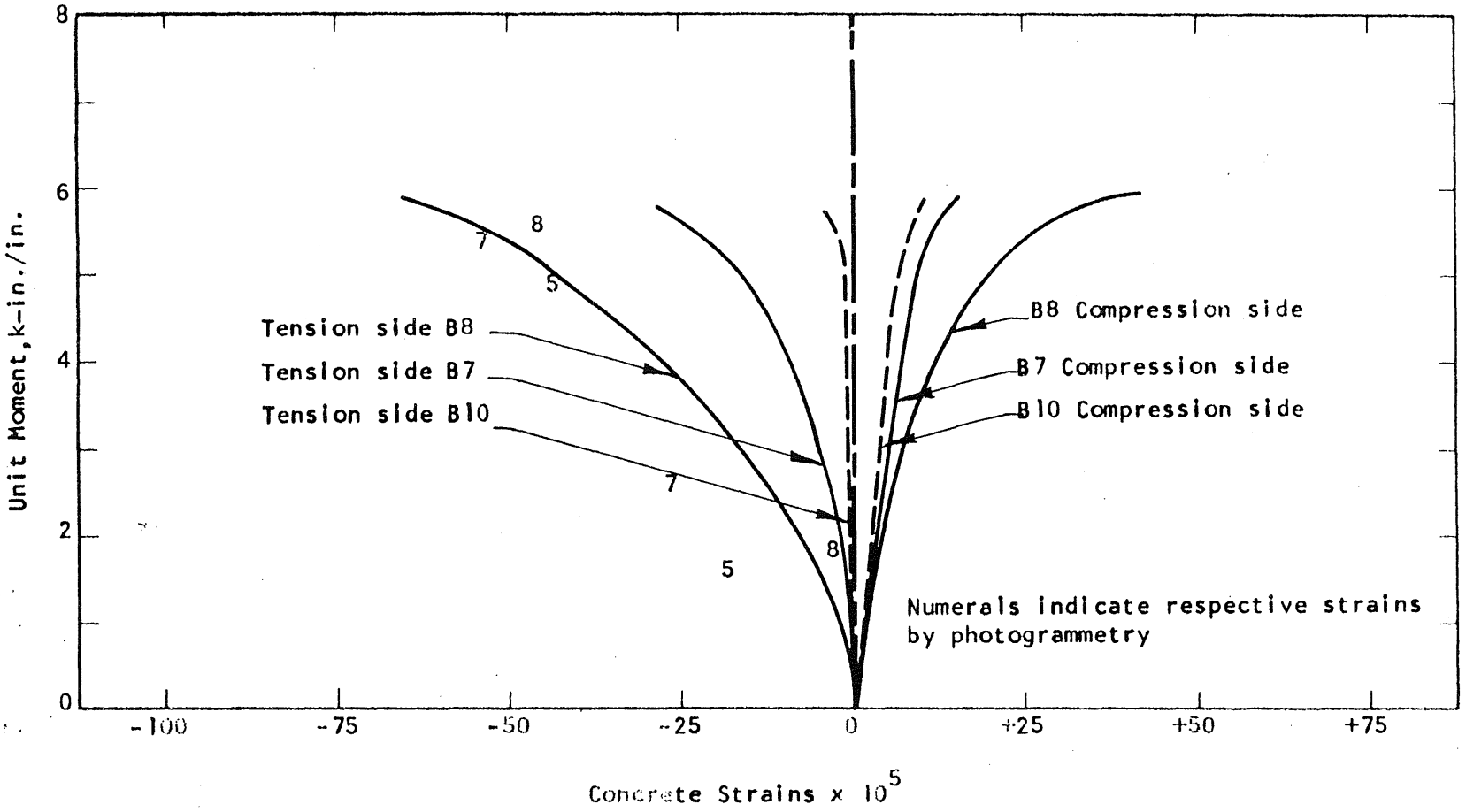

FIG. 4.35 TRANSVERSE STRAINS ON THE SURFACES OF SPECIMENS SUBJECTED TO UNIAXIAL BENDING

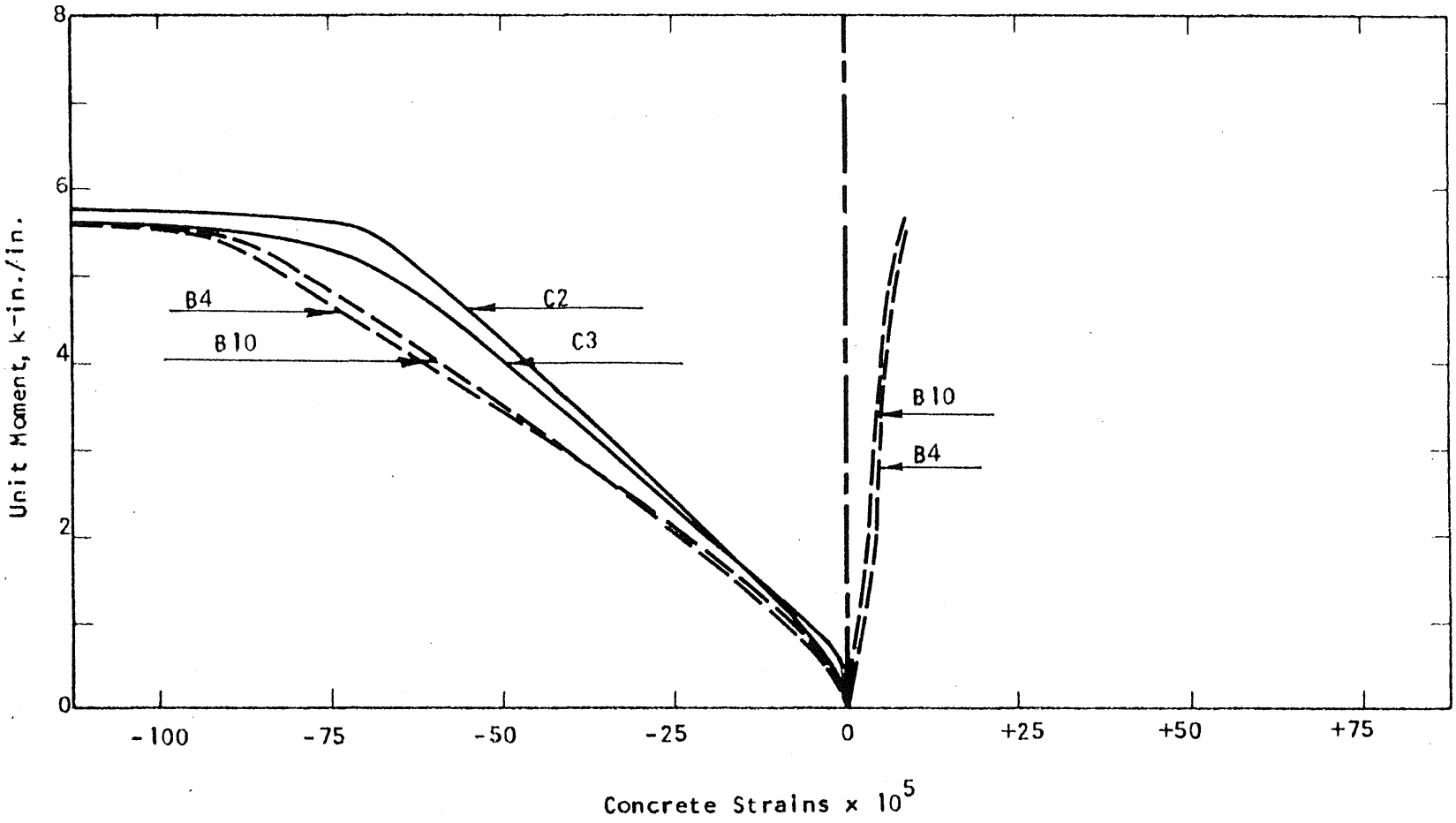

FIG. 4.36 STRAINS ON THE COMPRESSION SIDE OF SPECIMENS SUBJECTED TO ISOSTATIC MOMENT

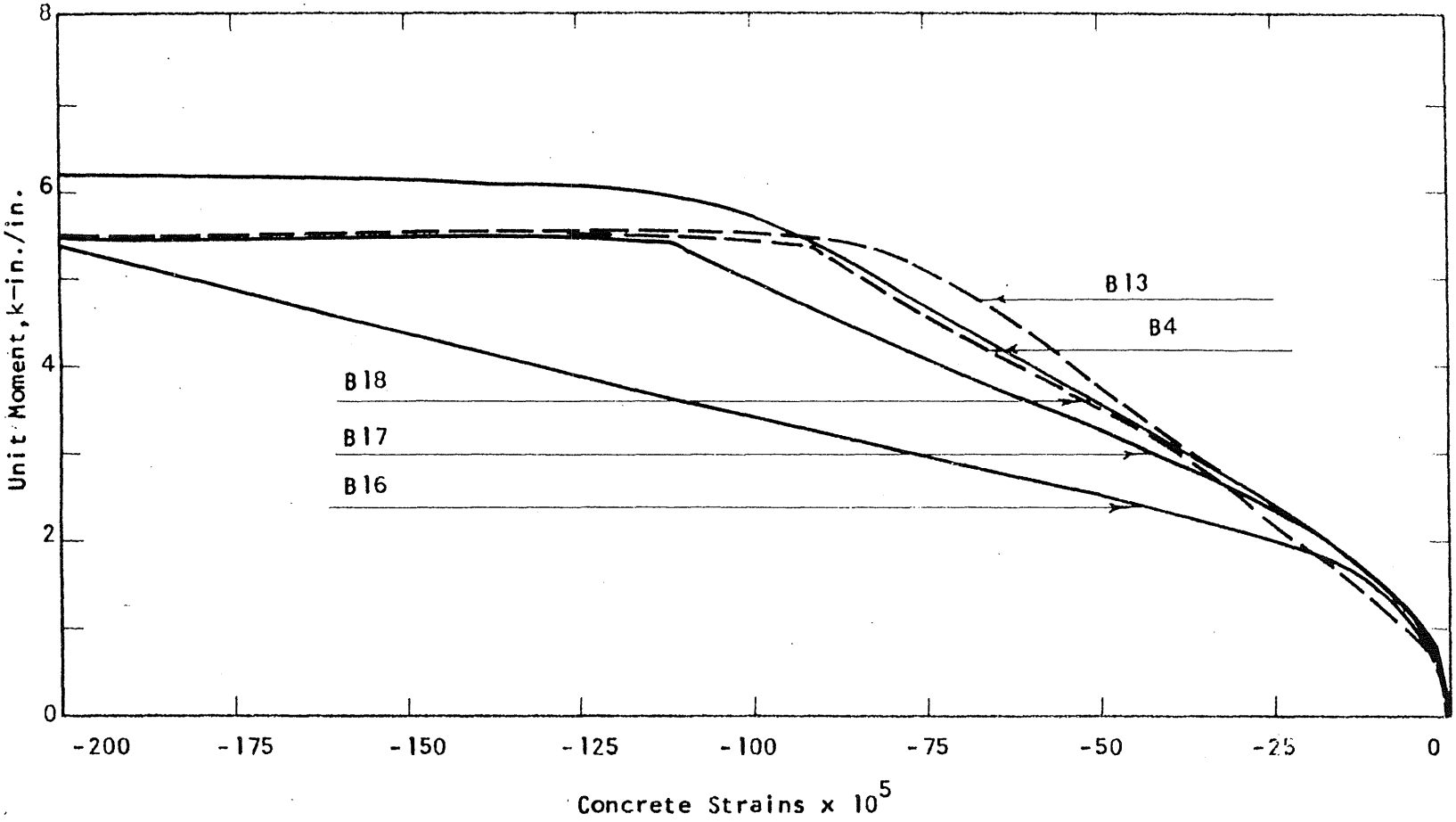

FIG. 4.37 COMPRESSIVE STRAINS IN THE DIRECTION OF A PRINCIPAL MOMENT IN SPECIMENS SUBJECTED TO PURE TORSION

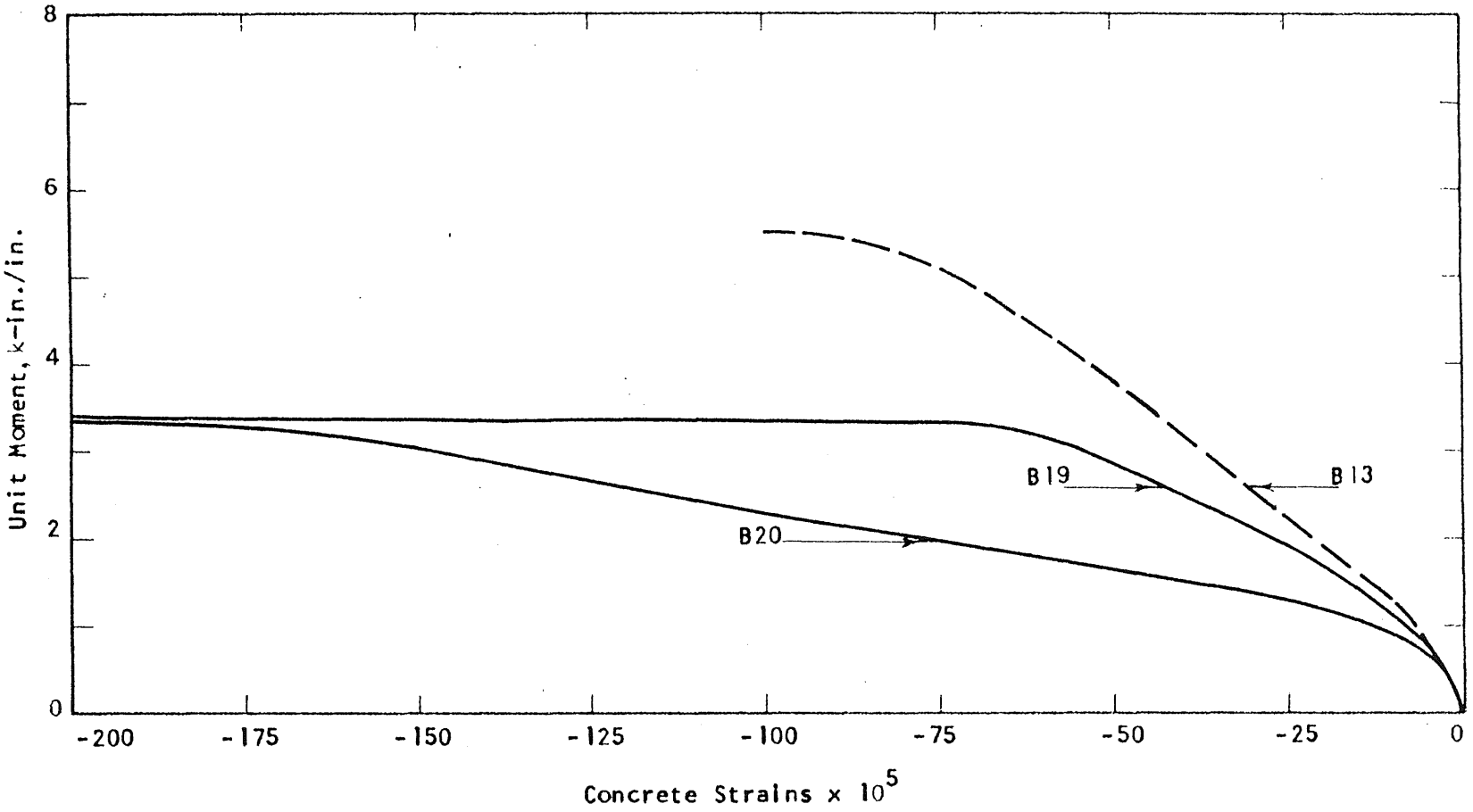

FIG. 4.38 COMPRESSIVE STRAINS IN THE DIRECTION OF A PRINCIPAL MOMENT IN SPECIMENS SUBJECTED TO PURE TORSION

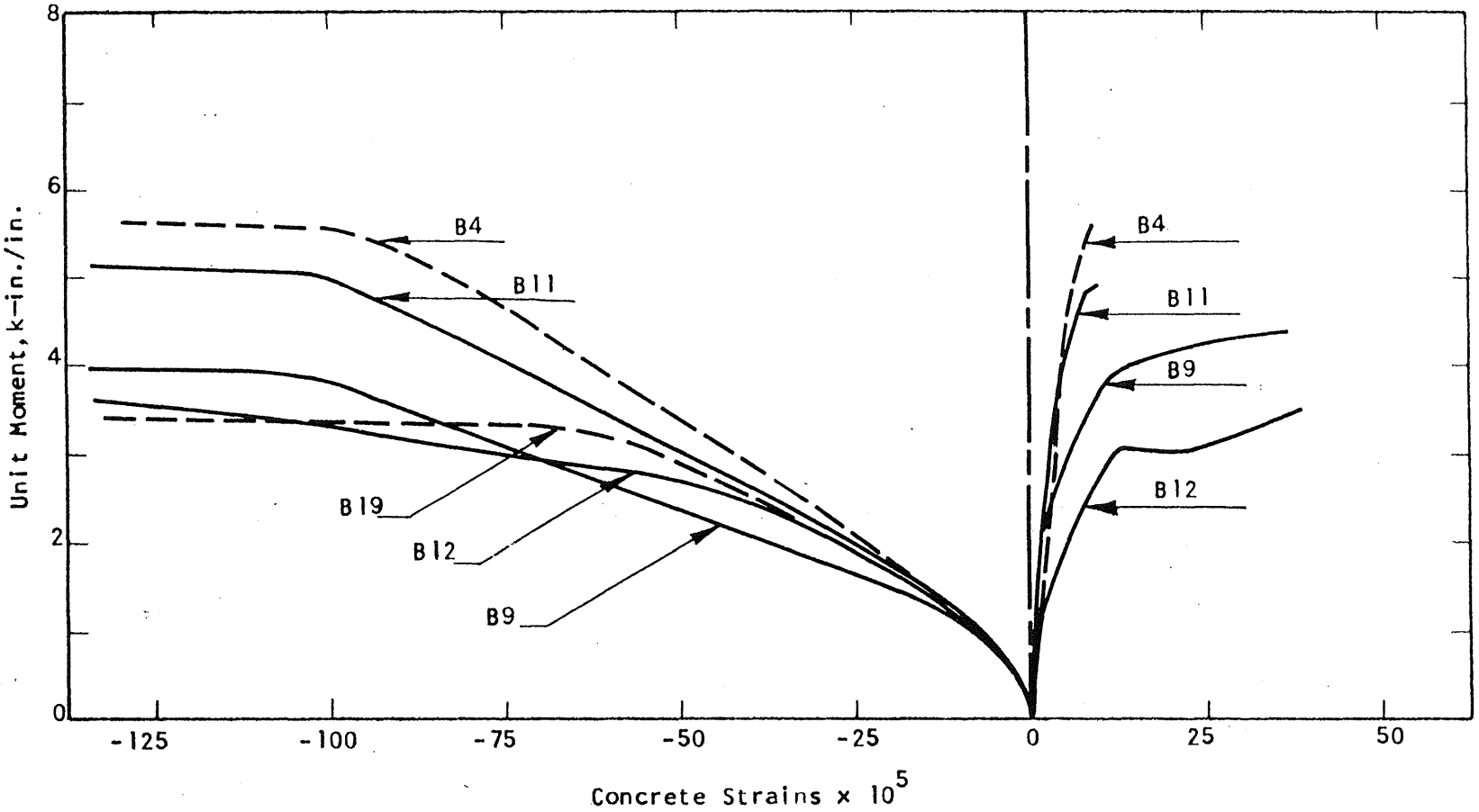

FIG. 4.39 STRAINS ON THE COMPRESSION SIDE OF SPECIMENS SUBJECTED TO UNIAXIAL MOMENT

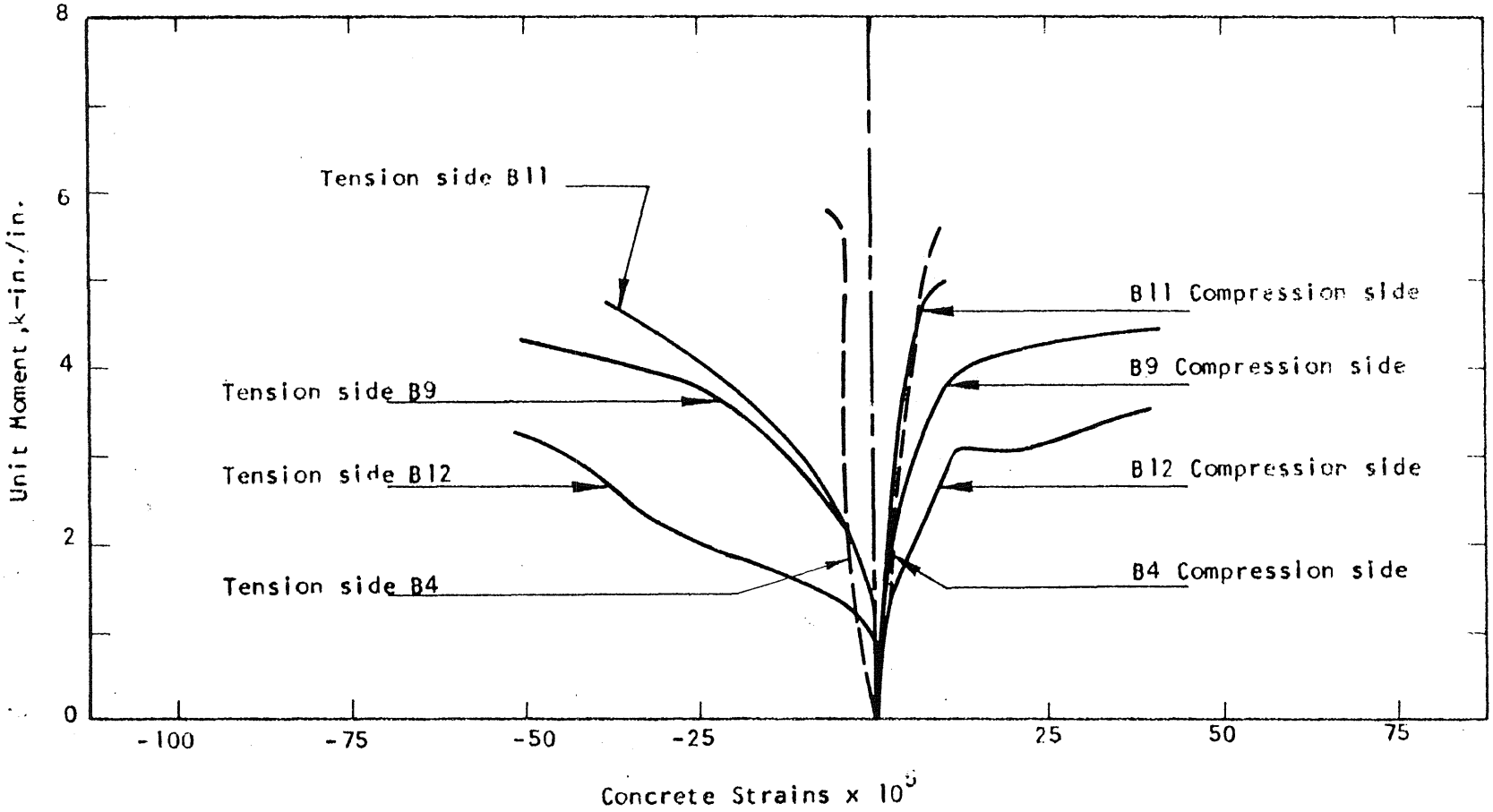

FIG. 4.40 TRANSVERSE STRAINS ON THE SURFACES OF SPECIMENS SUBJECTED TO UNIAXIAL BENDING

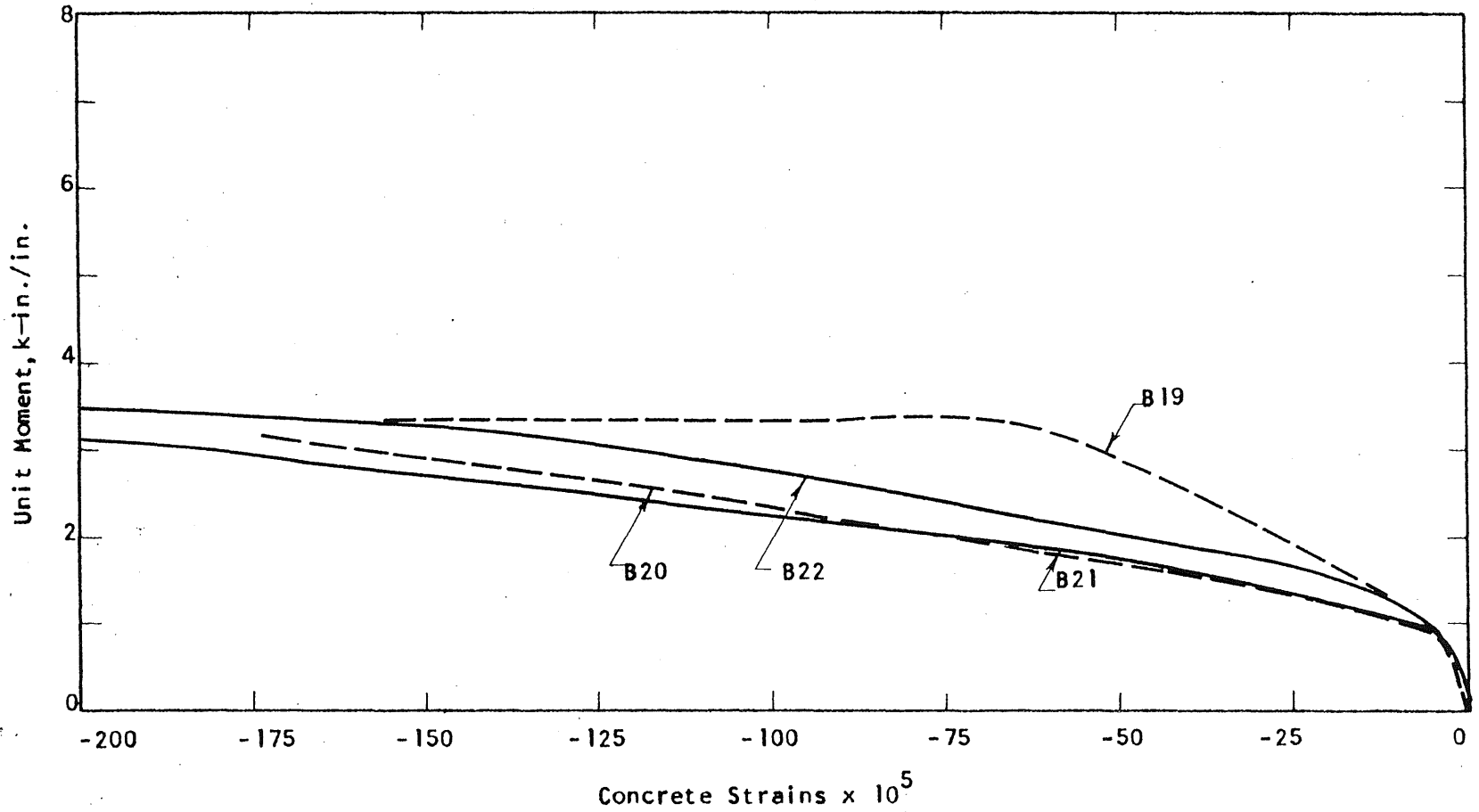

FIG. 4.41 COMPRESSIVE STRAINS IN THE DIRECTION OF A PRINCIPAL CURVATURE IN SPECIMENS SUBJECTED TO PURE TORSION

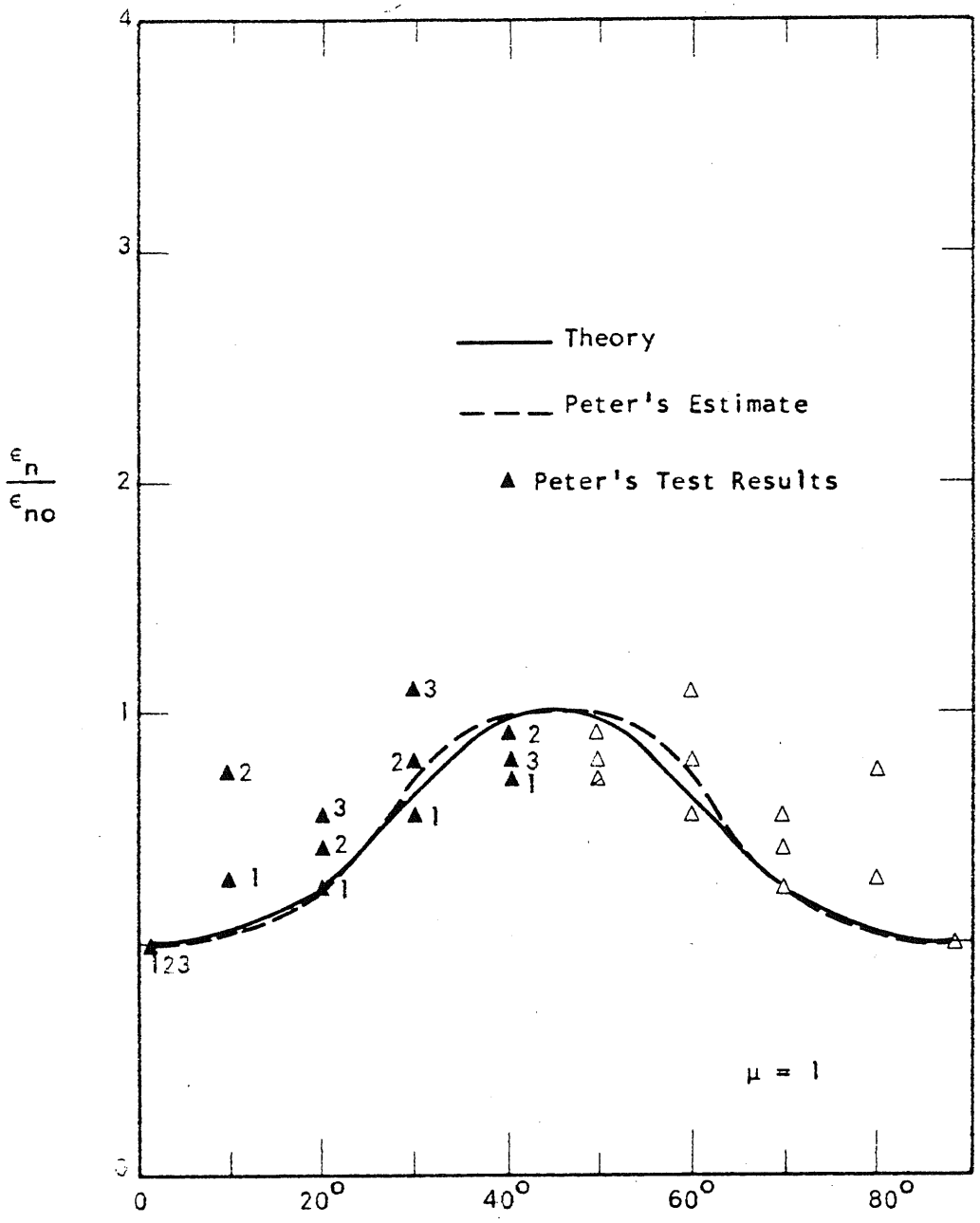

FIG. 4.42 ELONGATION OF AN ISOTROPICALLY REINFORCED ELEMENT SUBJECTED TO IN-PLANE FORCES

Note: Numerals in the figure indicate loading stages for a given specimen with a specific value of α. Hollow triangles are symmetrical counterparts of the solid ones.

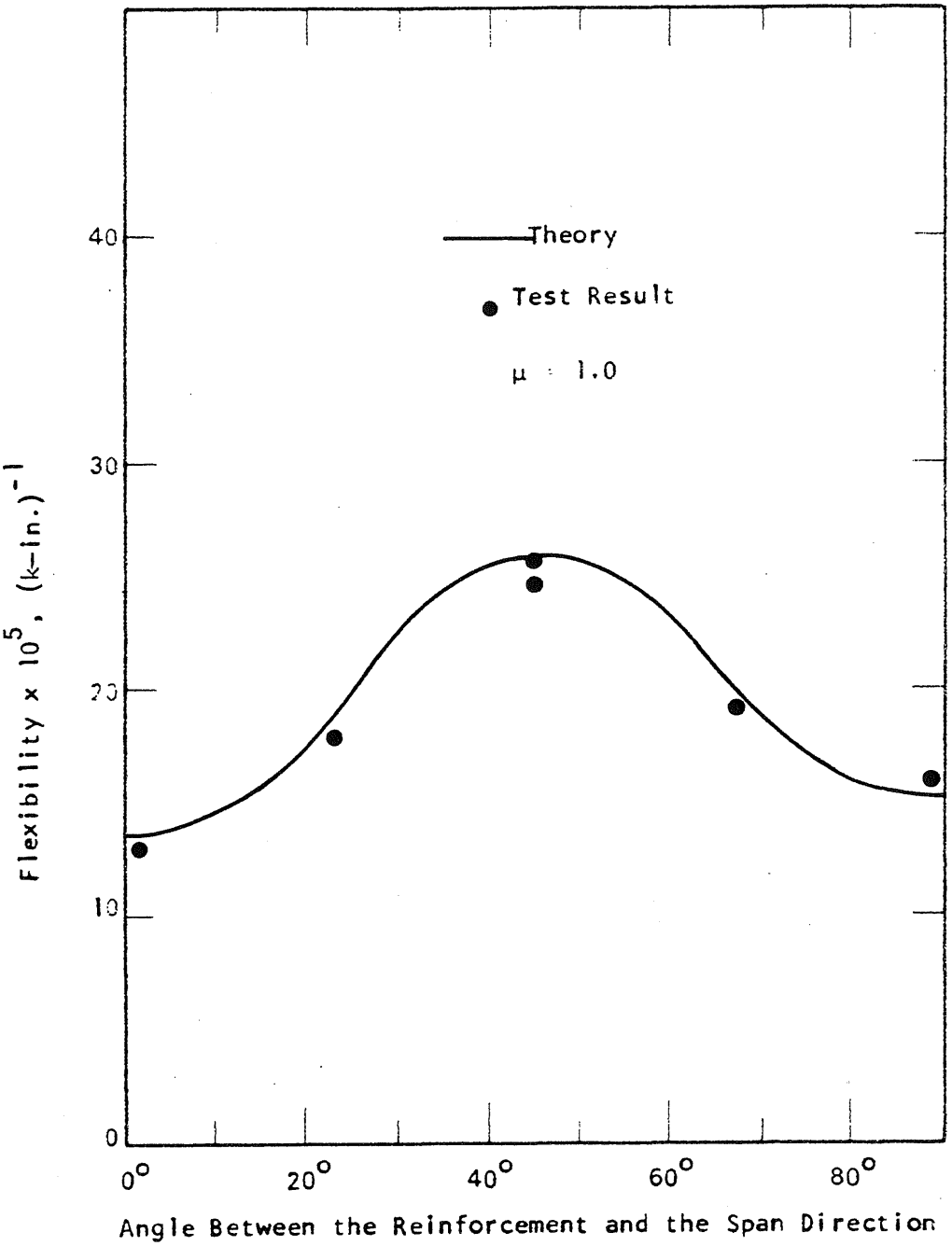

FIG. 4.43 FLEXIBILITY OF AN ISOTROPICALLY REINFORCED ELEMENT SUBJECTED TO UNIAXIAL MOMENT

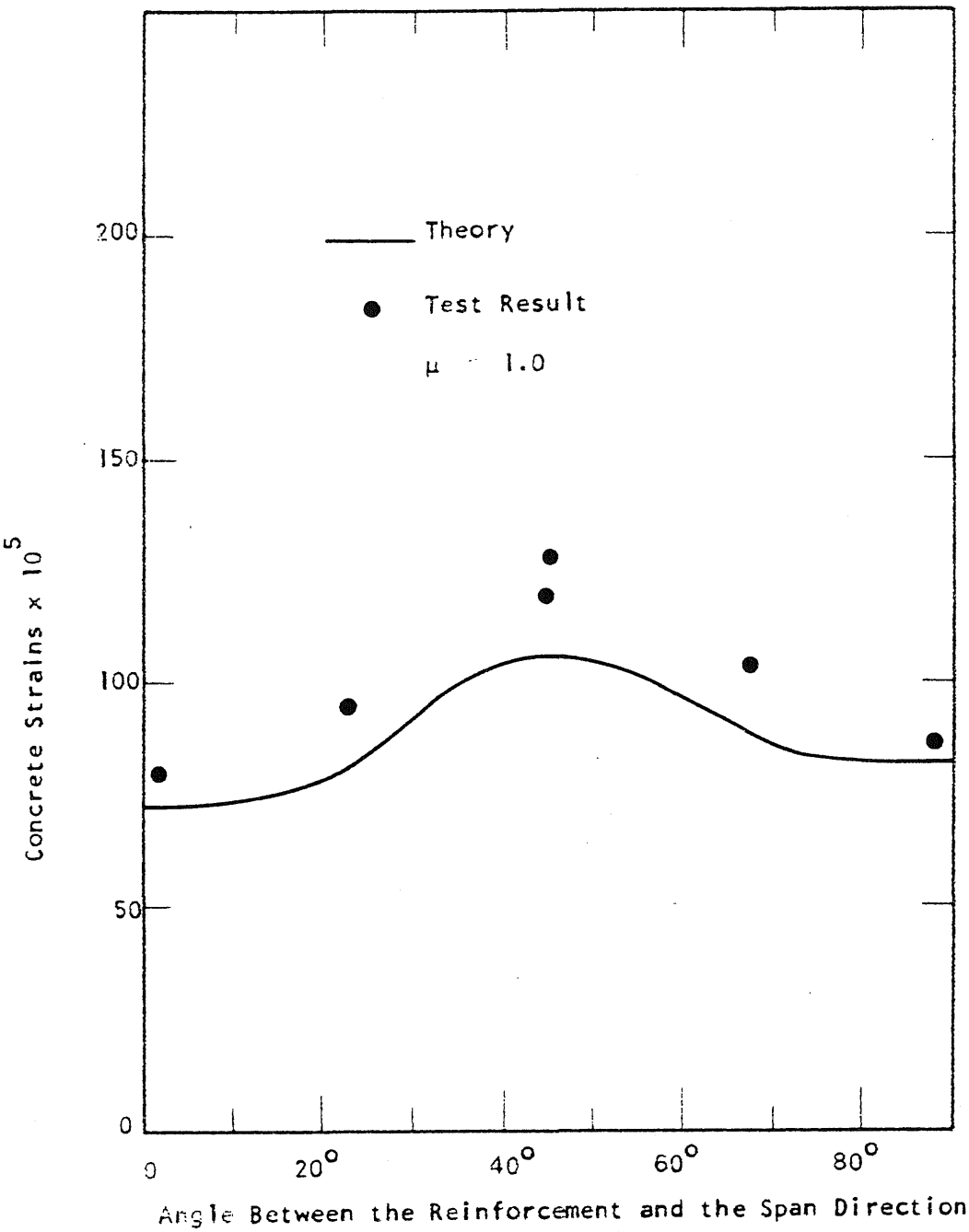

FIG. 4.44 CONCRETE STRAINS AT YIELDING IN A ISOTROPICALLY REINFORCED ELEMENT SUBJECTED TO UNIAXIAL ELEMENT

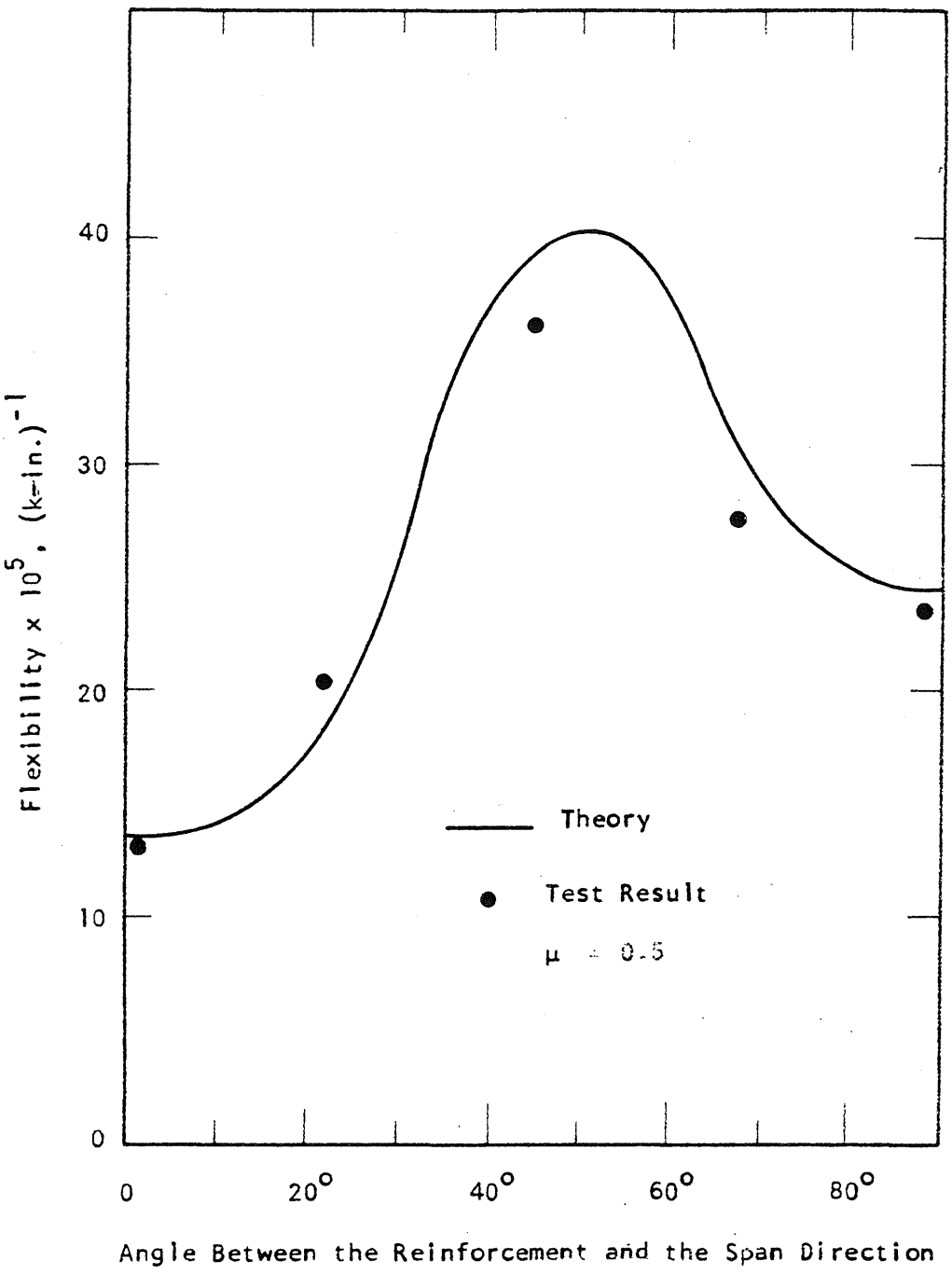

FIG. 4.45 FLEXIBILITY OF AN NONISOTROPICALLY REINFORCED ELEMENT SUBJECTED TO UNIAXIAL MOMENT

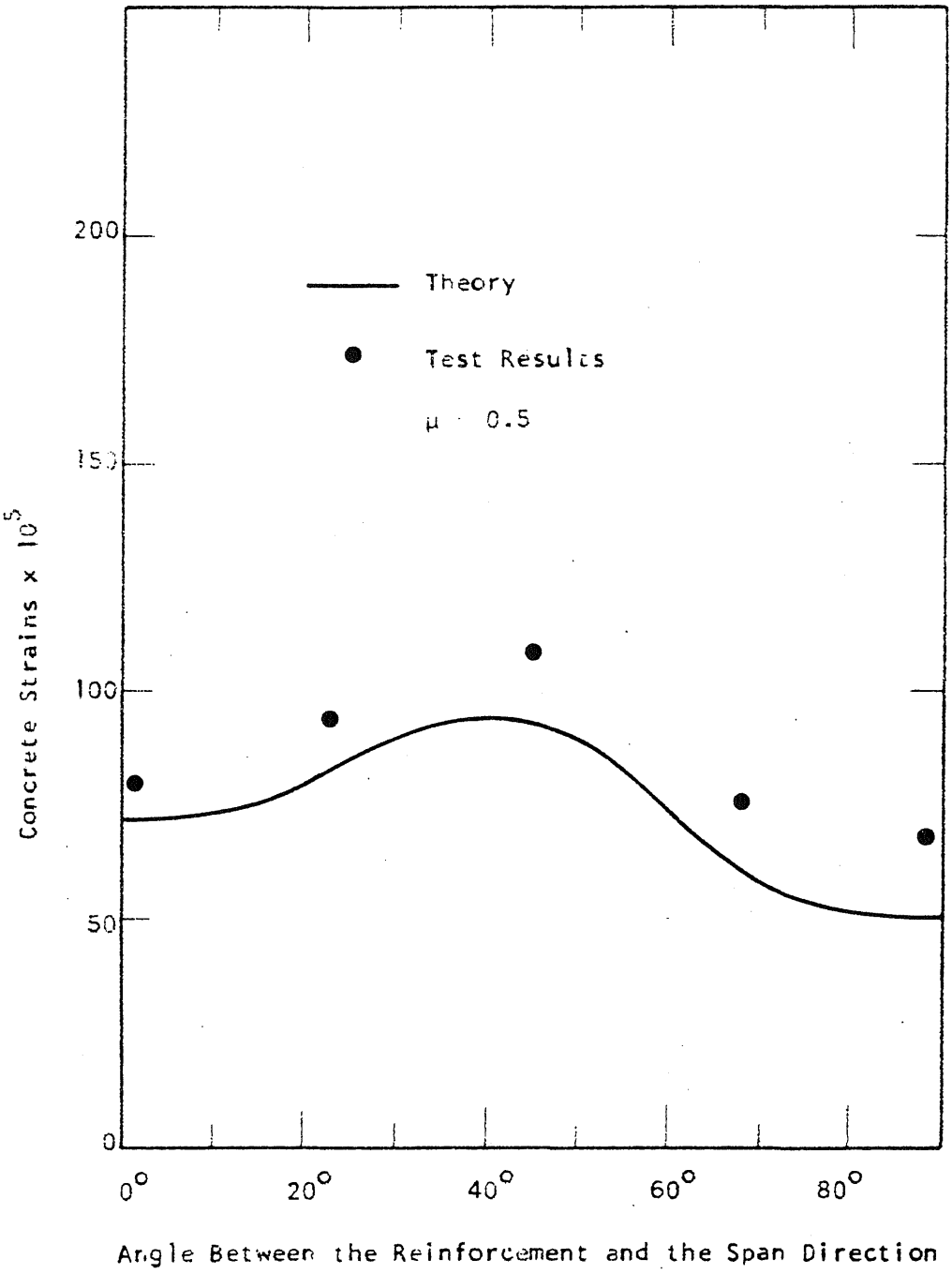

FIG. 4.46 CONCRETE STRAINS AT YIELDING IN AN ISOTROPICALLY REINFORCED ELEMENT SUBJECTED TO UNIAXIAL MOMENT

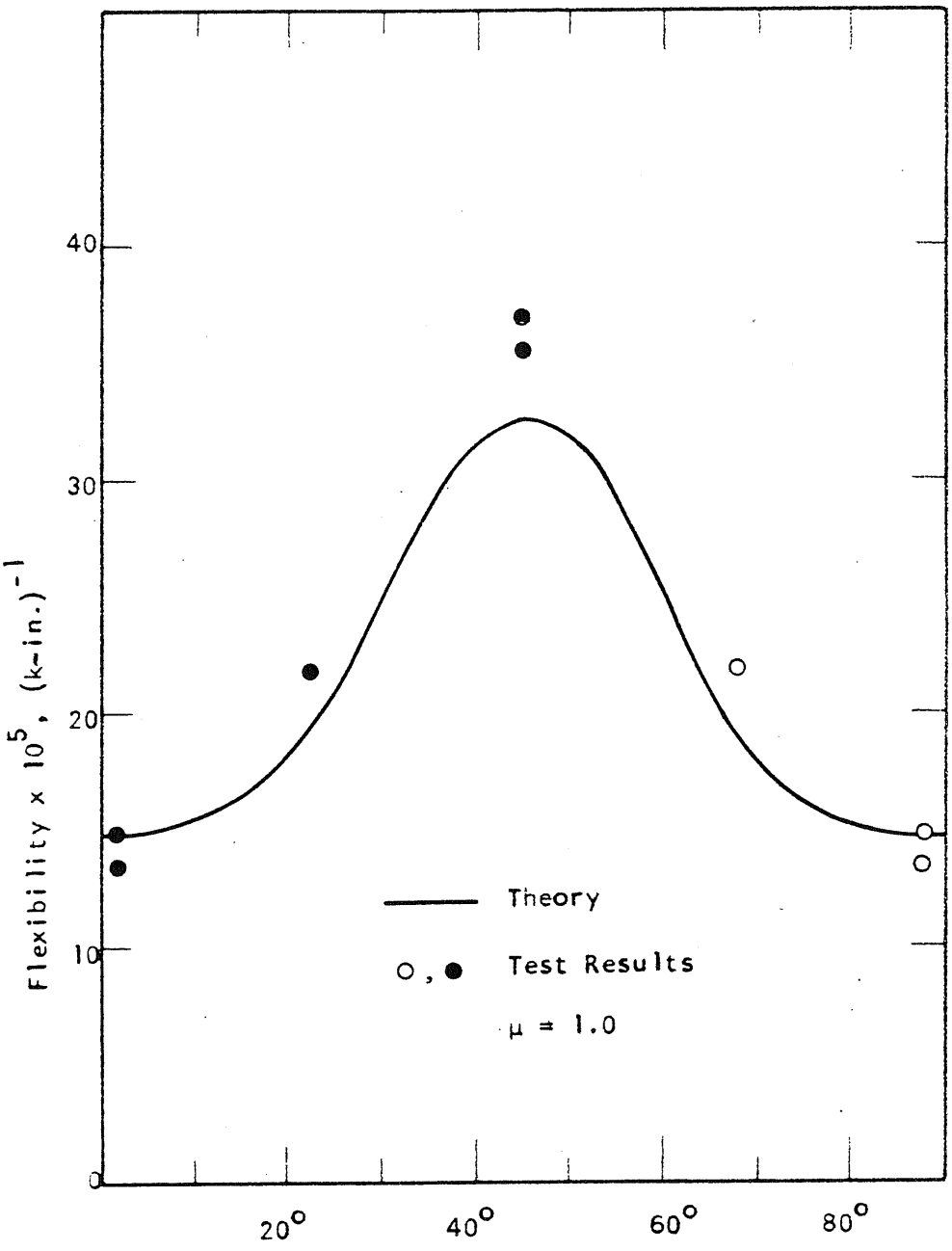

FIG. 4.47 FLEXIBILITY OF AN ISOTROPICALLY REINFORCED ELEMENT SUBJECTED TO TORSION

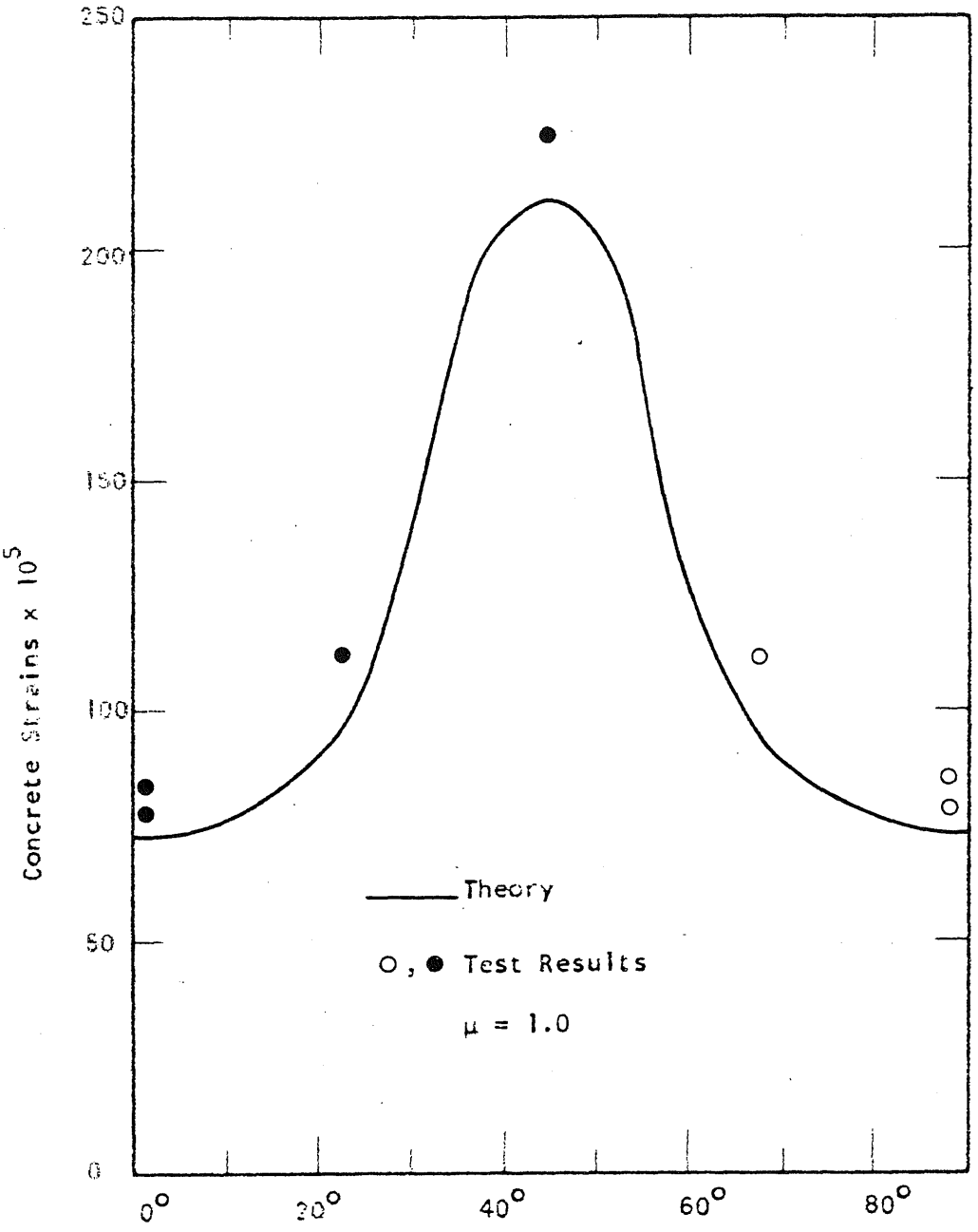

FIG. 4.48 CONCRETE STRAINS AT YIELDING IN A ISOTROPICALLY REINFORCED ELEMENT SUBJECTED TO TORSION

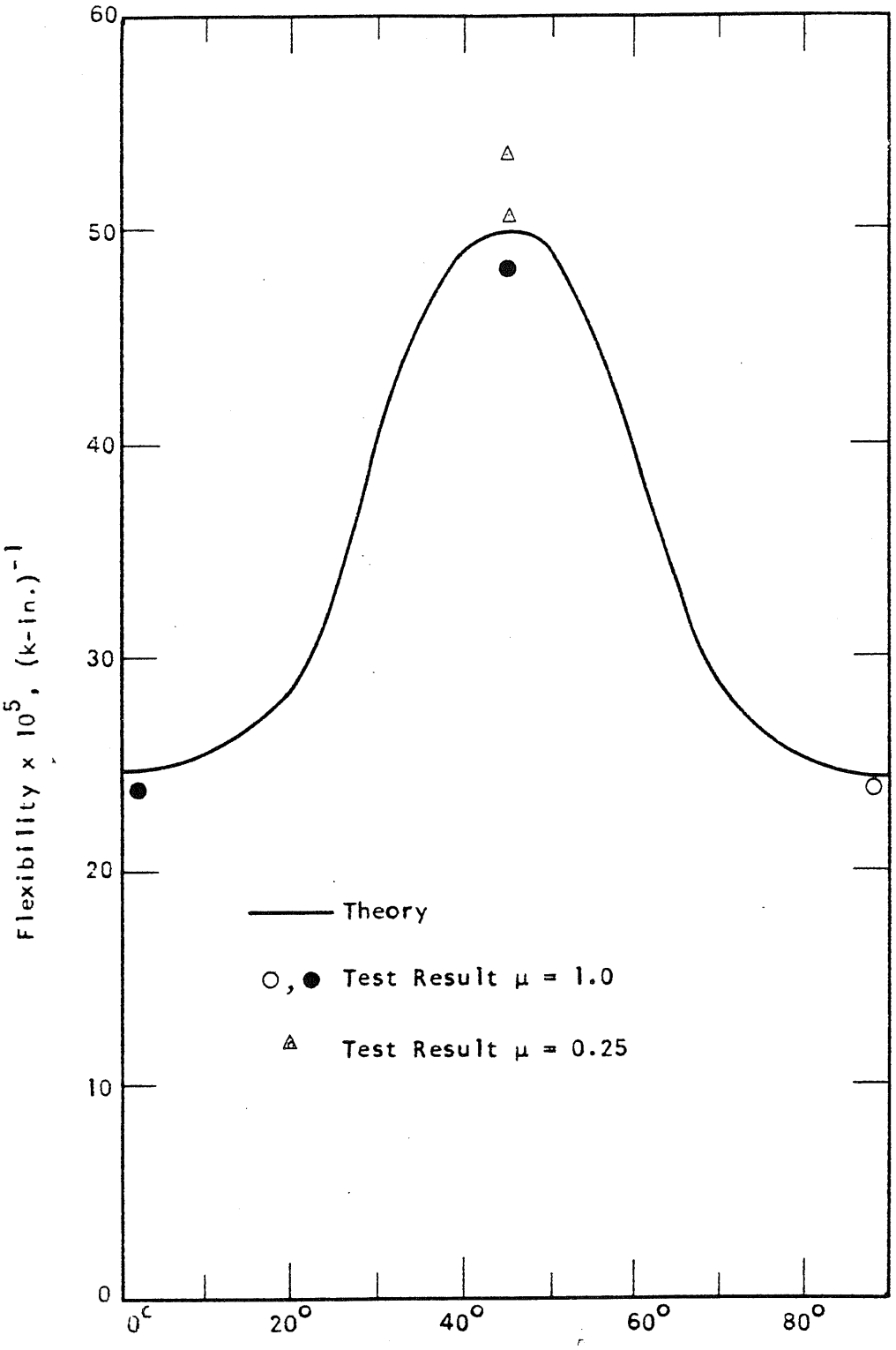

FIG. 4.49 FLEXIBILITY OF A REINFORCED ELEMENT SUBJECTED TO TORSION

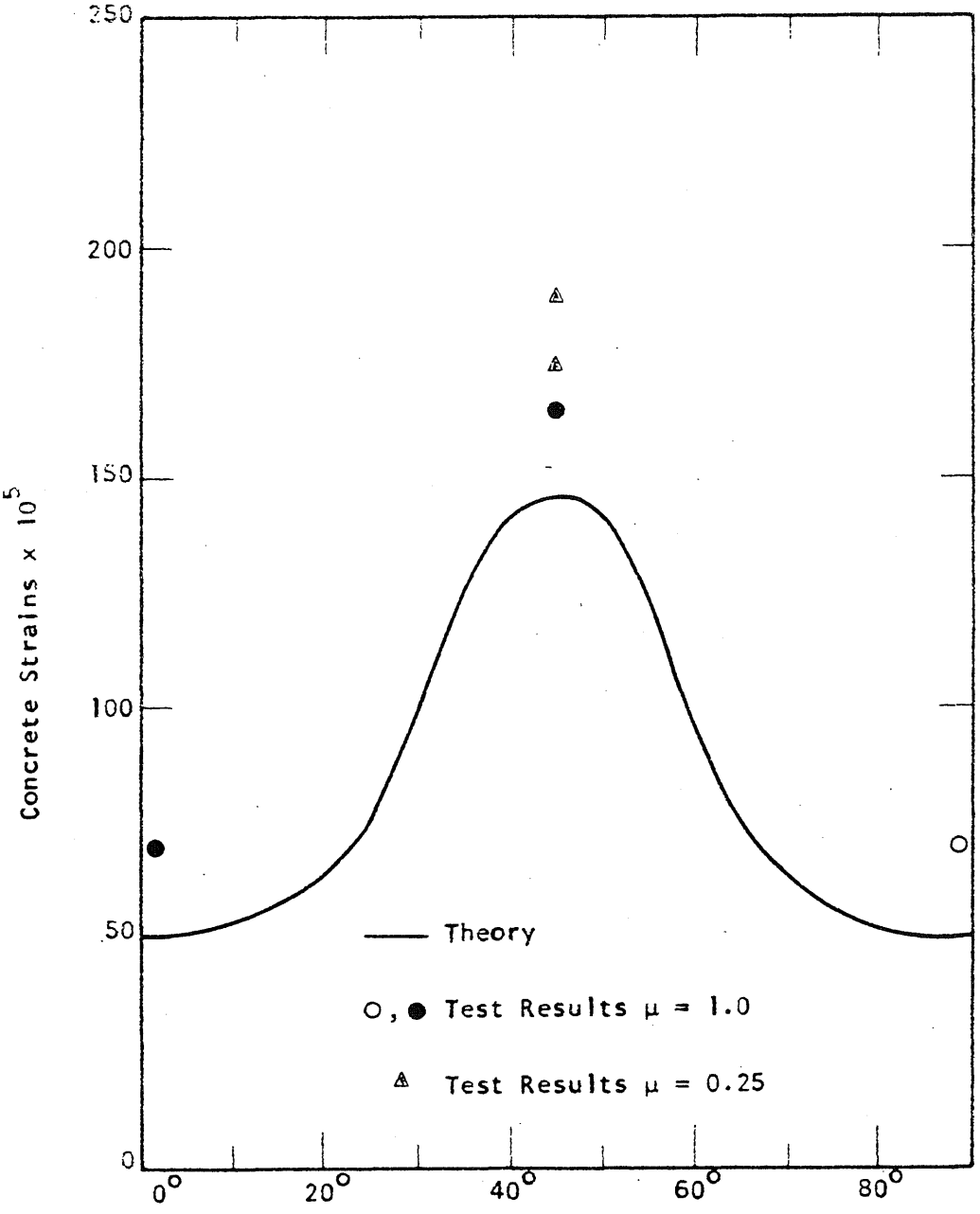

FIG. 4.50 CONCRETE STRAINS AT YIELDING IN A REINFORCED ELEMENT SUBJECTED TO TORSION

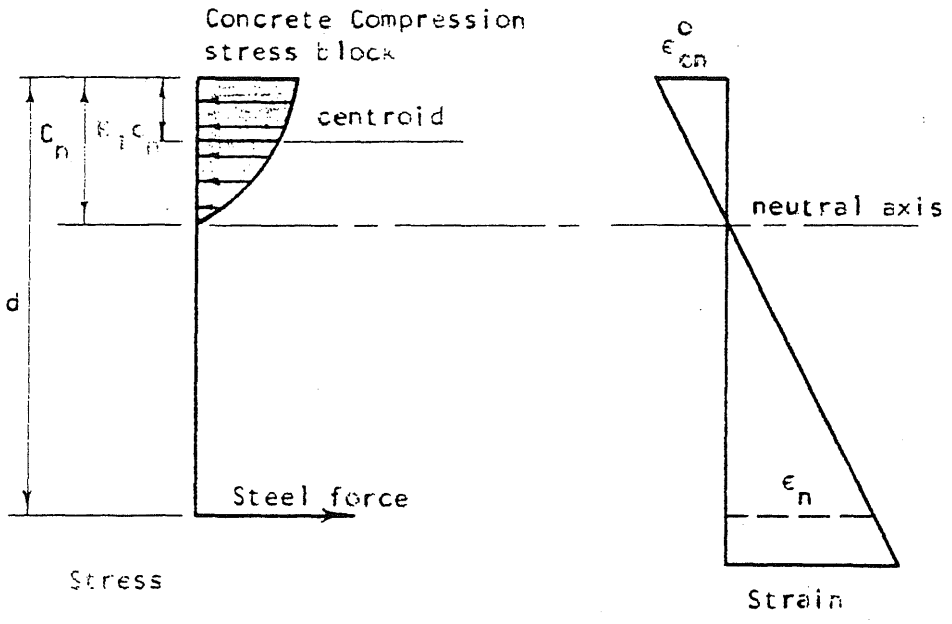

FIG. 5.1 STRESS AND STRAIN ASSUMPTIONS

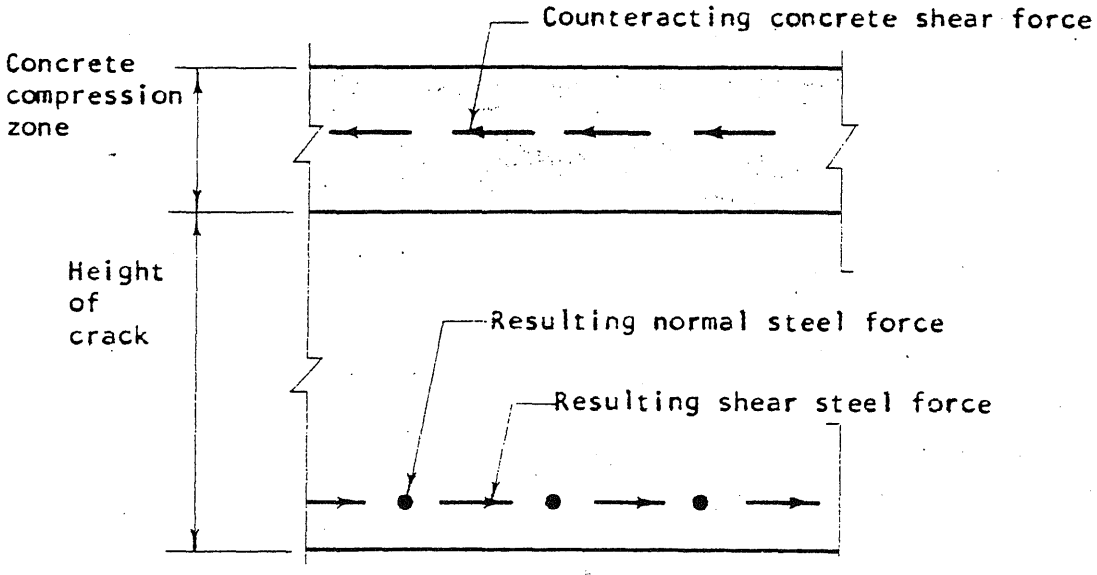

FIG. 5.2 SHEAR FORCES IN A NONISOTROPICALLY REINFORCED SECTION

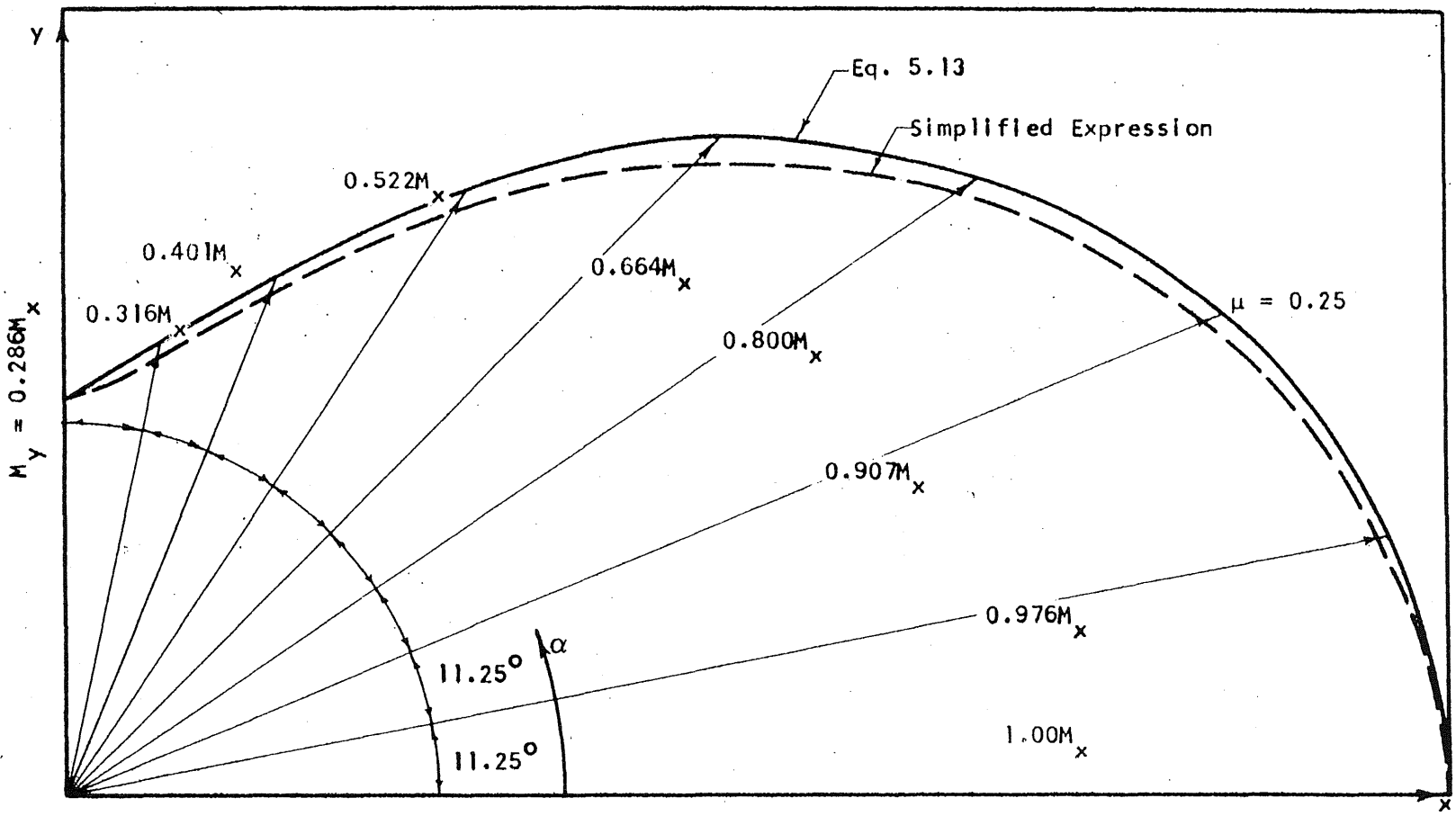

FIG. 5.3 RESISTING MOMENT AT YIELD LINES WITH VARIABLE ORIENTATION

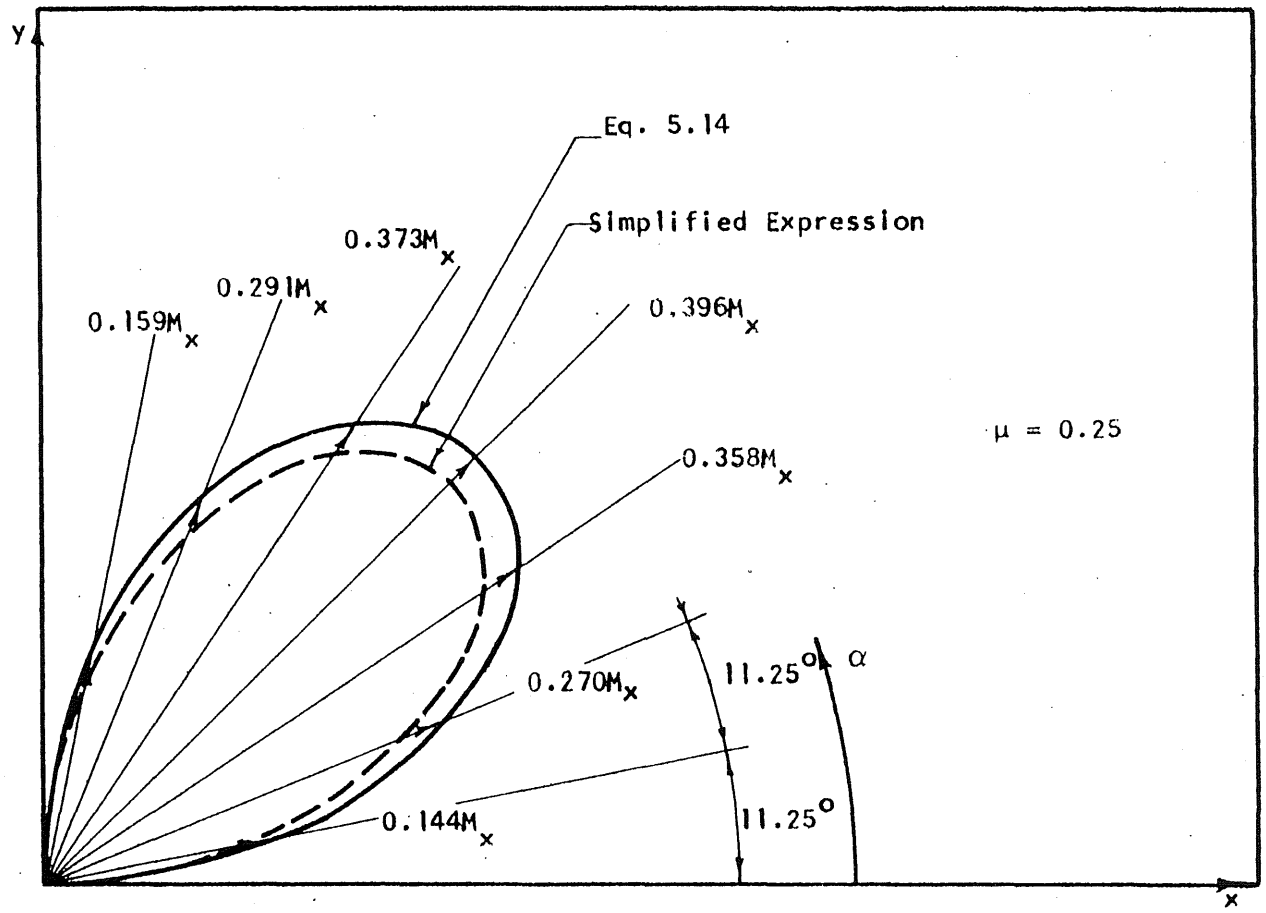

FIG. 5.4 RESISTING TWISTING MOMENT AT YIELD LINES WITH VARIABLE ORIENTATION

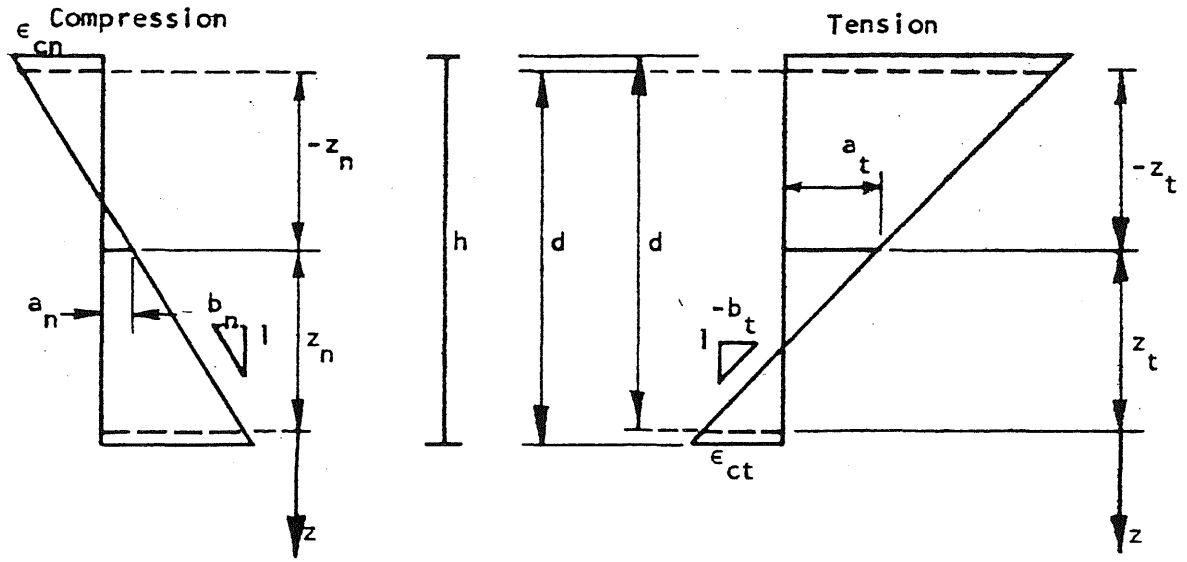

Strain in the n-direction

a

Strain in the t-direction

b

FIG. 5.5 STRAINS IN THE n- AND t-DIRECTIONS

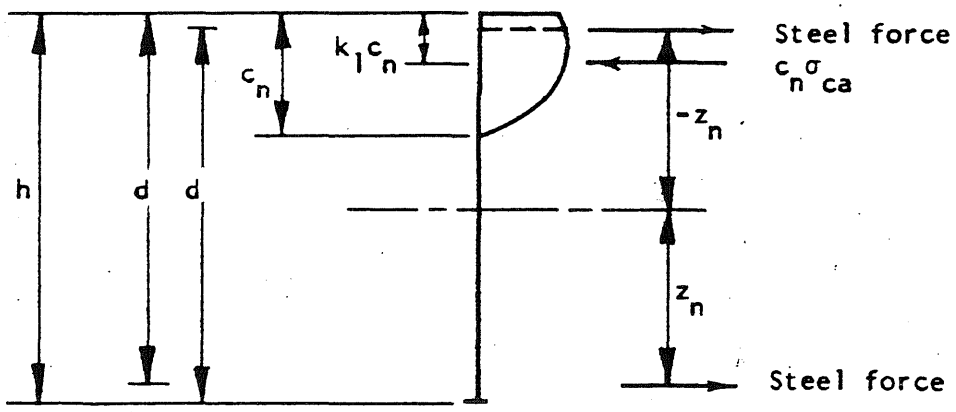

FIG. 5.6 FORCES IN A SECTION PERPENDICULAR TO THE n-DIRECTION

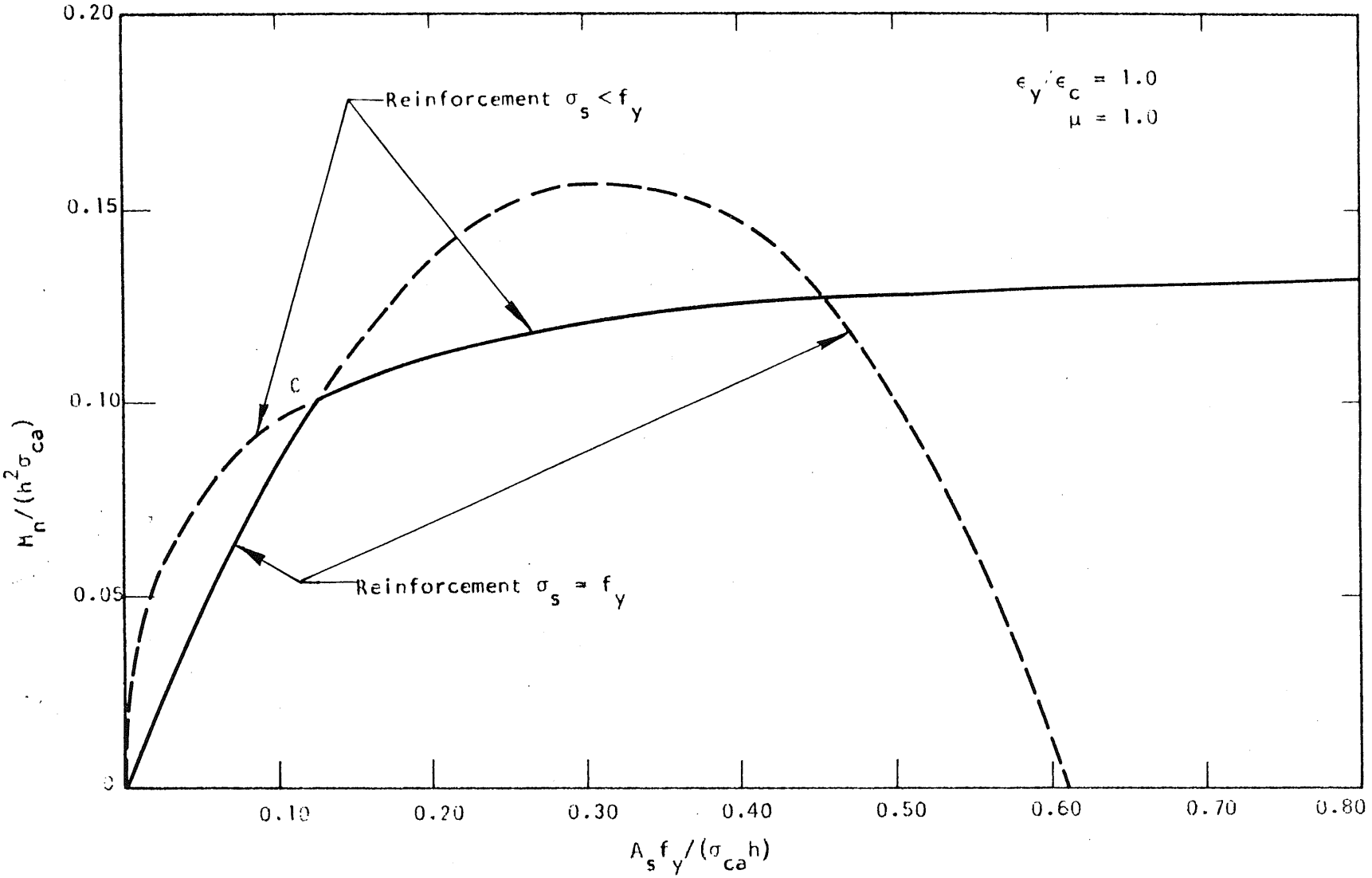

FIG. 5.7 TORSIONAL MOMENT CAPACITY OF A SPECIMEN WITH ISOTROPIC REINFORCEMENT INCLINED 45° TO THE PRINCIPAL MOMENTS

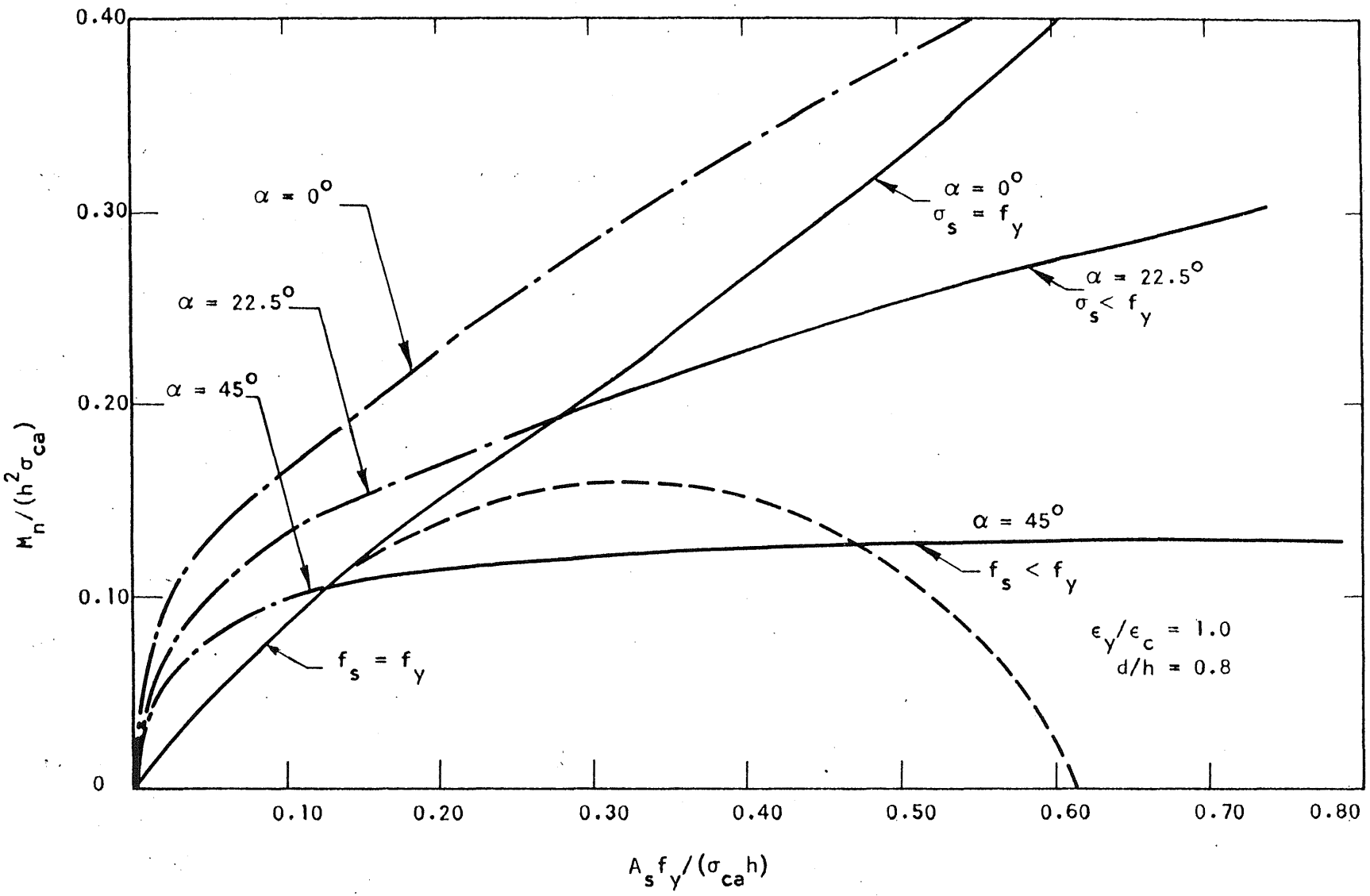

FIG. 5.8 TORSIONAL CAPACITY OF AN ISOTROPICALLY REINFORCED SPECIMEN WITH DIFFERENT INCLINATION OF REINFORCEMENT

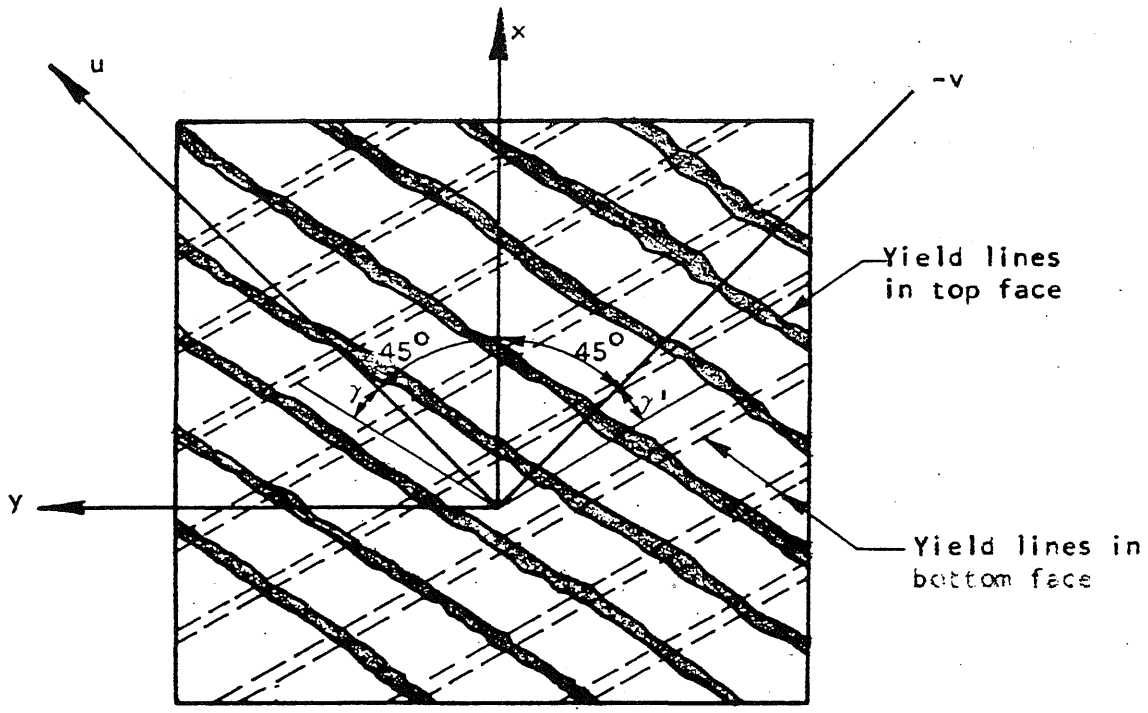

FIG. 5.9 YIELD LINES IN AN ELEMENT

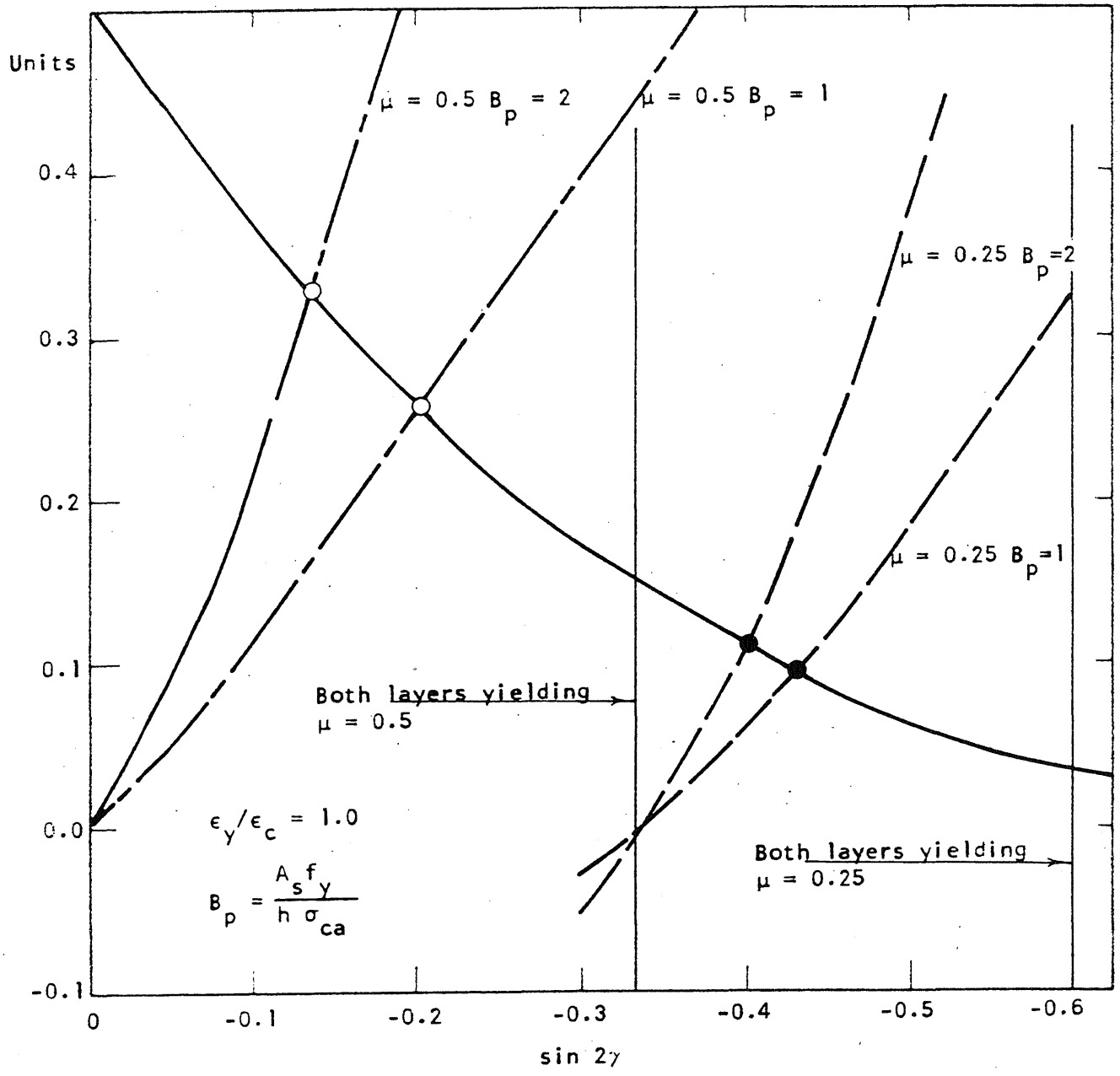

FIG. 5.10 SOLUTIONS OF EQUATION 5.70

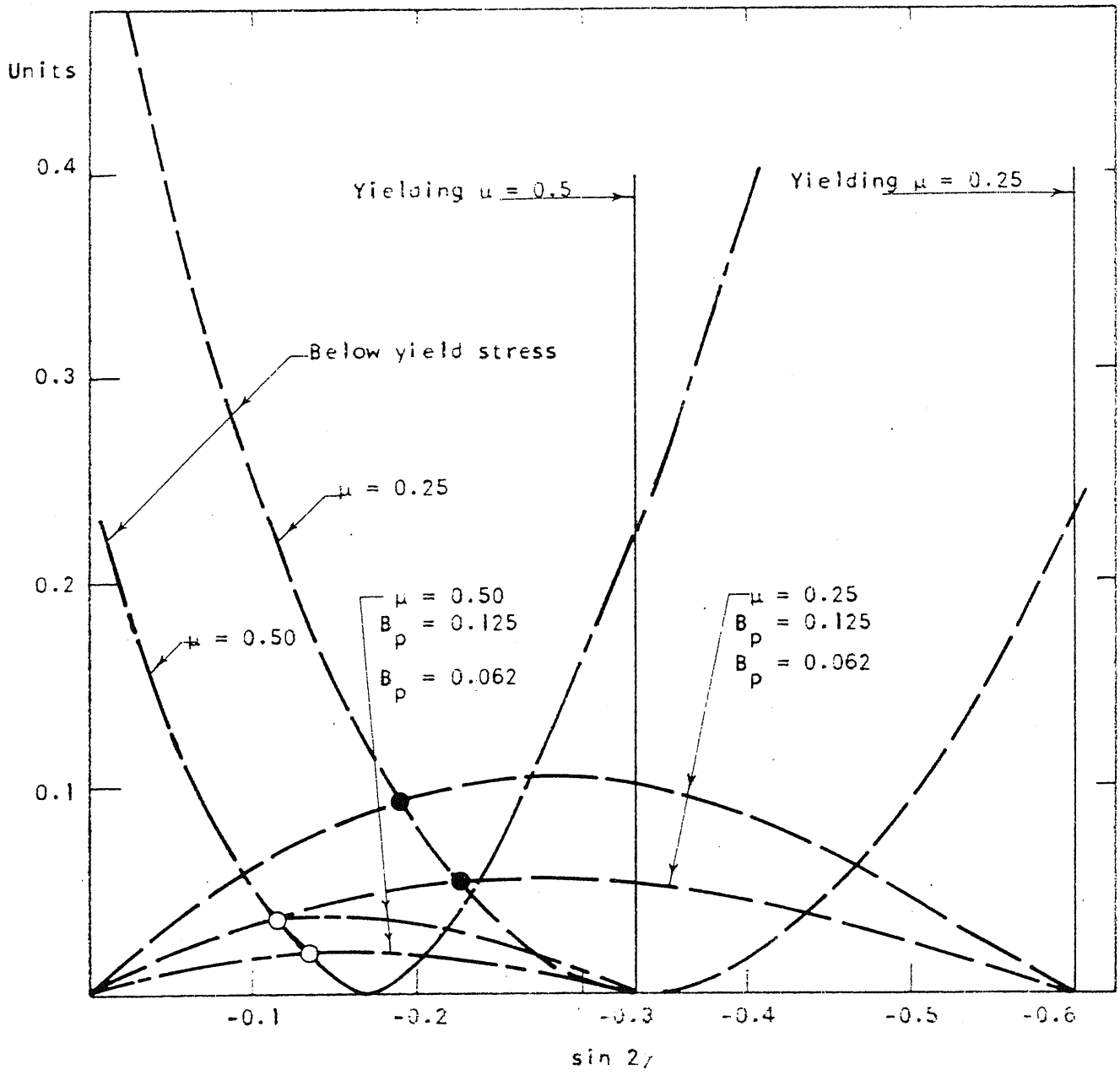

FIG. 5.11 DEVIATION OF THE DIRECTION OF THE "YIELD" LINE OVER- AND UNDER-REINFORCED SPECIMENS

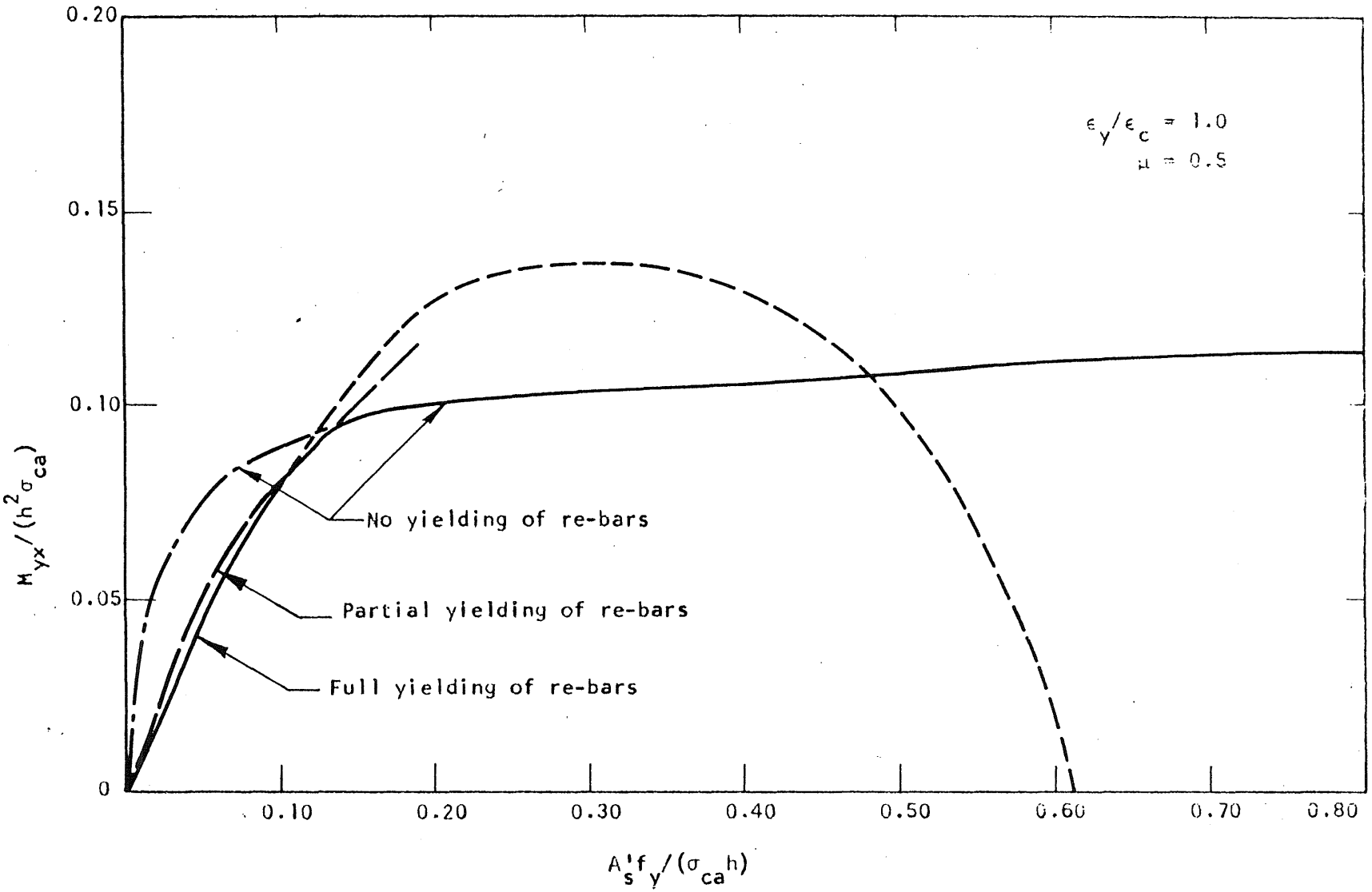

FIG. 5.12 TORSIONAL MOMENT CAPACITY OF A SPECIMEN WITH NONISOTROPIC REINFORCEMENT INCLINED 45° TO THE PRINCIPAL MOMENTS

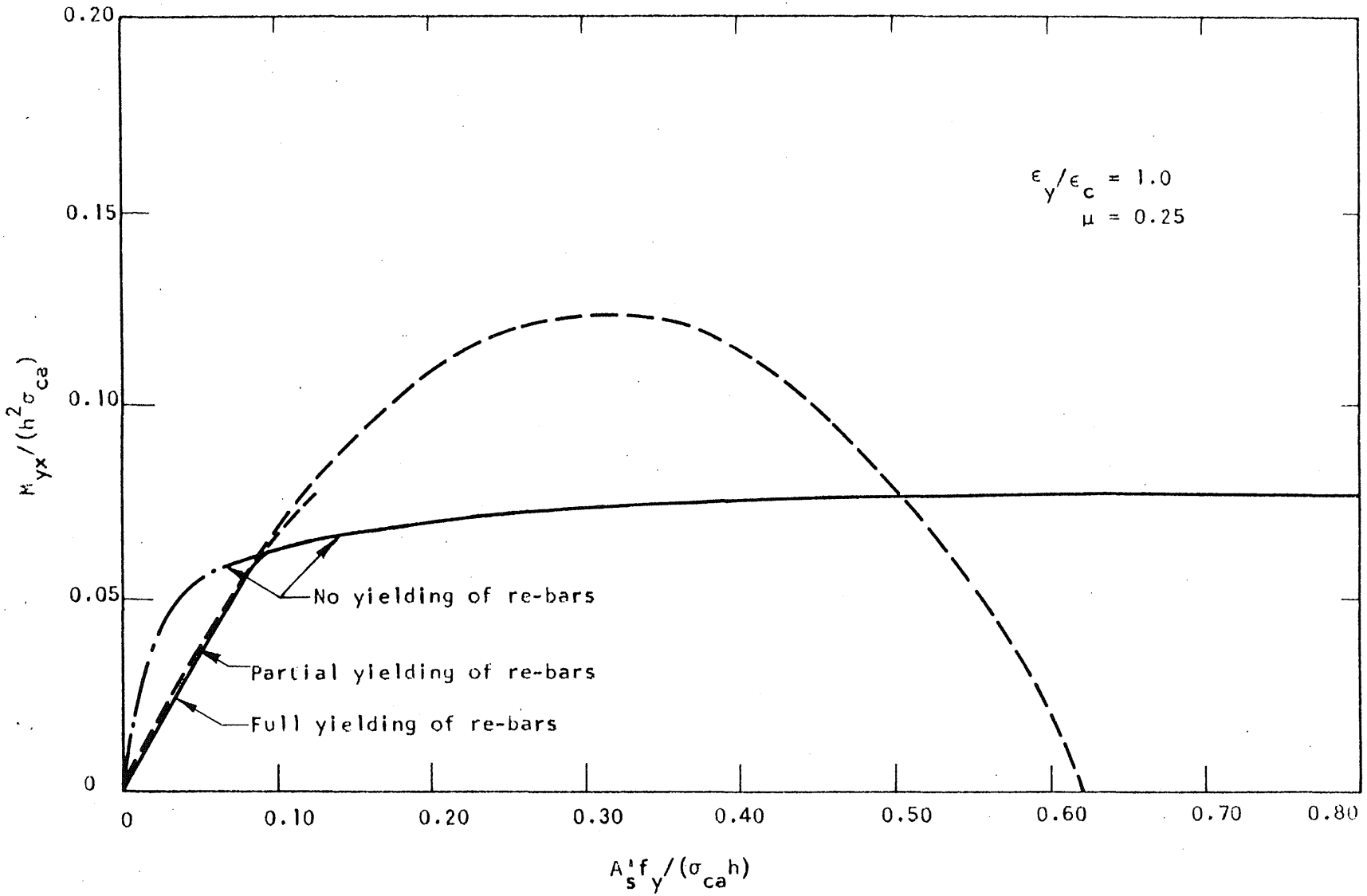

FIG. 5.13 TORSIONAL MOMENT CAPACITY OF A SPECIMEN WITH NONISOTROPIC REINFORCEMENT INCLINED 45^{o} TO THE PRINCIPAL MOMENTS

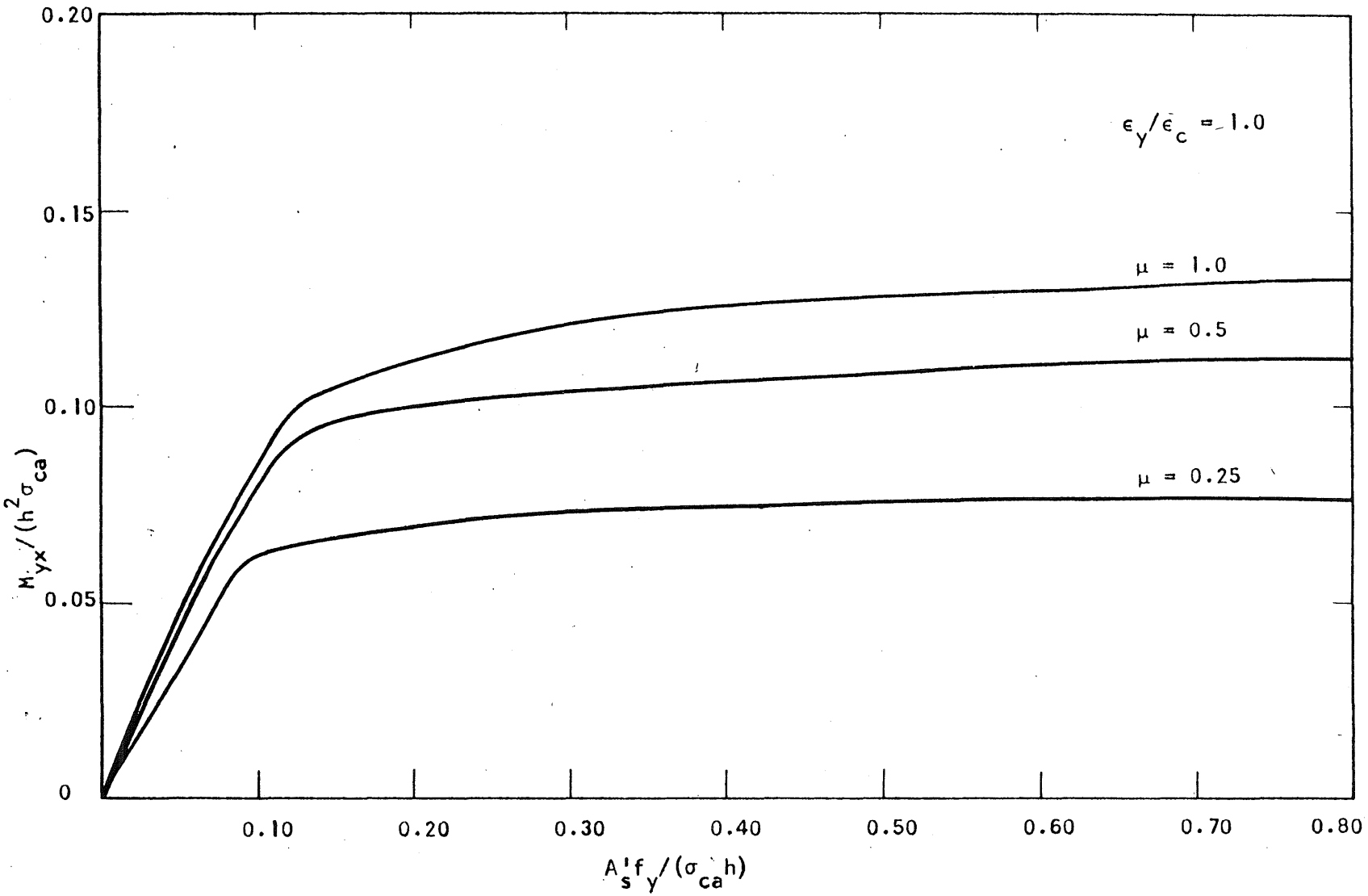

FIG. 5.14 TORSIONAL MOMENT CAPACITY AS A FUNCTION OF THE DISTRIBUTION OF REINFORCEMENT

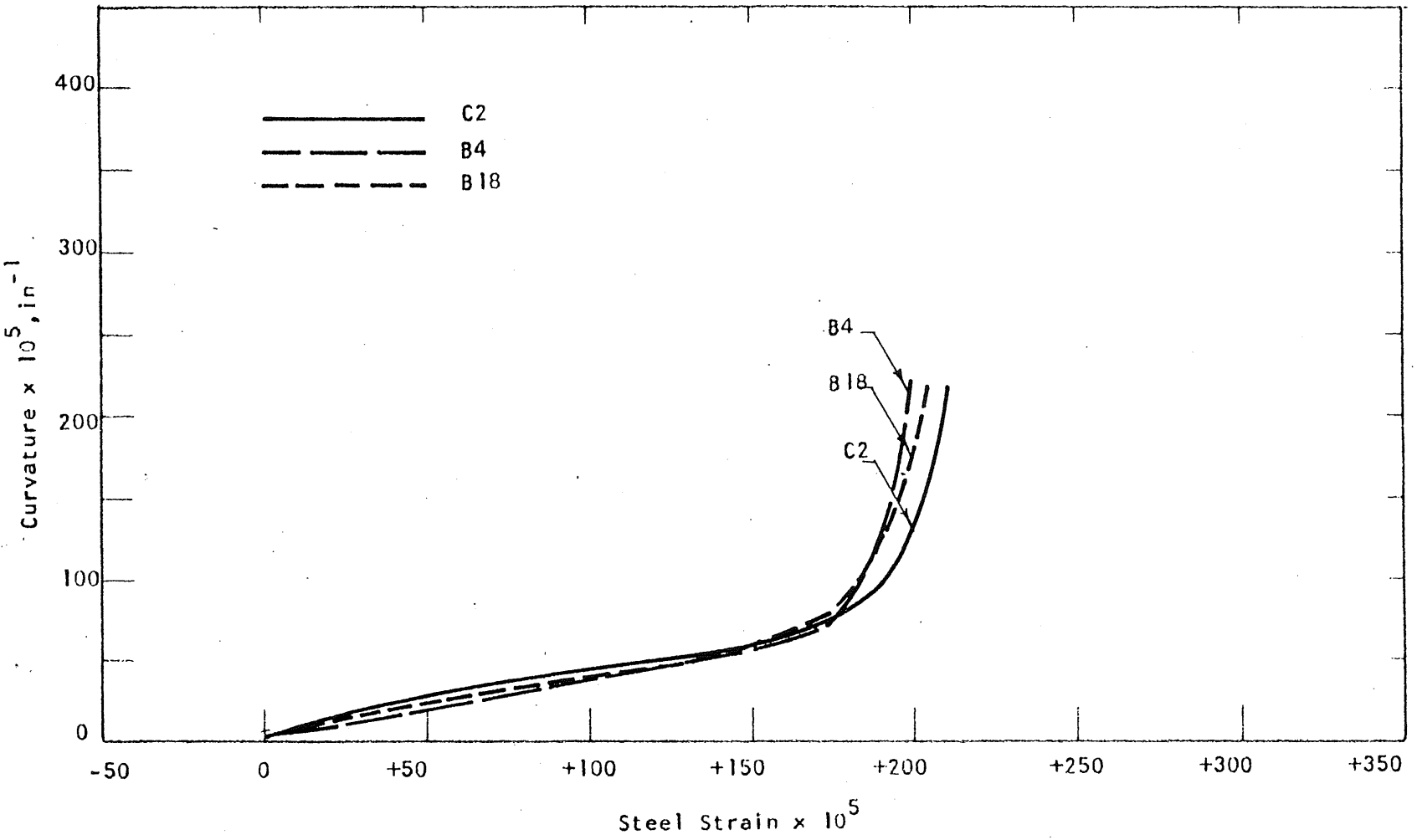

FIG. 5.15 CURVATURE-STRAIN RELATIONSHIPS FOR SPECIMENS SUBJECTED TO PRINCIPAL MOMENTS IN THE DIRECTIONS OF THE REINFORCEMENT

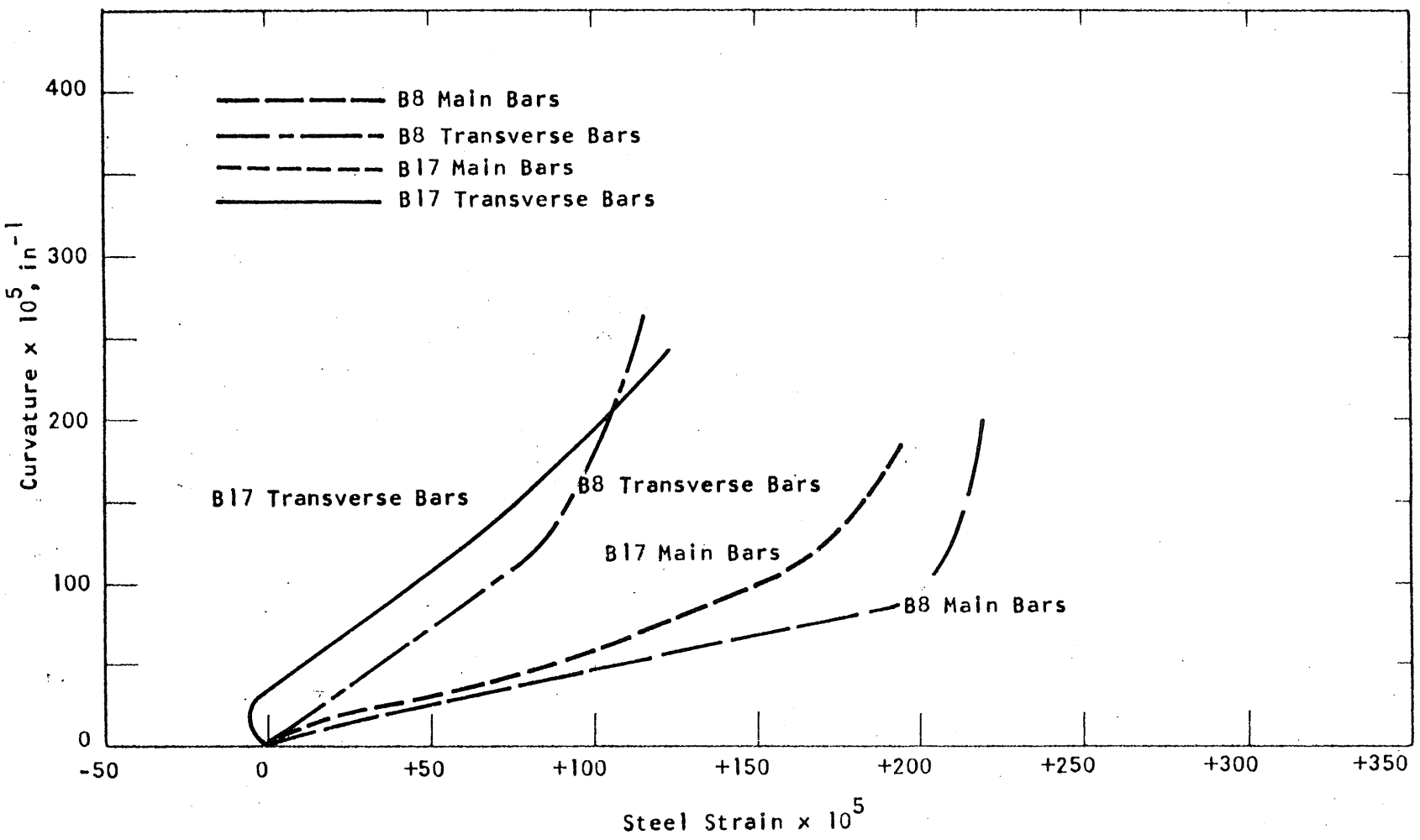

FIG. 5.16 CURVATURE-STRAIN RELATIONSHIP FOR SPECIMENS SUBJECTED TO PRINCIPAL MOMENTS MAKING 22 1/2° AND 67 1/2° TO THE DIRECTIONS OF THE REINFORCEMENT

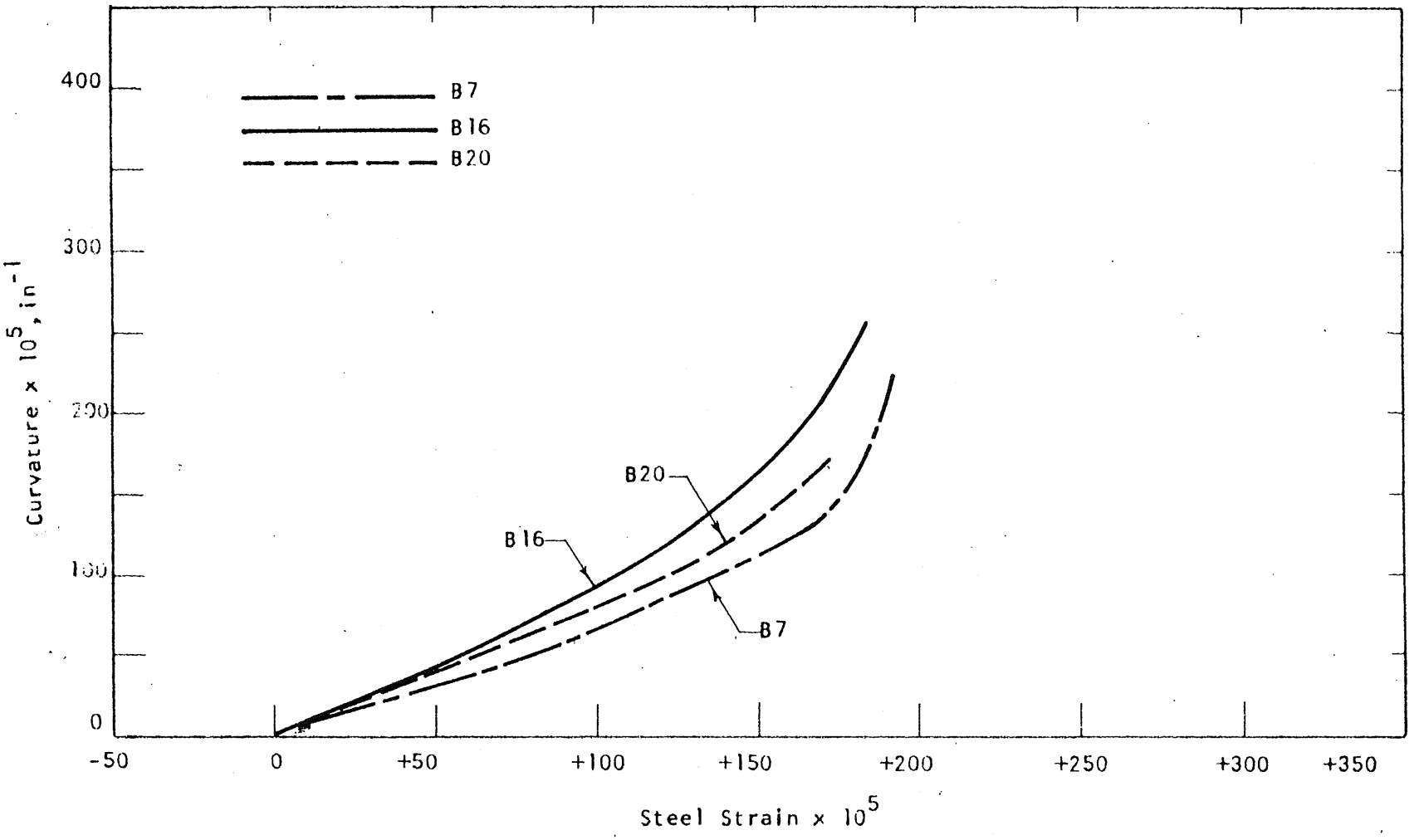

FIG. 5.17 CURVATURE-STRAIN RELATIONSHIPS FOR SPECIMENS SUBJECTED TO PRINCIPAL MOMENTS 45° TO THE DIRECTIONS OF THE REINFORCEMENT

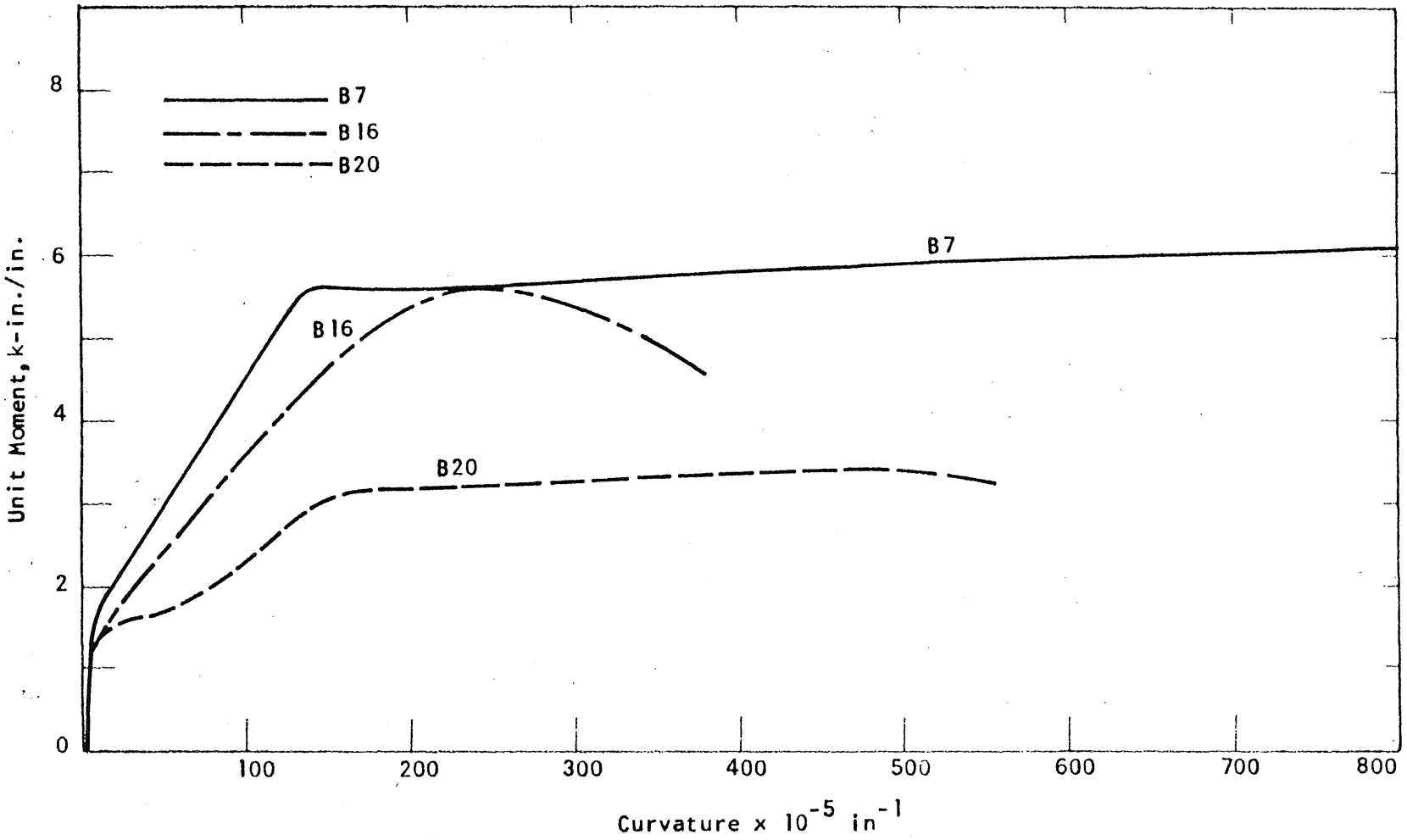

FIG. 5.18 MOMENT-CURVATURE RELATIONSHIPS FOR SPECIMENS SUBJECTED TO PRINCIPAL MOMENTS 45° TO THE DIRECTIONS OF THE REINFORCEMENT

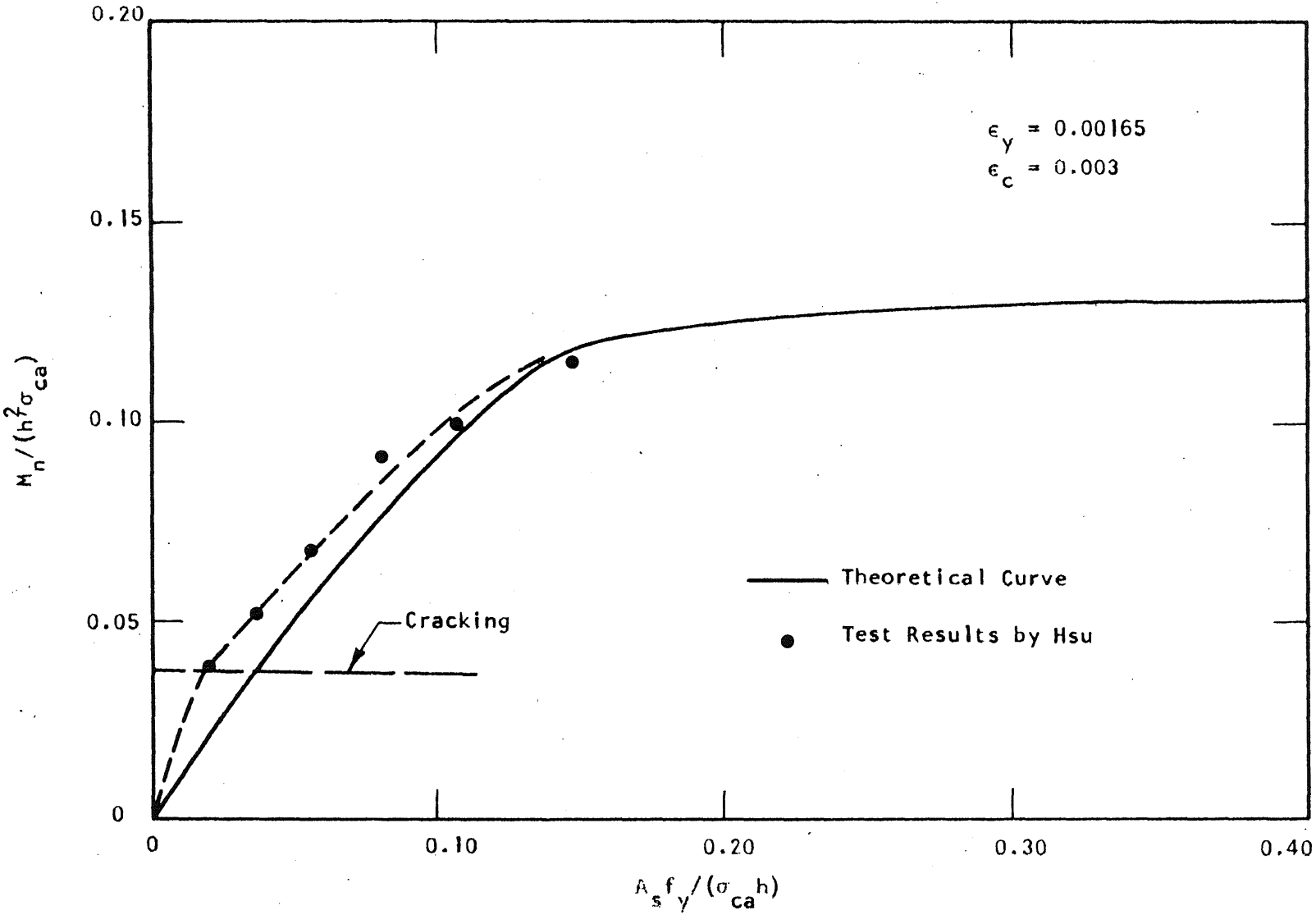

FIG. 5.19 TORSIONAL MOMENT CAPACITY OF A BEAM SPECIMEN

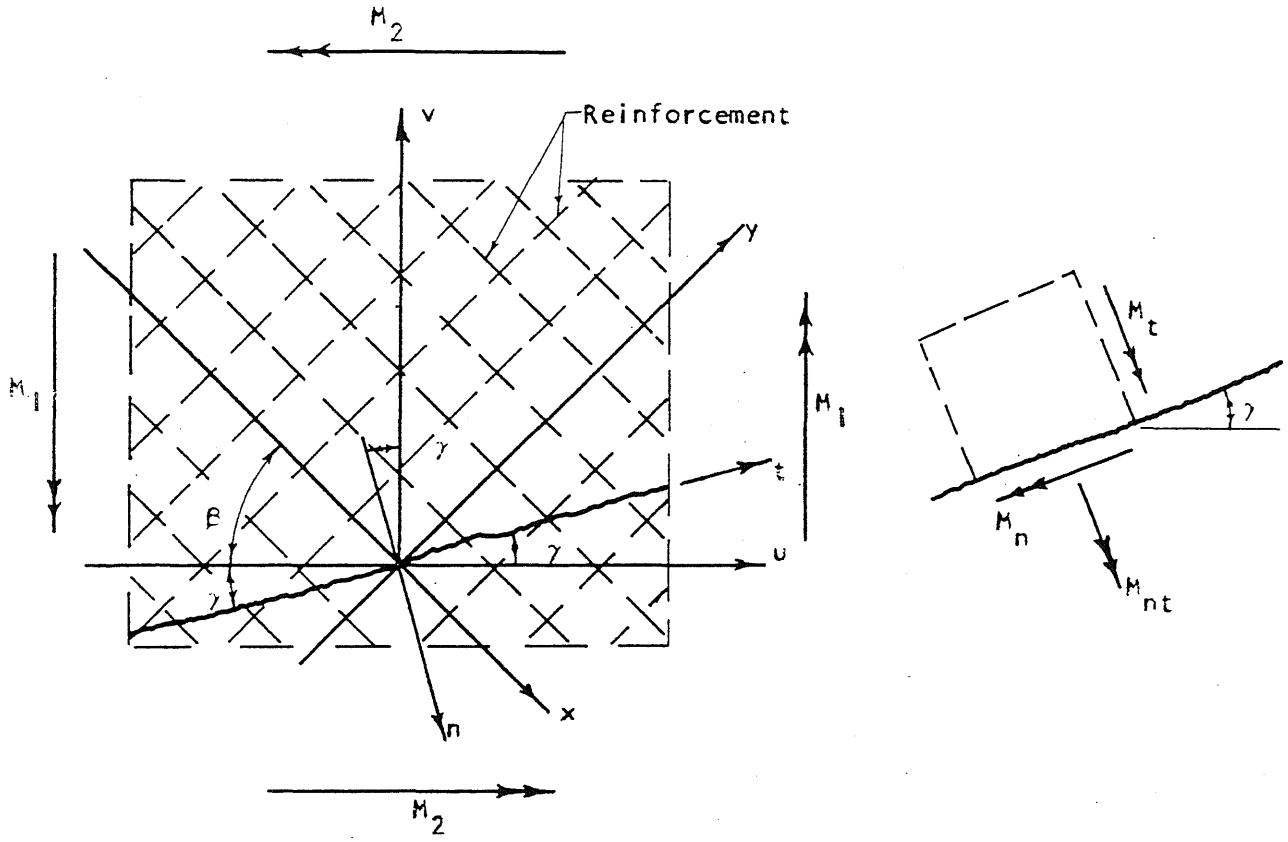

FIG. 6.1 ORIENTATION OF YIELD LINE

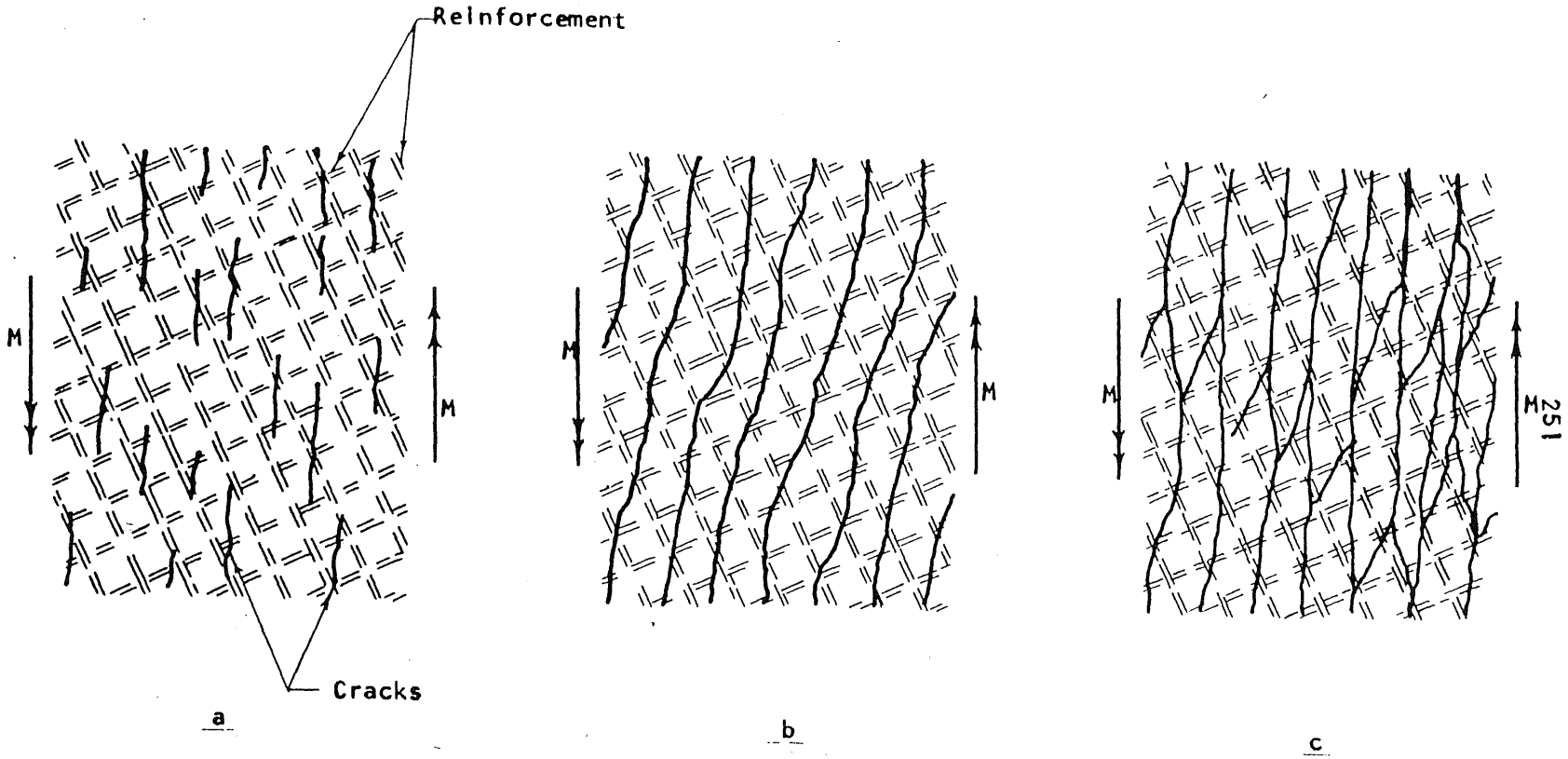

FIG. 6.2 THE DEVELOPMENT OF CRACKS DURING TESTING OF SPECIMEN B8

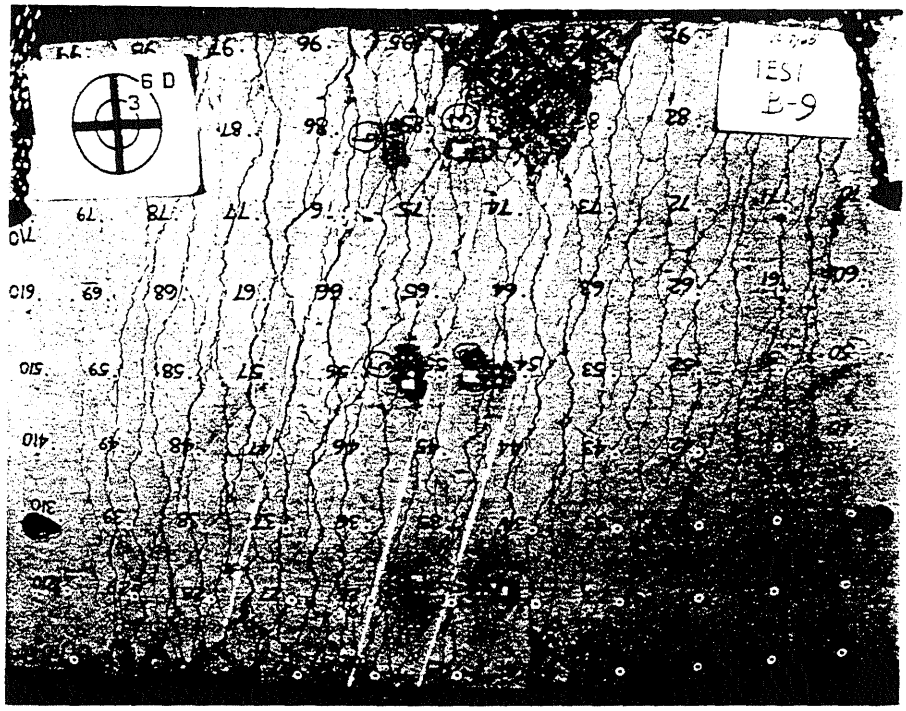

a

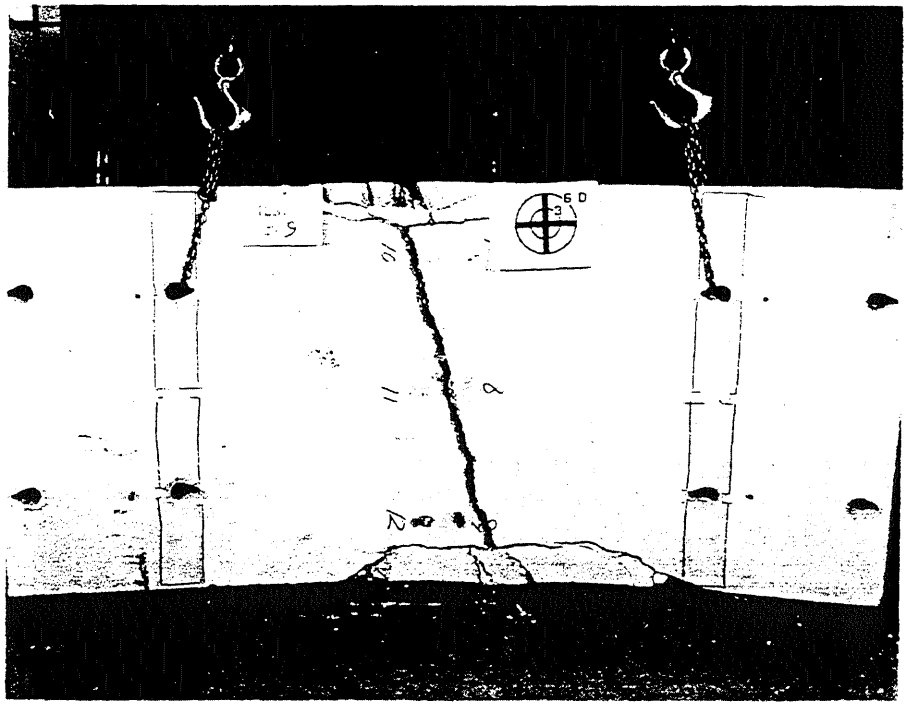

b

FIG. 6.3 YIELD LINES IN SPECIMEN B9

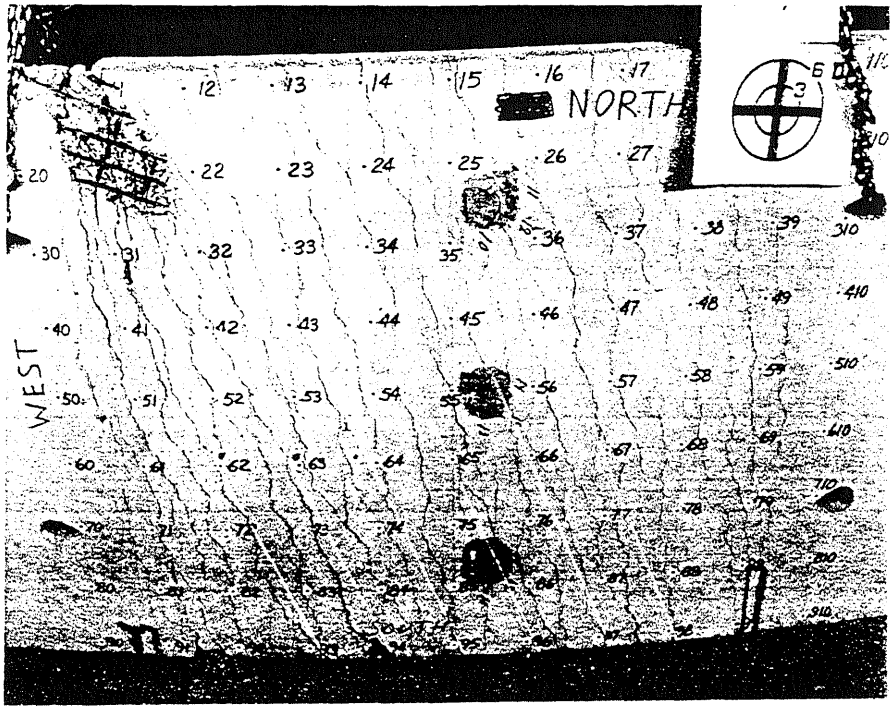

a

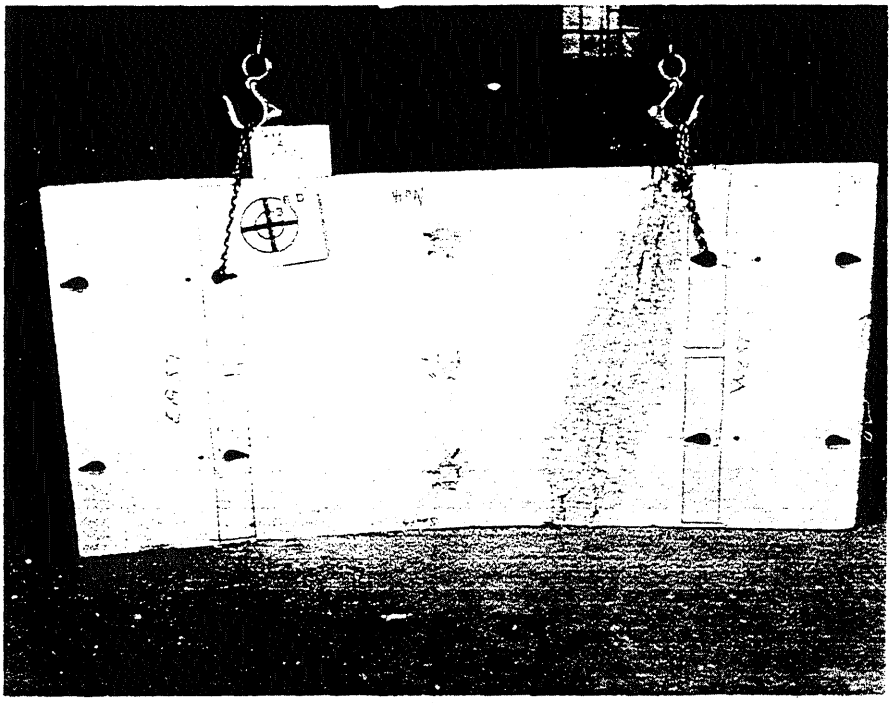

b

FIG. 6.4 YIELD LINES IN SPECIMEN B11

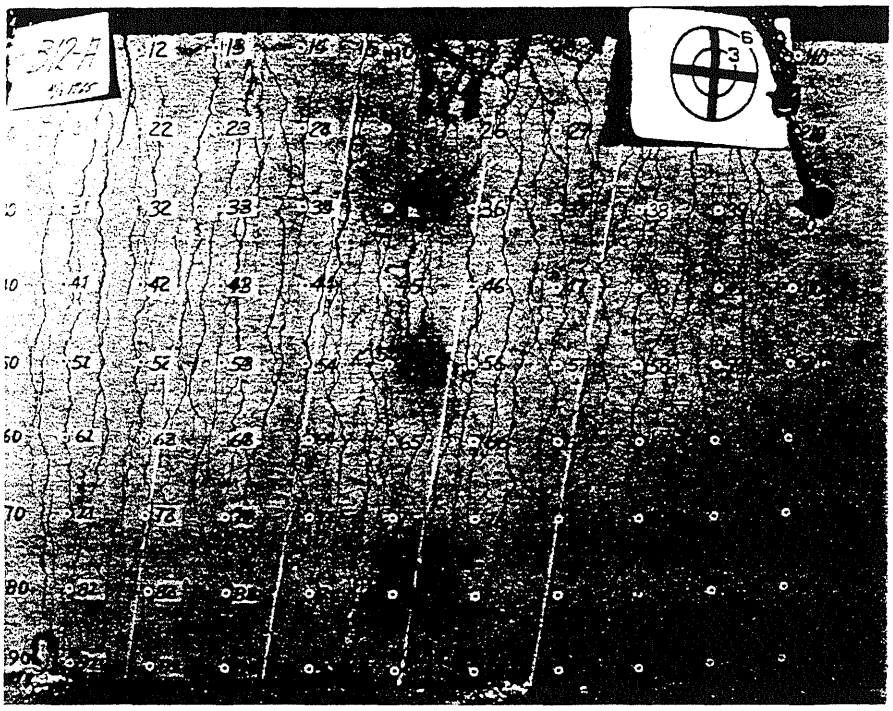

a

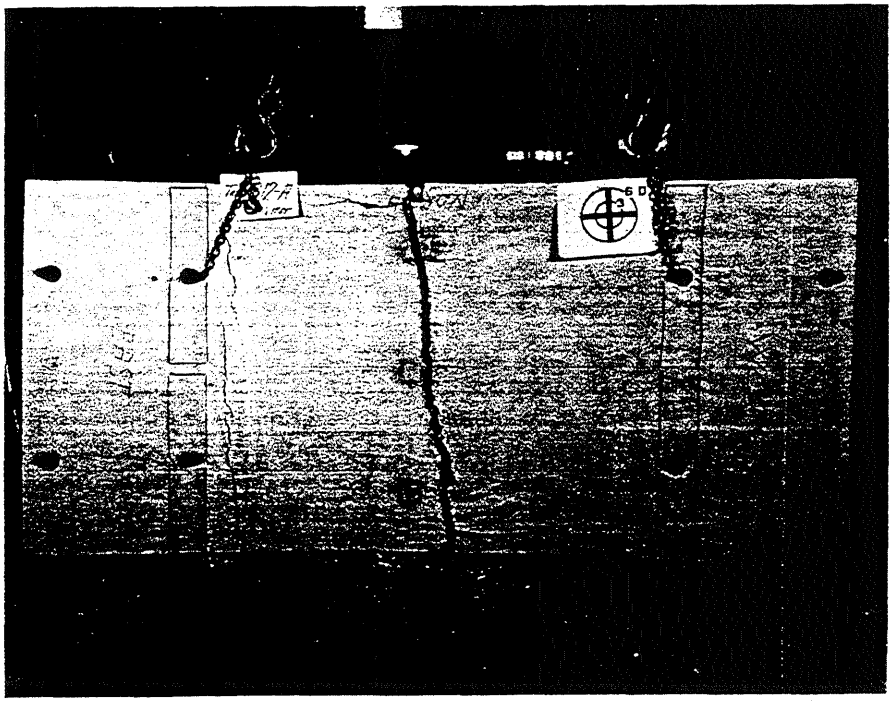

b

FIG. 6.5 YIELD LINES IN SPECIMEN B12

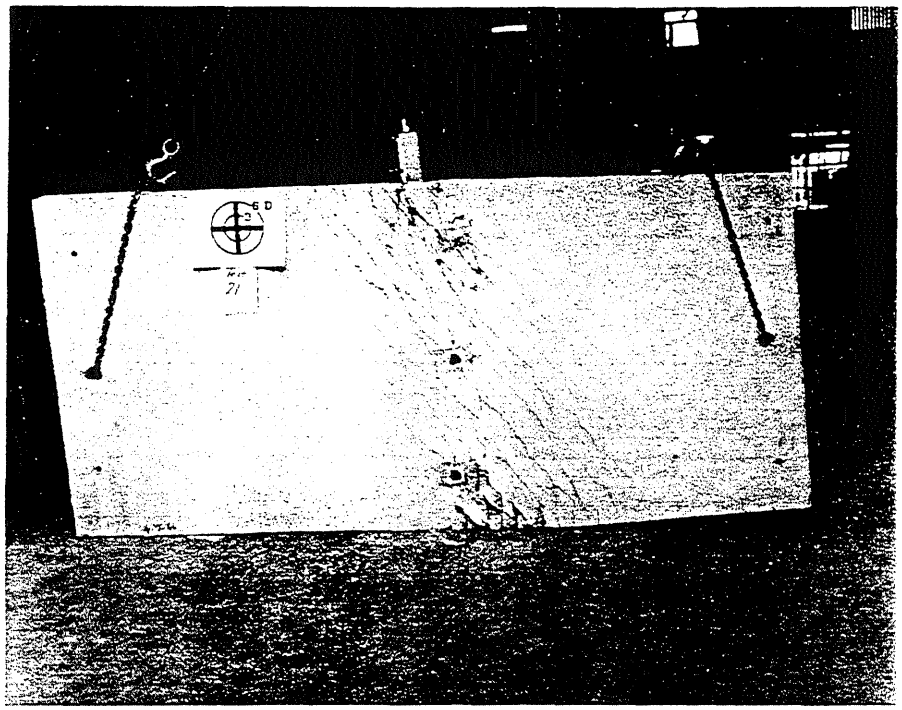

a

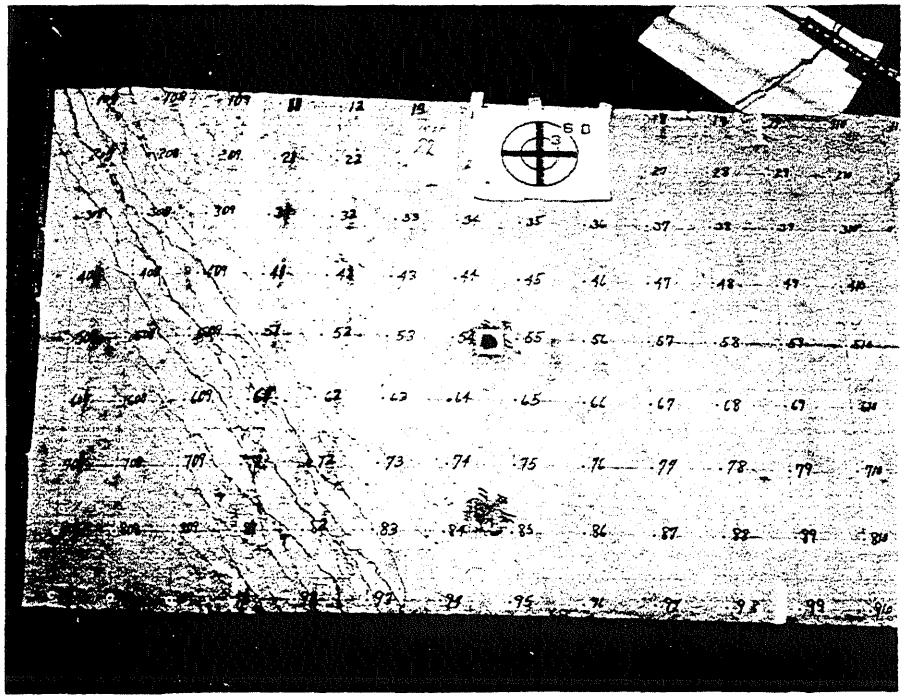

b

FIG. 6.6 YIELD LINES IN SPECIMEN B21 AND B22

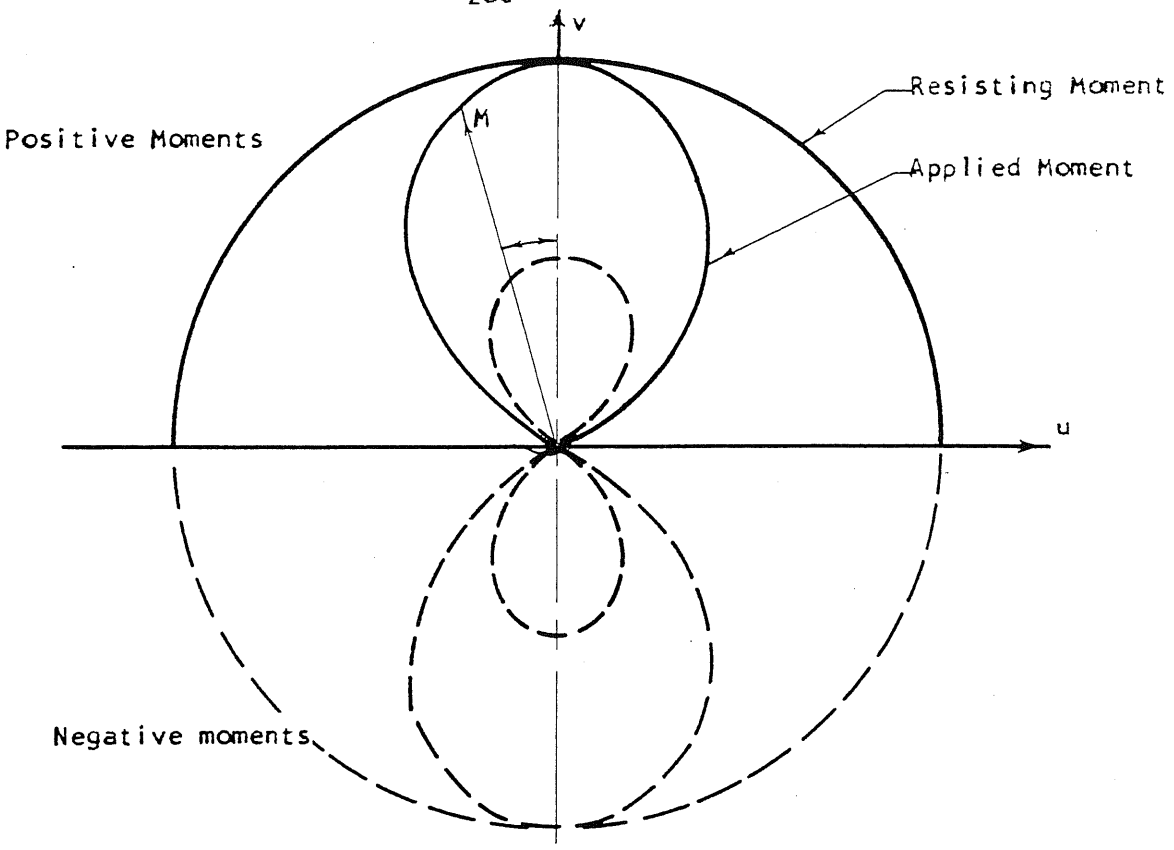

FIG. 7.1 ISOTROPICALLY REINFORCED ELEMENT SUBJECTED TO UNIAXIAL MOMENT

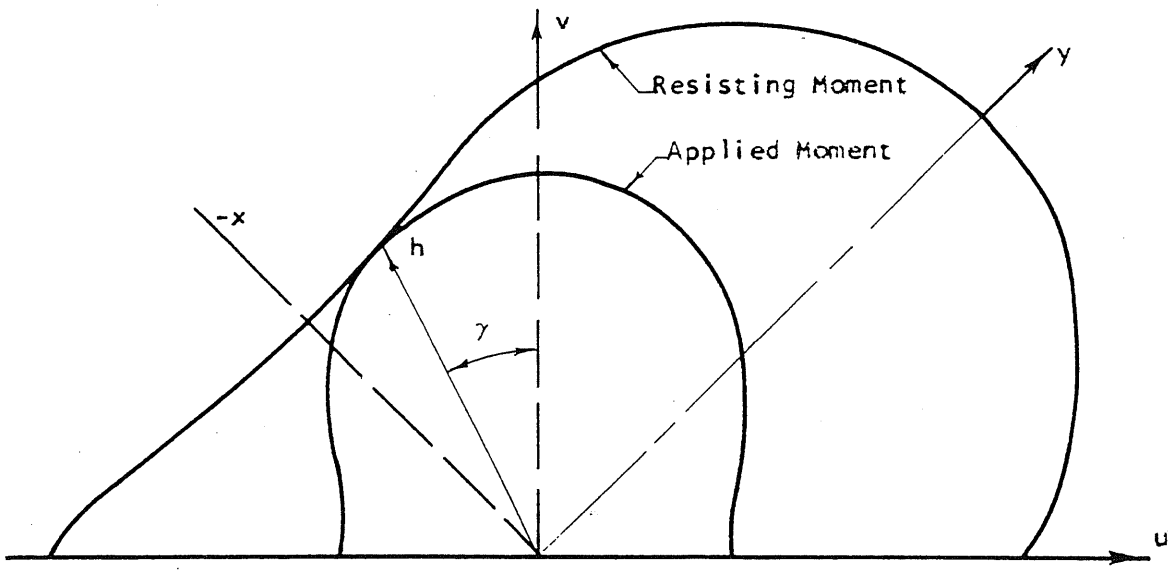

FIG. 7.2 NONISOTROPICALLY REINFORCED ELEMENT SUBJECTED TO BIAXIAL MOMENT

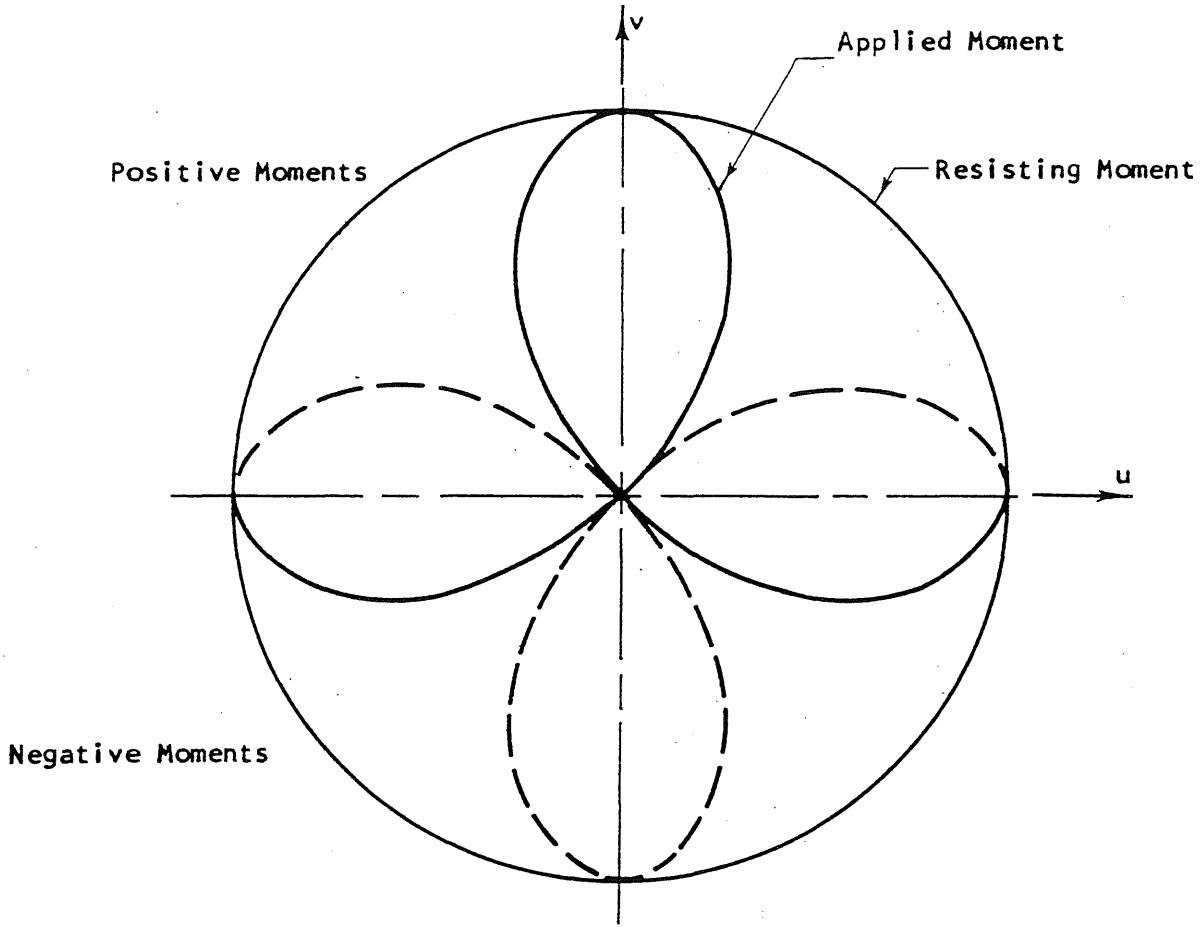

FIG. 7.3 ISOTROPICALLY REINFORCED ELEMENT SUBJECTED TO PURE TORSION

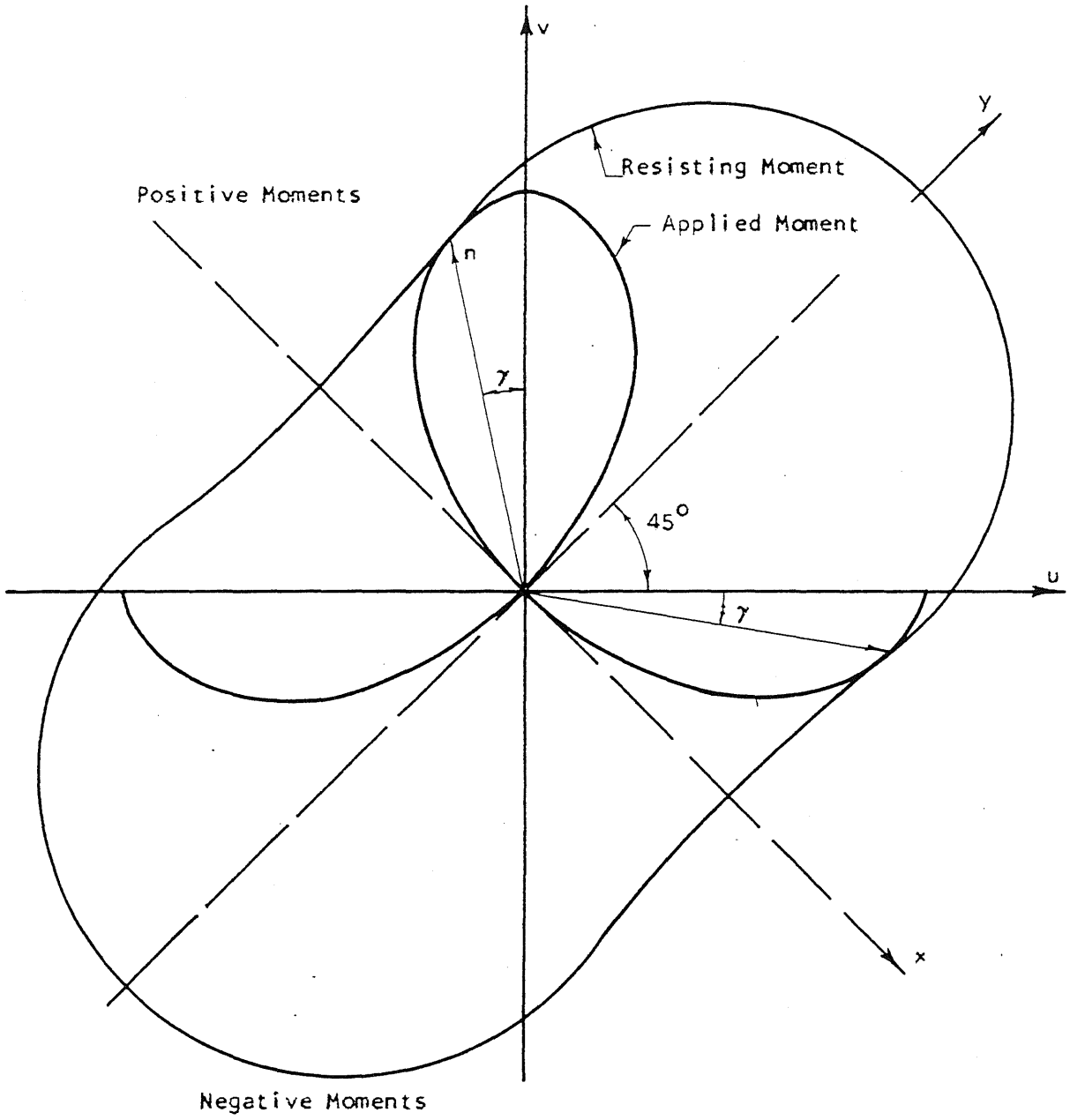

FIG. 7.4 NONISOTROPICALLY REINFORCED ELEMENT SUBJECTED TO PURE TORSION

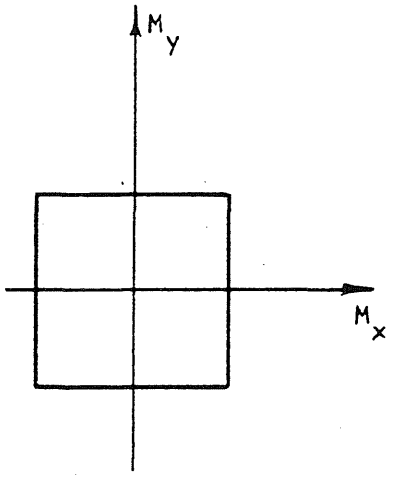

$A_s f_y = 0.125\sigma_{ca} h$

a

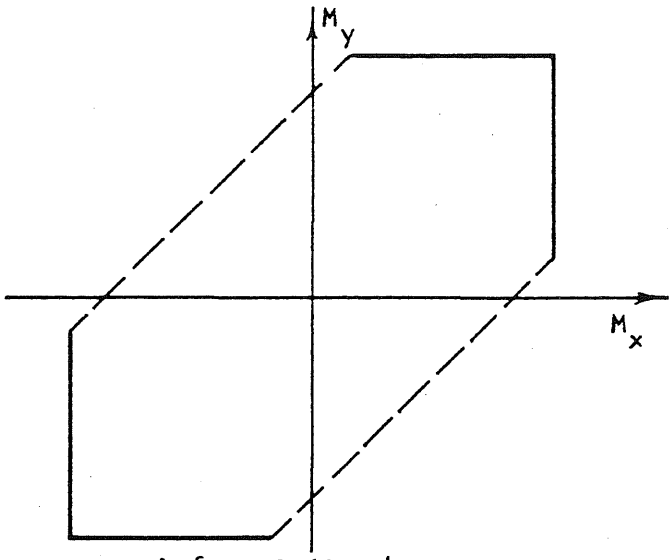

$A_s f_y = 0.40\sigma_{ca} h$

c

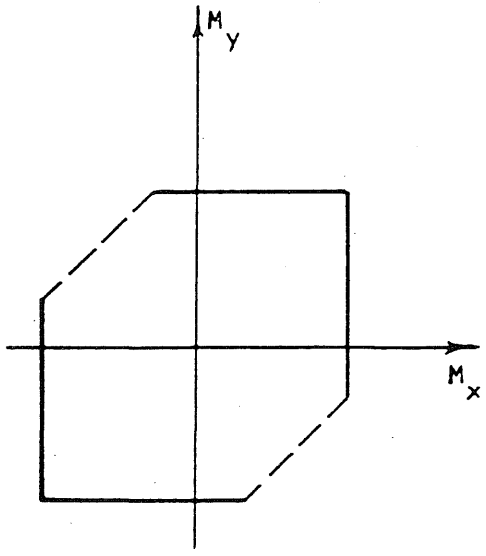

$A_s f_y = 0.25\sigma_{ca} h$

b

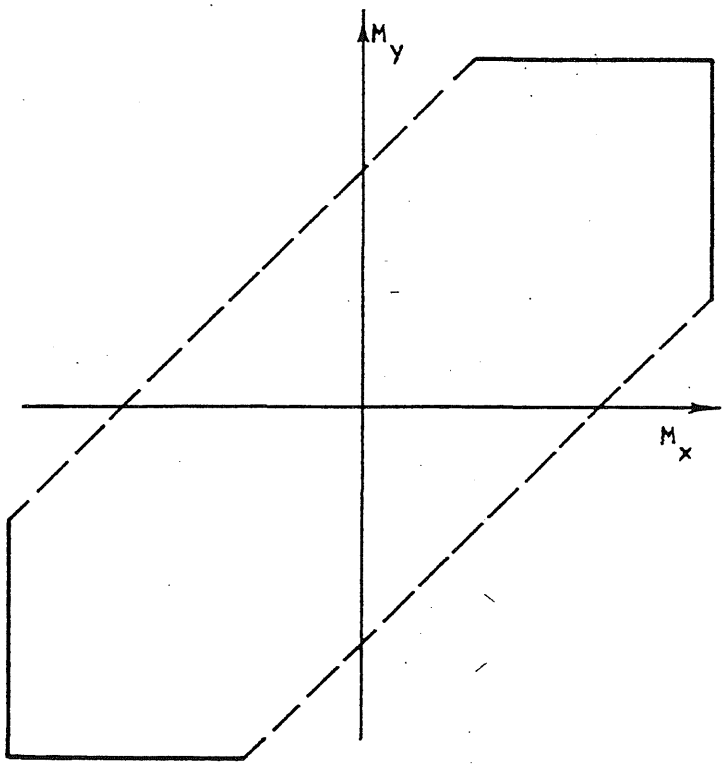

$A_s f_y = 0.60\sigma_{ca} h$

d

FIG. 7.5 YIELD-LINE CRITERIA IN CARTESIAN COORDINATES

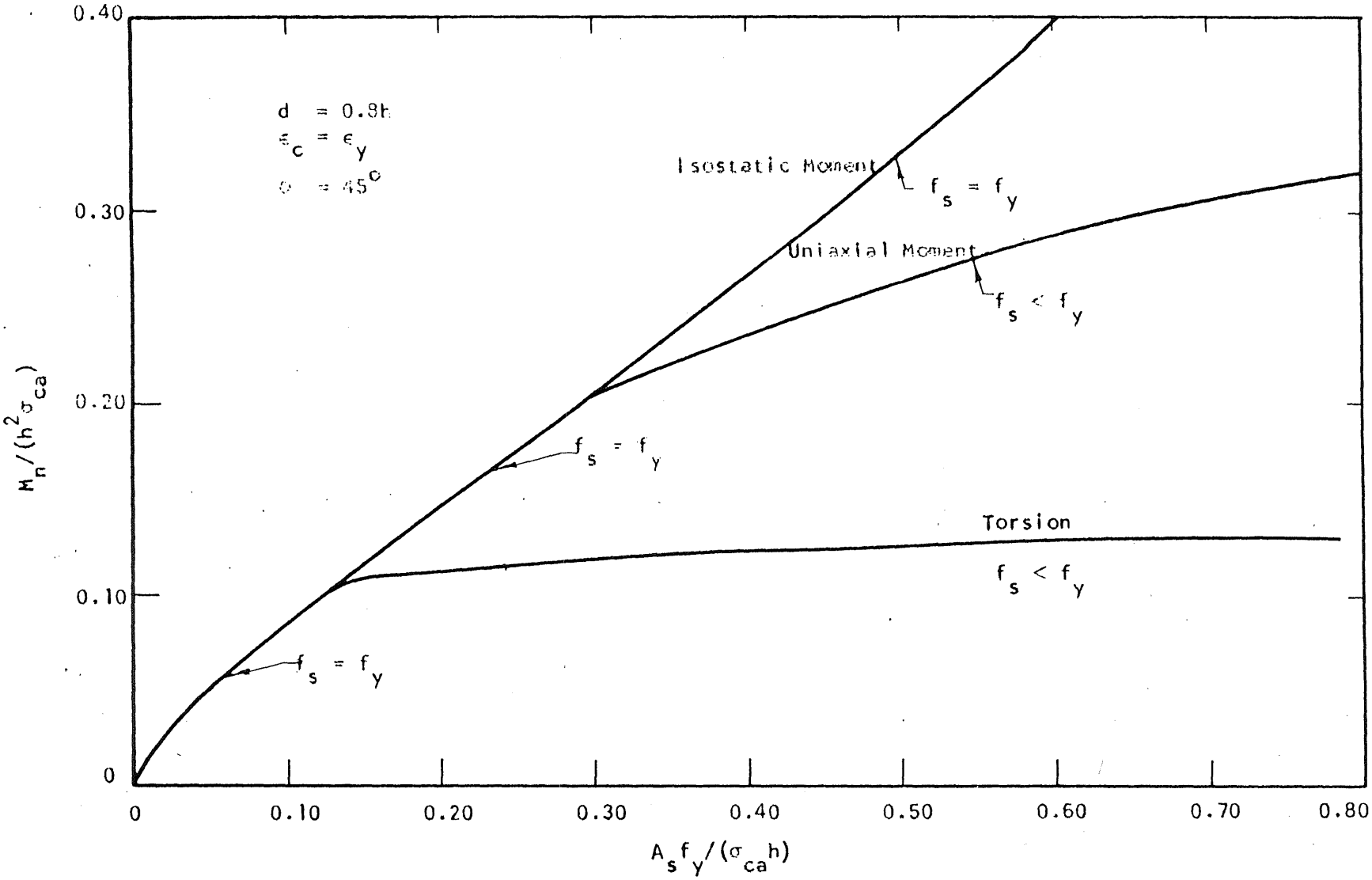

FIG. 7.6 OVERREINFORCED AND UNDERREINFORCED SECTIONS

APPENDIX A

DESCRIPTION OF EXPERIMENTAL METHODS AND TEST DATA

A.1 Introductory Remarks

This appendix gives a description of the experimental part of the investigation, which consisted of 22 test specimens. It reports the properties of the specimens, the test setup, the measurements made, and objective observations.

A.2 Materials

(a) Cement

Atlas brand high-early strength cement was used for all specimens.

(b) Aggregates

Wabash River sand and pea gravel were used for all specimens. Both aggregates have been used in this laboratory for many previous investigations and have passed the usual specification tests. The maximum size of the gravel was 3/8 in.

The origin of these aggregates is an outwash of the Wisconsin glaciation. The major constituents of the gravel were limestone and dolomite. The sand consisted mainly of quartz.

(c) Concrete Mixes

Mixes were designed by the trial-batch method. Three batches were ordinarily used in each specimen. Table A.1 lists the proportions of the concrete batches used in each specimen along with the slump,

compressive strength, splitting strength and age at the time of the testing of the specimen. Proportions are in terms of the dry weights of gravel and sand. The control cylinders were taken from the concrete that was placed in the testing area of the test specimens. The testing area could contain one, two or three batches, as indicated in Table A.1. The splitting strength was found from tests of 6 by 6-in. control cylinders loaded at 9.50 psi per sec. Strips of stiff fiber board of 1/8 in. thickness and 1/2 in. width were placed between the cylinder and the heads of the testing machine to distribute the load evenly along the length of the specimen. The compressive strength was determined from tests on 6 by 12-in. control cylinders loaded at 58 psi per sec.

(d) Reinforcement

Two shipments of No. 2 (0.25 in. diameter) deformed reinforcing bars were used for this series of twenty-two tests. The first shipment was used in specimens C1 through B17, and the second shipment was used for all other tests specimens. Both shipments were purchased in California from the Triangle Steel and Supply Company and annealed at 1200°F for two hours by the Fred A. Snow Company of Chicago (Fig. A.1).

The strain in the reinforcement during testing was obtained using foil strain gages placed on filed portions of the bars. The reduction in area due to filing was measured to be about three percent.

The reinforcing bars used in specimens B15 through B22 were welded at the ends. Tension tests of various types of welds showed that the welding had no significant effect on the yield stress or on the strain hardening of the reinforcing bars.

The yield stress, yield strain, and the strain at strain hardening listed in Table A.2 were all measured from tension tests performed on a Tinius Olsen testing machine using samples with five-in. effective lengths. The strain hardening was determined from the load-deformation diagrams of tests performed at 0.05 in. per minute strain rate, 0.5 in. per minute chart drive, and 6000 pound capacity. These diagrams are similar to the dotted curve shown in Fig. A.1. However, the elongation as indicated by the chart plots also included the slipping of the specimen in the grips of the machine. By calculating the percent slip on specimens of 5 and 10 in. effective lengths, an actual strain of 0.02 was found to correspond to one inch of elongation on the flat yielding portion of the load-deformation diagrams.

During the early stages of testing, C1 through B11, the results from the tension tests of the reinforcing bars were consistent enough to be combined. After B11, however, slight inconsistencies in the yield points forced the adoption of separate tests for the steel used in each slab. The yield stresses in the first shipment were quite consistent. This may be due to the fact that it was annealed in ten-ft lengths. The second shipment, however, was annealed in twenty-ft lengths and a significant variation in yield stresses was observed between bundles and between ends of a given bundle. To overcome this difficulty, accurate records were kept of the steel used in each slab. This helped maintain full control of steel characteristics within a given slab.

A.3 Description of Specimens

The test specimens were of two types: the "circular" test specimen designated "C" and the rectangular test specimen designated "B".

The thickness of the test specimens was close to 4.12 in. The thickness of the specimens was checked by a 0.001 in. dial gage which was fixed to a fork provided with levels in two perpendicular directions. The thickness was measured at 15 points evenly spaced within the test area. The cross section where the thickness appeared to be minimum was considered in the theoretical computations, see Table 3.1.

The circular test specimen "C" is shown in Fig. 4.20. The test area was within the 3-ft diameter circle in the center of the specimen. The test element was supported along the 3 ft 6 in. inner circle and loaded with downward forces on the 6-ft outer circle. The loading area contained six evenly placed slots to minimize the membrane forces outside the test area.

The rectangular test specimen "B" is shown in Fig. 4.19. The test area was 3 ft 6 in. by 4 ft for specimens subjected to uniaxial bending and 3 ft 6 in. by 6 ft 10 in. for specimens subjected to torsion. The uniaxial moment was introduced as shown in Fig. 4.19, while the torsion was introduced through channels clamped at either end of the specimen.

The reinforcement for the individual specimens will be described in Section A.8.

A.4 Casting and Curing

All concrete was mixed in a nontilting drum-type mixer of six cu. ft capacity. A butter mix of one cu. ft preceded the batches used in the test specimen. The total mix quantity was approximately 11 cu. ft. After a few trials it became evident that mixing in three

batches would give better results than could be obtained by mixing the whole quantity in two batches. The slump of the batches used in the test area was determined immediately after mixing.

The circular test specimens were cast in forms with a plastic-covered plywood bottom and steel-sheet sides. The rectangular test specimens were cast in forms with plastic-covered plywood bottom and sides. The sides were replaced by new ones as soon as they appeared to be worn. Holes were formed in the specimen for the loading and supporting rods to go through by screwing 4 in. pieces of steel pipe (2 in. diameter) to the bottom.

The test area was cast first, and then the loading areas. Three 6 by 12-in. cylinders were cast from each batch to be used in determining the compressive strength of the concrete. In addition, three 6 by 6-in. cylinders were cast from those batches placed in the test area for determination of the splitting strength.

The freshly cast concrete in the test specimen as well as in the control cylinders was vibrated with a high frequency internal vibrator. The top surfaces of the test specimens were troweled smooth and the cylinders were capped with a paste of neat cement two to four hours after casting. The forms for the test specimen were not struck until one day before testing. The specimen was covered on the second day after casting by wet burlap which was removed one or two days before testing. The forms of the cylinders were removed after one day and wrapped in wet burlap until one or two days before testing.

The reinforcement was placed in the form before casting. The bottom layer was supported by small pieces of steel rods which provided

a minimum concrete cover of 3/8 in. for the reinforcement. The top layers of the reinforcement were placed on "chairs" that provided the same concrete cover at the top as at the bottom.

A.5 Instrumentation

(a) Electric Strain Gages on Reinforcement

Two reinforcing bars in each layer of reinforcement were ordinarily instrumented with electric strain gages placed well within the test area. The gages used in the first specimens (up to and including B4) were Budd Metal Film gages C6-121. The limited capacity of these gages to measure strains beyond yielding of the bars was not completely satisfactory for this investigation. The following specimens were provided with HE-111-GF gages. The Budd gage C6-121 had a nominal gage length of 1/8 in. The HE-111-GF gage had a nominal gage length of 1/16 in. The surface of the reinforcing bar was prepared for the mounting of the gage by grinding down one rib of the deformed bars. Then the surface was cleaned using fine emery cloth and acetone. The C6-121 gages were mounted using Eastman 910 cement as the bonding agent, while the HE-111-6F gages were mounted using Duco cement and were "baked" in an oven at a temperature of 200°F for two hours immediately after installation. The lead wires were soldered to the gages and insulated with tape before the gages were waterproofed with a synthetic rubber coating, "Gagekote #2." The location of the strain gages are shown in the figures describing results.

(b) Electric Strain Gages on Concrete

The concrete strains were measured on the top and bottom face of the specimens. The strains were measured with SR-4 Type A3

gages which have a nominal gage length of 3/4 in. and a width of 3/8-in. This type was used on specimens subjected to isostatic and uniaxial moment. For the specimens subjected to torsion, 45° rosette-gages, SR-4, Type AR-1-S-6, were used. Each element in the rosette gage had the same characteristics as Type A3. The concrete at locations of the strain gages was smoothed with fine sand paper and cleaned with compressed air and acetone. The use of compressed air appeared to be particularly effective. A layer of Eastman 910 cement was applied to the concrete surface and 6A-1A Accelerator to the gage. The gages were pressed against the concrete for 30 seconds or more during the application process. Most of the gages were placed well inside the test area. The location of the strain gages are indicated with the presentation of the results.

(c) Mechanical Dial Gages

The curvatures of the specimens were measured by equally spaced dial gages on light steel bridges. The larger type of the bridges had 5 dial gages spaced 7.5 in. apart, while the smaller type bridge had 3 dial gages 3 in. apart. The dial gages were Federal, Ames, and Starret gages with 0.001 in. divisions. For the circular specimens two bridges of the larger type were used to measure the curvatures in two directions. For the specimens subjected to uniaxial moment, the curvatures were measured by two bridges in the span direction and one bridge in the transverse direction, all bridges being of the larger type. For the specimens subjected to torsion, three of the larger bridges were mounted in a "rosette" form so that the curvature in any direction could be obtained. The small bridges were welded together into a triangular shape for additional measurements in all torsion specimens and a few of the

uniaxially bent specimens. The larger bridges were placed under the specimens and could not be moved during the testing. The smaller bridges could be moved freely on the top surface to the desired location any time during the testing period.

(d) Measurements by Photogrammetry

An attempt was made to measure curvatures and strains by photogrammetry. The procedure and results are briefly described in Appendix B.

A.6 Loading and Supporting Systems

A special loading and supporting system was constructed for this investigation. The main object was to eliminate undue influence from the load and the supports during the stage at which the test specimen would have significant deformations. In other words, the object was to maintain full control of the boundary conditions at all stages of the loading.

(a) Loading and Supporting System of Specimens Subjected to Uniaxial Moment

Figure A.2 illustrates the system used. The specimens were suspended from a 18 by 20-in. steel box beam by two steel rods. All the steel hangers were 5/8 in. high strength "Stressteel" rods. All hangers were provided with a convex spherical washer in each end which was matched with a corresponding concave spherical setting in the connection. The two leverarms under the support beam (Fig. A.2) divided the load equally between the supports under the test specimen. Two other identical leverarms transferred and distributed the jack loads to the specimen. The leverarms consisted of two channels 6 x 2-in. (13 lb/ft) spaced at 1.875 in. Bolts with a 1.0 in. hole perpendicular to the bolt axis for the hangers were placed in the space between the channels.

The bolts were free to rotate. Hence, the loading and supporting system had 24 hinges, which should provide equally distributed load and support forces and should prevent undesirable twisting moments caused by the deformation of the specimen. Before loading, the 1.4-kip specimen and equipment could easily be rotated by pushing lightly up or down on the side of the specimen with the fingers. The rotational resistance under partial and full load was measured repeatedly by a third set of jack and dynamometer located at the side of the specimen. The results showed that the rotational friction moment was less than three percent of the introduced moment. Although the above magnitude is small, the actual frictional moment was apparently significantly lower, because the mentioned three percent resulted from several degrees rotation, and the resisting rotational moment appeared to rise with increasing rotation.

The loads were introduced by two hydraulic jacks connected to one common electric pump. The 30-ton jacks were Simplex, Model R315. The loads, both at the load and the support locations, were transferred to the concrete surface by steel blocks measuring 3 by 20-in. A block was stiffened by two 1/2 by 3 by 20-in. steel plates in order to minimize the bending. The stiffeners can be seen in Fig. A.2 and A.4. A plate of 1.0 in. thick hard rubber was placed between the steel block and the concrete surface. At large deformations such as those shown in Fig. A.3 and A.4, it was necessary to insert wooden wedges between the rubber plate and the specimen in order to prevent sliding of the shoes.

(b) Loading and Supporting System of Specimens Subjected to Torsional Moment

Most of the equipment used for uniaxially bent specimens was also used for torsion specimens. The system can be seen in Fig. A.5 and

A.6. Two channels 5 x 1 3/4-in. (6.7 lb/ft) were clamped to either end by three 1.0 in. bolts. Hard 1.0 in. thick rubber plates were placed between the channels and the concrete surface. The specimen was suspended at two diagonally opposite corners by hangers which were provided with the usual hinged connections in either end. The hinges of the channels were also of the same type as those in leverarms used for the uniaxial bent specimens. Because of the large deformations, it was necessary to provide two Simplex jacks at either loading corner. Even this arrangement had to be reset. Each jack had a 5 in. stroke. The majority of the torsion tests had a maximum deflection at any corner that was more than 20 in. measured relative to a plane passing through the location of the other corners of the deflected plate.

(c) Loading and Supporting System of Specimens Subjected to Isostatic Moment

Figures A.7 and A.8 show the loading and supporting system for a circular test specimen. The specimen was suspended from the three corners of a triangular frame placed on top of the 18 by 20-in. beam, Fig. A.7. Three leverarms distributed the supporting forces to six steel blocks placed in a circle of 3 ft 6 in. diameter. The blocks were 3 by 15-in. and formed a hexagon around the test area. The blocks were stiffened with two 2 1/2 by 15-in. steel plates, and a one in. thick rubber layer was placed between the steel blocks and the concrete. Three leverarms under the specimen transferred the forces from three hydraulic jacks to each of the six loading "wings" along a circle with a 6 ft diameter. The load blocks on the wings and the leverarms above the test plate were the same as those described for the uniaxially bent specimens, while each of the leverarms below was made of two 6 x 2-in. channels (13 lb/ft) of

40 in. length. Either end of every high strength steel hanger was hinged by means of a spherical washer and setting. The 36 hinges insured an even distribution of the applied moment regardless of the deformation of the test specimen. The three Simplex jacks were connected to one electric pump.

(d) Load Measurements

The loads were measured by means of 30,000 lb. capacity dynamometers made for this investigation. The dynamometers were placed between the jacks and the loading frame constructed of heavy I-10 steel sections. The dynamometer essentially consisted of a ring of T-1 steel located between two steel plates. The ring had a 4 in. diameter with respect to its centerline. The cross section of the steel ring was 0.6 in. in the radial direction and the height was 0.825 in. The ring rested on three 3/4-in. steel balls located between the ring and the plate, 120° apart. Under loading, three other 3/4 in. steel balls located between the supporting balls exposed the steel ring to bending and torsion. The strains were registered by eight SR-4 Type A7 gages evenly distributed around the ring. The strain gages were connected in a four arm bridge system and to a Baldwin strain indicator. The calibration of the dynamometer was in the order of 4 lb. per division. Unfortunately, the calibration curves were not perfectly straight lines. Therefore the actual calibration curves were used to graphically convert the readings into loads. The dynamometers were recalibrated near the middle and at the end of the test series. No significant changes were observed.

A.7 Test Procedure

The yield load was ordinarily reached in 12 to 14 increments, and the ultimate load was reached in 20 to 25 increments. Before yielding the increments were equal load increments. After yielding the increments were related to an increase of the curvature of 50 to 100 x 10^{-5}/in. Immediately after each increment of load or curvature, the dynamometers readings were taken. Thereafter all deflection and strain measurements were read and the moment arms for the loads were checked. Photographs for photogrammetry were taken at approximately every third increment in the first half of the test series, but this number was later reduced. This procedure usually took three men five to ten minutes for each test increment. At the completion of the readings, the loads on the dynamometers were checked. Cracks usually appeared after three or four load increments. All the specimens, except one (B13), were loaded to complete failure. Specimen B13 manifested exceptional ductility and the testing was stopped because of fear of damaging the testing equipment. Each test took from five to eight hours. Control specimens were tested concurrently or immediately after the test, except for specimen B14, whose control specimens were tested three days after the slab specimen.

A.8 Description of the Individual Tests of the Test Series

The test results and observations of the individual tests are reported in this section. A survey of the test specimens, their properties and test results are given in Table 3.1.

The tests will be reported in the following sequence: (a) specimens subjected to isostatic moment, (b) specimens subjected to uniaxial moment, and (c) specimens subjected to torsion.

(a) Specimens Subjected to Isostatic Moment

The first series consisted of three specimens subjected to isostatic bending. The three specimens had the same reinforcement. The reinforcement is shown in Fig. 3.9 and A.9. No. 2 (0.25 in. diam.) bars were placed in pairs in order to improve the conditions for casting and vibration. The first layer of reinforcement had a 3-in. spacing between pairs and the second layer was spaced at 2.75 in. between the pairs of bars. The latter spacing was narrower to compensate for the shorter internal moment arm of the second layer. The amount of steel in the first layer was approximately one percent of the effective cross section. The loading areas or the wings were extra reinforced with u-shaped No. 3 (3/8 in.) bars (Fig. 3.9 and A.9). The moment capacity was made 50 percent higher in the loading area than in the test area.

Specimen C1

Test specimen C1 was the first test specimen to be tested and was a test of the loading and supporting system as well as of the specimen. Strain measurements were reduced to a minimum.

After nine load increments, corresponding to a unit moment of 1.45 k-in./in., the first cracks appeared at the slots. After two more load increments, or at a total unit moment of 2.32 k-in./in., the cracks were spread over the entire test area. The crack pattern was uniform over the test area. The cracks had a tendency to coincide with the reinforcing bars (Fig. A.10). The directions of reinforcement coincided with the directions of the coordinate system drawn on the surface. The squares of the coordinate system were 4 by 4-in., while the average "crack square" was about 3 by 3-in. which corresponds to the reinforcing bar spacing. The cracks widened equally over the test area. At the corners of the slots, however, the cracks became wider than elsewhere

in the plate. Figure A.11 shows a close up photograph of this phenomenon. Because of the stiffness of the loading wings, the compatibility conditions resulted in a concentration of the curvature in the corner of the slot. During this test series, the use of 12 wings instead of six was considered in order to reduce the concentration of curvature. It was found from this first test, however, that the middle part of the test area could be strained far beyond yielding before crushing took place at the slots. Within this deformation range a change from 6 to 12 wings was not likely to have any effect on the 30-in. diameter middle area where the deflection and strain measurements were obtained.

The theoretical deformed shape of an isotropically reinforced element subjected to an isostatic moment is spherical. Such a shape was indicated by the readings of the two dial-gage bridges, but even more illustrative were the results from the photogrammetry shown in Fig. A.12. The contour lines are as circular as can be expected, considering that the element after yielding was in a state of near instability in which small imperfections might give preference to deformations in one direction. Figure A.13 shows the compression side after collapse. Crushing at every corner is visible. The crushing was most extensive at the farthest wing in the photograph and preceded the collapse of this wing. As seen in Fig. 3.9 and A.9, the reinforcement entered the wings at different angles. It entered two wings parallel to the wings' axes and entered the other wings at inclined angles. It is interesting to note that one of the latter wings collapsed first, although these should be the stronger ones according to the "kinking" theory.

The dead load moment was computed by calculating the weight of a concrete wing and weighing the loading equipment directly on a scale.

The dead load moment of the test area itself was small and was ignored. The curvature was measured by the gage bridges mounted from one slot corner to another (marked with chalk lines in Fig. A.13) so that they crossed each other at 60°. The moment-curvature relationship is shown in Fig. A.14. The 2-in. diameter holes in the plate restricted the magnitude of plate deformations and the load had to be removed while the supporting and loading blocks were reset causing the discontinuity of the curve in Fig. A.14.

The strain measurements on the compression side, shown versus the unit moment in Fig. A.15, indicated that the strains on the compression side were equal in all directions and the compressive concrete behaved approximately linearly elastic up to yield. The compressive strains in the center of the element at collapse were nearly 0.15 percent, but since the strains at the slot corners were considerably higher, the strain readings at the middle give no information of the strain capacity for the specimen.

Specimen C2

While C1 had an unusually high concrete strength (f'_c = 6610 psi), C2 had a more common concrete strength (f'_c = 4580 psi). The first cracks were observed at the slots after four load increments and at a unit moment of 1.13 k-in./in. At the sixth increment, at a unit moment of 1.89 k-in./in., the cracks had spread uniformly over the entire test area. As Fig. 3.8 and A.16 show, the crack pattern in the test area formed a nearly perfect square network. The holes in the plate were made pear-shaped to allow greater deformation before the steel hangers touched the concrete. The curvature could be increased to several times that at yield without any resetting. The specimen appeared to be extremely ductile, as is reflected by the moment-curvature relationship in Fig. A.18. The orientation of

the deflection measurement bridges was changed so that the bridges were perpendicular to each other. Thus, the curvatures in Fig. A.18 are the averages of the curvatures from the two bridges. The collapse occurred at a curvature of 850×10^{-5} in.$^{-1}$. At ultimate load it looked like the specimen was going to fail along several lines simultaneously. Finally, crushing took place along two lines as seen in Fig. A.17. (The directions of the reinforcement coincided with those of the strain gages.)

The strain readings shown in Fig. A.19 indicate that the compressive concrete strains were close to 0.3 percent at ultimate load, which supports the observation that the entire test area was about to fail simultaneously.

The curvature-strain relationships of Fig. A.20 and A.21 indicate that the steel strains were equal throughout the test area. Beyond the yield strain, 173×10^{-5}, the readings became unstable and inconsistent, which makes the vertical trend in Fig. A.20 questionable. The constant strain in Fig. A.20 may be due to separation of the gages from the steel. Or the vertical curve might indicate that bending took place somewhere outside the area influencing the strain gages.

Test Specimen C3

The concrete quality in specimen C3 was reduced to f'_c = 2700 psi. Surprisingly, the first cracks at the slots were not observed before the fifth load increment at a moment of 1.36 k-in./in., which is within the same range as the cracking moment for specimen C2. Figure A.22a shows the crack pattern, a uniformly distributed square grid of approximately 3 by 3-in. The failure occurred across a root of a wing as shown in Fig. A.22b. The directions of the reinforcement coincided with the system lines of the strain gages.

The moment-curvature relationship is shown in Fig. A.23. The ductility was significantly less than for specimen C2. Evidently, the wings collapsed before the whole ductility was utilized in the testing area. The concrete strain readings, Fig. A.24, also indicated that the test area was not strained to its capacity. Figure A.25 and A.26 illustrate the uniform distribution of the strains of the reinforcement in the test area.

The data from deflection and strain measurements confirmed that the test areas in all circular specimens were in a state of isostatic bending. It could also be concluded that the ductilities of the test areas of C1 and C3 probably were greater than indicated by the measurements. This point appears to be less important as long as the flat portion of the moment-curvature relationship of all specimens was observed, and the measured ductility can be assumed to be satisfactory for the yield-line theory.

(b) Specimens Subjected to Uniaxial Moment

Ten specimens were subjected to uniaxial moment. The concrete quality was in the moderately high range, from 3500 to 5500 psi. All specimens, except B13, were reinforced at one face only. The specimens were provided with 50 percent extra reinforcement in the loading zone to insure that failure took place in the test area.

Test Specimen B4

Specimen B4 was chosen as a "standard" specimen to be used for direct comparison with the other specimens without any intermediate theoretical computations. The specimen was actually a simple beam with the effective longitudinal No. 2 (1/4 in.) reinforcing bars in pairs spaced at 3 in. For consistency, a second layer of reinforcement was

placed in the transverse direction with the No. 2 bars in pairs spaced at 2.75 in. Although this layer did not affect the strength of the specimen, it appeared to influence the cracking. The crack pattern is shown in Fig. 3.6a and A.27. The chalk lines indicate the position of the reinforcing bars. The average crack spacing was approximately equal to the spacing of the reinforcement.

This specimen possessed very high ductility. When the slopes of the ends of the plate reached about 10^{o}, the loading blocks began to slide and the moment arm of the loads were difficult to measure accurately. The high ductility is illustrated in Fig. A.28 and A.29. The latter reflects the irregularities caused by the sliding of the loading blocks which started at a curvature of 500×10^{-5} in.$^{-1}$. It is interesting to note that the maximum compressive strains (Fig. A.30) were only slightly higher than those of the circular specimen C2. The transverse strains, plotted in Fig. A.31, appeared to rise rapidly before cracking and hardly showed any increase between cracking and yielding. This pattern, which is contrary to that of the compressive longitudinal stresses, is difficult to explain by Poisson's ratio. The transverse strains should also be reflected by the strain gages on the transverse bars given in Fig. A.33. As this is not the case, it may be concluded that the strain readings for small strains at the order of 5×10^{-5} were unreliable. The strain readings from the longitudinal reinforcing bars in Fig. A.32 show a consistent trend with a minimum scatter up to yielding. In order to evaluate the strains beyond yielding, the steel strains are compared with the curvature in Fig. A.34 and A.35. As it is seen, the readings beyond yield were poor. Consequently, it was decided to replace the gages of Type C6-121 with Type HE-111-GF.

Specimen B5

Specimen B5 was the first specimen in which bond problems with the reinforcement were encountered. The reinforcing bars were at an angle of 45° with the longitudinal axis as shown in Fig. A.36. It was decided to test two specimens with inclined reinforcement without any special arrangement for increasing the bond at the end of the bars. The behavior of the specimen under loading was as expected up to a load close to the predicted yield load. Cracking began between 1.0 and 2.0 k-in./in. applied moment, and the cracks spread uniformly over the test area. At a moment of 5.0 k-in./in., the curvature suddenly concentrated at either side of the test area as shown in Fig. A.37. The concrete popped up, lifted by the reinforcing bars as seen in Fig. A.38. Some of the bars may have lost all bond with the concrete over a considerable length. The resisting moment dropped off and the middle part that had had a smooth curve became nearly straight again, as is shown by the photograph in Fig. A.39.

The effective width of an element was considered to correspond to the cross section in the test area which had the least number of bars crossing it. This consideration allowed the bars a 2 to 3 in. anchorage length in either end.

The moment-curvature relationship in Fig. A.40 supports the description above. It should be noted that the measurement bridge did not register the concentrated curvature (Fig. A.39). The transverse concrete strains on the compression side (Fig. A.41) show a definite trend of the effect of the resulting transverse forces introduced by the inclined reinforcement (and Poisson's ratio, which appeared to play

a minor role). Figure A.42 indicates that the longitudinal compressive strains in the middle part of the specimen reached only 125 x 10^{-5} before failure. From the steel strains, Fig. A.43, it can be concluded that the specimen was close to yield; some of the bars reached yield and some were close to yielding.

Specimen B6

Specimen B6 had the same reinforcement as the previous specimens (C1-B5), but the directions of the reinforcement were at 22.5° and 67.5° to the longitudinal axis as shown in Fig. A.44. This arrangement gave the more important layer of reinforcing bars an anchorage length of up to 6 in., and the element possessed some ductility as expressed by the moment-curvature relationship in Fig. A.46. The cracks deviated some from the transverse direction indicating the dominant role of the reinforcing bars at 22.5° to the longitudinal direction (Fig. A.45a). The failure appeared to be a bond failure with scaling of the concrete cover as shown in Fig. A.45b. The compressive concrete strain reached about 50 percent of the concrete strain capacity, Fig. A.47. Figure A.49 is an interesting picture of the strains in the two directions of reinforcement. The effect of the layer at 67.5° is surprisingly high, but may be explained by the inclined crack pattern shown in Fig. A.45a where the cracks deviated about 10° from the transverse direction in such a way as to increase the stresses in the layer which was stressed less.

Specimen B7

Test B7 was a repetition of B5 except that each reinforcing bar was provided with a double hook in either end and the pairs of

reinforcing bars were split so that the spacing was reduced by one-half. The hooks may be seen in the photograph in Fig. A.50. The effectiveness of the hooks may be best illustrated by the side view at ultimate load in Fig. A.52a and b and by the moment-curvature relationship shown in Fig. A.55.

The crack spacing appeared to be smaller in cases where the directions of the reinforcement were different than those of the principal moments. In Fig. A.51 the distances between the coordinate points are 5 in., and several cracks can be observed between two points. There was a striking difference between the crack spacing in this specimen and specimens with the reinforcing bars in the longitudinal and transverse direction (B4 and B10). Hence, this indicates that formulae which predict crack width and crack spacing for beams can hardly be applied to slabs.

An interesting phenomenon was the large transverse force introduced by the reinforcement. Before the ultimate load was reached, the transverse force began to crush the concrete on the sides, Fig. A.52b. The corresponding moment caused wide longitudinal cracks in the compression side of the specimen, Fig. A.54. At ultimate load the transverse forces seemed to split the concrete as is seen in Fig. A.53.

The closely cracked surface caused the concrete strain readings to scatter more than usual. The plotted results in Fig. A.56 reflect, however, the high transverse compressive strains in the side where the reinforcement was located. The corresponding tensile strains in the opposite side are plotted in Fig. A.58. It should be noted that longitudinal compressive strains were read beyond 450×10^{-5} (Fig. A.59).

The effectiveness of the hooks of the reinforcing bars were checked by several strain gages. From equilibrium, the forces in the very end of the bar should be one-half of the stress at some distance from the edge, provided the bond is complete. Thus Fig. A.60 indicates that the bond was satisfactory. Large-deformation strain gages of type HE-111-GF were located on the steel in order to measure deformations beyond yield, but the results in Fig. A.61 and A.62 show that the new gages did not improve the large-deformation measurements significantly.

Specimen B8

Specimen B8 had isotropic reinforcement, No. 2 bars (0.25 in. diam.) spaced at 1.5 in. in the first layer and at 1.375 in. in the second layer. The bars had double hooks at either end as for B7 and all the following specimens subjected to uniaxial bending, Fig. A.63. The reinforcement directions were at 22.5° and 67.5° to the span direction.

It was interesting to observe the development of the crack pattern. The cracks appeared and spread over the test area perpendicular to the direction of the span. With application of further load, the cracks began to combine in a direction so as to avoid the more effective reinforcement at 22.5° to the span. After first yielding, however, the force in the bars at 22.5° in the span was gradually less dominating and the yield lines eventually become approximately perpendicular to the span. The yield lines can be seen distinctly in Fig. 3.6c, while traces of some of the "rotated" cracks are also visible. The longitudinal cracks on the compression side in Fig. A.64 indicate strong transverse forces from the reinforcement in this case also, but while the strain readings in the transverse direction on the tension side are scattered, the readings on the compression side show the expected trend (Fig. A.66 and A.68).

Specimen B9

Specimen B9 was the first specimen with nonisotropic reinforcement, Fig. A.72. The first layer of No. 2 bars was spaced at 3 in.; the second layer at 1.375 in. After the cracks were initiated perpendicular to the span direction, the direction of the cracks gradually rotated with increasing load until yielding of the reinforcement took place. The final yield line direction is shown in Fig. 6.3 and A.73. This rotation of about 18° required a substantial twisting moment along the yield line because there was no external twisting moment. The presence of an internal twisting moment is supported by the photographs in Fig. A.74 and A.75. There was a difference in steel strains in the two layers as shown in Fig. A.81, where gages 23 and 24 represent the first (weak) layer and gages 27 and 28 represent the second layer. At first yield, the strains in the first layer were approximately 50 percent higher than those in the second layer, which theoretically corresponds to a rotation of the crack by 6° from the transverse direction. After full yielding had taken place, the strains for gages 23, 24, 27 and 28 were 0.01139, 0.01397, 0.00215 and 0.00281, which theoretically corresponds to a rotation of approximately 20°. That most of the rotation took place after the first yield was supported by direct observations.

Specimen B10

Specimen B10 was the second "standard" specimen. The second layer was the more effective layer. The reinforcement was isotropic. For consistency the bars were spread out and provided with hooks in either end, Fig. A.82. The crack-spacing averaged about 1.5 in., which was also the spacing for the transverse reinforcement. Figure A.84 shows

the compression side after failure. The wooden wedges under the loading and supporting blocks shown in Fig. A.85 had a slope of 12° and were inserted when the slope of the load area exceeded 7.5°. The load had to be taken off in order to insert the wedges, which explains the irregularity in the moment-curvature curve in Fig. A.86. The strain readings are shown in Fig. A.87-A.91.

Specimen B11

Specimen B11 had nonisotropic reinforcement. The first layer of No. 2 bars were spaced at 1.5 in. and were at an angle of 22.5° with the direction of the span (Fig. A.92). The second layer of bars were spaced 2.75 in. apart and were at 67.5° to the span direction. The development of the cracks and yield lines were similar to that of B9. The yield lines and the crushing zone are shown in Fig. 6.4a and b.

Because of the twisting of the specimen caused by the nonisotropic reinforcement (Fig. A.93), the principal concrete strains no longer were in the longitudinal and transverse direction, and 45° rosette gages were used. The results are shown in Fig. A.95-A.100. The gages on the reinforcement near the ends of the bars should not be considered as being representative of the average steel strains in the test area (Fig. A.101 and A.102). Because of the waterproofing that covered the gage and the gage's environment, the bond between the hook and a gage placed 2-3 in. from it may be assumed to be very small. Therefore, the results of the end gages may be assumed to be indicative of the hook stresses.

Specimen B12

This third specimen with nonisotropic reinforcement had the same amount and distribution of reinforcement as the preceding specimens B9 and B11, but the heavier layer was placed at an angle of 67.5° to the span direction, Fig. A.103. The yield-line pattern is shown in Fig. 6.5 and Fig. A.104. Although the rotation of the yield lines was one-half of that in either B9 or B11, the specimen had a significant twisting deformation, as can be seen in Fig. A.106. The moment-curvature relationship in Fig. A.107 and the steel strains in Fig. A.114 and A.115 indicate that the heavier layer of reinforcement played a minor role at the first yielding of the reinforcements but became more effective with increasing curvature.

Specimen B13

Test specimen B13 was a "standard" specimen, isotropically reinforced in the top and bottom, Fig. A.116. The crack pattern shown in Fig. A.117 was similar to that of B10, as would be expected. The specimen possessed very high ductility, as is indicated in Fig. A.4, and was the only specimen that was not loaded to complete failure. The moment-curvature and strain readings are shown in Fig. A.118 through A.123.

Specimens Subjected to Torsion

Because a torsional moment produces tensile stresses in both top and bottom sides of an element, all torsional test specimens were provided with reinforcement repeated in the top and bottom faces. Since a torsional specimen has no "tension" side, "compression" side, or "span" direction, the locations and directions have been defined as follows: The references

to top and bottom of the specimens are with respect to their position during the test. The longitudinal or the x-direction coincides with the longer sides of the specimen, while the transverse or y-direction is parallel to the shorter sides. The reinforcement layers are counted from top to bottom. Nine specimens were tested in torsion, seven isotropically reinforced and two reinforced nonisotropically. The effective widths of the specimens were computed assuming the yield line would appear along a section that avoided reinforcing bars at the edge as much as possible.

Specimen B14

The isotropic reinforcement is shown in Fig. A.124. The directions of the reinforcement were in the longitudinal and transverse directions, that is, 45° to the applied principal moments.

Specimens B14 and B15 were tested with particular attention to the edge problems. Because the directions of the edges do not coincide with one of the principal moments, a concentrated shear force (called a "nodal" force in the yield line theory) trying to rip the plate from the edge will occur at the edge. Even though all bars were doubly hooked at both ends, the shear force cracked the side between the vertical hooks and ripped the plate as shown in Fig. A.125. The edge failure occurred immediately before yielding as the moment-curvature plot in Fig. A.126 indicates. The strain readings are plotted in Fig. A.127 through A.134.

Specimen B15

Specimen B15 had the same reinforcement as B14 except that it was rotated 45° to the longitudinal axis, as is shown in Fig. A.135.

It was difficult to decide whether the edge failure in the preceding test was due to bond failure or a pure shear failure. To prevent bond failure all reinforcement was welded together in this specimen. Tests of welded bars in a testing machine revealed no change in the stress-strain relationship for the bars. The welding led to a definite improvement in slab performance. As indicated by the moment-curvature relationship in Fig. A.138, the element reached yield and possessed a ductility corresponding to a deformation three times that at yielding. Figures A.145 and A.146 show that the tension reinforcement was strained well beyond the yield point. Still the failure seemed to be due to an edge failure, and this time it appeared to be a definite shear failure (Fig. A.137a and b).

Specimen B16

The reinforcement in B16, shown in Fig. A.147a, was equal to that of B14, but the details at the edge were handled differently. As may seem from Fig. A.147b, the reinforcing bars were welded to No. 2 vertical bars 3.75 in. long. To take the shear, No. 3 (0.375 in. diam.) bars inclined 45° were welded to the reinforcement. No extra "moment" reinforcement was added, but two bars in either side were moved towards the shear reinforcement to provide a connection. This solution appeared to be satisfactory. Figure A.148a shows the specimen under ultimate load with the edge still intact.

The moment-curvature relationship, Fig. A.149, indicates that the element was "overreinforced" or at the "balance" point. The crushing of the top face, Fig. A.148a, supported this impression. The concrete compressive strains plotted in Fig. A.154 increased very rapidly after cracking, but, because of an increasing number of cracks, the strain

readings became unreliable before the assumed crushing strain of the concrete was reached. Figures A.156 and A.157 show that the steel strains barely reached the yield strain. This may be even more emphasized by the plotted curvature-strain relationship in Fig. A.158 and A.159. Therefore, the slab element may be assumed to have been precisely at the "balance" point under the given conditions

Specimen B17

Specimen B17 had isotropic reinforcement placed at 22.5° and 67.5° to the longitudinal direction (Fig. A.160). The arrangement of the reinforcement at the edges of B16 as shown in Fig. A.147b was retained for the remaining specimens of the test series. The moment-curvature relationship, Fig. A.163, shows that B17 possessed extensive ductility. There was no distinct yield point. The reason for the absence of a distinct yield point may be explained by studying the steel strains in Fig. A.170-A.173. The less effective bars, which started out in compression, were gradually strained in tension and finally these bars approached the yield point at very large slab deformations.

At the last stage before collapse, bending in one direction became dominant. Figure A.161a shows that the compressive stresses in the top face almost eliminated the yield lines in the perpendicular direction, while Fig. A.161b shows how the tension lines were dominating in the bottom face.

Specimen B18

The reinforcement was inclined 45° to the longitudinal axis and was the same as for B15 (Fig. A.135) with the exception of the details at the edges. The behavior of the element indicated clearly

that the element was underreinforced. The yield lines were at 45° to the longitudinal axis and were very wide before the crushing appeared on the opposite side, see Fig. A.174 and A.175. The moment-curvature relationships are shown in Fig. A.176. The ductility presented by this curve refers to the curvature of the middle 25 in. of the test area. After yielding the curvature began to concentrate along the line that later turned into the crushing line shown in Fig. A.174. This concentration of the curvature after yielding is also demonstrated by the curvature-steel strain relationship plotted in Fig. A.185 and A.186.

Specimen B19

Specimen B19 had isotropic reinforcement in top and bottom inclined 45° to the longitudinal axes. The spacing of the reinforcing bars was 3 in. in the first and fourth layers and 2.75 in. in the second and third layers, Fig. A.187. The shear reinforcement at the edge was reduced to one-half of that in the preceding test specimens. At a principal curvature of 500×10^{-5}, the shear reinforcement broke in a weld. The weld appeared to have about one-half the cross section that it should have had. The failure of the weld indicates that the shear reinforcement was stressed considerably. The connection was rewelded and the testing continued. Figure A.190 shows the location of the broken shear reinforcement.

Specimen B20

Specimen B20 had the same reinforcement as B19, but with the reinforcing bars in the longitudinal and transverse direction. The reinforcement is shown in Fig. A.200 and A.201. Figure A.202 shows the yield lines at 45° and Fig. A.203 illustrates the amount of the twisting of the element. The moment-curvature relationship is given in Fig. A.204.

Specimen B20 was similar to B18 with exception of the amount of reinforcement. The behavior of the two specimens again supports the idea that B18 had a "balanced" amount of reinforcement while B20 was underreinforced. This is also supported by the strain readings given in Fig. A.205 through A.214.

Specimen B21

The test series was concluded with two nonisotropically reinforced specimens. According to the theory derived in this investigation, the difference between the nonisotropic and the isotropic cases will not be significant until the ratio of the amount of the reinforcement in the two directions is 0.30 or lower. In this investigation the reinforcement was reduced in the longitudinal direction to one fourth of that used in the transverse direction, as shown in Fig. A. 215. The moment-curvature relationship (Fig. A.219) was similar to that of B20, but the final yield line deviated 15-18° from the direction of the principal moment which was at 45° to the longitudinal direction. The line of crushed concrete can be seen in Fig. A.216. The open yield lines occurring in the opposite side are shown in Fig. A.217. Two "sets" of cracks may be seen: (1) the cracks that appeared at the first cracking at 45° to the vertical in the photograph, and (2) the final yield lines that are partly former cracks and partly lines "leaping" from one crack to another which finally resulted in the yield lines deviating 15-18° from the initial crack direction.

Specimen B22

Specimen B22 was a repetition of B21 except for one detail concerning the consideration of the dead load moment. It is evident

that the dead load moment introduces a uniaxial moment component in the torsion specimen. Thus, the torsion test was not a "pure torsion test", although it was not possible to observe the effect of the comparatively small dead load even at the stage of the cracking. The cracks formed at 45° to the longitudinal axis as if no uniaxial moment component were present. Most of the torsion specimens failed by crushing of the concrete on the top surface, a bias possibly introduced by the dead load moment. But even then, not all failed in this manner. In computation of the applied moment, the dead load moment was taken into account by adding its 45° component to the torsional moment.

From the theory derived in the text, the resistance against torsion is not higher than that provided by the "weakest side" of the element. It should therefore be possible to "overreinforce" the bottom side and let it take care of the dead load moment. Thus, the top layer would determine the torsional resistance. The dead load moment in B22 required approximately the strength of 1.5 longitudinal bars. Therefore, two extra bars were placed in the bottom of specimen B22 as may be seen in Fig. A.228. In this test the applied moment was <u>not</u> considered to include the dead load and the comparison between the computed and measured moment supports the assumption that the dead load was taken care of in this way. The results also support the idea that the torsional resistance cannot be increased by strengthening one side only. The yield-line pattern is shown in Fig. 6.6b, and the moment-curvature relationship is shown in Fig. A.230. The relatively high moment is due to a higher yielding stress in the reinforcement, see Table 3.1. The strain readings are plotted in Fig. A.231 through A.238.

TABLE A.1

PROPERTIES OF CONCRETE MIXES

Mark / Batch →	Compressive Strength, f'_c psi 1	2	3	Splitting Strength, f'_t psi 1	2	3	C:S:G by weight	Water / Cement	Slump in. 1 2 3	Age at Test Days
C1	6610	----	----	---	---	---	1:2.8:3.1	0.68	3.2,3.5,---	25
C2	4580	----	----	407	---	---	1:2.8:3.1	0.68	3.0,---,---	8
C3	2700	----	----	216	---	---	1:3.9:4.3	0.92	1.5,---,---	7
B4	4250	5225	----	329	406	---	1:2.8:3.1	0.68	2.0,2.5,---	8
B5	4790	4910	----	281	269	---	1:2.8:3.1	0.68	1.5,2.25,--	9
B6	4895	4895	----	377	362	---	1:2.8:3.1	0.68	---,---,---	8
B7	5220	5025	----	---	---	---	1:2.7:3.0	0.67	2.0,3.0,---	7
B8	3635	3805	----	328	333	---	1:2.7:3.0	0.67	3.0,3.0,---	7
B9	4050	3595	----	370	396	---	1:2.7:3.0	0.67	3.0,3.0,---	7
B10	4790	5040	----	369	349	---	1:2.7:3.0	0.67	5.0,3.5,---	7
B11	4850	4740	----	403	389	---	1:2.7:3.0	0.67	2.0,2.5,---	7
B12	5310	5040	----	370	350	---	1:2.7:3.0	0.67	3.0,4.0,---	7
B13	3910	4575	----	326	381	---	1:2.7:3.0	0.67	5.5,6.0,---	7
B14	6075	6000	----	360	359	---	1:2.7:3.0	0.67	3.5,3.5,---	10
B15	5475	5040	----	338	357	---	1:2.7:3.0	0.67	4.0,4.0,---	7
B16	4925	4545	----	307	324	---	1:2.7:3.0	0.67	5.5,6.5,---	7
B17	5920	5265	4875	379	356	---	1:2.7:3.0	0.67	4.5,5.0,---	7
B18	5210	4855	5055	400	351	---	1:2.7:3.0	0.67	4.0,6.5,6.5	7
B19	5465	4975	5595	407	313	---	1:2.7:3.0	0.67	4.5,6.5,5.0	8
B20	5225	5830	5405	313	419	---	1:2.7:3.0	0.67	2.5,5.5,5.5	9
B21	5500	5205	4830	371	403	---	1:2.7:3.0	0.67	3.0,6.0,6.0	8
B22	5760	5300	5300	418	432	---	1:2.7:3.0	0.67	1.5,1.5,6.5	7

TABLE A.2

STEEL PROPERTIES

No. 2 (0.25 in. diam.) Deformed Reinforcing Bars

Test	Average Yield Stress psi	Average Yield Strain ($E = 29 \times 10^6$ psi)	Strain at Strain Hardening	Comments
B1-B11	50,000	1.72×10^{-3}	.020	First Shipment
B12	47,600	1.64×10^{-3}	.020	
B13	47,900	1.65×10^{-3}	.020	
B14	47,900	1.65×10^{-3}	.020	
B15	47,900	1.65×10^{-3}	.020	
B16	48,300	1.67×10^{-3}	.020	
B17	50,800	1.75×10^{-3}	.020	
B18	56,100	1.93×10^{-3}	.023	Second Shipment
B19	53,100	1.83×10^{-3}	.023	
B20	51,750	1.78×10^{-3}	.023	
B21	47,800	1.65×10^{-3}	.023	
B22	53,750	1.83×10^{-3}	.023	

Welded

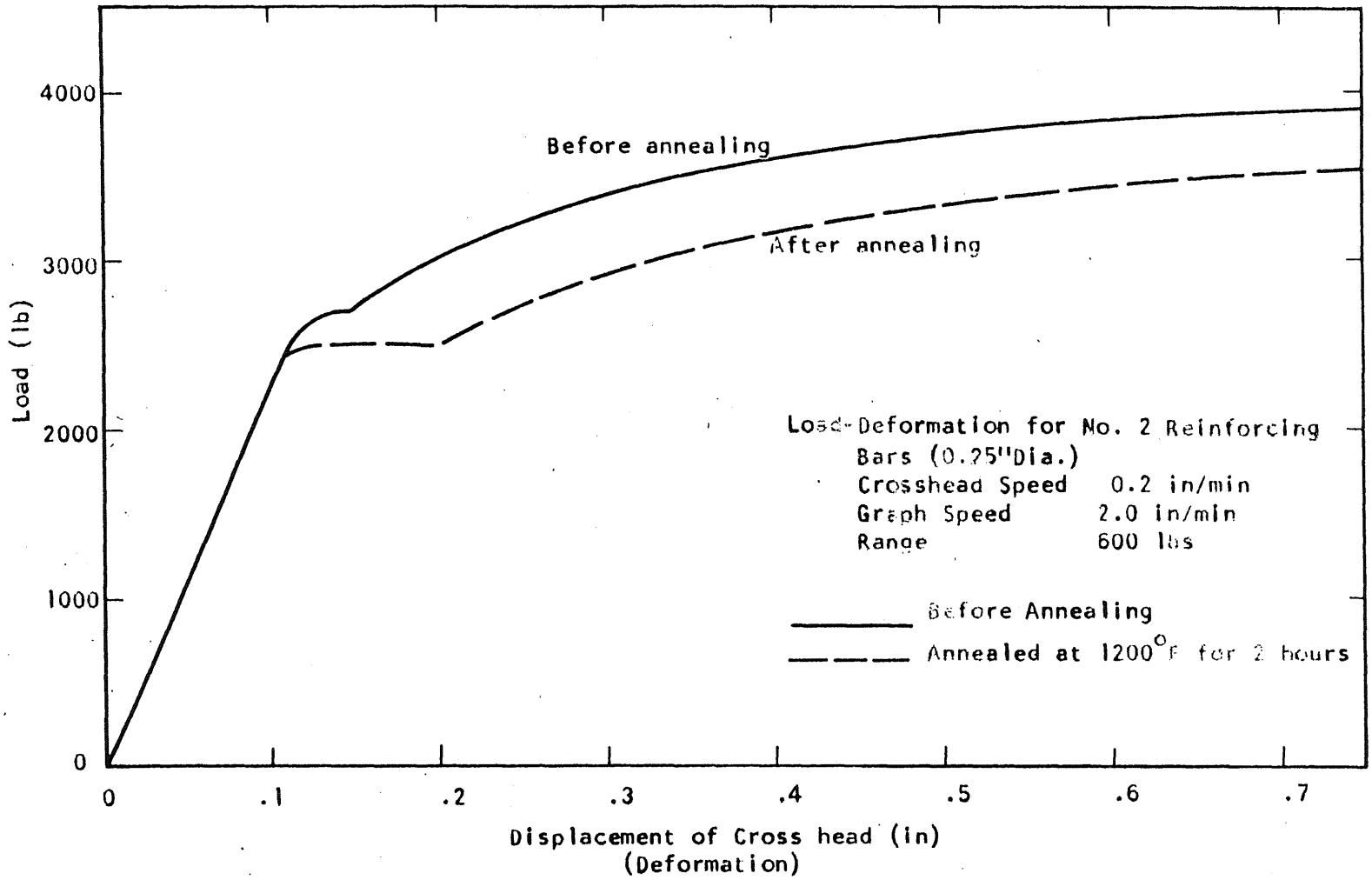

FIG. A.1 ANNEALING OF STEEL

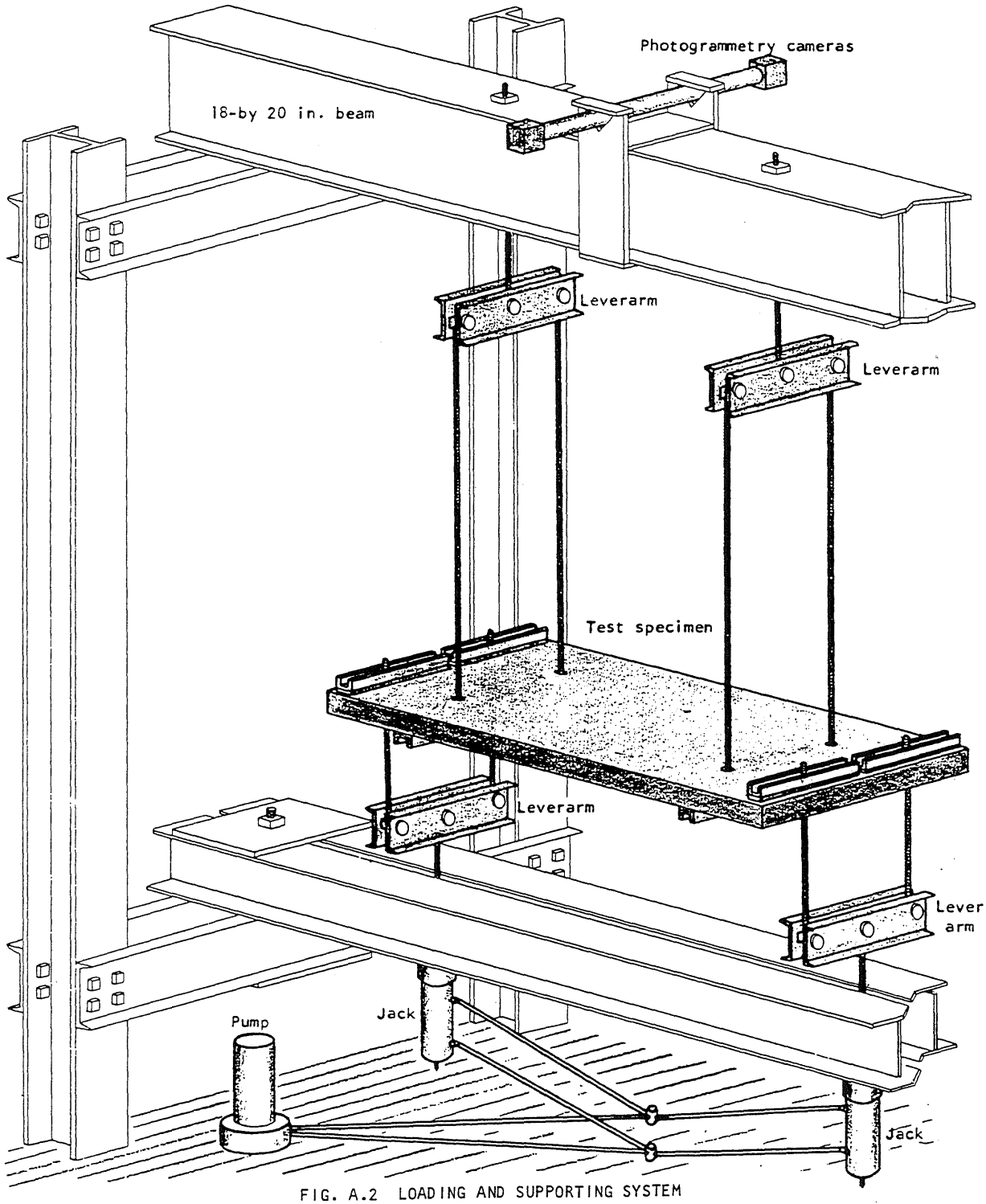

FIG. A.2 LOADING AND SUPPORTING SYSTEM

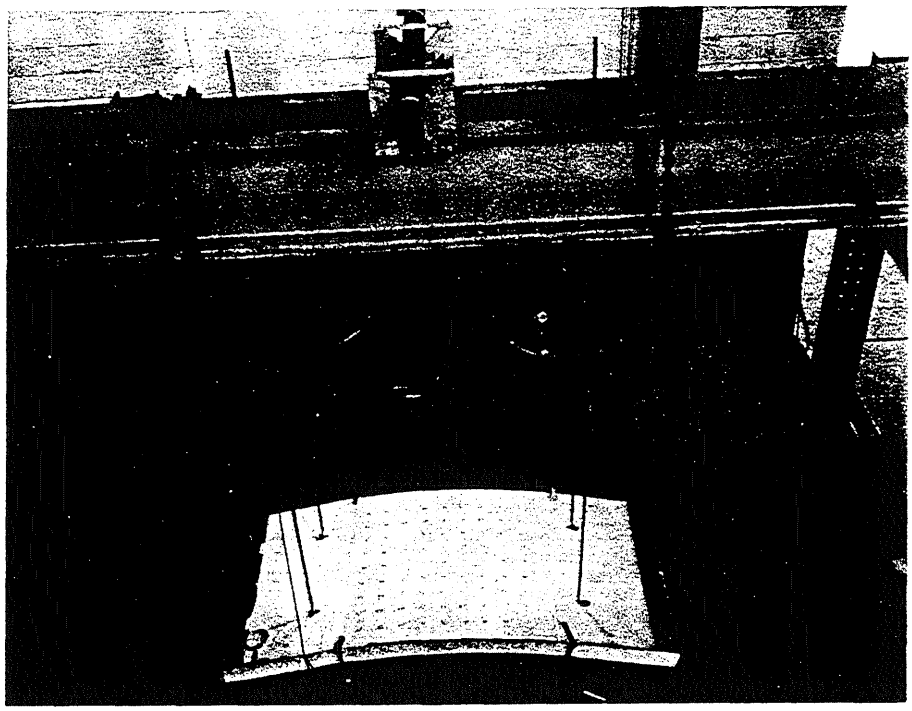

FIG. A.3 SPECIMEN (B4) SUBJECTED TO UNIAXIAL MOMENT

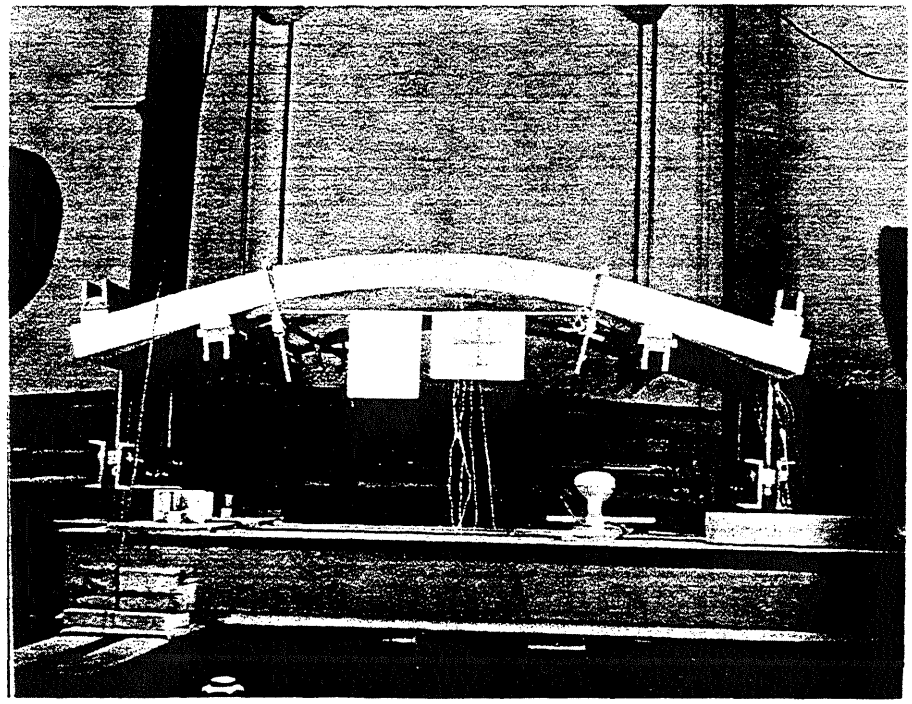

FIG. A.4 SPECIMEN (B13) SUBJECTED TO UNIAXIAL MOMENT

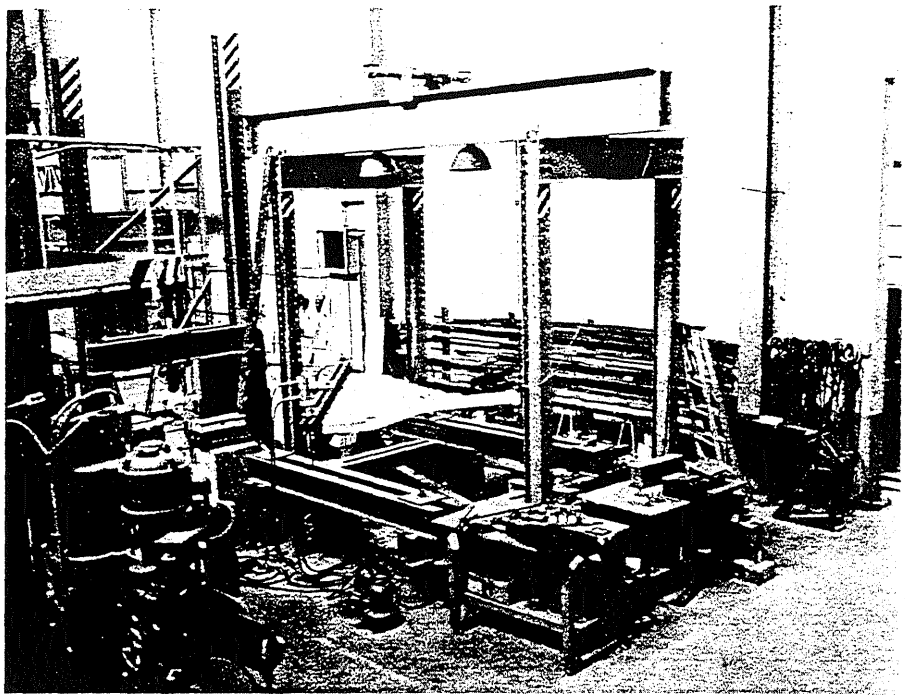

FIG. A.5 SPECIMEN (B16) SUBJECTED TO TORSION

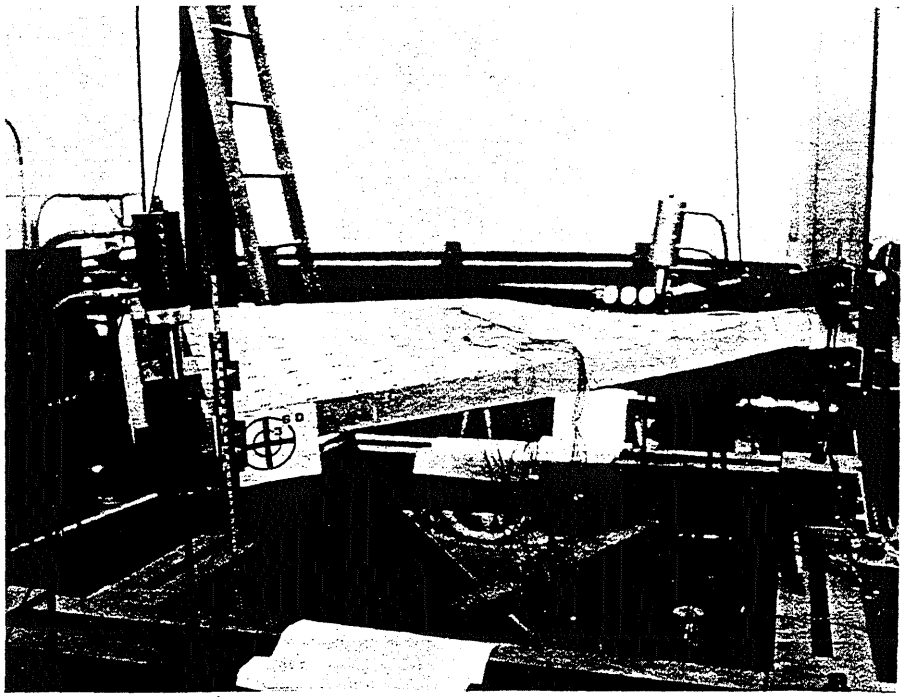

FIG. A.6 SPECIMEN (B22) SUBJECTED TO TORSION

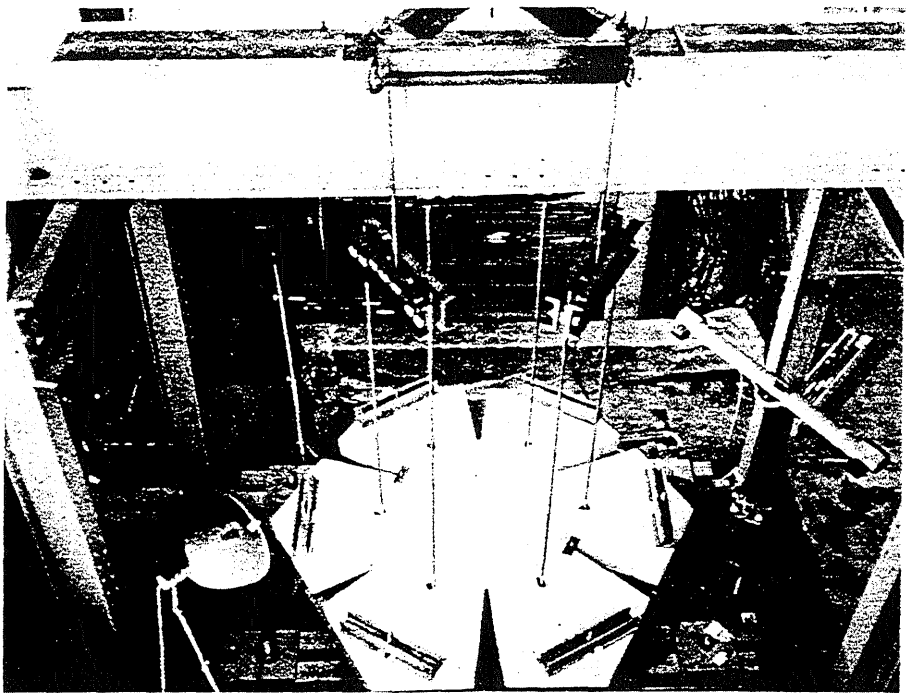

FIG. A.7 CIRCULAR SPECIMEN (C2) SUBJECTED TO ISOSTATIC MOMENT

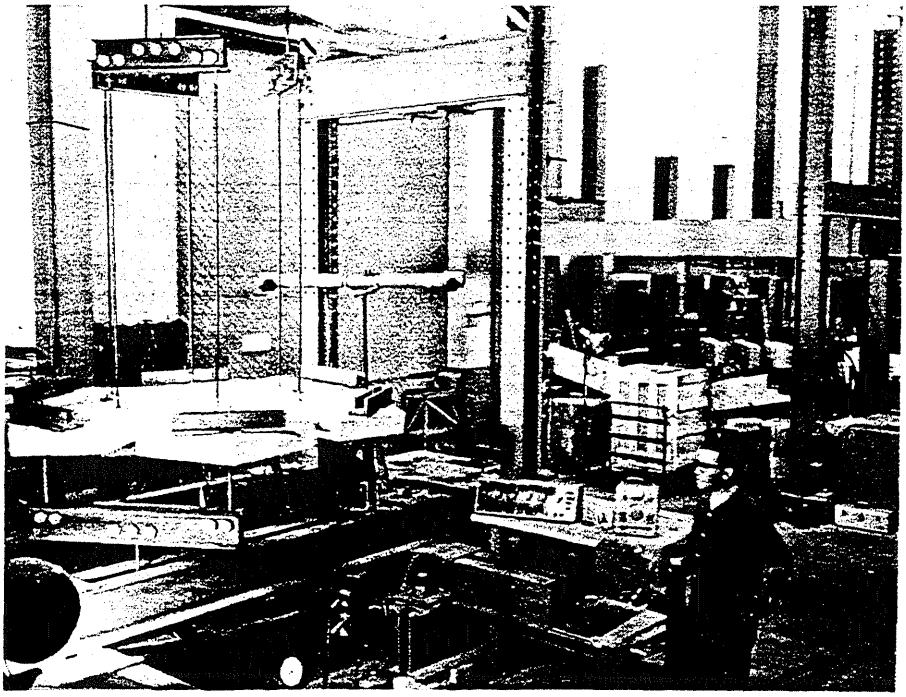

FIG. A.8 CIRCULAR SPECIMEN (C2) SIDE VIEW

FIG. A.9 REINFORCEMENT IN SPECIMEN C1

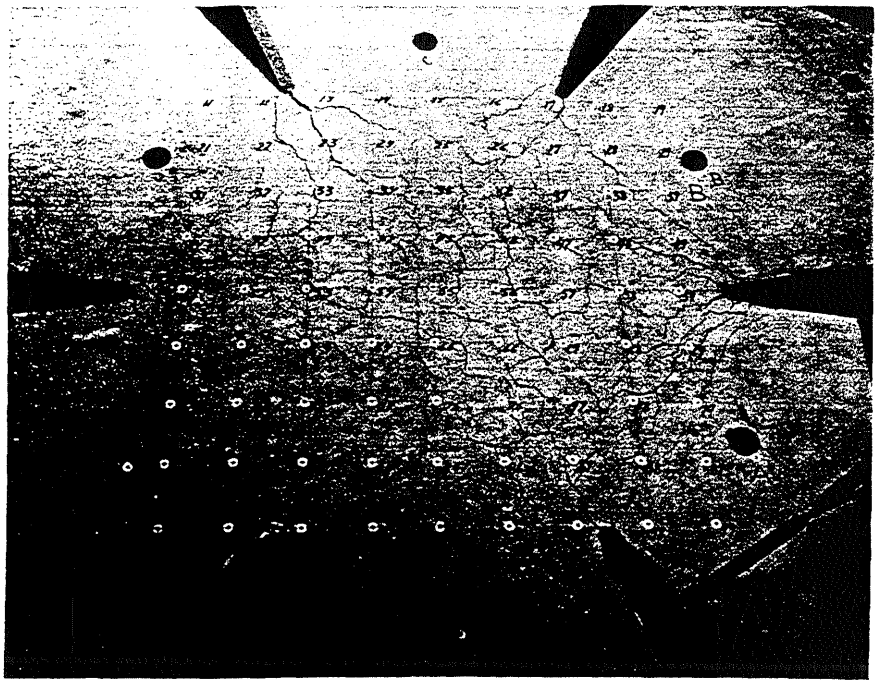

FIG. A.10 CRACK PATTERN IN TOP SURFACE OF C1

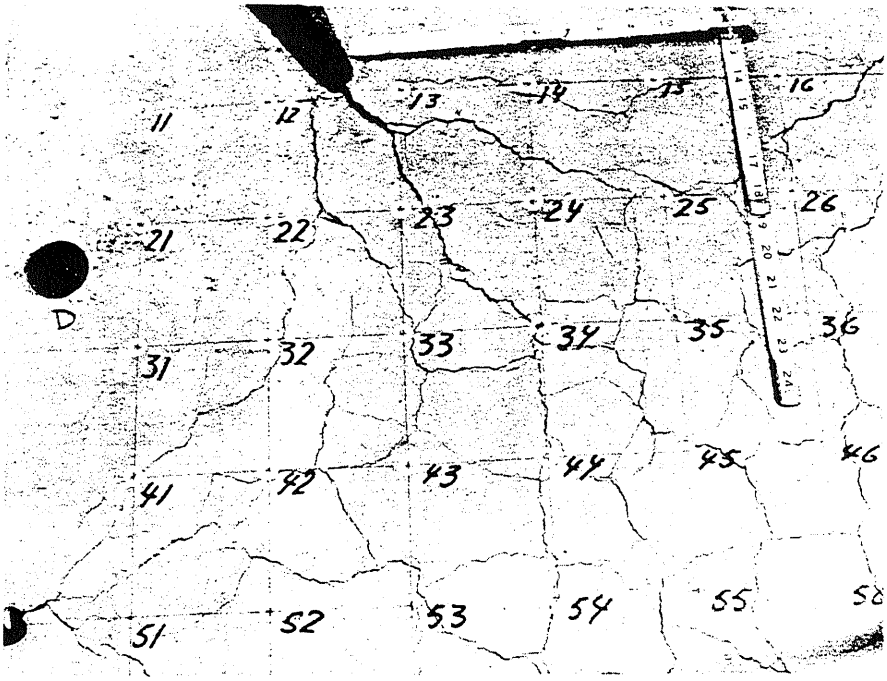

FIG. A.11 CRACK PATTERN IN TOP SURFACE OF C1

FIG. A.13 BOTTOM SURFACE OF C1

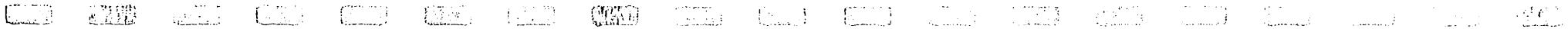

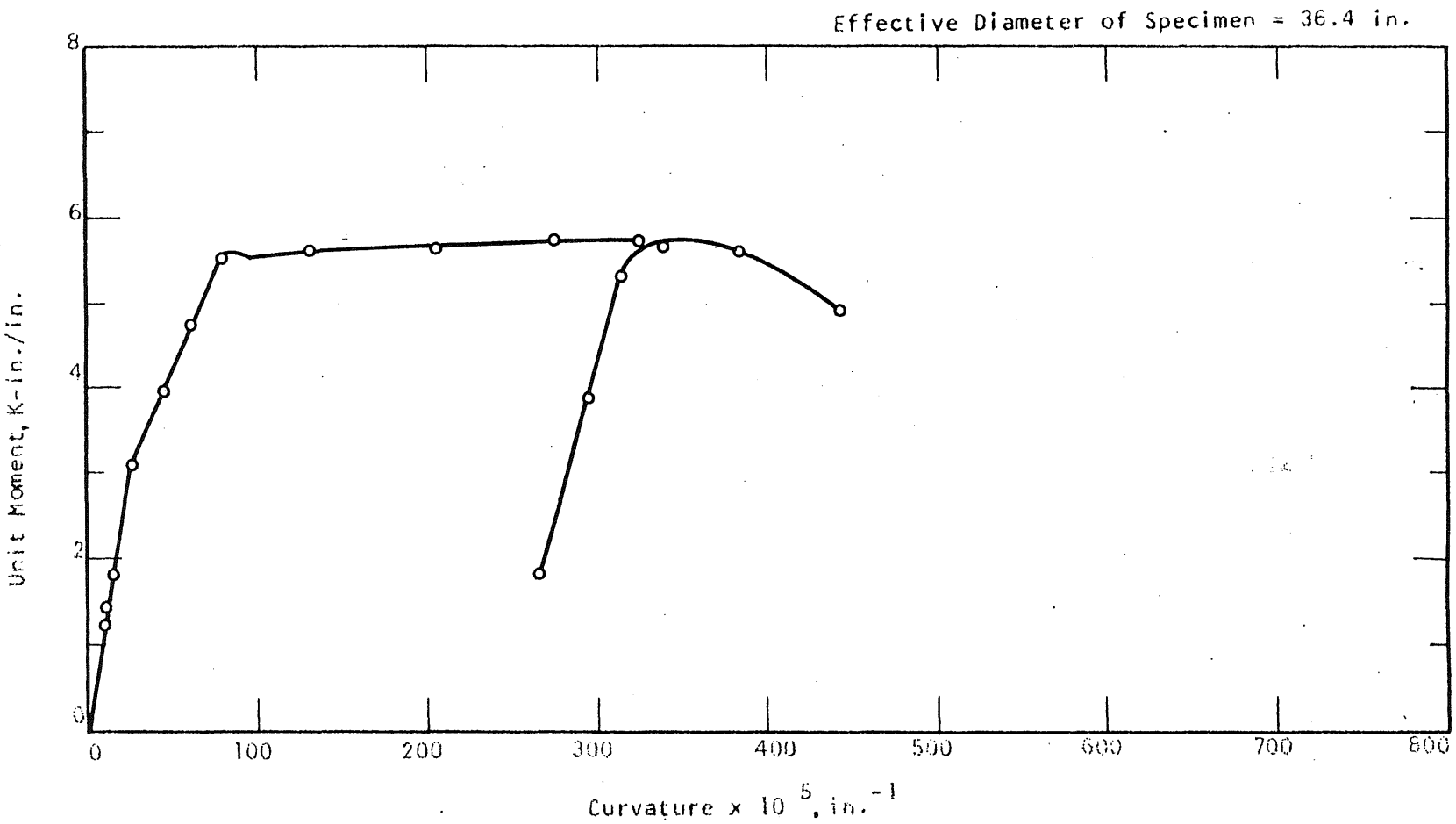

FIG. A.14 MOMENT-CURVATURE PLOT FOR SPECIMEN C1

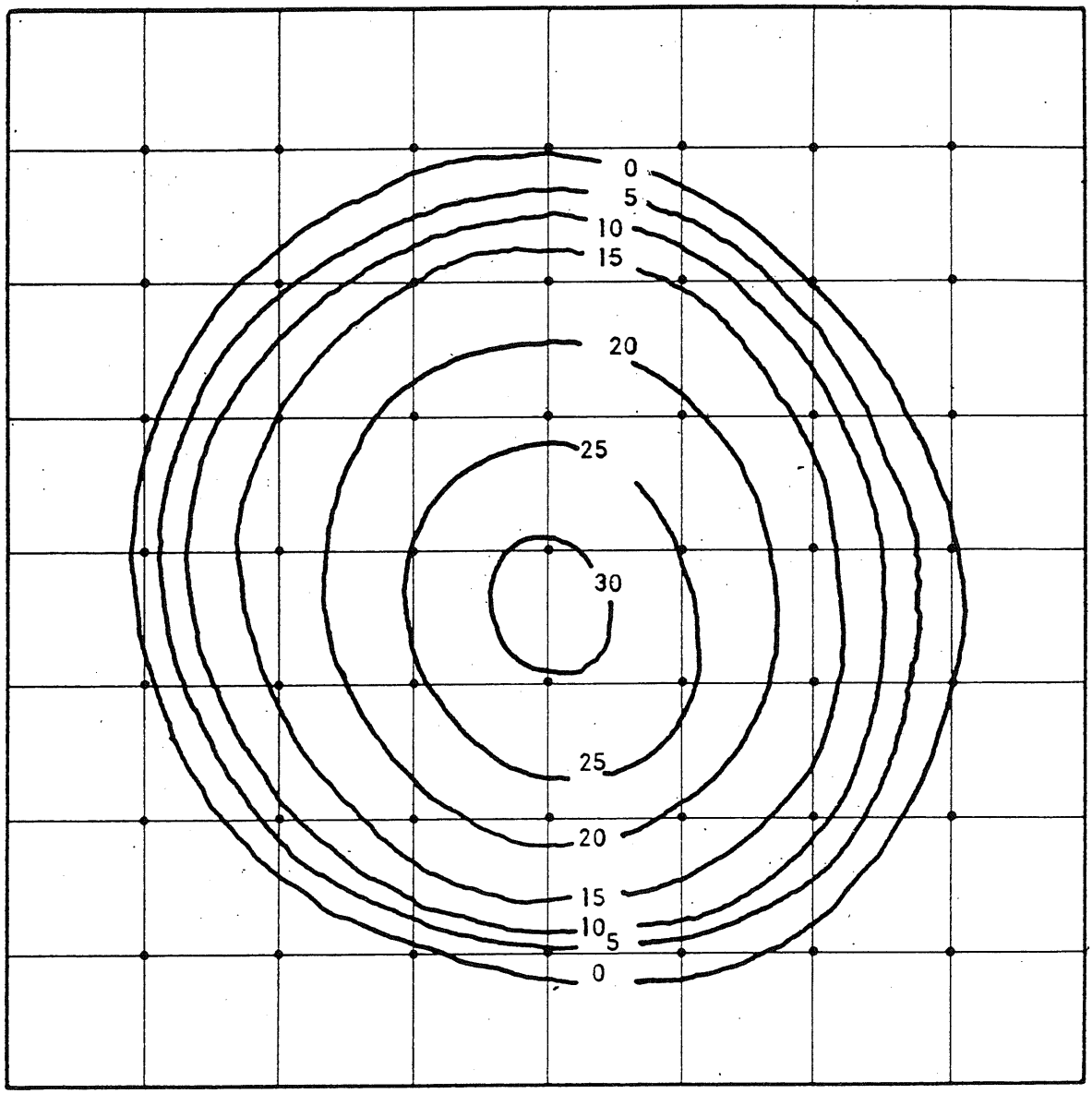

Grid 4 by 4 in. Contour Interval = 0.05 in.

FIG. A.12 SURFACE OF THE TEST AREA OF A TEST SPECIMEN ("C1") SUBJECTED TO BIAXIAL BENDING

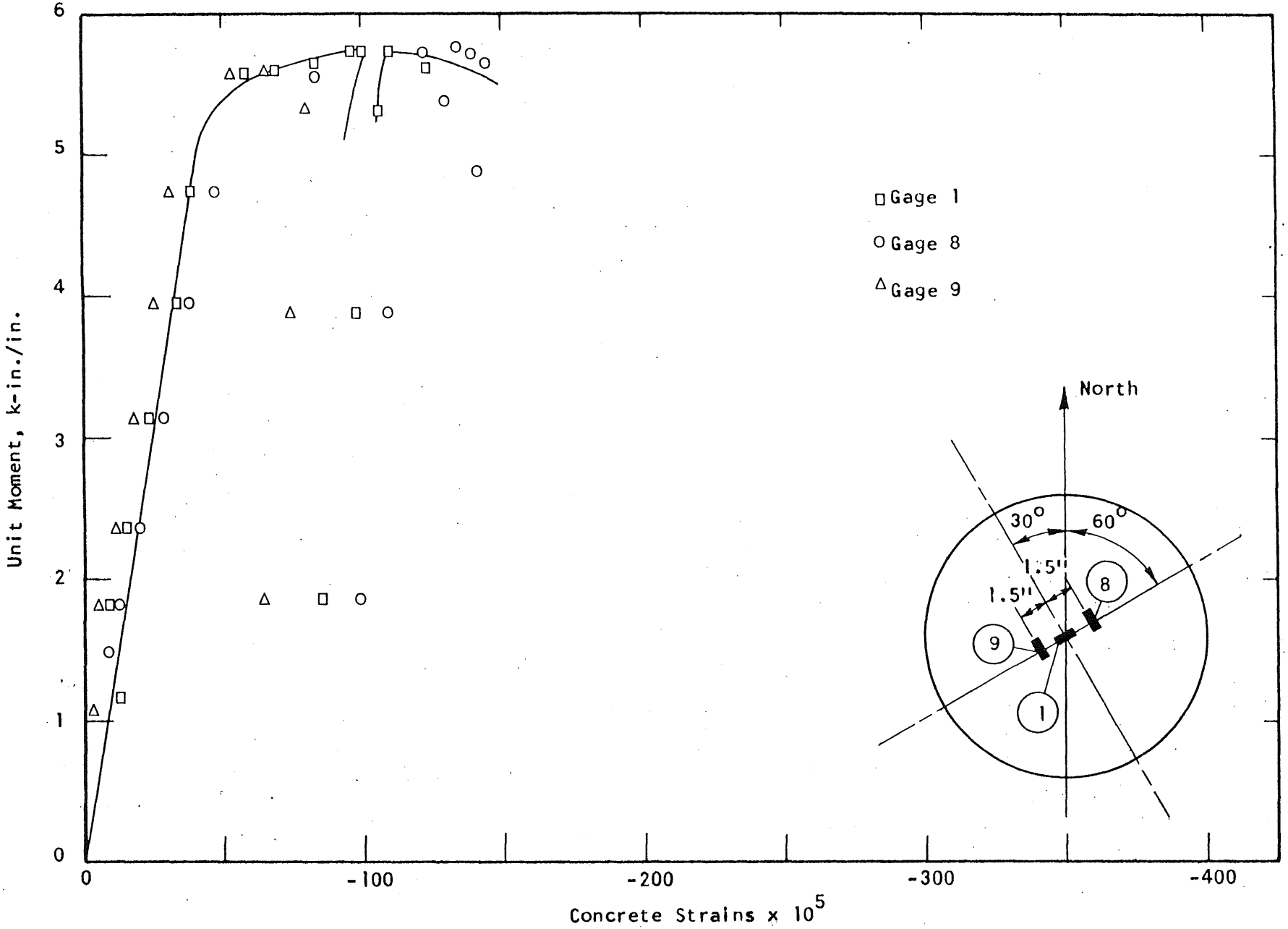

FIG. A.15 CONCRETE STRAIN PLOT, COMPRESSION SIDE OF SPECIMEN C1

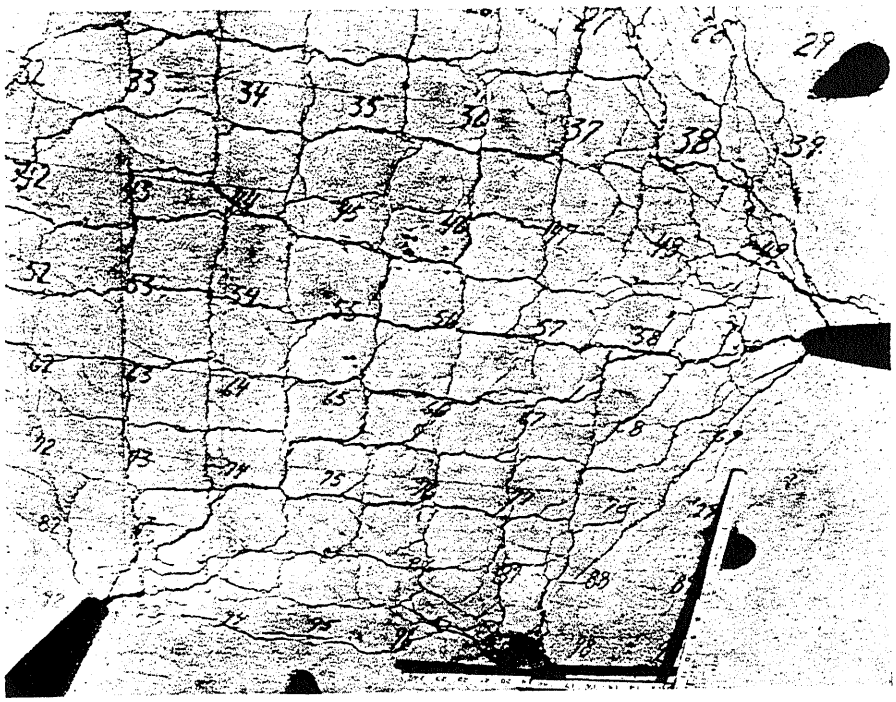

FIG. A.16 CRACK PATTERN IN TOP SURFACE OF C2

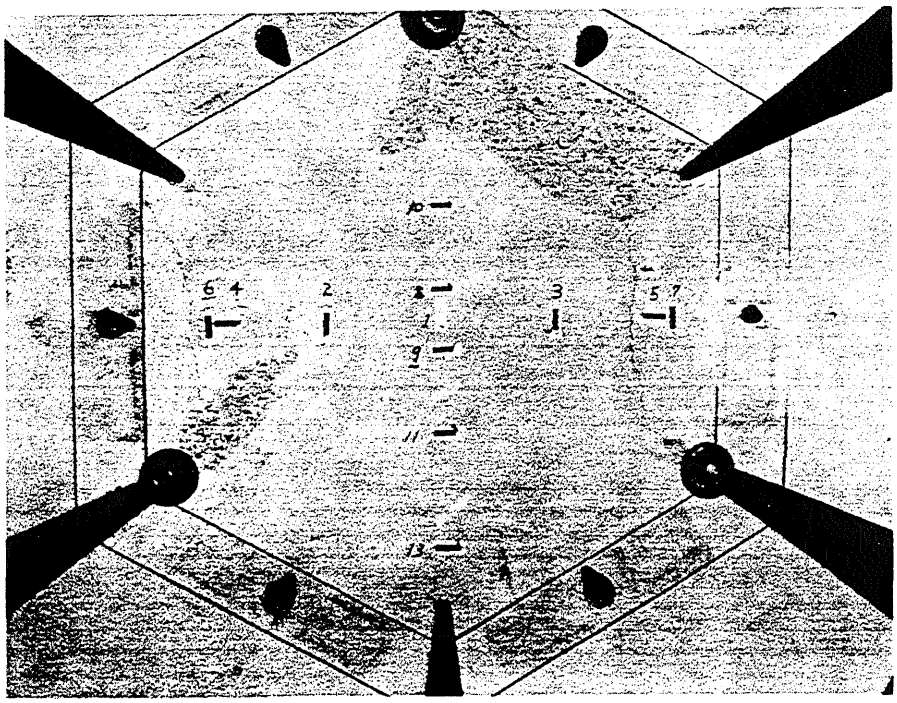

FIG. A.17 BOTTOM SURFACE OF C2

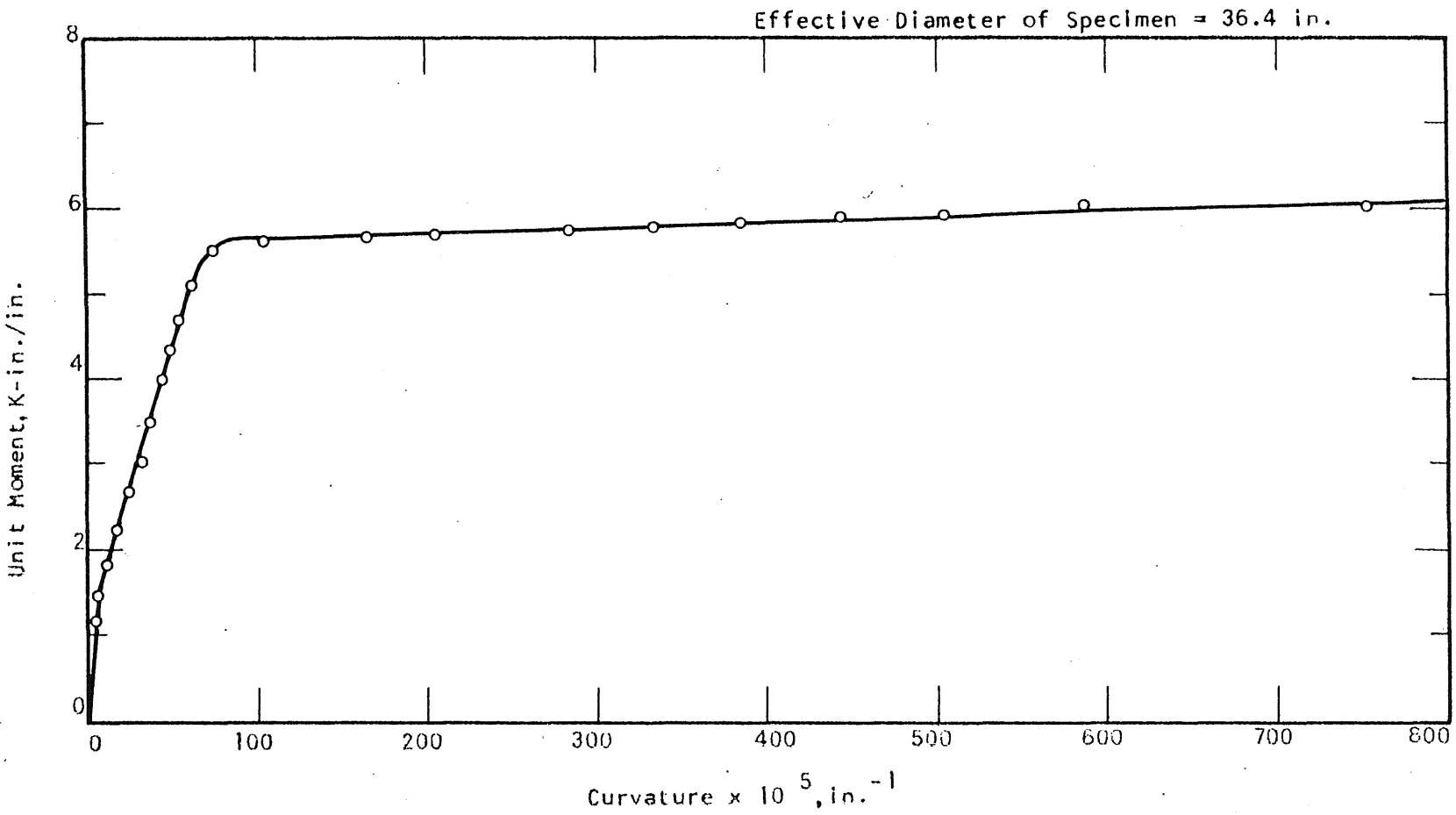

FIG. A.18 MOMENT-CURVATURE PLOT FOR SPECIMEN C2

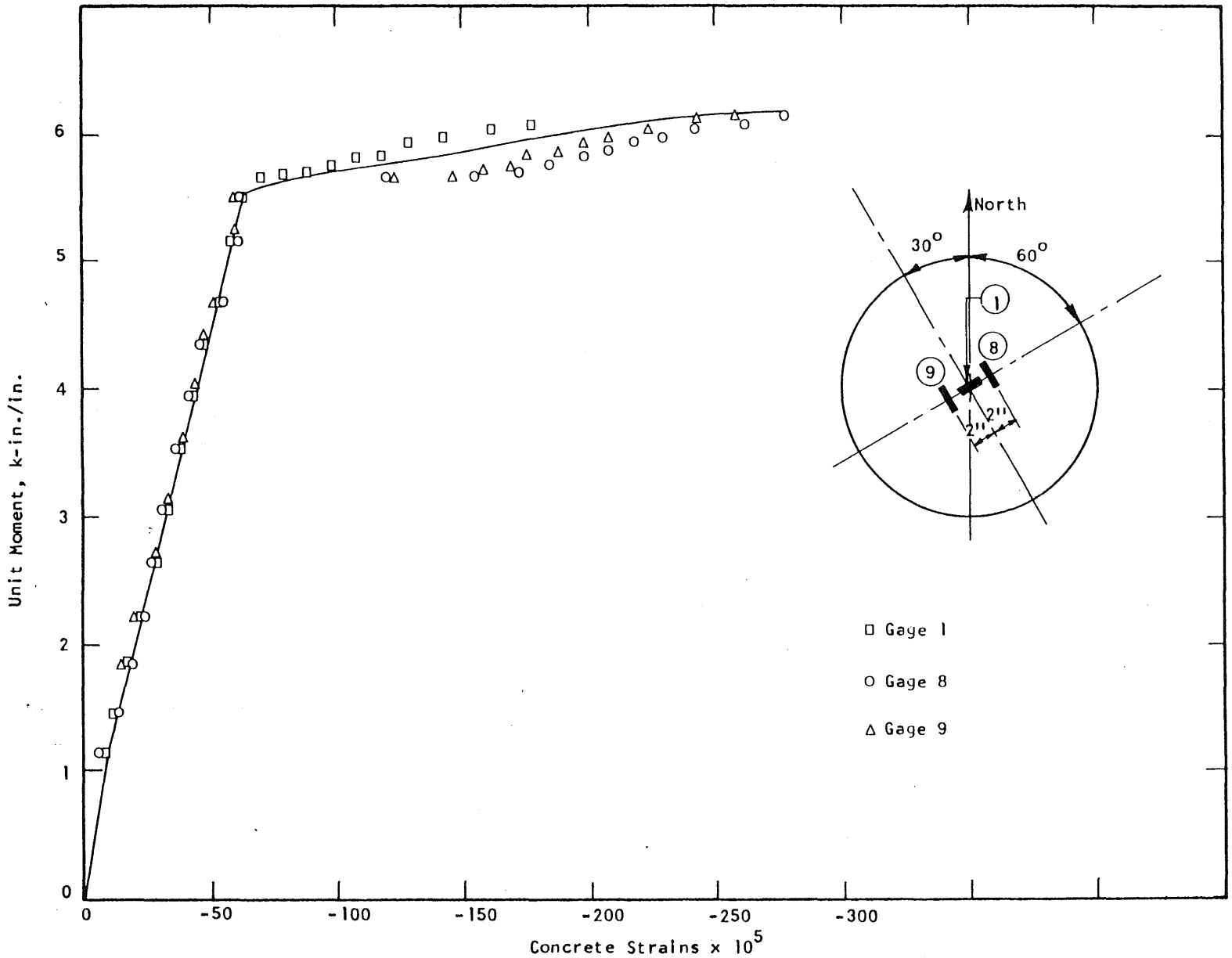

FIG. A.19 CONCRETE STRAIN PLOT, COMPRESSION SIDE OF SPECIMEN C2

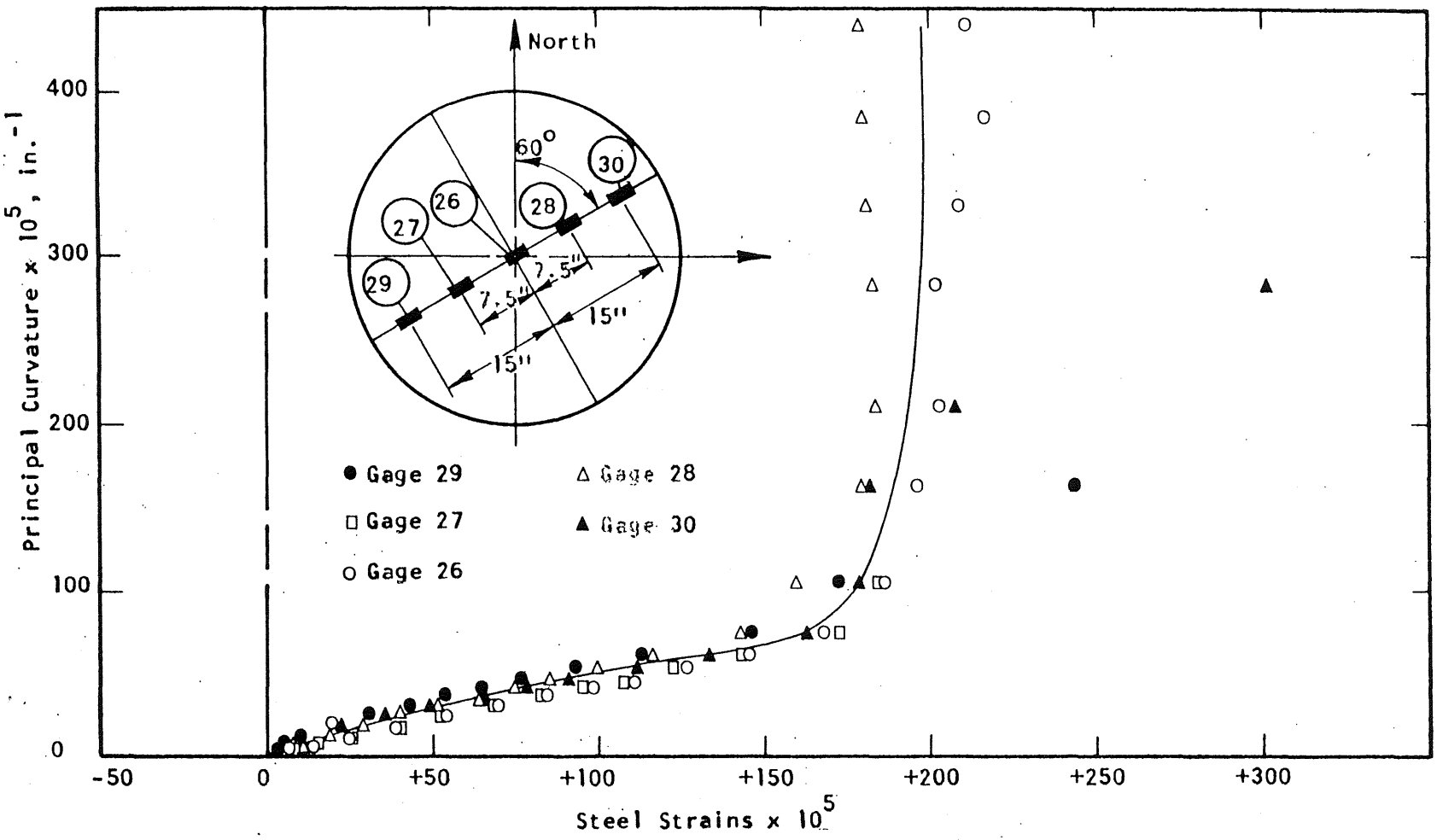

FIG. A.20 STEEL STRAIN PLOT, SPECIMEN C2

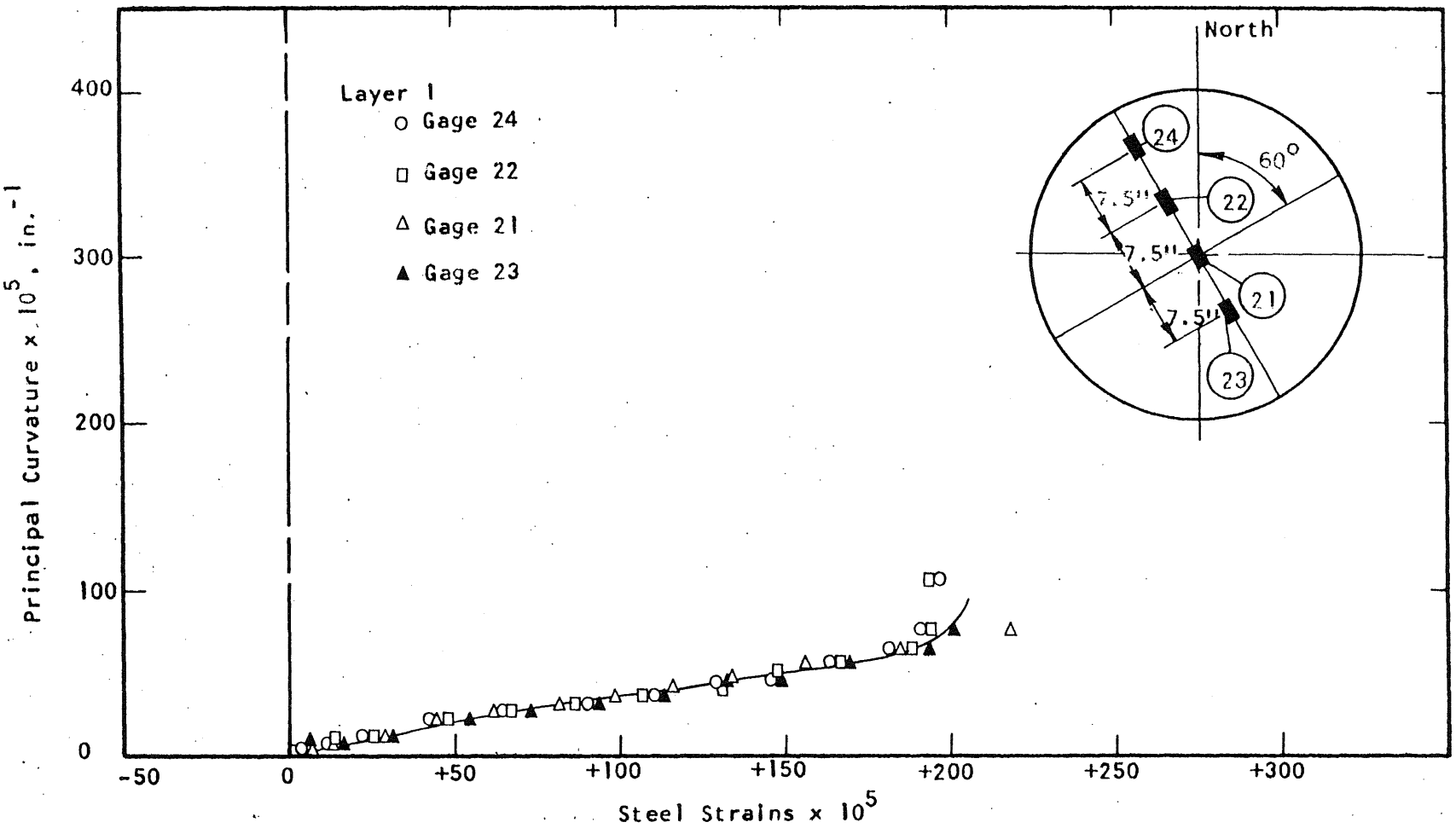

FIG. A.21 STEEL STRAIN PLOT, SPECIMEN C2

a Top Surface of C3

b Bottom Surface of C3

FIG. A.22 CRACK PATTERNS IN SPECIMEN C3

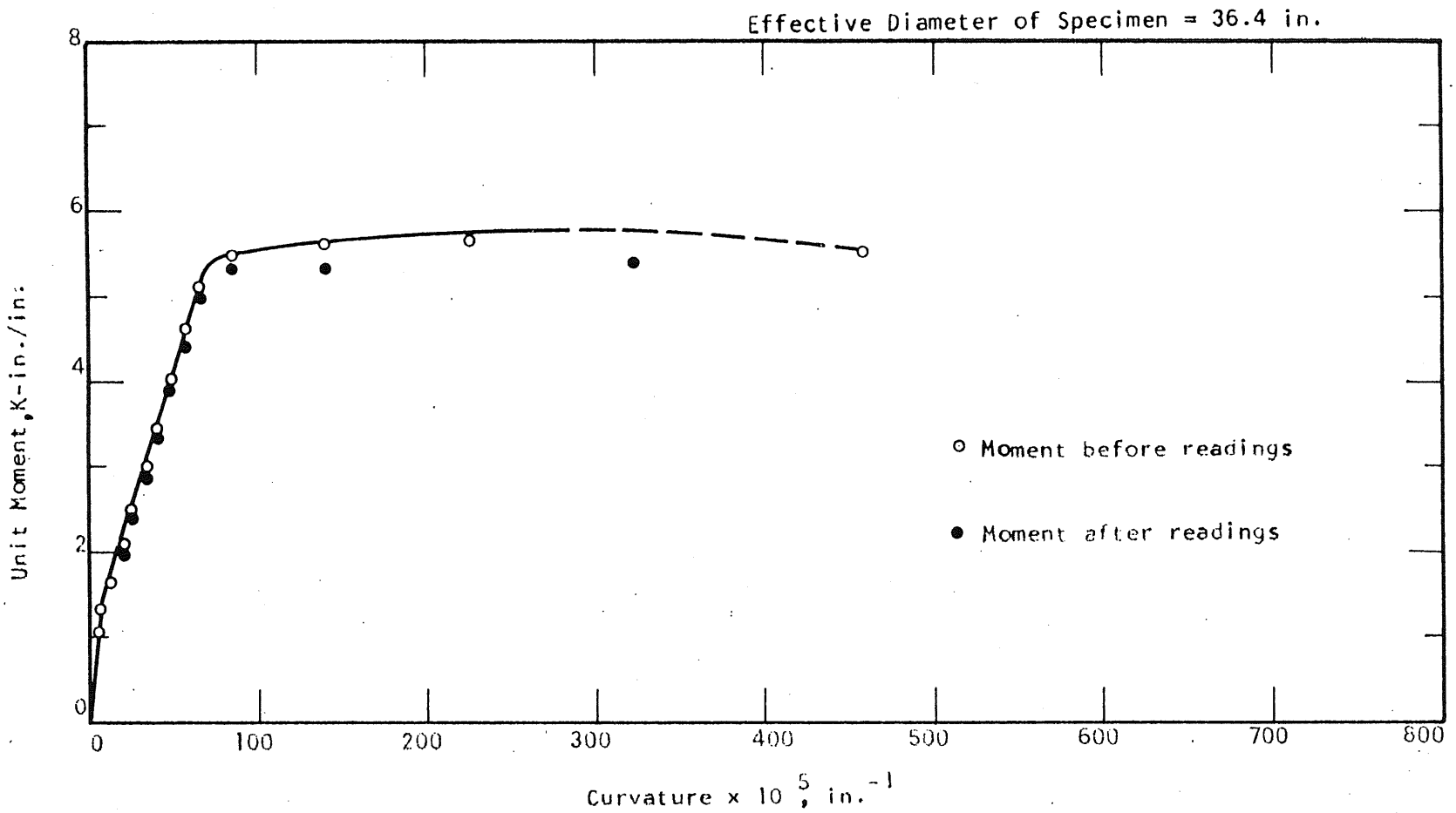

FIG. A.23 MOMENT-CURVATURE PLOT FOR SPECIMEN C3

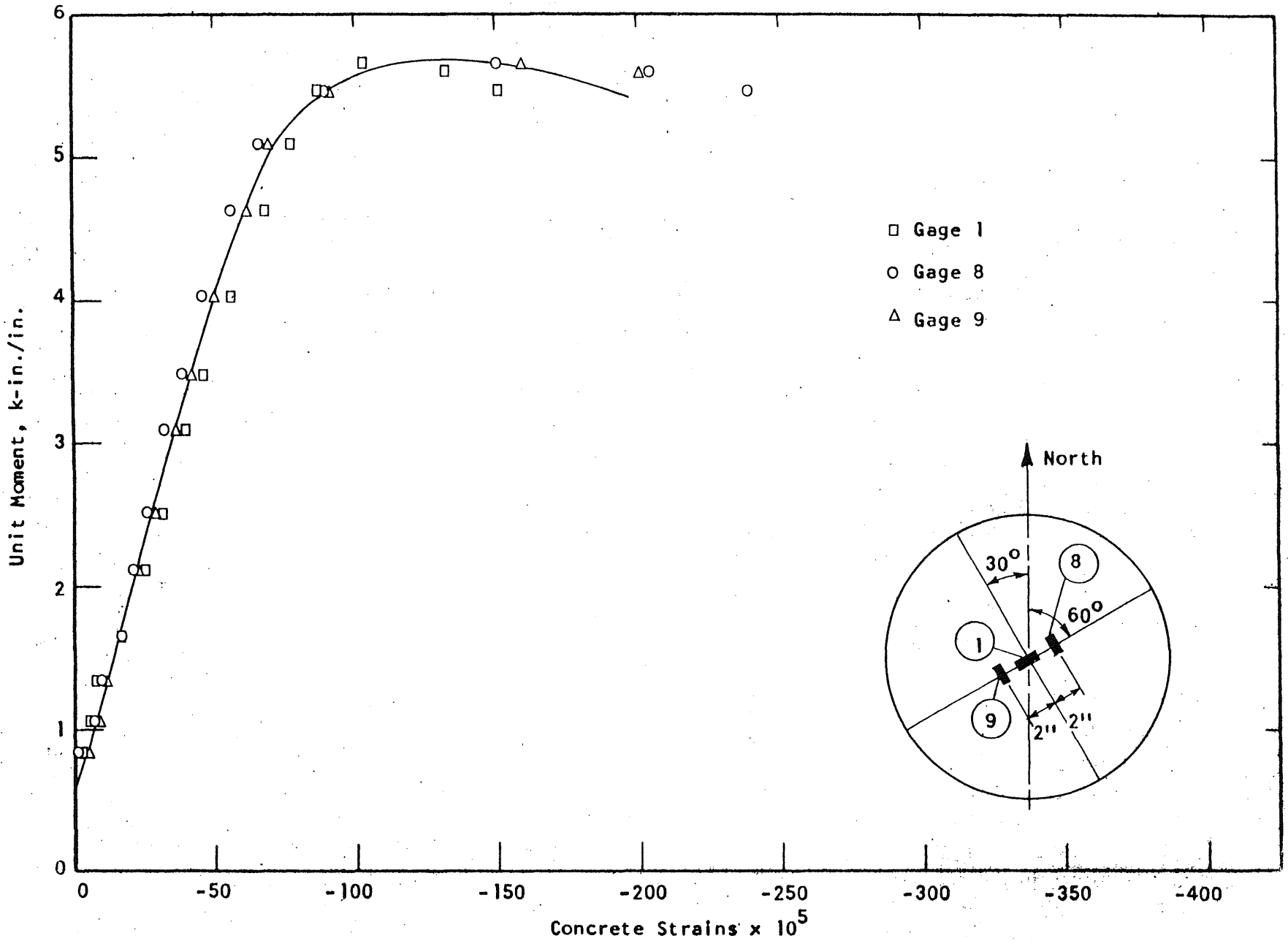

FIG. A.24 CONCRETE STRAIN PLOT, COMPRESSION SIDE OF SPECIMEN C3

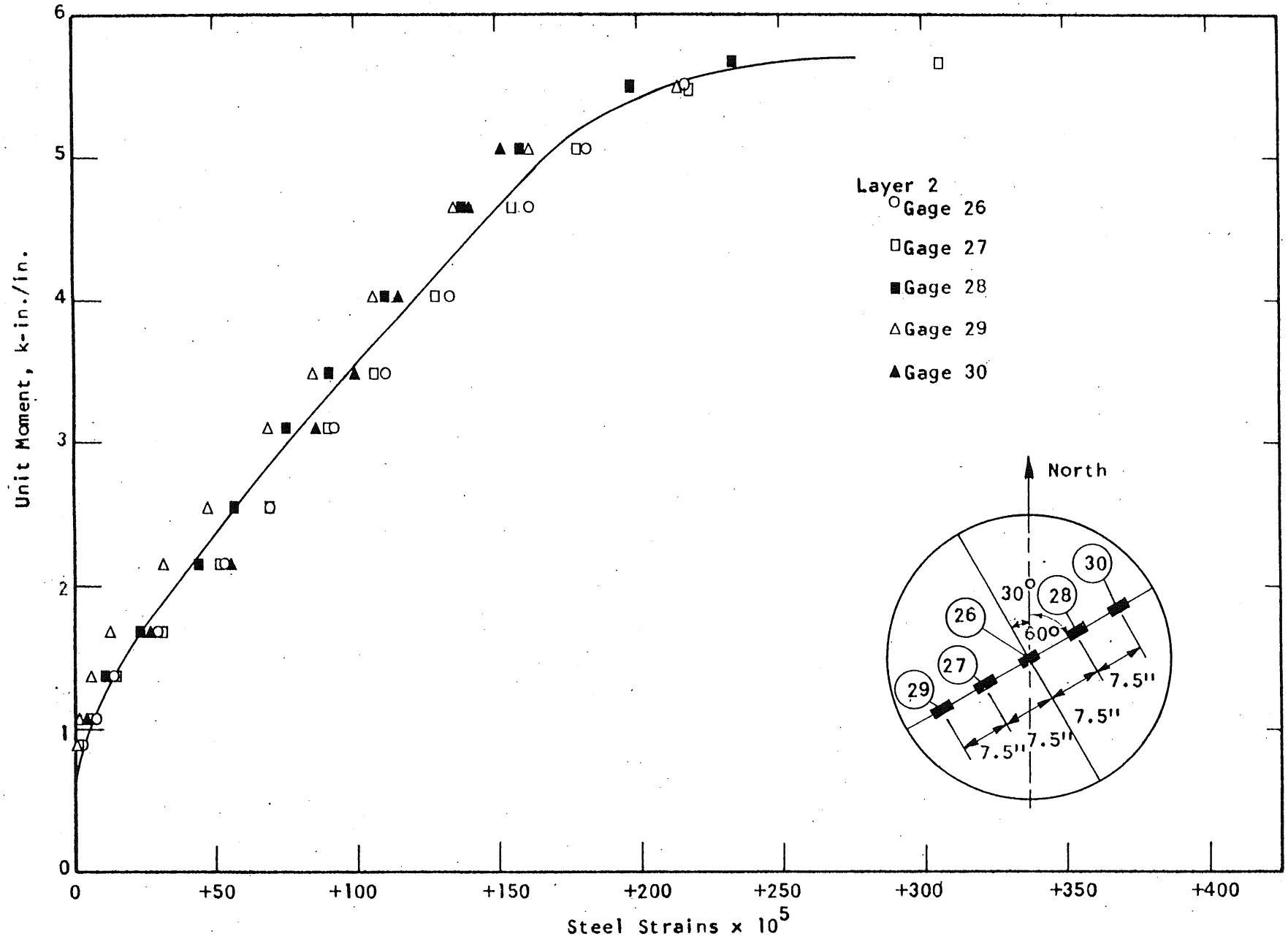

FIG. A.25 STEEL STRAIN PLOT, SPECIMEN C3

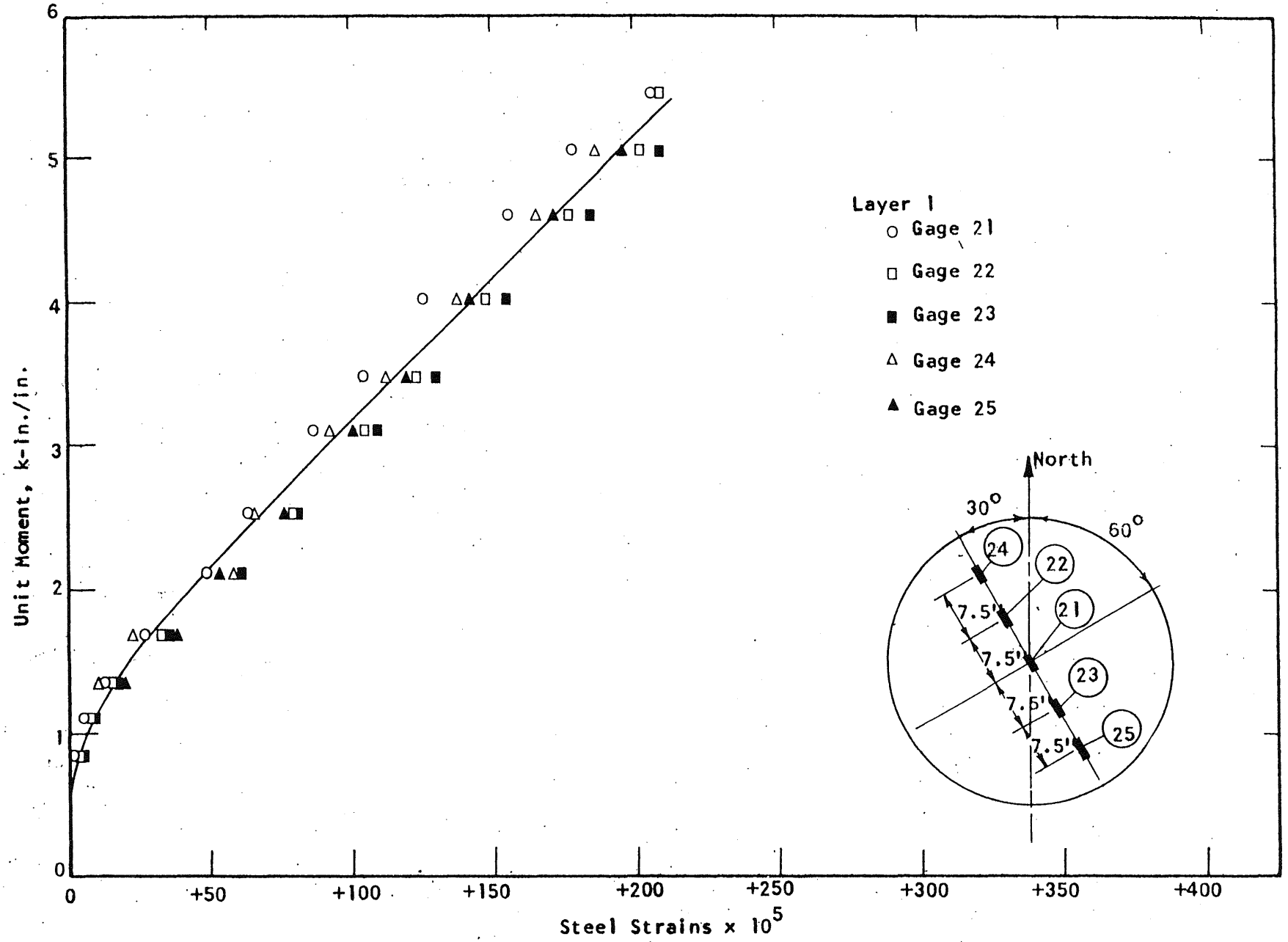

FIG. A.26 STEEL STRAIN PLOT, SPECIMEN C3

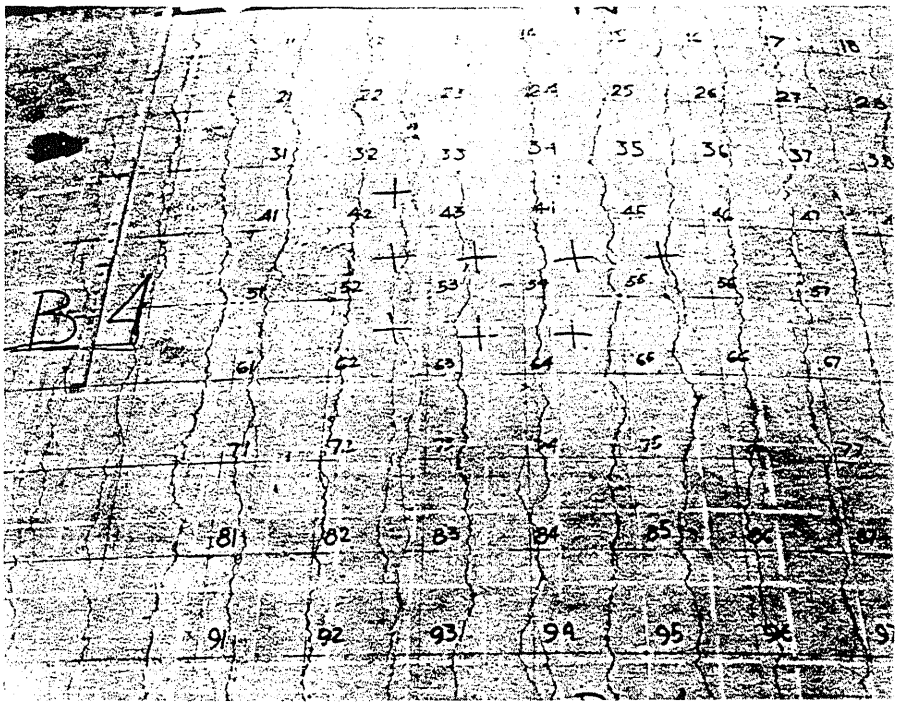

FIG. A.27 CRACK PATTERN IN TOP SURFACE OF B4

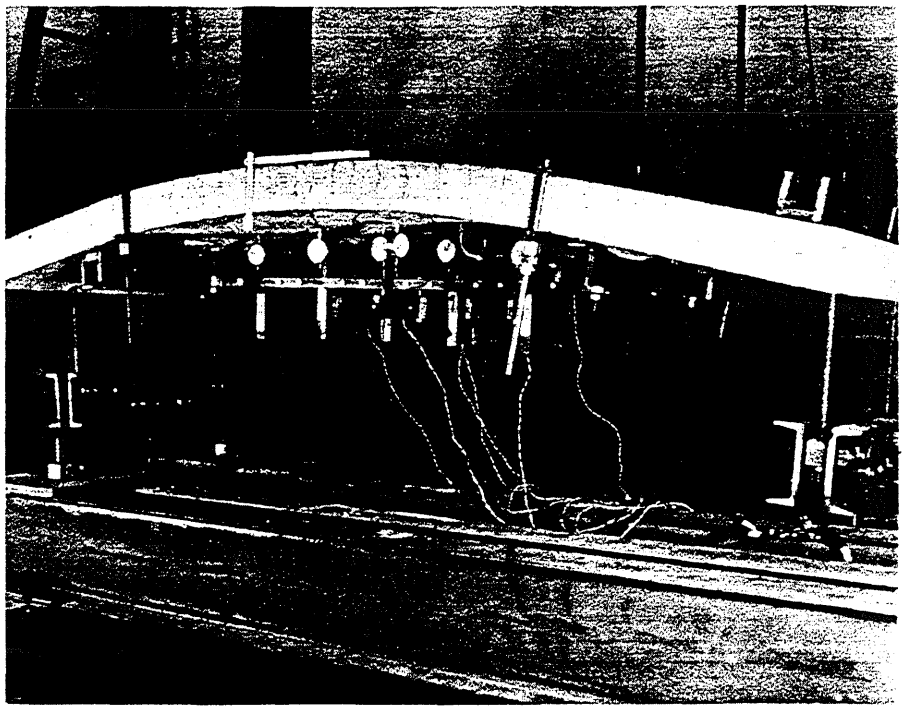

FIG. A.28 SIDE VIEW OF B4

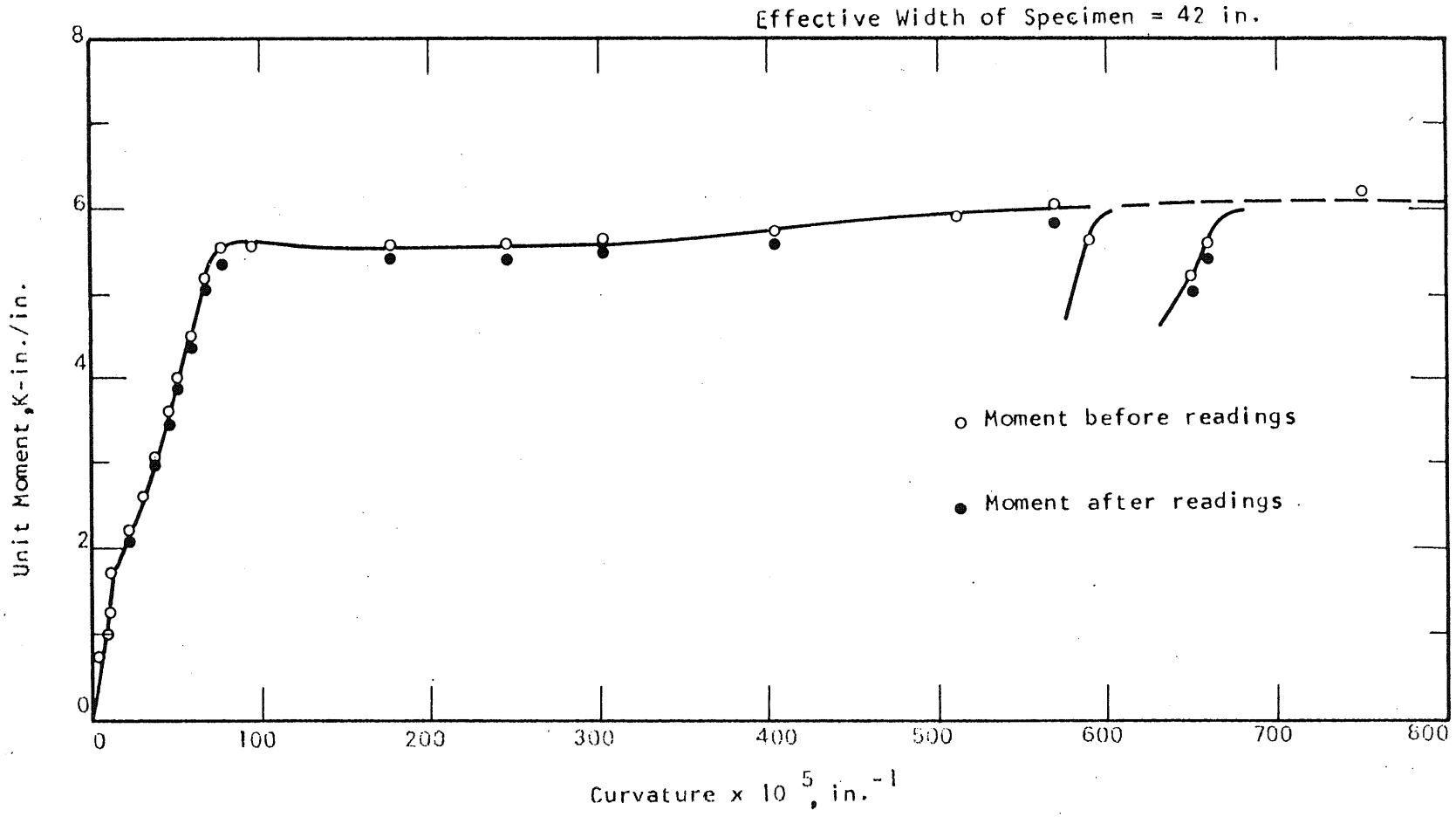

FIG. A.29 MOMENT-CURVATURE PLOT FOR SPECIMEN B4

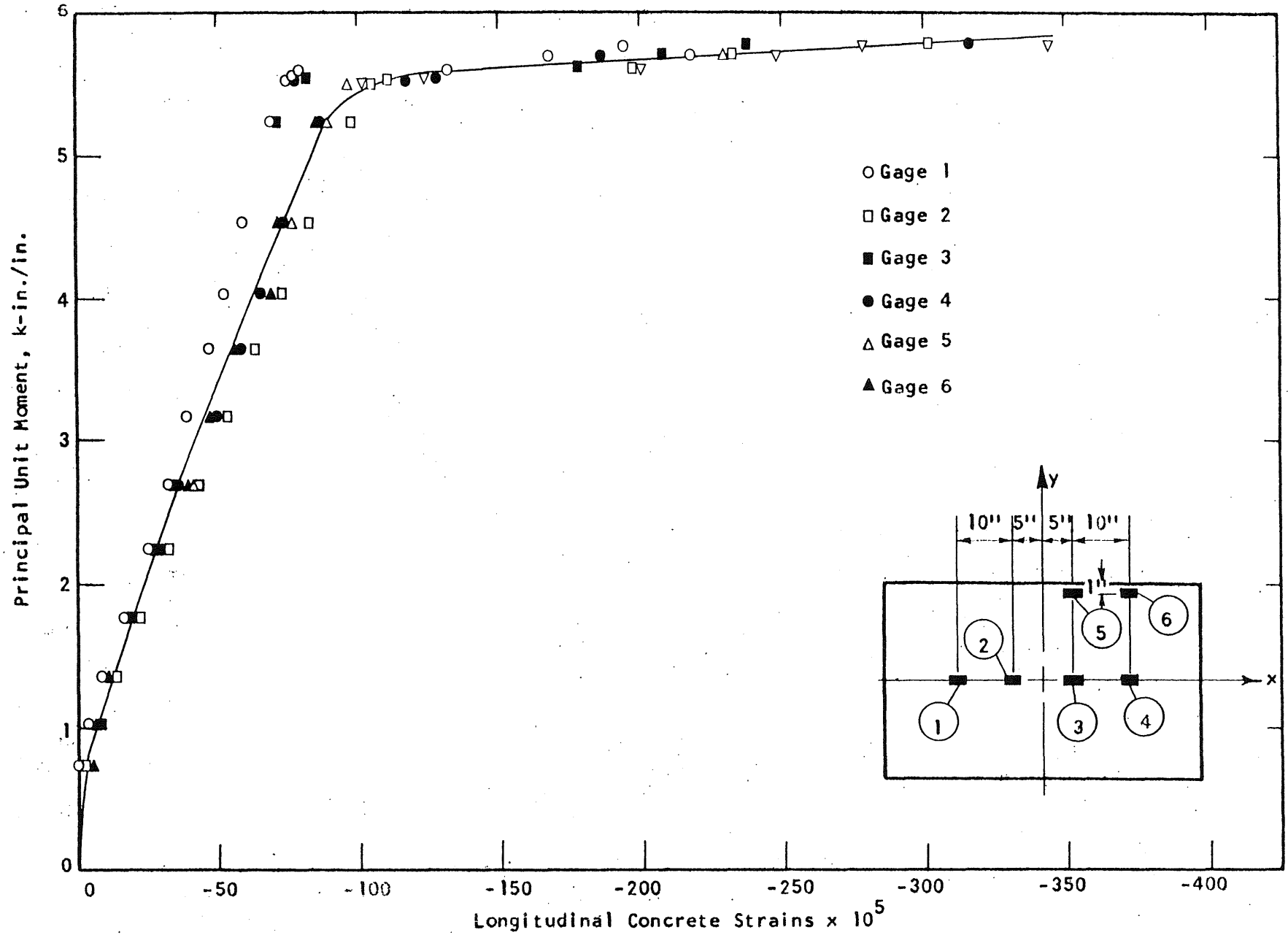

FIG. A.30 CONCRETE STRAIN PLOT, COMPRESSION SIDE OF SPECIMEN B4

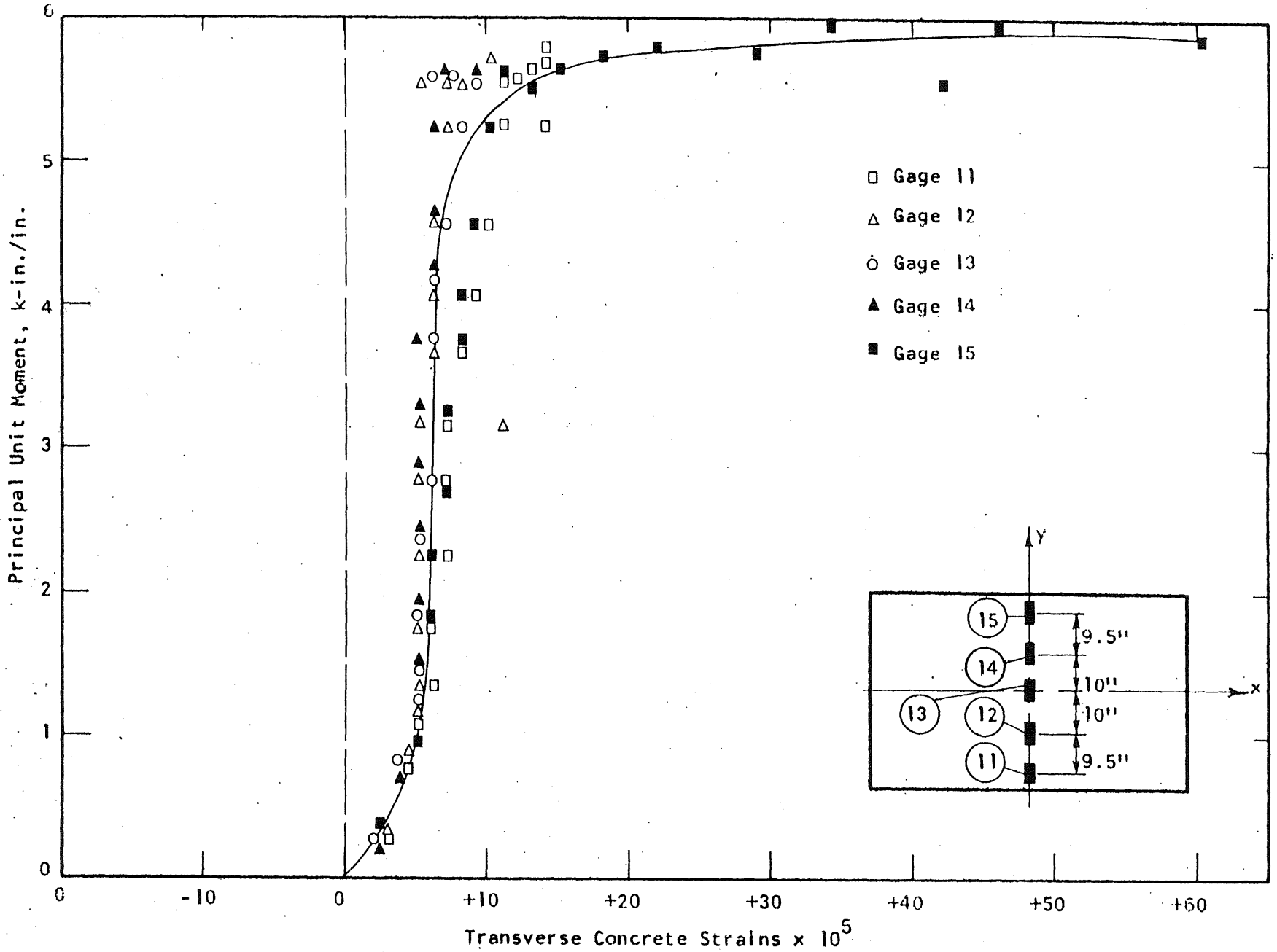

FIG. A.31 CONCRETE STRAIN PLOT, COMPRESSION SIDE OF SPECIMEN B4

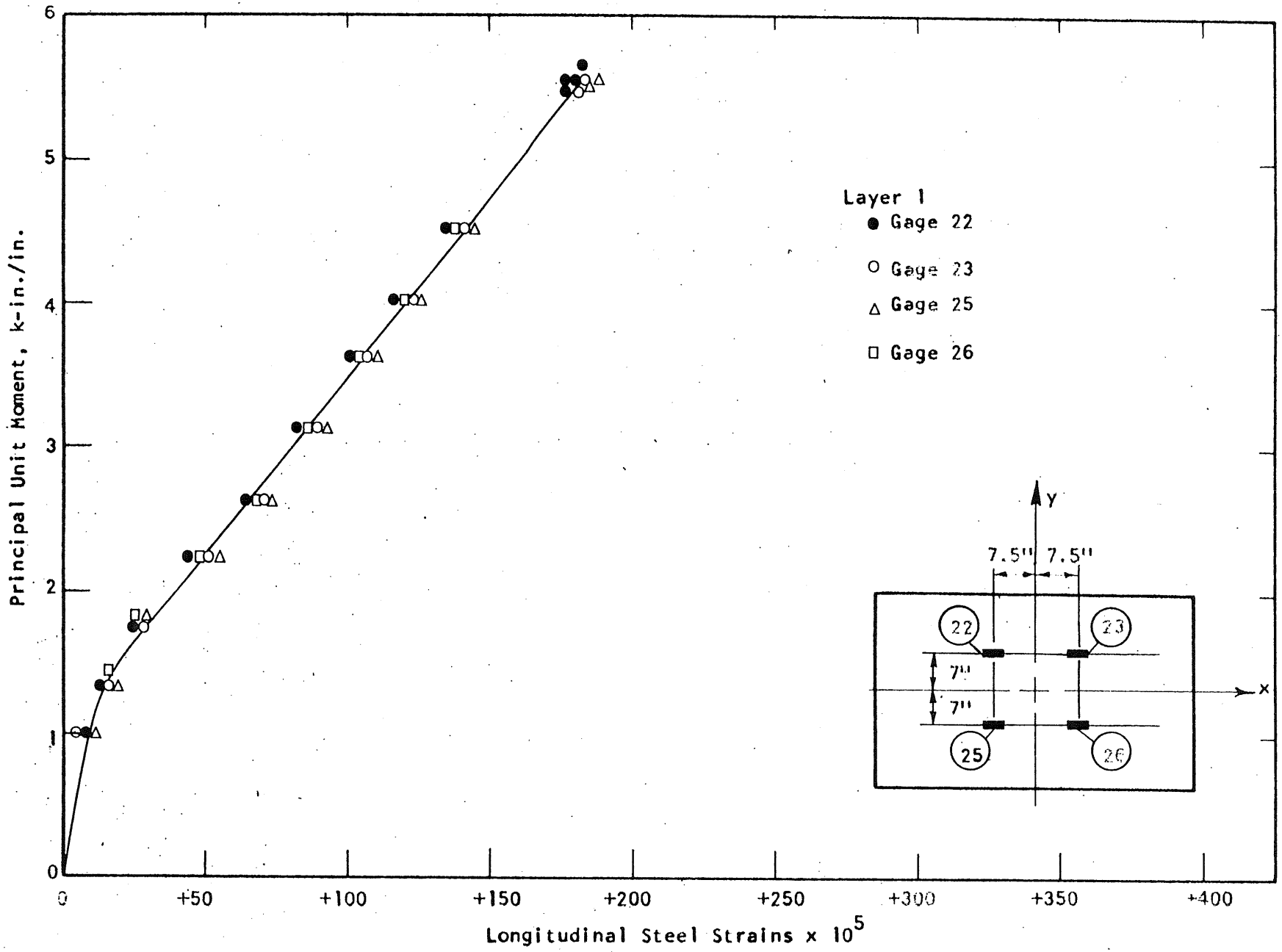

FIG. A.32 STEEL STRAIN PLOT, SPECIMEN B4

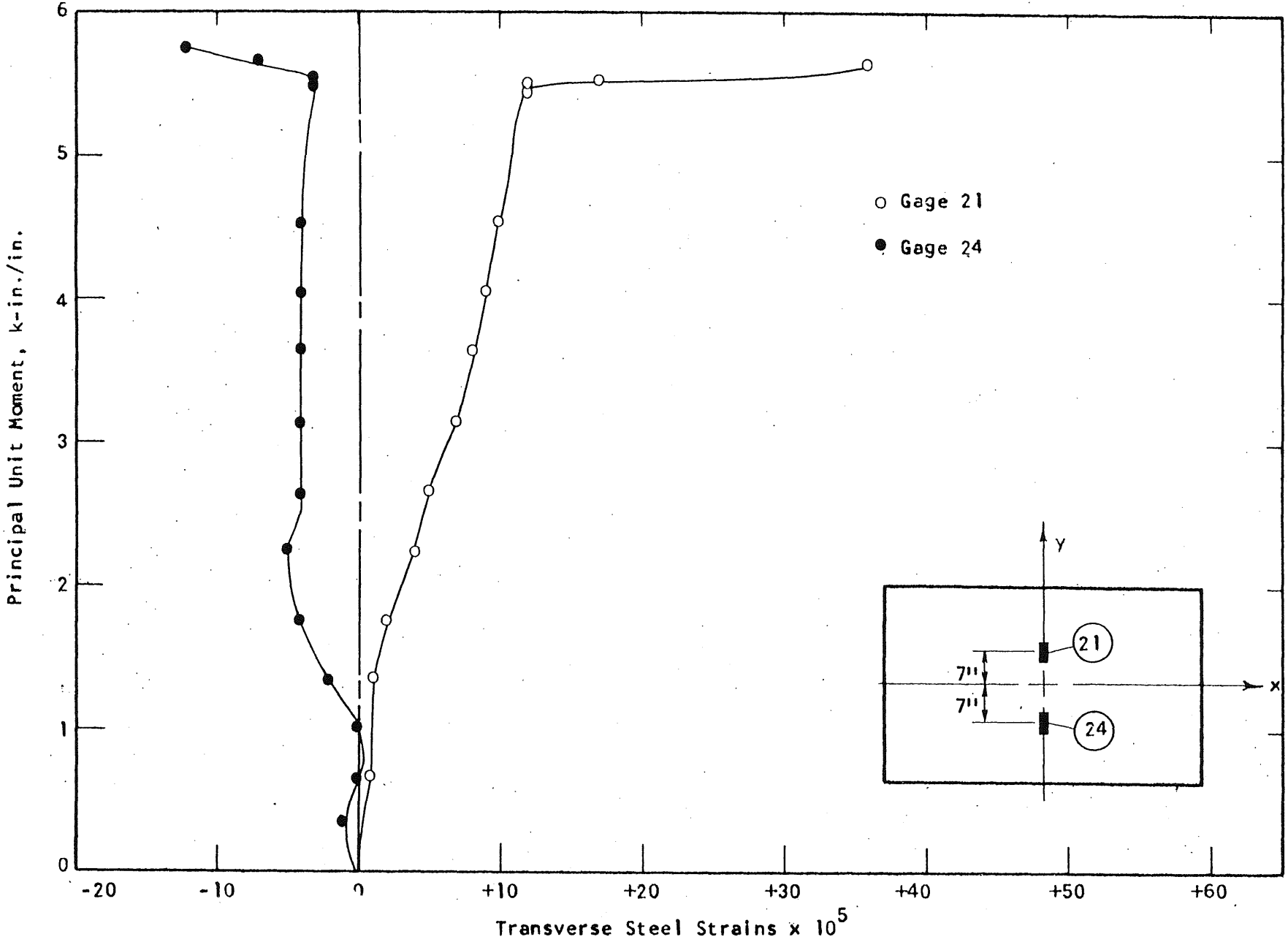

FIG. A.33 STEEL STRAIN PLOT, SPECIMEN B4

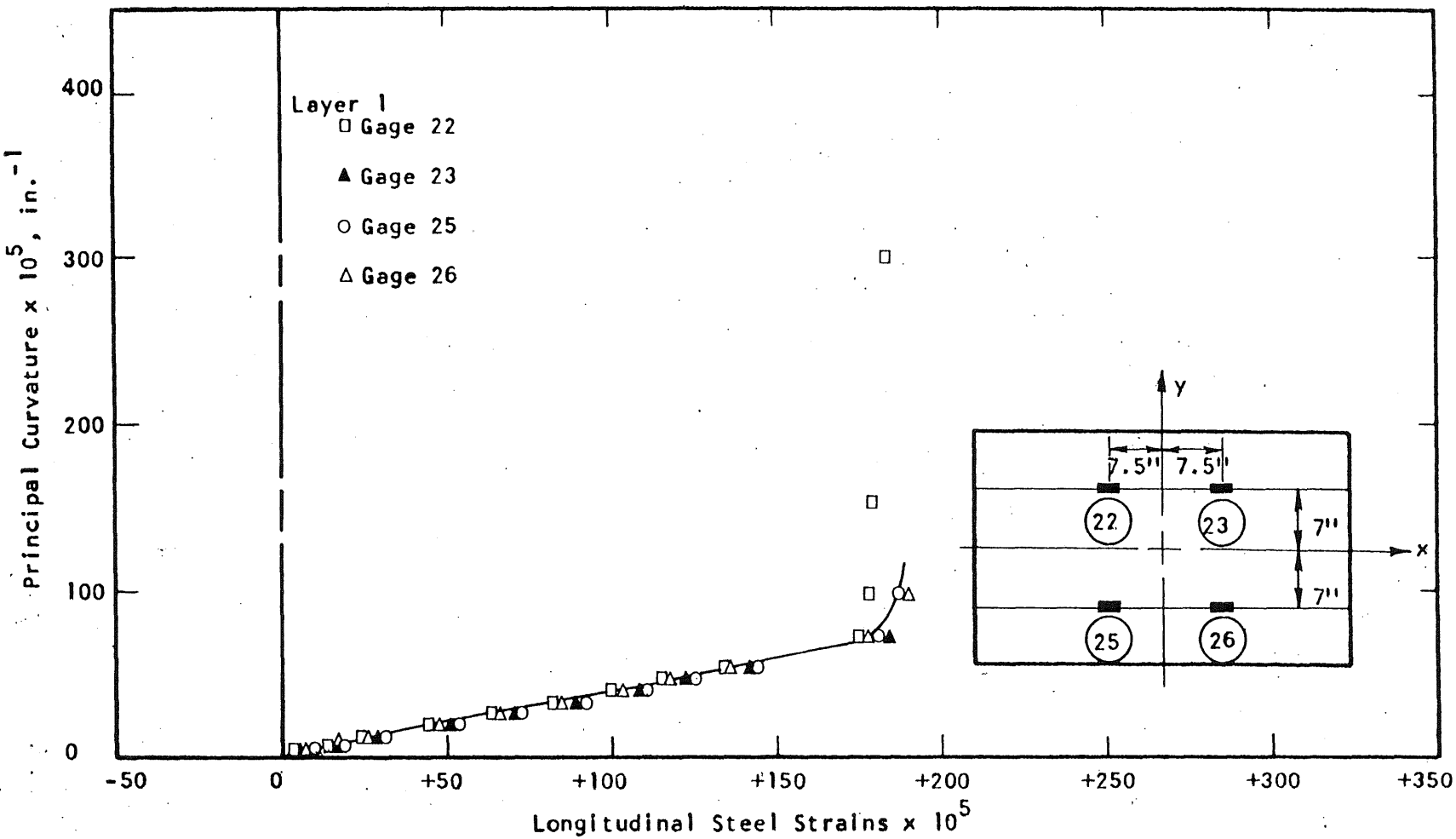

FIG. A.34 STEEL STRAIN PLOT, SPECIMEN B4

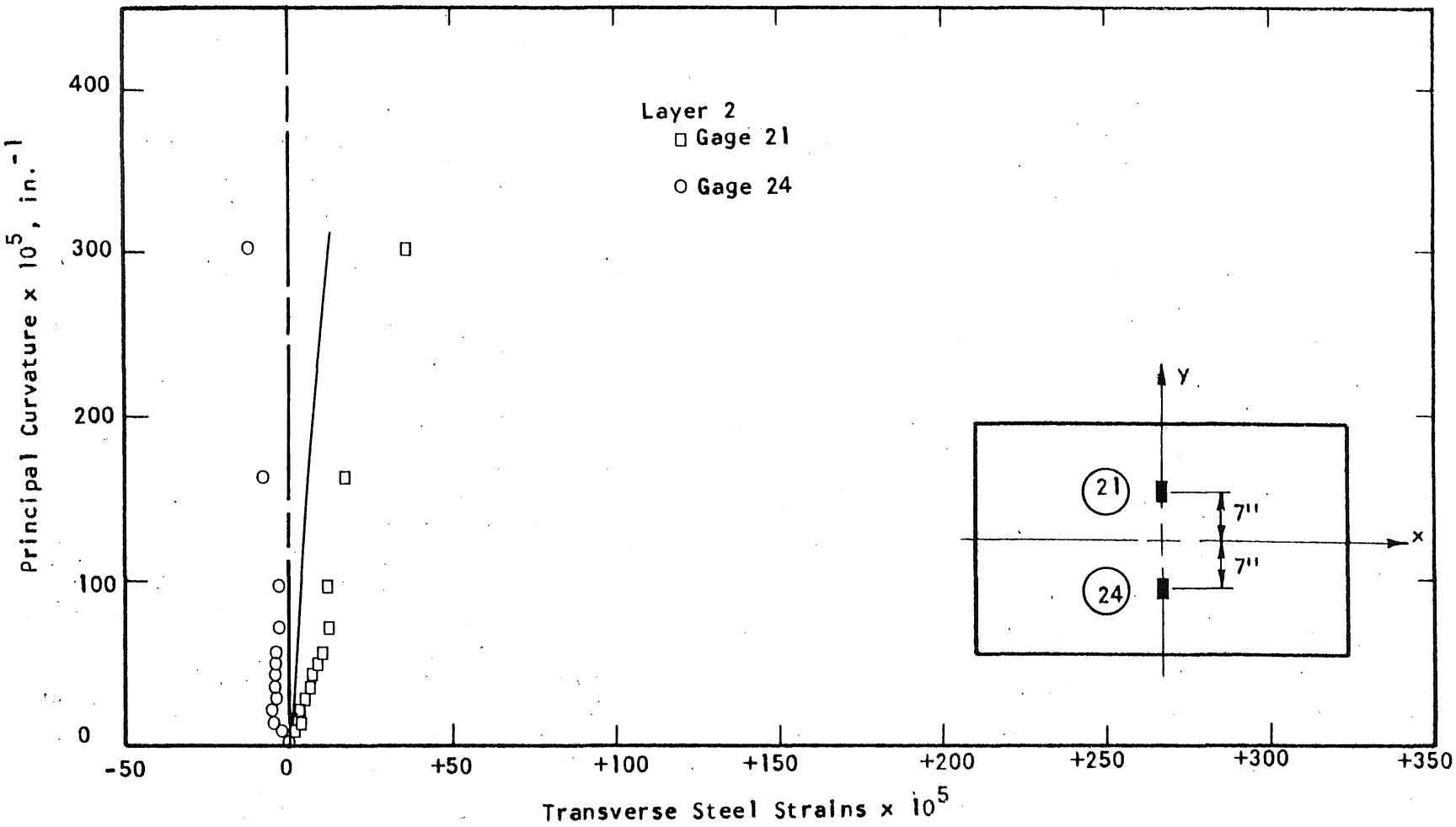

FIG. A.35 STEEL STRAIN PLOT, SPECIMEN B4

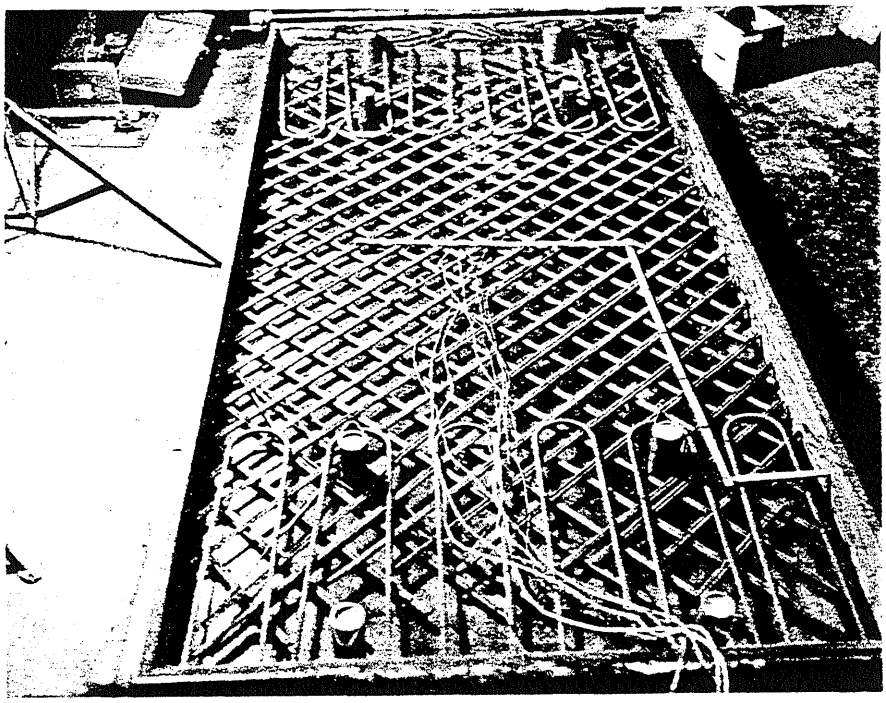

FIG. A.36 REINFORCEMENT IN SPECIMEN B5

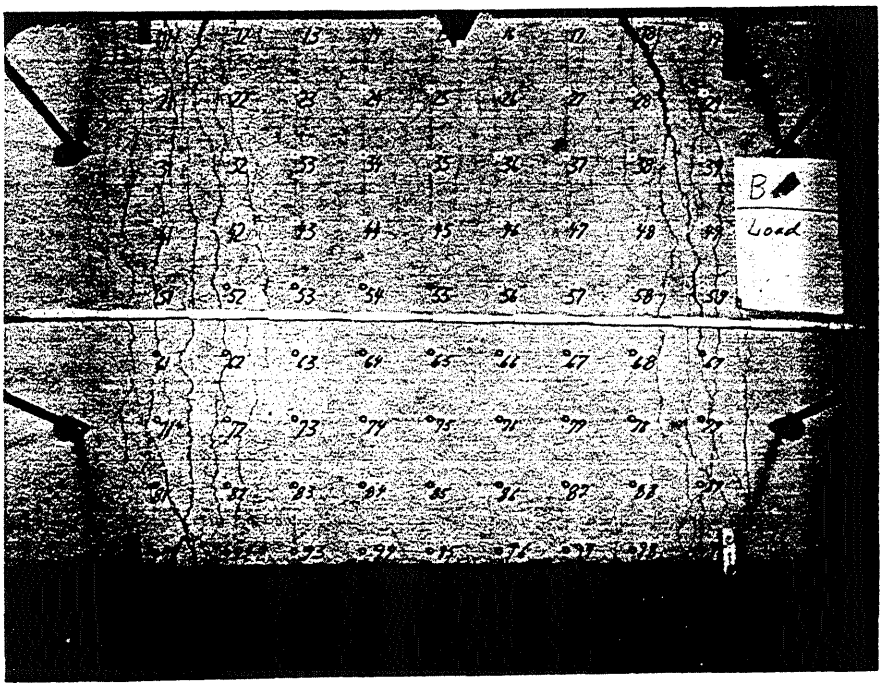

FIG. A.37 CRACK PATTERN IN TOP SURFACE OF B5

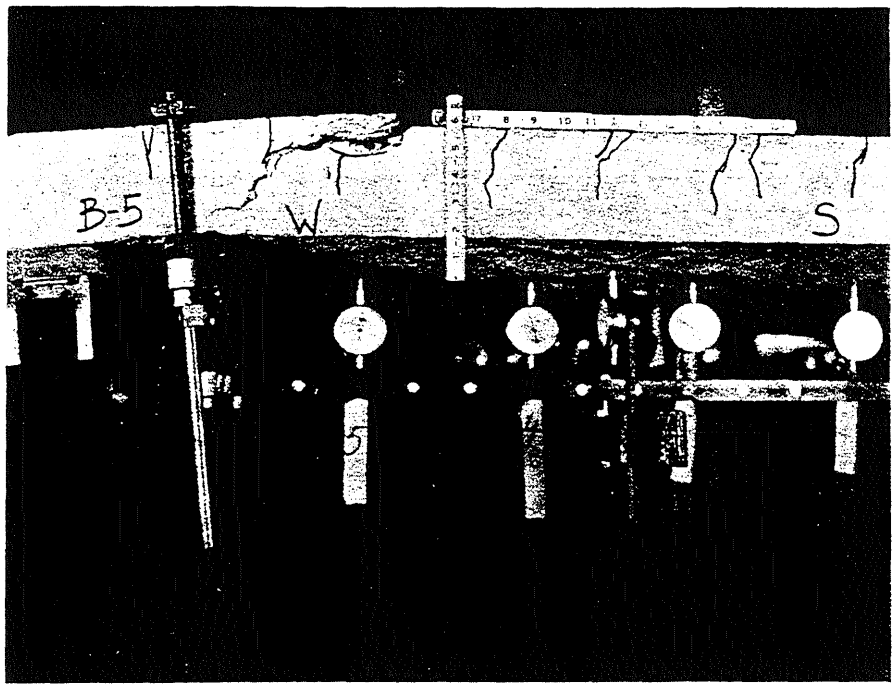

FIG. A.38 CLOSE-UP OF B5

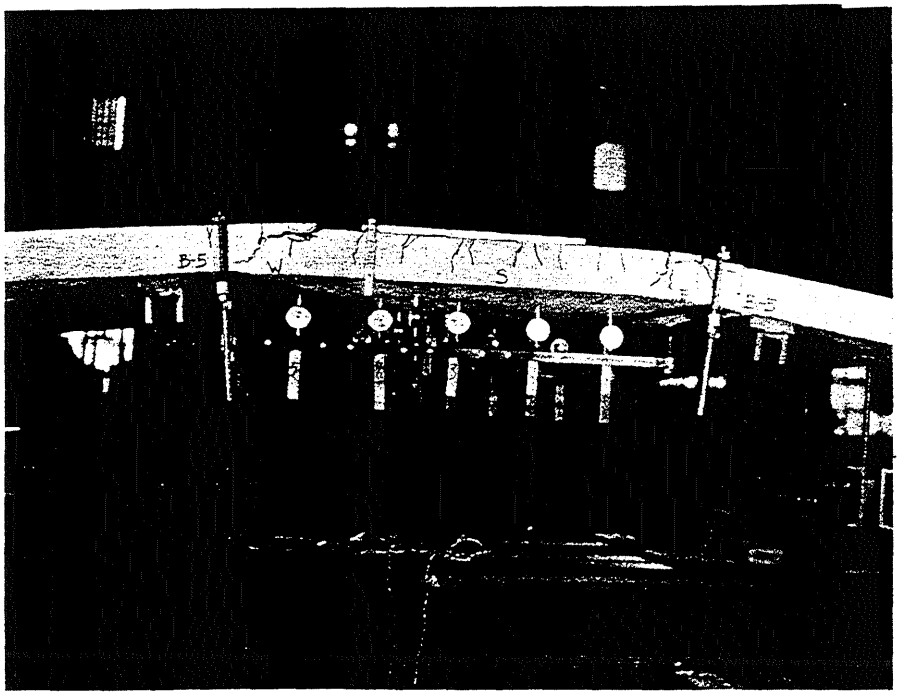

FIG. A.39 SIDE VIEW OF B5

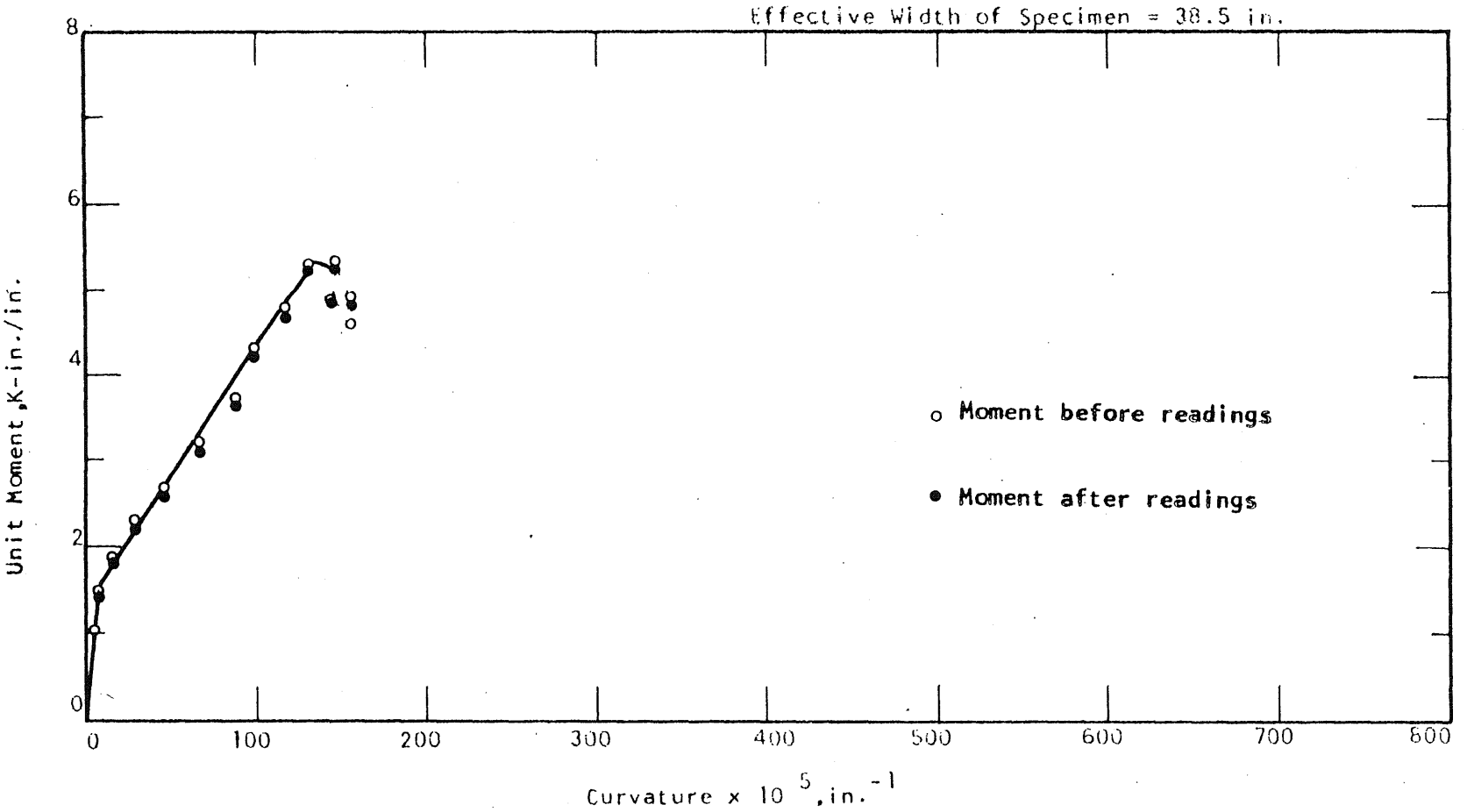

FIG. A.40 MOMENT-CURVATURE PLOT FOR SPECIMEN B5

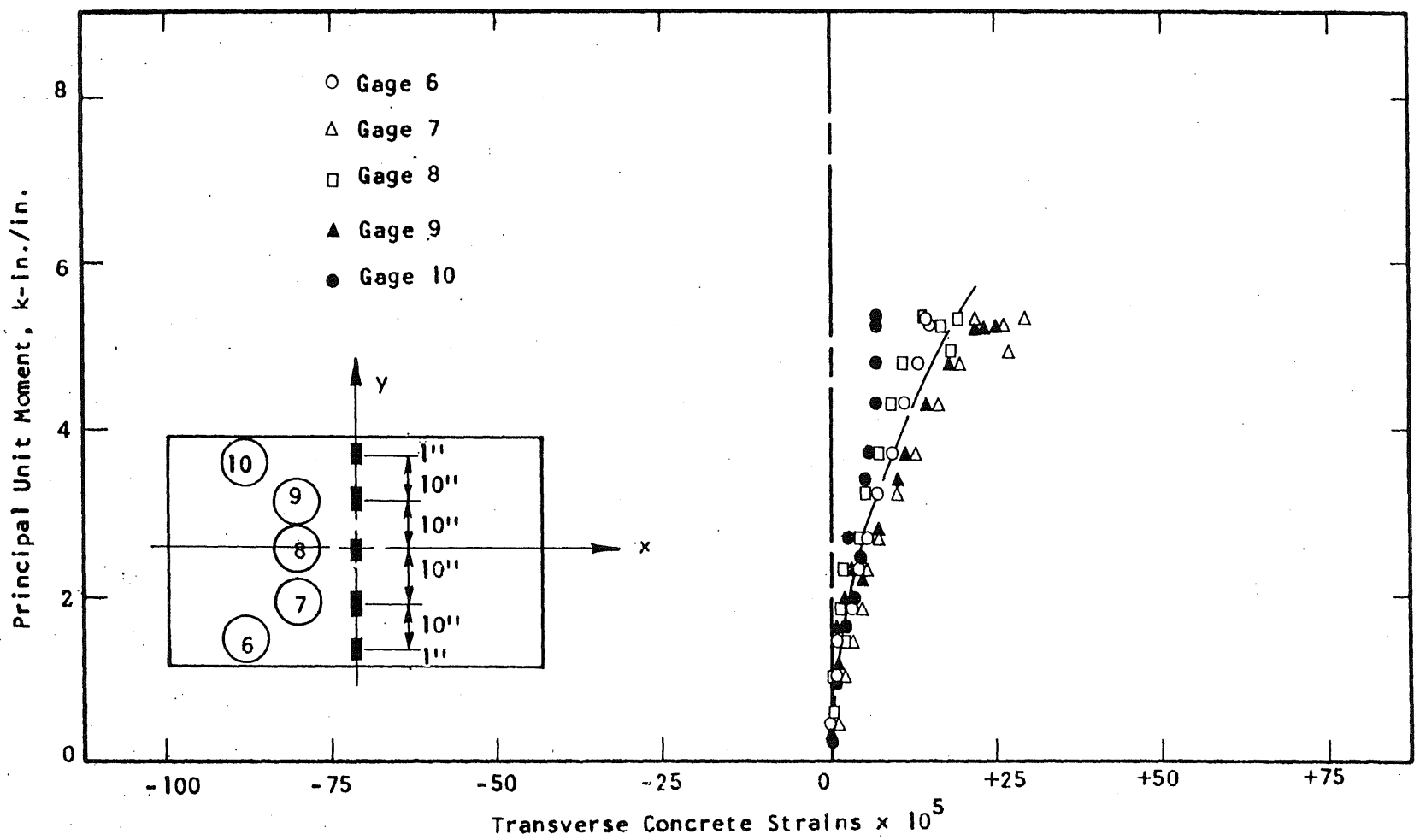

FIG. A.41 CONCRETE STRAIN PLOT, COMPRESSION SIDE OF SPECIMEN B5

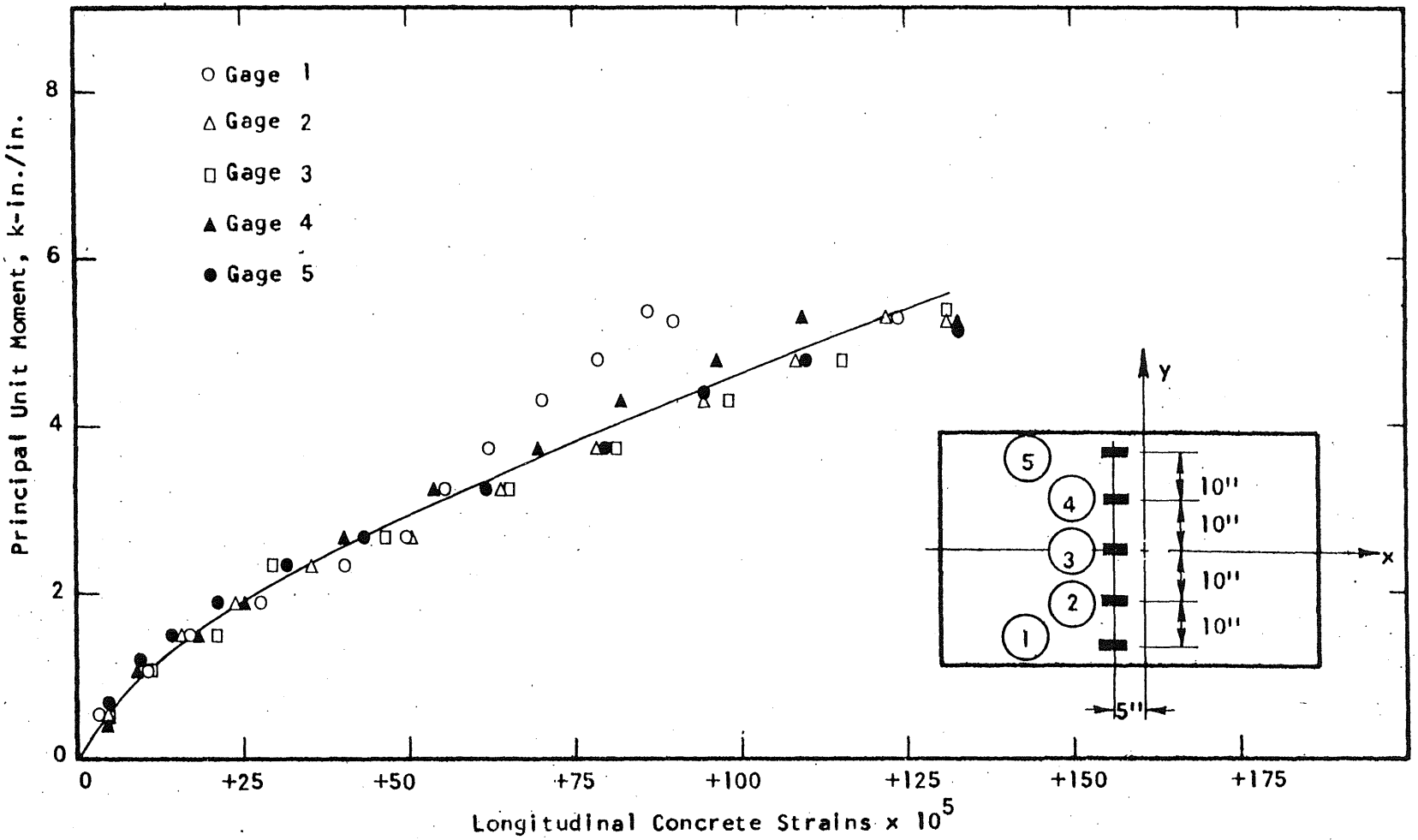

FIG. A.42 CONCRETE STRAIN PLOT, COMPRESSION SIDE OF SPECIMEN B5

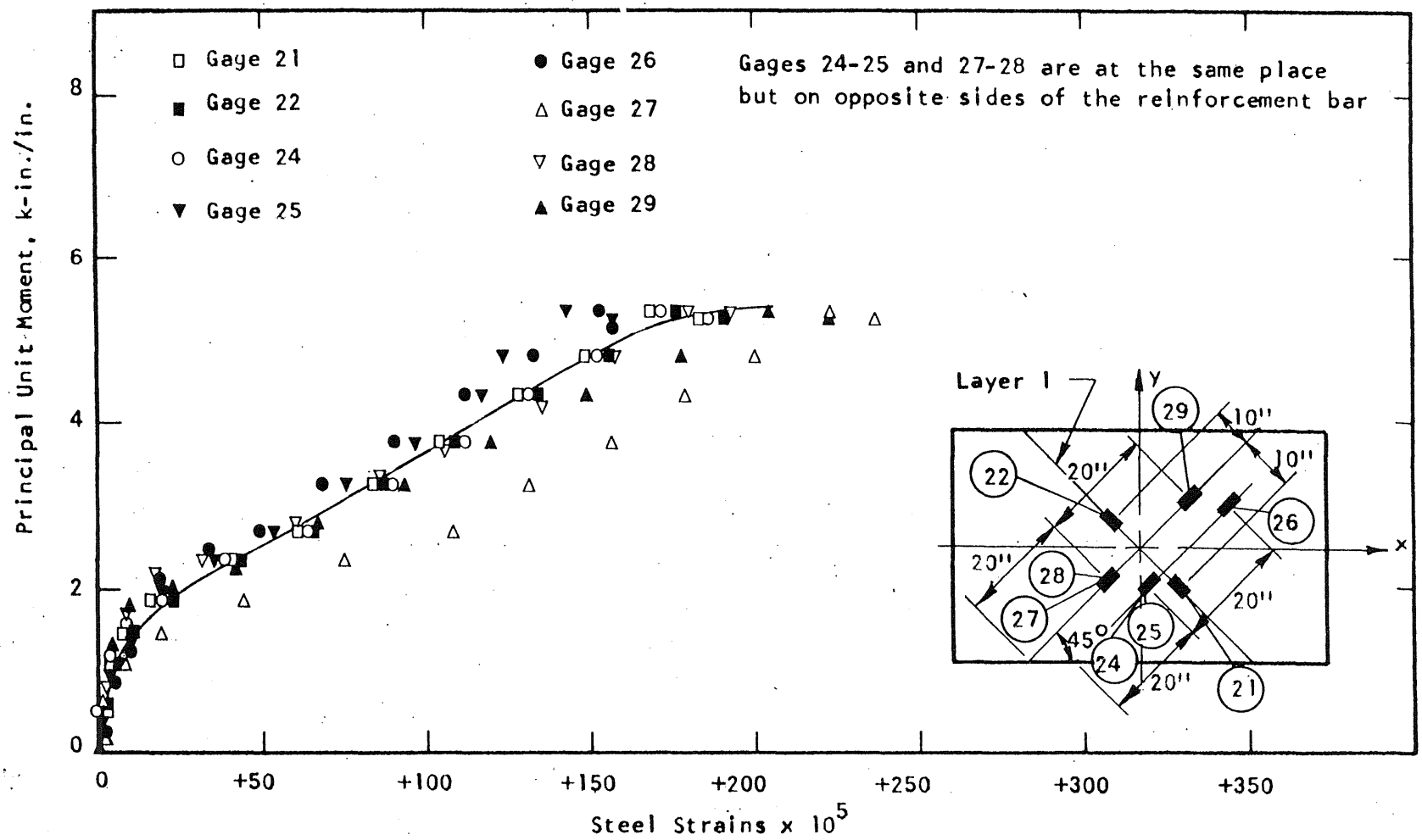

FIG. A.43 STEEL STRAIN PLOT, SPECIMEN B5

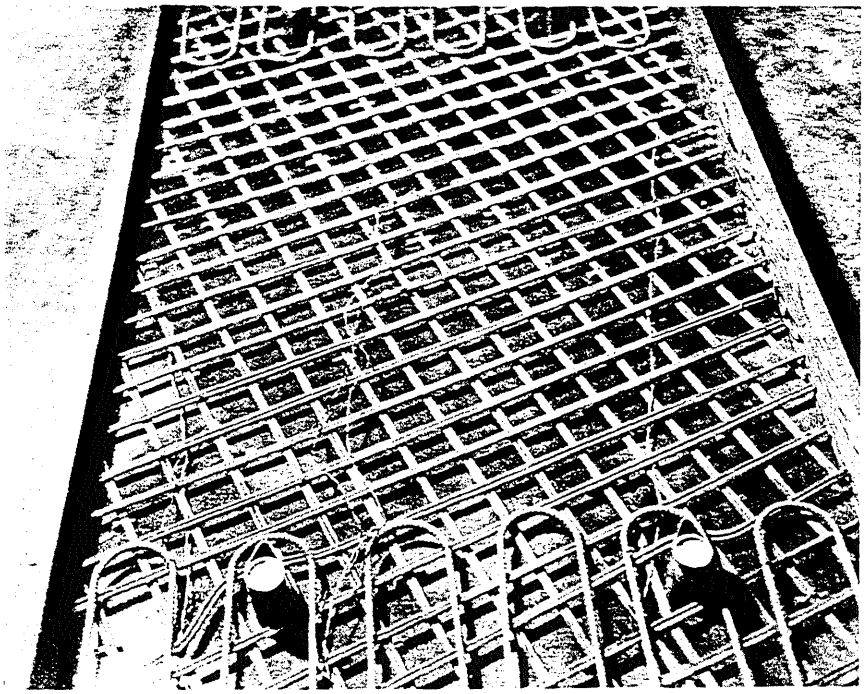

FIG. A.44 REINFORCEMENT IN SPECIMEN B6

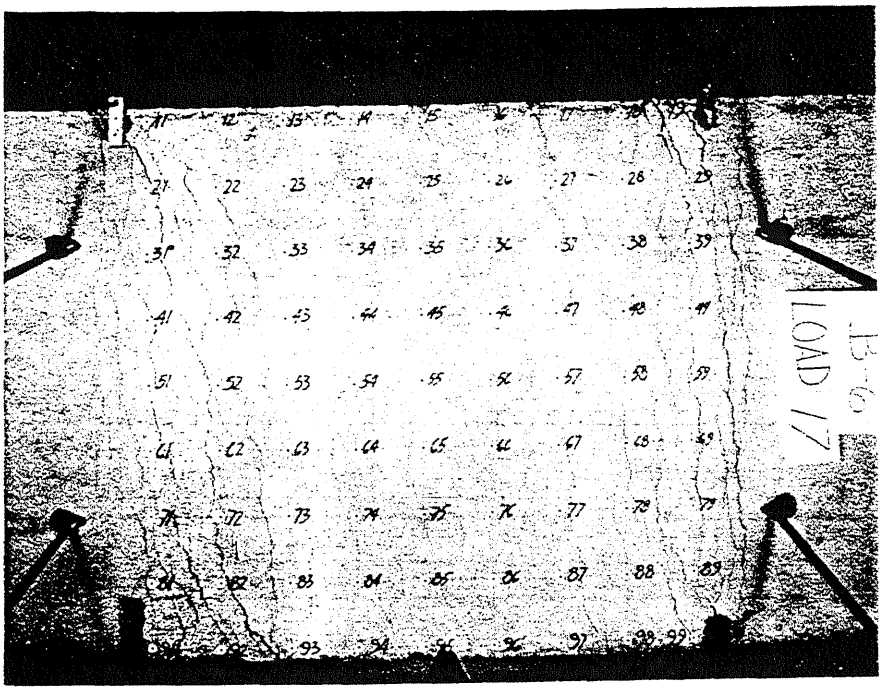

a Crack Pattern in Top Surface of B6

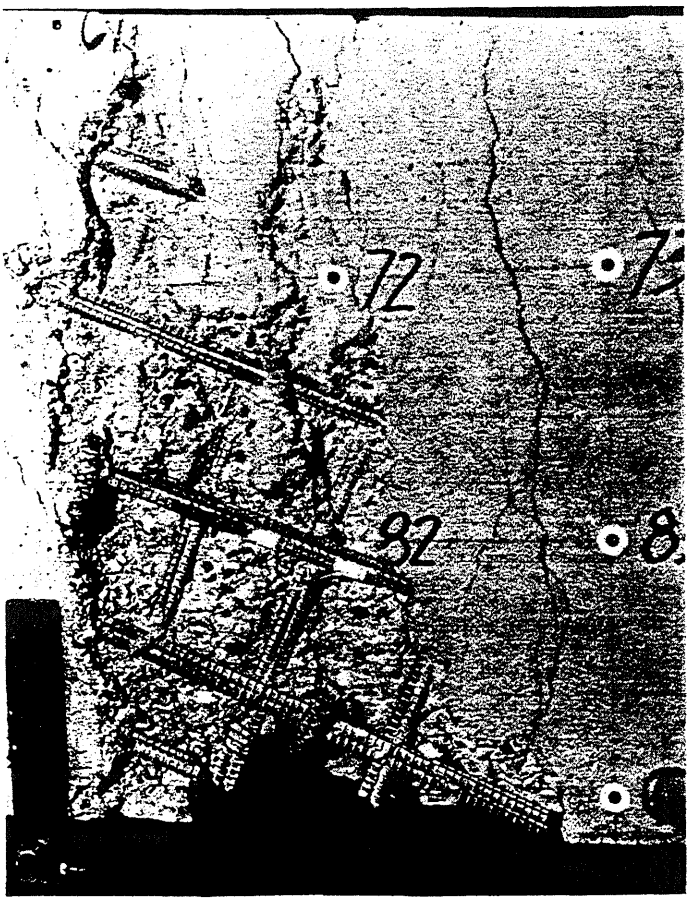

b Close-up of Top Surface of B6

FIG. A.45 CRACK PATTERN OF SPECIMEN B6

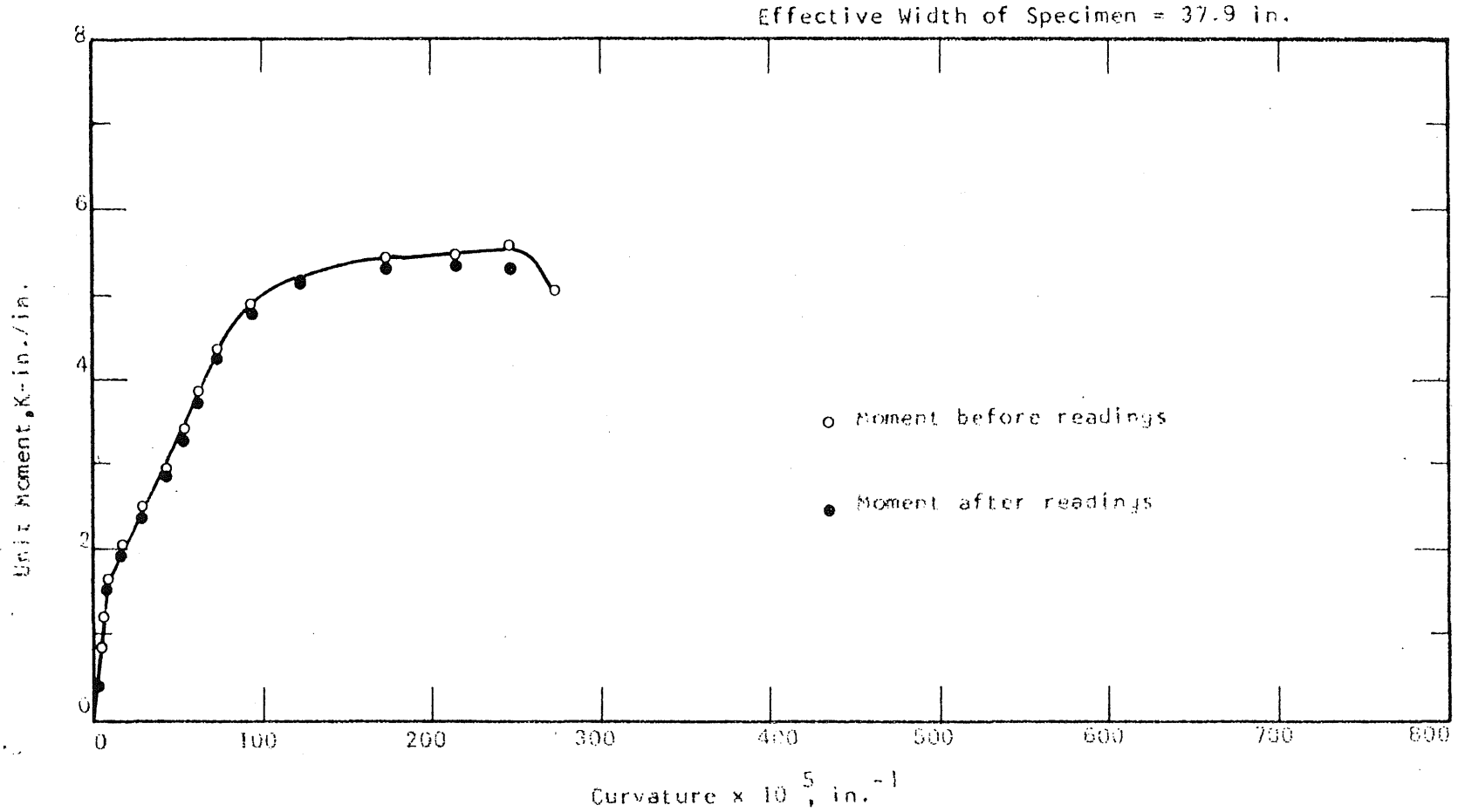

FIG. A.46 MOMENT-CURVATURE PLOT FOR SPECIMEN B6

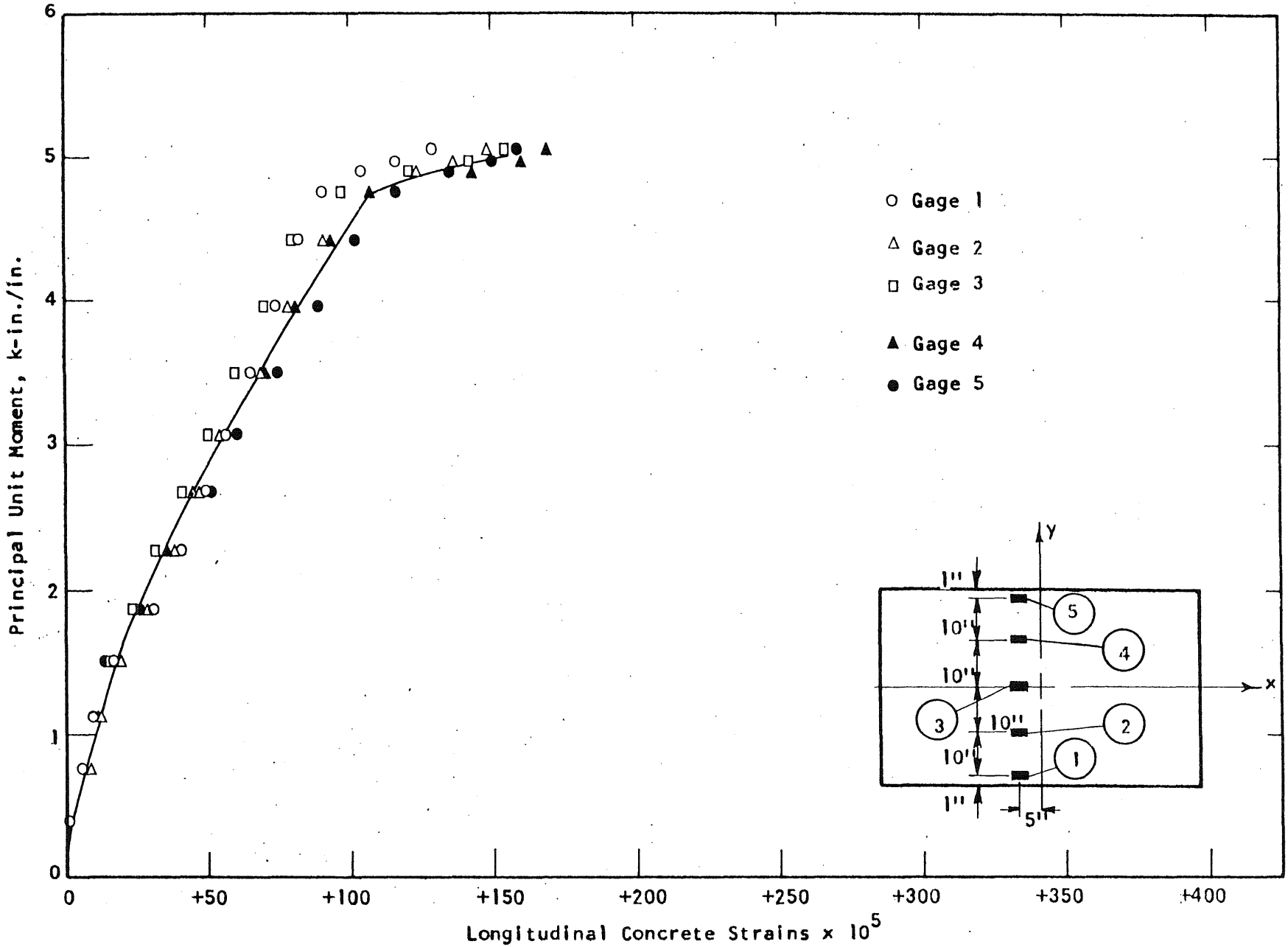

FIG. A.47 CONCRETE STRAIN PLOT, COMPRESSION SIDE OF SPECIMEN B6

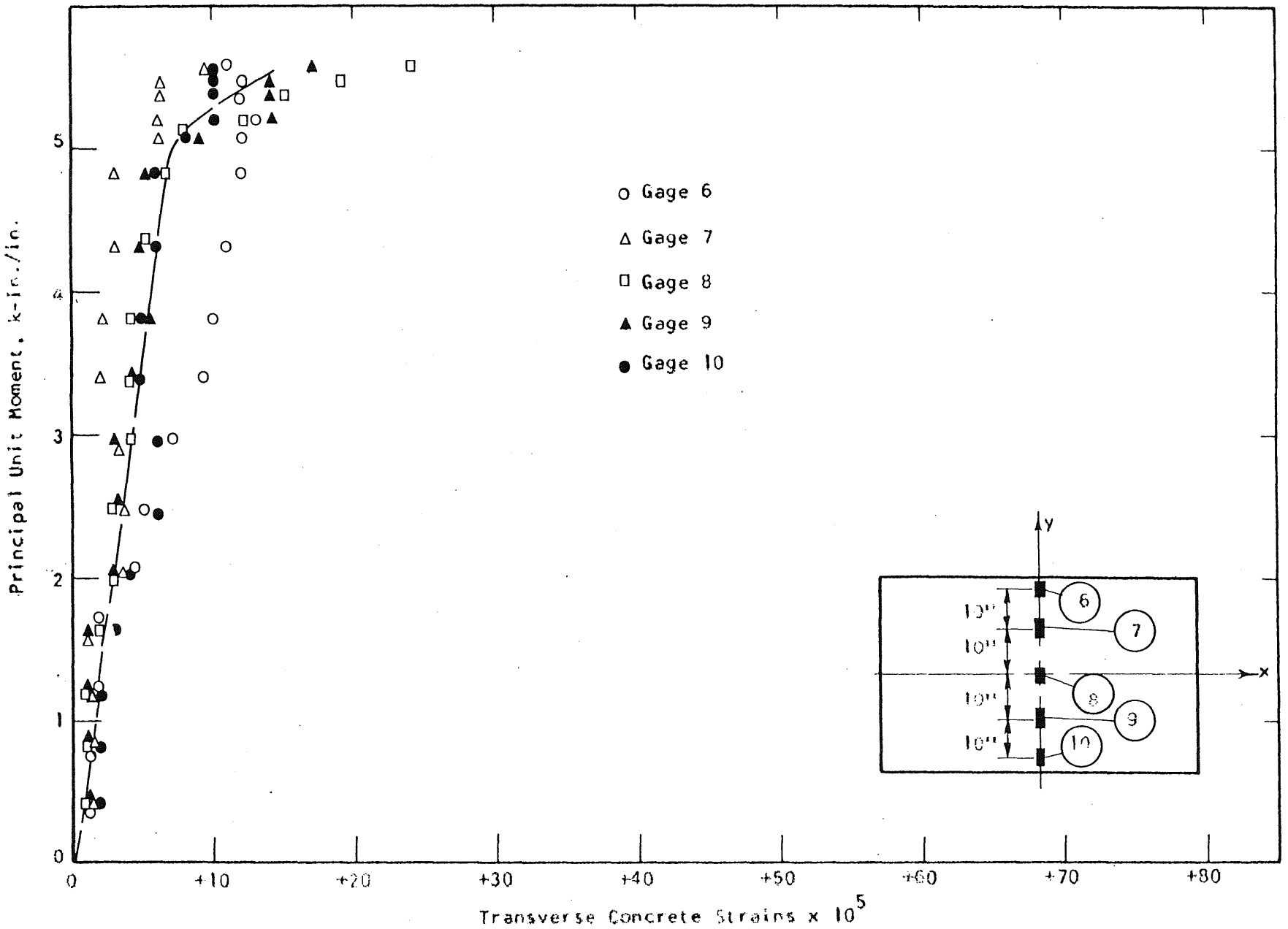

FIG. A.48 CONCRETE STRAIN PLOT, COMPRESSION SIDE OF SPECIMEN B6

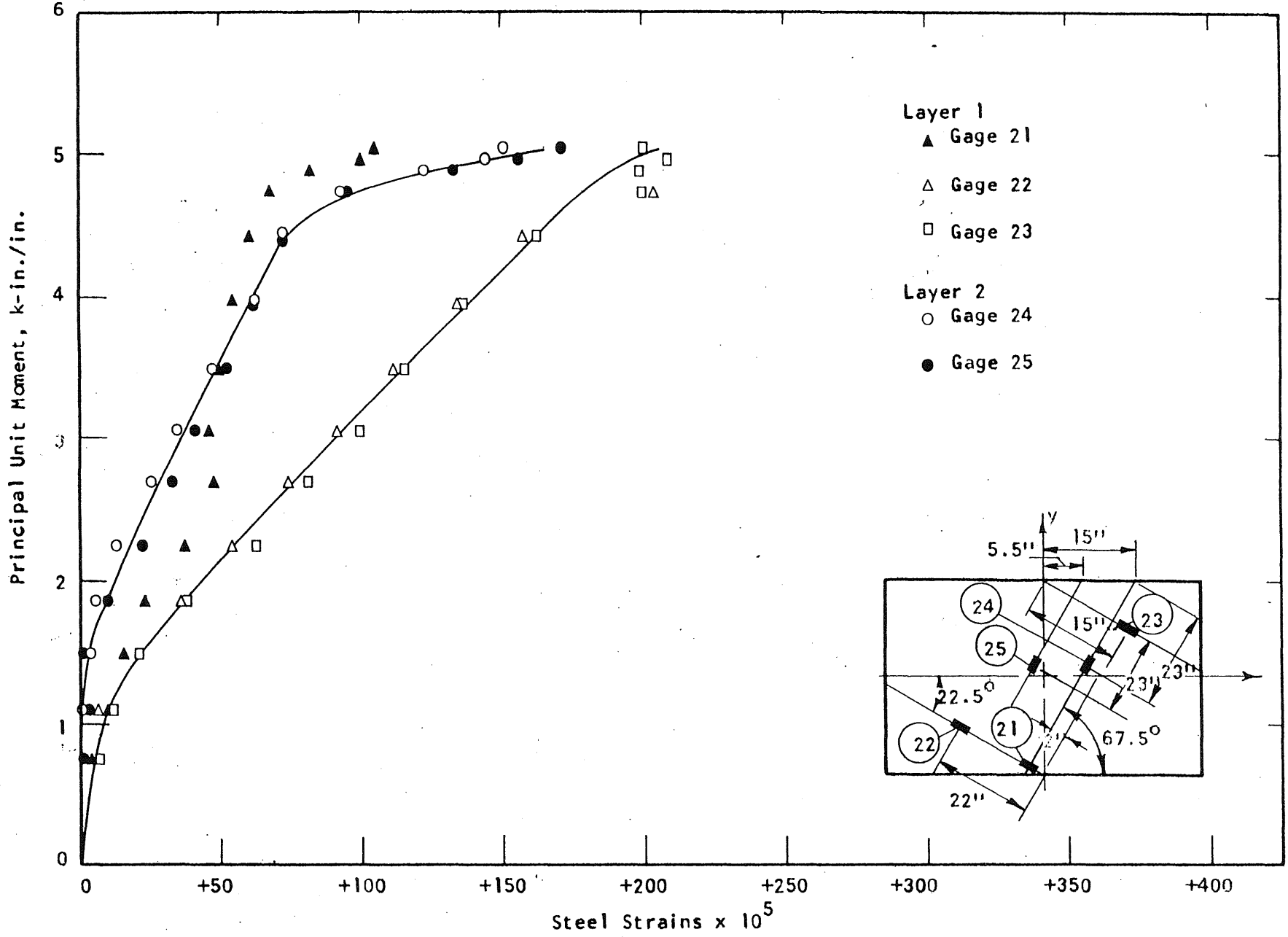

FIG. A.49 STEEL STRAIN PLOT, SPECIMEN B6

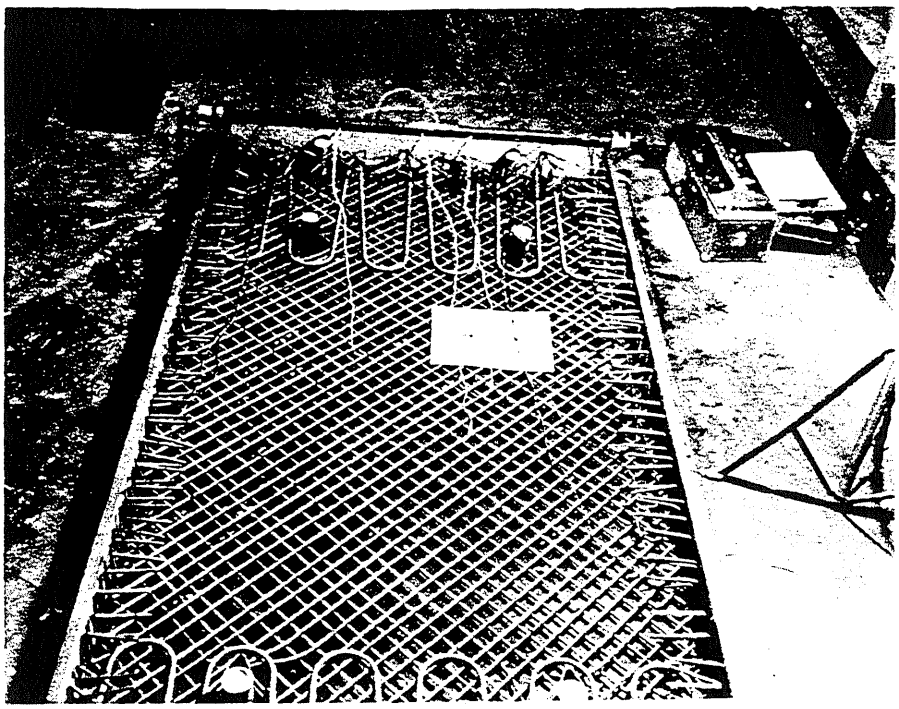

FIG. A.50 REINFORCEMENT IN SPECIMEN B7

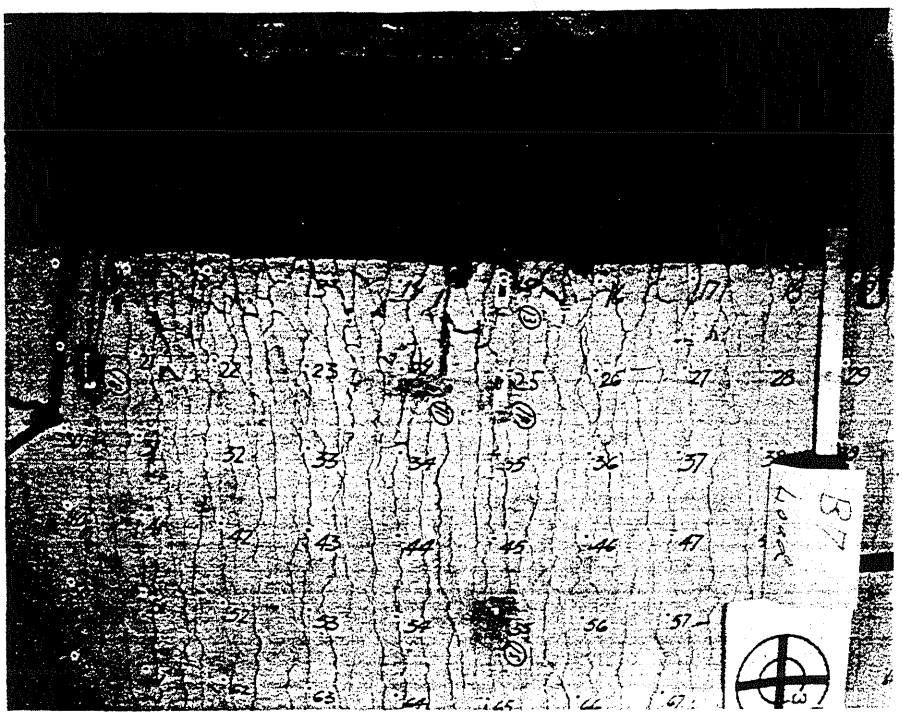

FIG. A.51 CRACK PATTERN ON TOP SURFACE OF B7

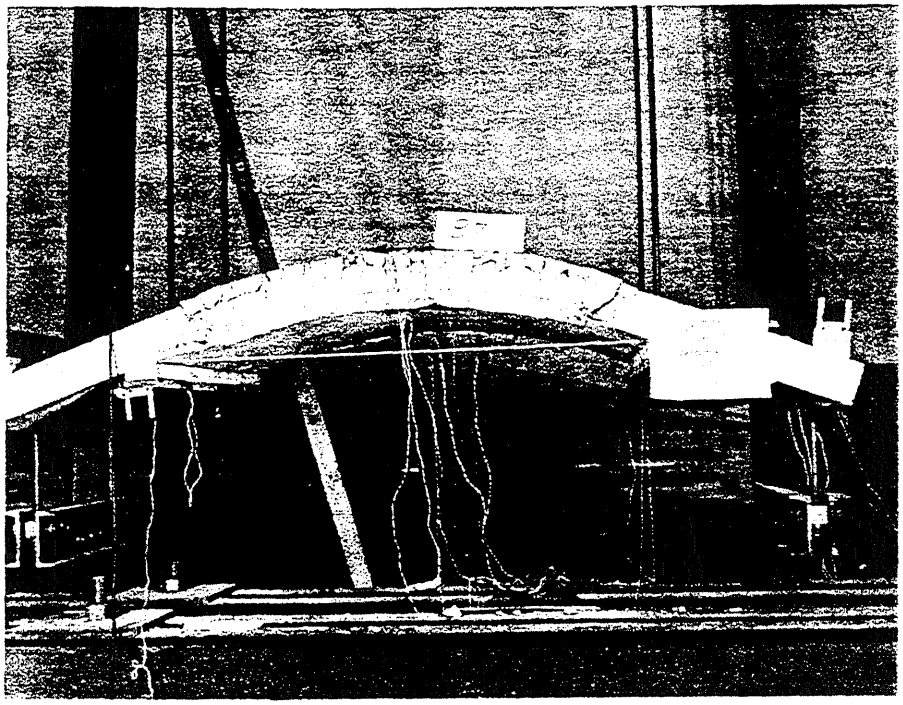

a Side View

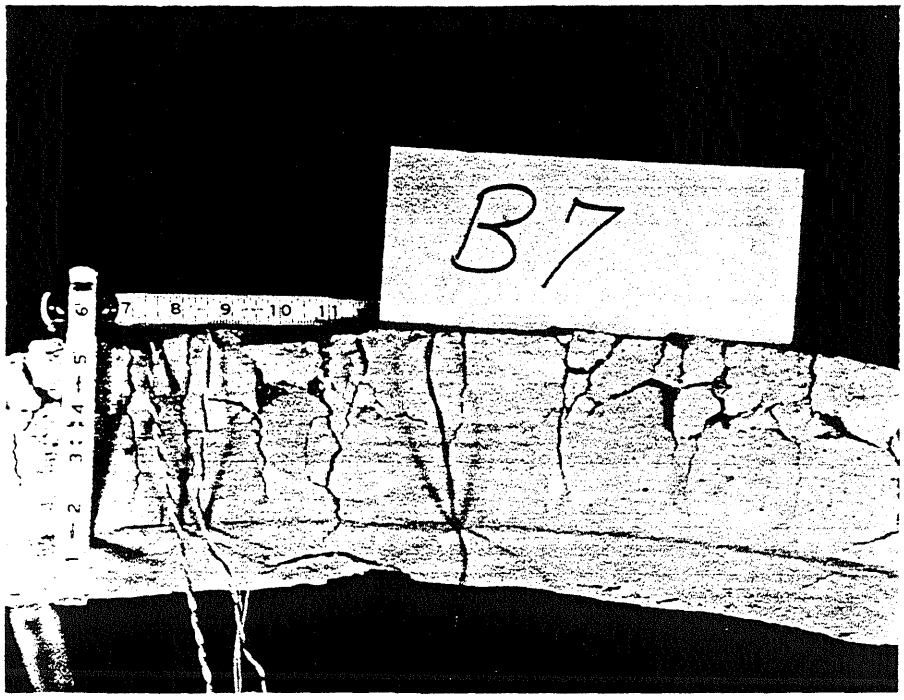

b Close-up

FIG. A.52 SIDE VIEWS OF SPECIMEN B7

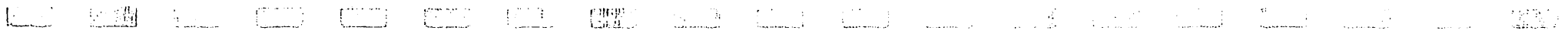

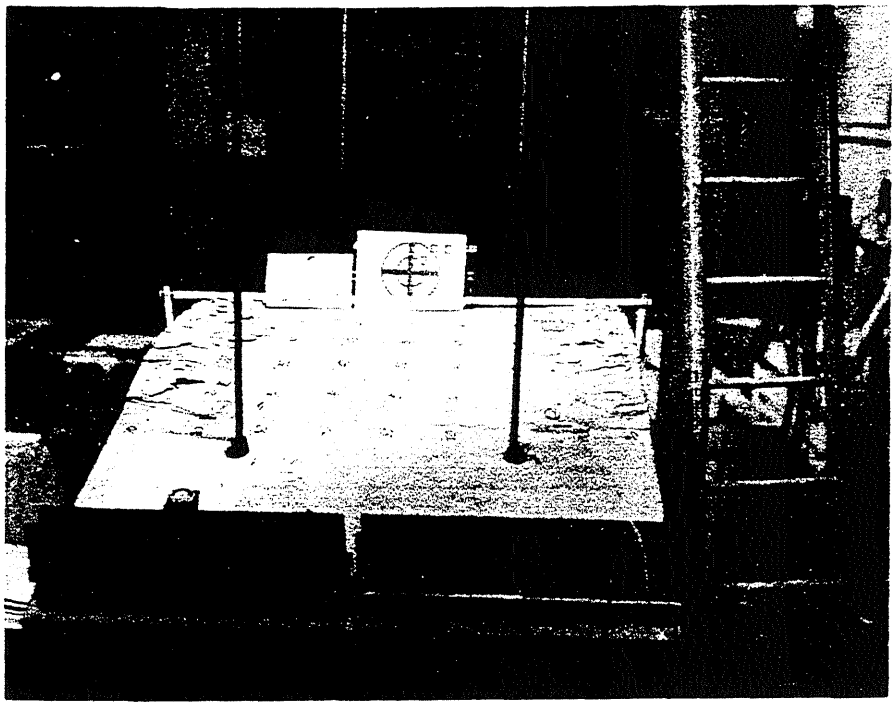

FIG. A.53 END VIEW OF B7

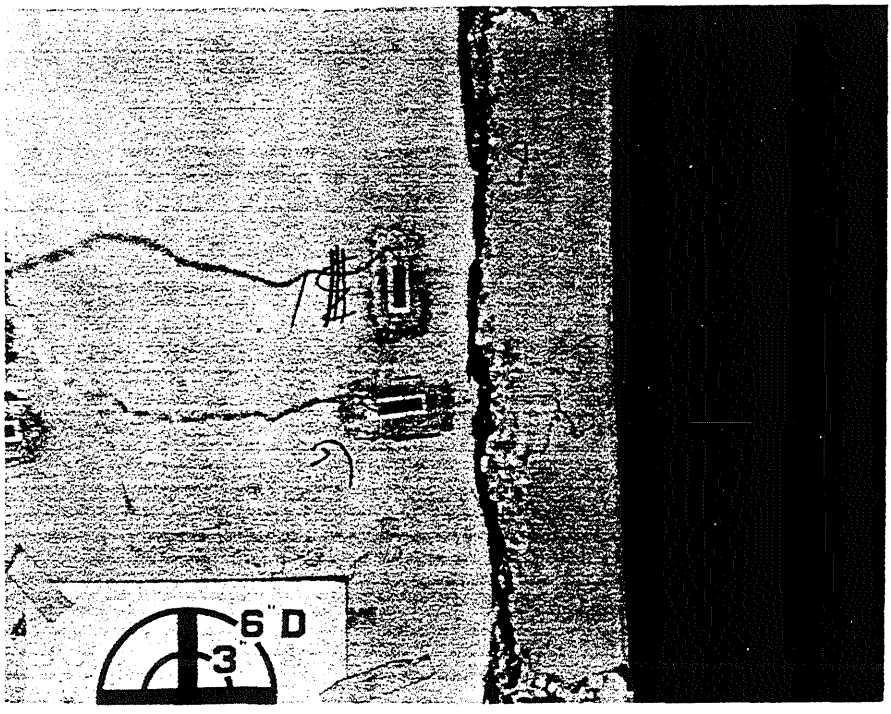

FIG. A.54 CRACK ON BOTTOM FACE OF B7

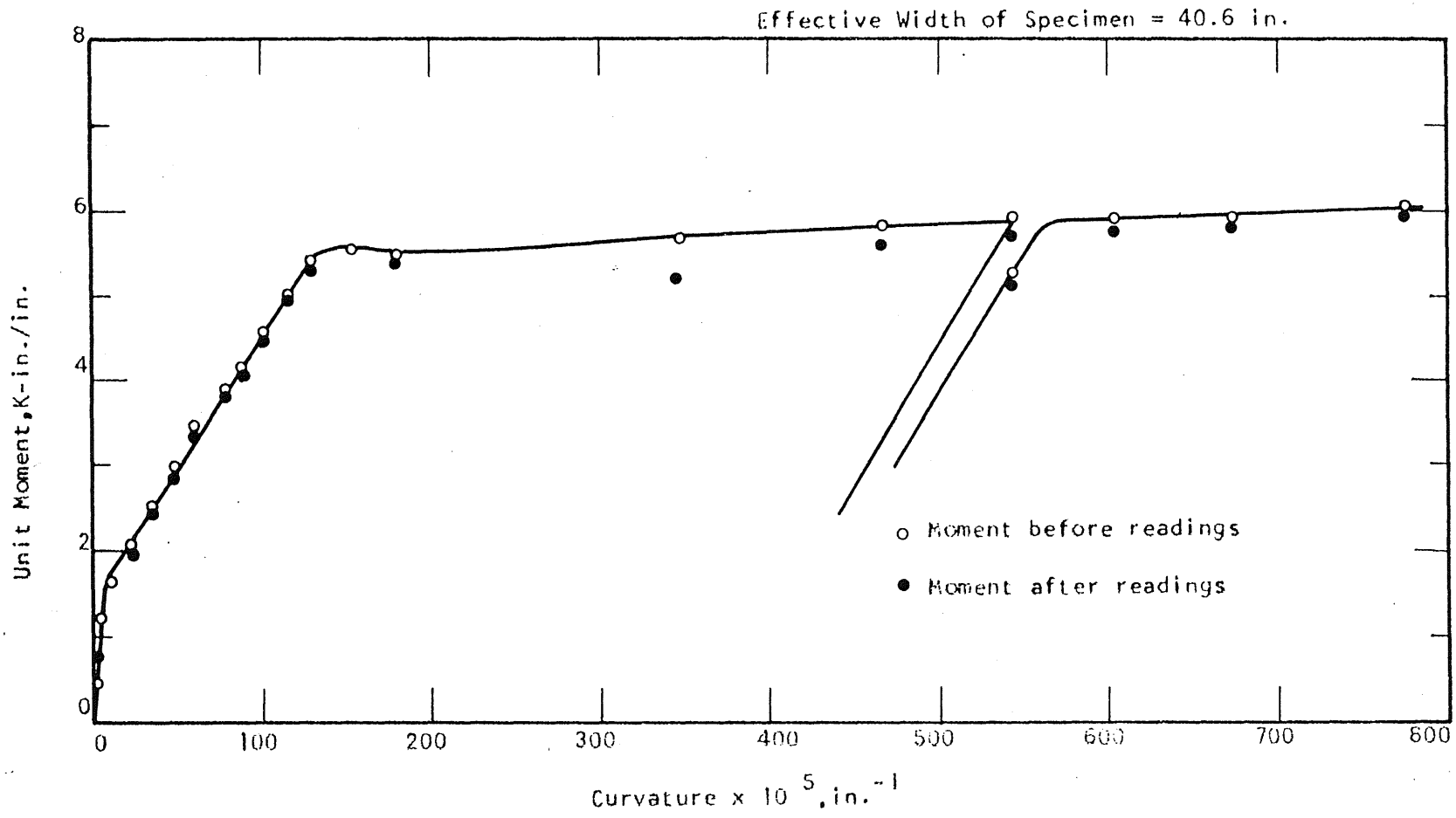

FIG. A.55 MOMENT-CURVATURE PLOT FOR SPECIMEN B7

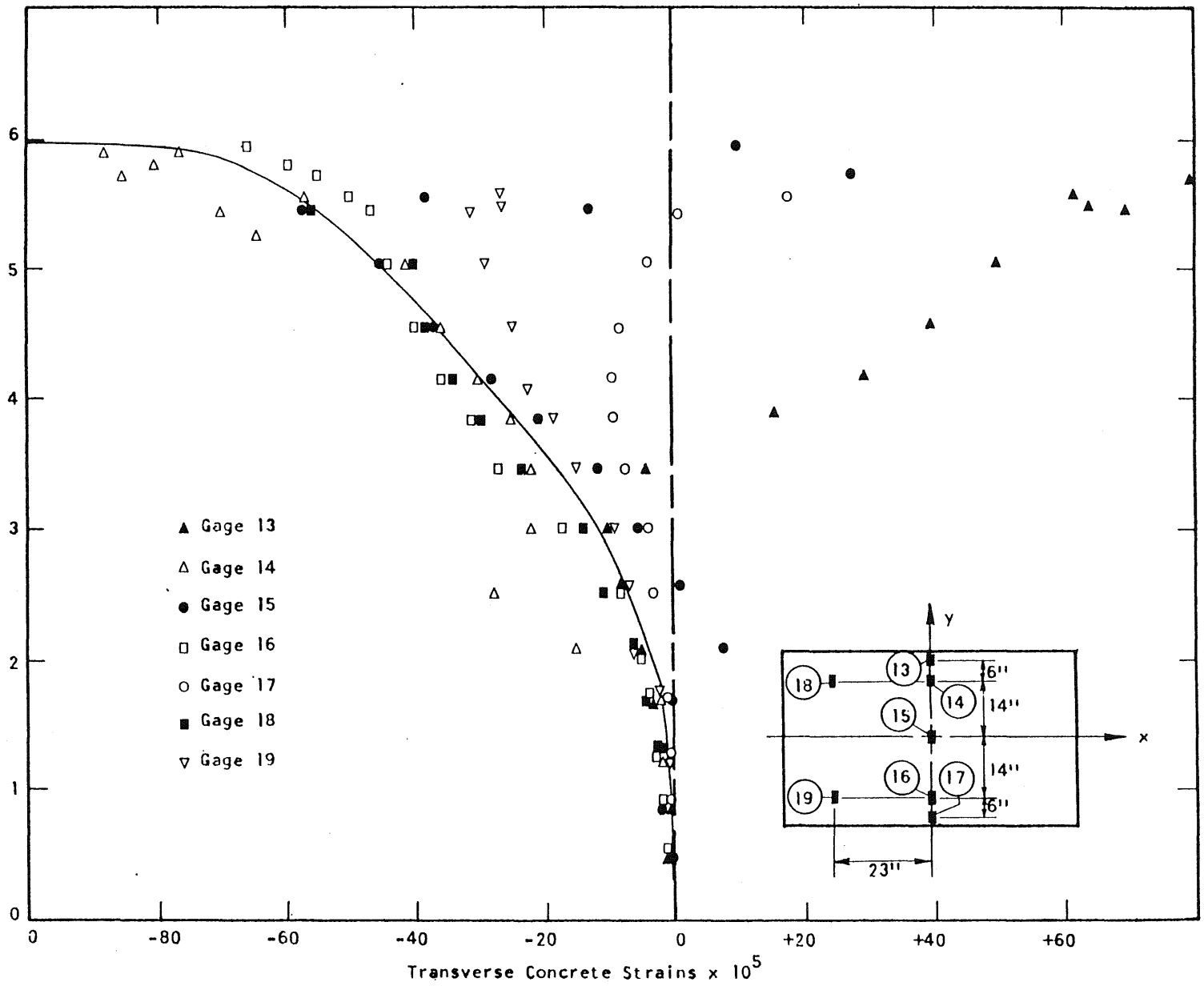

FIG. A.56 CONCRETE STRAIN PLOT, TENSION SIDE OF SPECIMEN B7

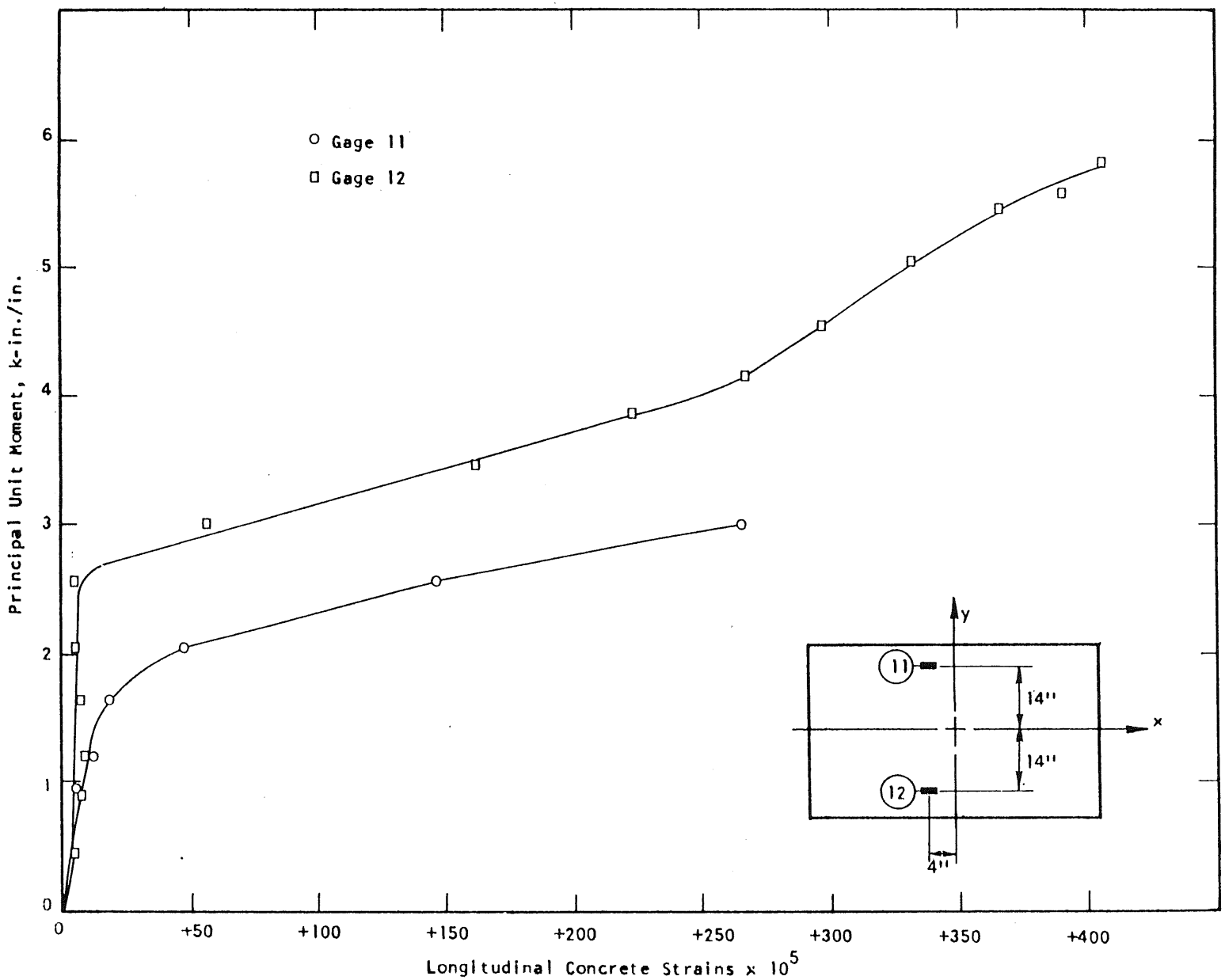

FIG. A.57 CONCRETE STRAIN PLOT , TENSION SIDE OF SPECIMEN B7

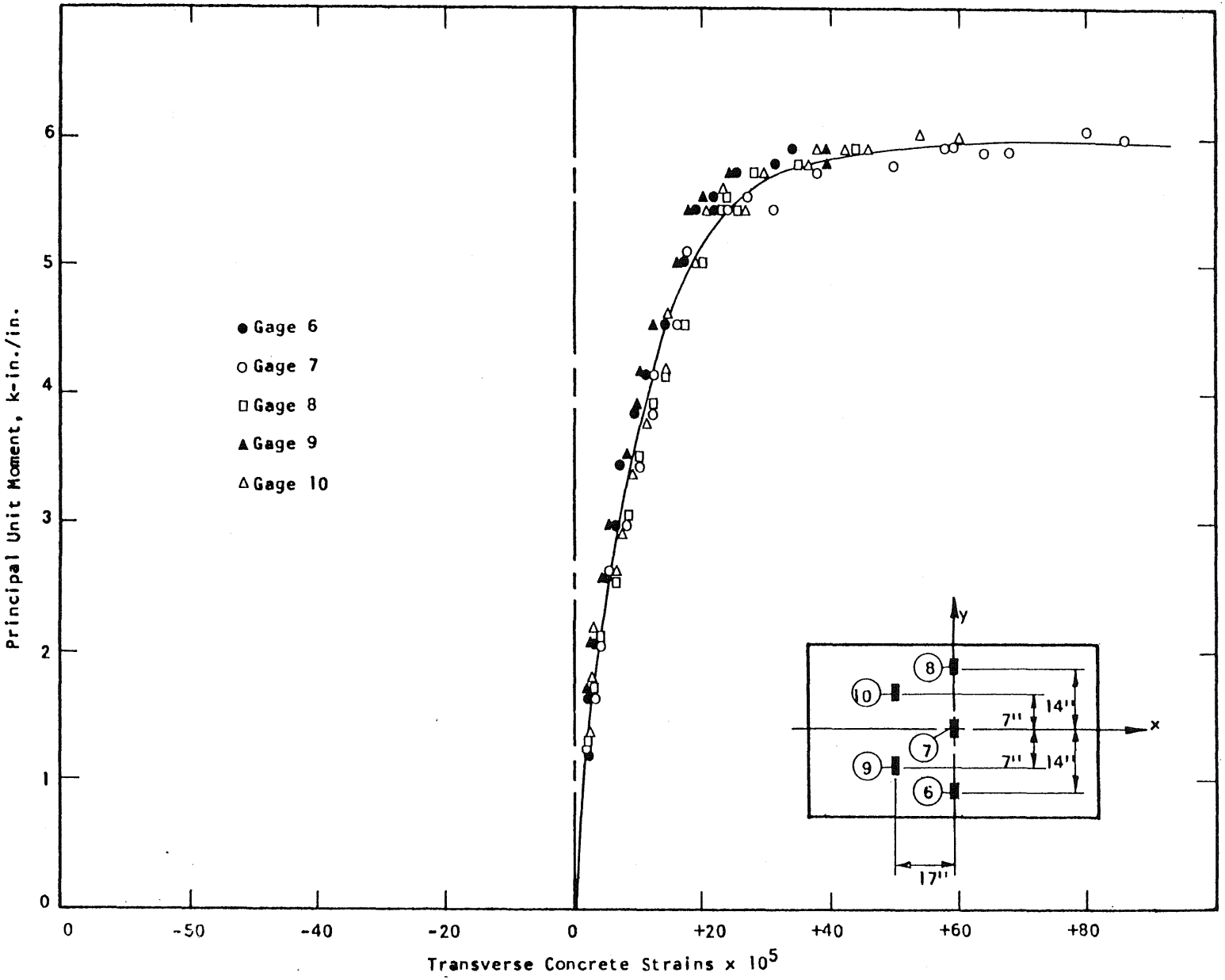

FIG. A.58 CONCRETE STRAIN PLOT, COMPRESSION SIDE OF SPECIMEN B7

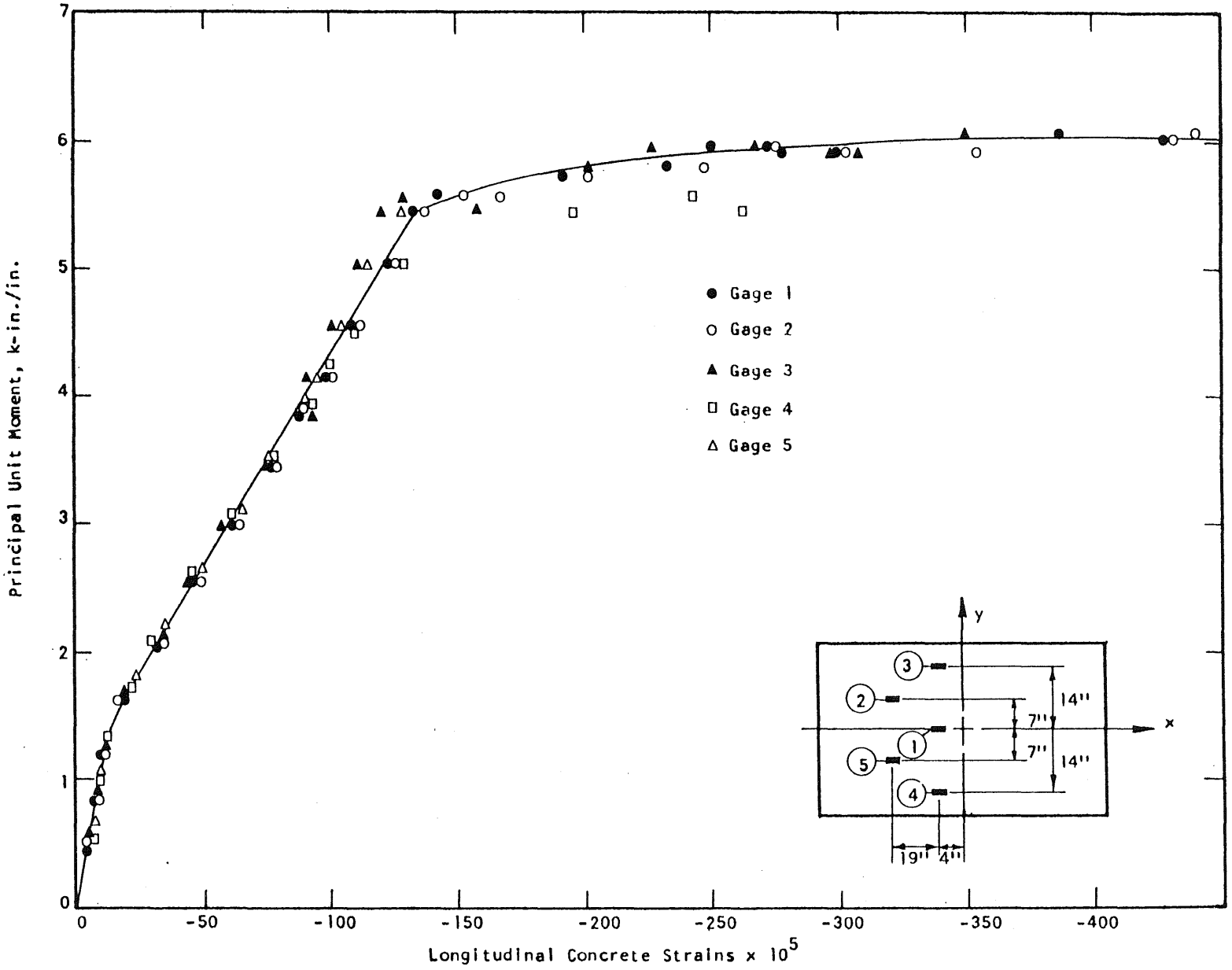

FIG. A.59 CONCRETE STRAIN PLOT, COMPRESSION SIDE OF SPECIMEN B7

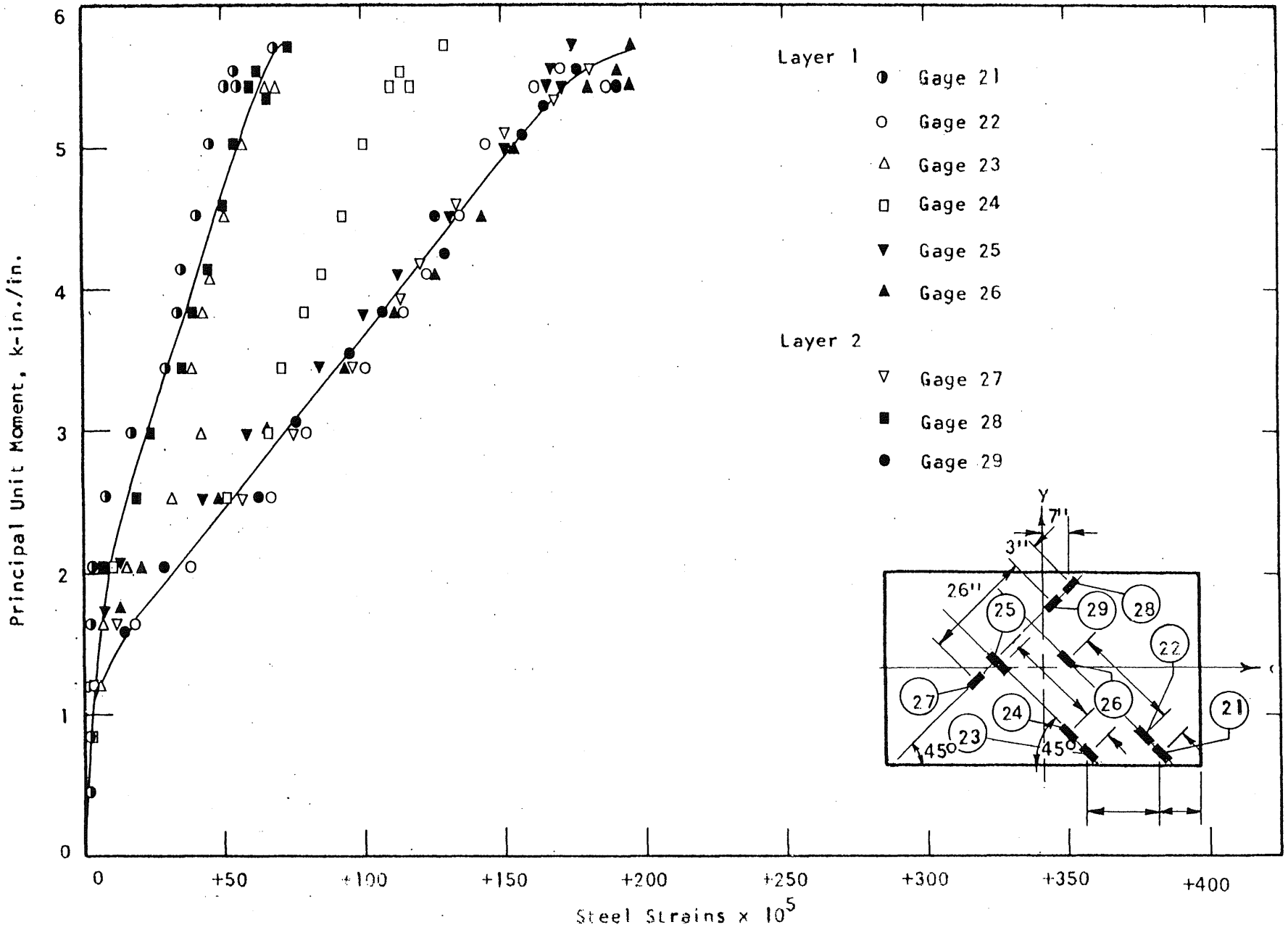

FIG. A.60 STEEL STRAIN PLOT, SPECIMEN B7

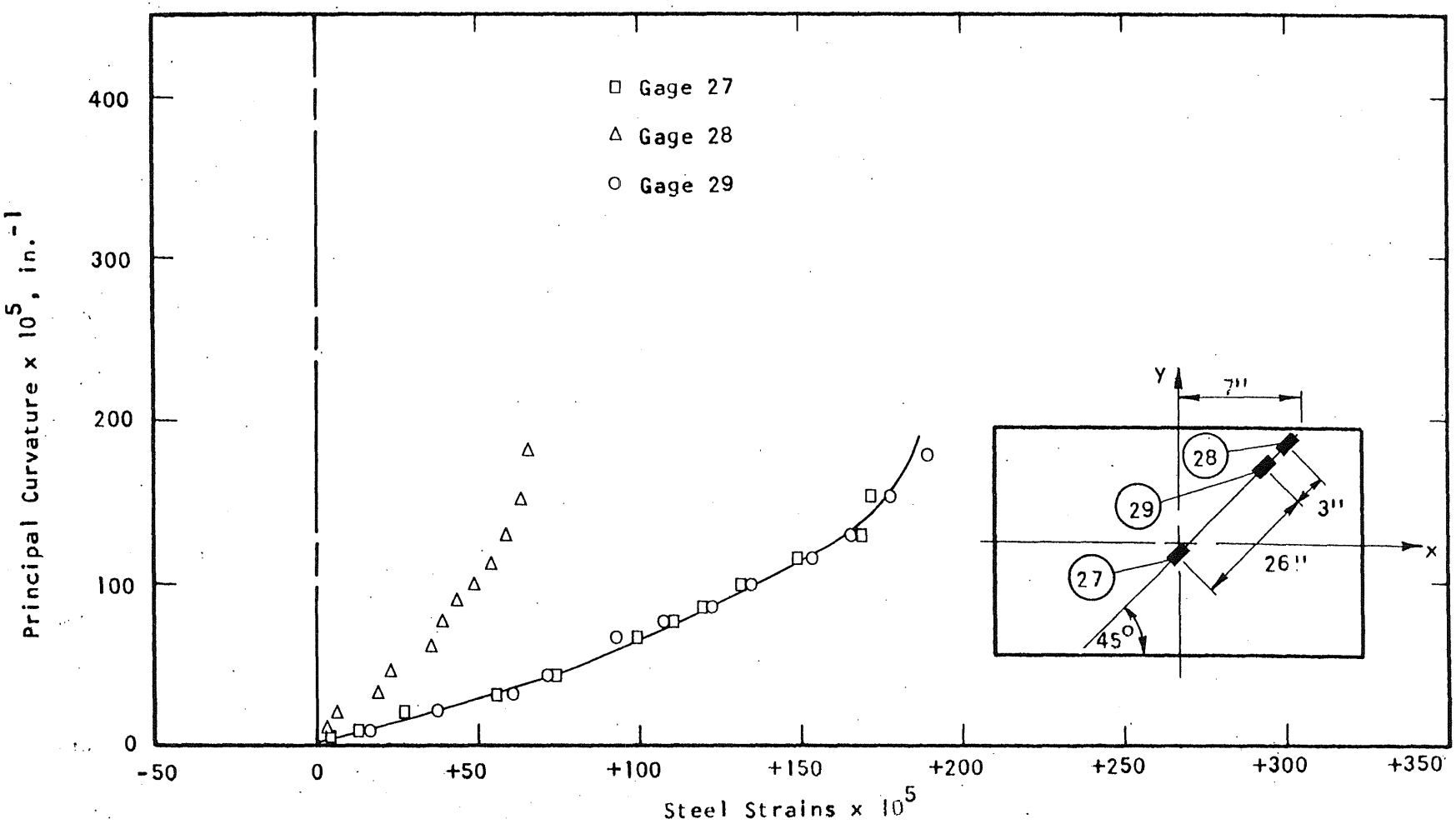

FIG. A.61 STEEL STRAIN PLOT, SPECIMEN B7

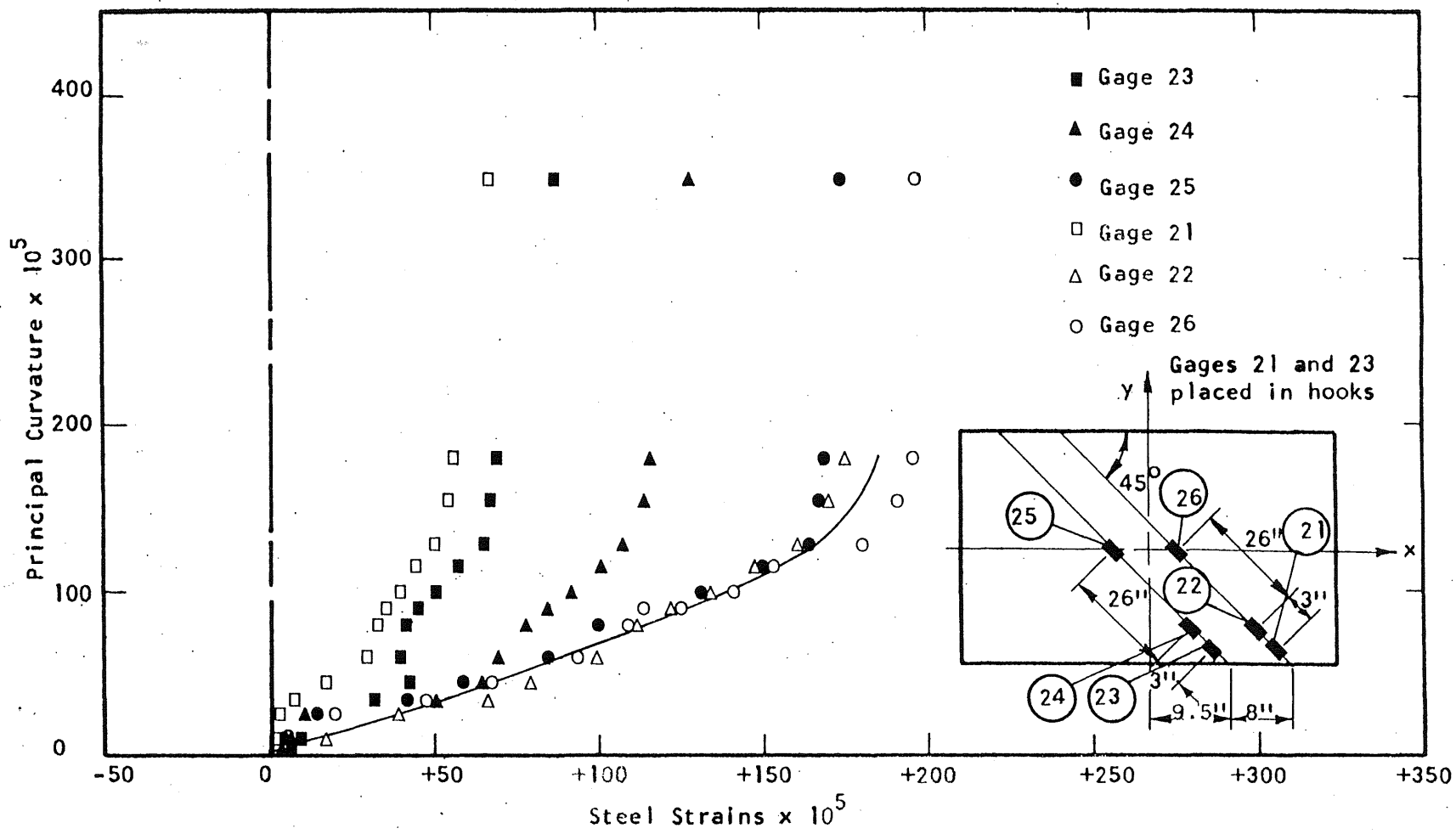

FIG. A.62 STEEL STRAIN PLOT, SPECIMEN B7

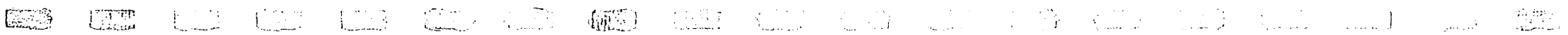

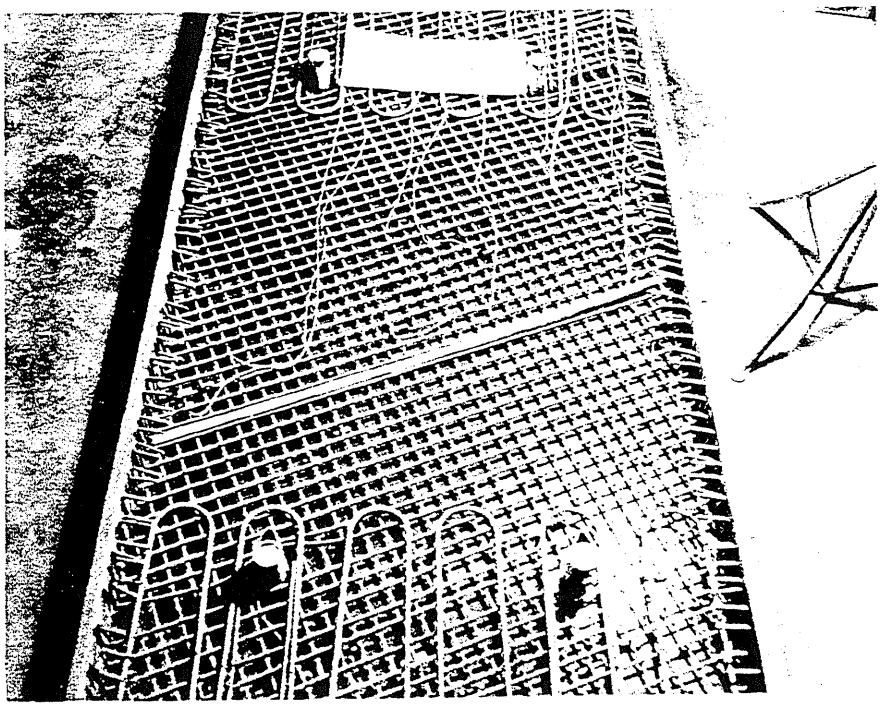

FIG. A.63 REINFORCEMENT IN SPECIMEN B8

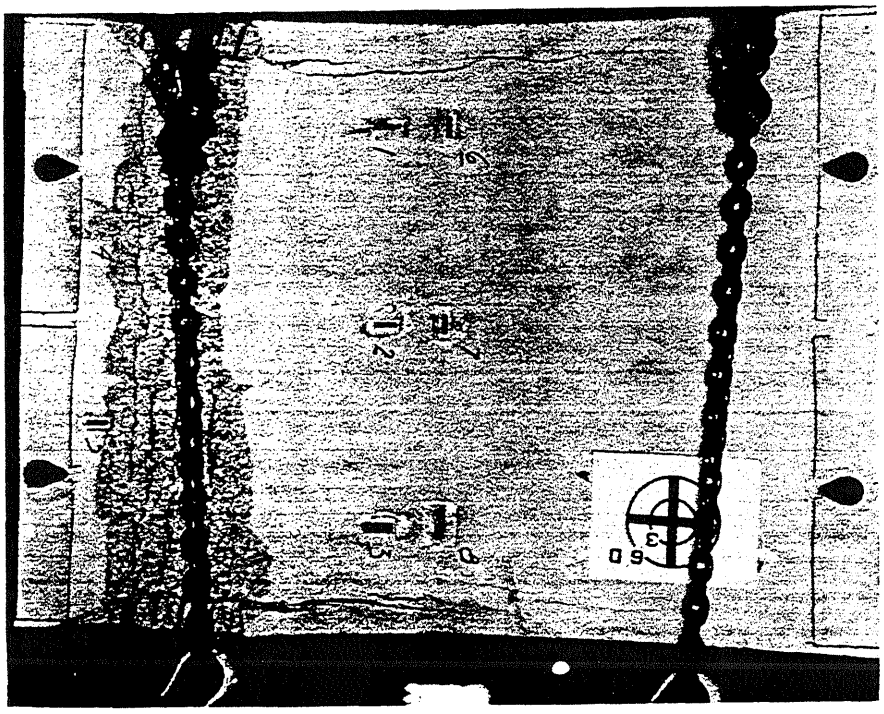

FIG. A.64 BOTTOM SURFACE OF B8

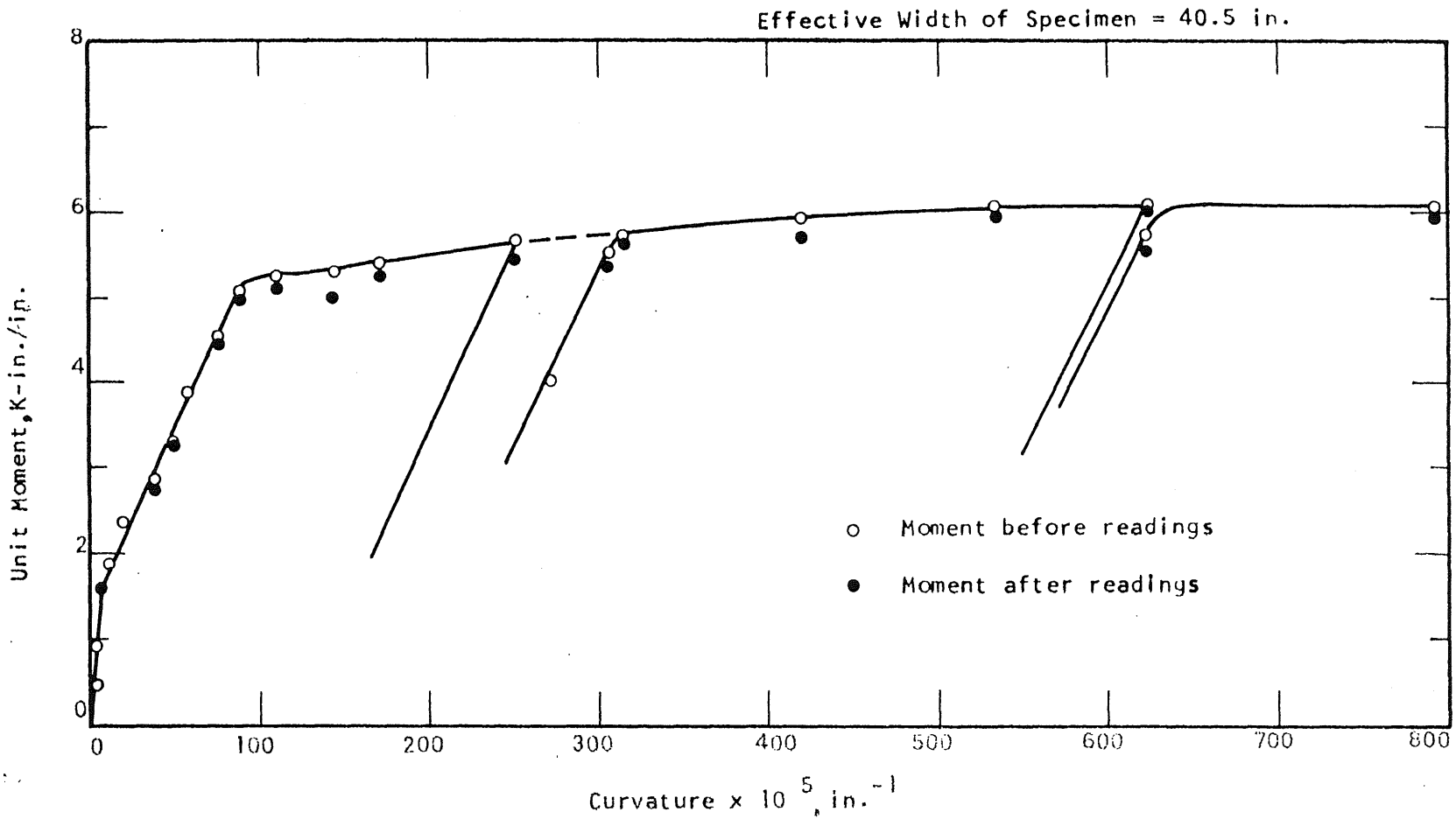

FIG. A.65 MOMENT-CURVATURE PLOT FOR SPECIMEN B8

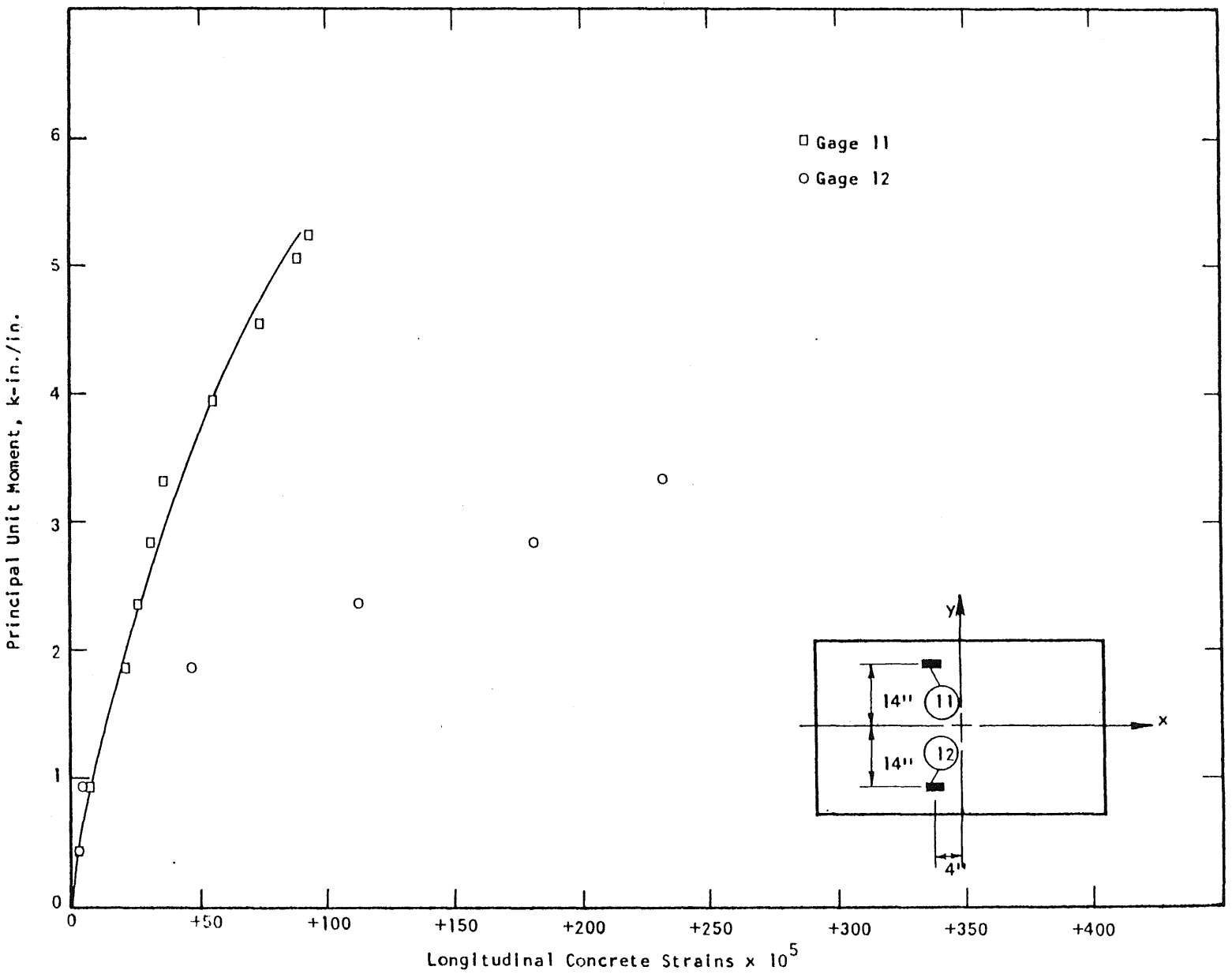

FIG. A.66 CONCRETE STRAIN PLOT, TENSION SIDE OF SPECIMEN B8

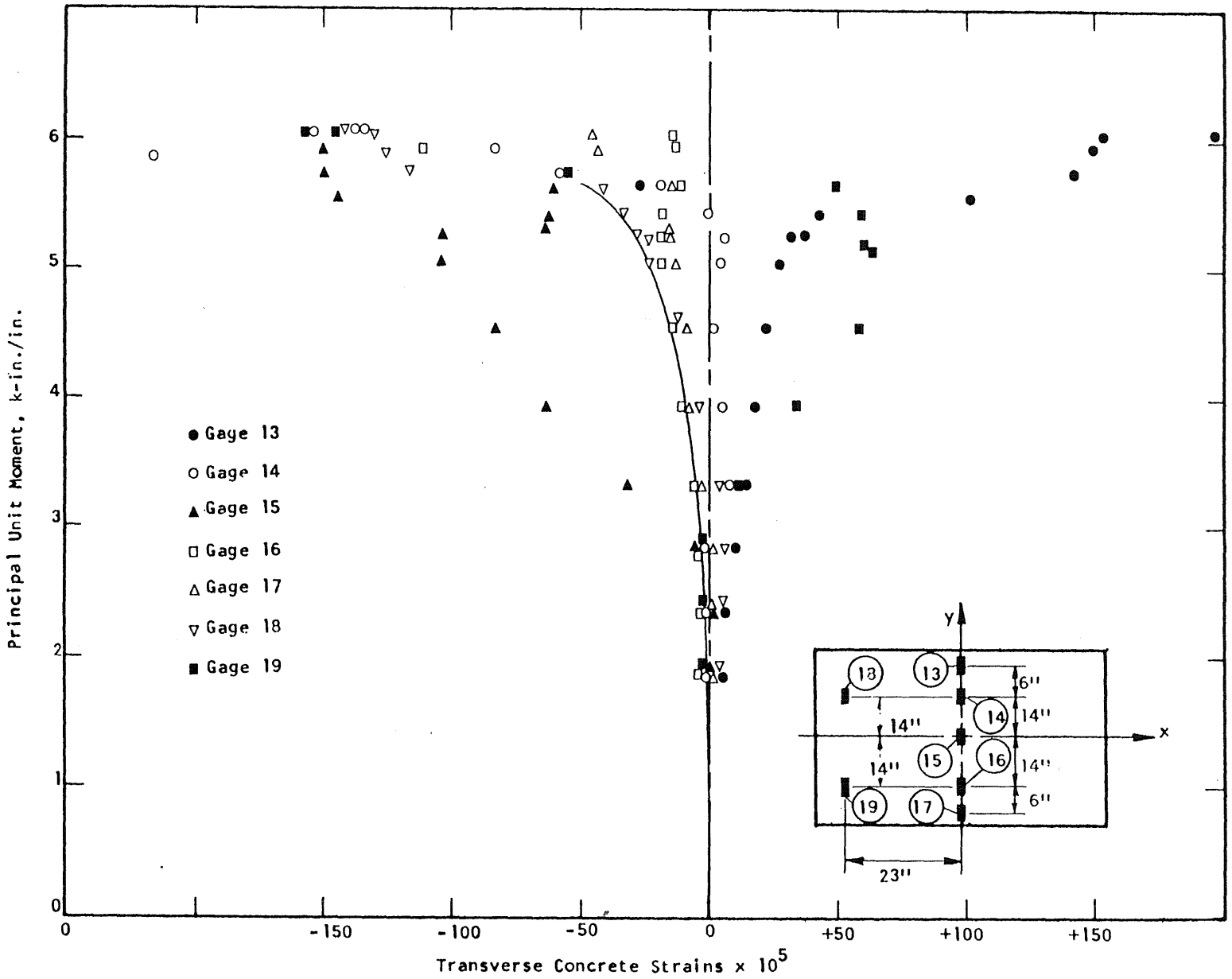

FIG. A.67 CONCRETE STRAIN PLOT, TENSION SIDE OF SPECIMEN B8

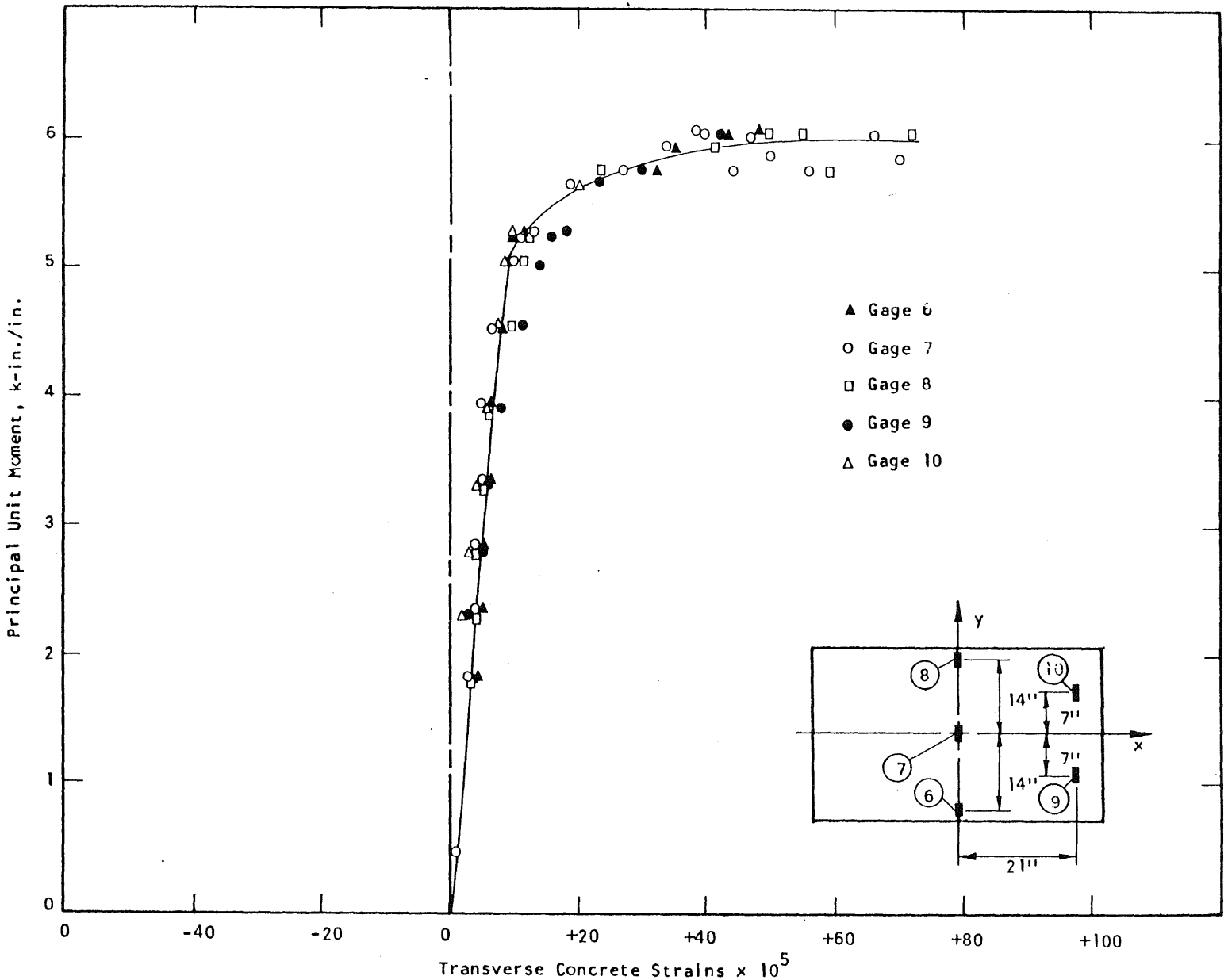

FIG. A.68 CONCRETE STRAIN PLOT, COMPRESSION SIDE OF SPECIMEN B8

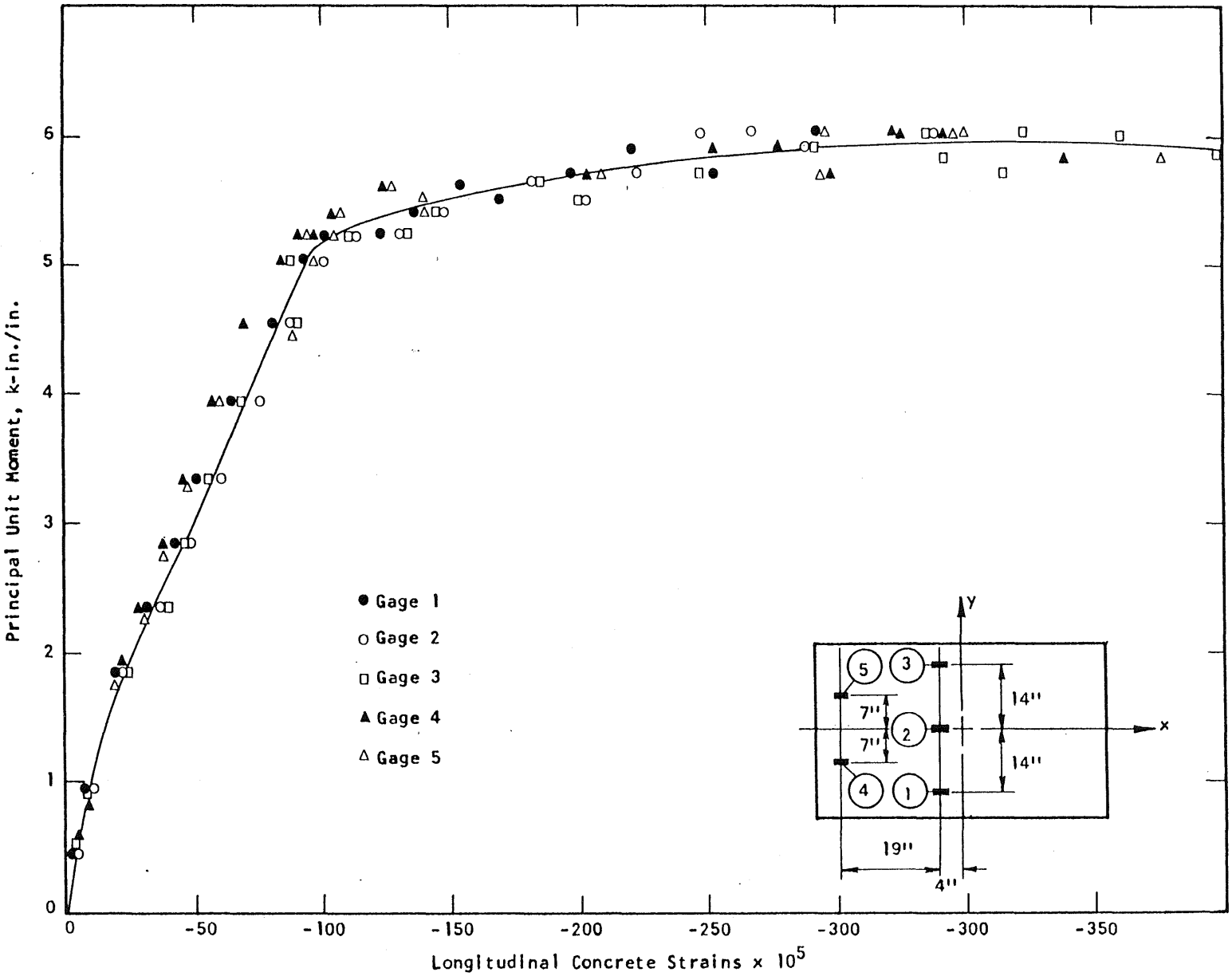

FIG. A.69 CONCRETE STRAIN PLOT, COMPRESSION SIDE OF SPECIMEN B8

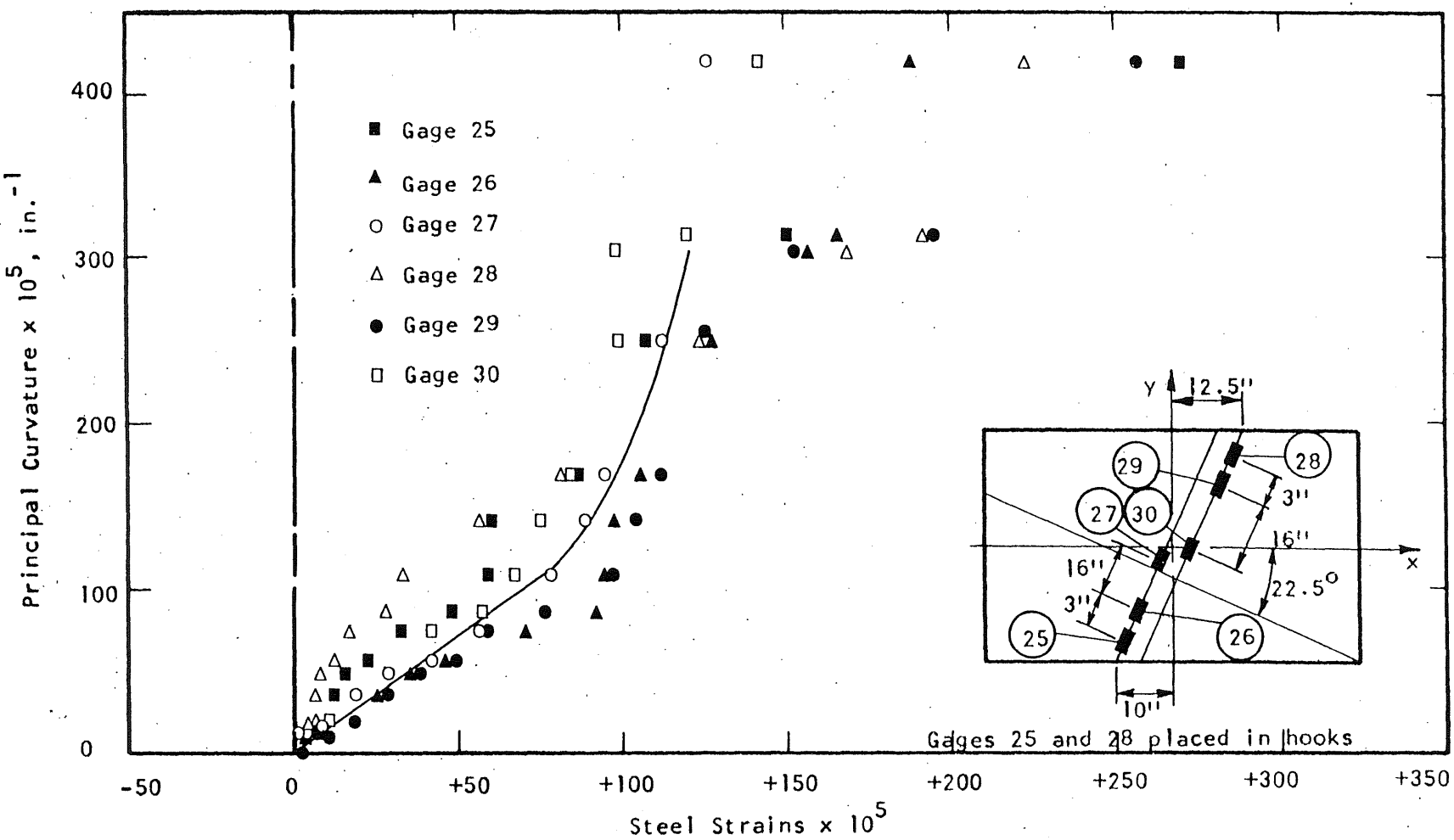

FIG. A.70 STEEL STRAIN PLOT, SPECIMEN B8

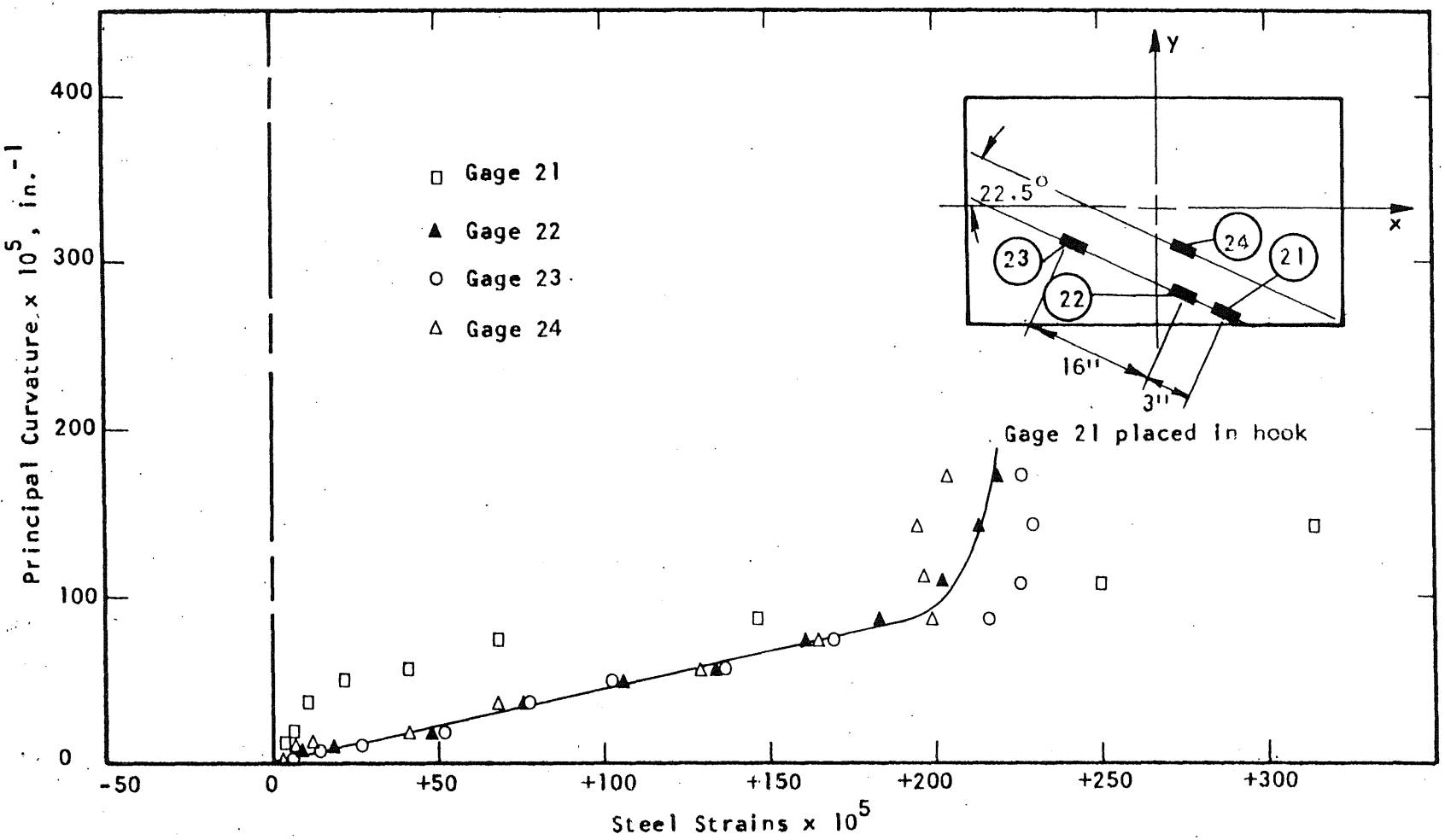

FIG. A.71 STEEL STRAIN PLOT, SPECIMEN B8

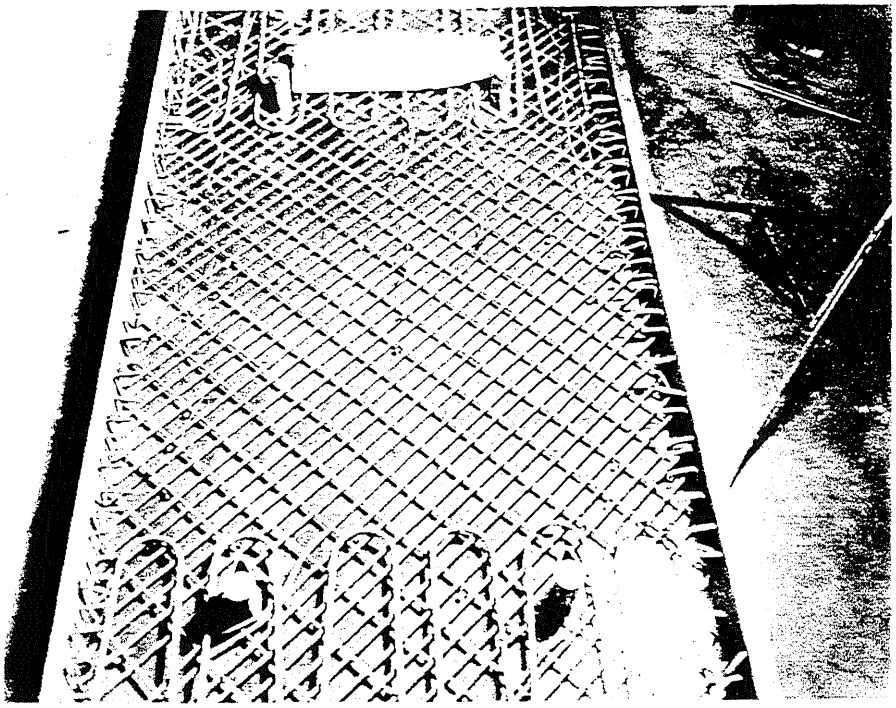

FIG. A.72 REINFORCEMENT IN SPECIMEN B9

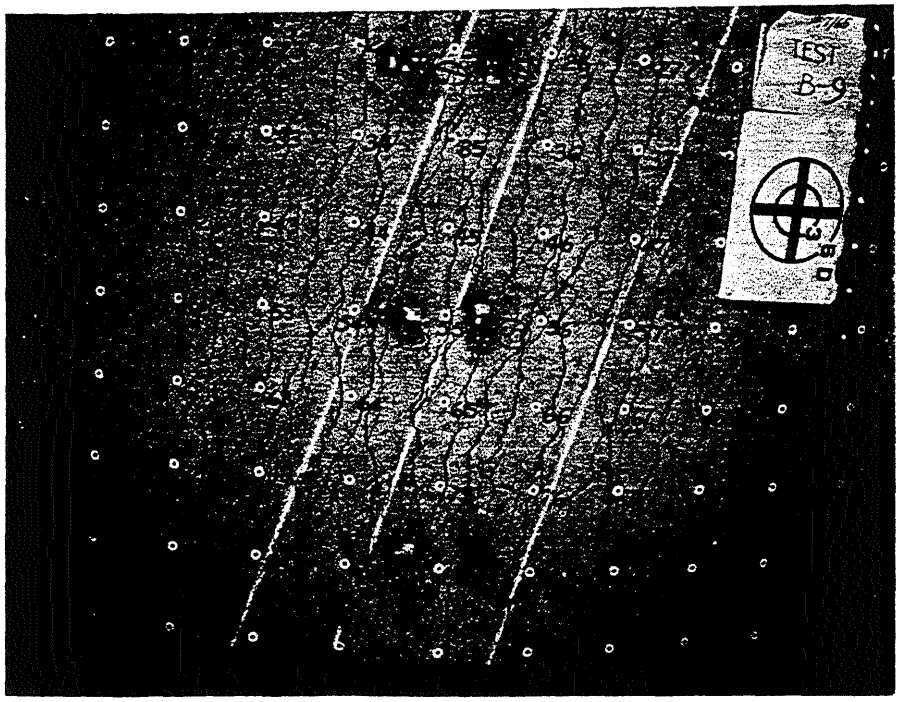

FIG. A.73 CRACK PATTERN IN TOP SURFACE OF B9

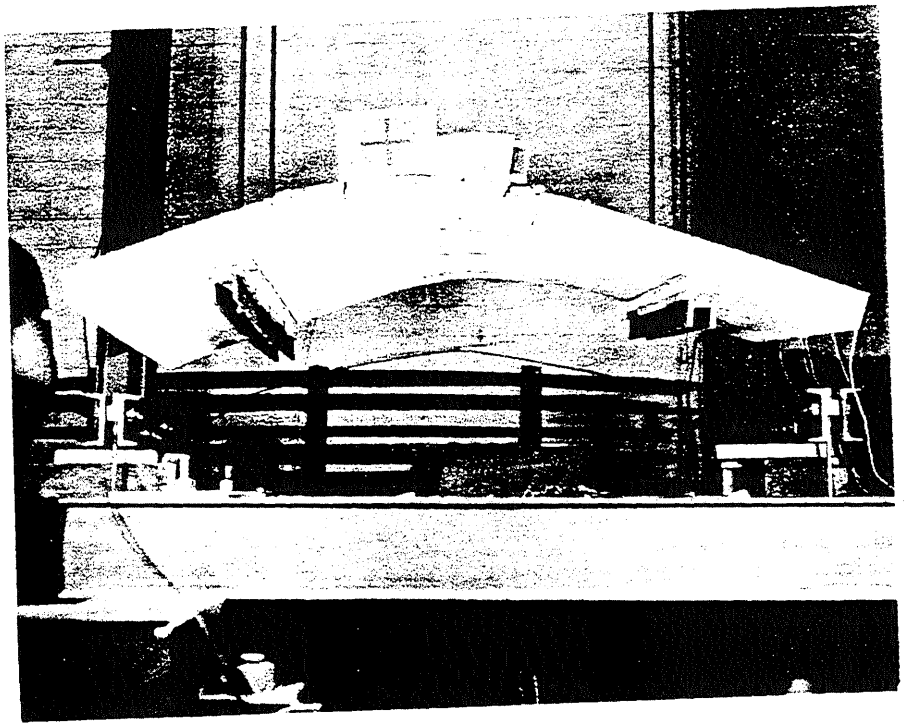

FIG. A.74 SIDE VIEW OF B9

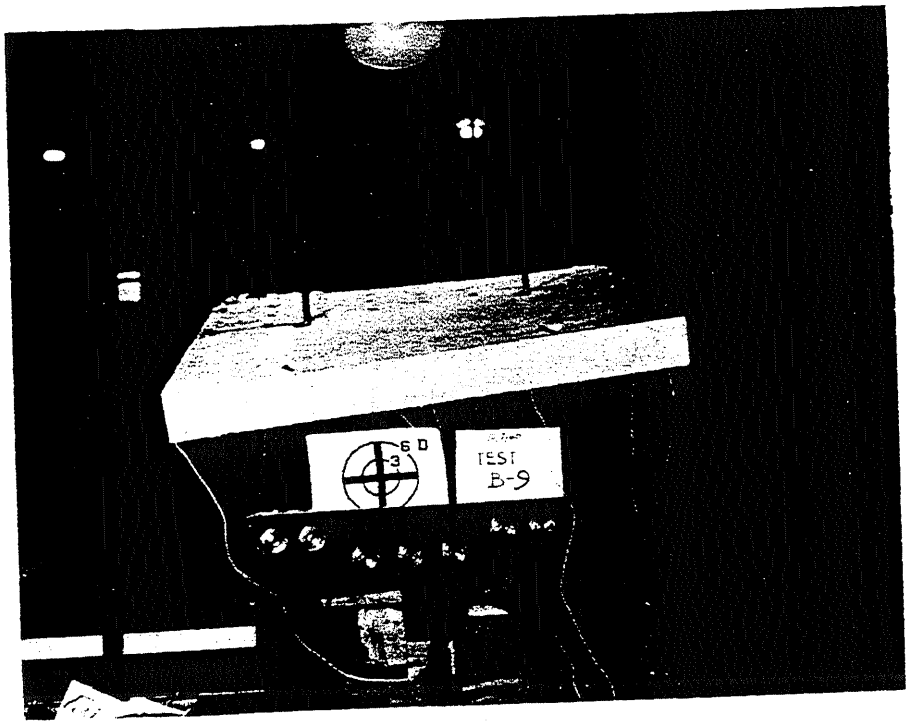

FIG. A.75 END VIEW OF B9

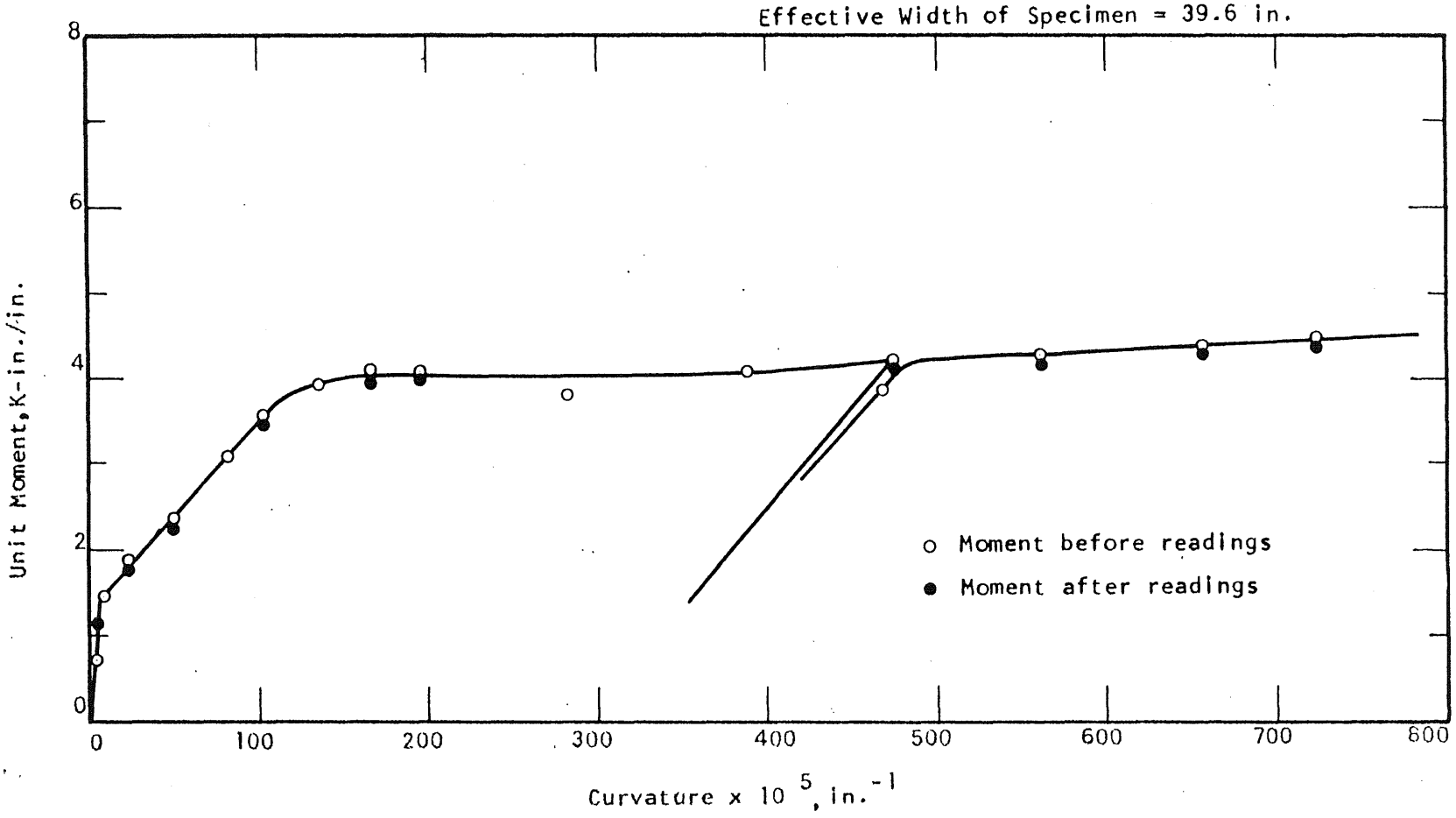

FIG. A.76 MOMENT-CURVATURE PLOT FOR SPECIMEN B9

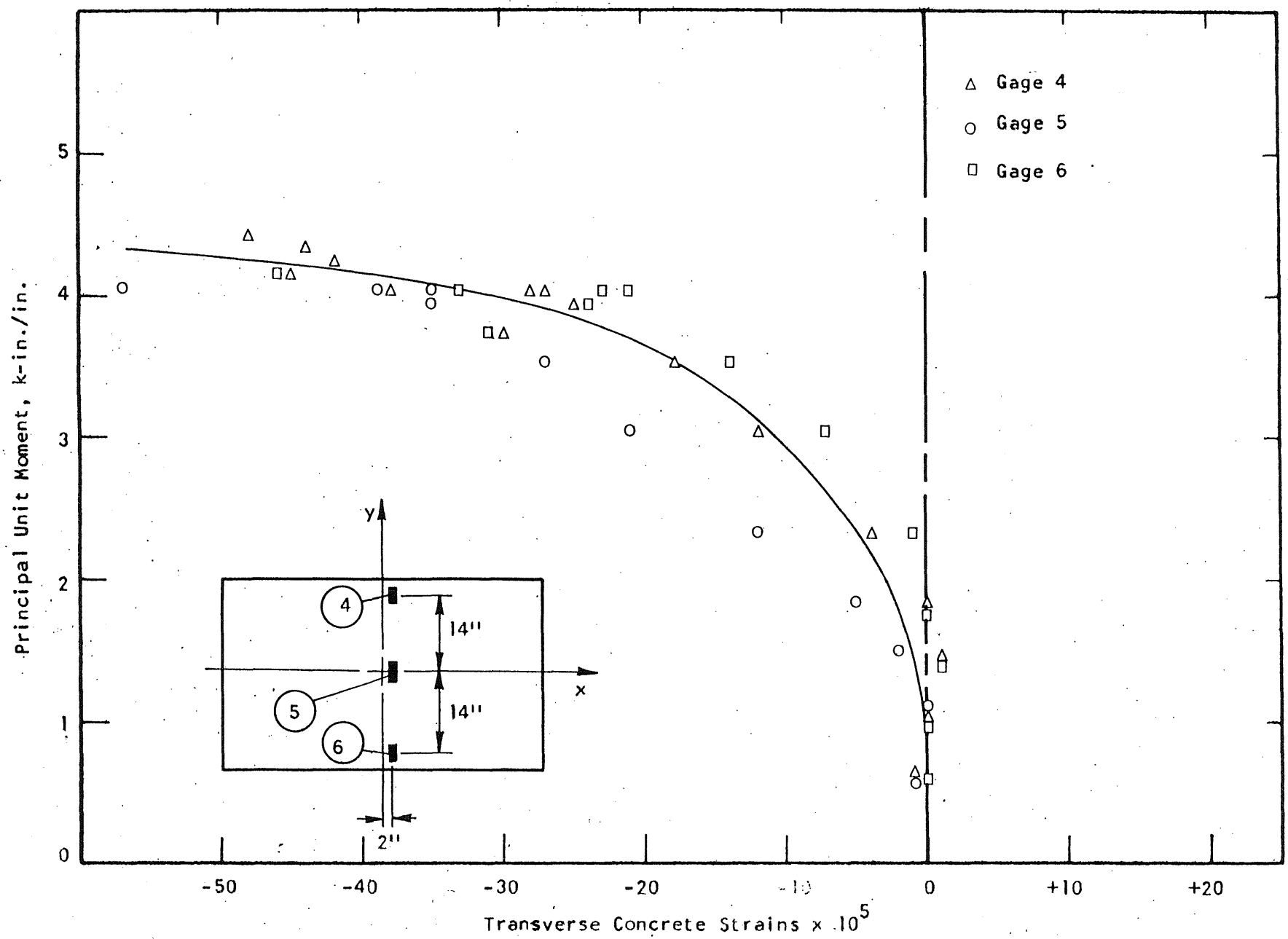

FIG. A.77 CONCRETE STRAIN PLOT, TENSION SIDE OF SPECIMEN B9

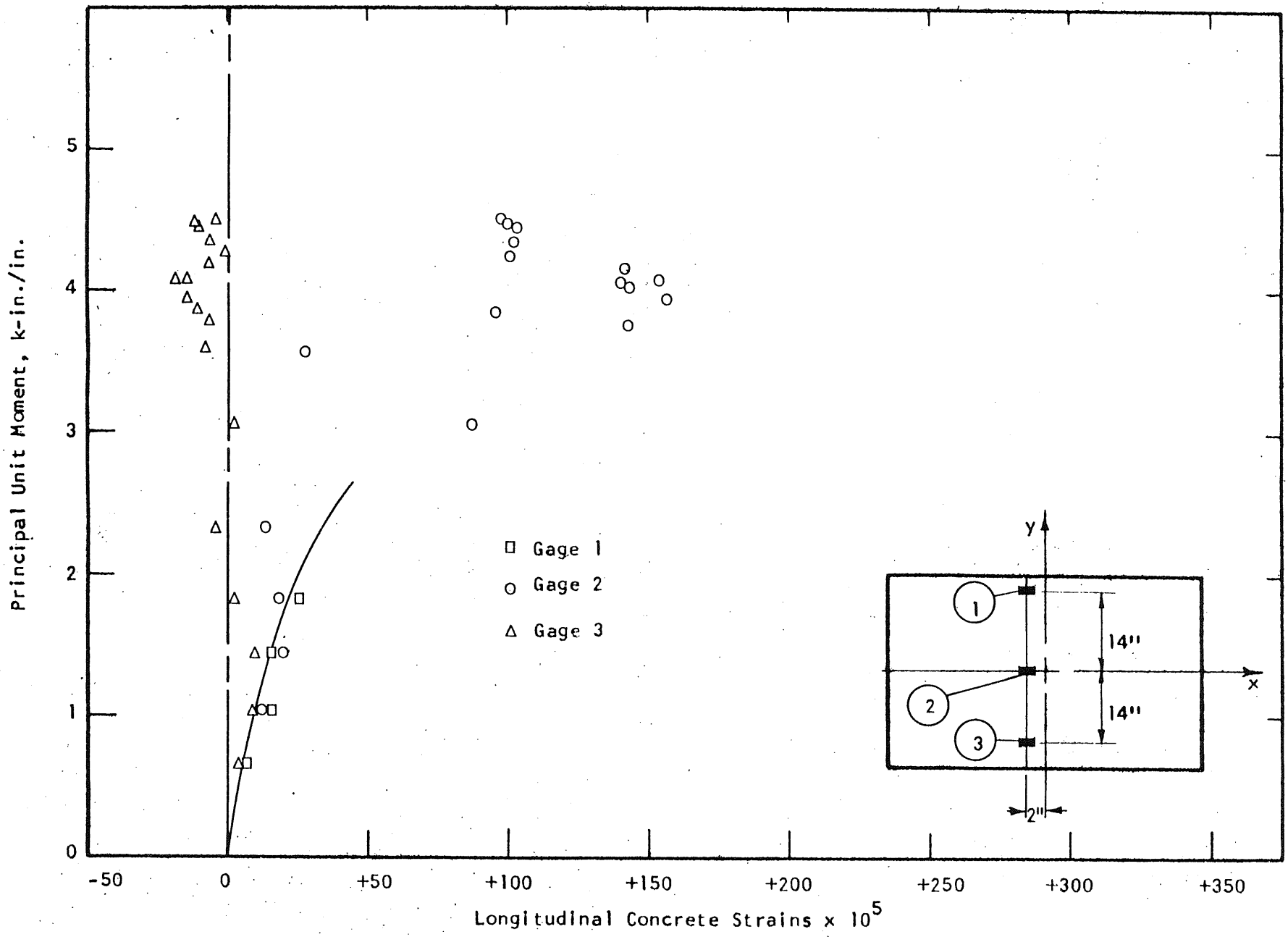

FIG. A.78 CONCRETE STRAIN PLOT, TENSION SIDE OF SPECIMEN B9

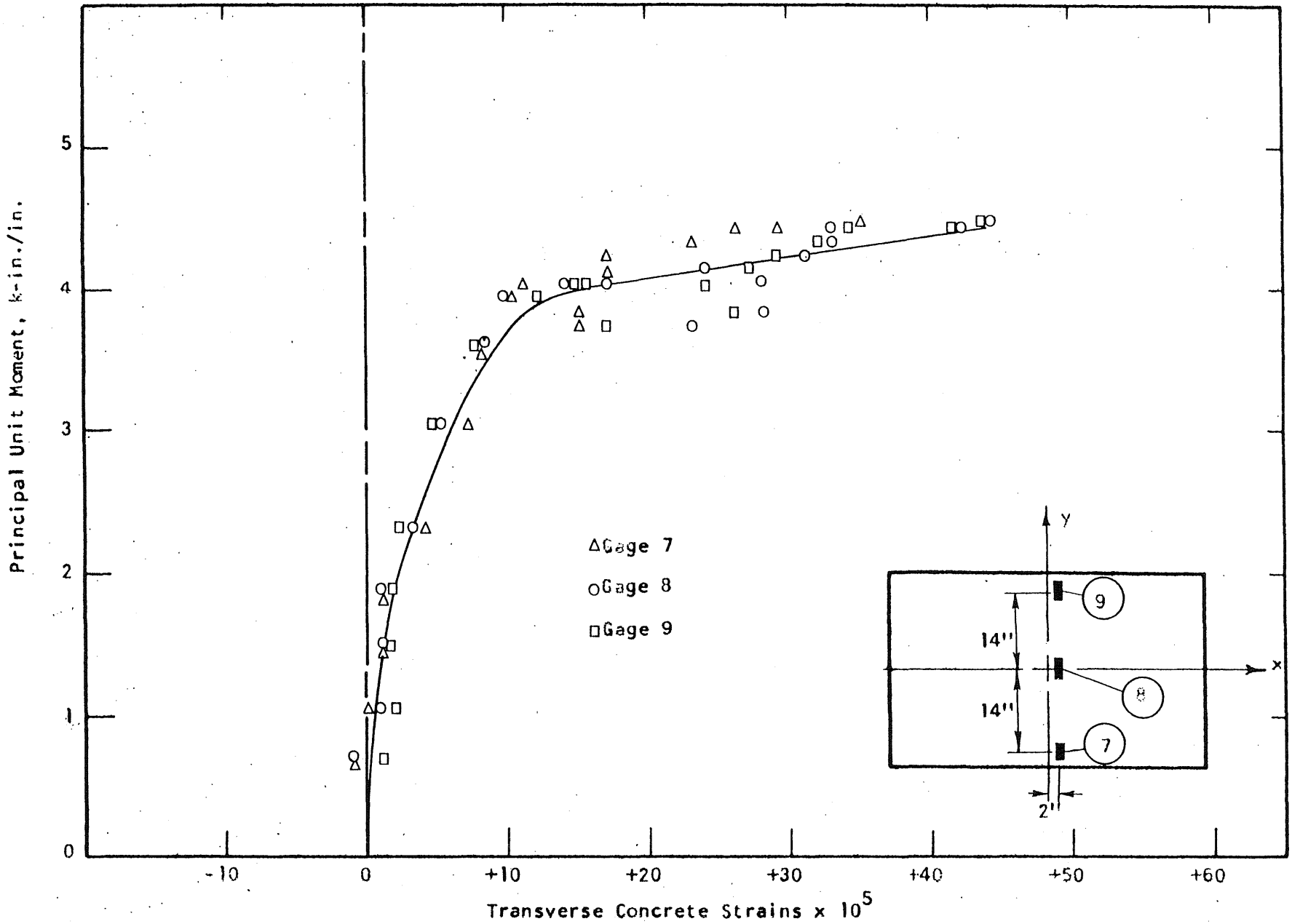

FIG. A.79 CONCRETE STRAIN PLOT, COMPRESSION SIDE OF SPECIMEN B9

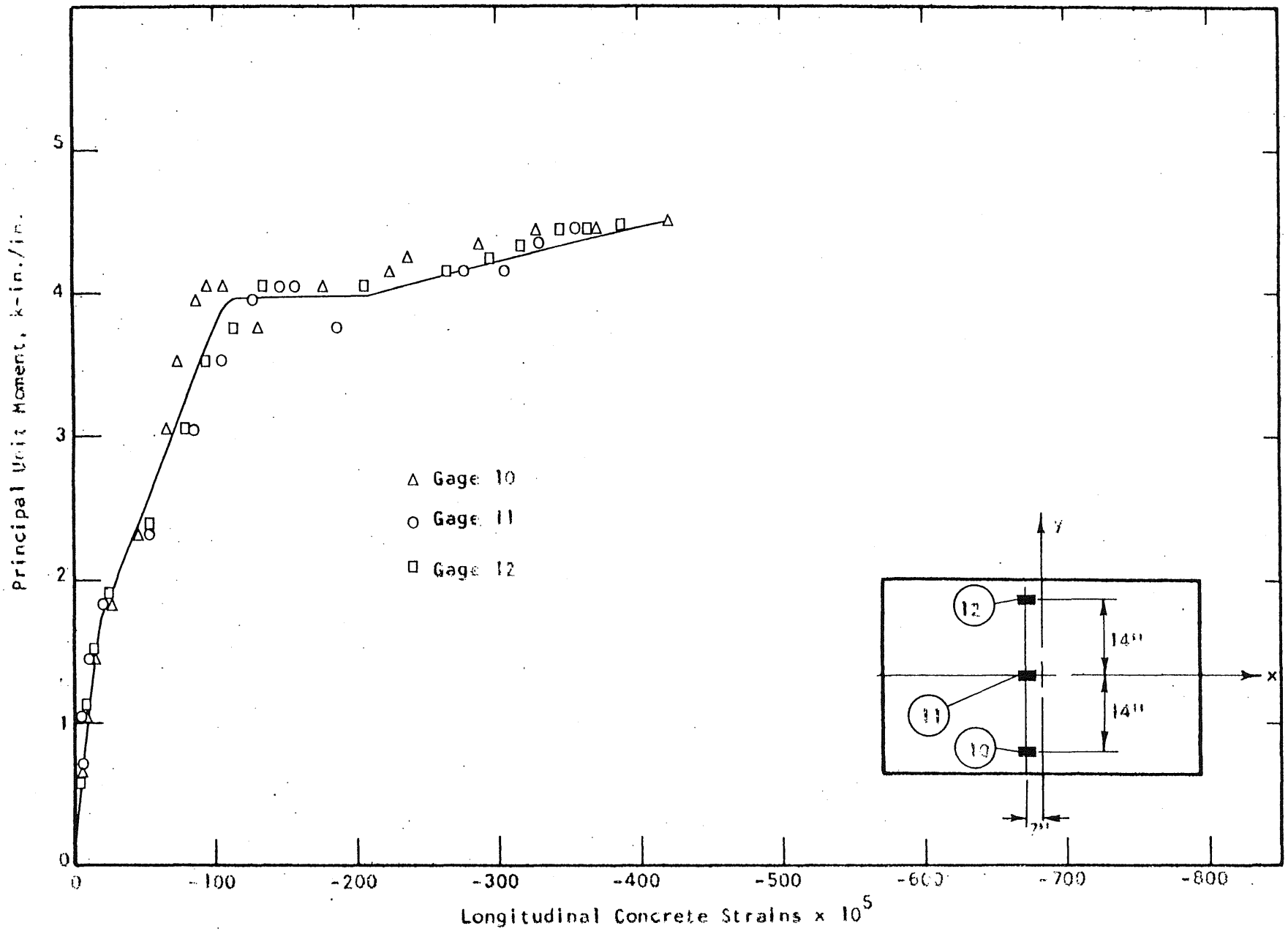

FIG. A.80 CONCRETE STRAIN PLOT, COMPRESSION SIDE SPECIMEN B9

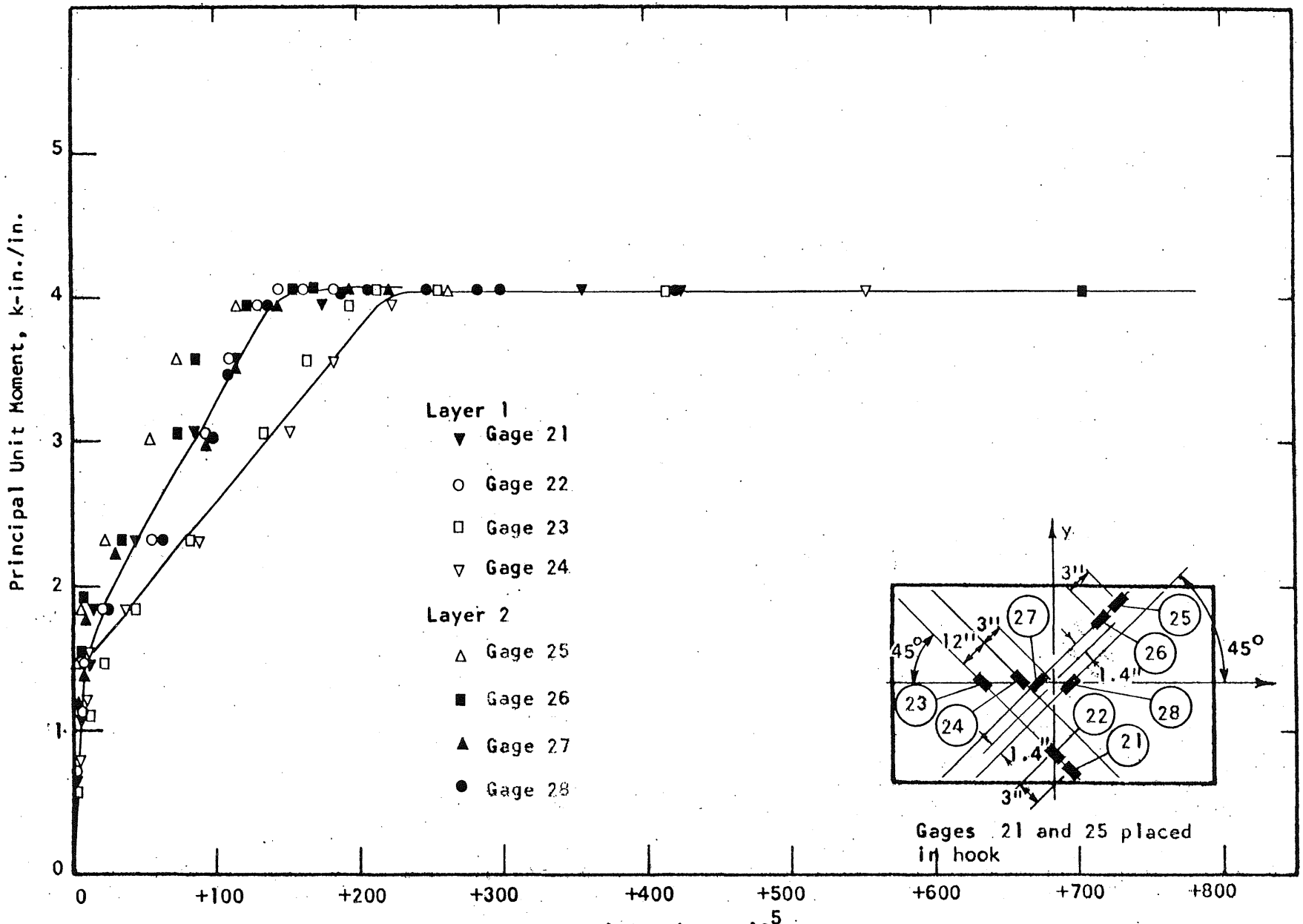

FIG. A.81 STEEL STRAIN PLOT, SPECIMEN B9

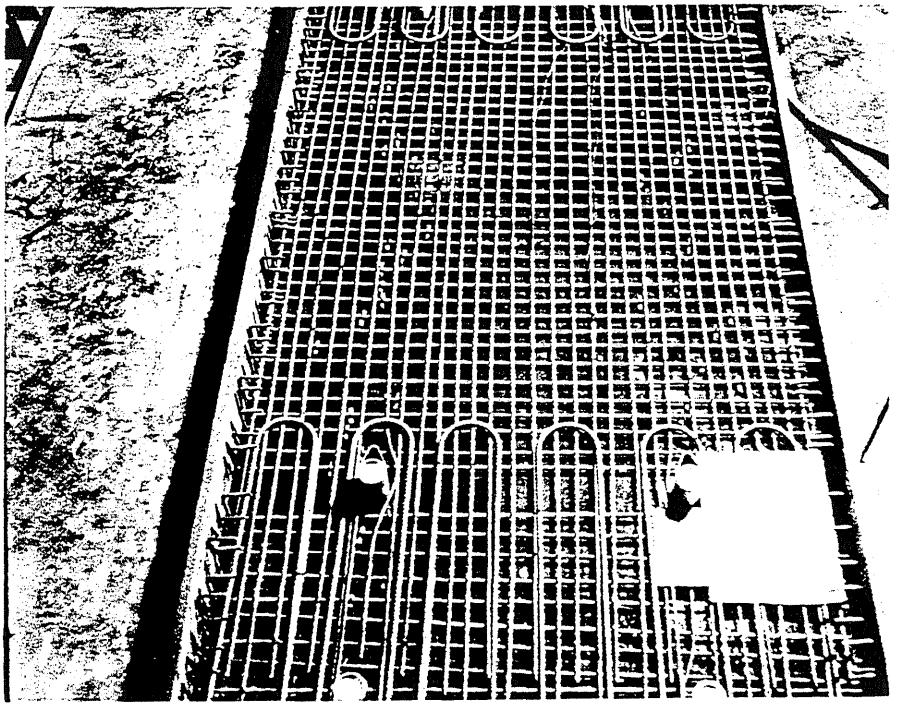

FIG. A.82 REINFORCEMENT IN SPECIMEN B10

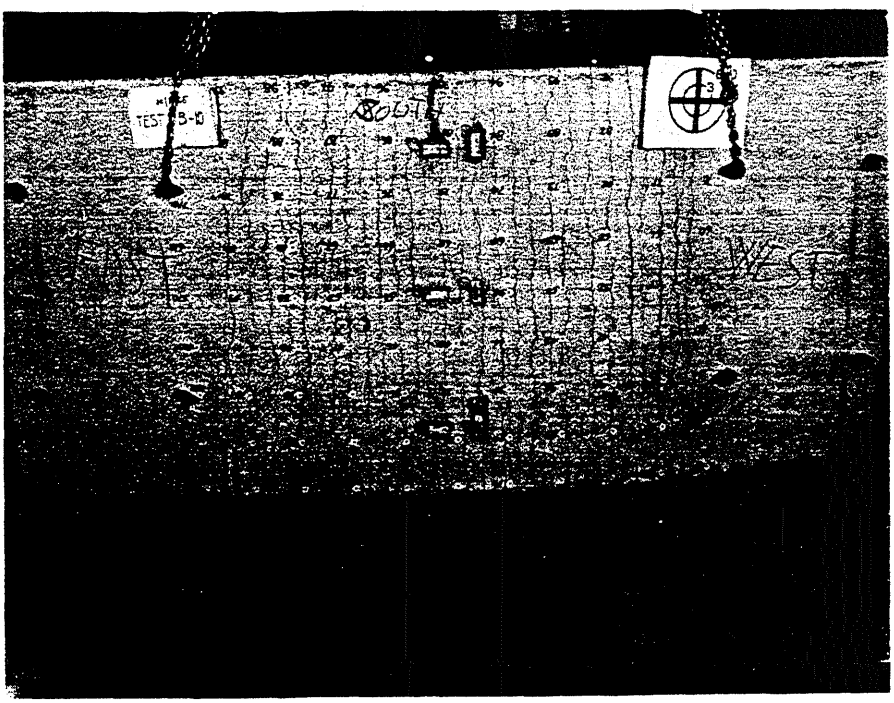

FIG. A.83 CRACK PATTERN IN TOP SIDE OF B10

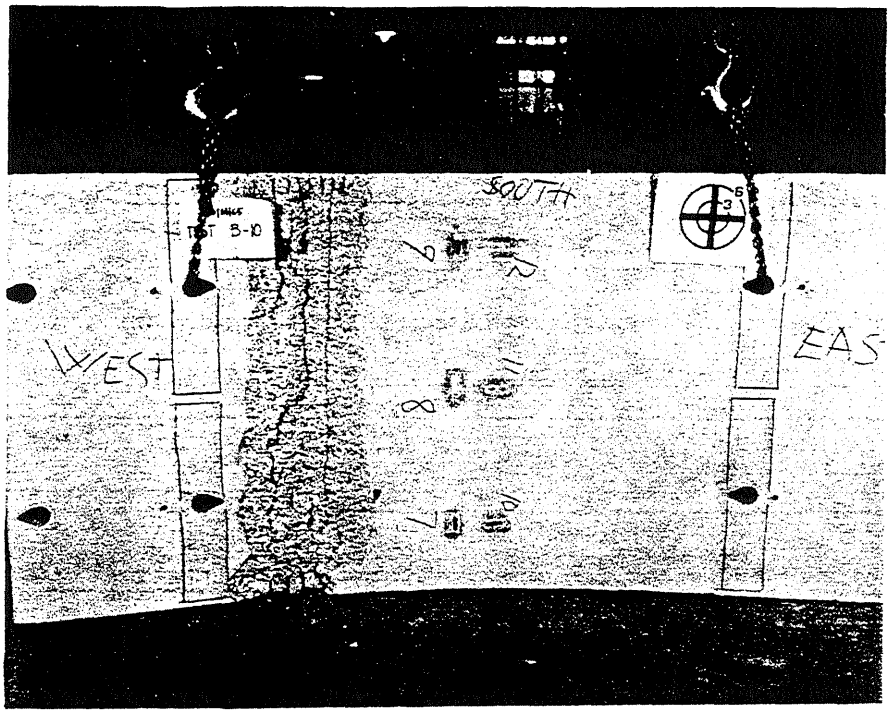

FIG. A.84 BOTTOM SURFACE OF B10

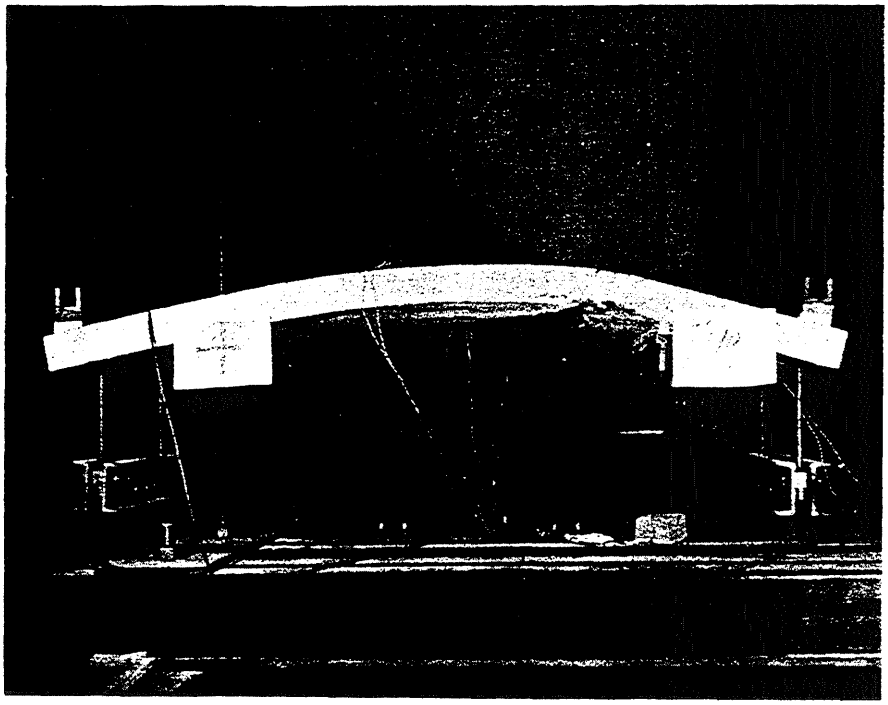

FIG. A.85 SIDE VIEW OF B10

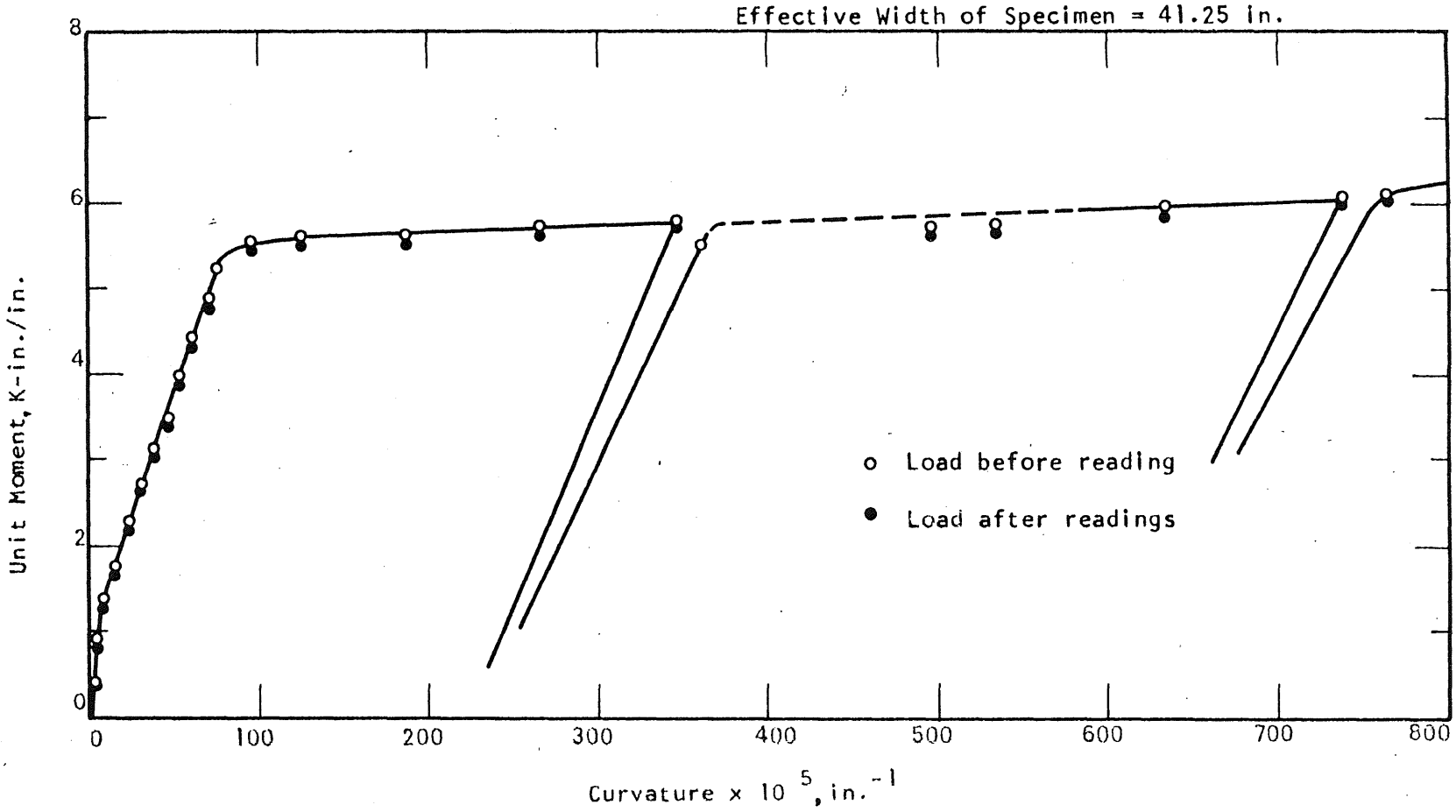

FIG. A.86 MOMENT-CURVATURE PLOT FOR SPECIMEN B10

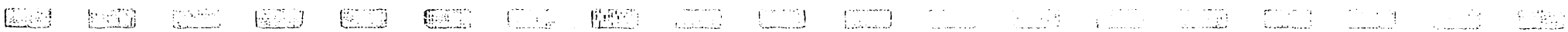

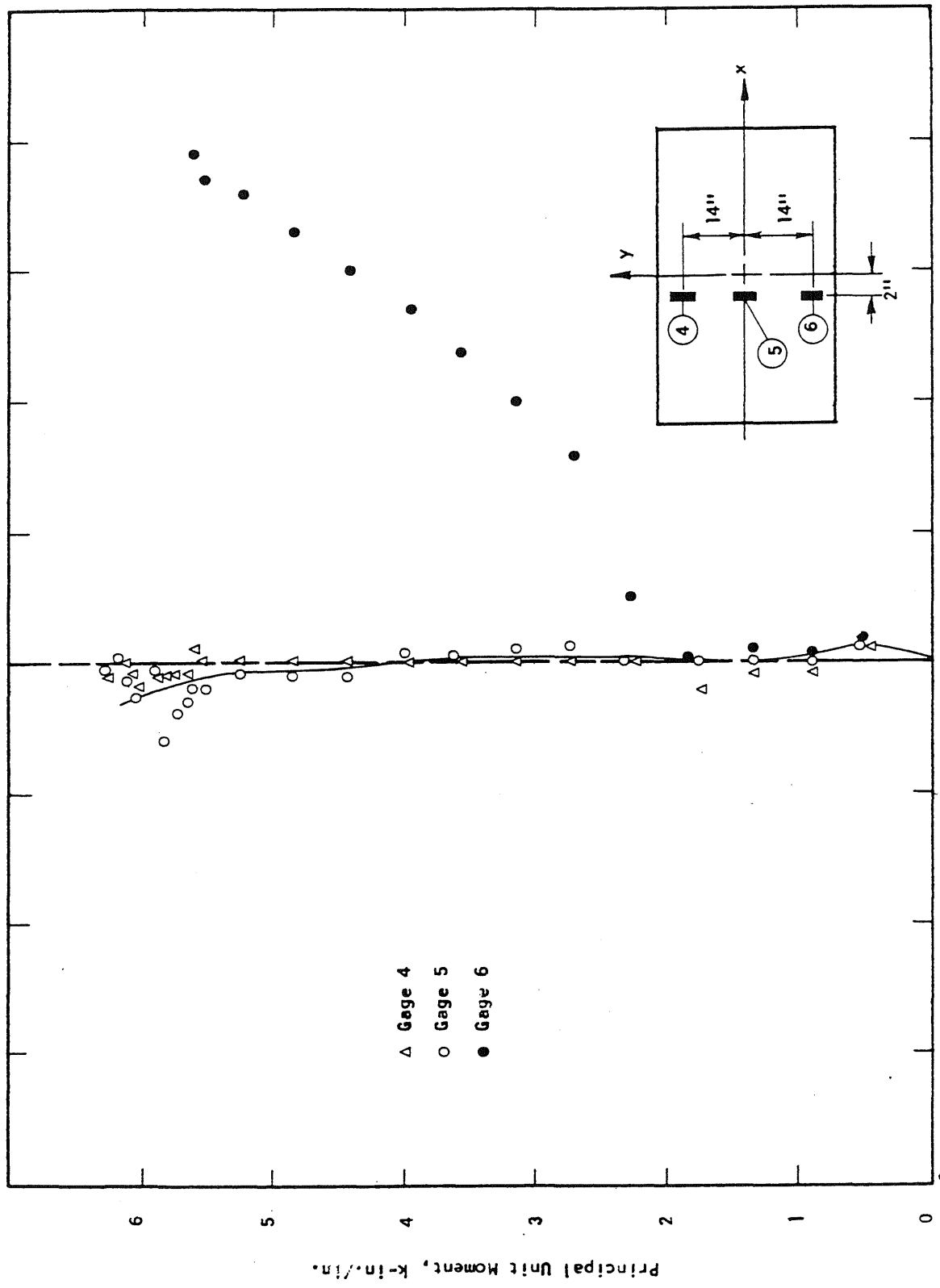

FIG. A.87 CONCRETE STRAIN PLOT , TENSION SIDE OF SPECIMEN B10

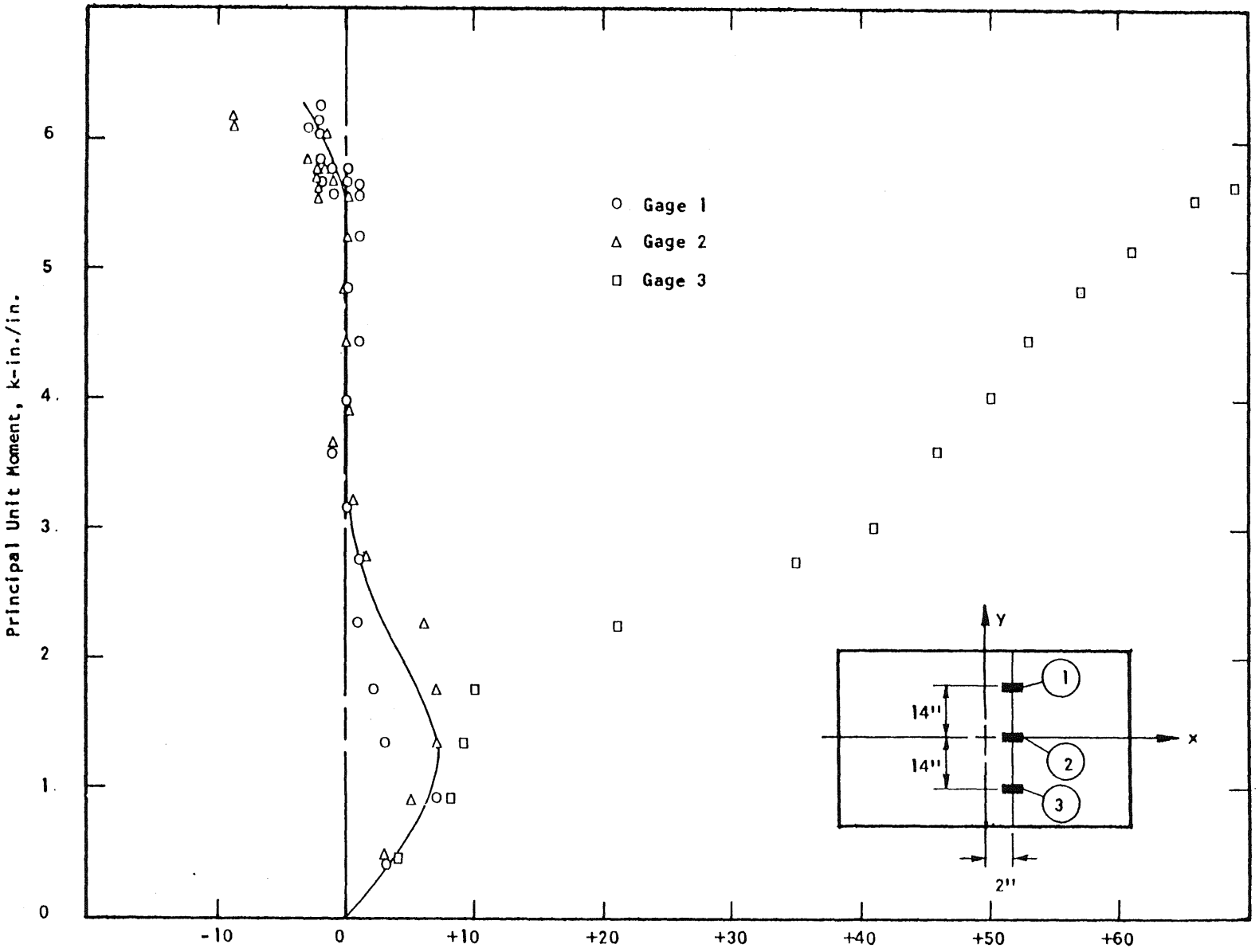

FIG. A.88 CONCRETE STRAIN PLOT, TENSION SIDE OF SPECIMEN B10

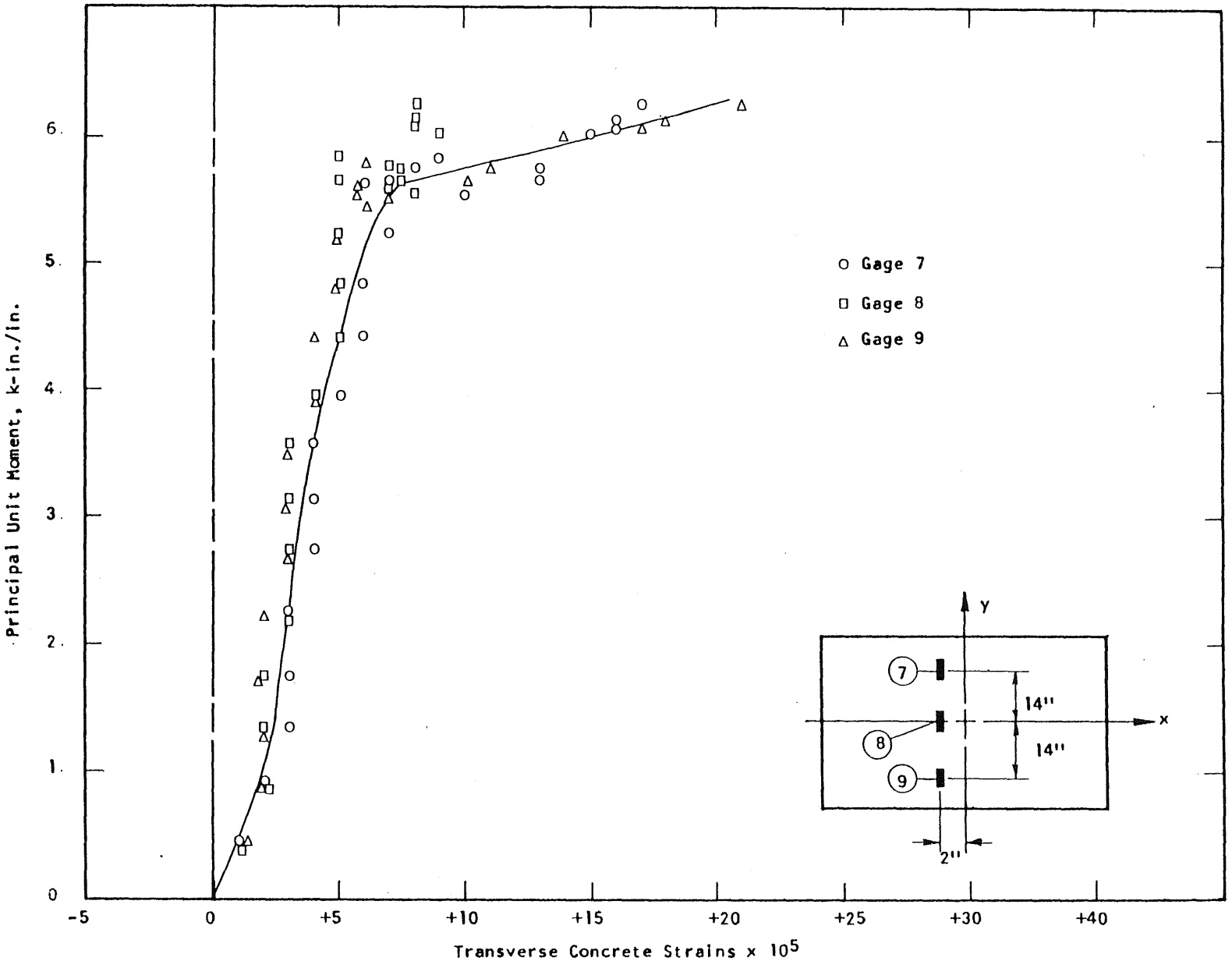

FIG. A.89 CONCRETE STRAIN PLOT, COMPRESSION SIDE OF SPECIMEN B10

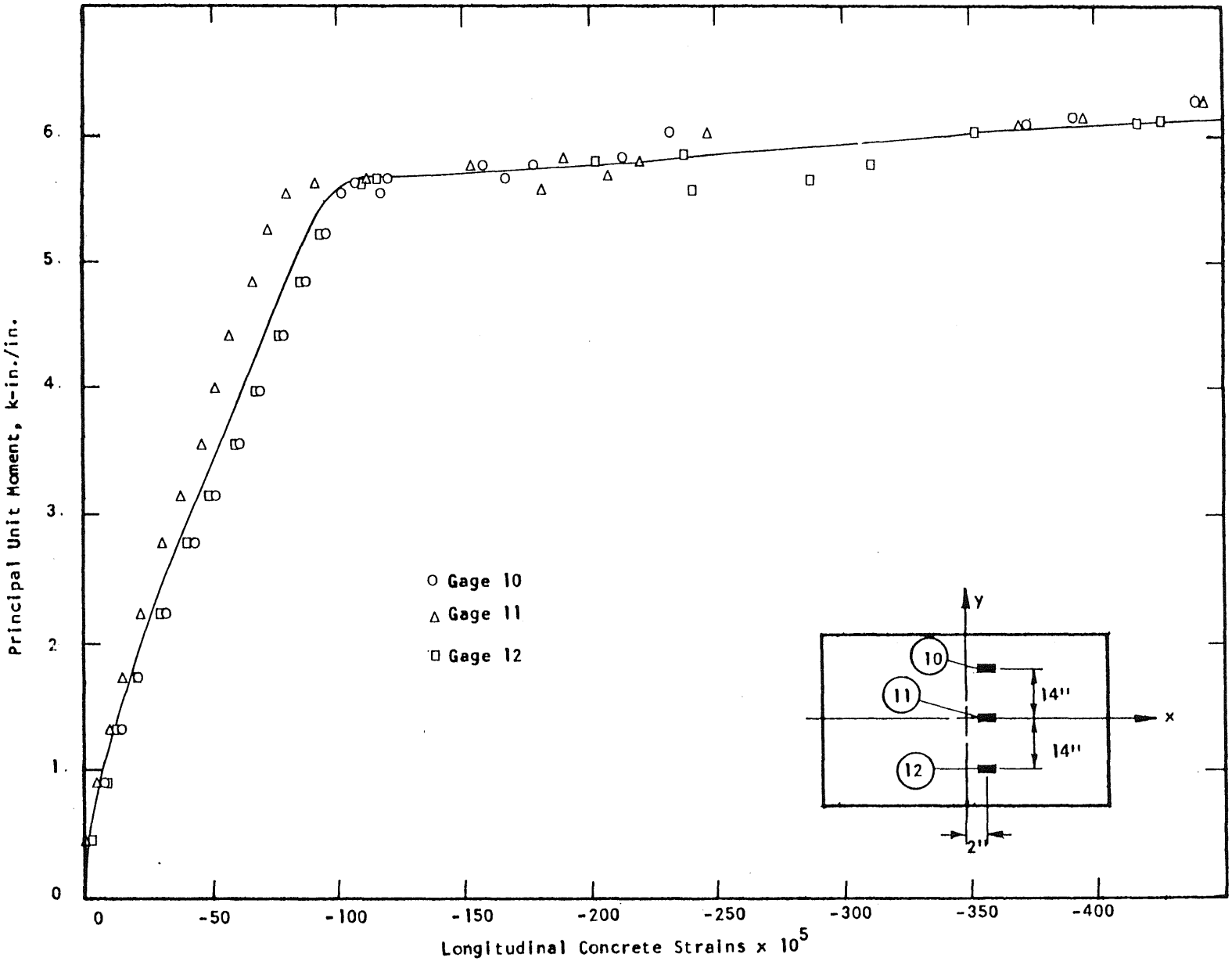

FIG. A.90 CONCRETE STRAIN PLOT , COMPRESSION SIDE OF SPECIMEN B10

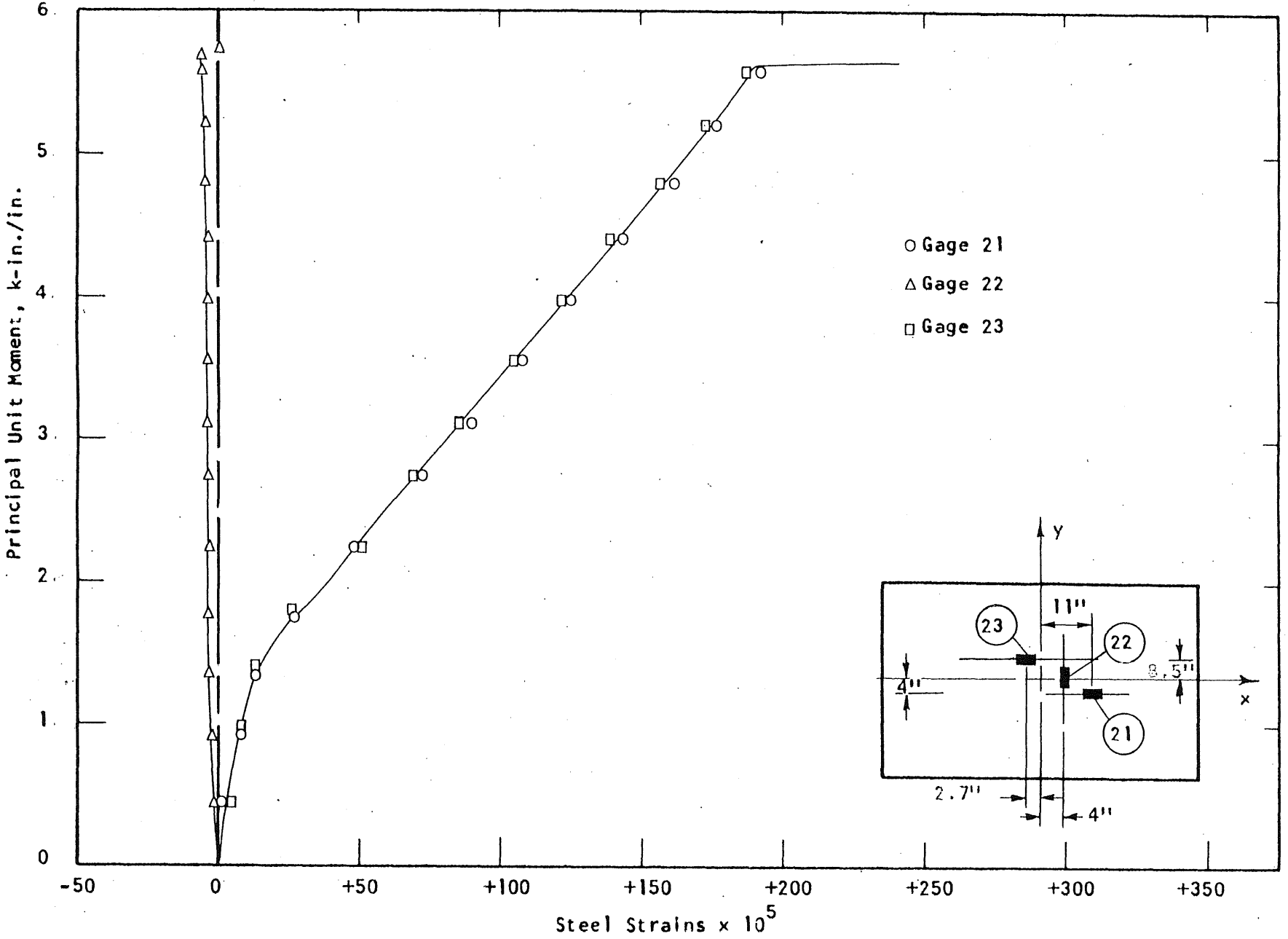

FIG. A.91 STEEL STRAIN PLOT, SPECIMEN B10

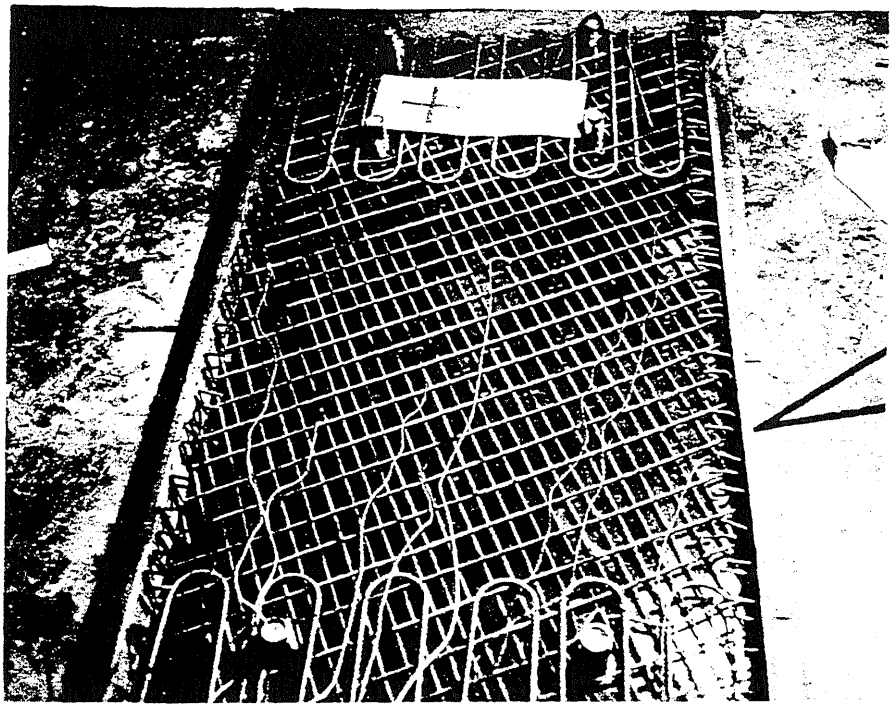

FIG. A.92 REINFORCEMENT IN SPECIMEN B11

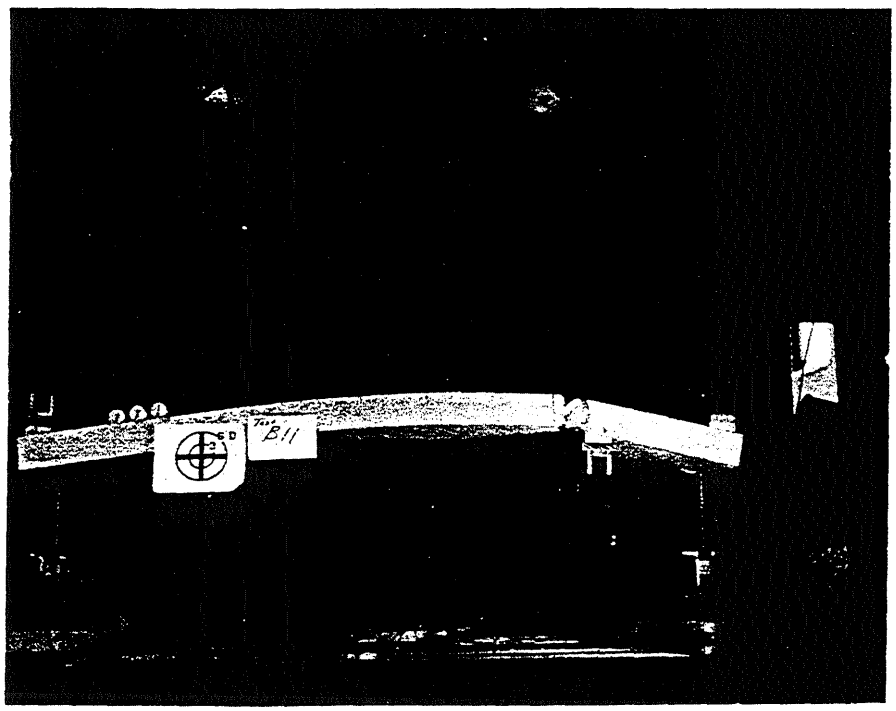

FIG. A.93 SIDE VIEW OF B11

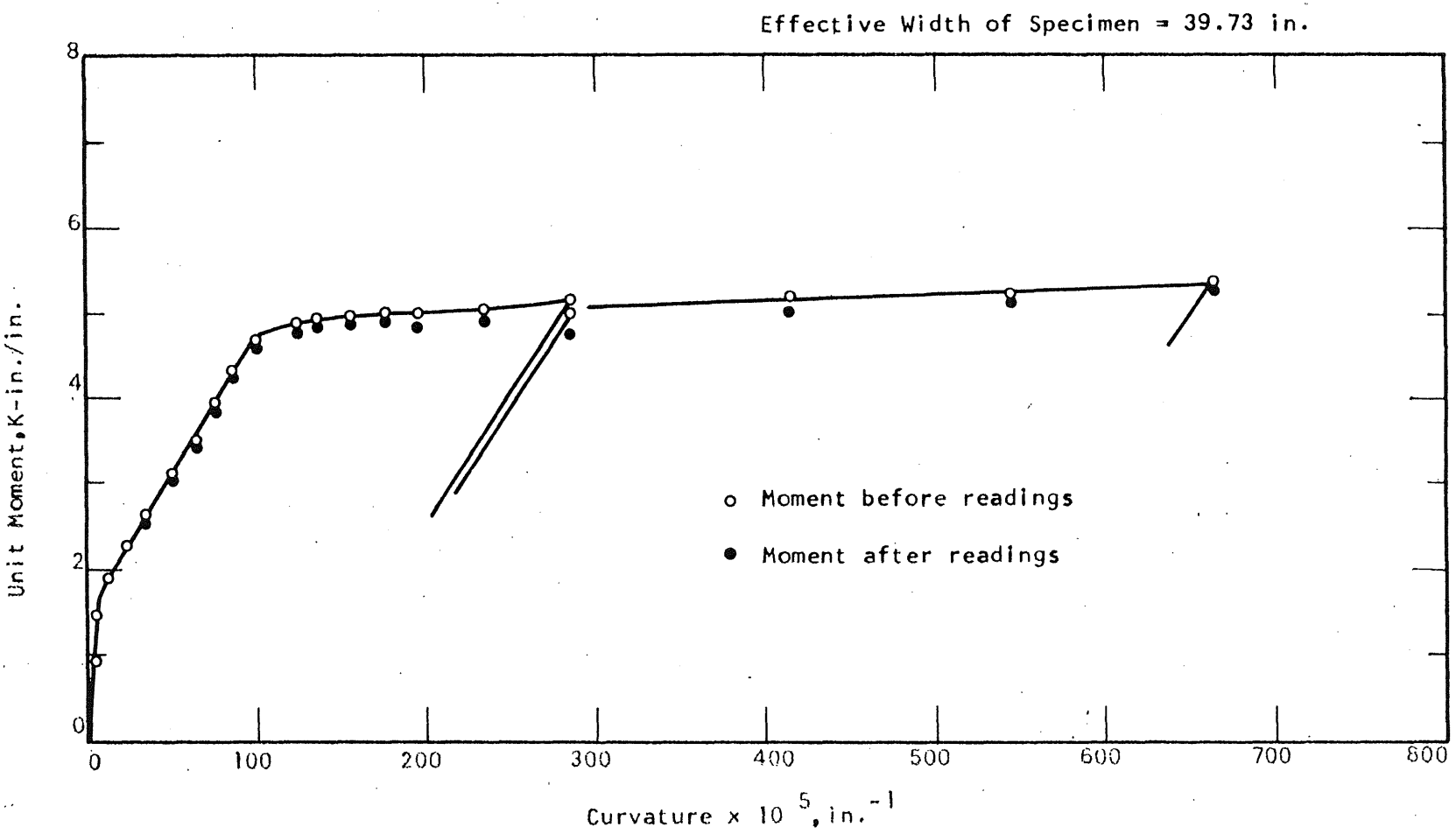

FIG. A.94 MOMENT-CURVATURE PLOT FOR SPECIMEN B11

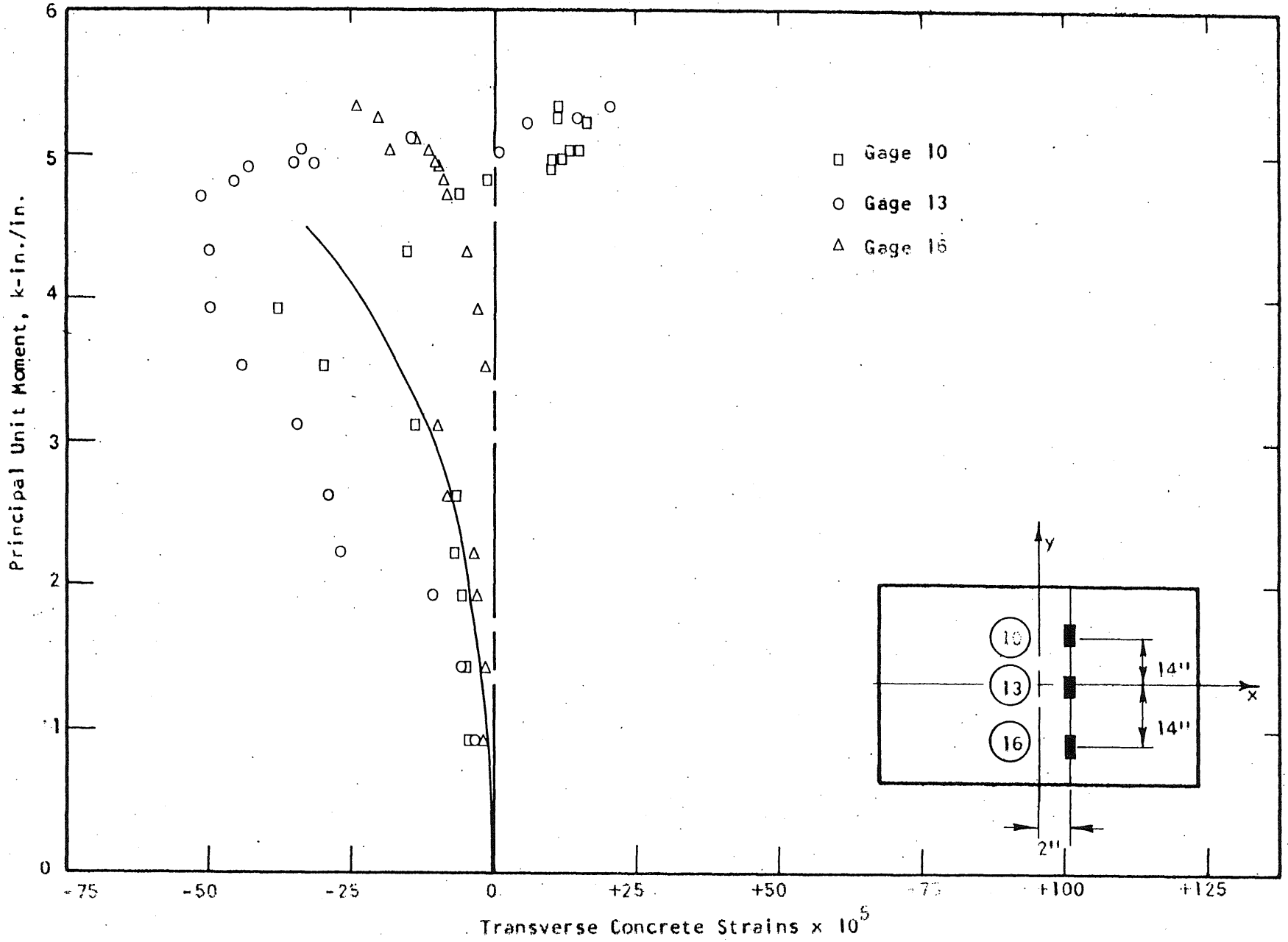

FIG. A.95 CONCRETE STRAIN PLOT, TENSION SIDE OF SPECIMEN B11

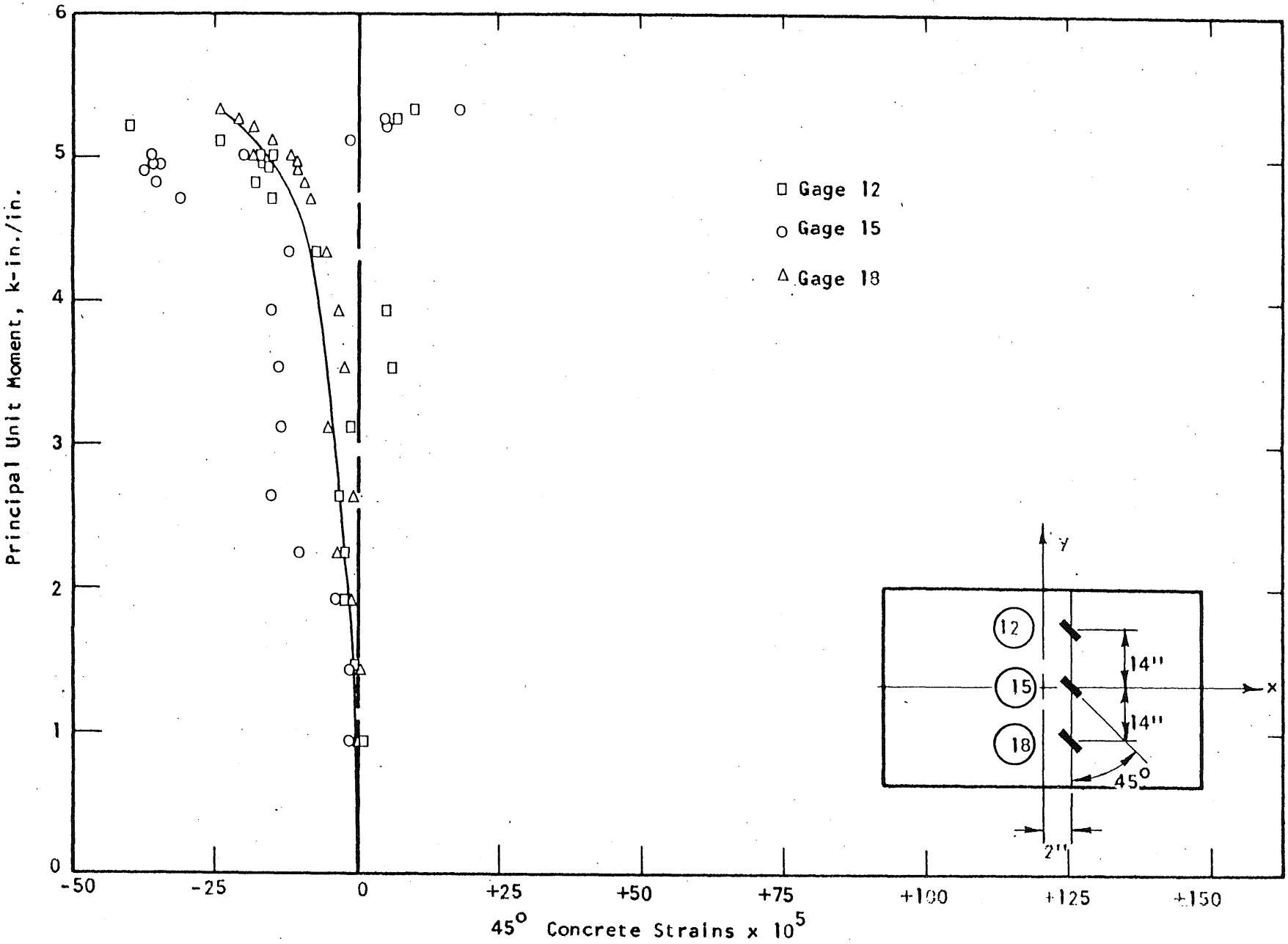

FIG. A.96 CONCRETE STRAIN PLOT, TENSION SIDE OF SPECIMEN B11

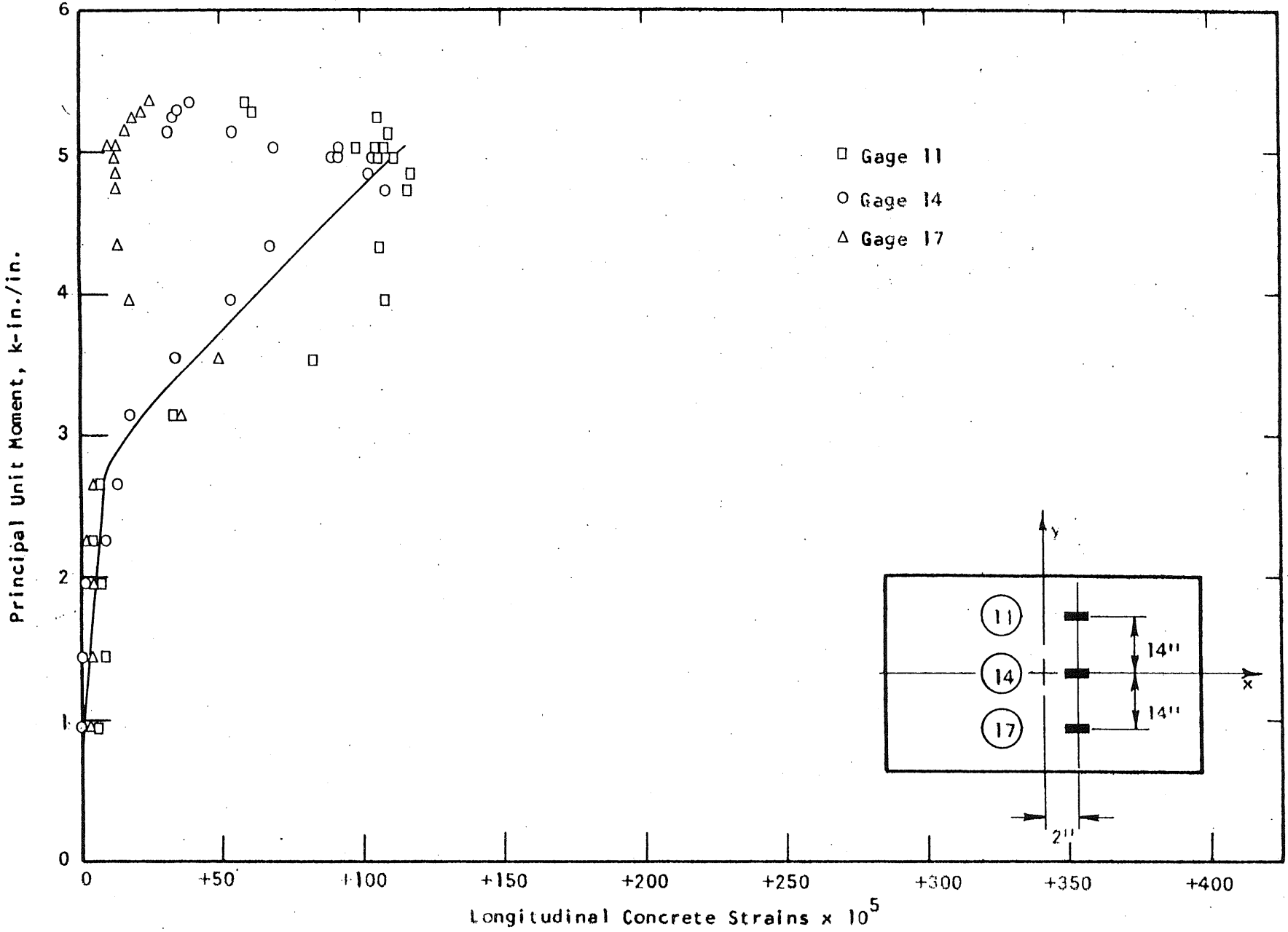

FIG. A.97 CONCRETE STRAIN PLOT, TENSION SIDE OF SPECIMEN B11

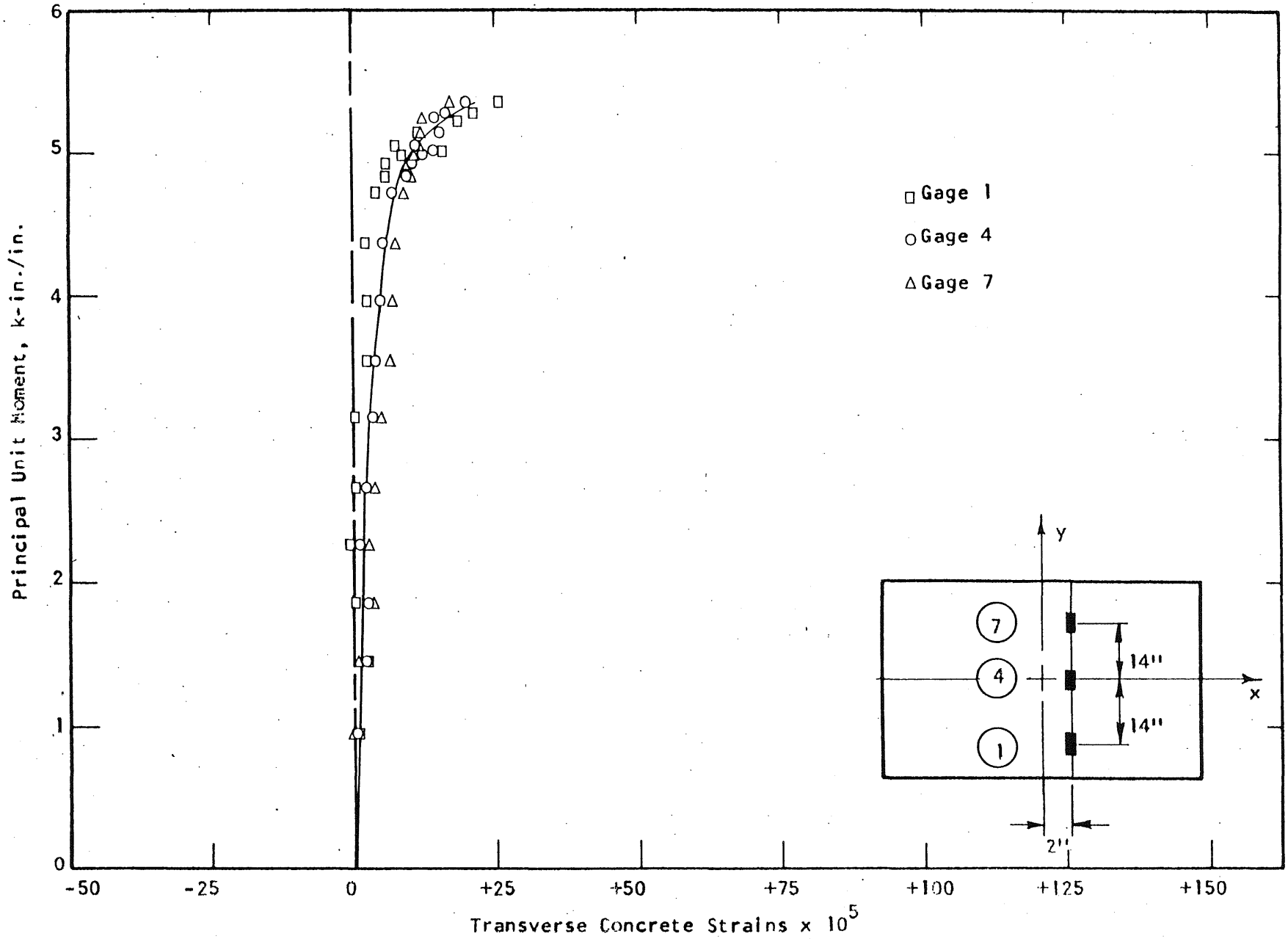

FIG. A.98 CONCRETE STRAIN PLOT, COMPRESSION SIDE OF SPECIMEN B11

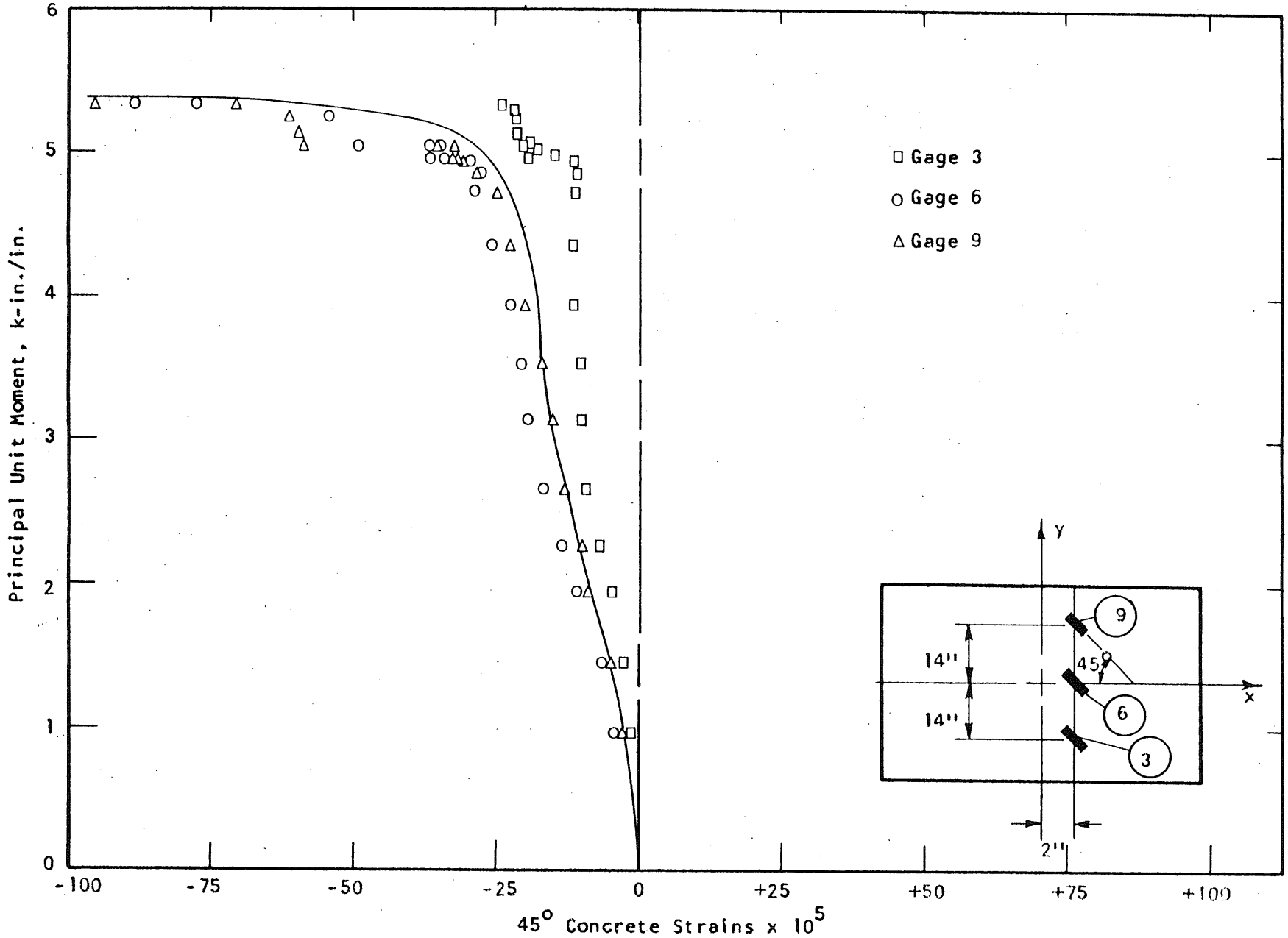

FIG. A.99 CONCRETE STRAIN PLOT, COMPRESSION SIDE OF SPECIMEN B11

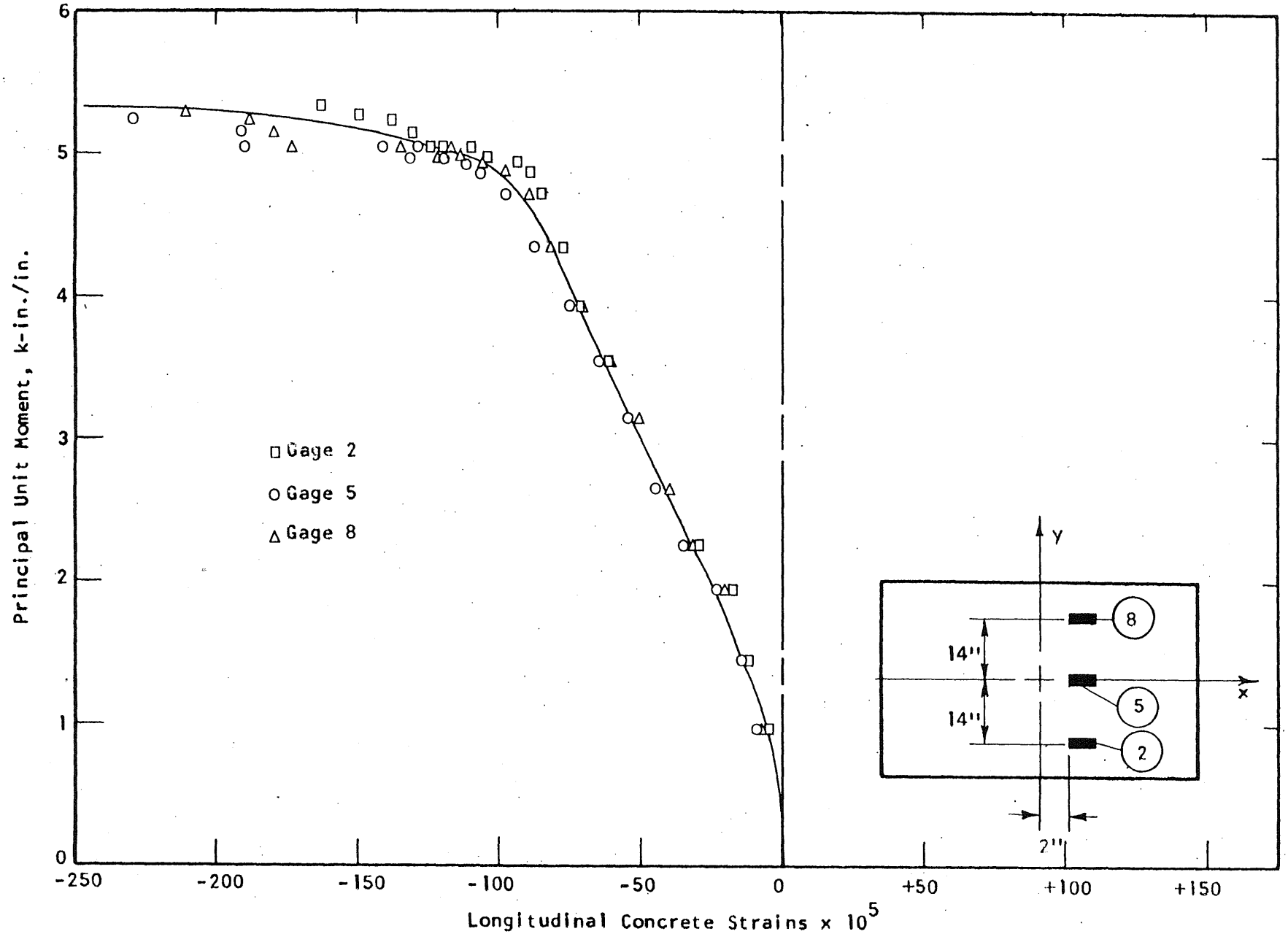

FIG. A.100 CONCRETE STRAIN PLOT, COMPRESSION SIDE OF SPECIMEN B11

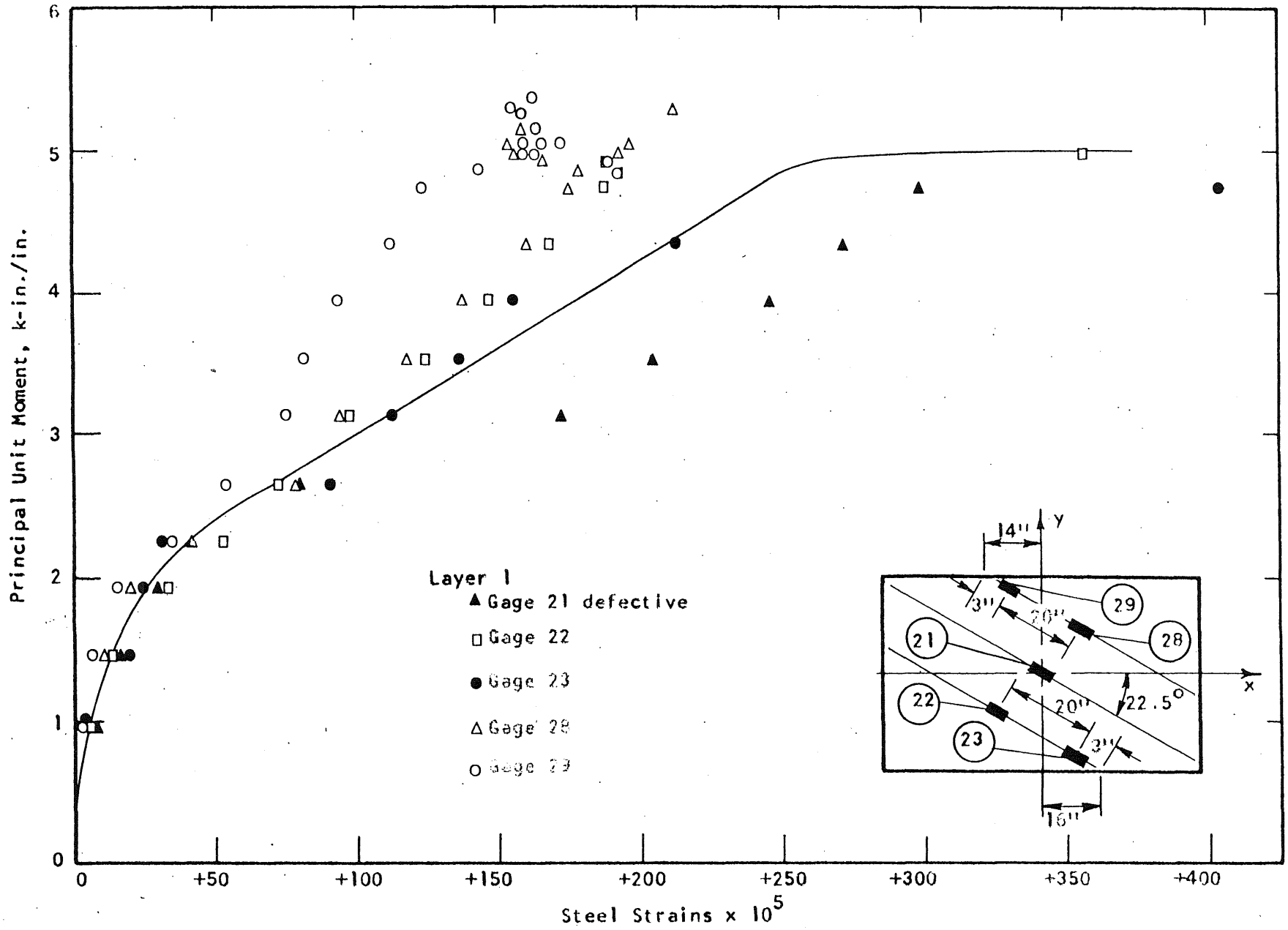

FIG. A.101 STEEL STRAIN PLOT, SPECIMEN B11

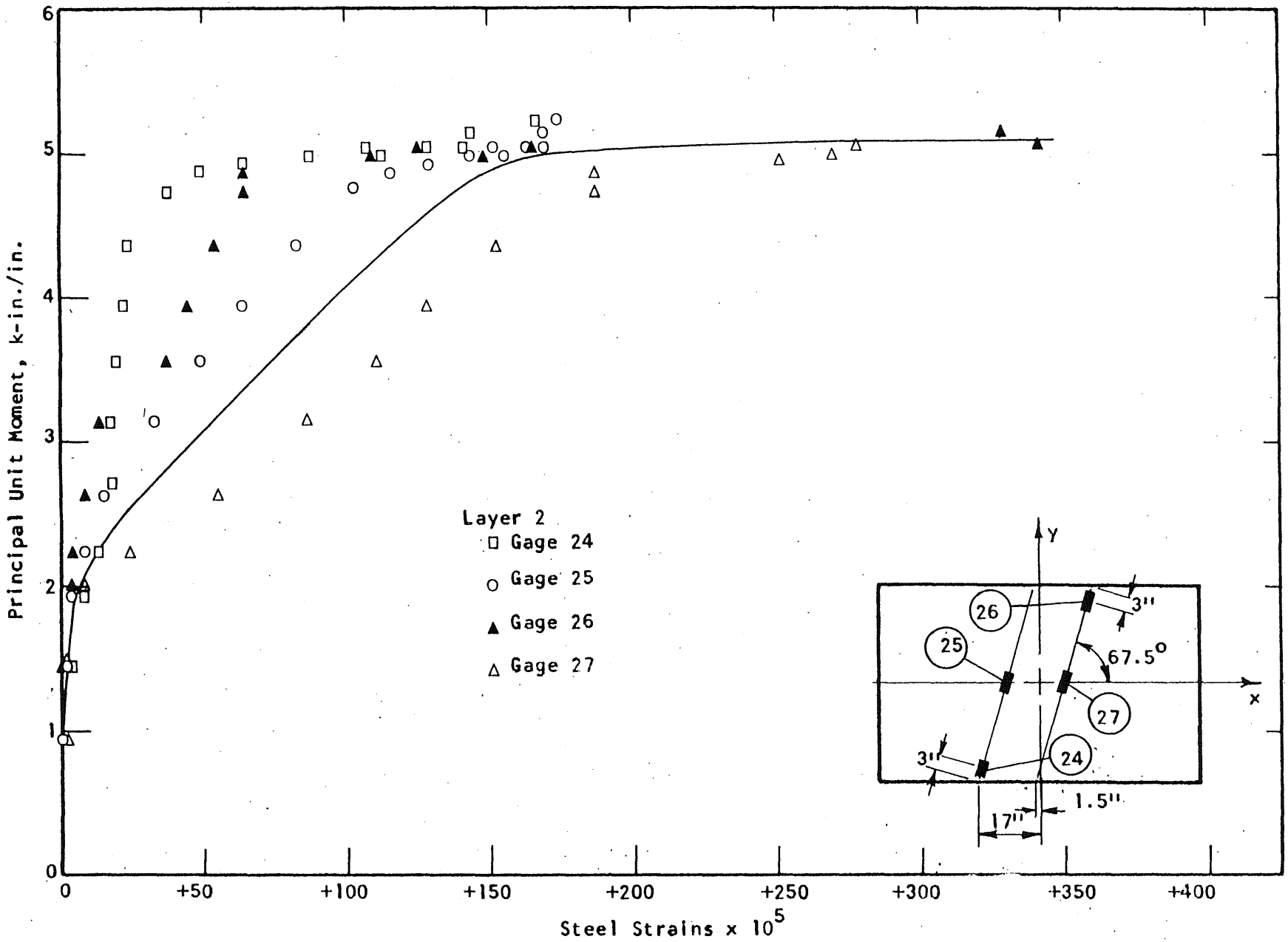

FIG. A.102 STEEL STRAIN PLOT, SPECIMEN B11

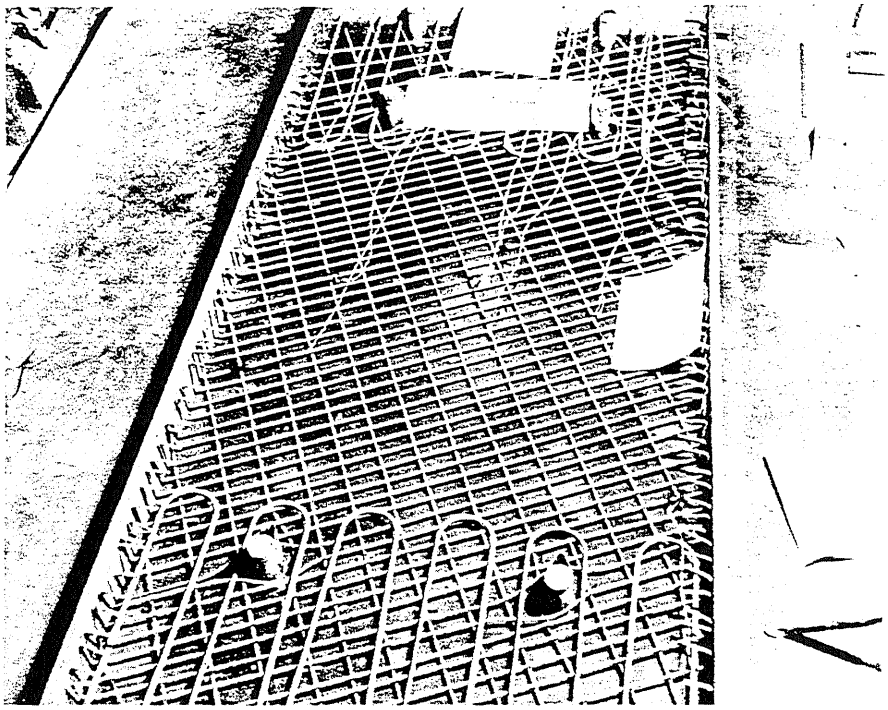

FIG. A.103 REINFORCEMENT IN SPECIMEN B12

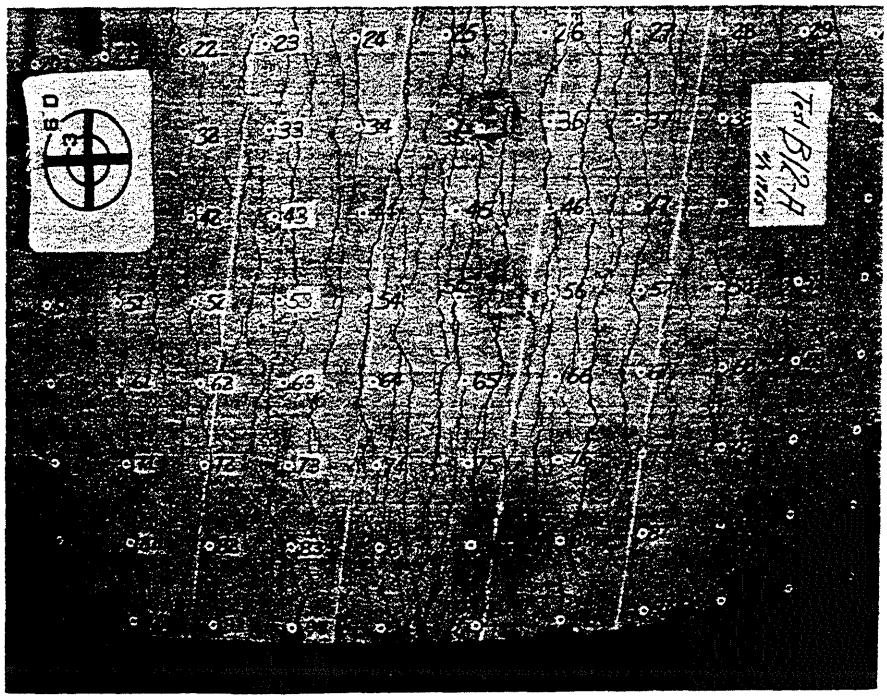

FIG. A.104 CRACK PATTERN IN TOP SURFACE OF B12

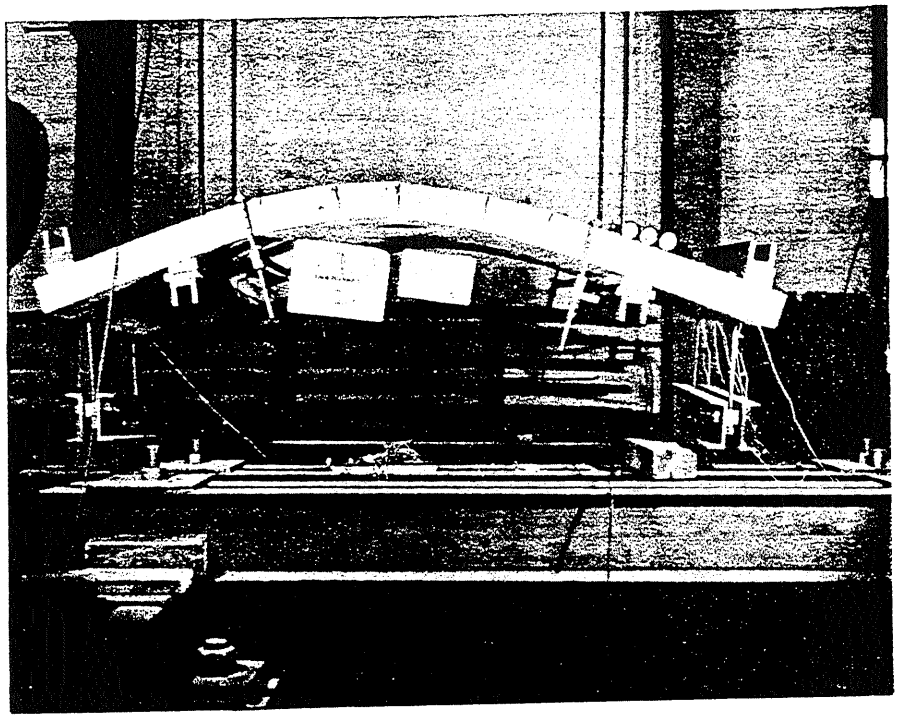

FIG. A.105 SIDE VIEW OF B12

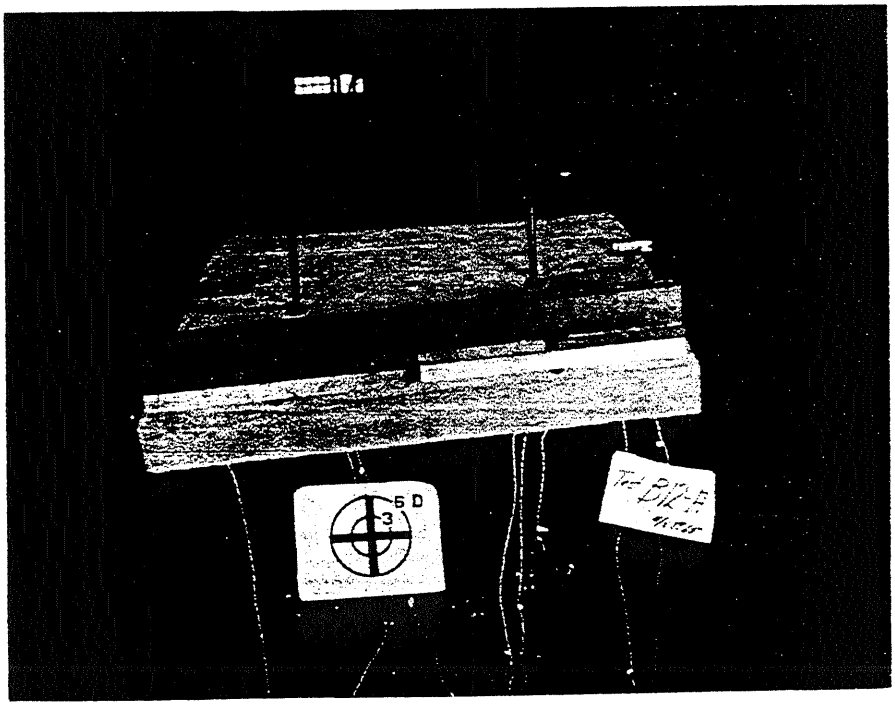

FIG. A.106 END VIEW OF B12

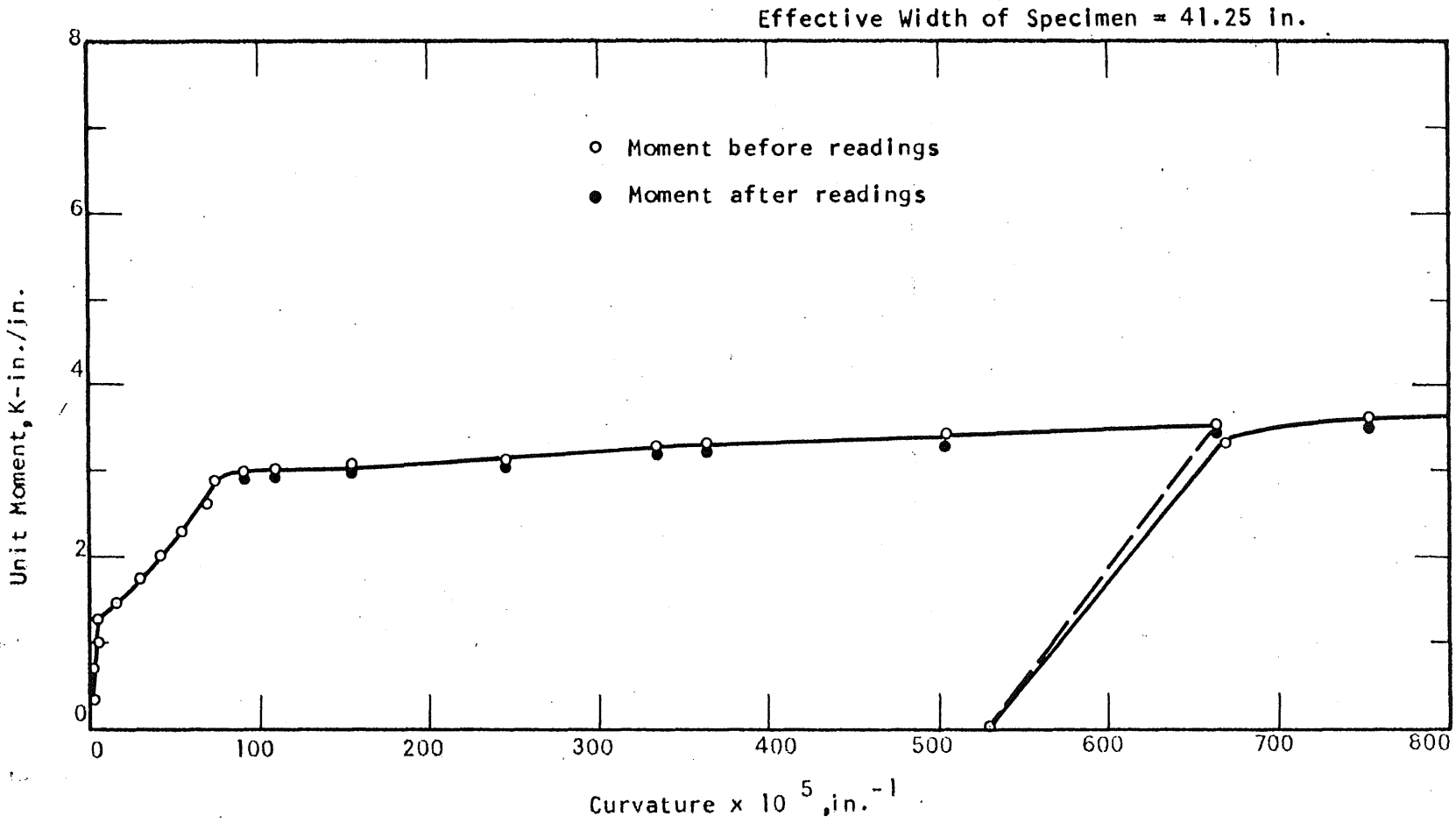

FIG. A.107 MOMENT-CURVATURE PLOT FOR SPECIMEN B12

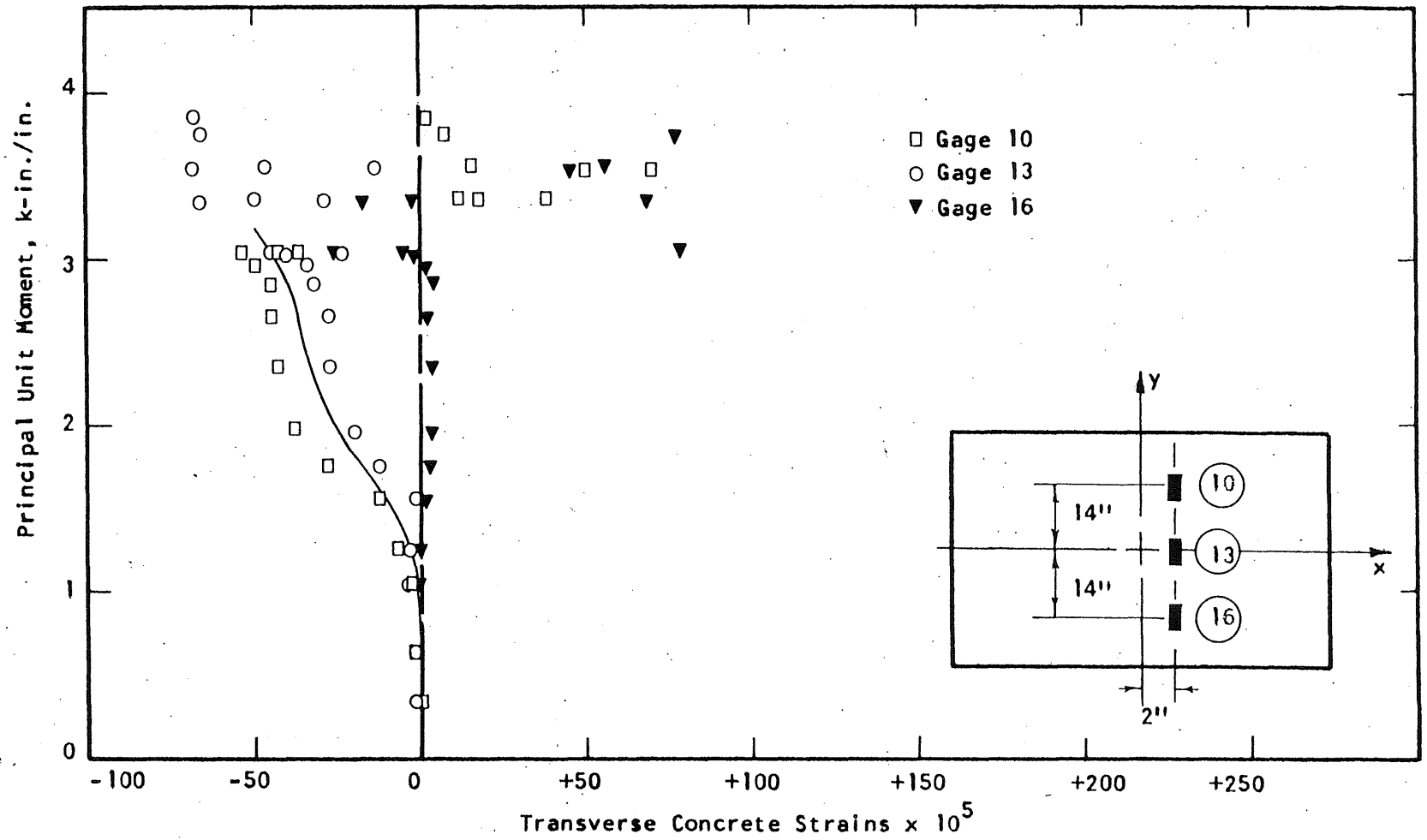

FIG. A.108 CONCRETE STRAIN PLOT, TENSION SIDE OF SPECIMEN B12

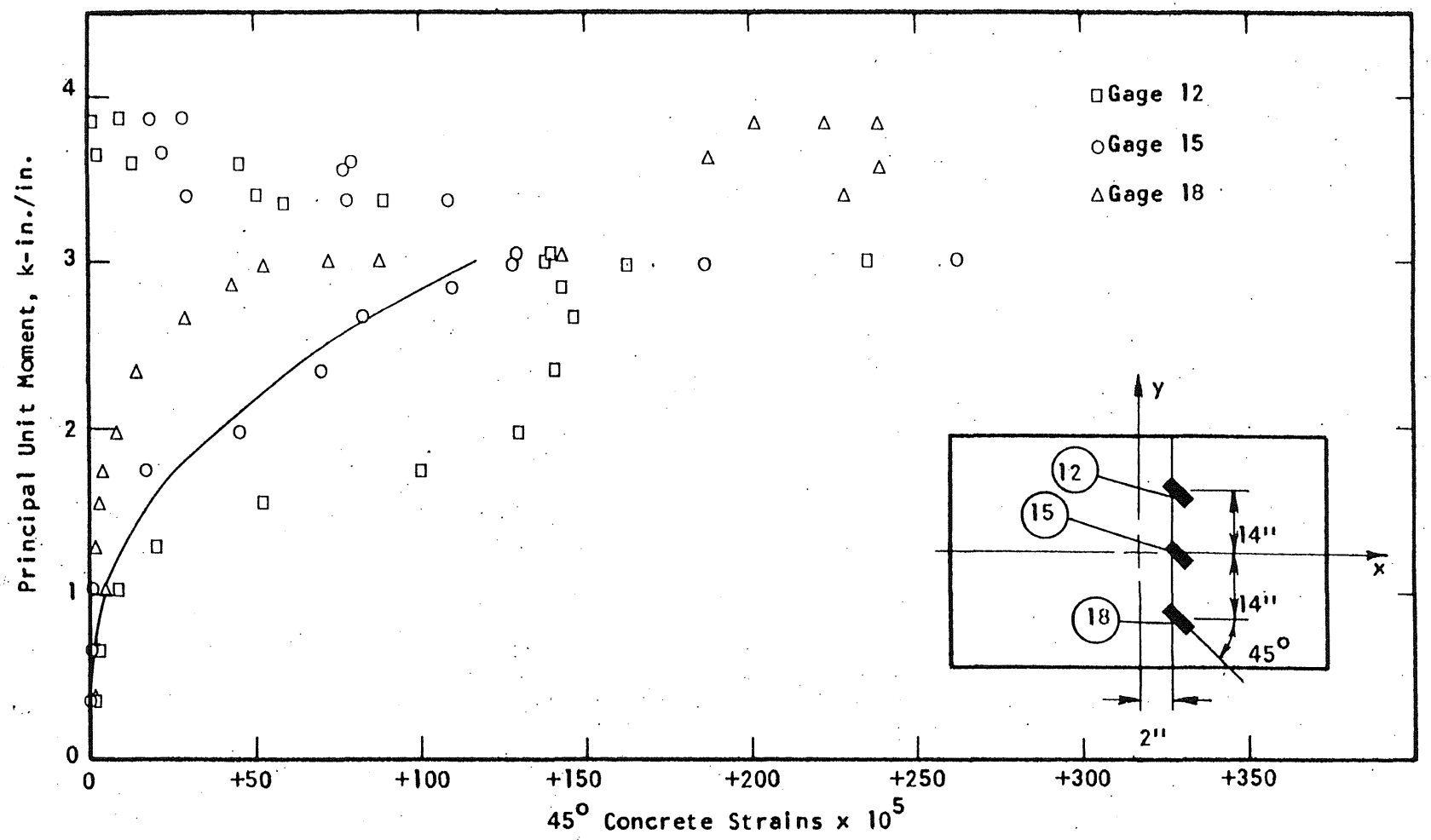

FIG. A.109 CONCRETE STRAIN PLOT, TENSION SIDE OF SPECIMEN B12

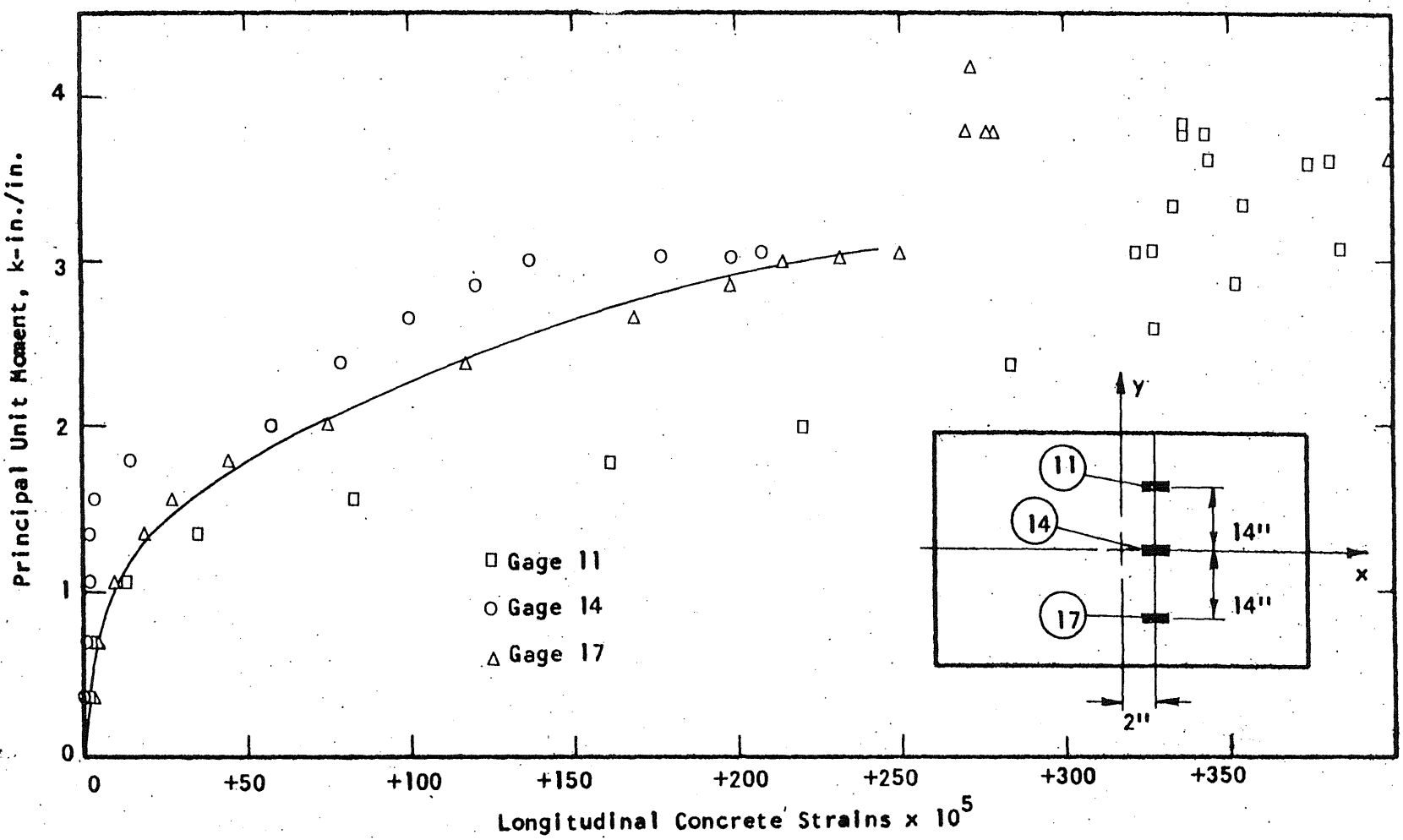

FIG. A.110 CONCRETE STRAIN PLOT, TENSION SIDE OF SPECIMEN B12

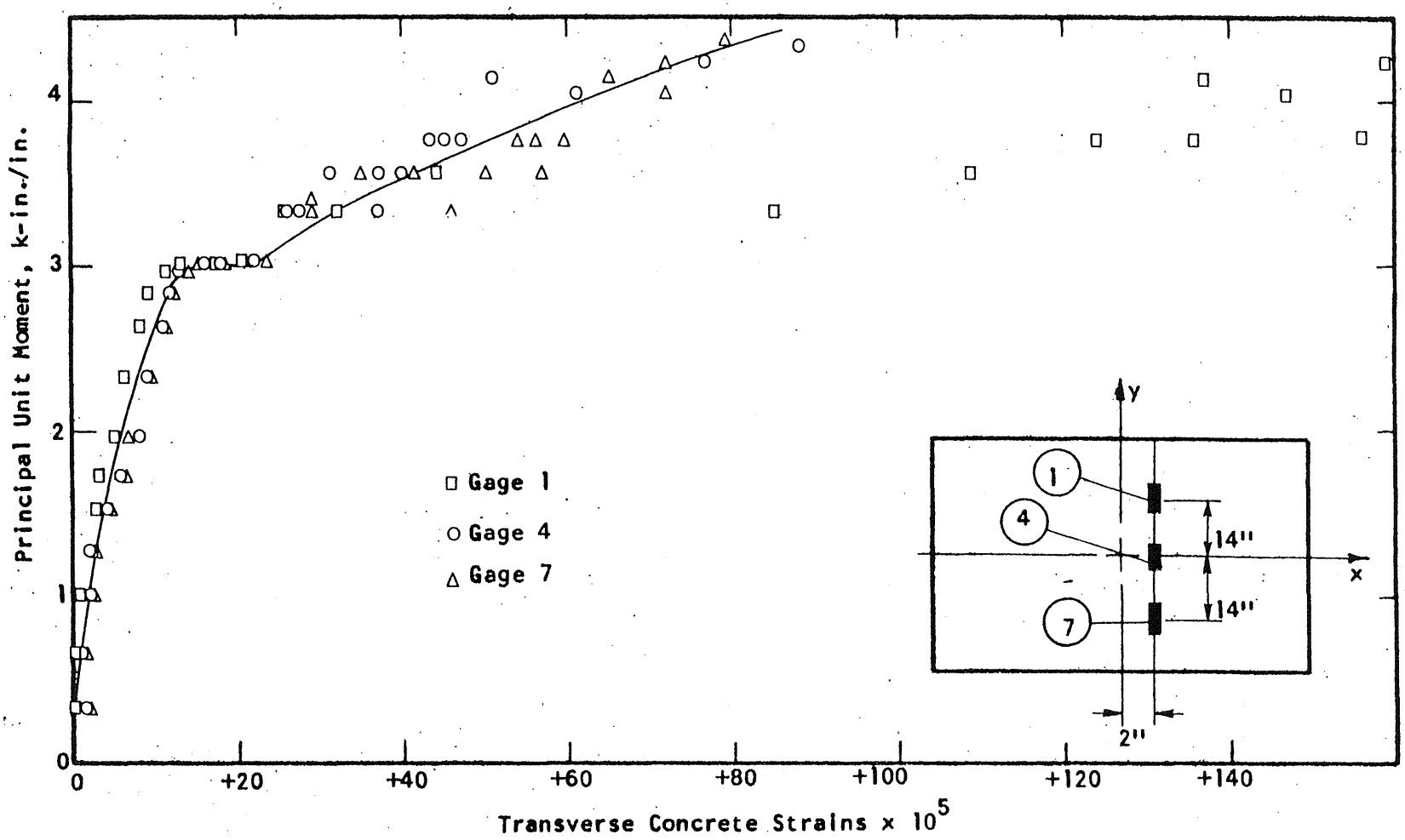

FIG. A.111 CONCRETE STRAIN PLOT, COMPRESSION SIDE OF SPECIMEN B12

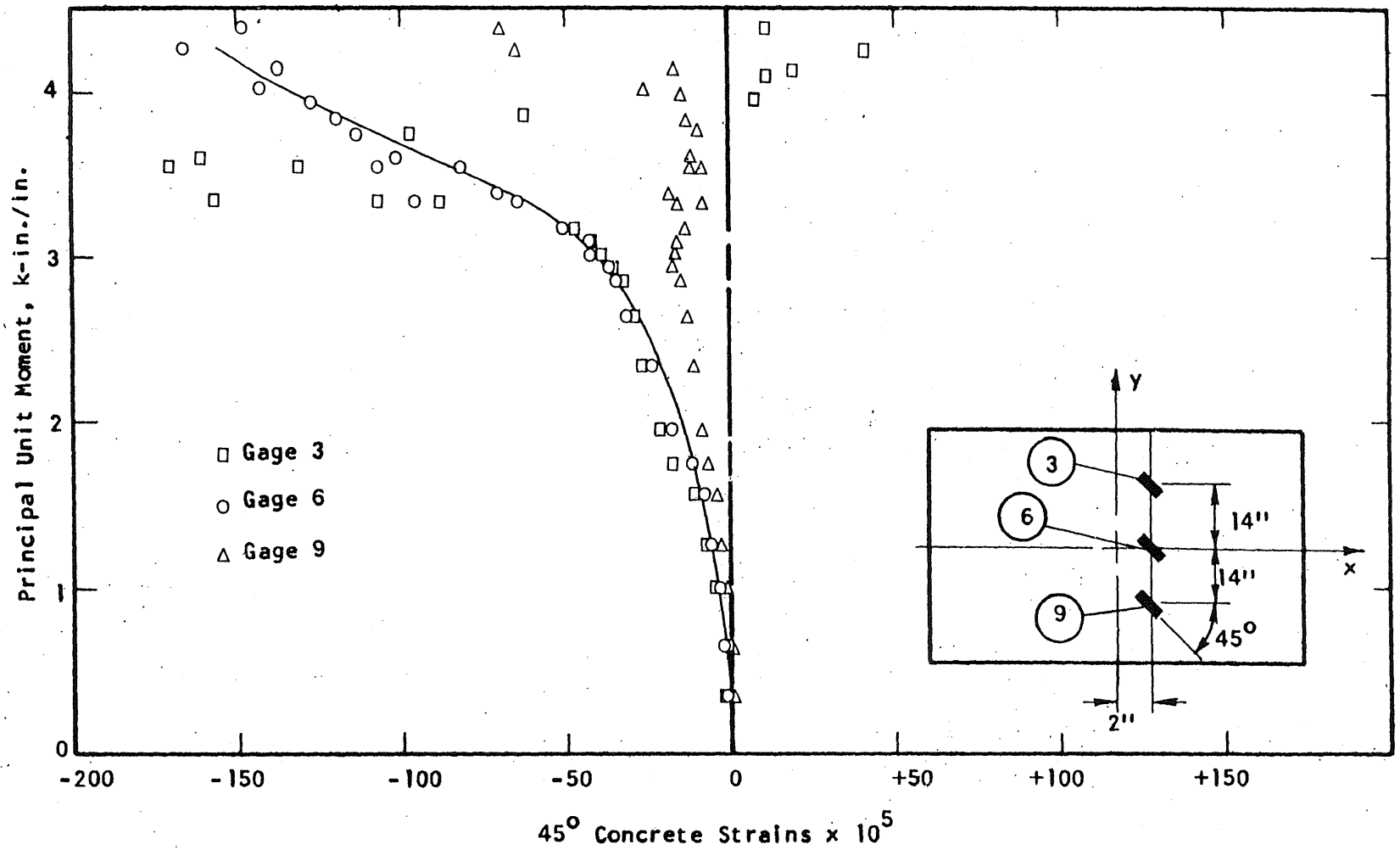

FIG. A.112 CONCRETE STRAIN PLOT, COMPRESSION SIDE OF SPECIMEN B12

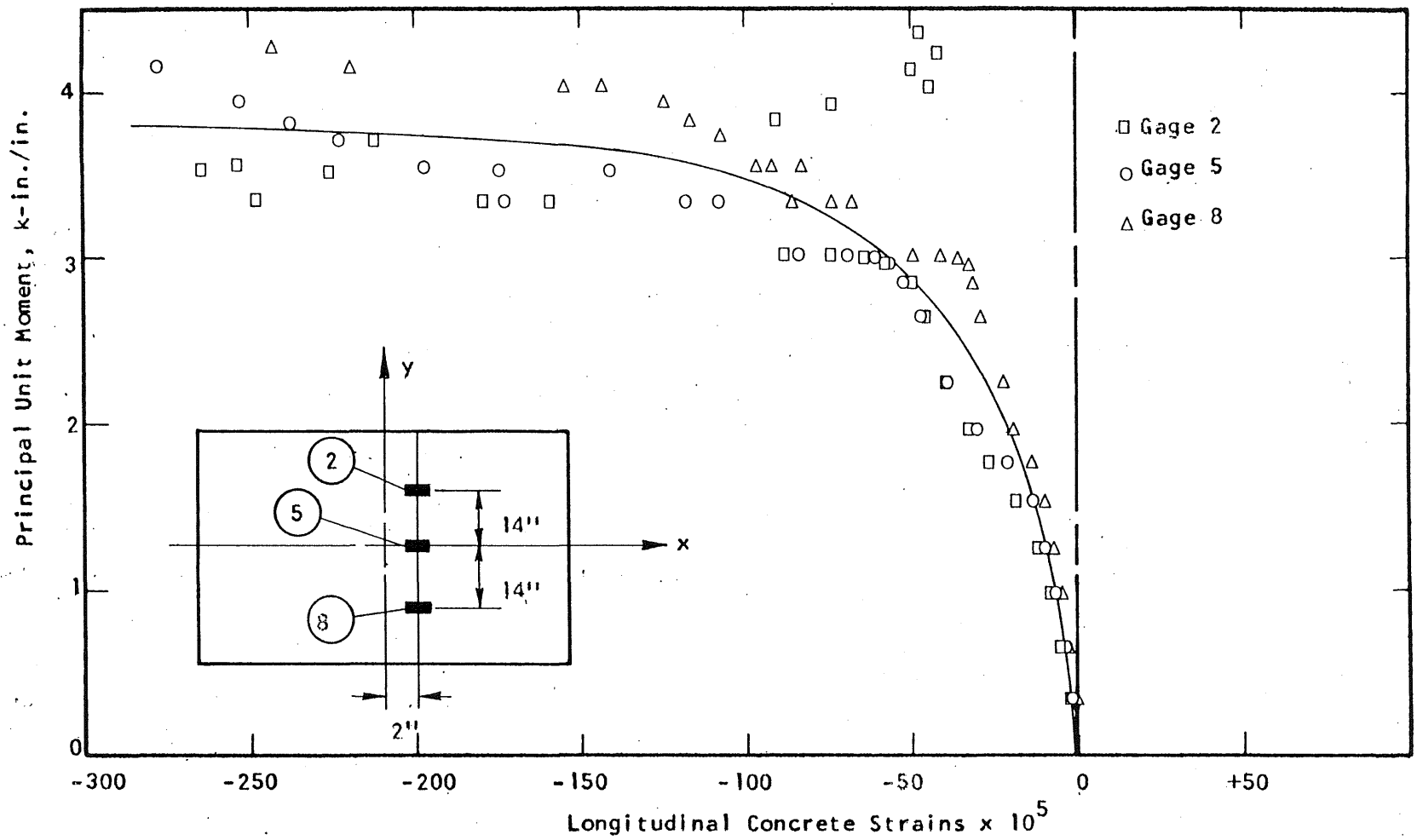

FIG. A.113 CONCRETE STRAIN PLOT, COMPRESSION SIDE OF SPECIMEN B12

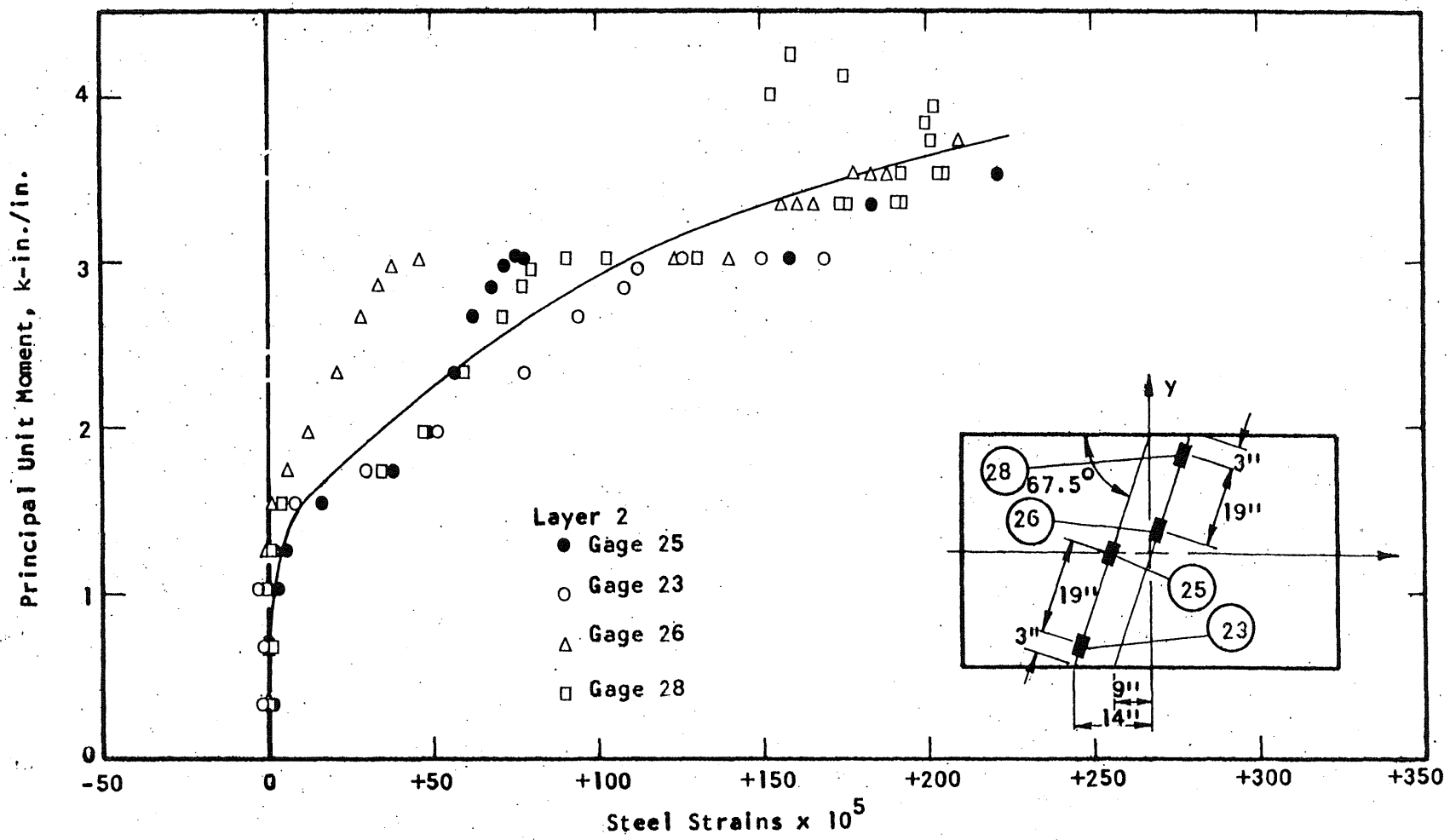

FIG. A.114 STEEL STRAIN PLOT, SPECIMEN B12

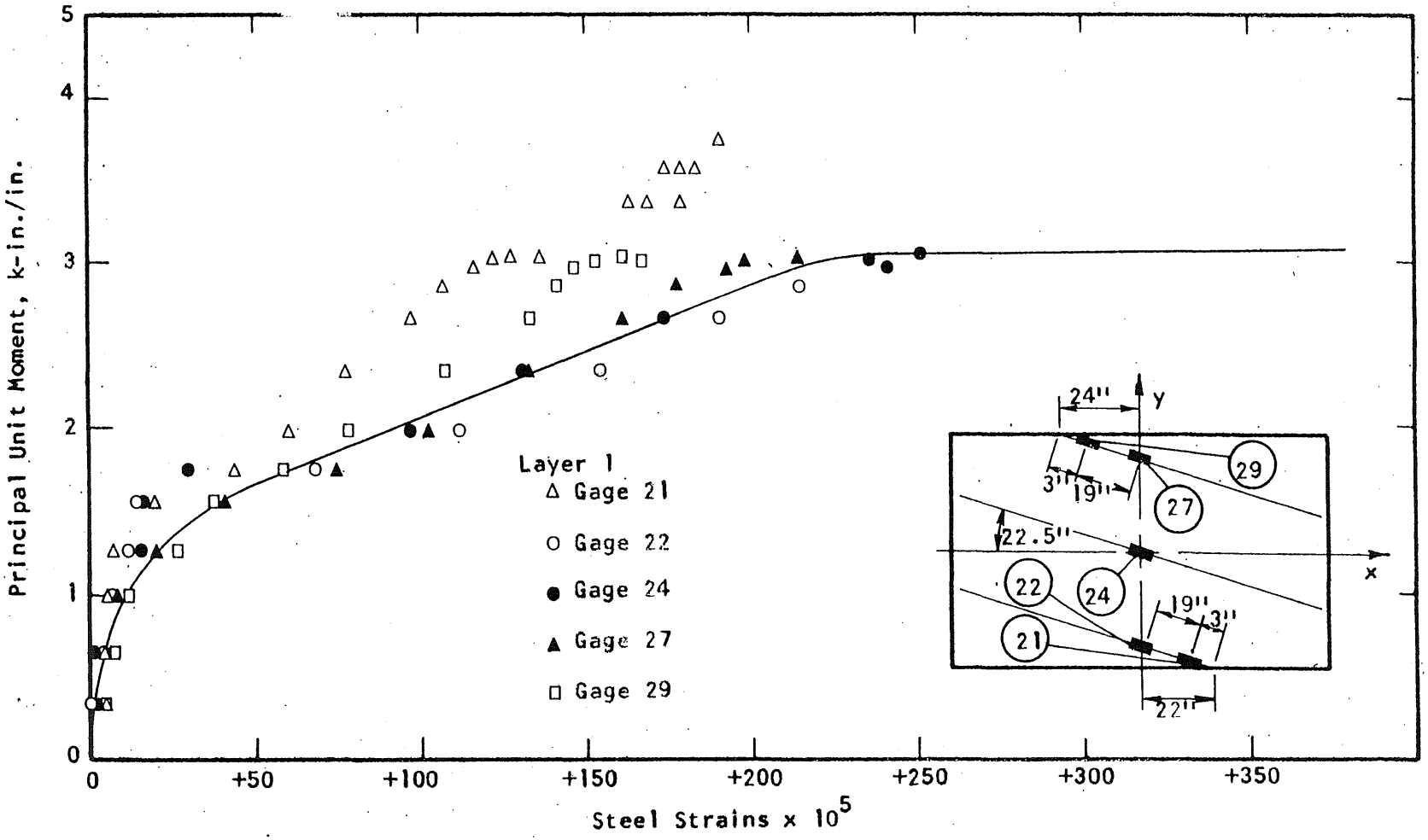

FIG. A.115 STEEL STRAIN PLOT, SPECIMEN B12

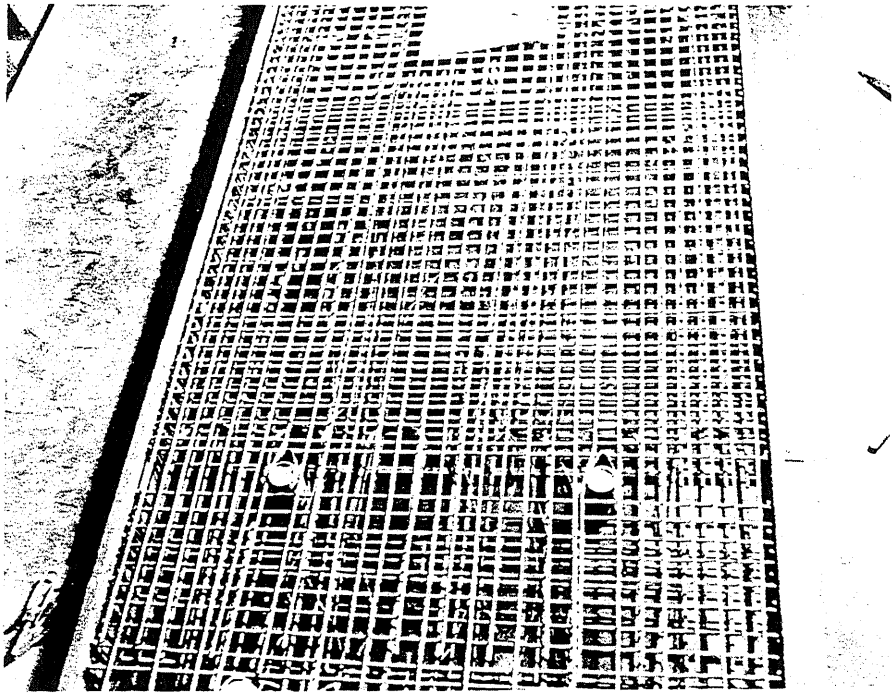

FIG. A.116 REINFORCEMENT IN SPECIMEN B13

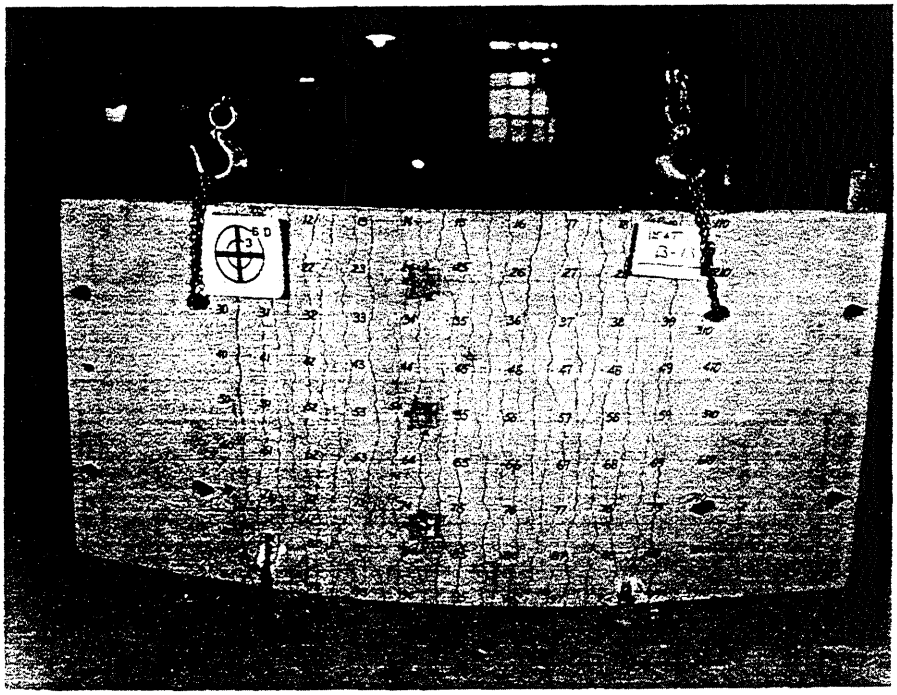

FIG. A.117 CRACK PATTERN IN TOP SURFACE OF B13

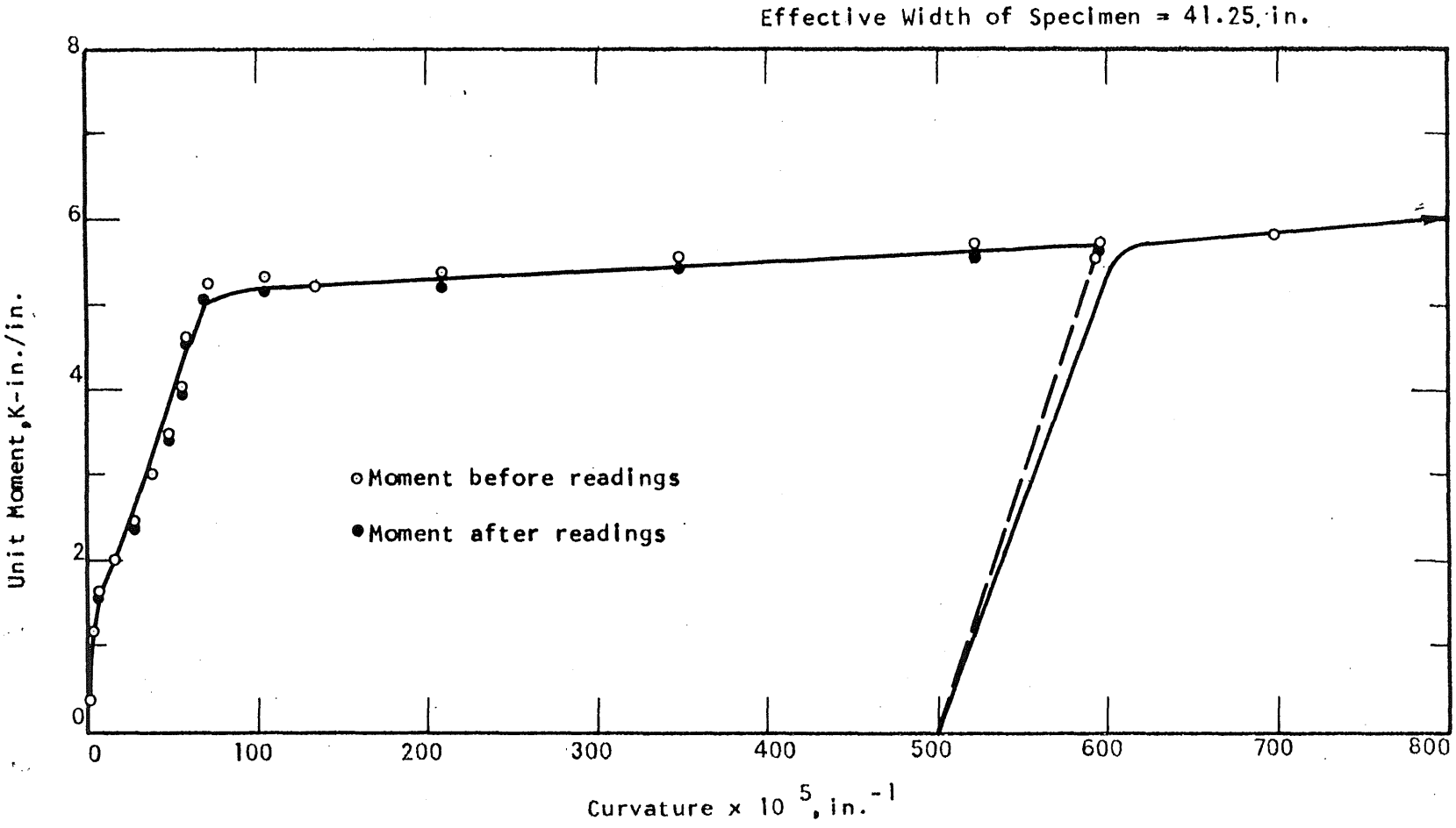

FIG. A.118 MOMENT-CURVATURE PLOT FOR SPECIMEN B13

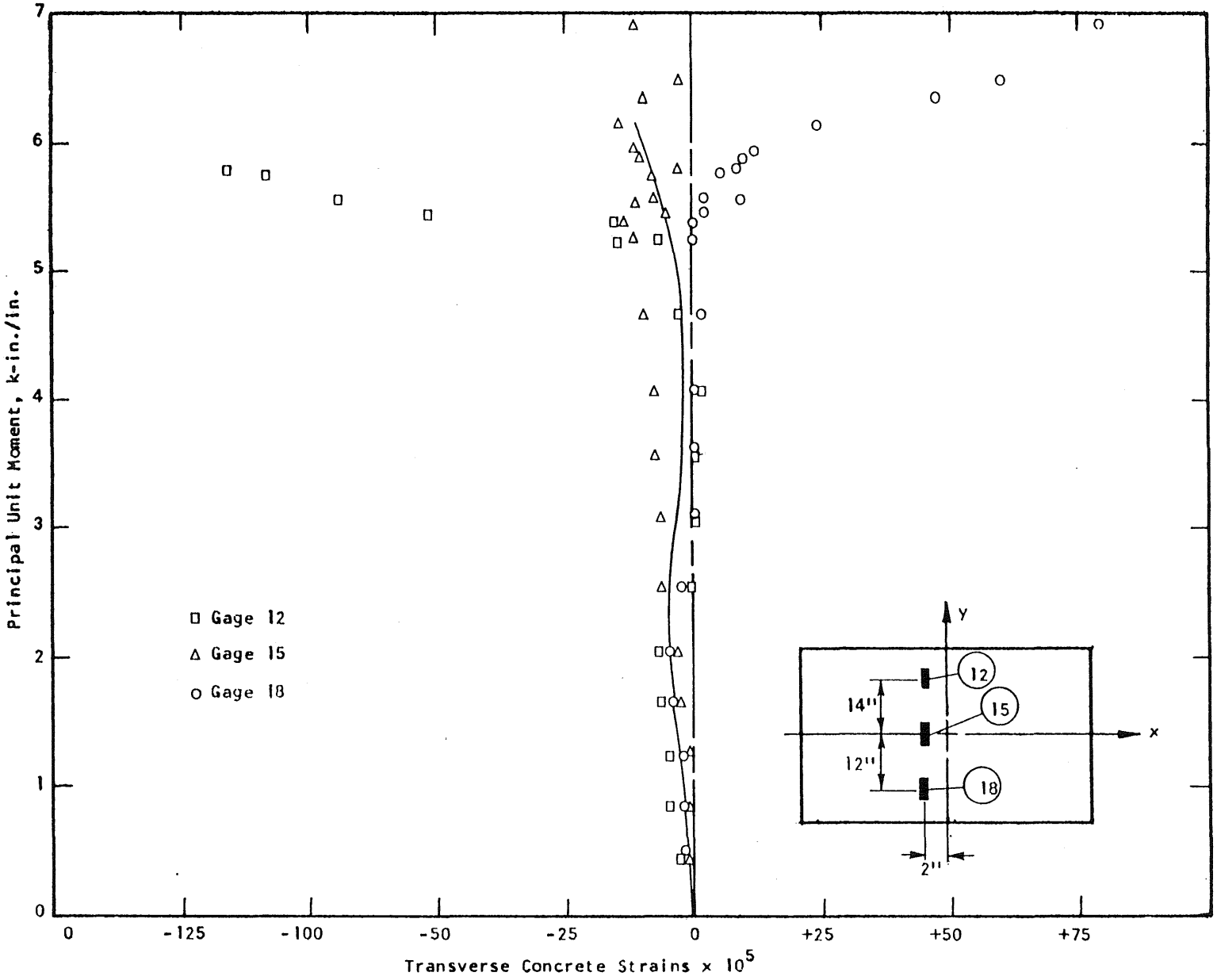

FIG. A.119 CONCRETE STRAIN PLOT, TENSION SIDE OF SPECIMEN B13

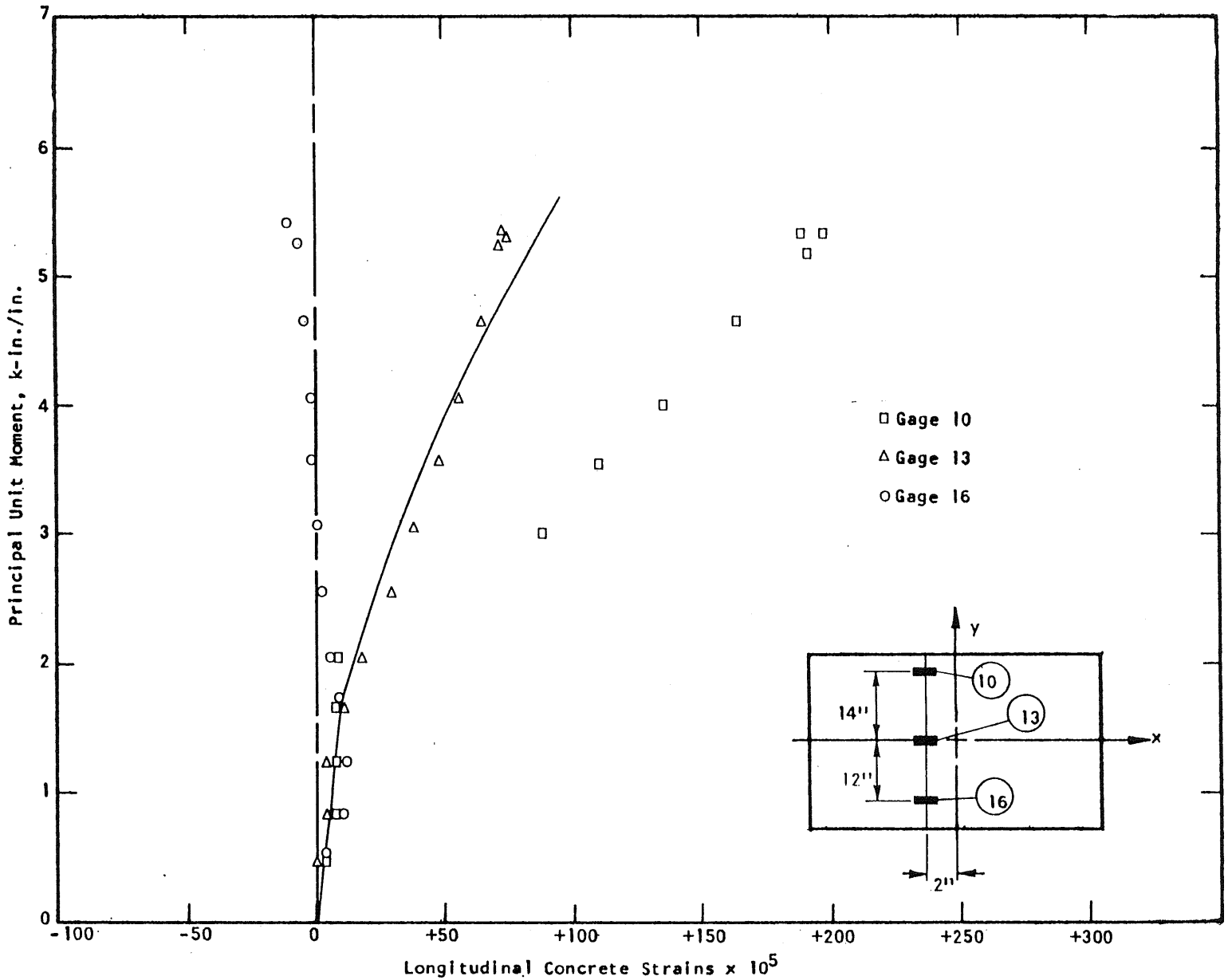

FIG. A.120 CONCRETE STRAIN PLOT, TENSION SIDE OF SPECIMEN B13

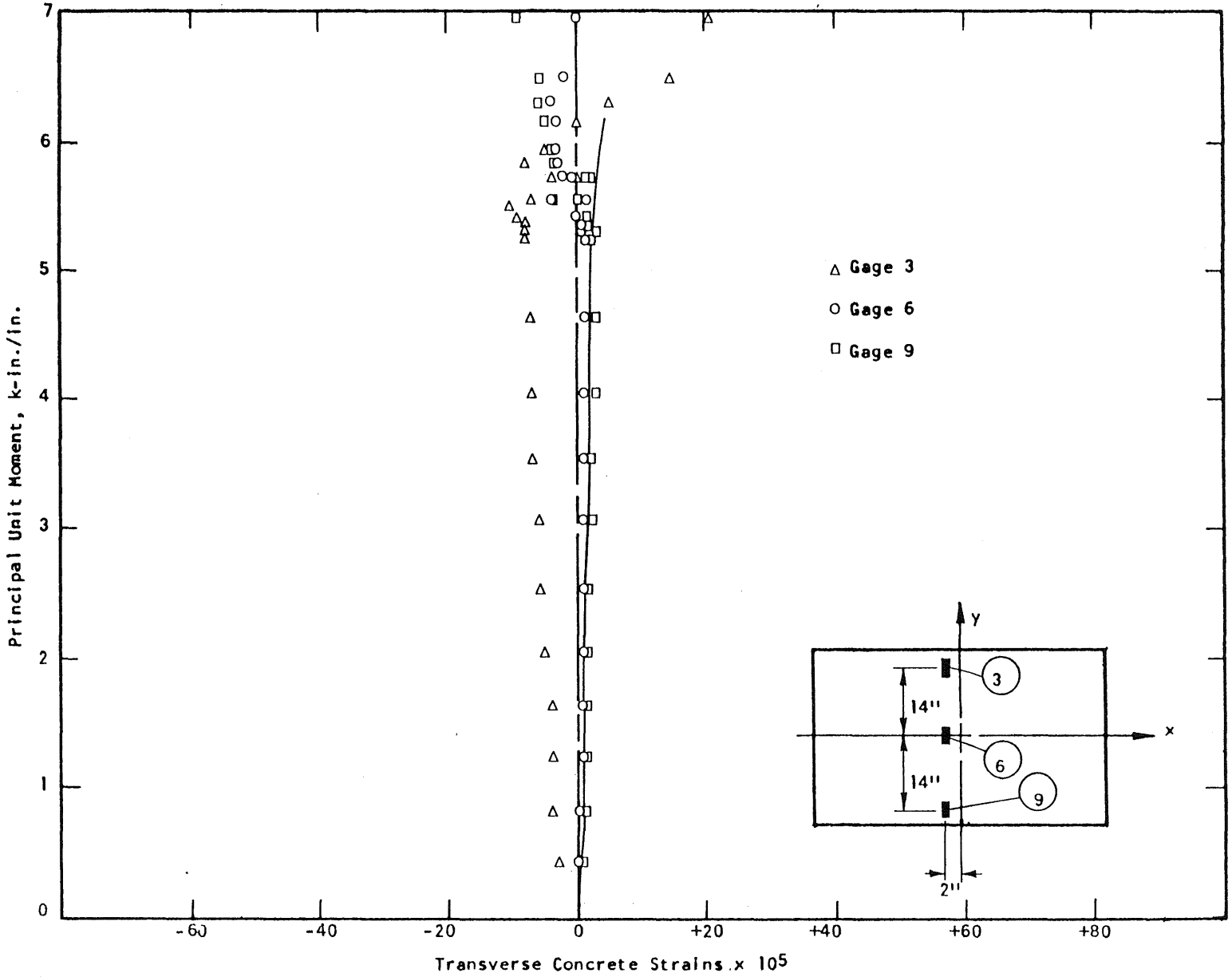

FIG. A.121 CONCRETE STRAIN PLOT - COMPRESSION SIDE OF SPECIMEN B13

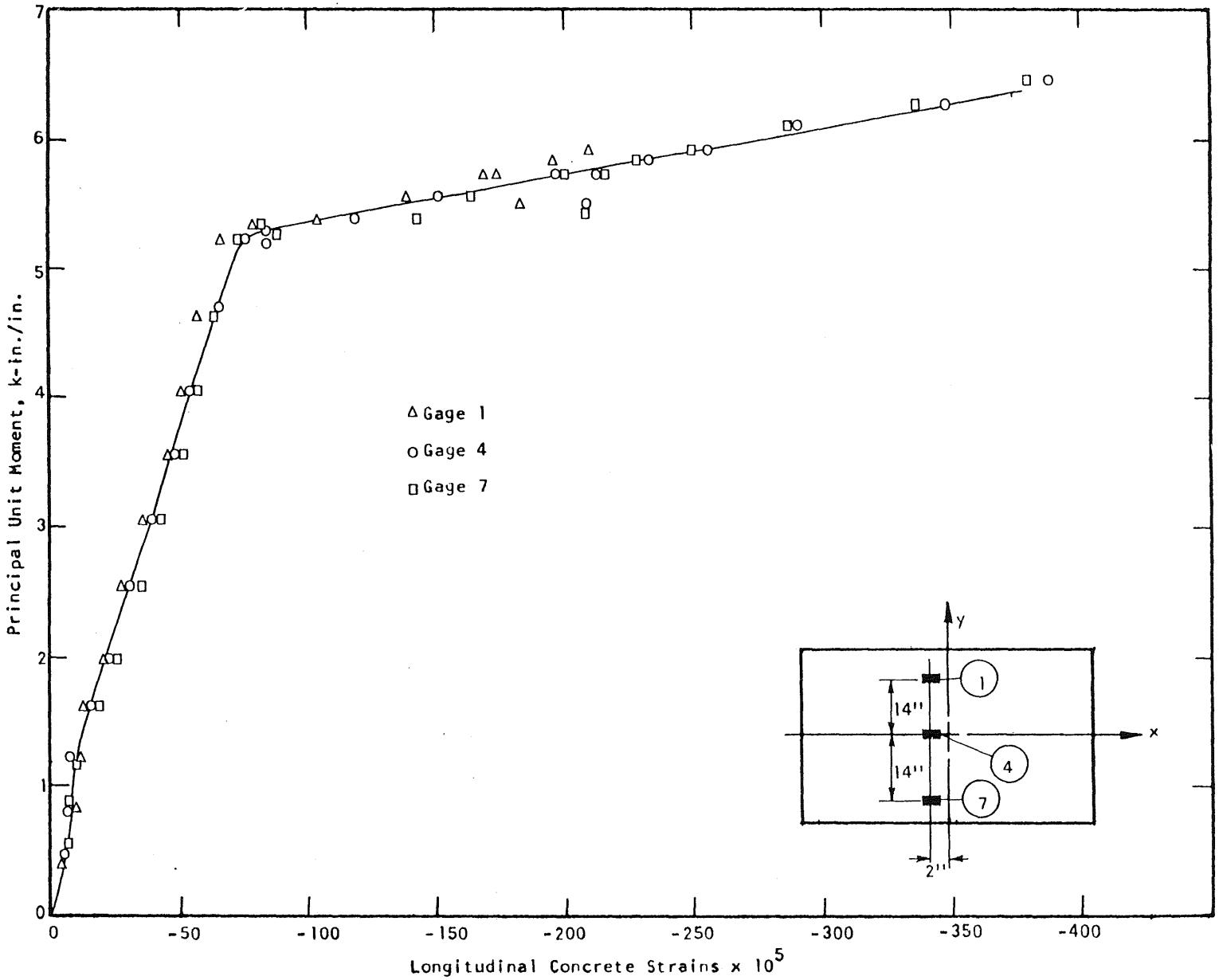

FIG. A.122 CONCRETE STRAIN PLOT , COMPRESSION SIDE OF SPECIMEN B13

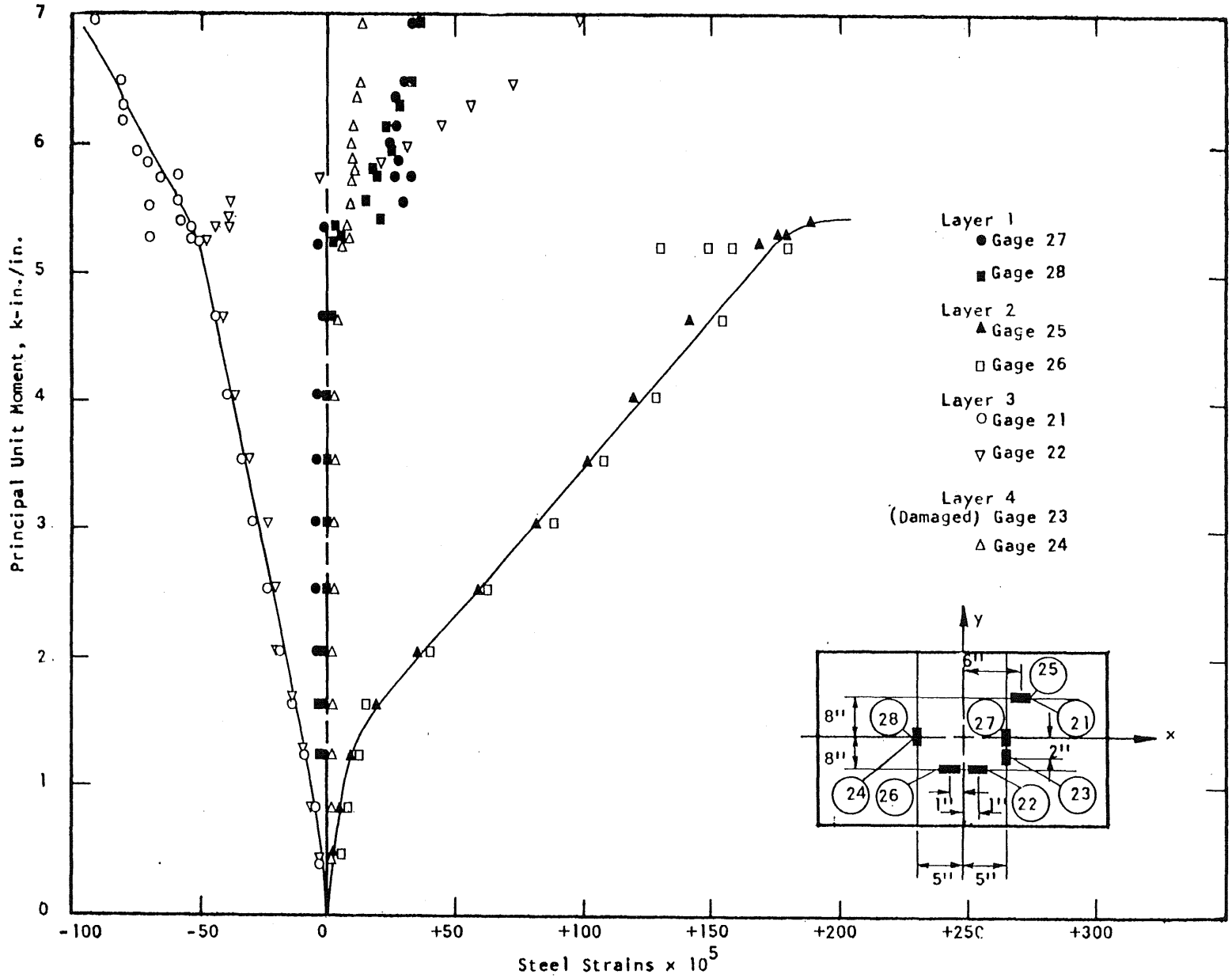

FIG. A.123 STEEL STRAIN PLOT, SPECIMEN B13

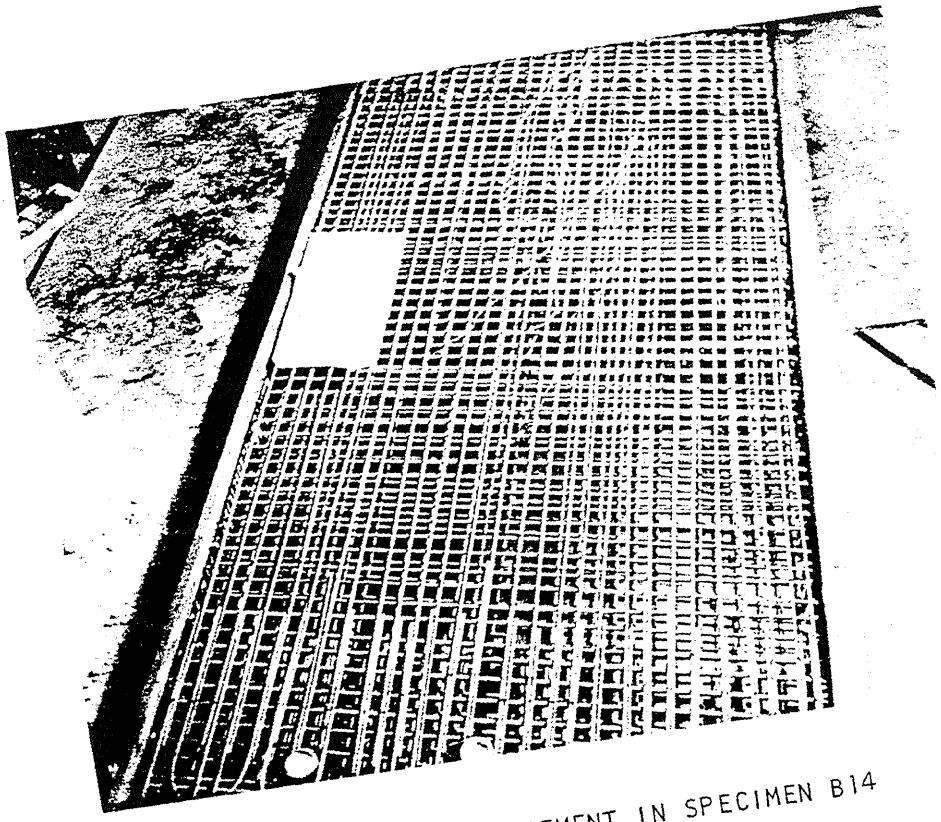

FIG. A.124 REINFORCEMENT IN SPECIMEN B14

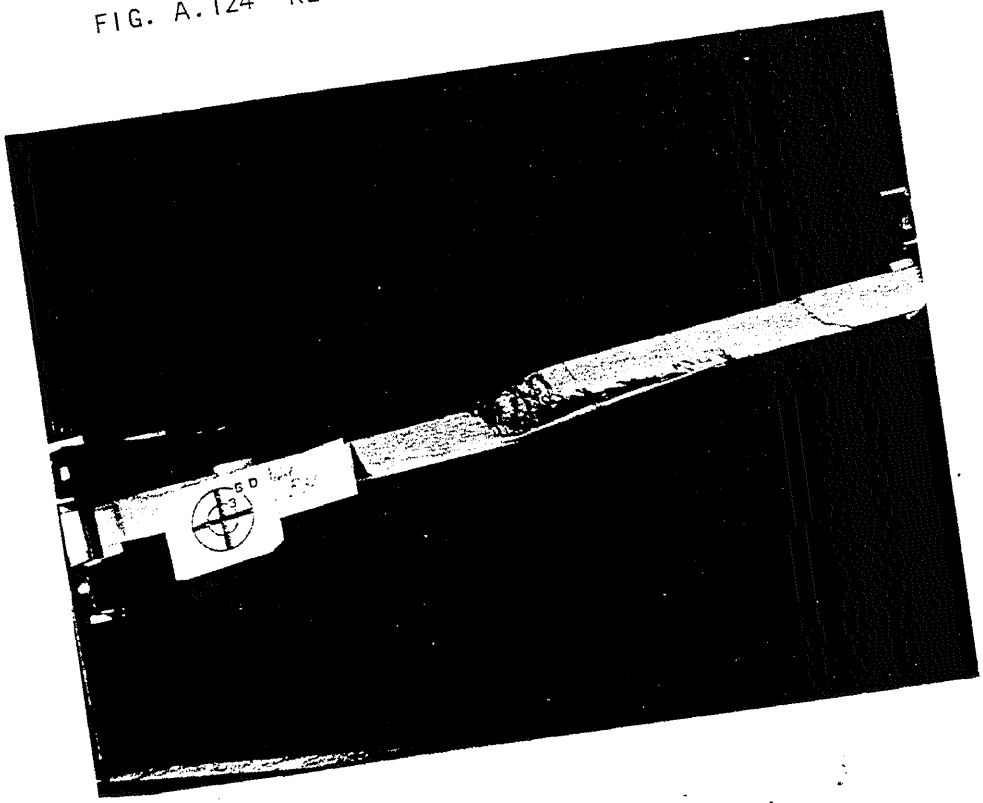

FIG. A.125 SIDE VIEW OF B14

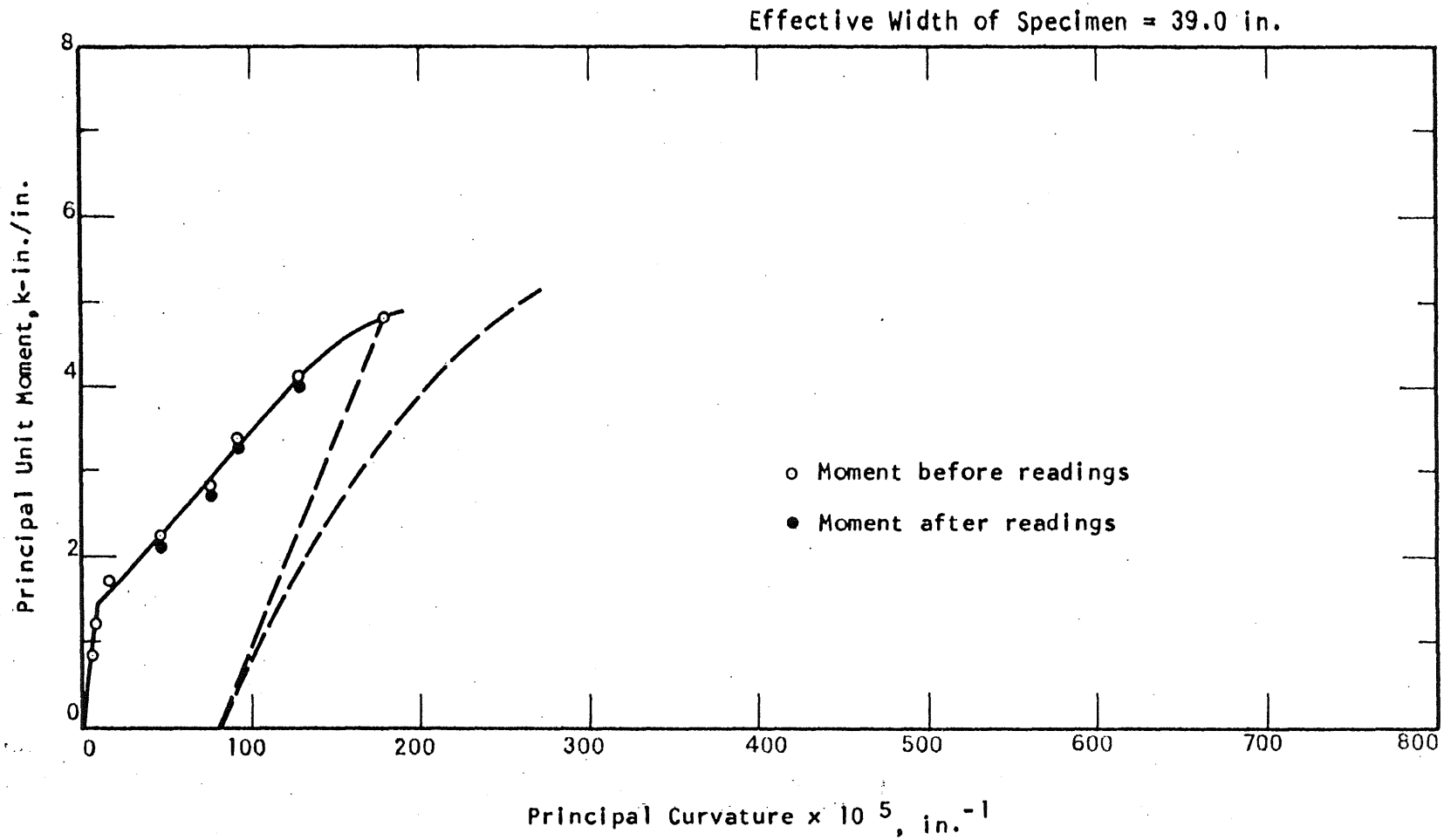

FIG. A.126 MOMENT-CURVATURE PLOT FOR SPECIMEN B14

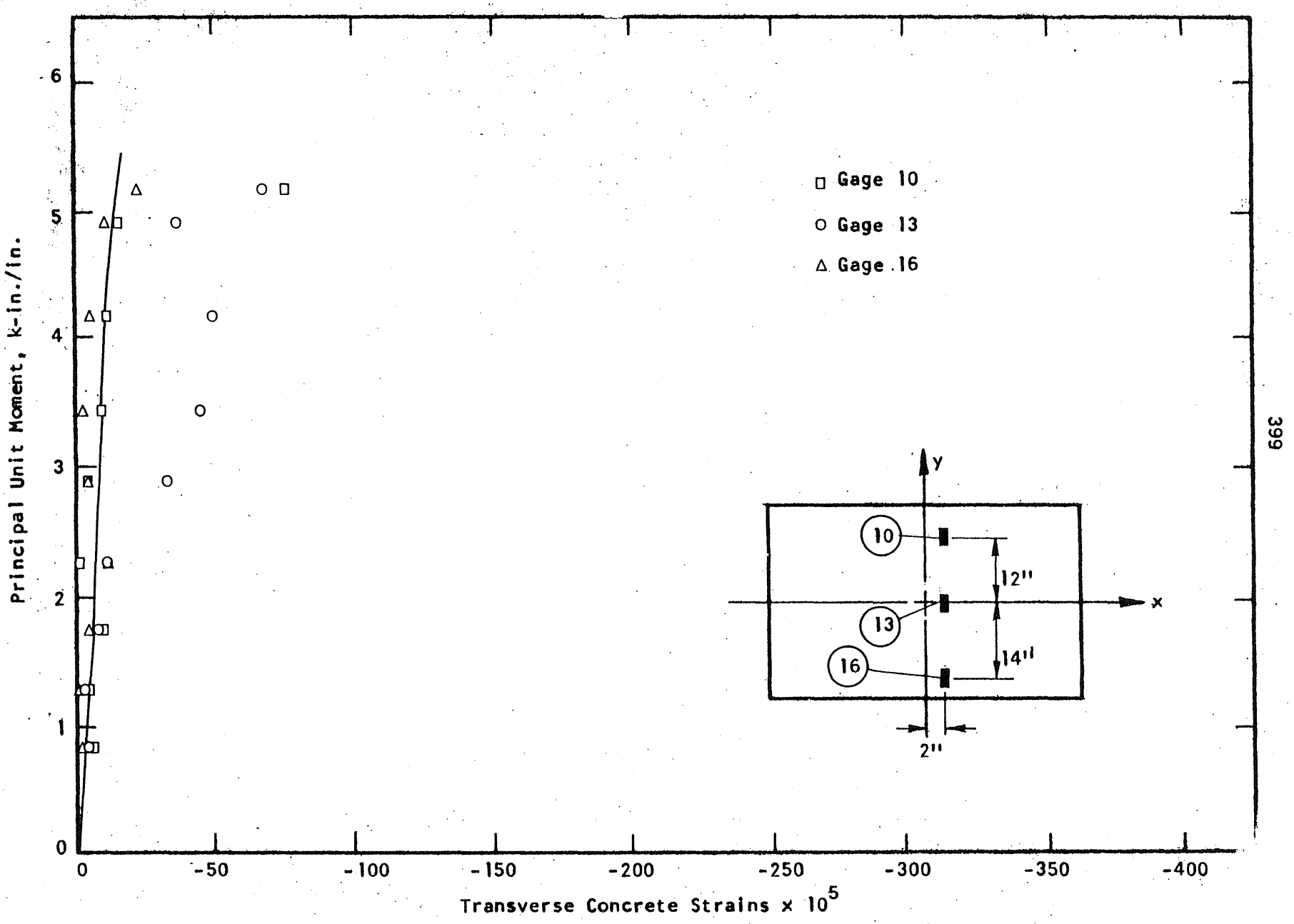

FIG. A.127 CONCRETE STRAIN PLOT, TOP SIDE OF SPECIMEN B14

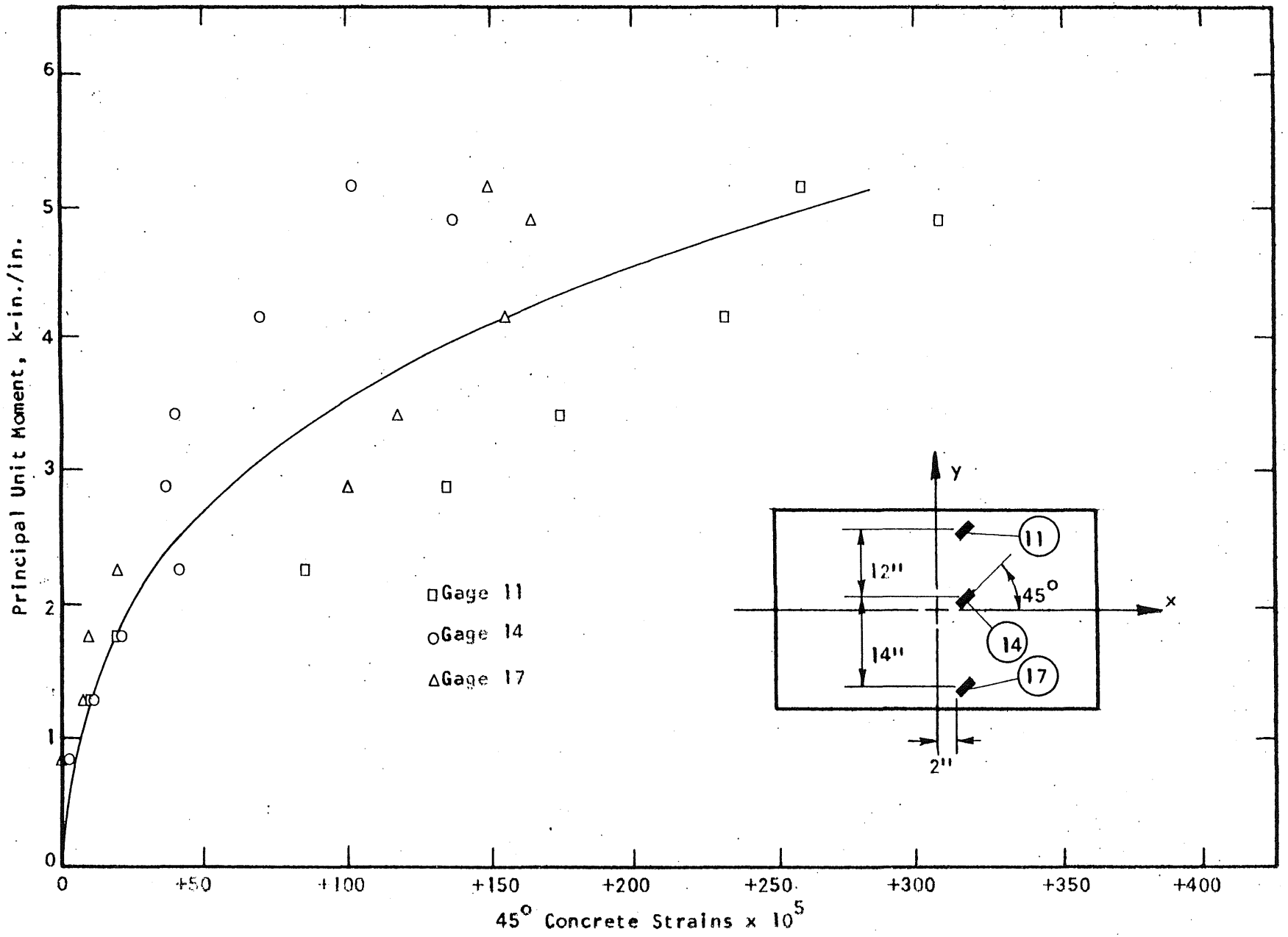

400

FIG. A.128 CONCRETE STRAIN PLOT, TOP SIDE OF SPECIMEN B14

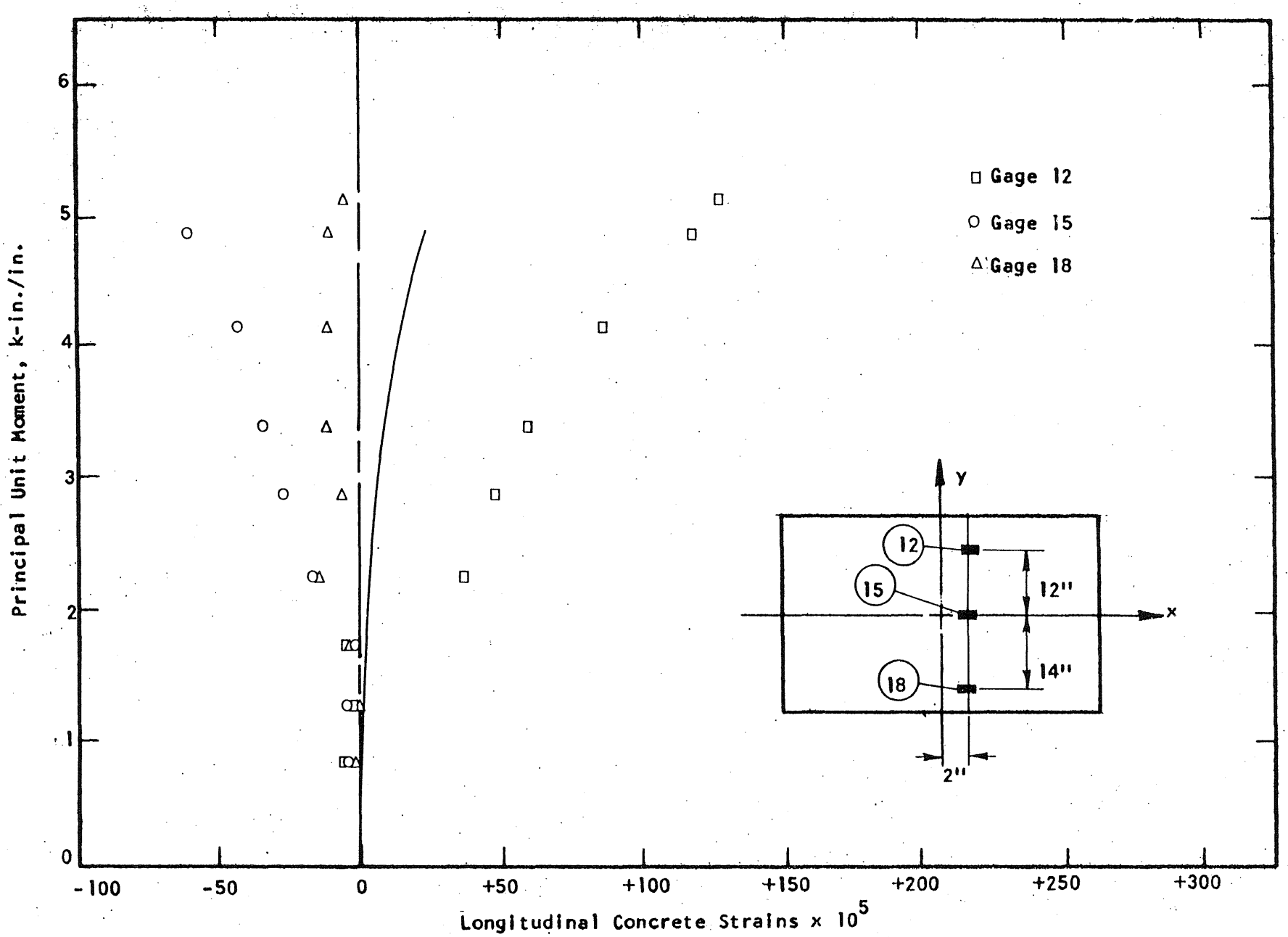

FIG. A.129 CONCRETE STRAIN PLOT, TOP SIDE OF SPECIMEN B14

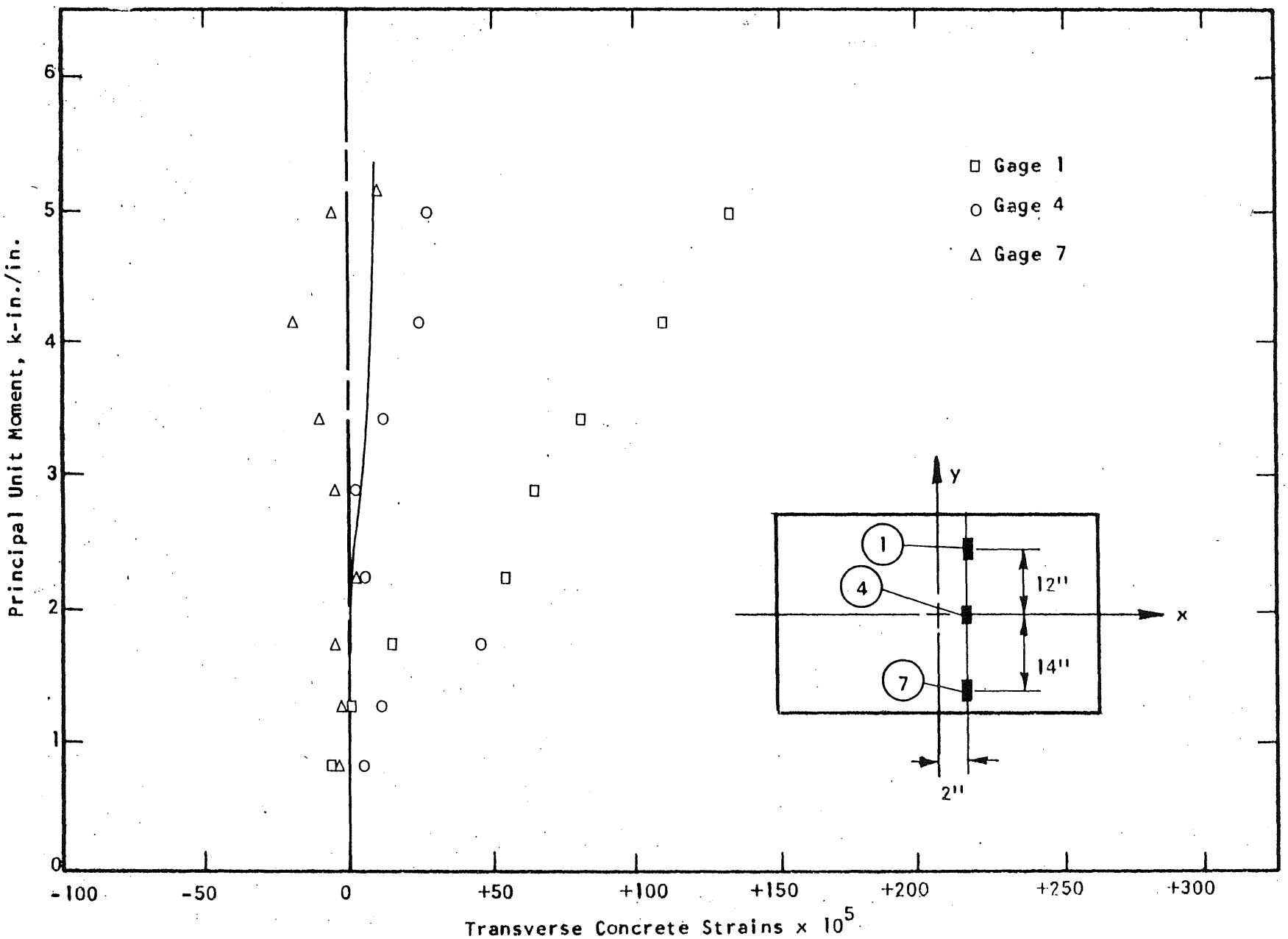

FIG. A.130 CONCRETE STRAIN PLOT, BOTTOM SIDE OF SPECIMEN B14

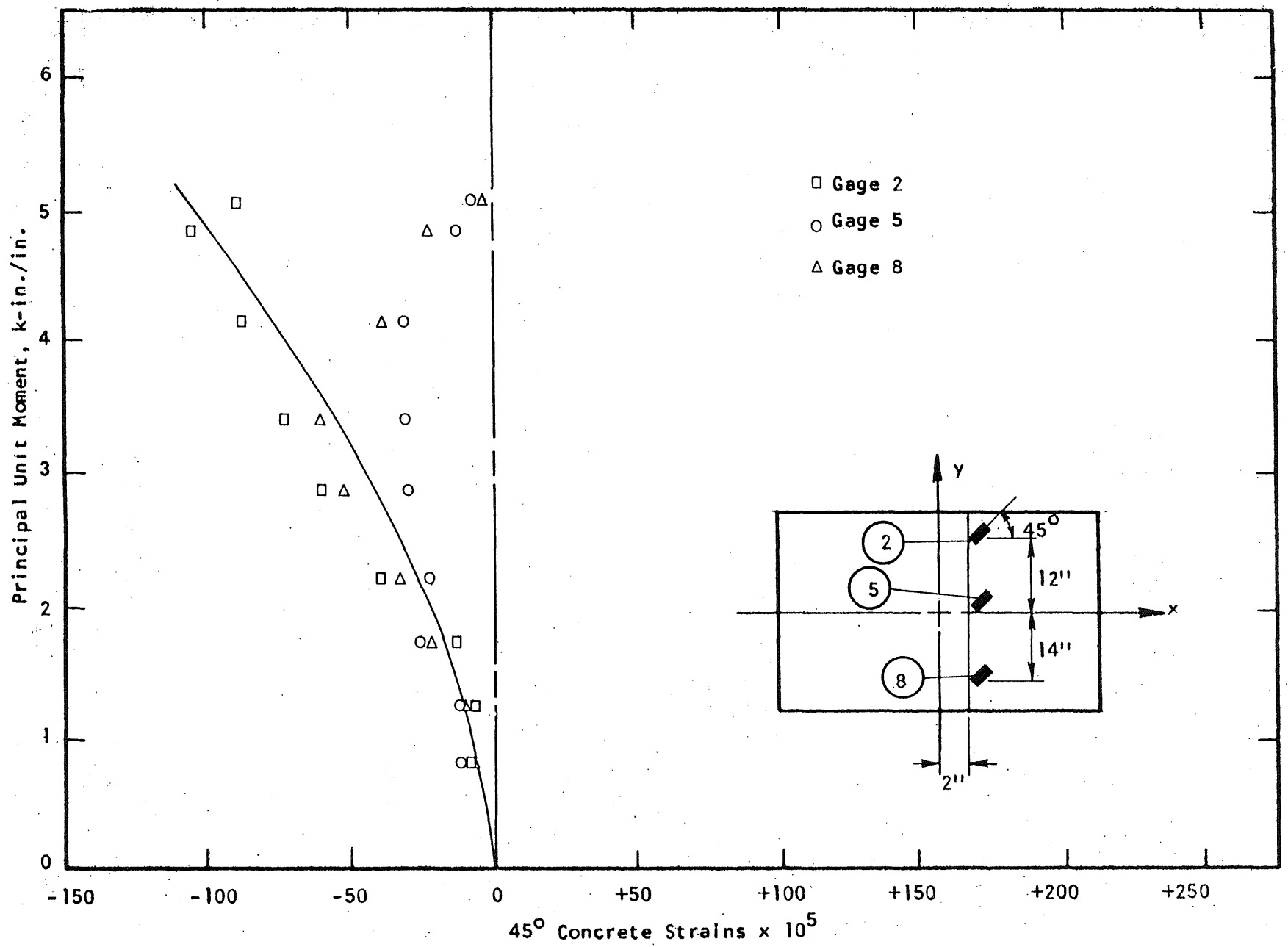

FIG. A.131 CONCRETE STRAIN PLOT, BOTTOM SIDE OF SPECIMEN B14

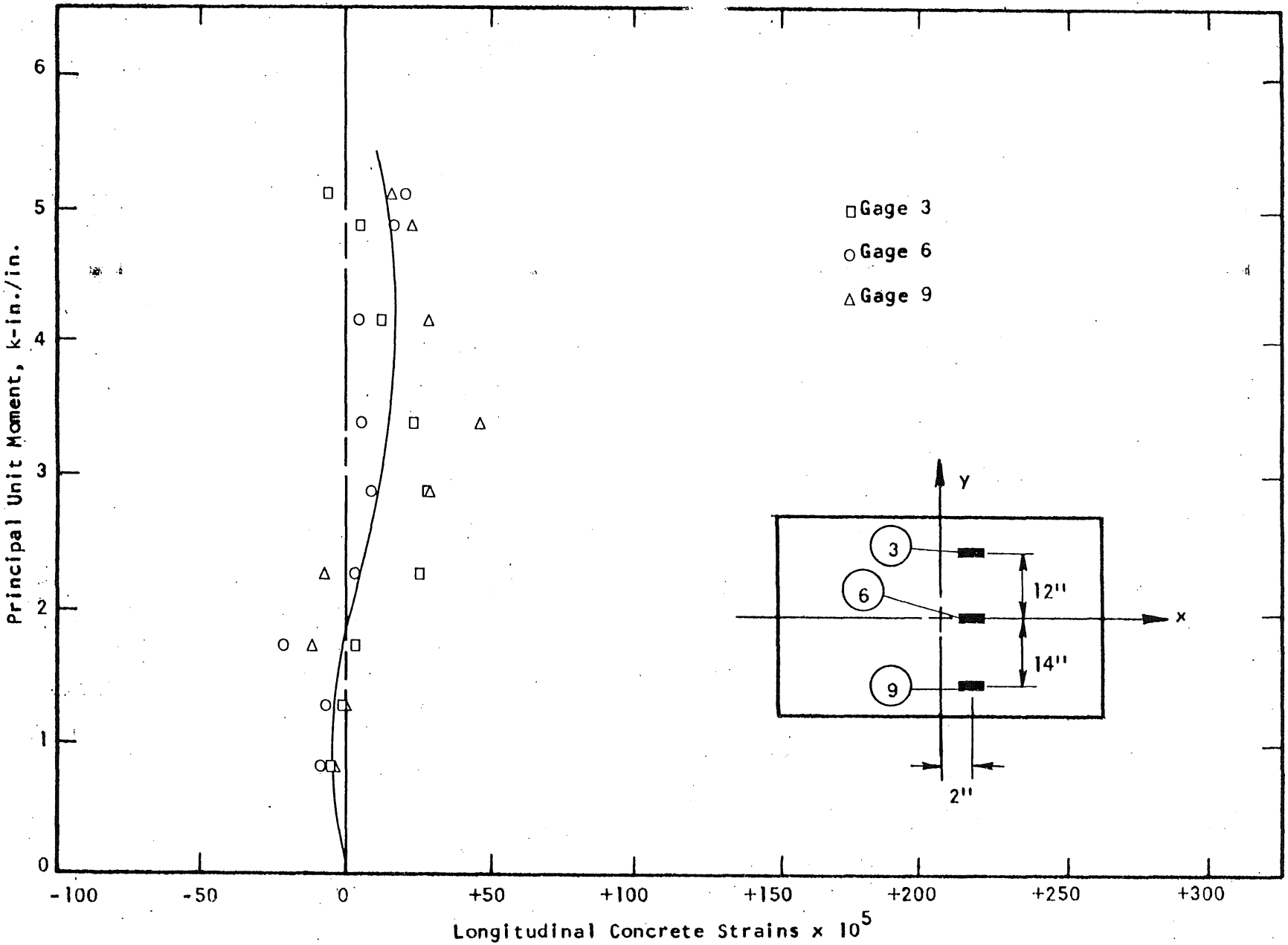

FIG. A.132 CONCRETE STRAIN PLOT, BOTTOM SIDE OF SPECIMEN B14

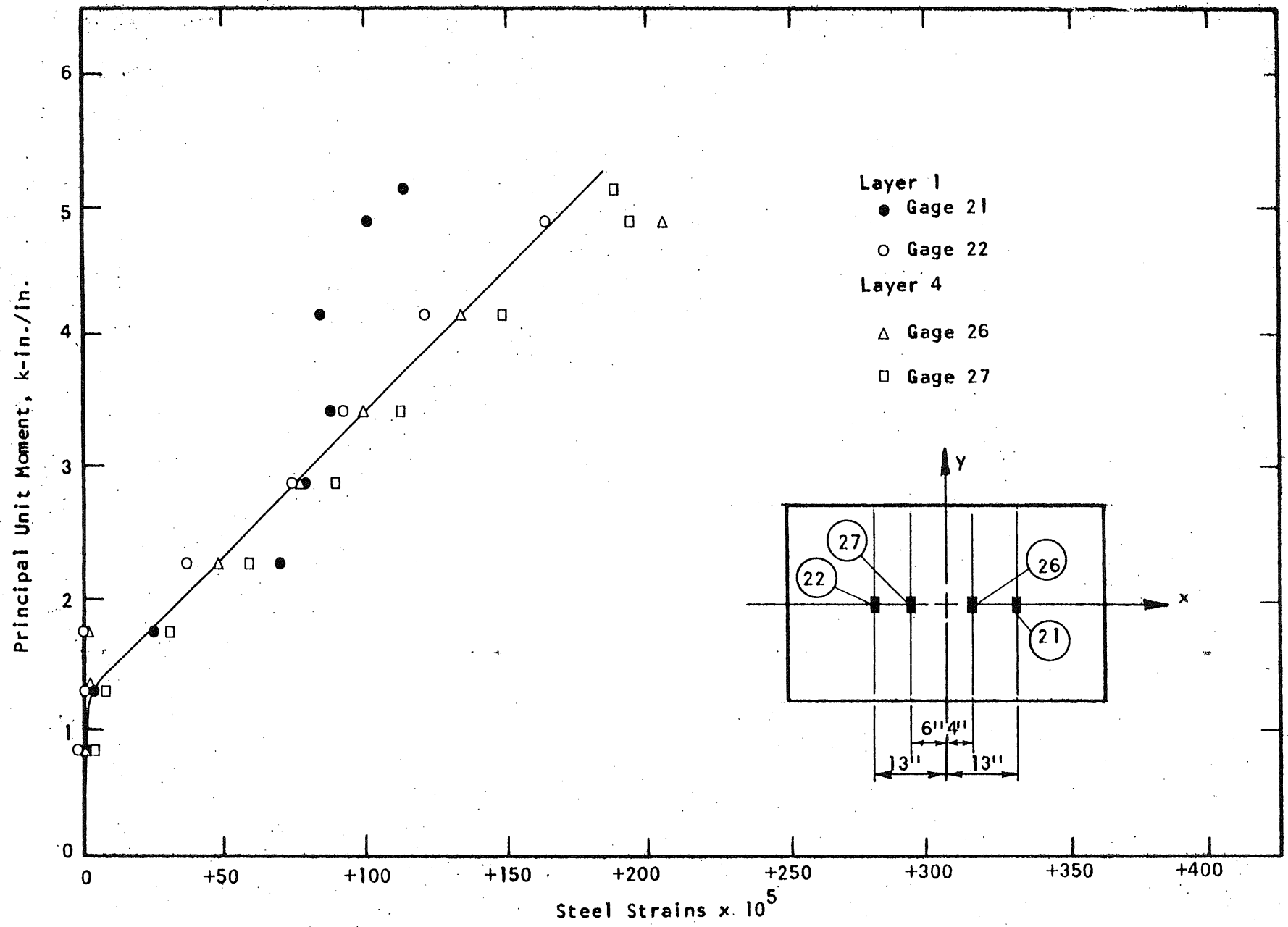

FIG. A.133 STEEL STRAIN PLOT, SPECIMEN B14

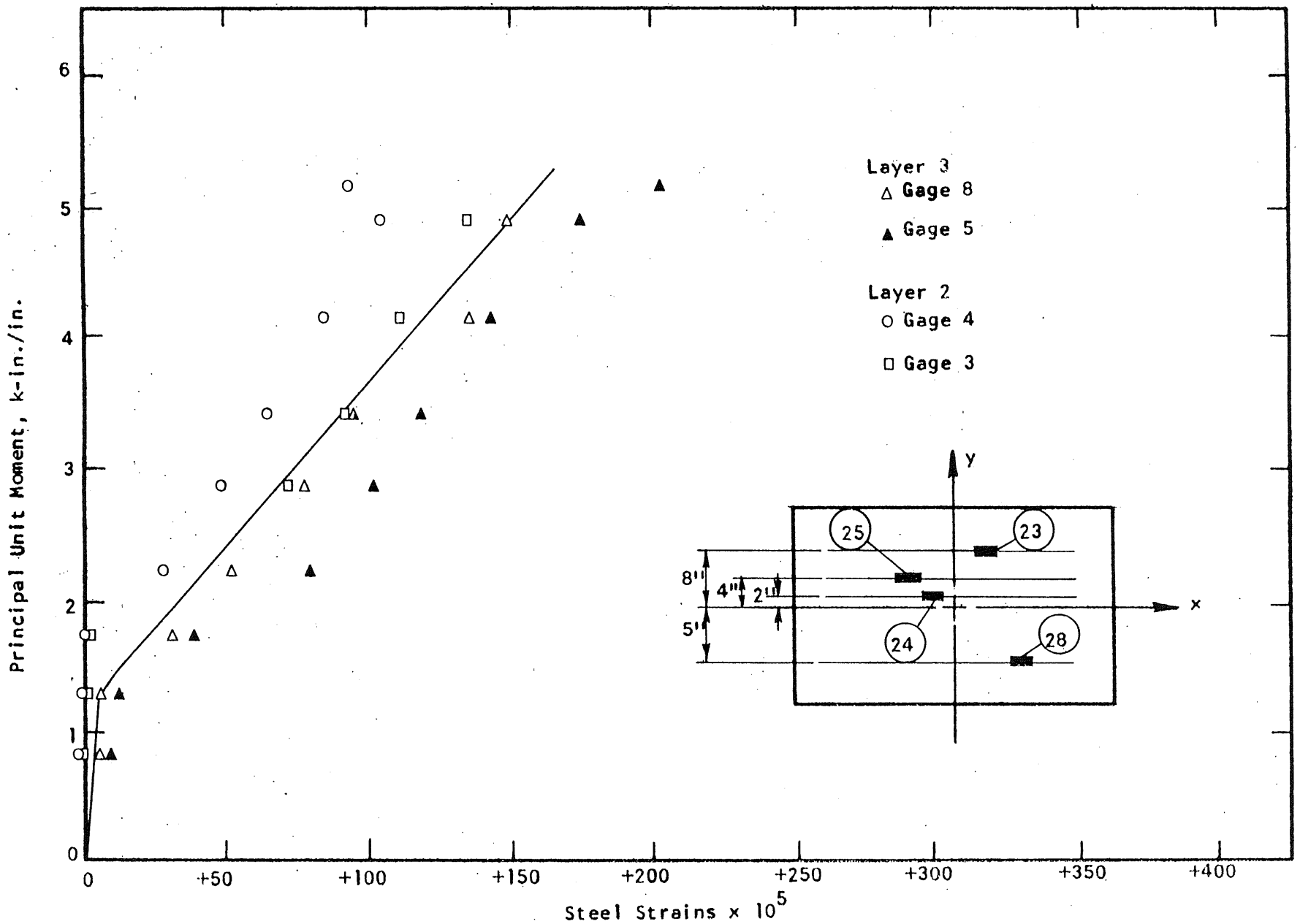

FIG. A.134 STEEL STRAIN PLOT, SPECIMEN B14

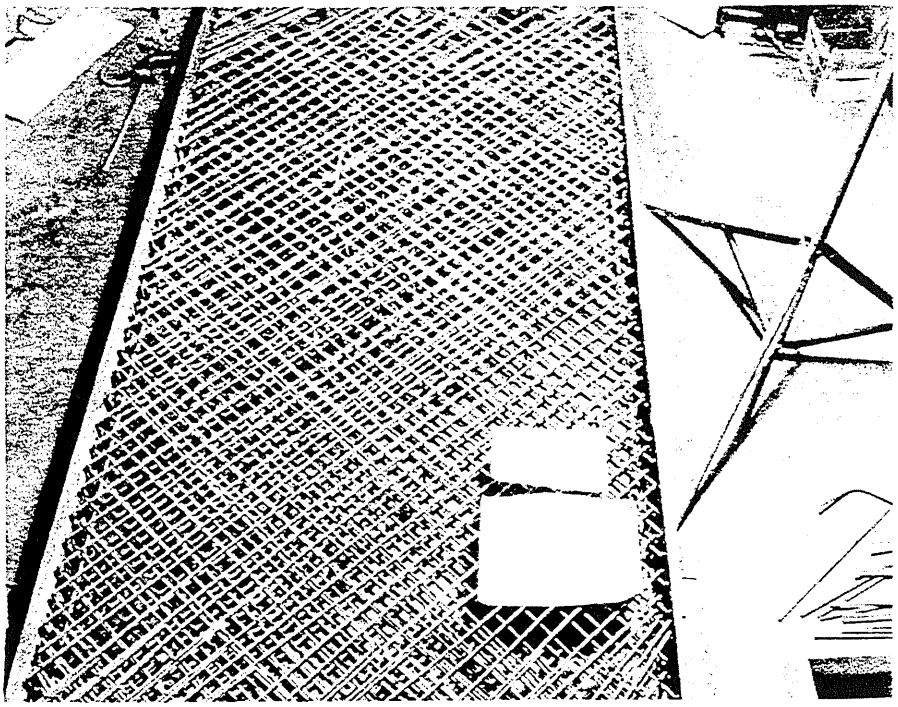

FIG. A.135 REINFORCEMENT IN SPECIMEN B15

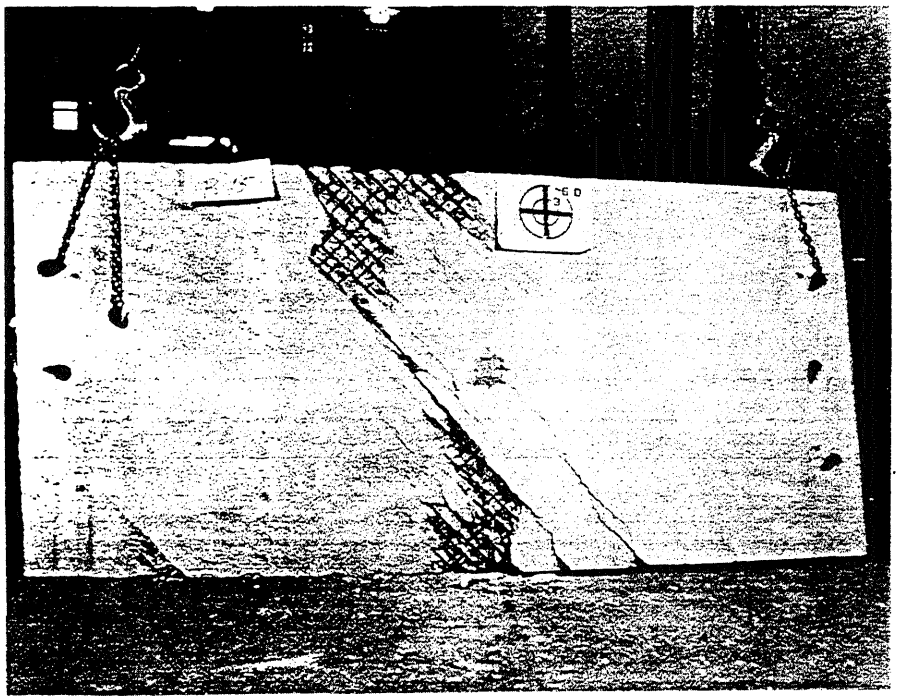

FIG. A.136 CRACK PATTERN IN BOTTOM SURFACE OF B15

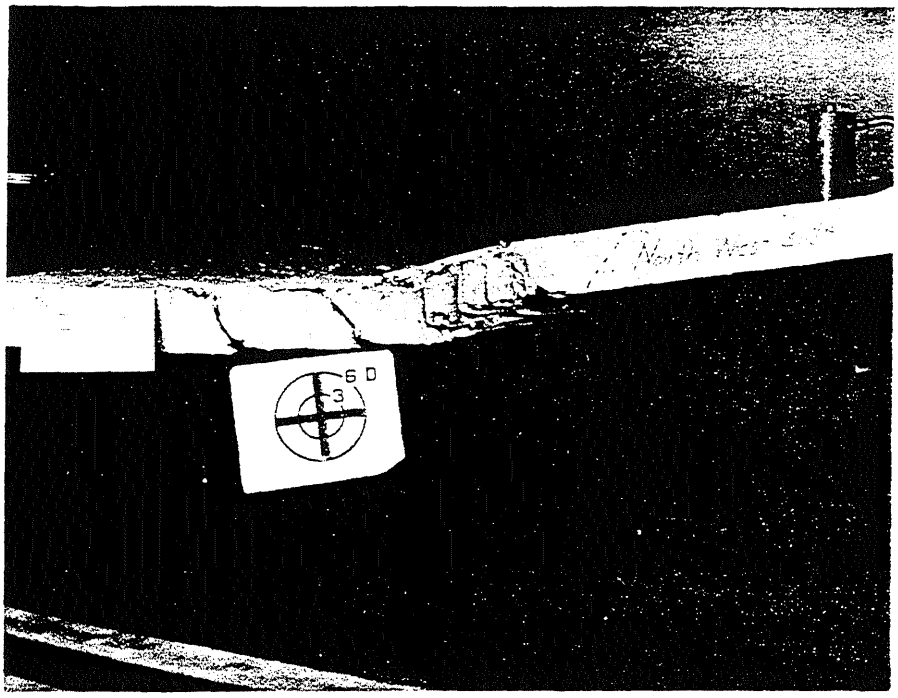

a

b

FIG. A.137 SIDE VIEWS OF SPECIMEN B15

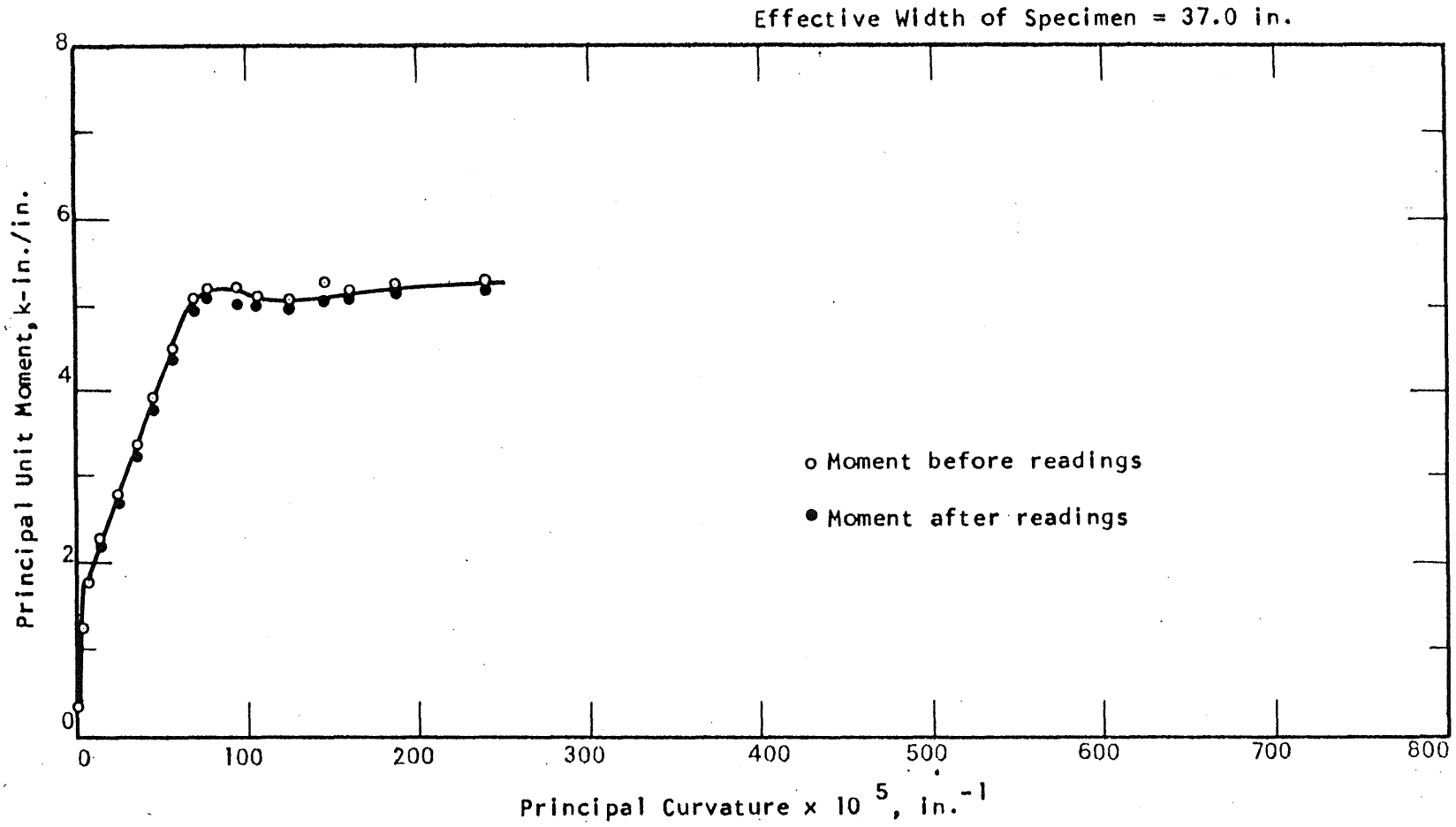

FIG. A.138 MOMENT-CURVATURE PLOT FOR SPECIMEN B15

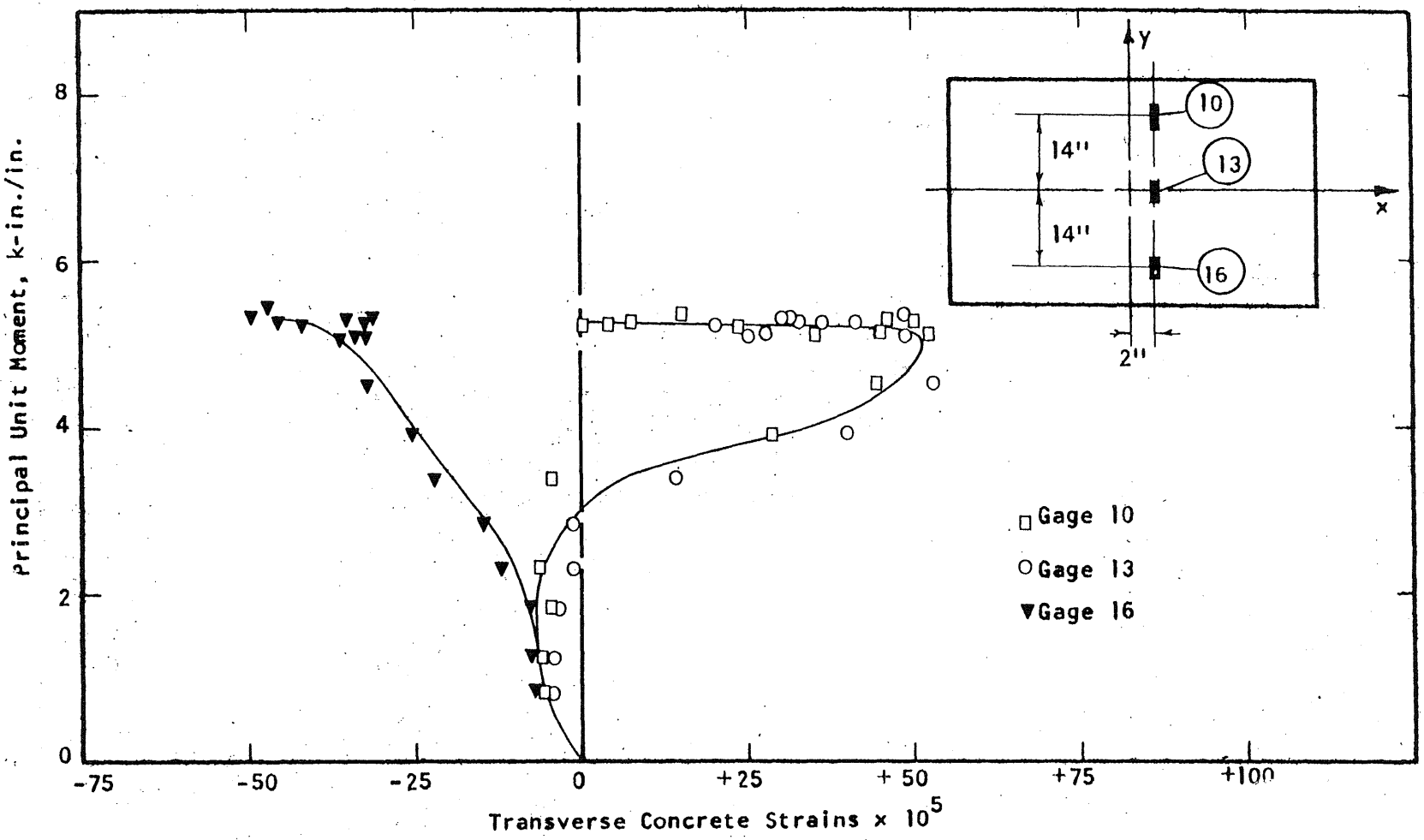

FIG. A.139 CONCRETE STRAIN PLOT, TOP SIDE OF SPECIMEN B15

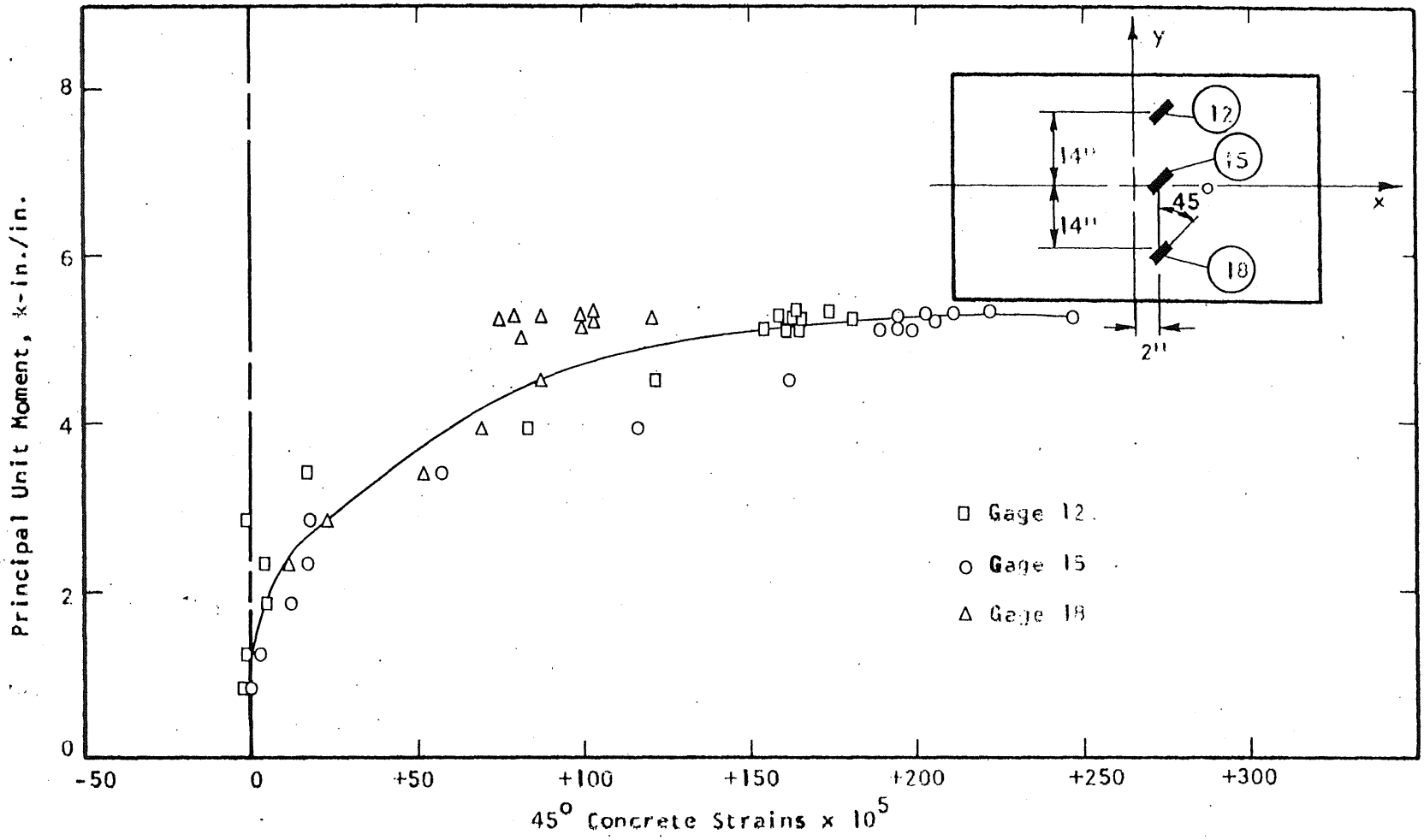

FIG. A.140 CONCRETE STRAIN PLOT, TOP SIDE OF SPECIMEN B15

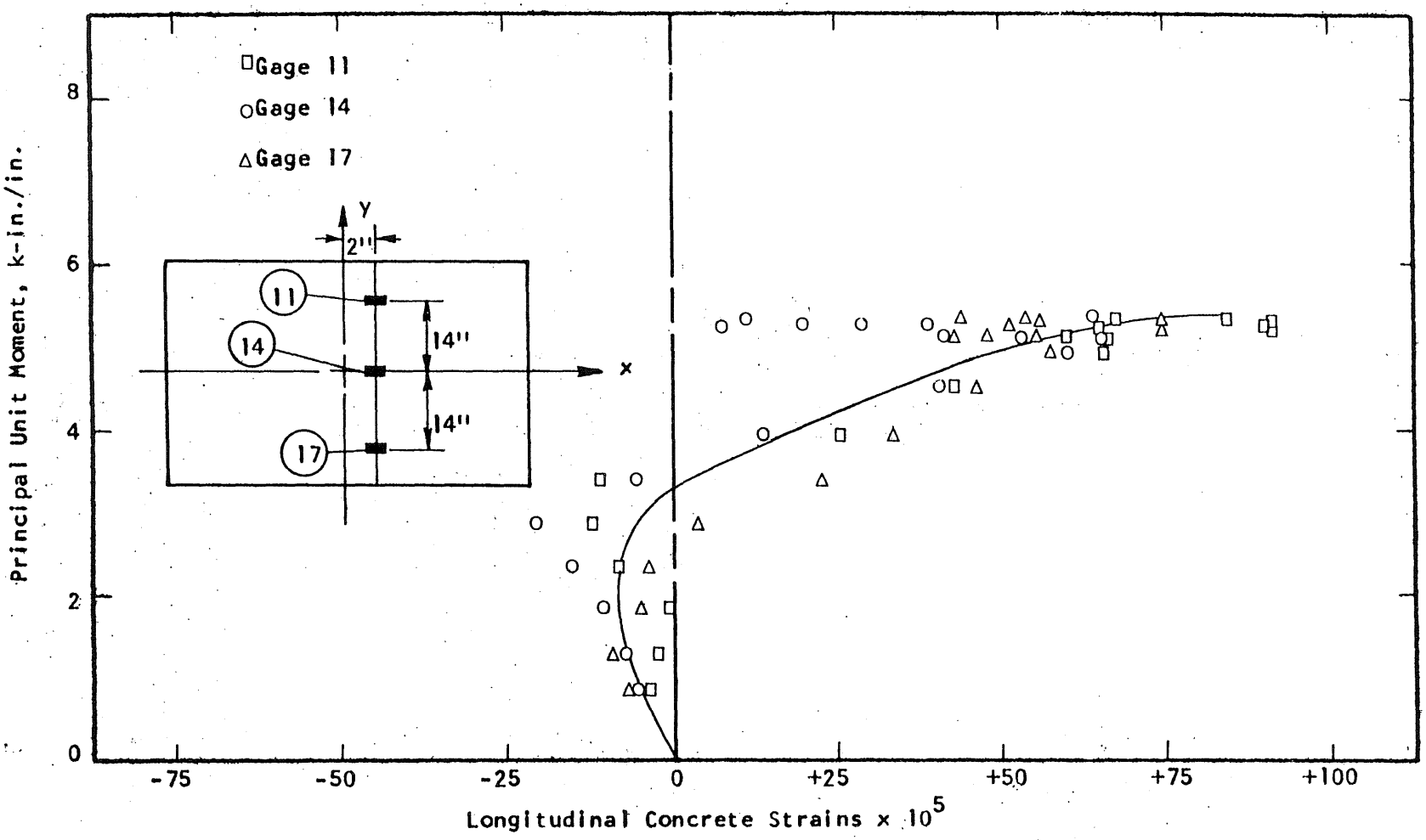

FIG. A.141 CONCRETE STRAIN PLOT, TOP SIDE OF SPECIMEN B15

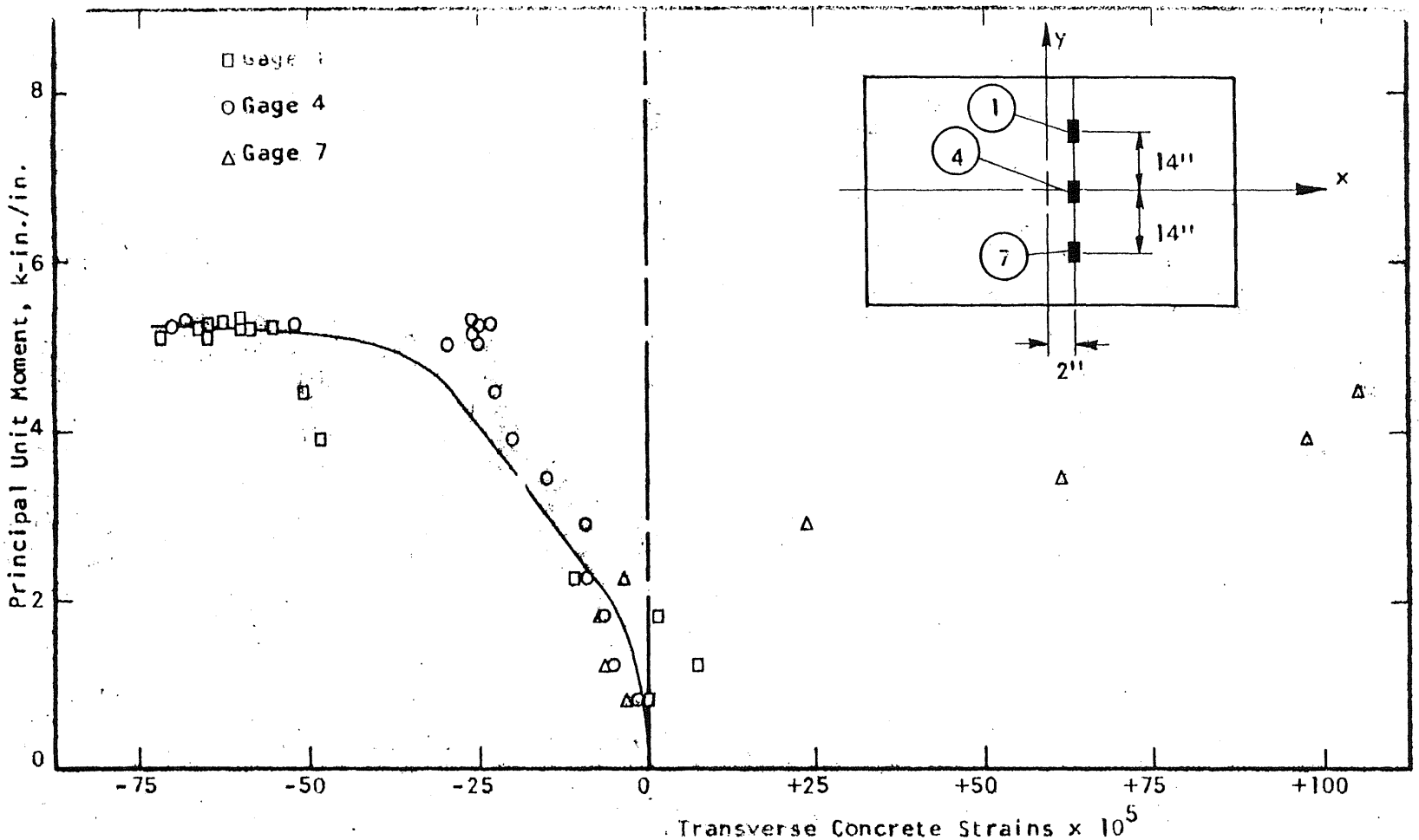

FIG. A.142 CONCRETE STRAIN PLOT, BOTTOM SIDE OF SPECIMEN S15

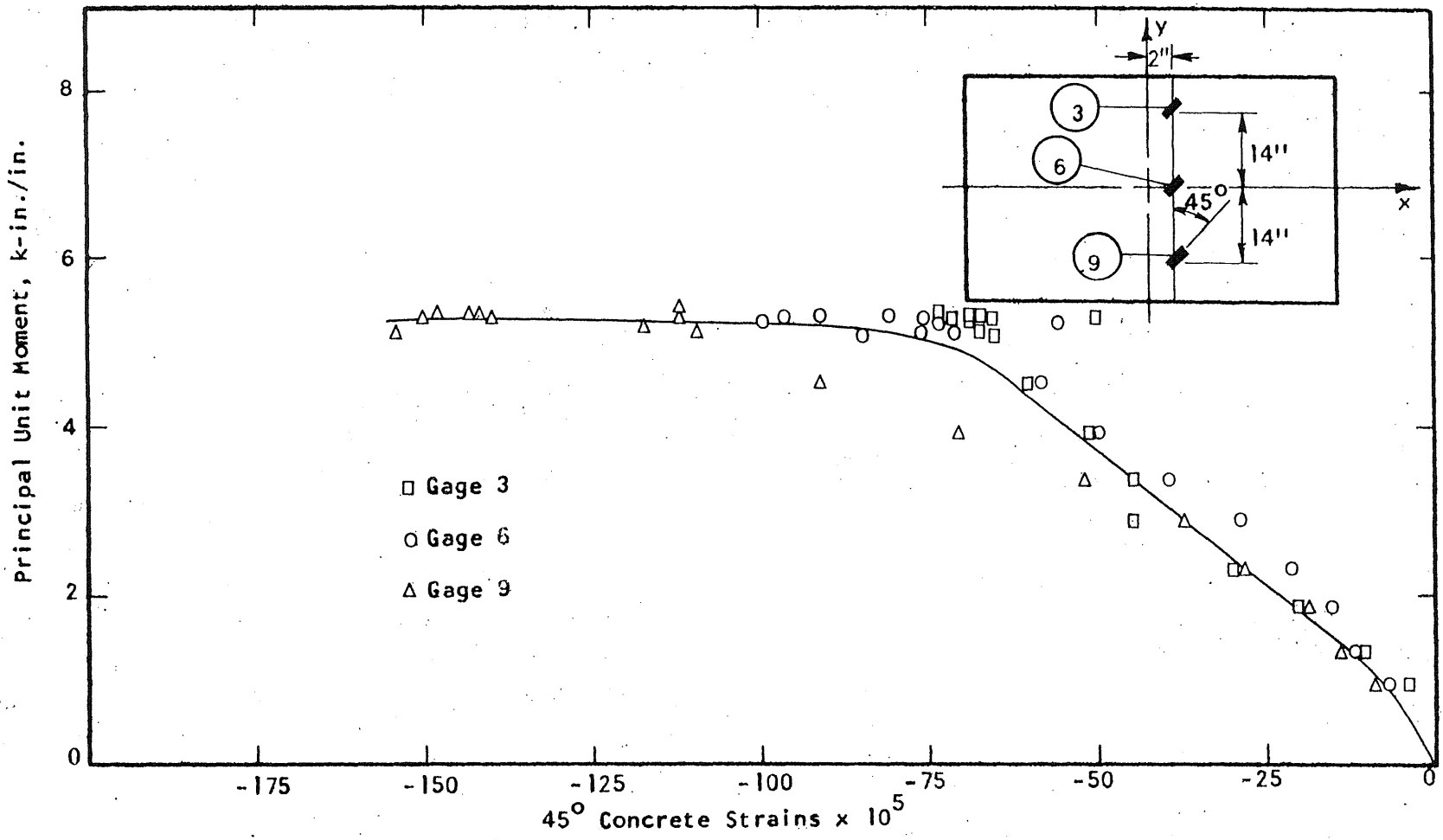

FIG. A.143 CONCRETE STRAIN PLOT, BOTTOM SIDE OF SPECIMEN B15

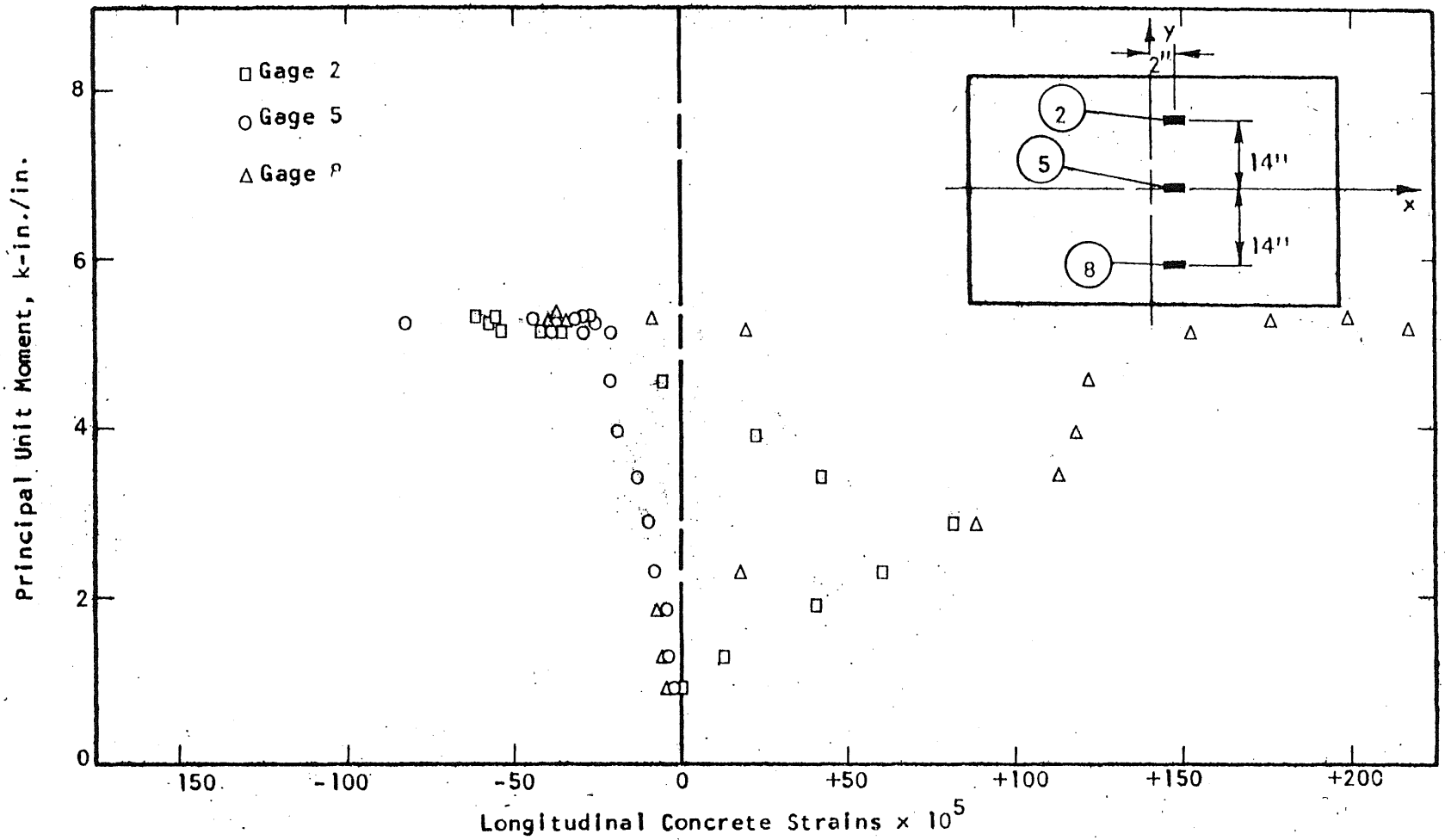

FIG. A.144 CONCRETE STRAIN PLOT, BOTTOM SIDE OF SPECIMEN B15

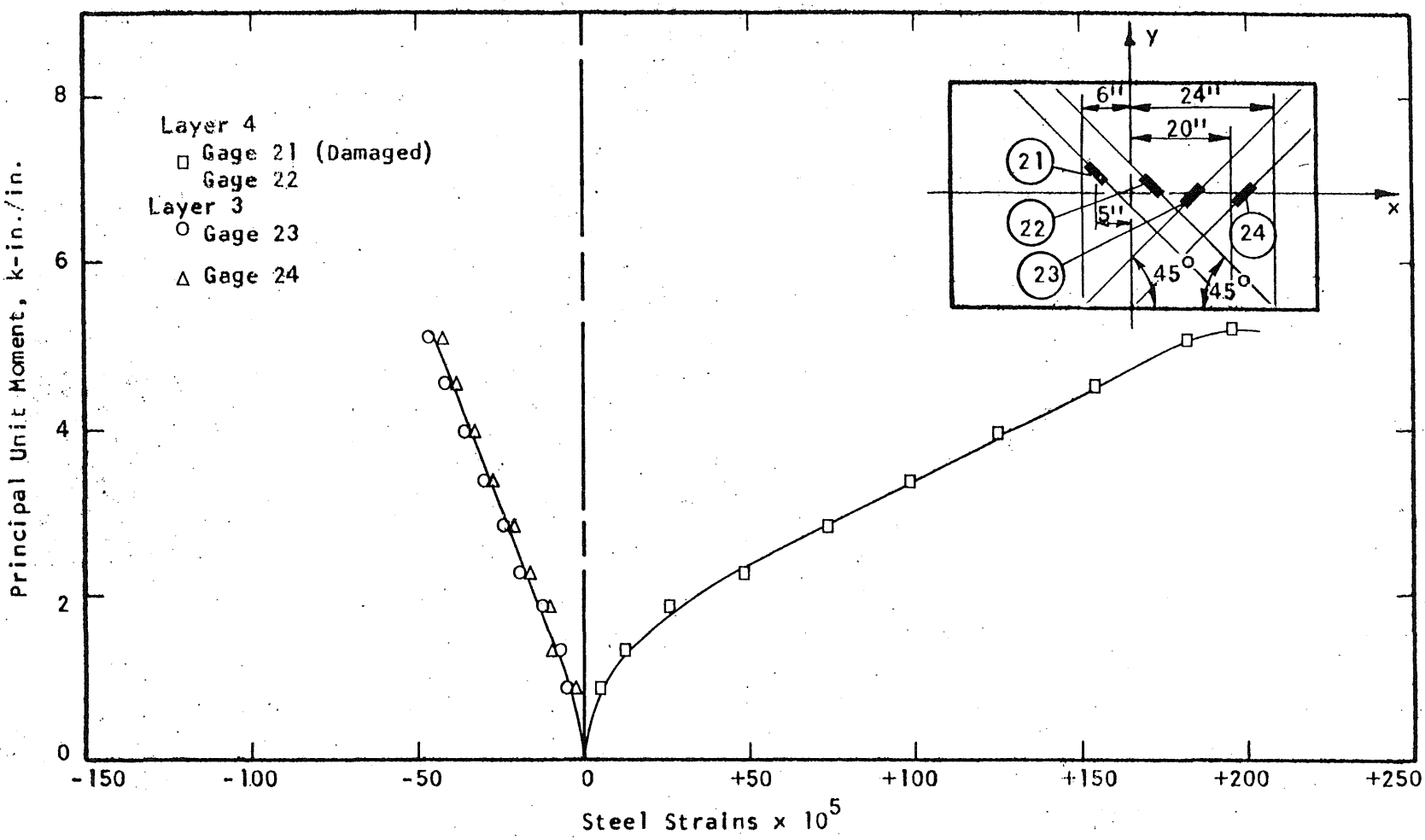

FIG. A.145 STEEL STRAIN PLOT, SPECIMEN B15

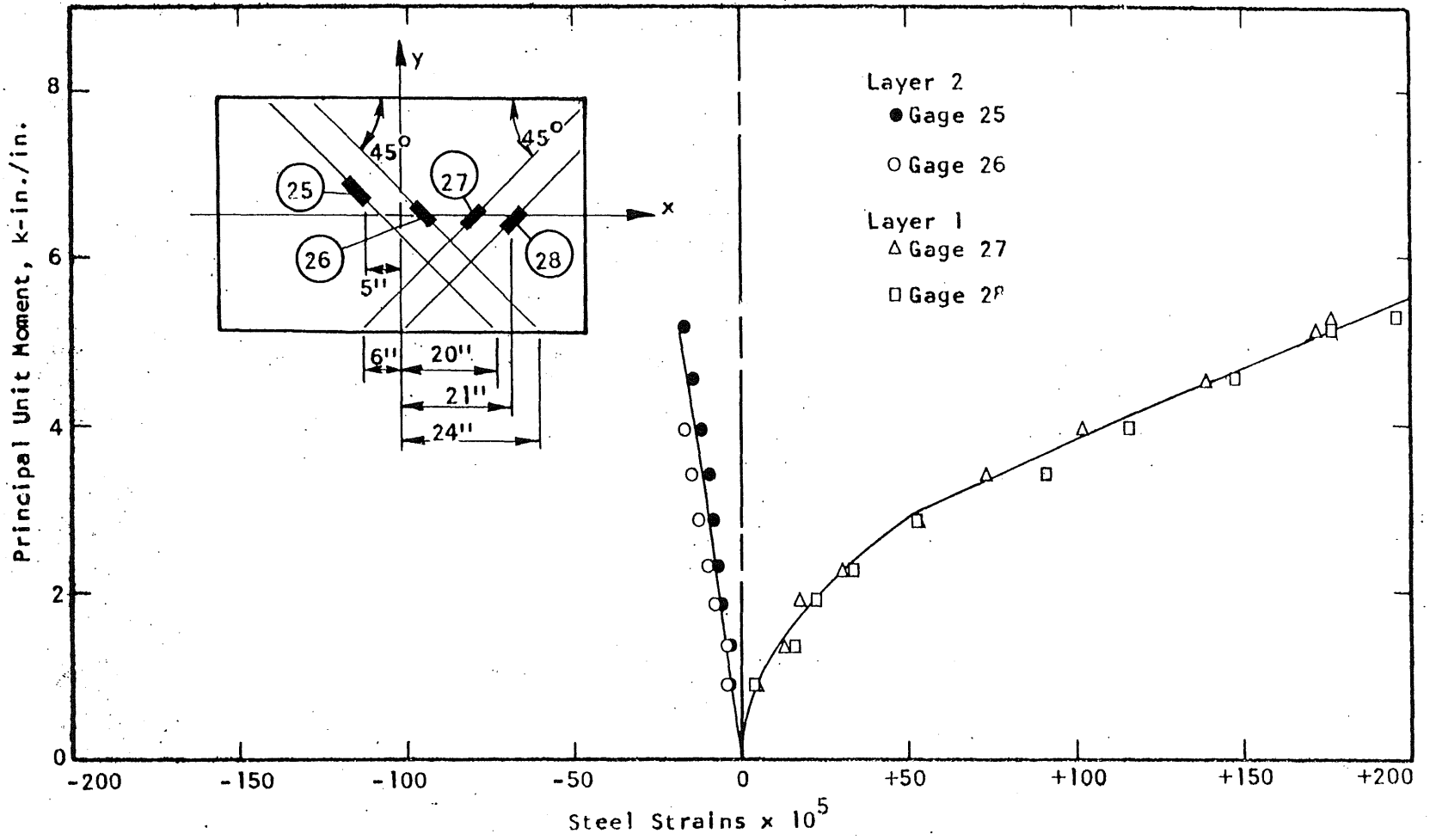

FIG. A.146 STEEL STRAIN PLOT, SPECIMEN B15

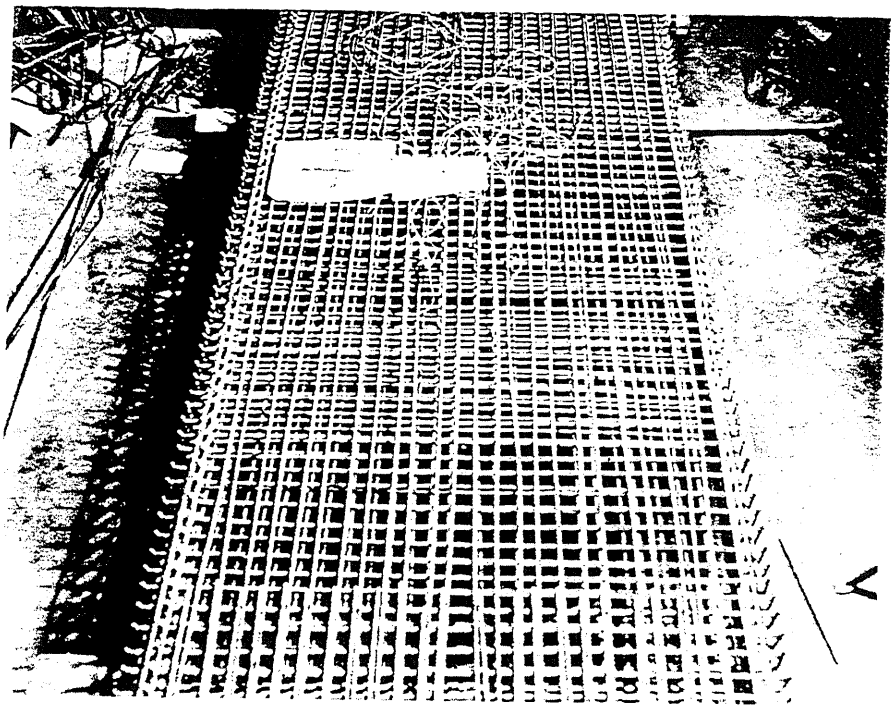

a Reinforcement with Strain Gages Connected

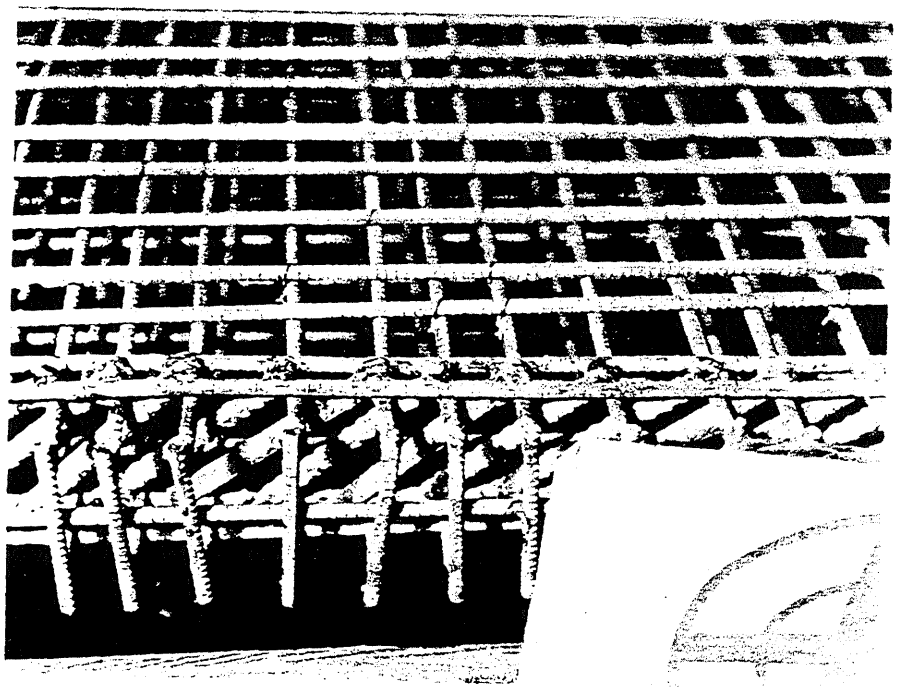

b Close-up Side View of Reinforcement in B16

FIG. A.147 . REINFORCEMENT IN SPECIMEN B16

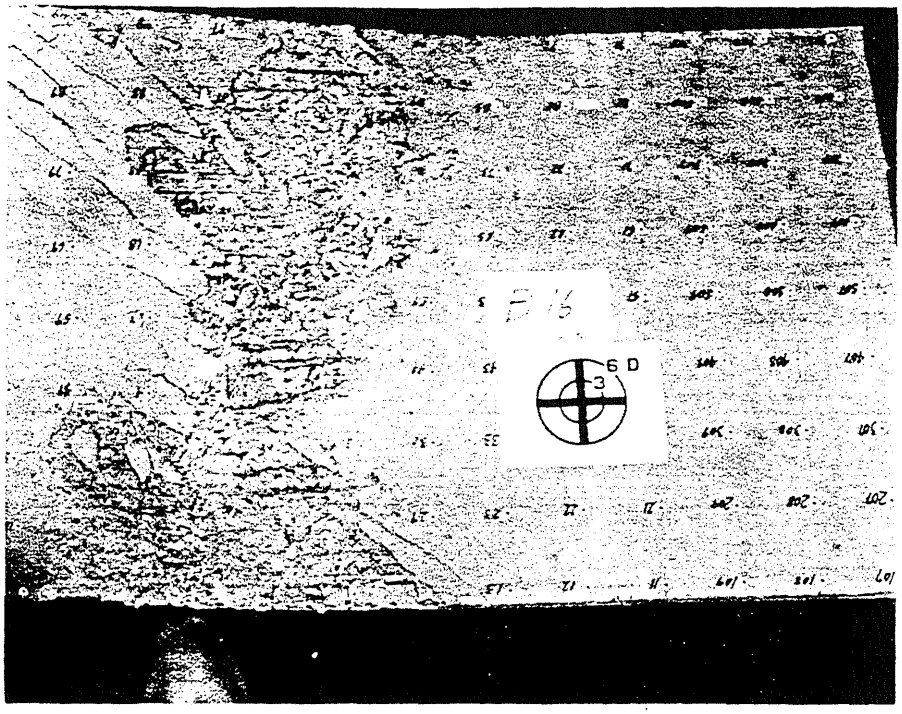

a Crack Pattern in Top Surface of B16

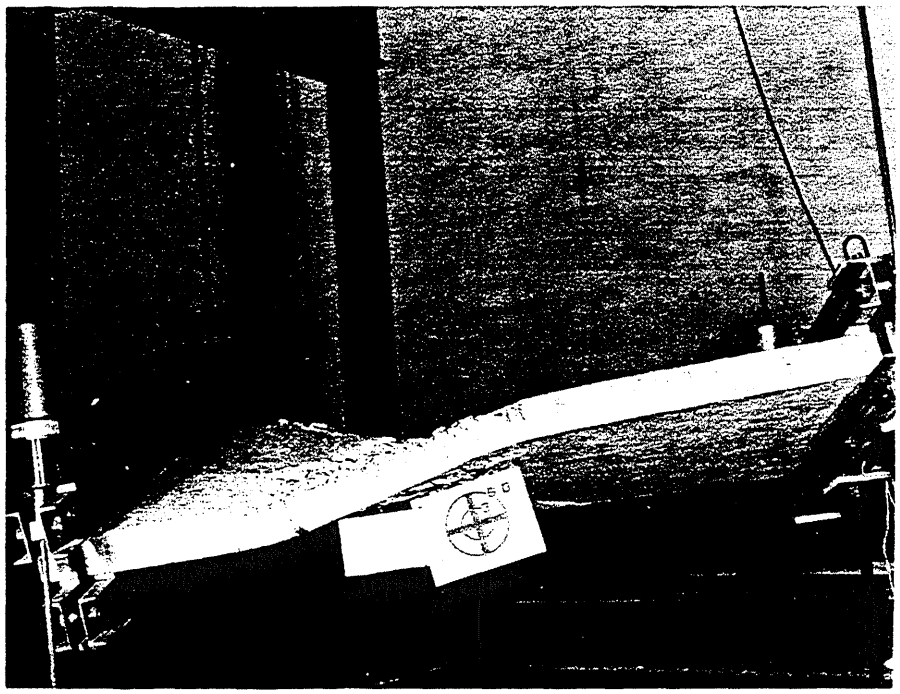

b Side View of Cracked Specimen B16

FIG. A.148 CRACK PATTERN OF SPECIMEN B16

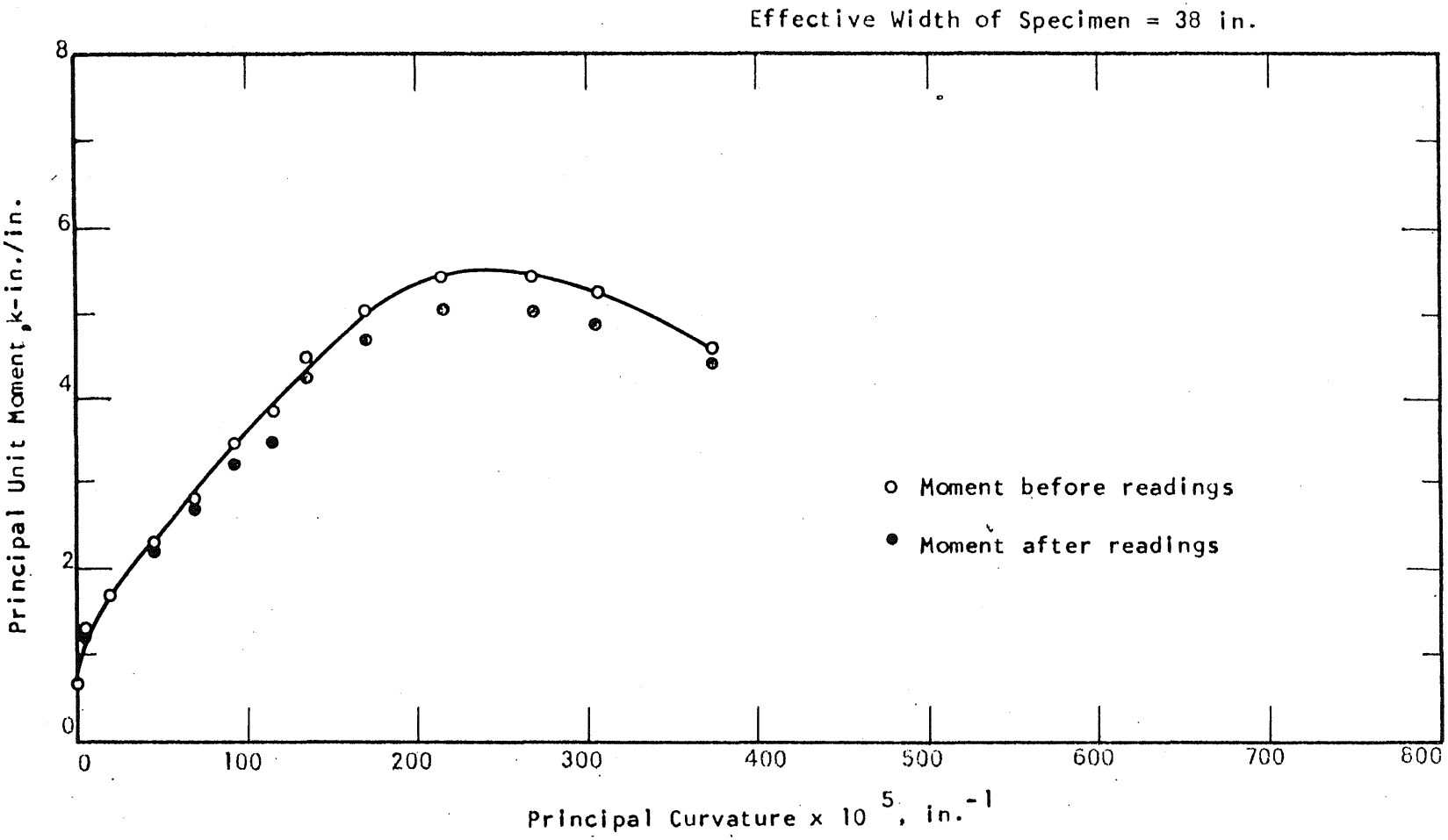

FIG. A.149 MOMENT-CURVATURE PLOT FOR SPECIMEN B16

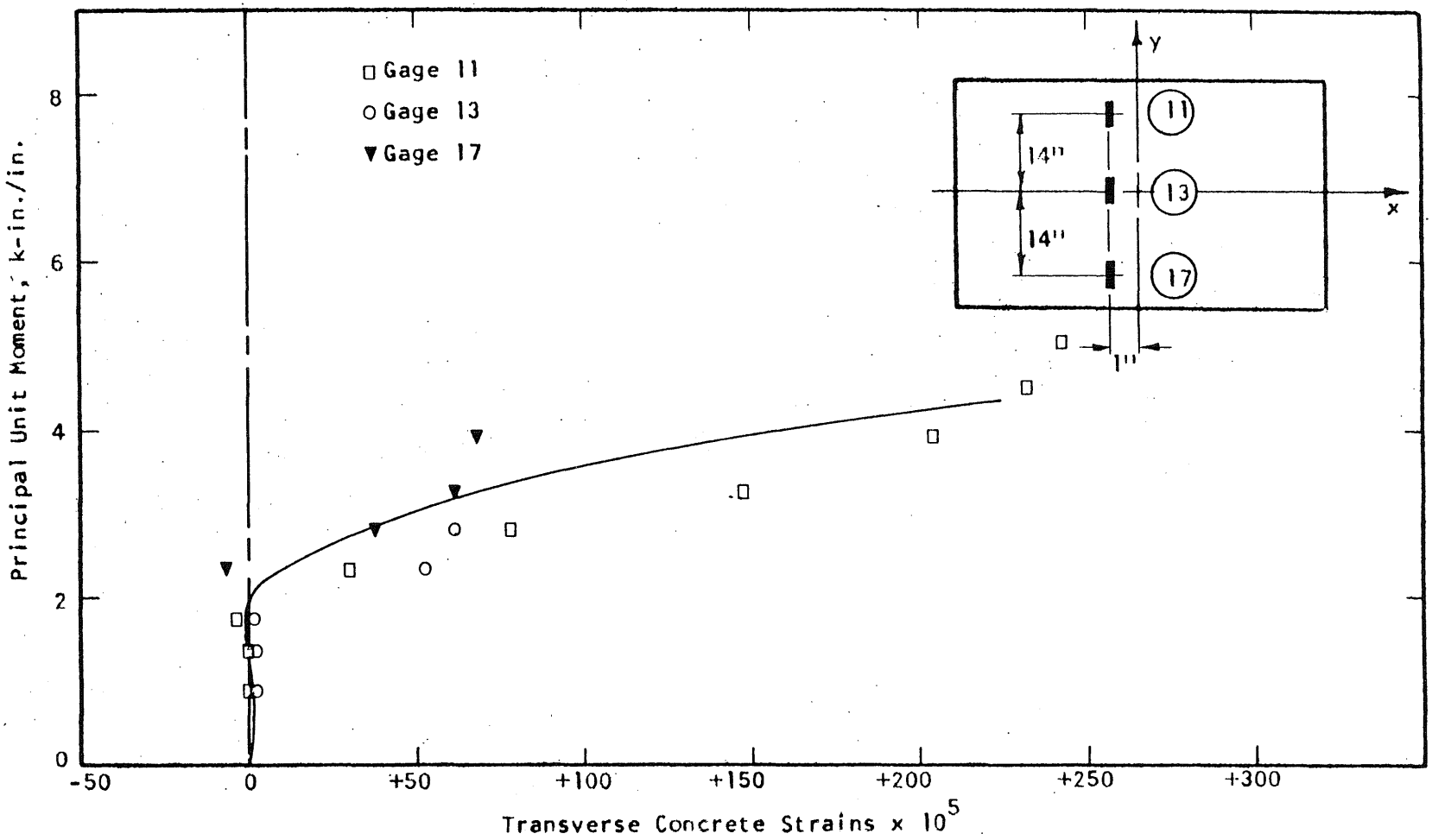

FIG. A.150 CONCRETE STRAIN PLOT, TOP SIDE OF SPECIMEN B16

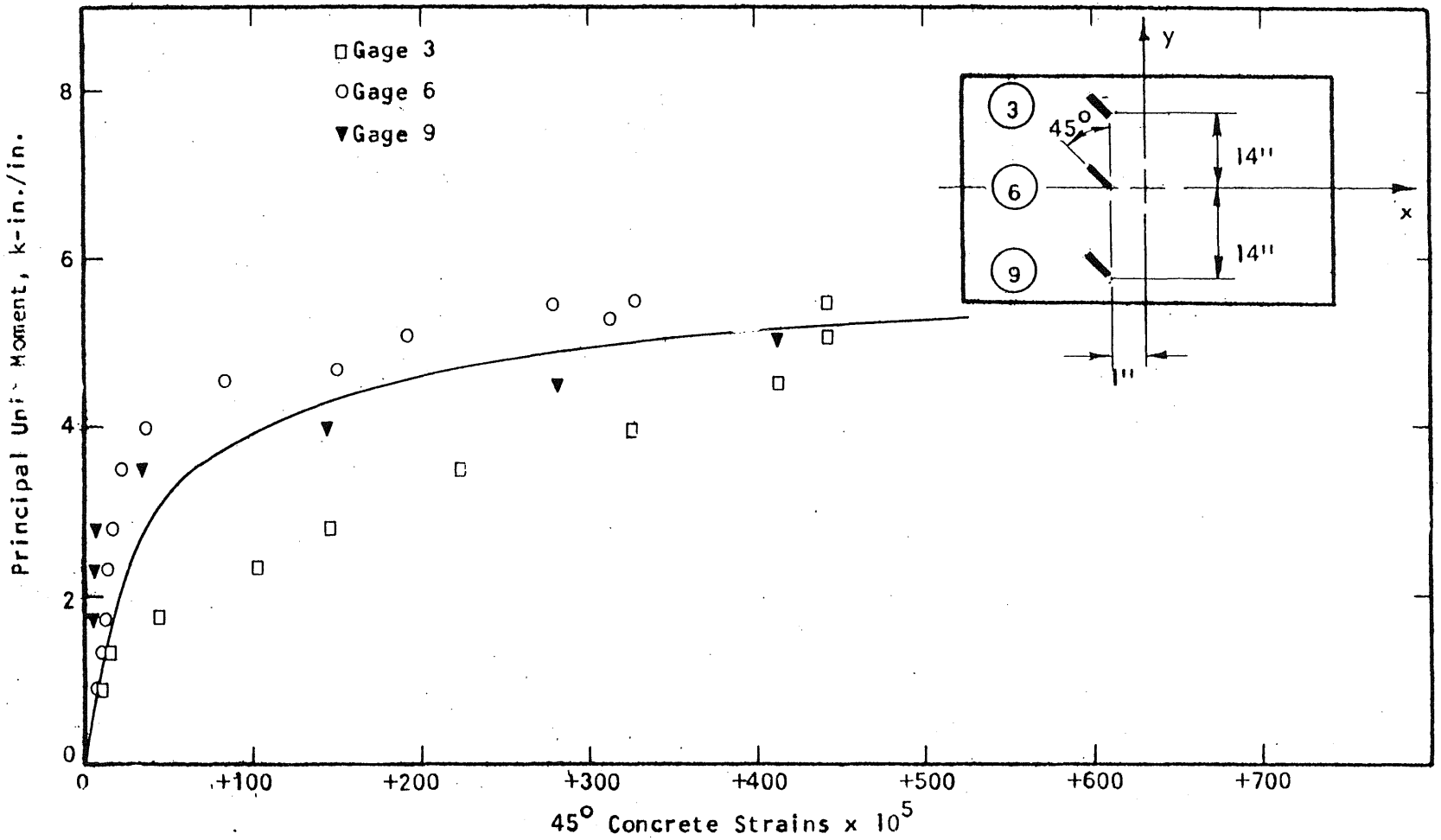

FIG. A.151 CONCRETE STRAIN PLOT, BOTTOM SIDE OF SPECIMEN B16

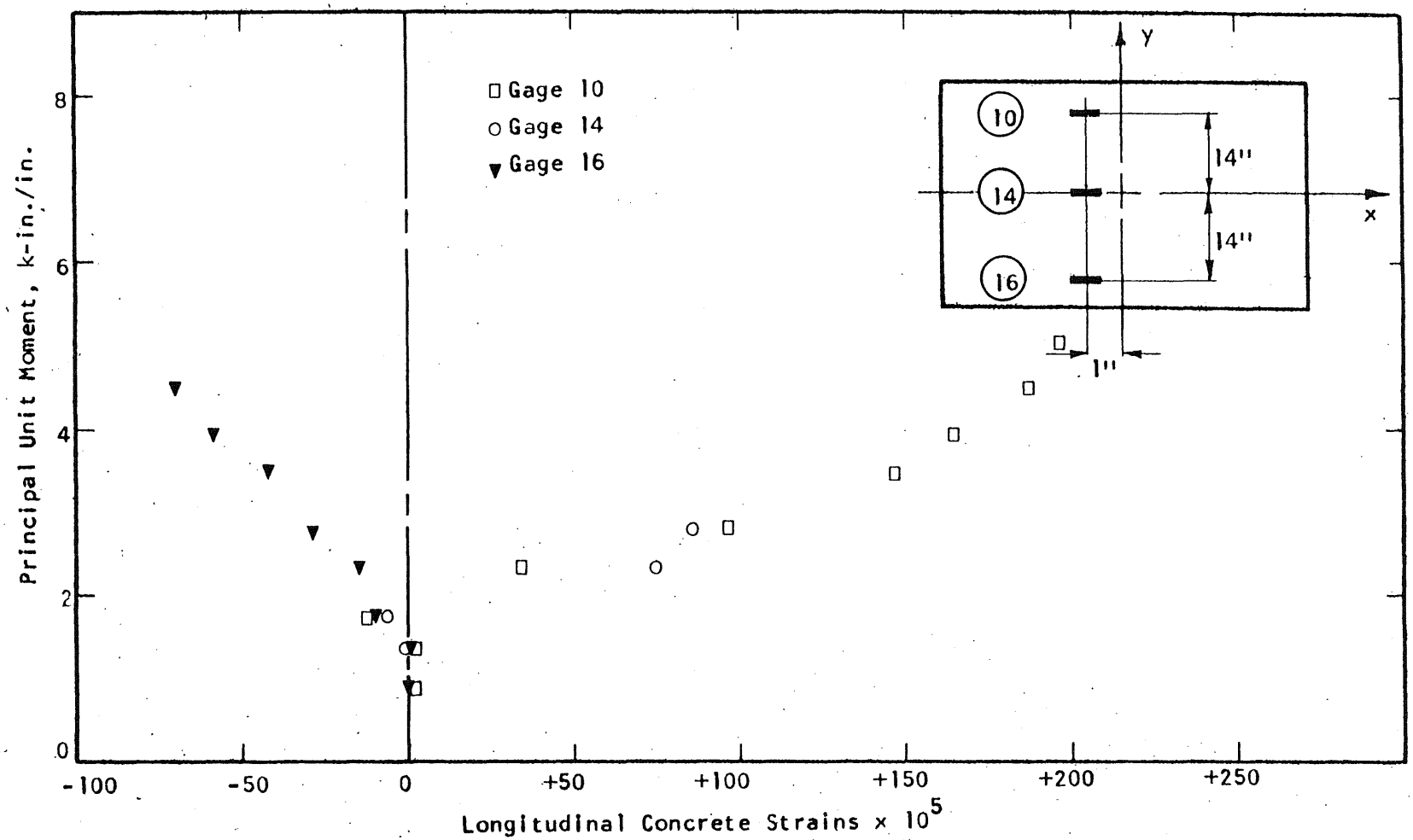

FIG. A.152 CONCRETE STRAIN PLOT, TOP SIDE OF SPECIMEN B16

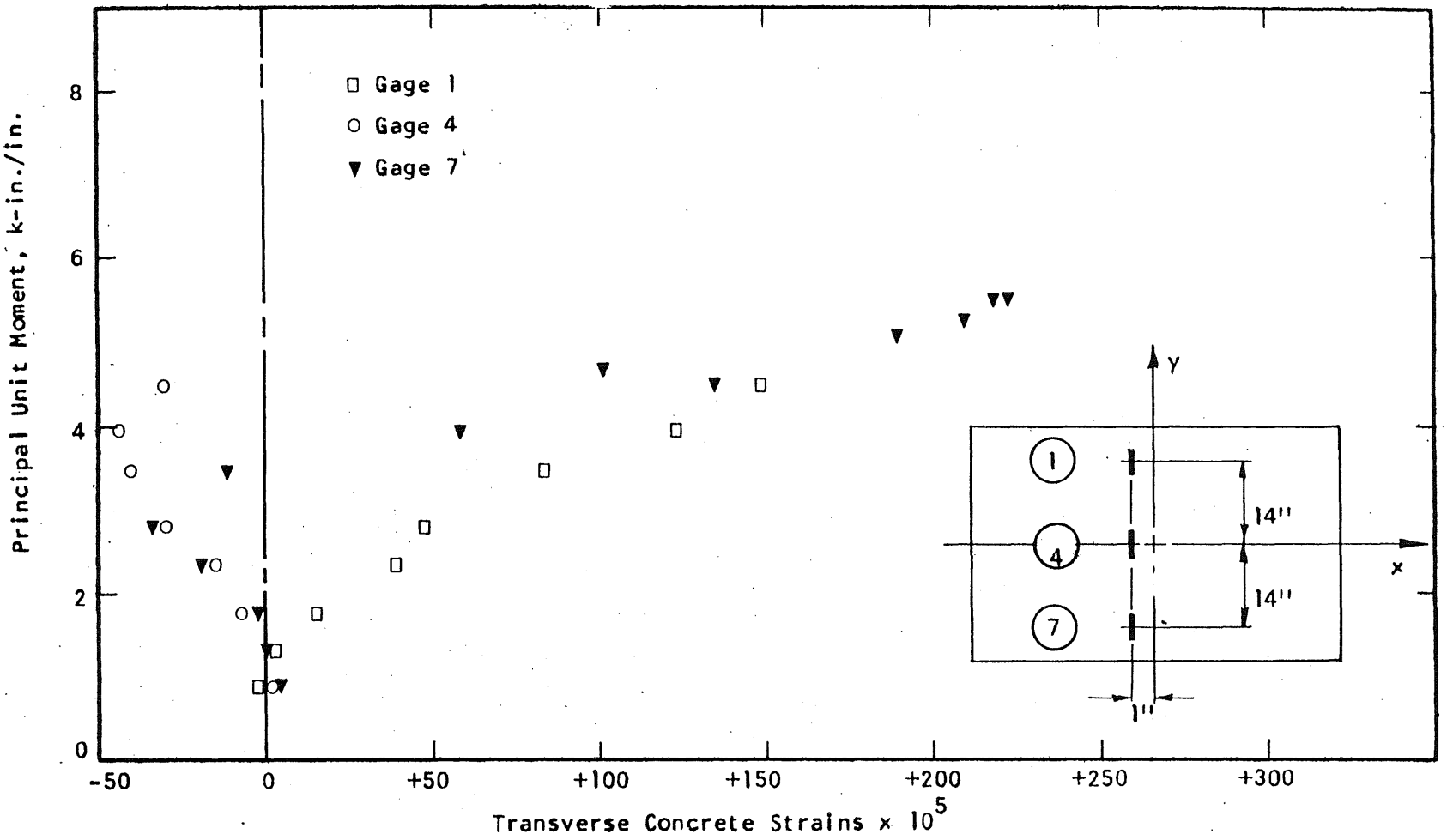

FIG. A.153 CONCRETE STRAIN PLOT, BOTTOM SIDE OF SPECIMEN B16

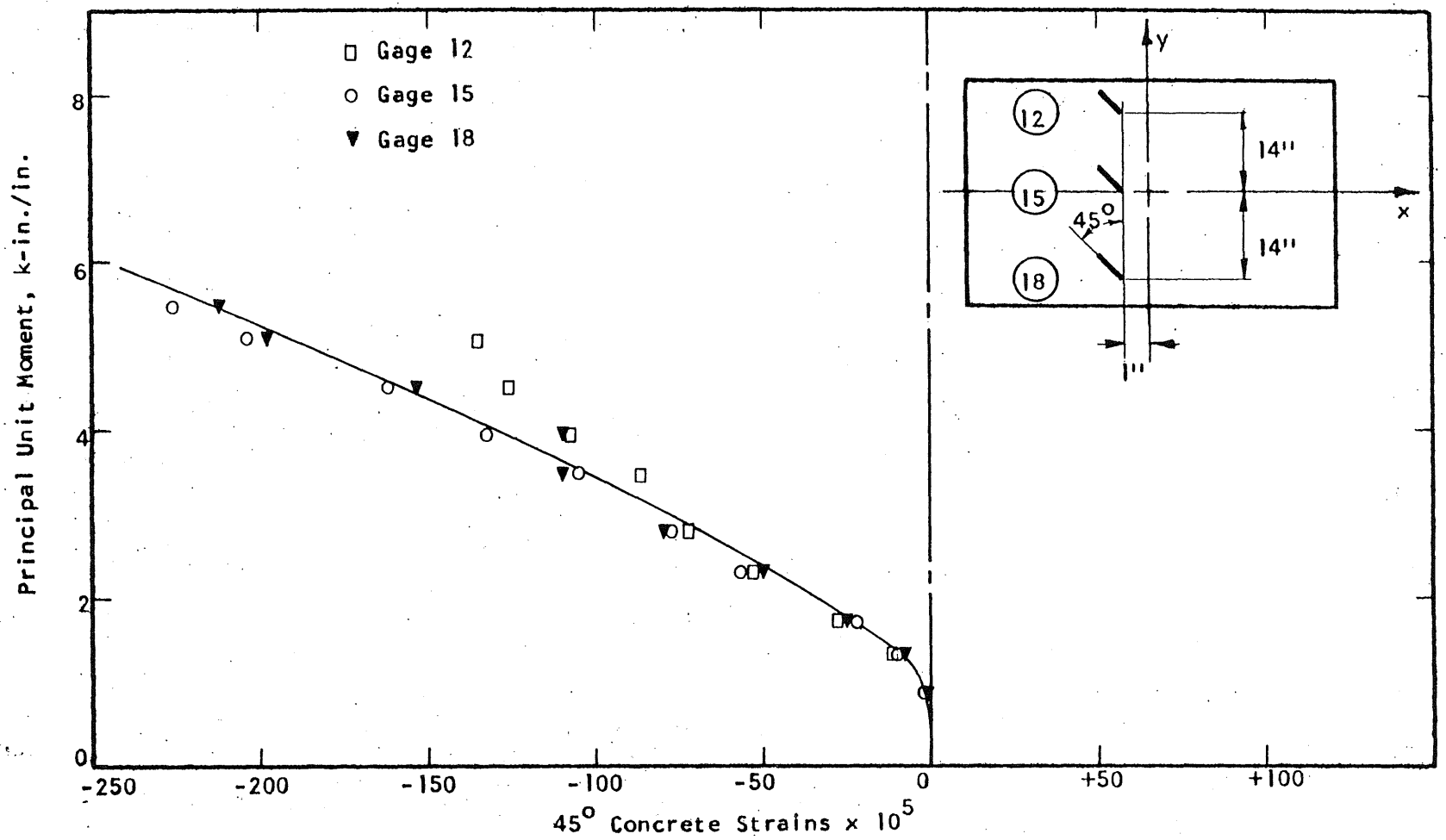

FIG. A.154 CONCRETE STRAIN PLOT, TOP SIDE OF SPECIMEN B16

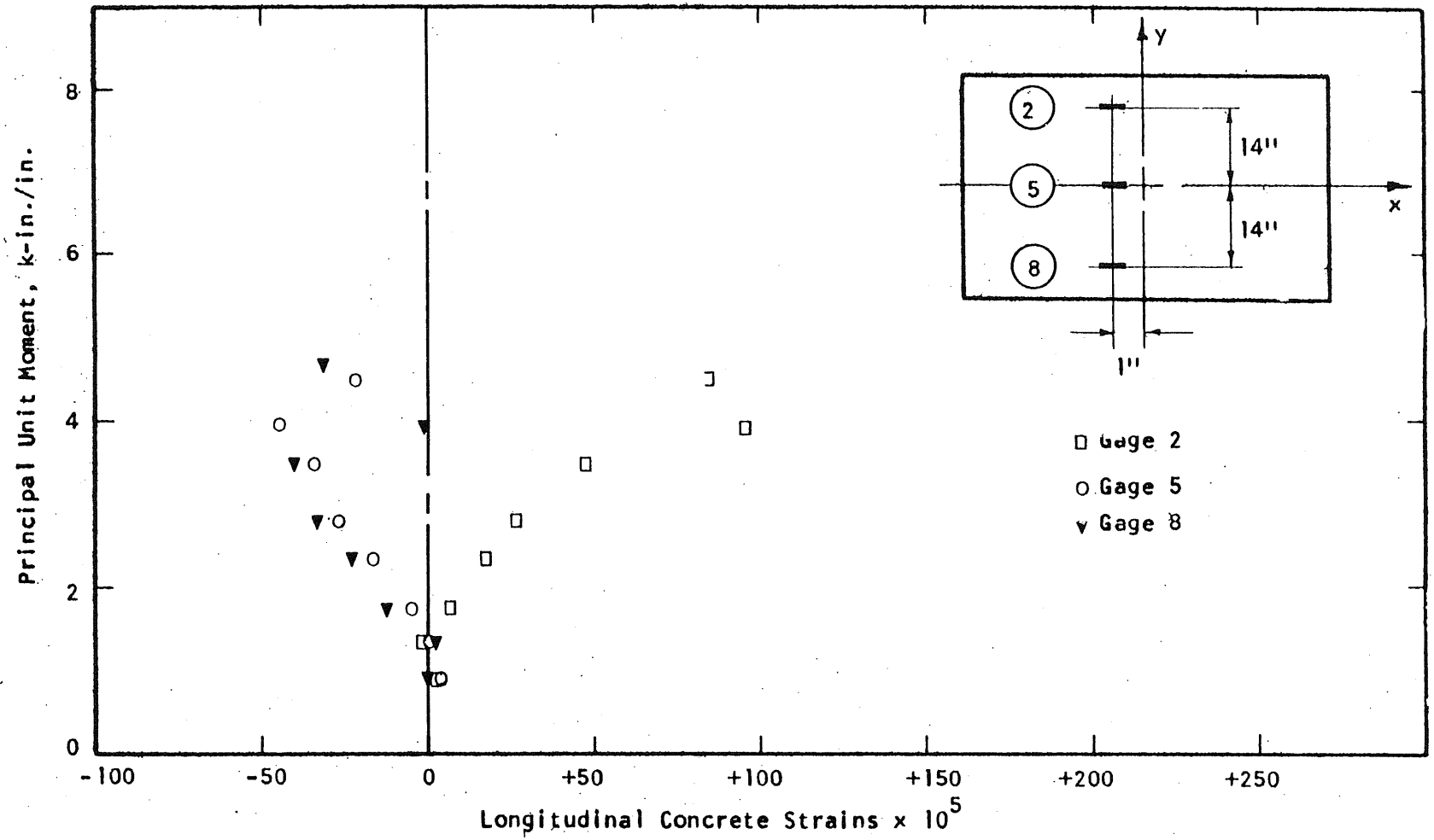

FIG. A.155 CONCRETE STRAIN PLOT, BOTTOM SIDE OF SPECIMEN B16

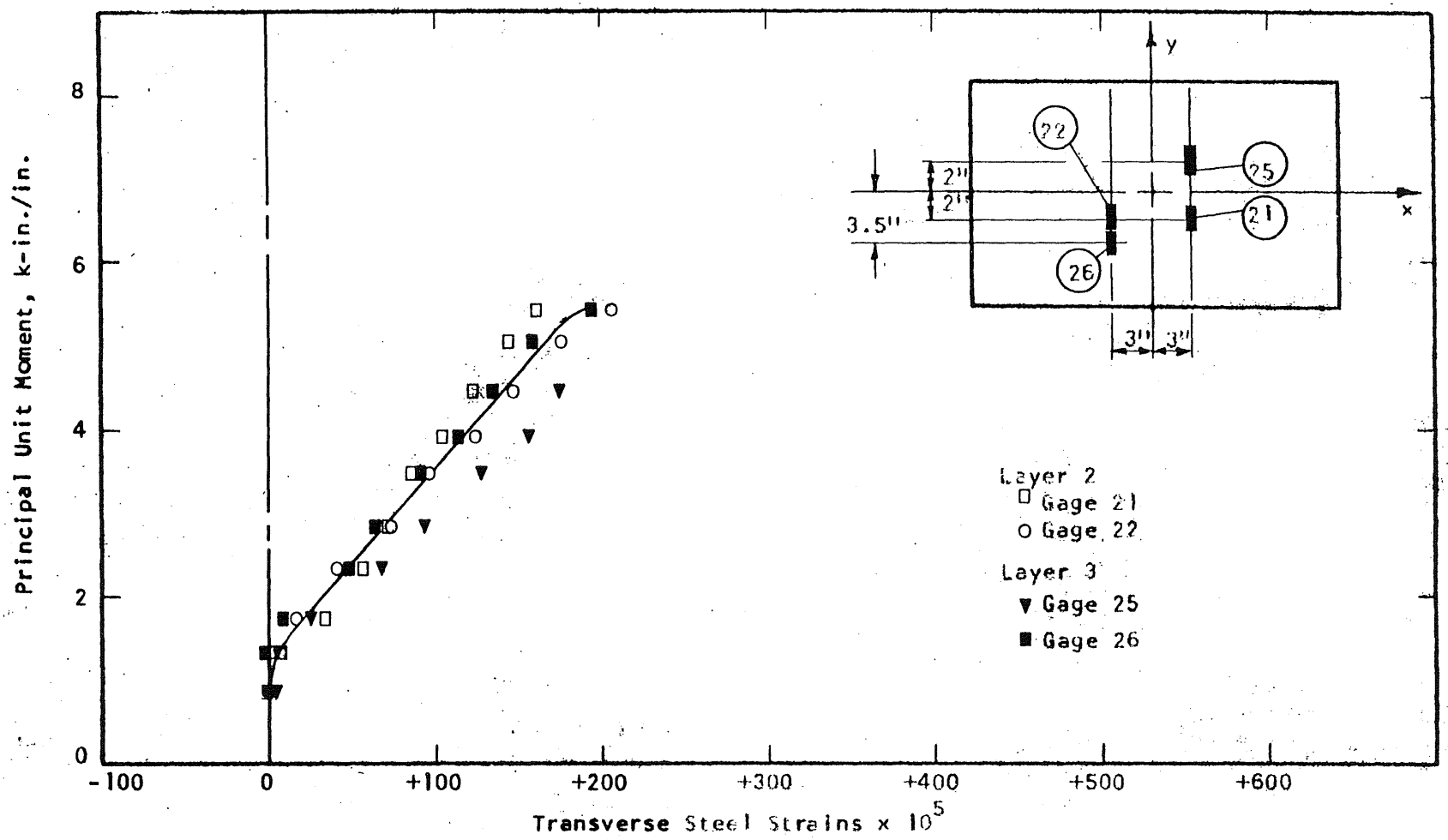

FIG. A.156 STEEL STRAIN PLOT, SPECIMEN B16

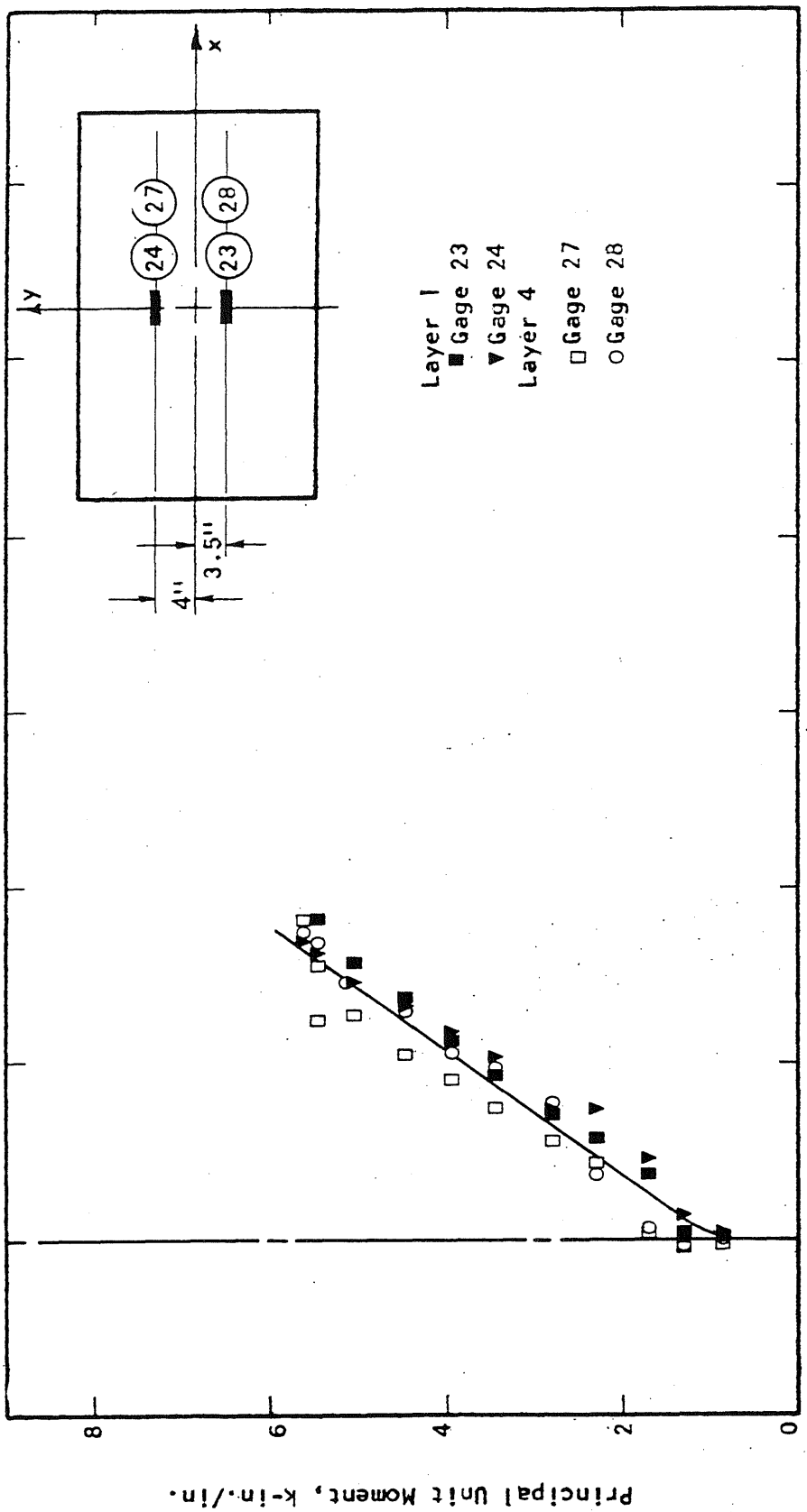

FIG. A.157 STEEL STRAIN PLOT, SPECIMEN B16

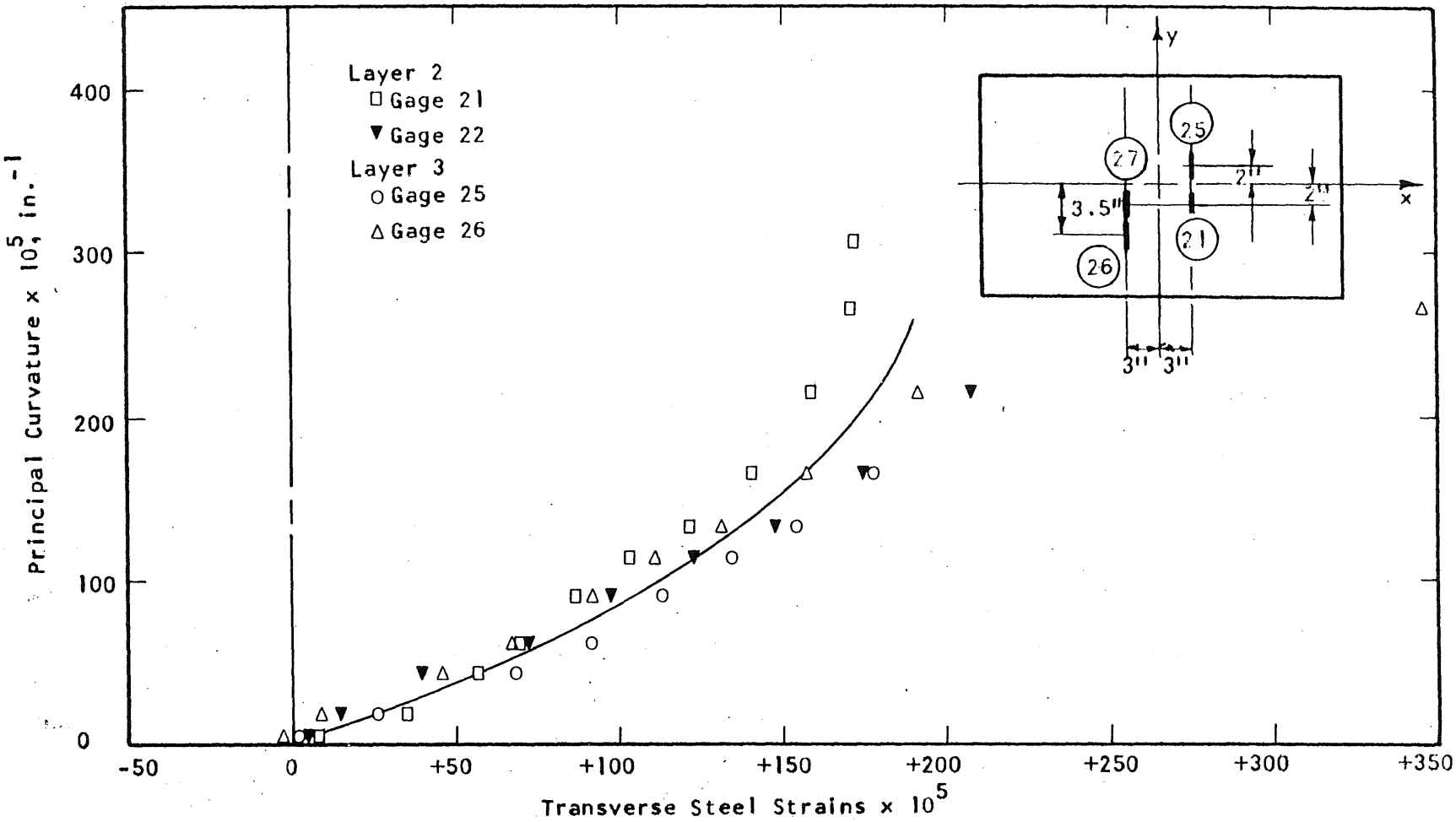

FIG. A.158 STEEL STRAIN PLOT, SPECIMEN B16

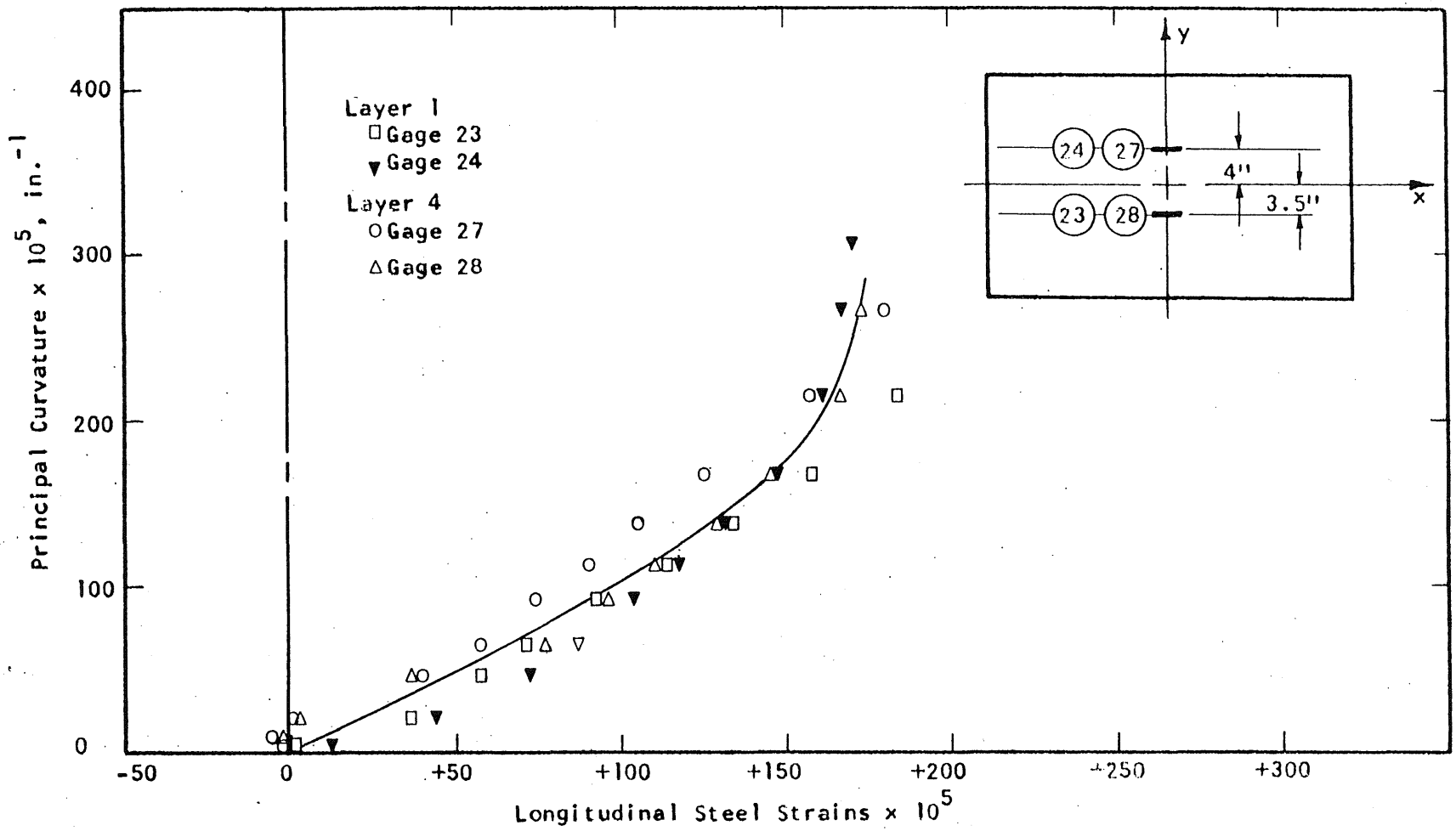

FIG. A.159 STEEL STRAIN PLOT, SPECIMEN B16

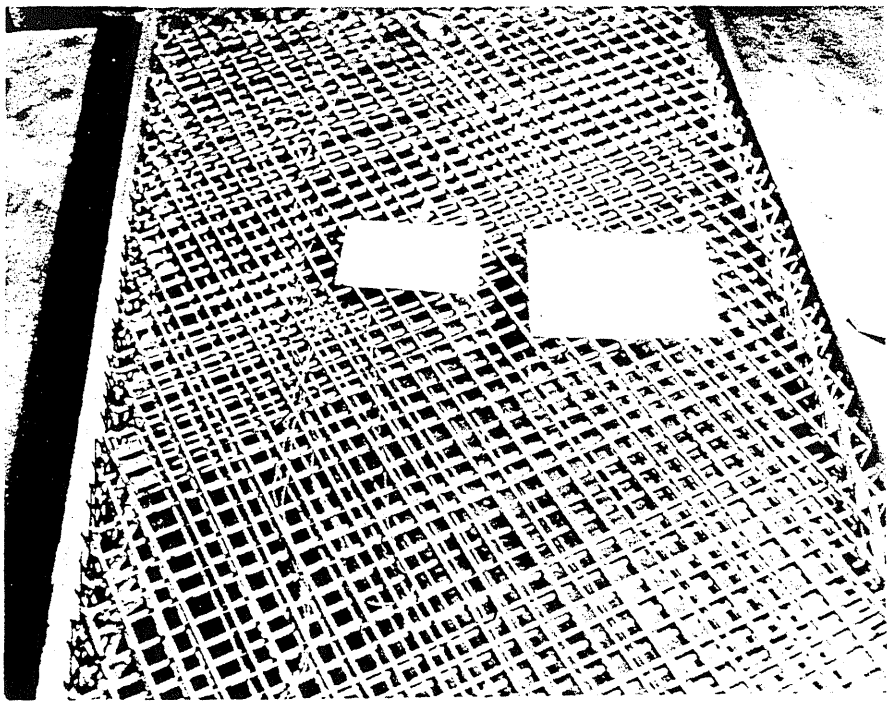

FIG. A.160 REINFORCEMENT IN SPECIMEN B17

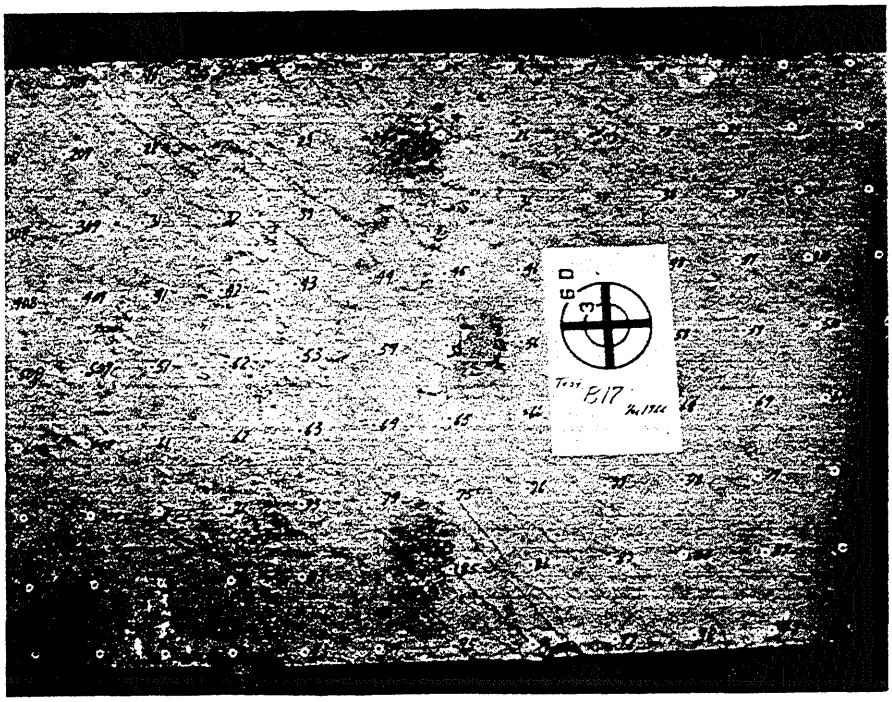

FIG. A.161a CRACK PATTERN IN TOP SURFACE OF B17

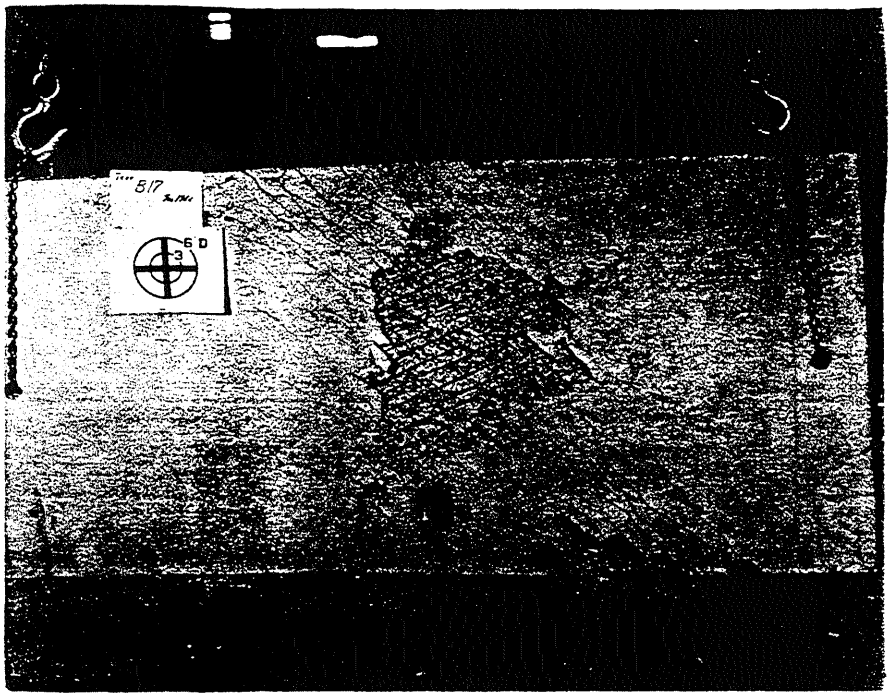

FIG. A.161b CRACK PATTERN IN BOTTOM SURFACE OF B17

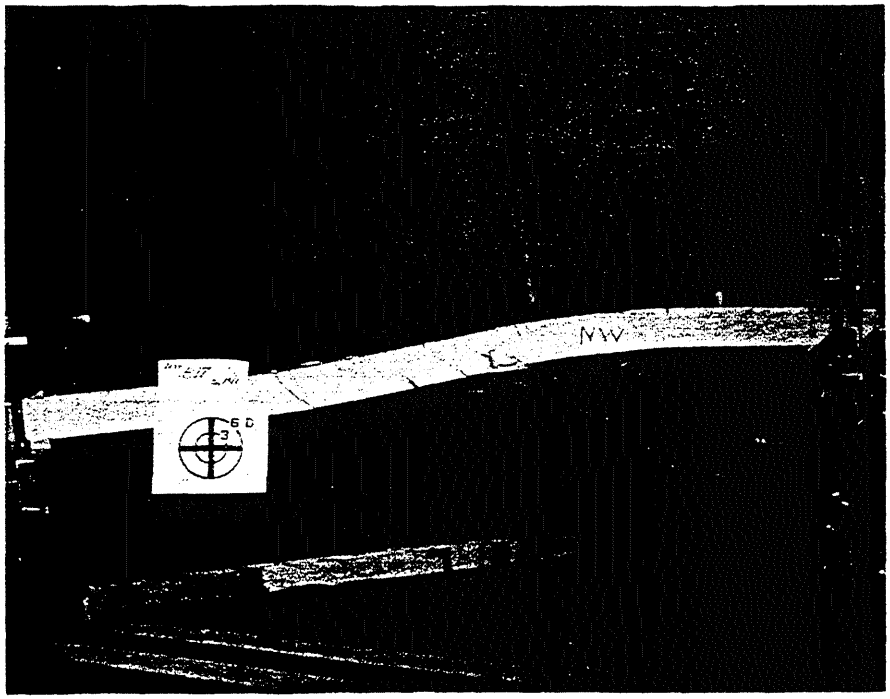

FIG. A.162 SIDE VIEW OF B17

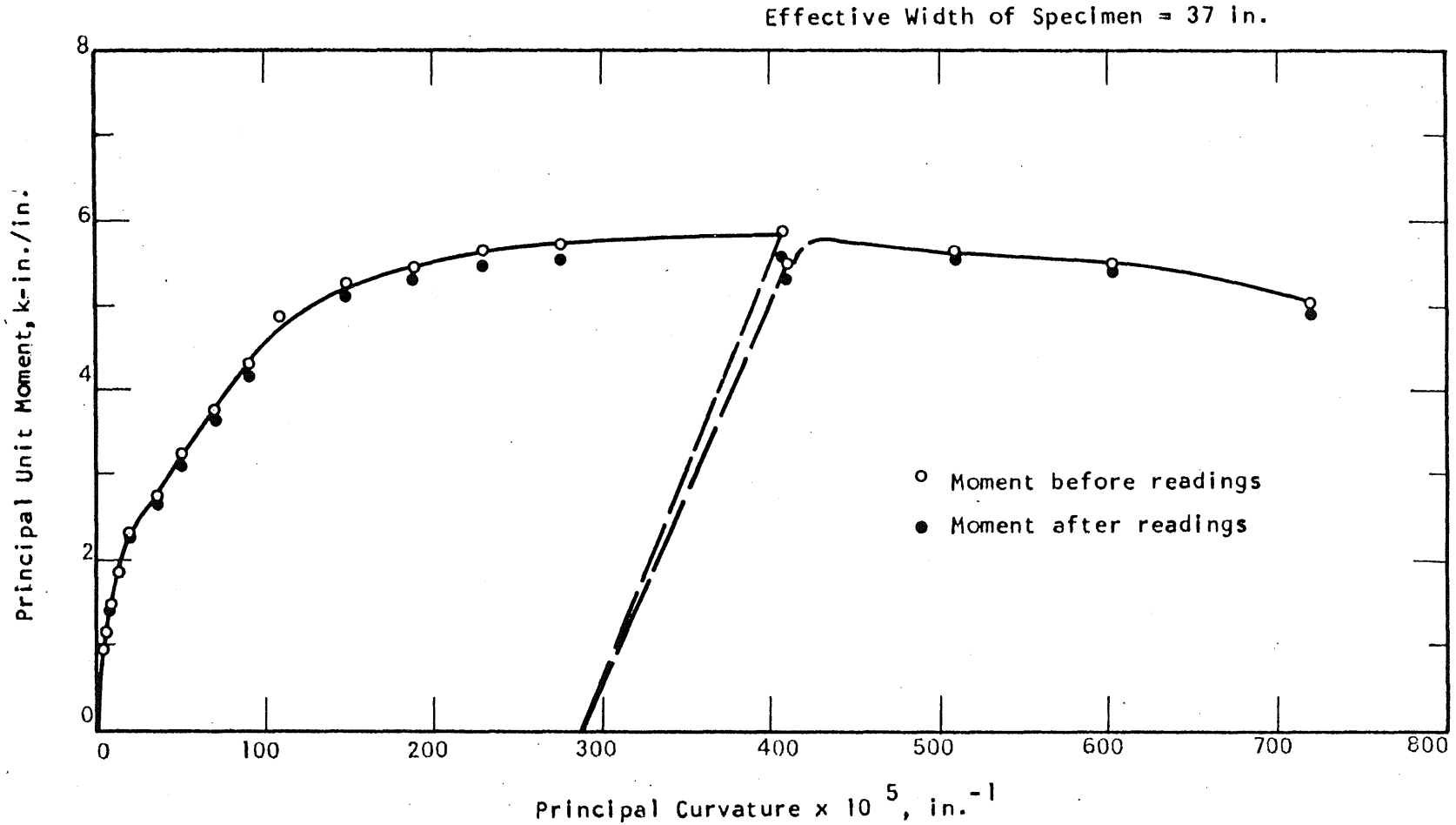

FIG. A.163 MOMENT-CURVATURE PLOT FOR SPECIMEN B17

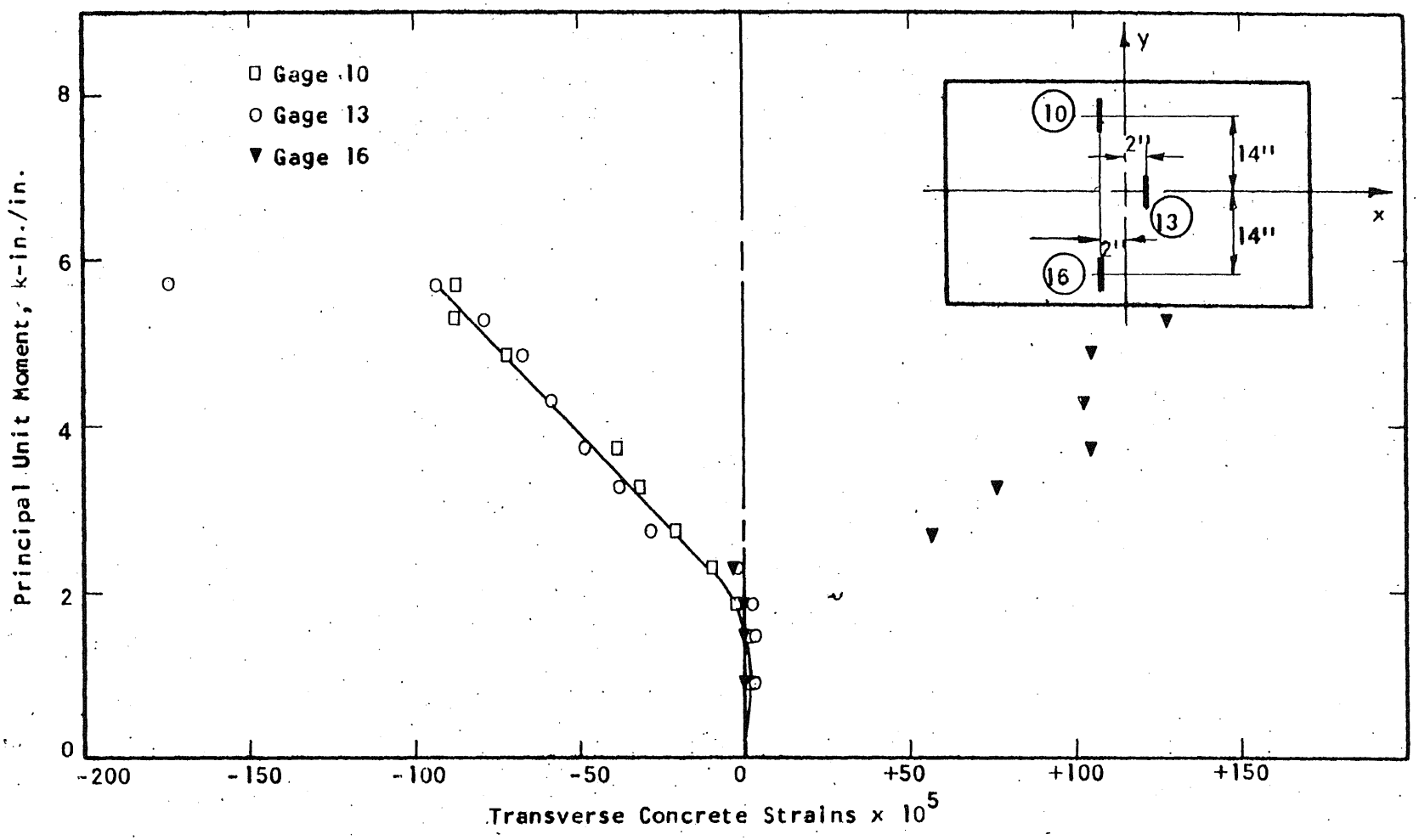

FIG. A.164 CONCRETE STRAIN PLOT, TOP SIDE OF SPECIMEN B17

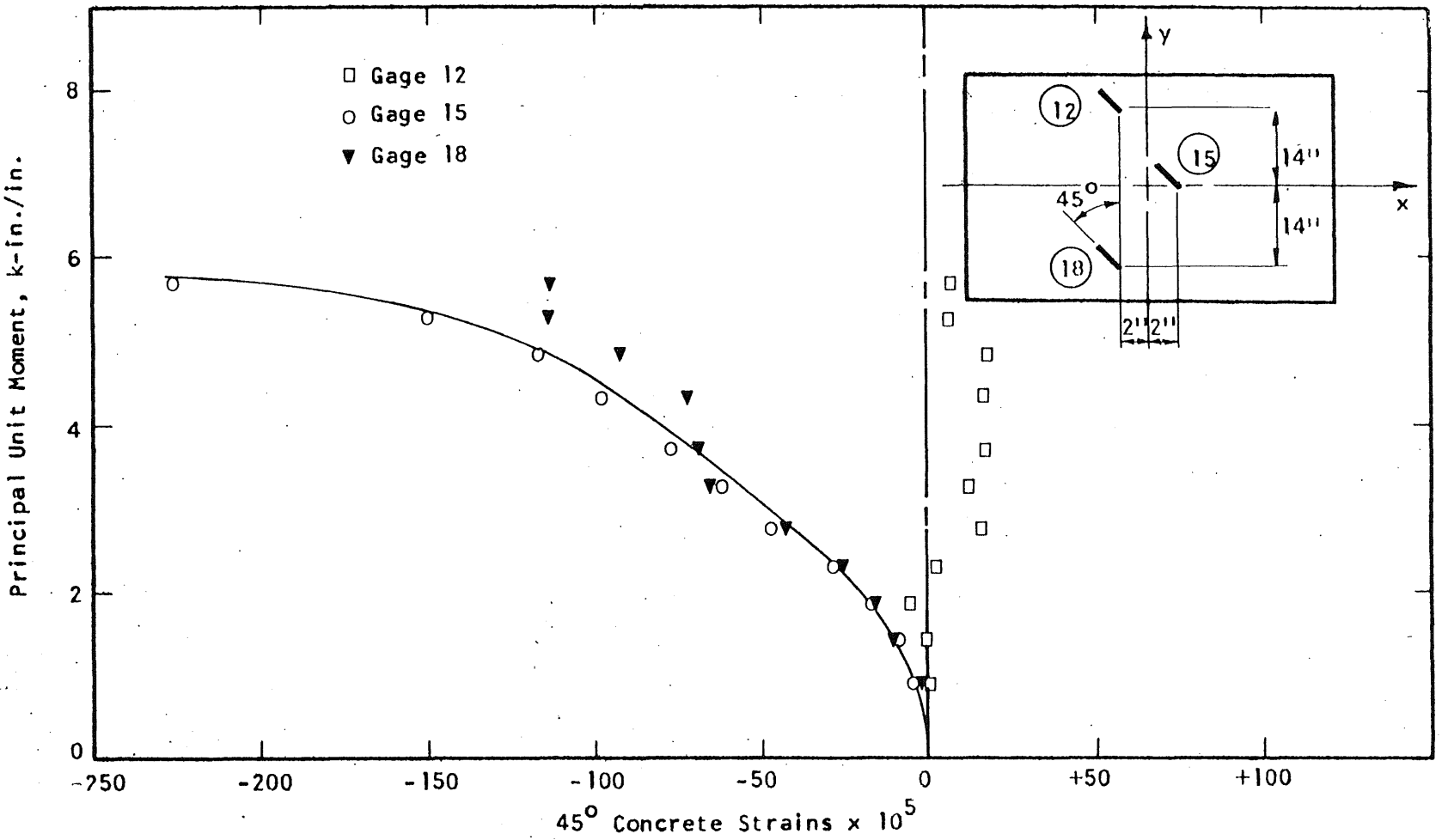

FIG. A.165 CONCRETE STRAIN PLOT, TOP SIDE OF SPECIMEN B17

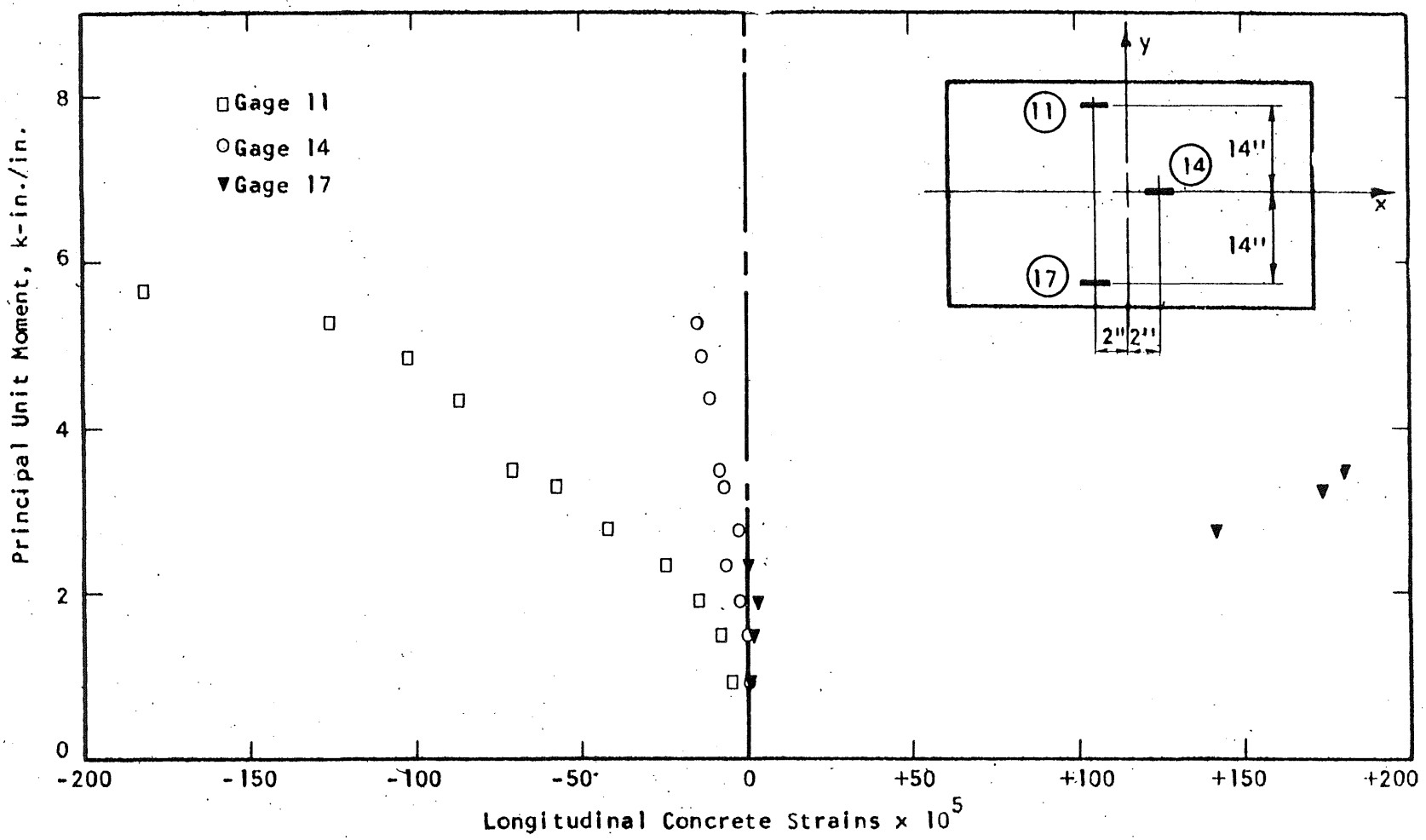

FIG. A.166 CONCRETE STRAIN PLOT, TOP SIDE OF SPECIMEN B17

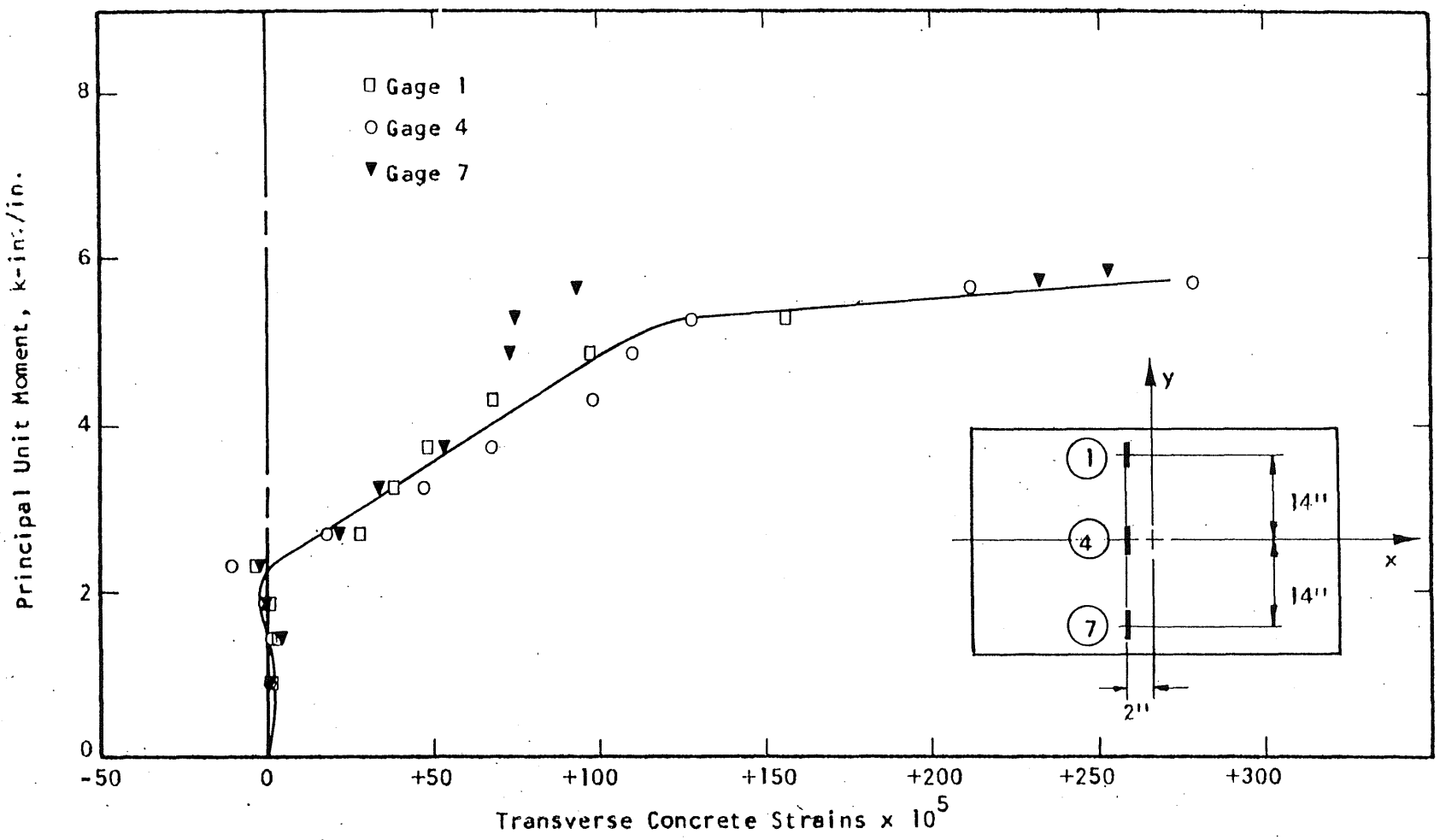

FIG. A.167 CONCRETE STRAIN PLOT, BOTTOM SIDE OF SPECIMEN B17

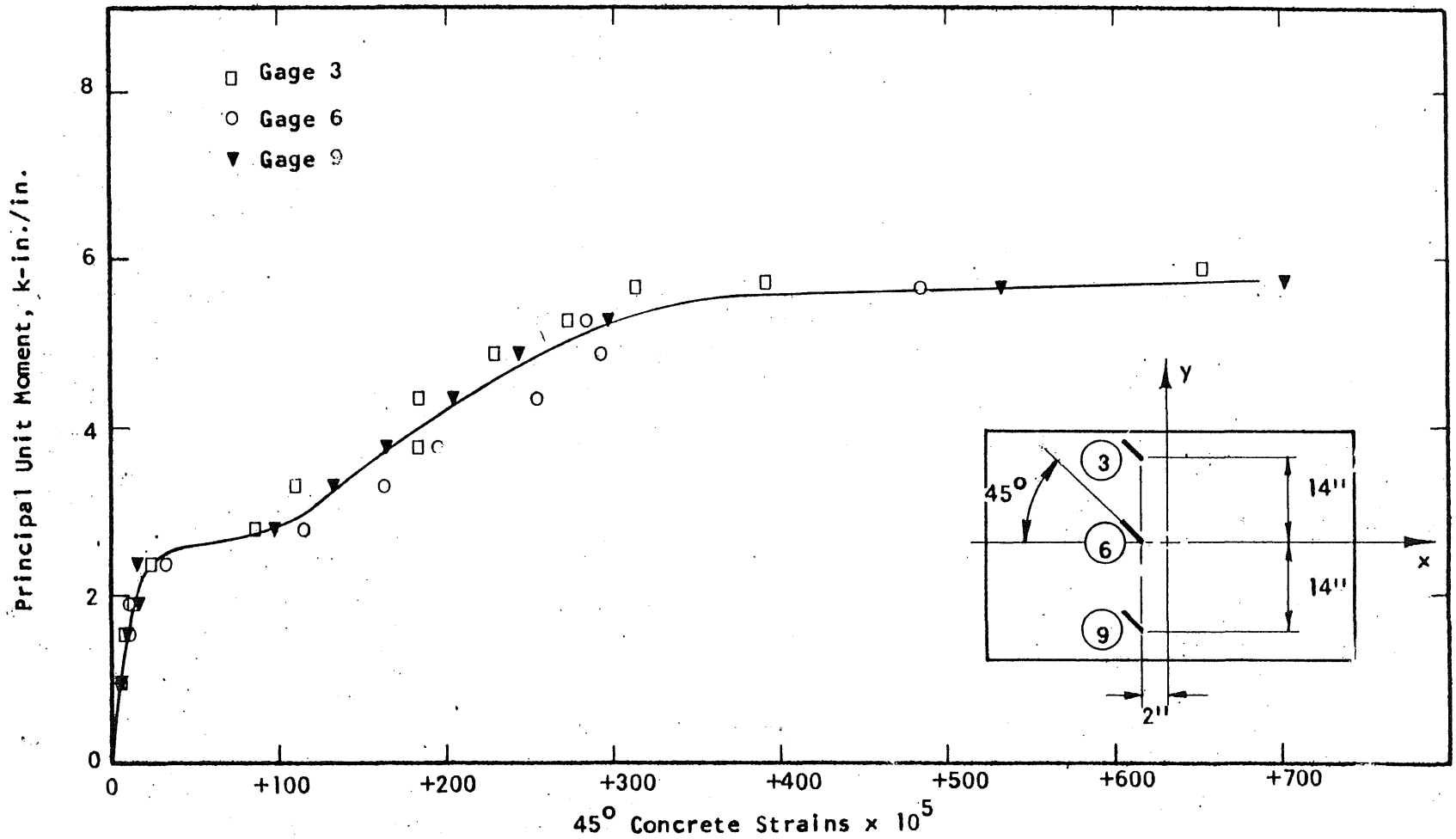

FIG. A.168 CONCRETE STRAIN PLOT, BOTTOM SIDE OF SPECIMEN B17

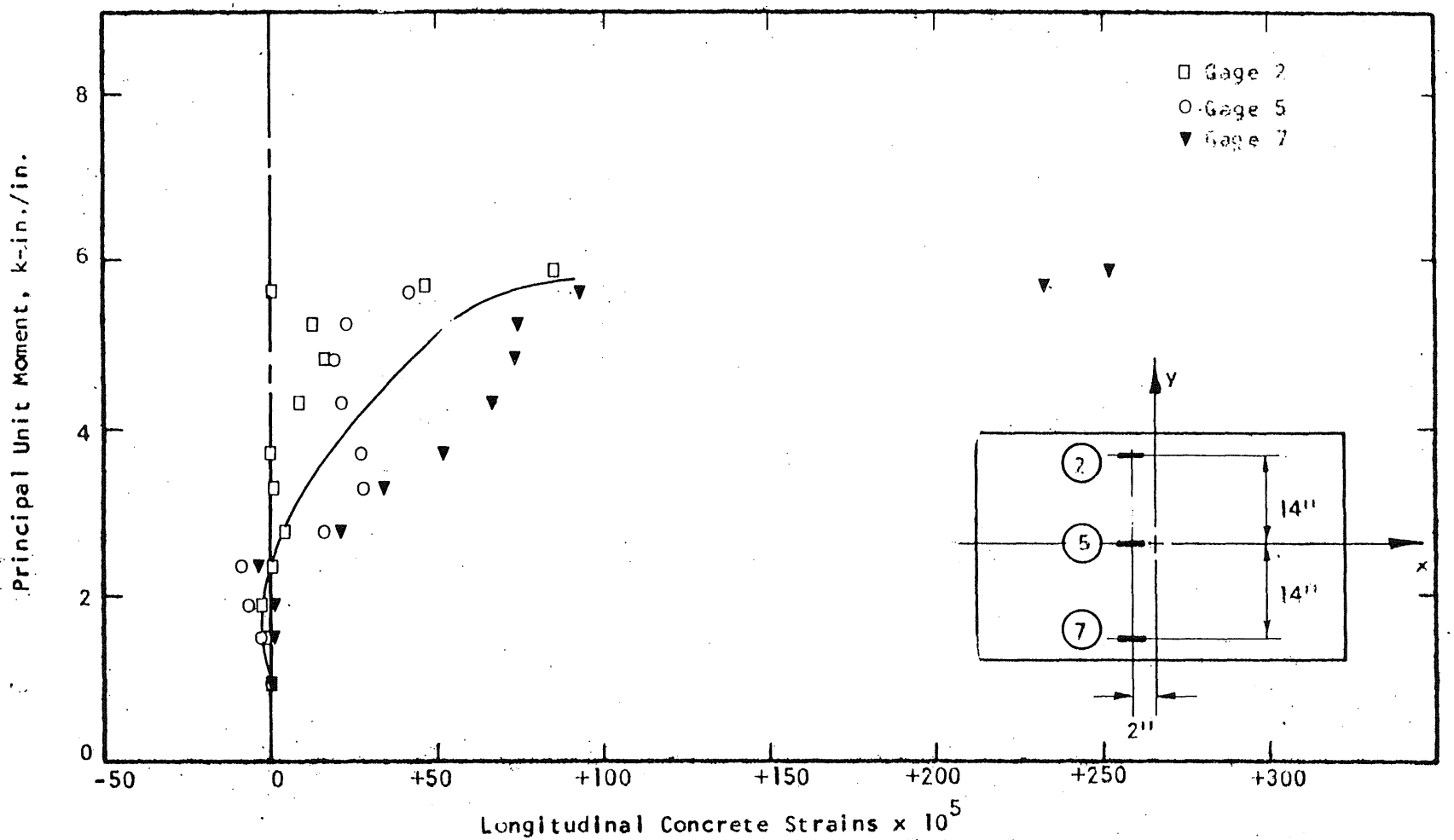

FIG. A.169 CONCRETE STRAIN PLOT, BOTTOM SIDE OF SPECIMEN B17

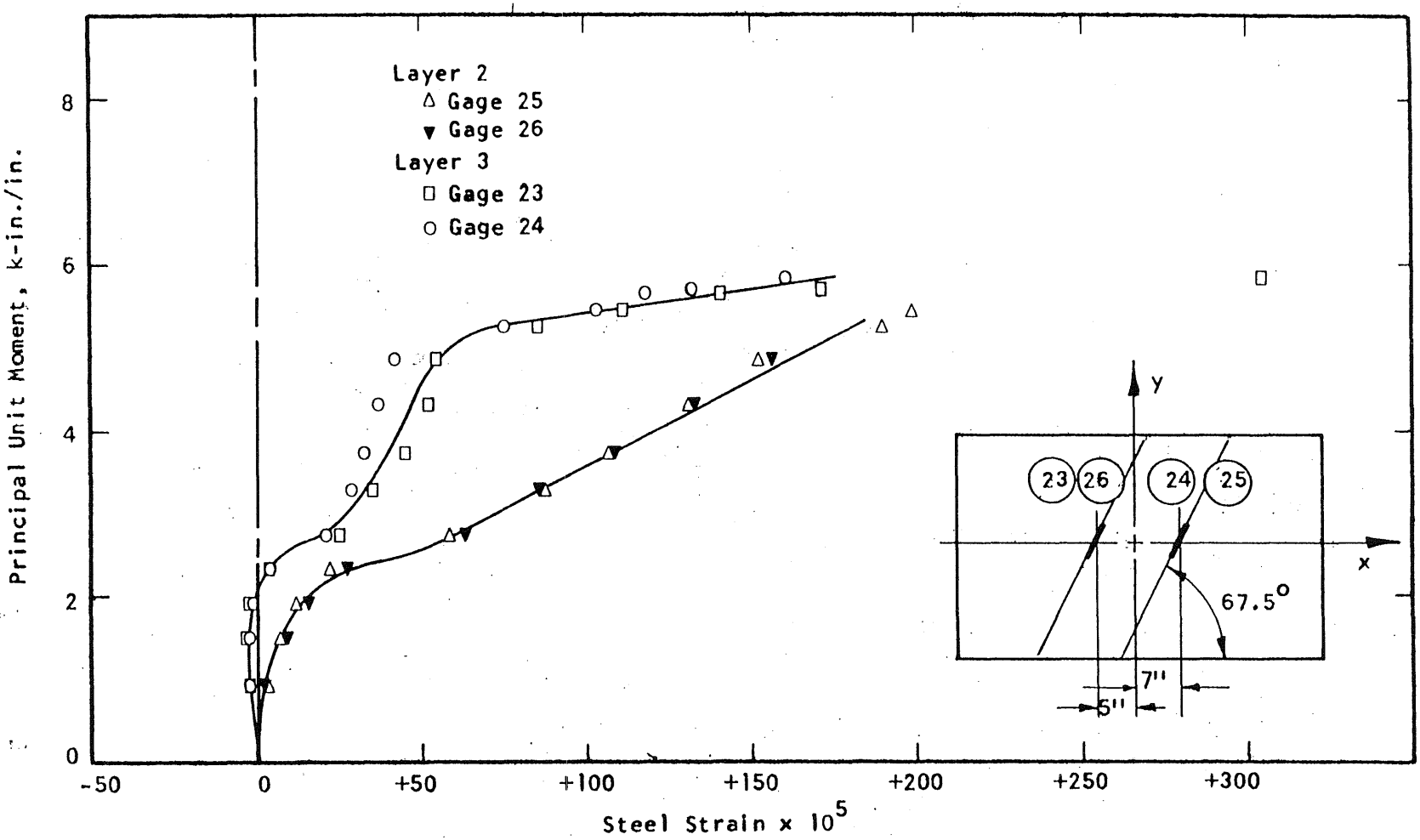

FIG. A.170 STEEL STRAIN PLOT, SPECIMEN B17

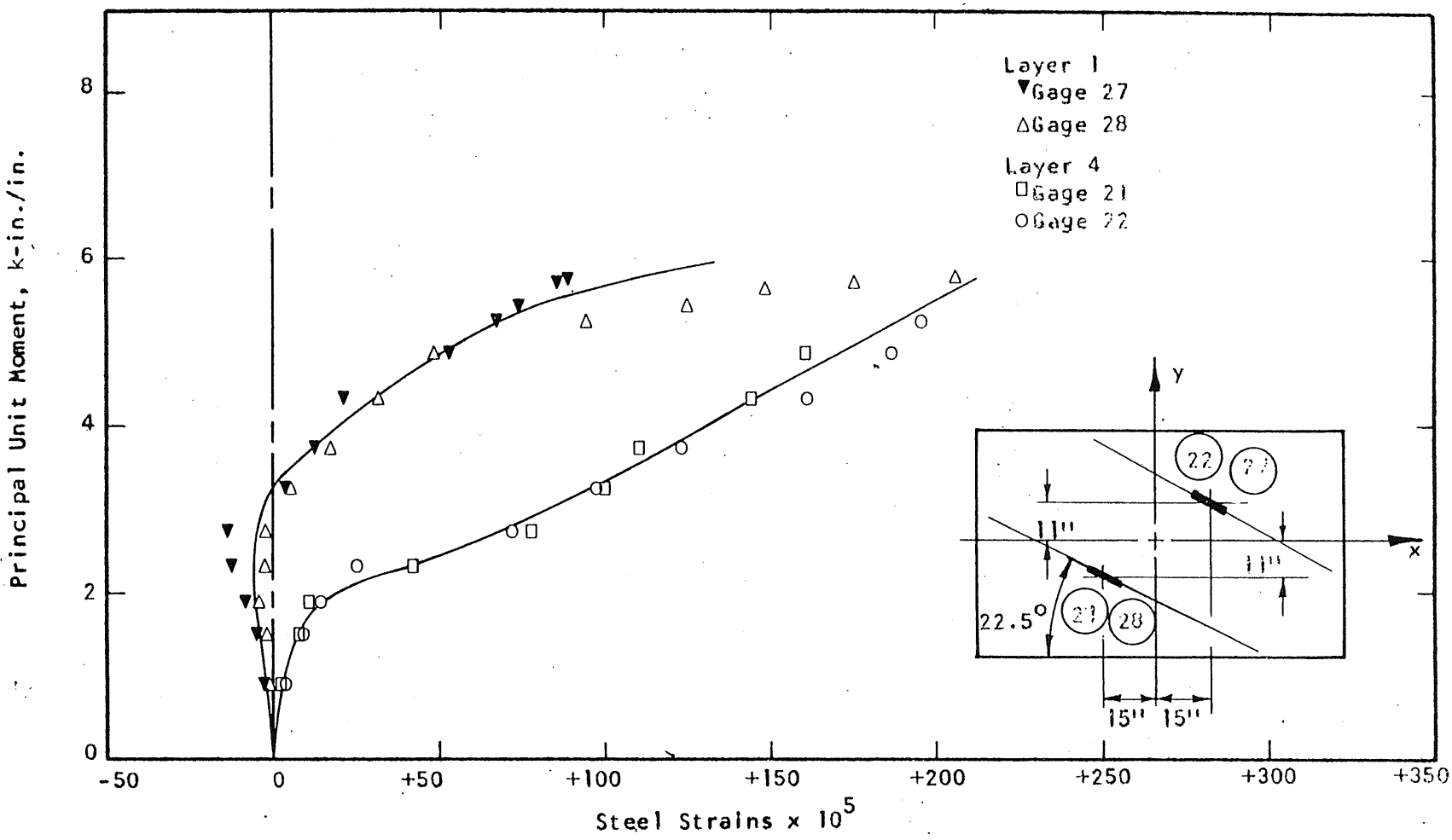

FIG. A.171 STEEL STRAIN PLOT, SPECIMEN B17

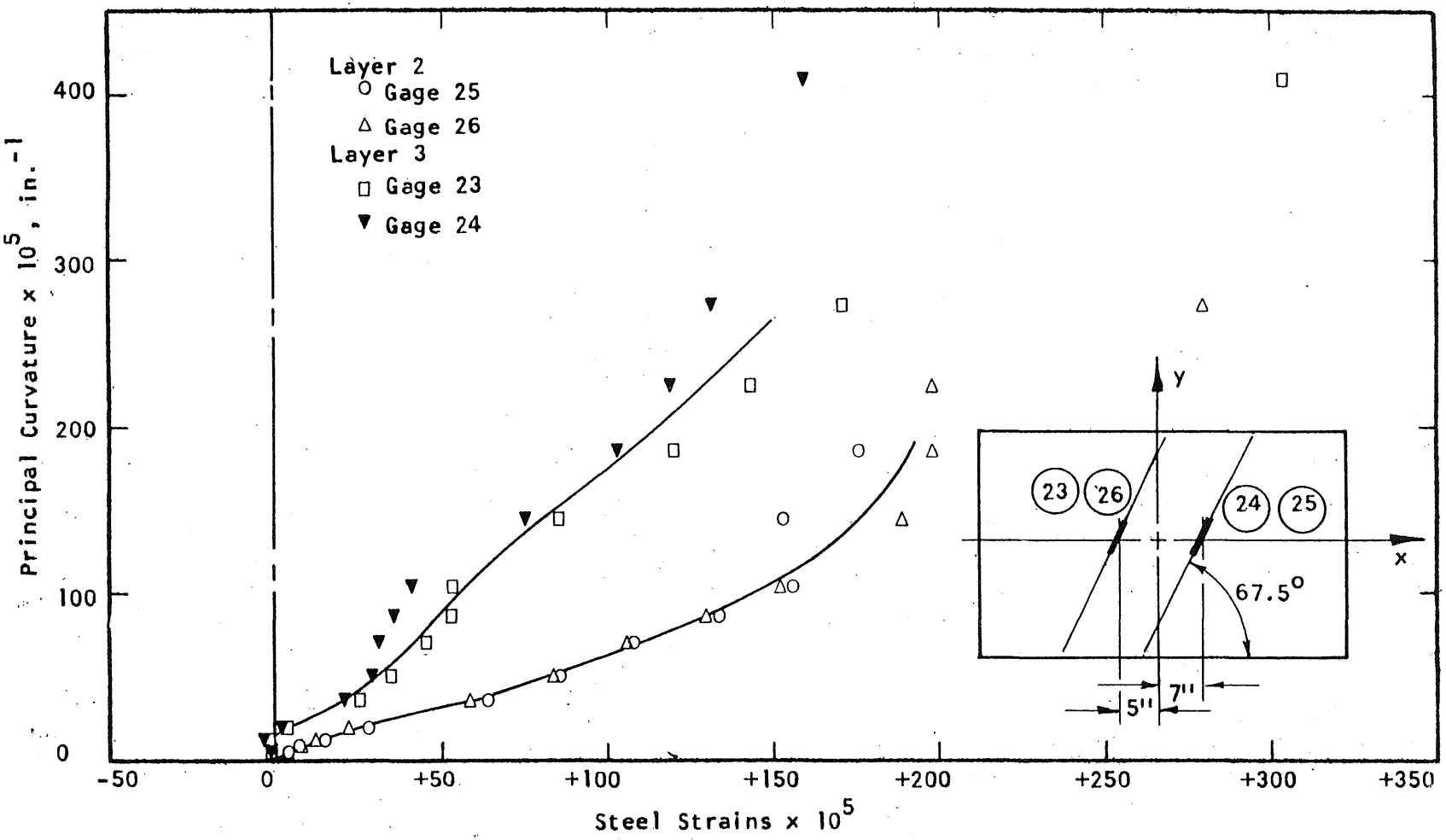

FIG. A.172 STEEL STRAIN PLOT, SPECIMEN B17

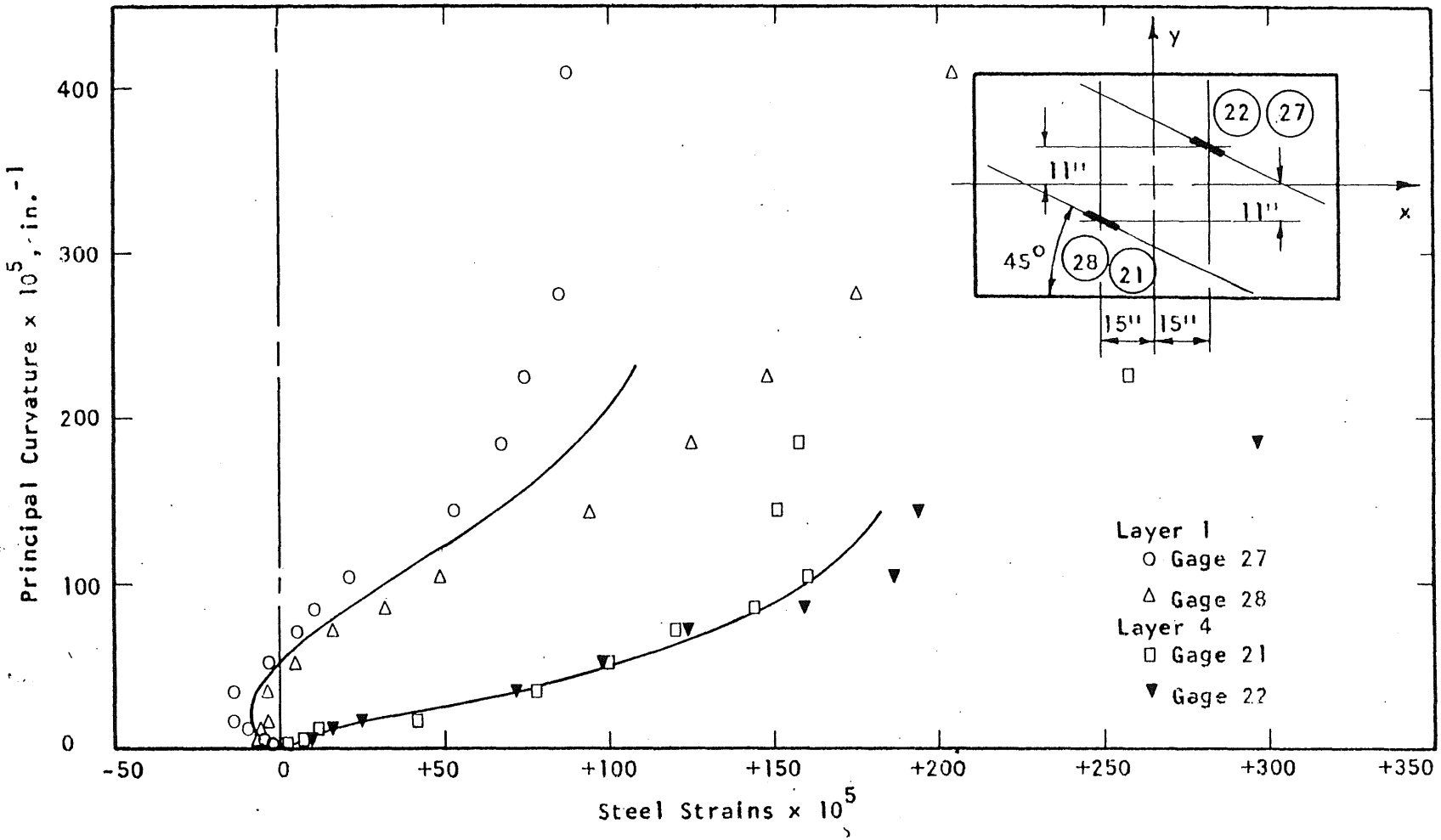

FIG. A.173 STEEL STRAIN PLOT, SPECIMEN B17

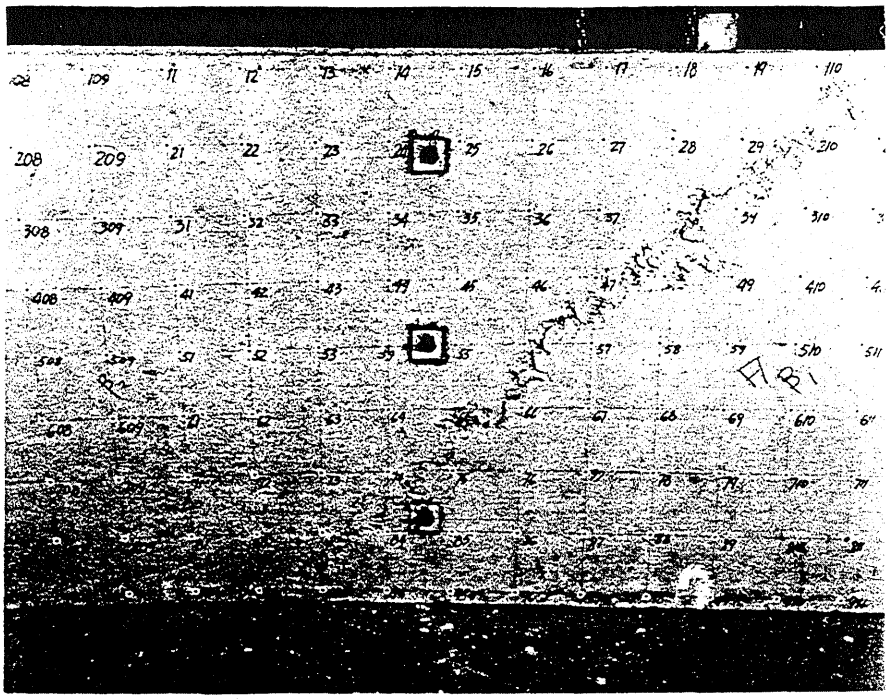

FIG. A.174 CRACK PATTERN IN TOP SURFACE OF B18

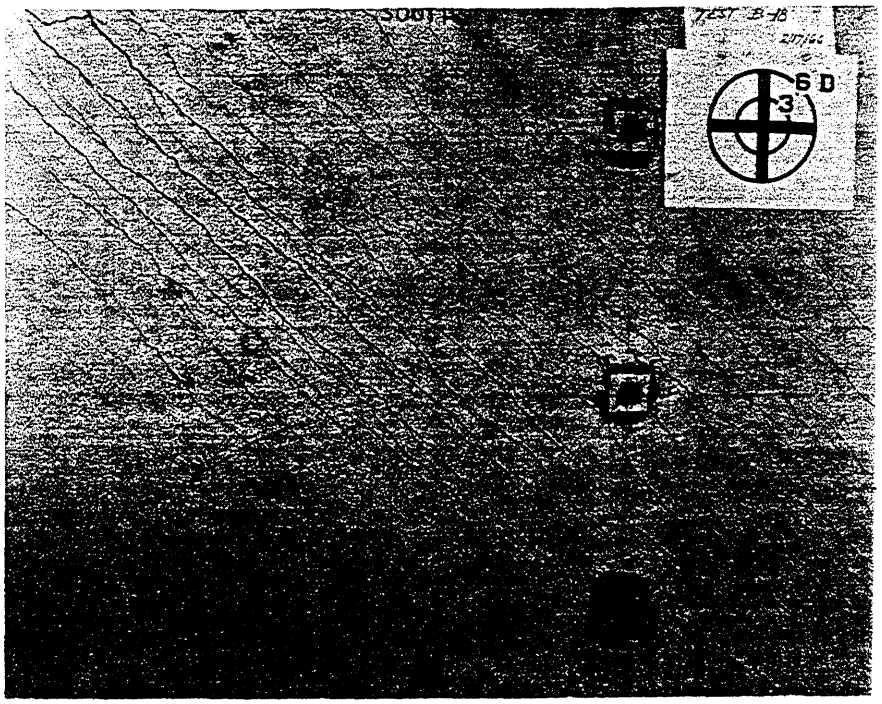

FIG. A.175 CRACK PATTERN IN BOTTOM SURFACE OF B18

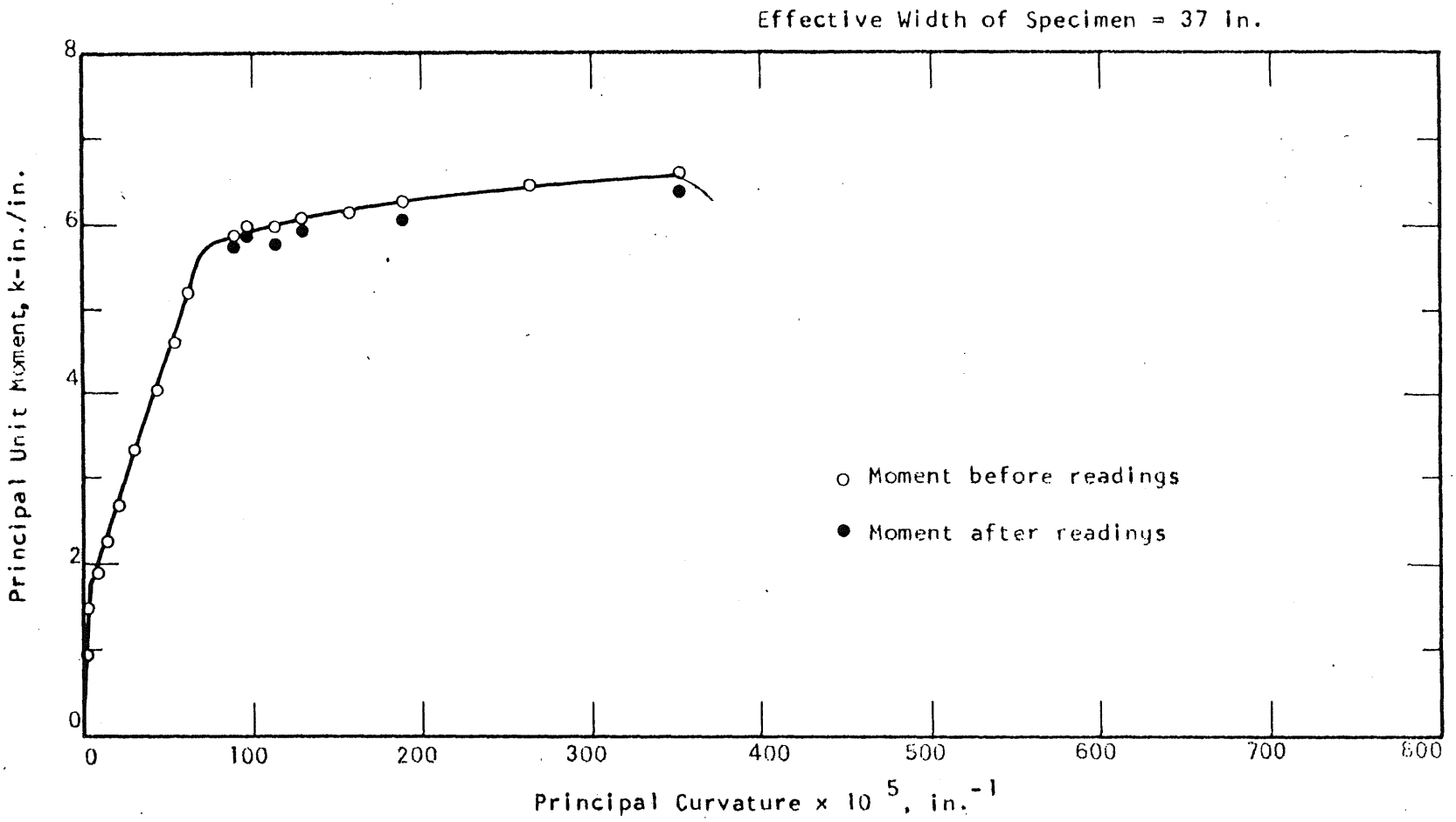

FIG. A.176 MOMENT-CURVATURE PLOT FOR SPECIMEN B18

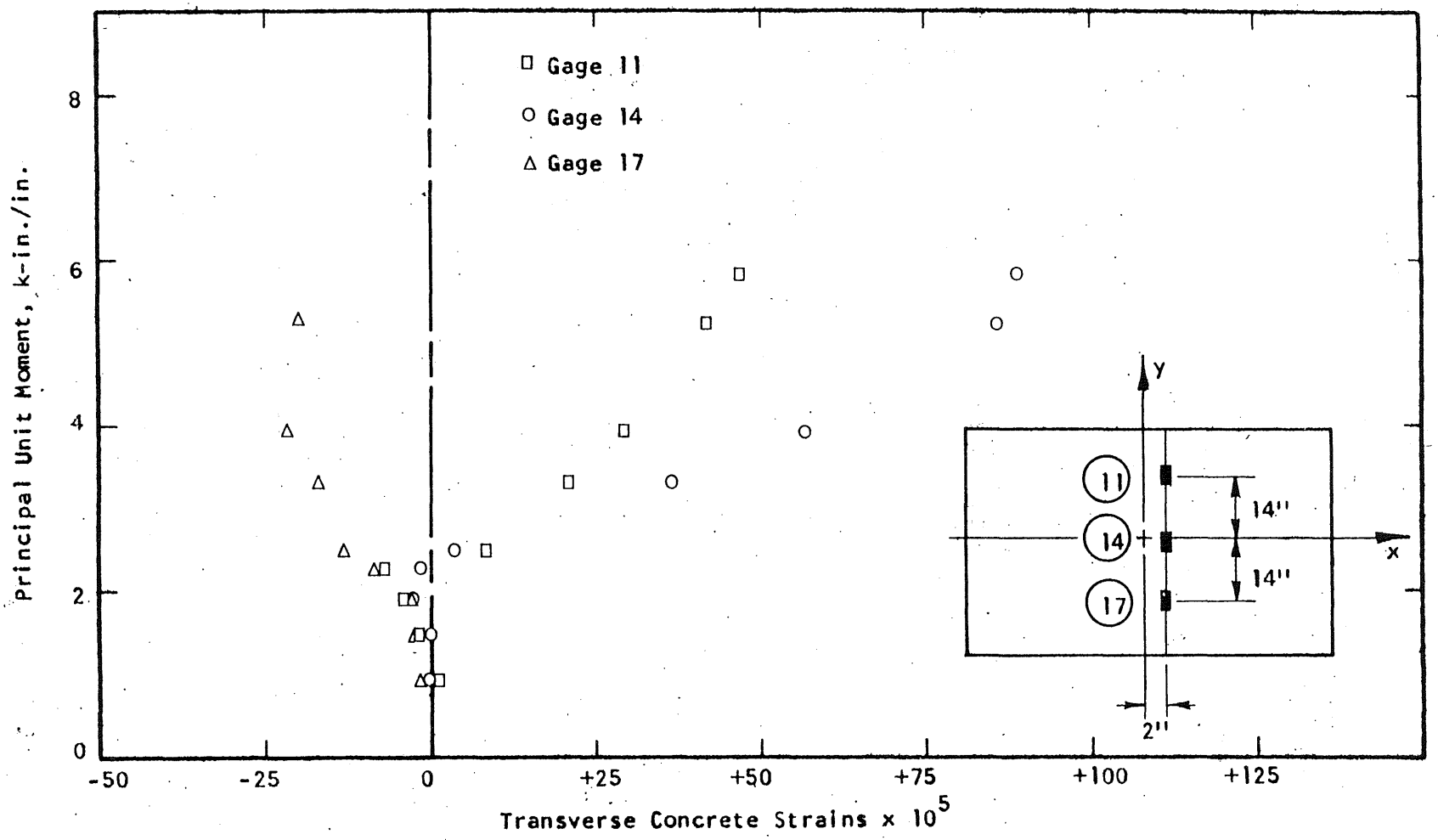

FIG. A.177 CONCRETE STRAIN PLOT, TOP SIDE OF SPECIMEN B18

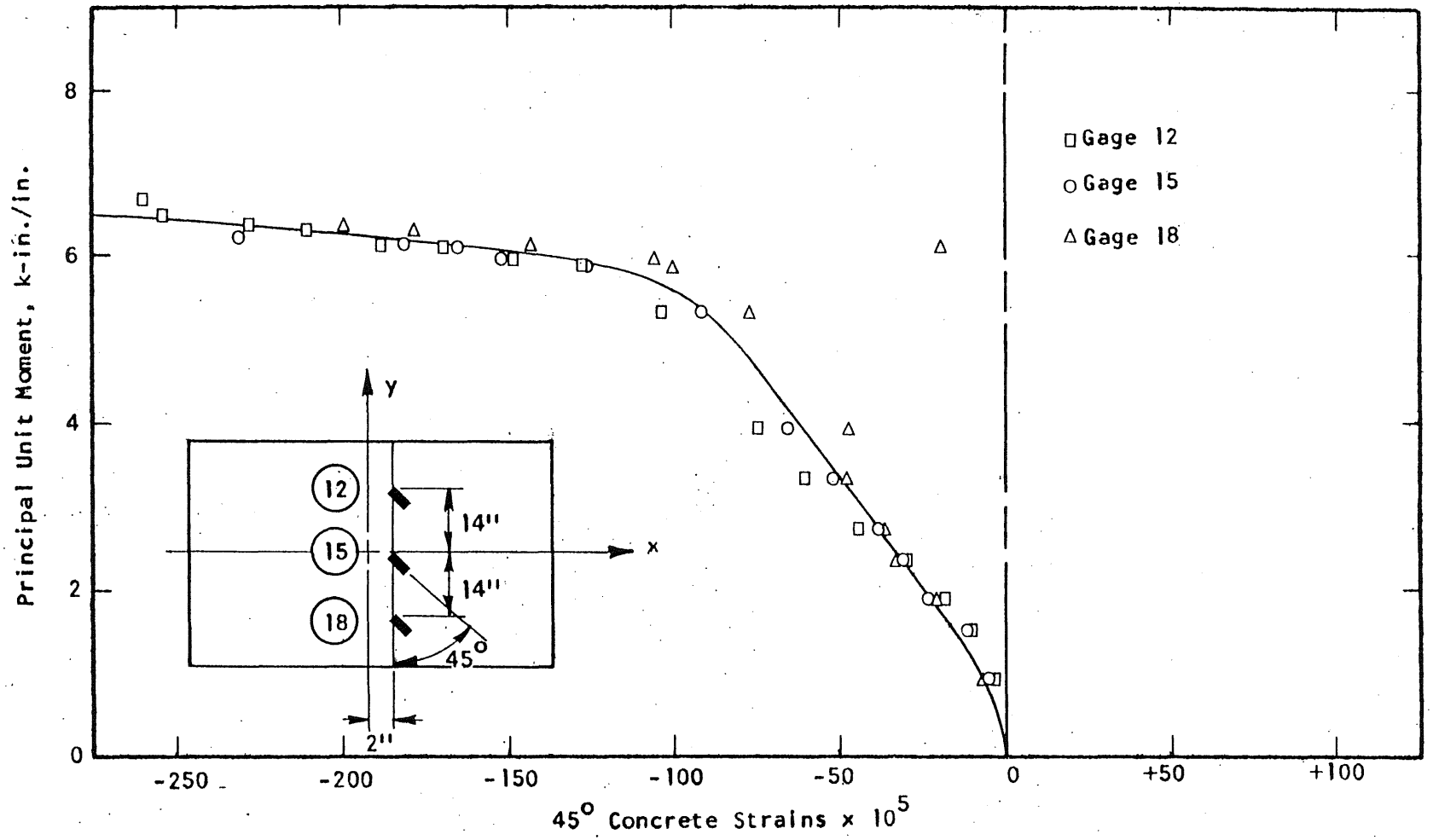

FIG. A.178 CONCRETE STRAIN PLOT, TOP SIDE OF SPECIMEN B18

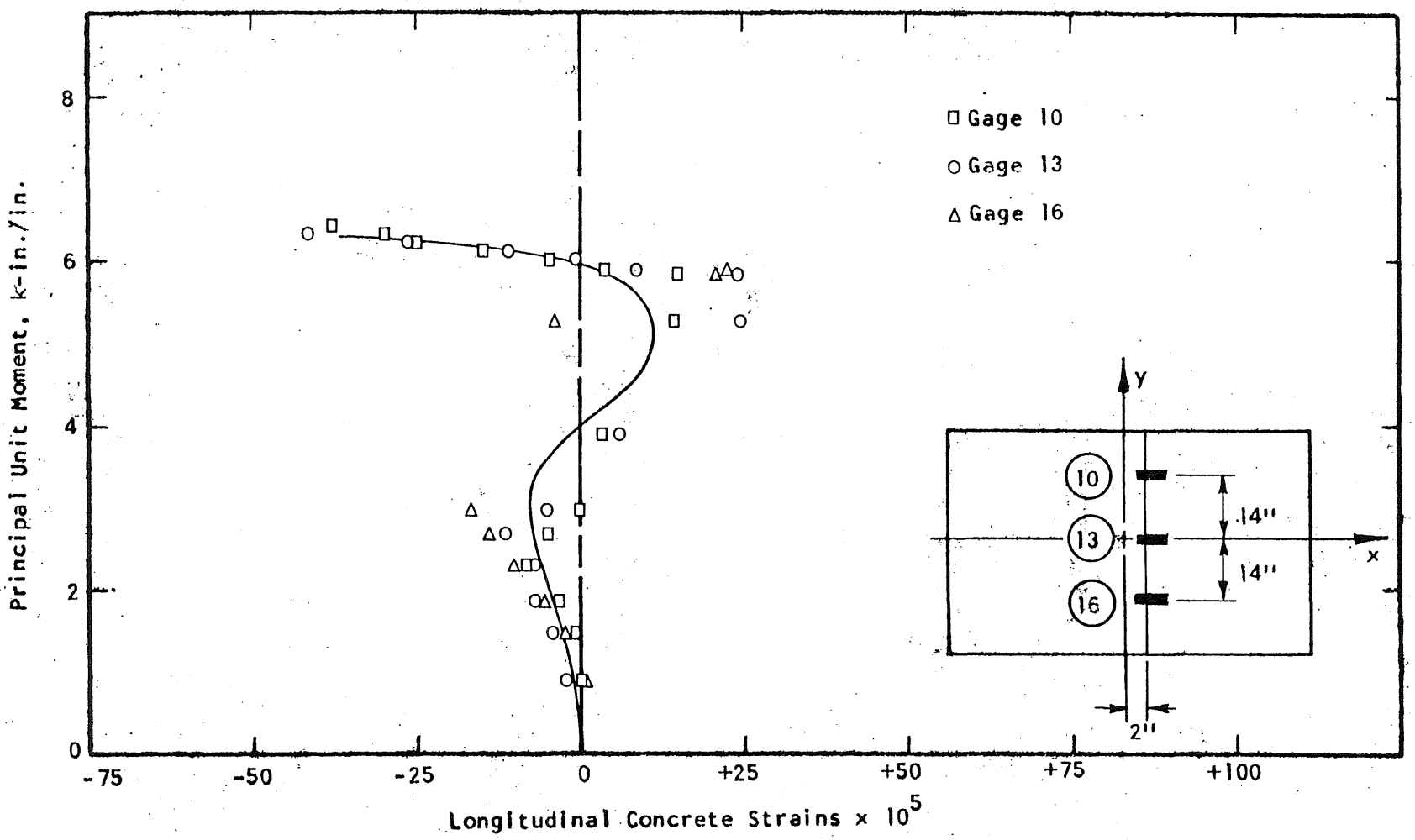

FIG. A.179 CONCRETE STRAIN PLOT, TOP SIDE OF SPECIMEN B18

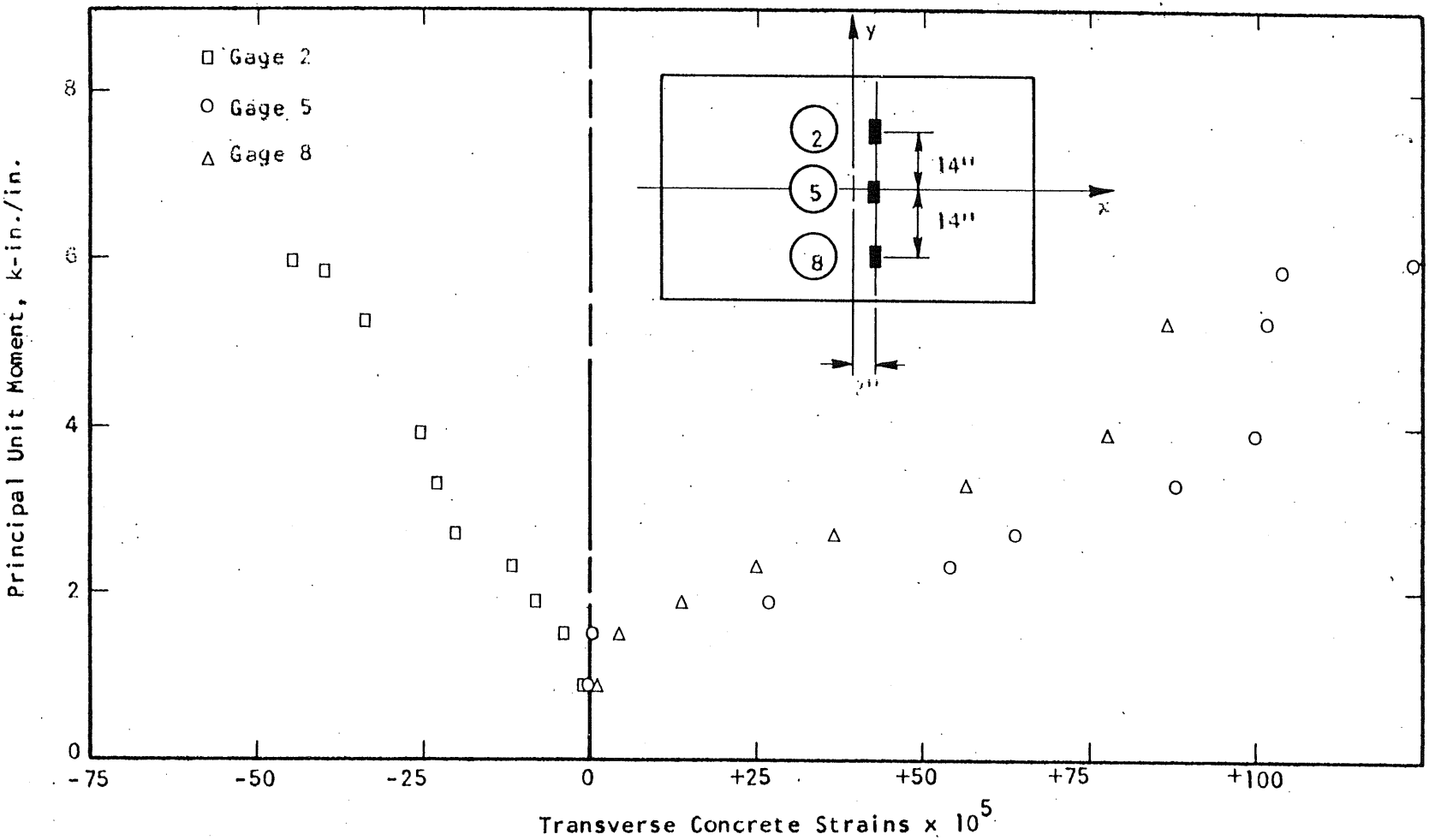

FIG. A.180 CONCRETE STRAINS, BOTTOM SIDE OF SPECIMEN B18

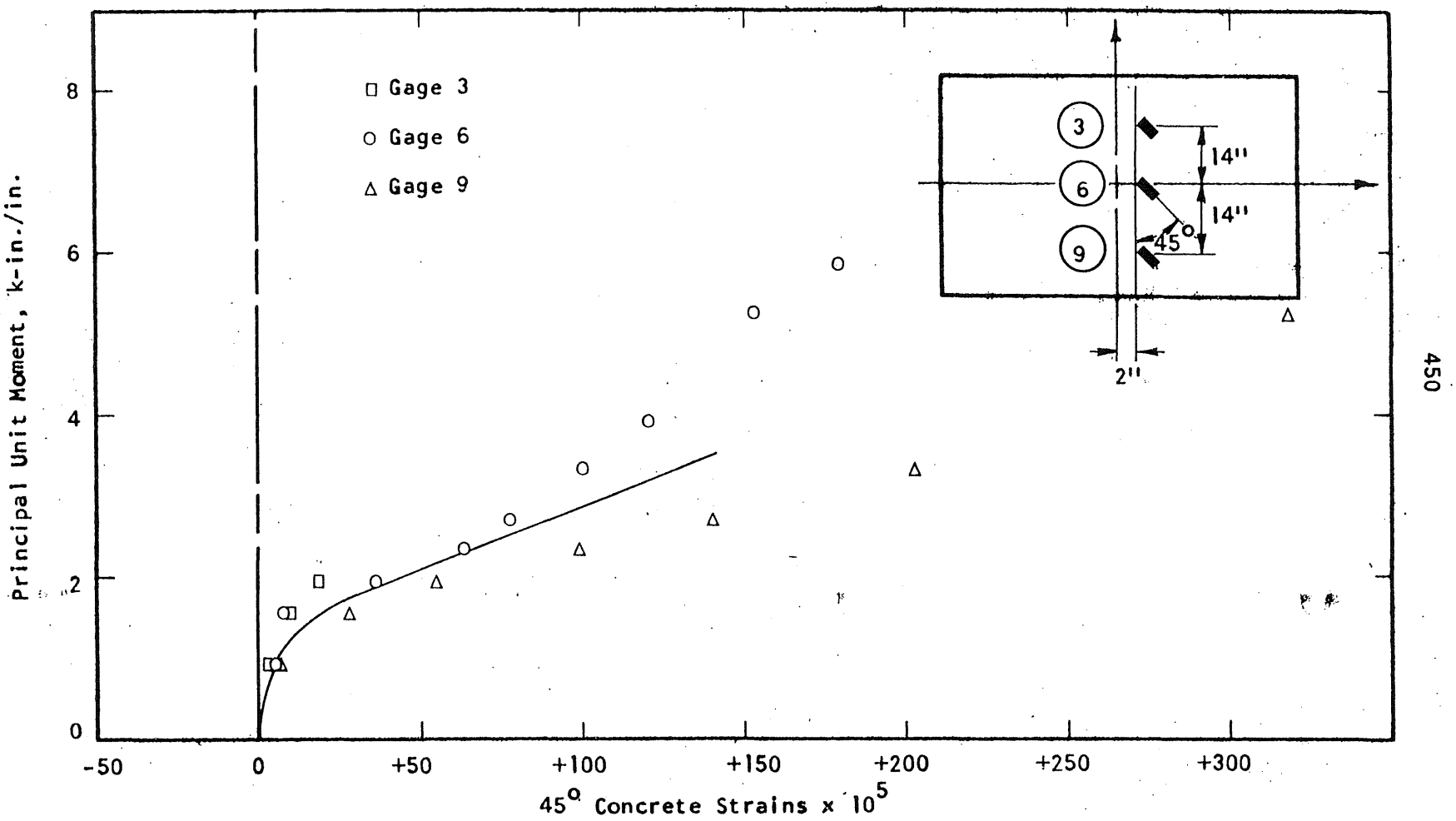

FIG. A.181 CONCRETE STRAIN PLOT, BOTTOM SIDE OF SPECIMEN B18

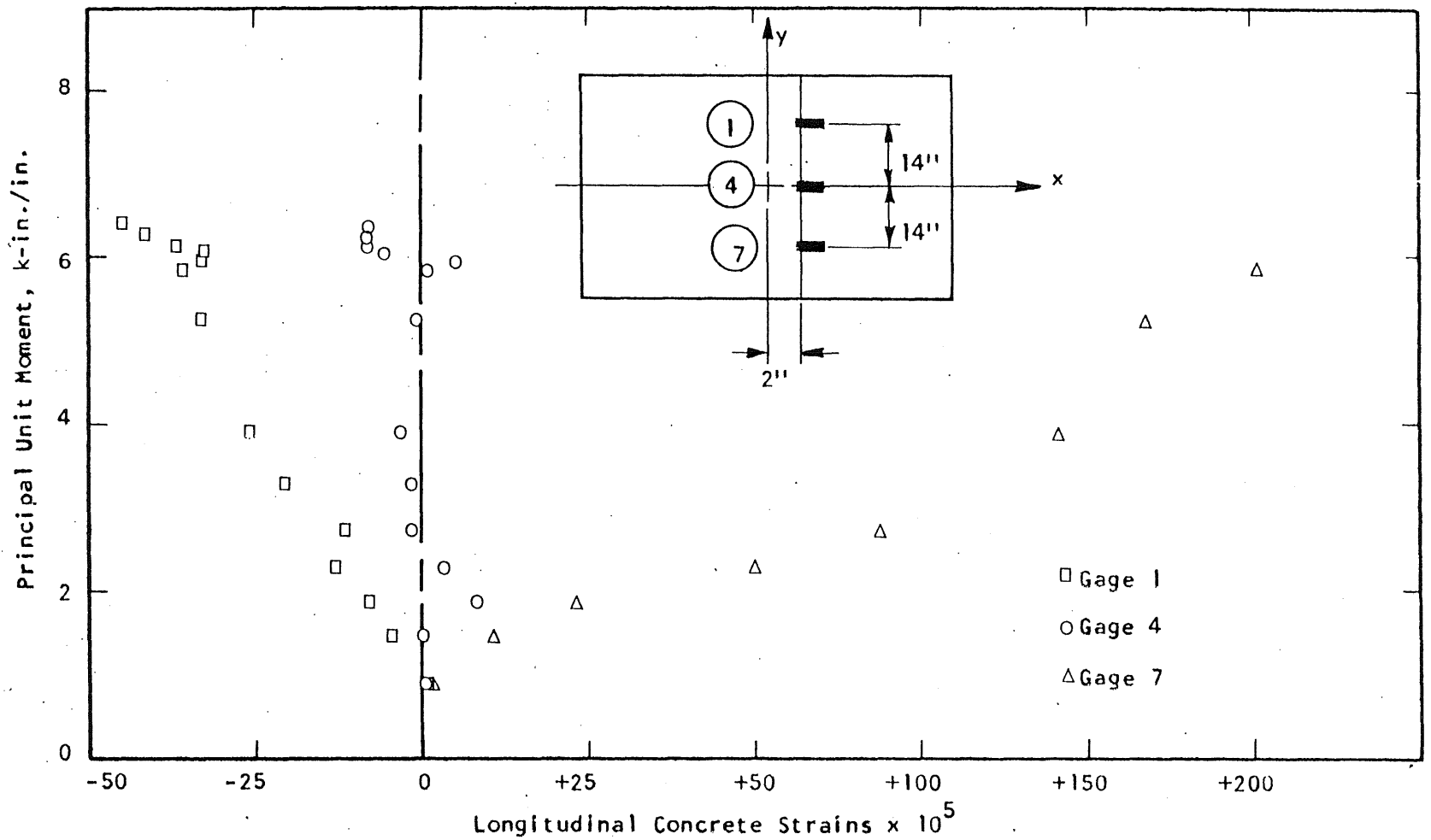

FIG. A.182 CONCRETE STRAIN PLOT, BOTTOM SIDE OF SPECIMEN B18

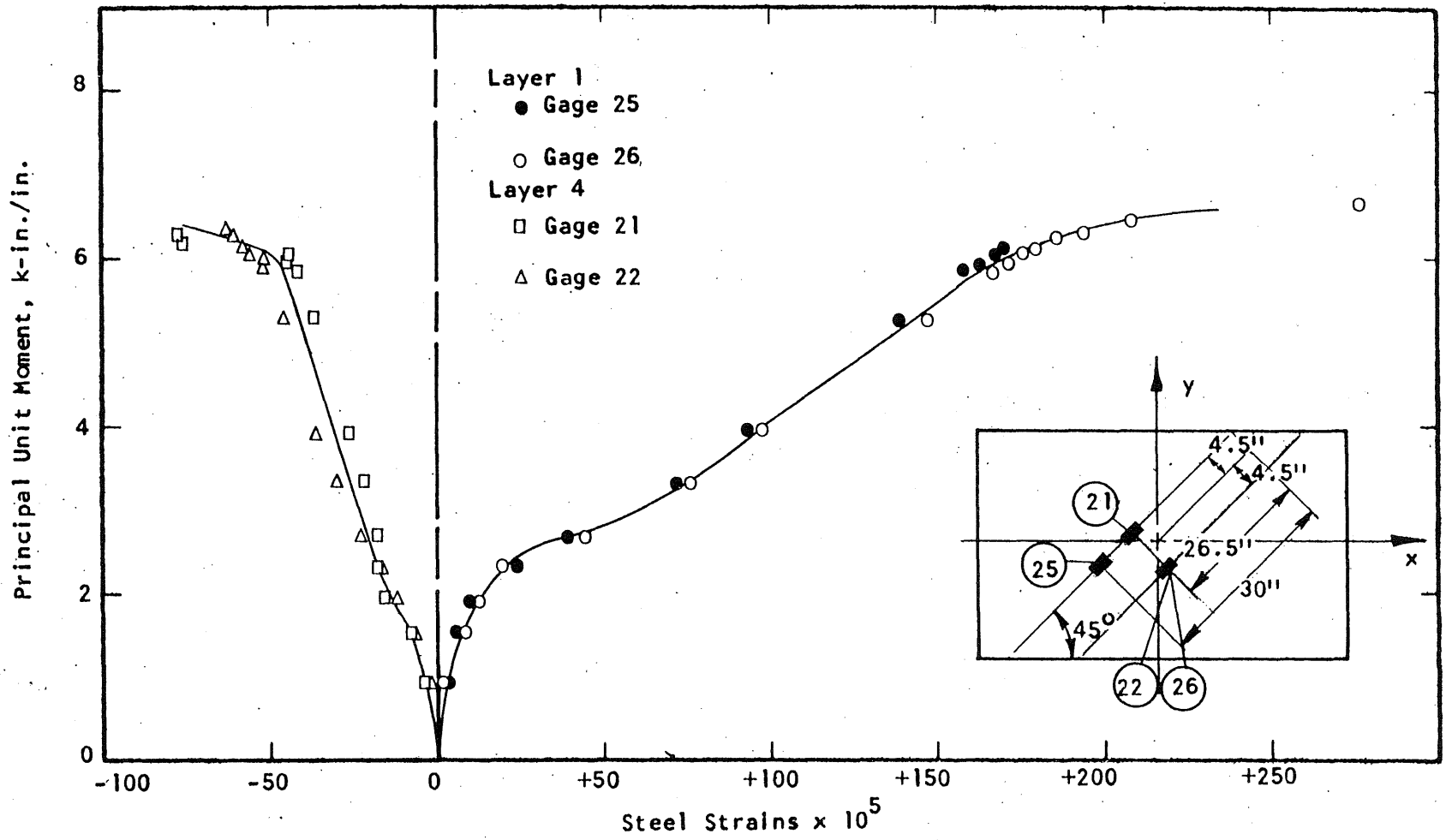

FIG. A.183 STEEL STRAIN PLOT, SPECIMEN B18

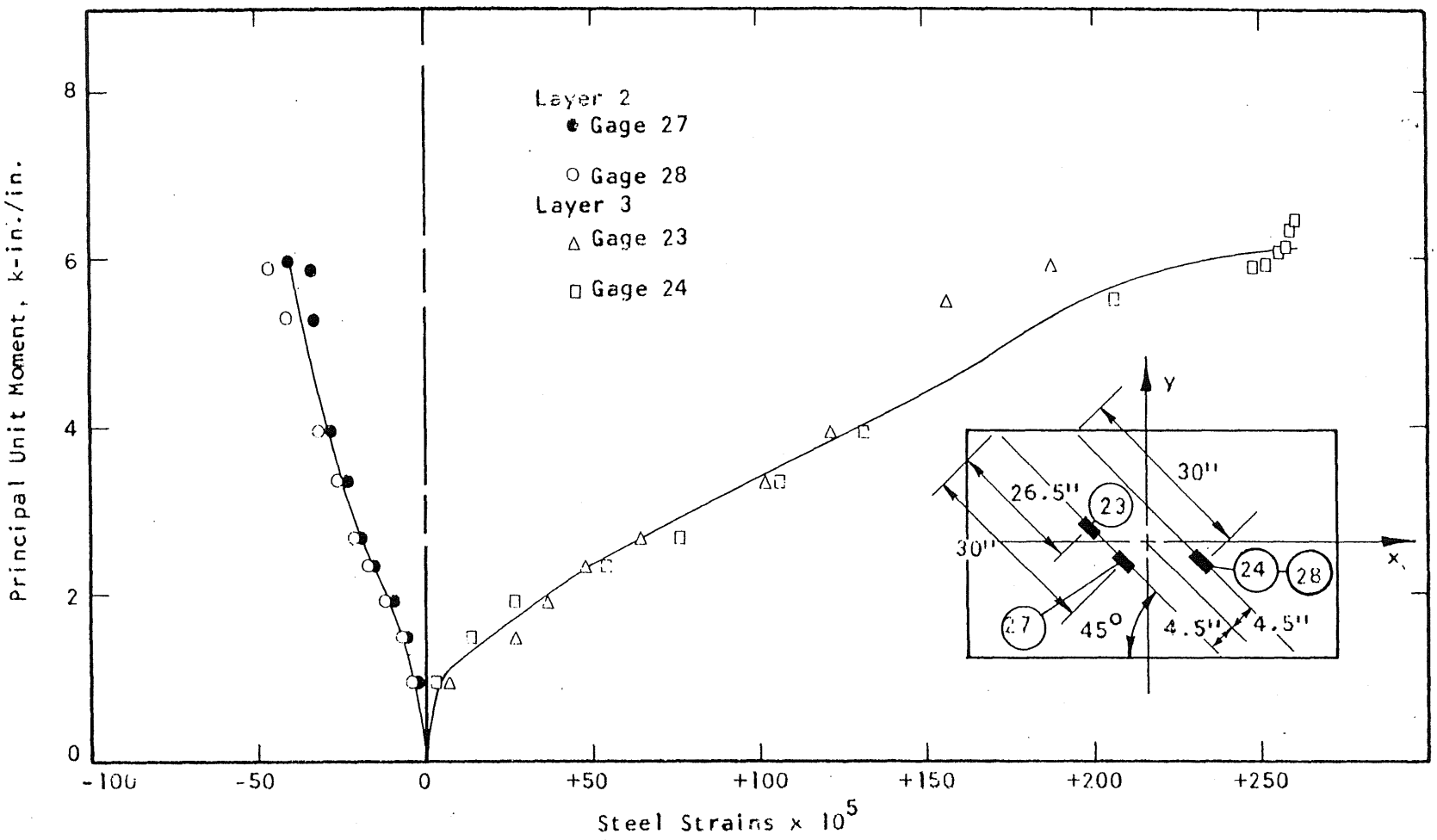

FIG. A.184 STEEL STRAIN PLOT, SPECIMEN B18

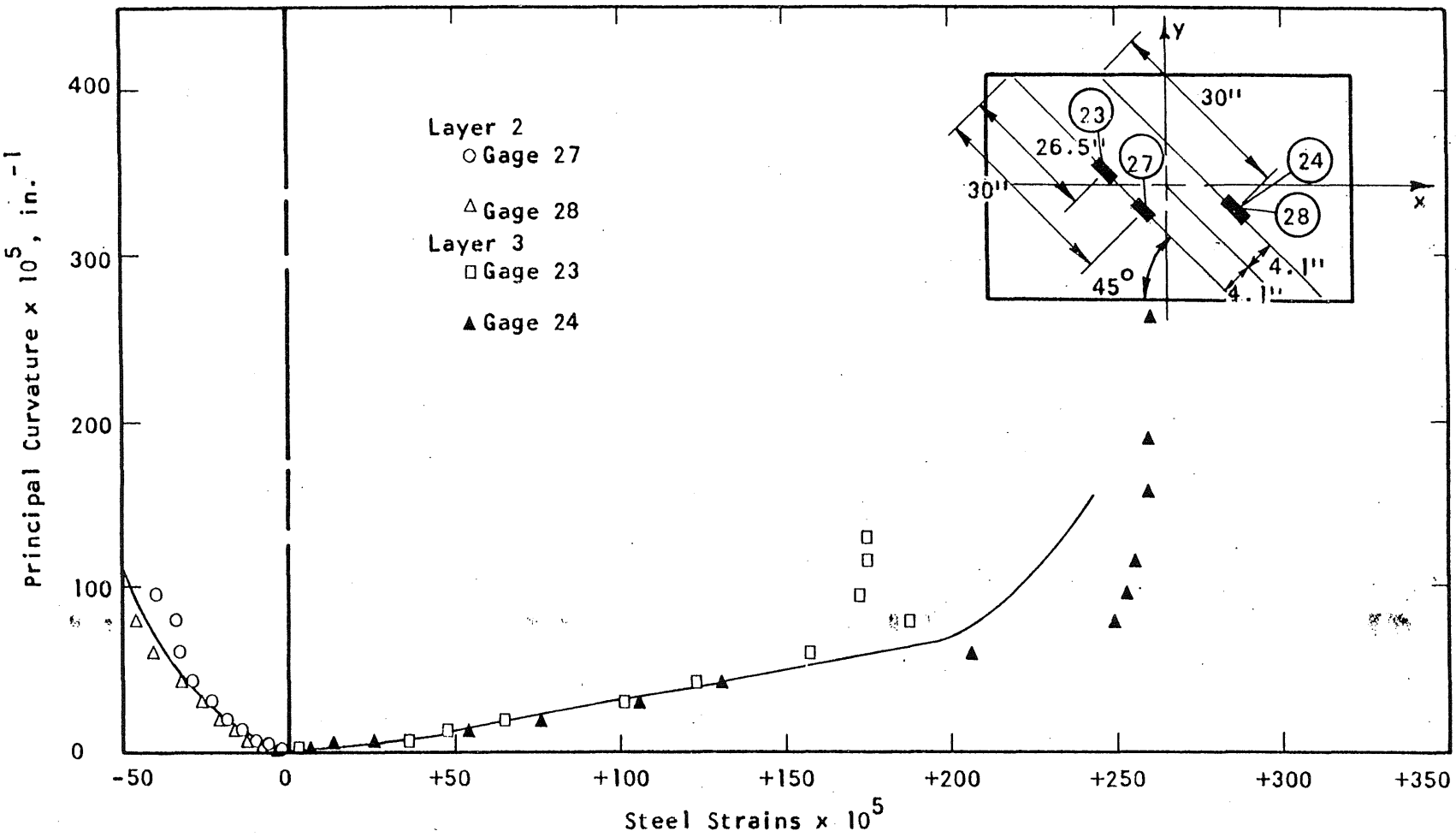

FIG. A.185 STEEL STRAIN PLOT, SPECIMEN B18

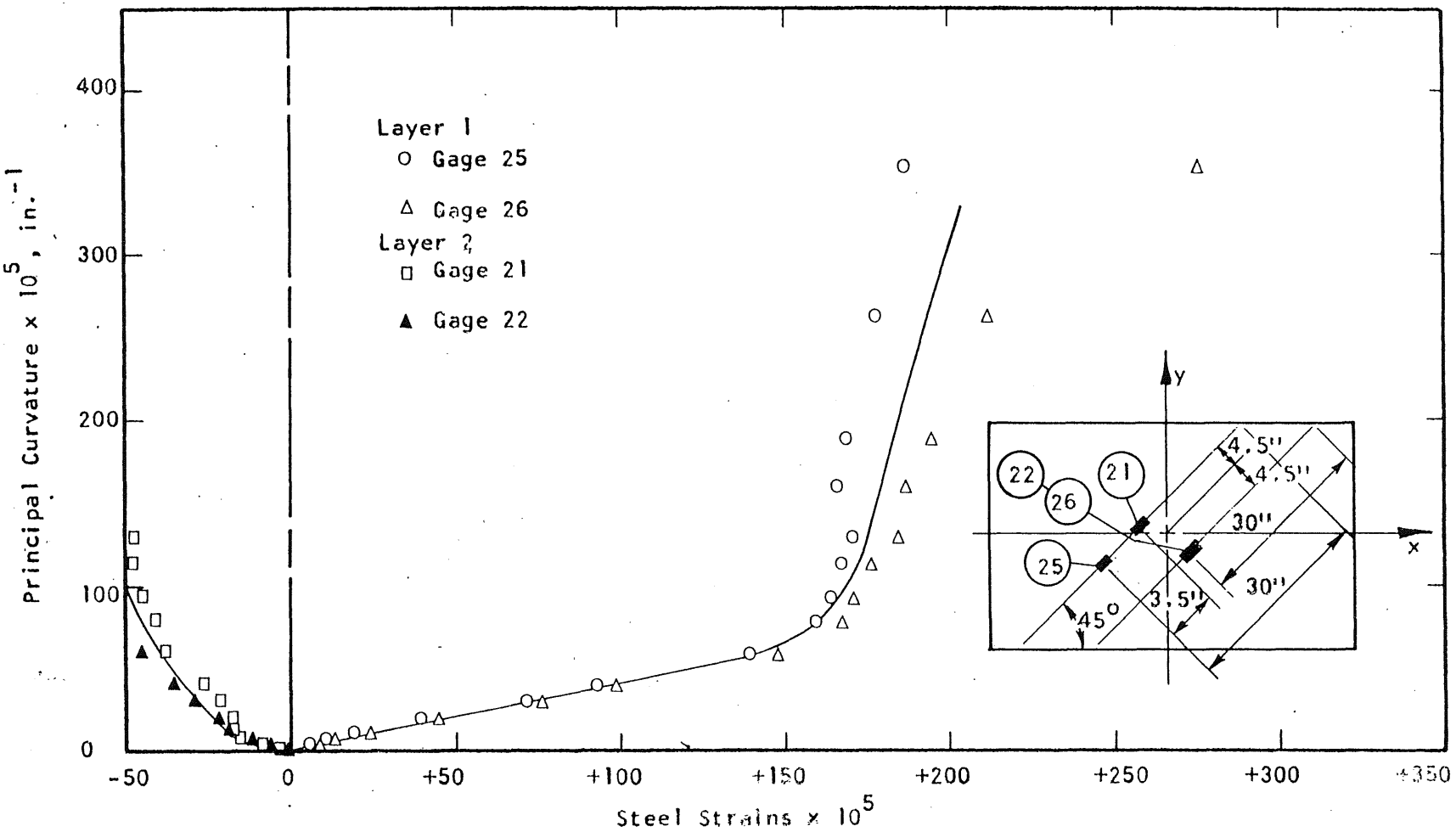

FIG. A.186 STEEL STRAIN PLOT, SPECIMEN B18

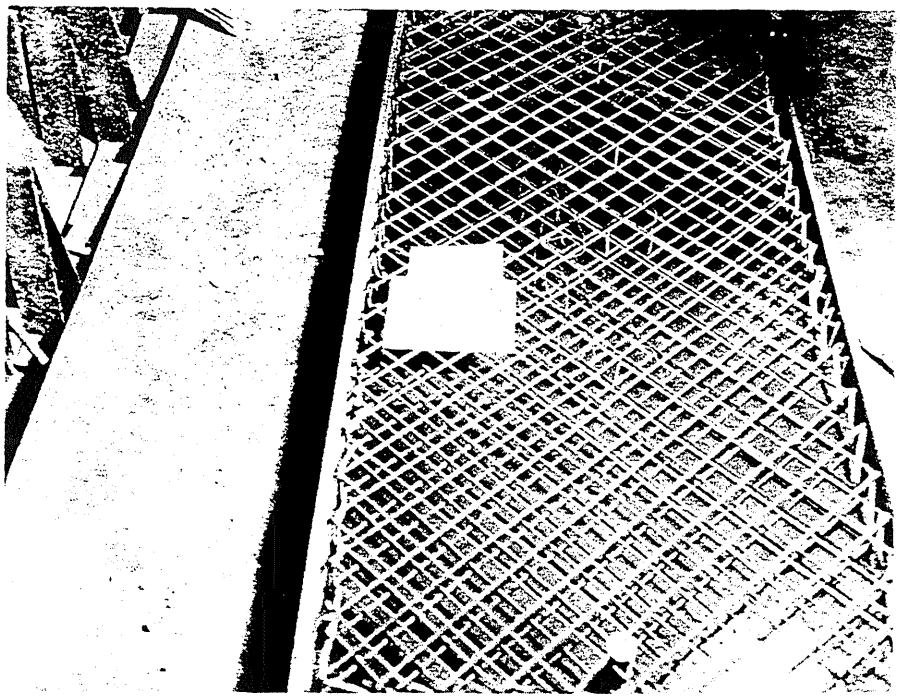

FIG. A.187 REINFORCEMENT IN SPECIMEN B19

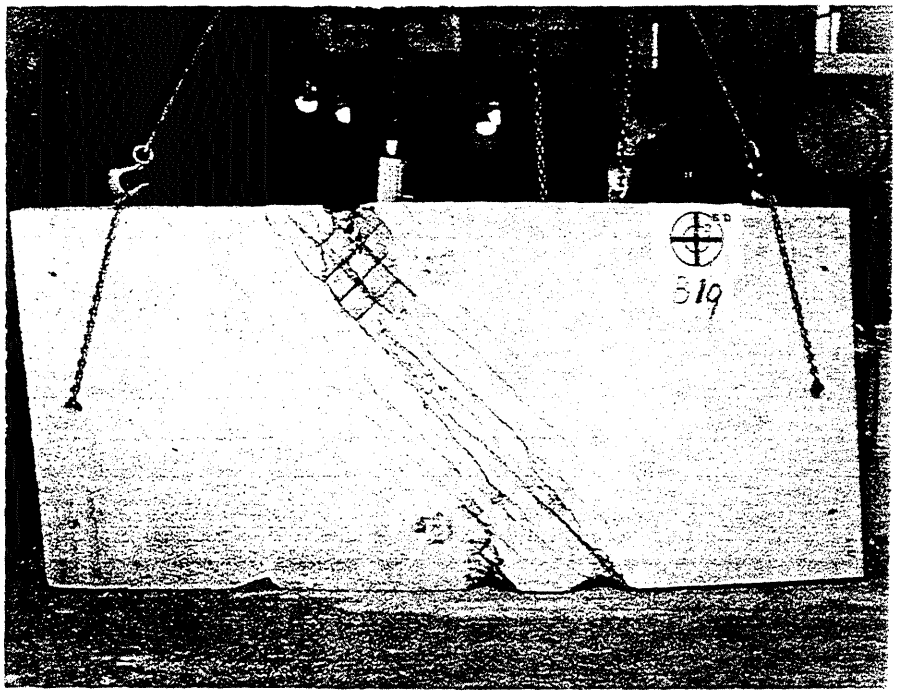

FIG. A.188 CRACK PATTERN IN BOTTOM SURFACE OF B19

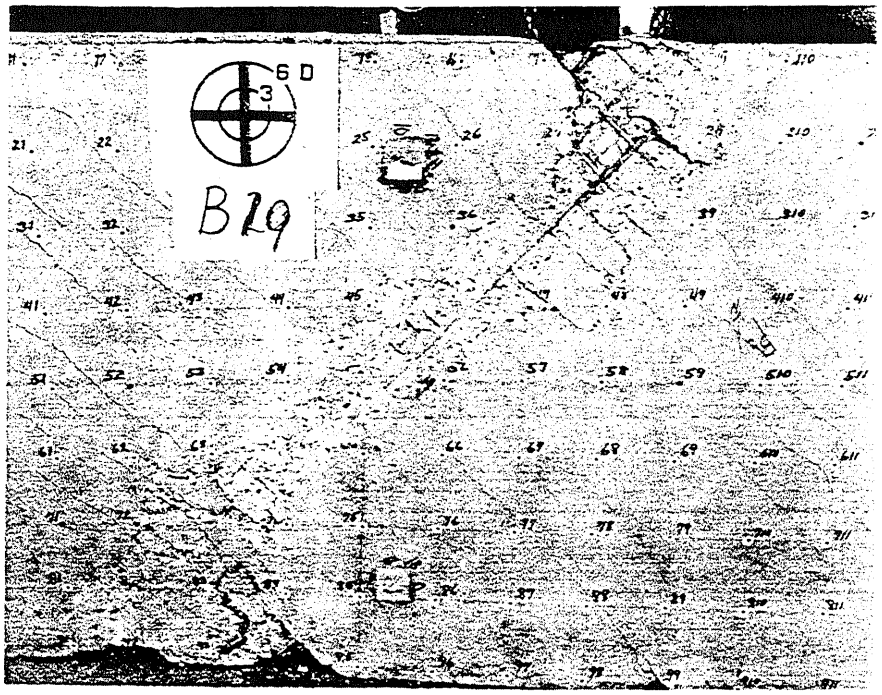

FIG. A 189 CRACK PATTERN IN TOP SURFACE OF B19

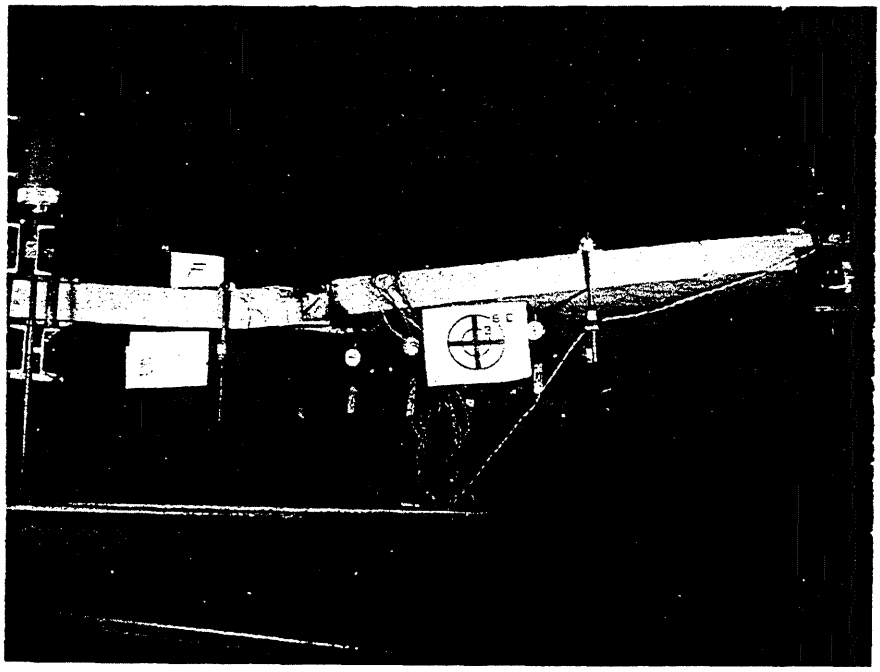

FIG. A.190 SIDE VIEW OF B19

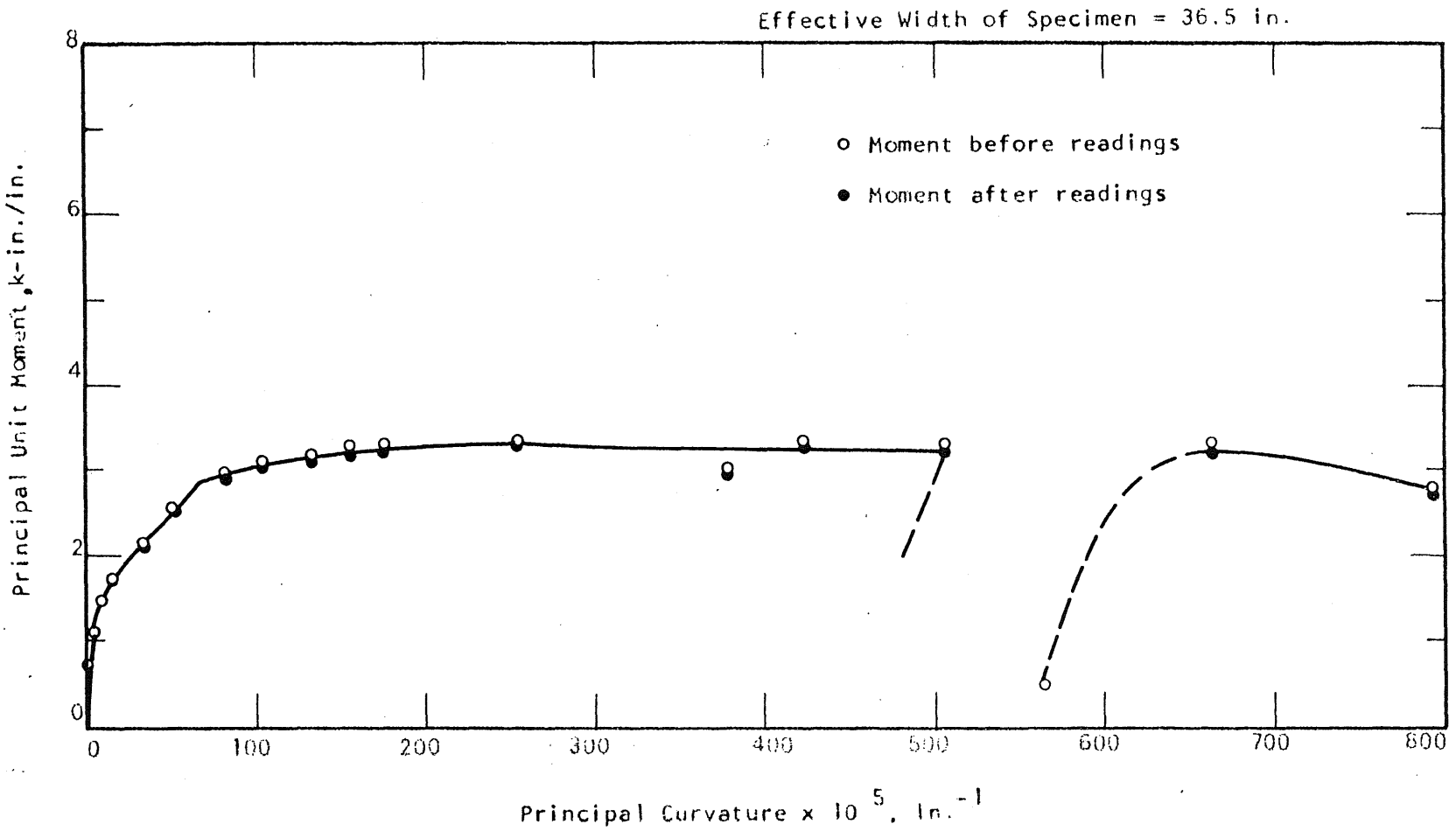

FIG. A.191 MOMENT-CURVATURE PLOT FOR SPECIMEN B19

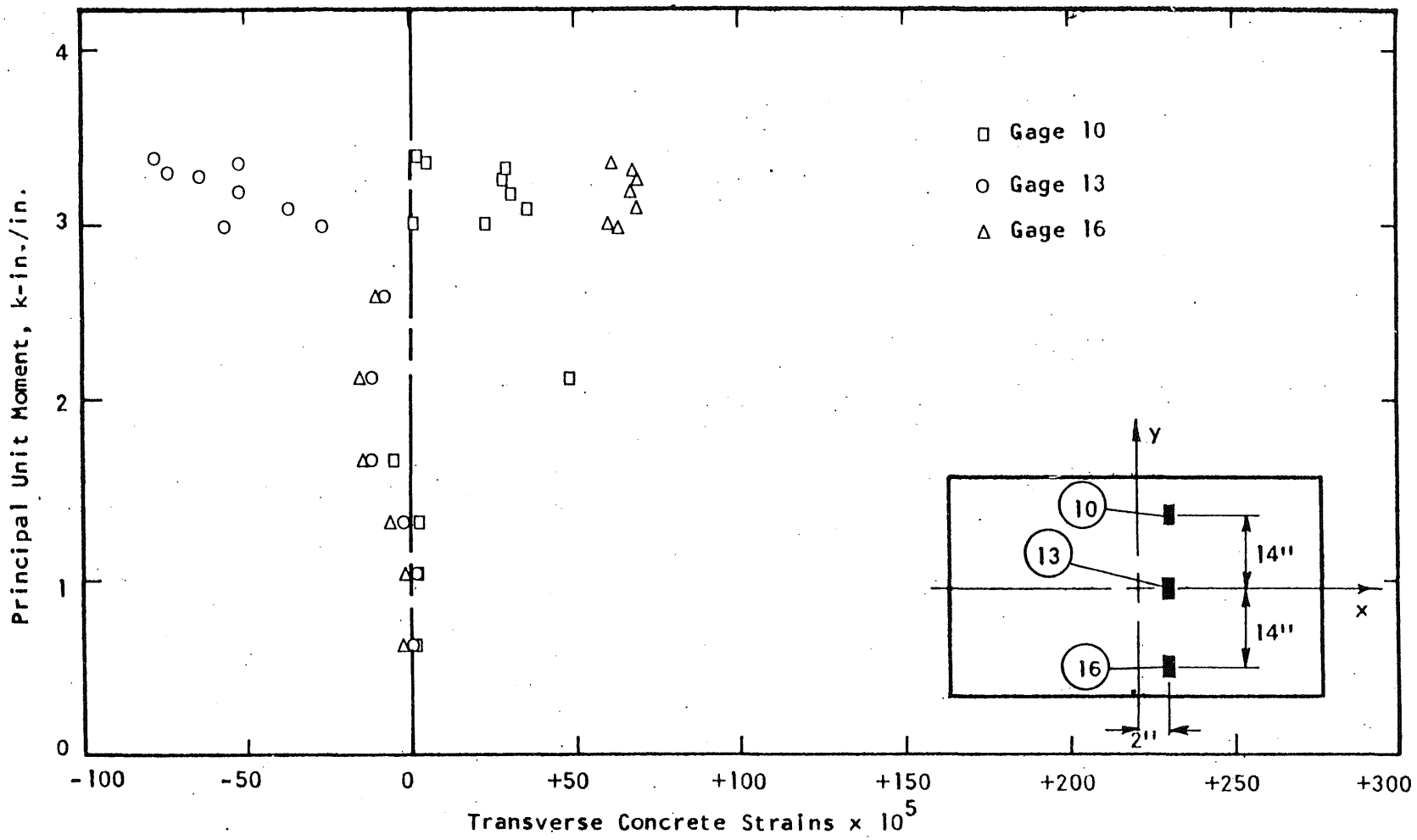

FIG. A.192 CONCRETE STRAIN PLOT, TOP SIDE OF SPECIMEN B19

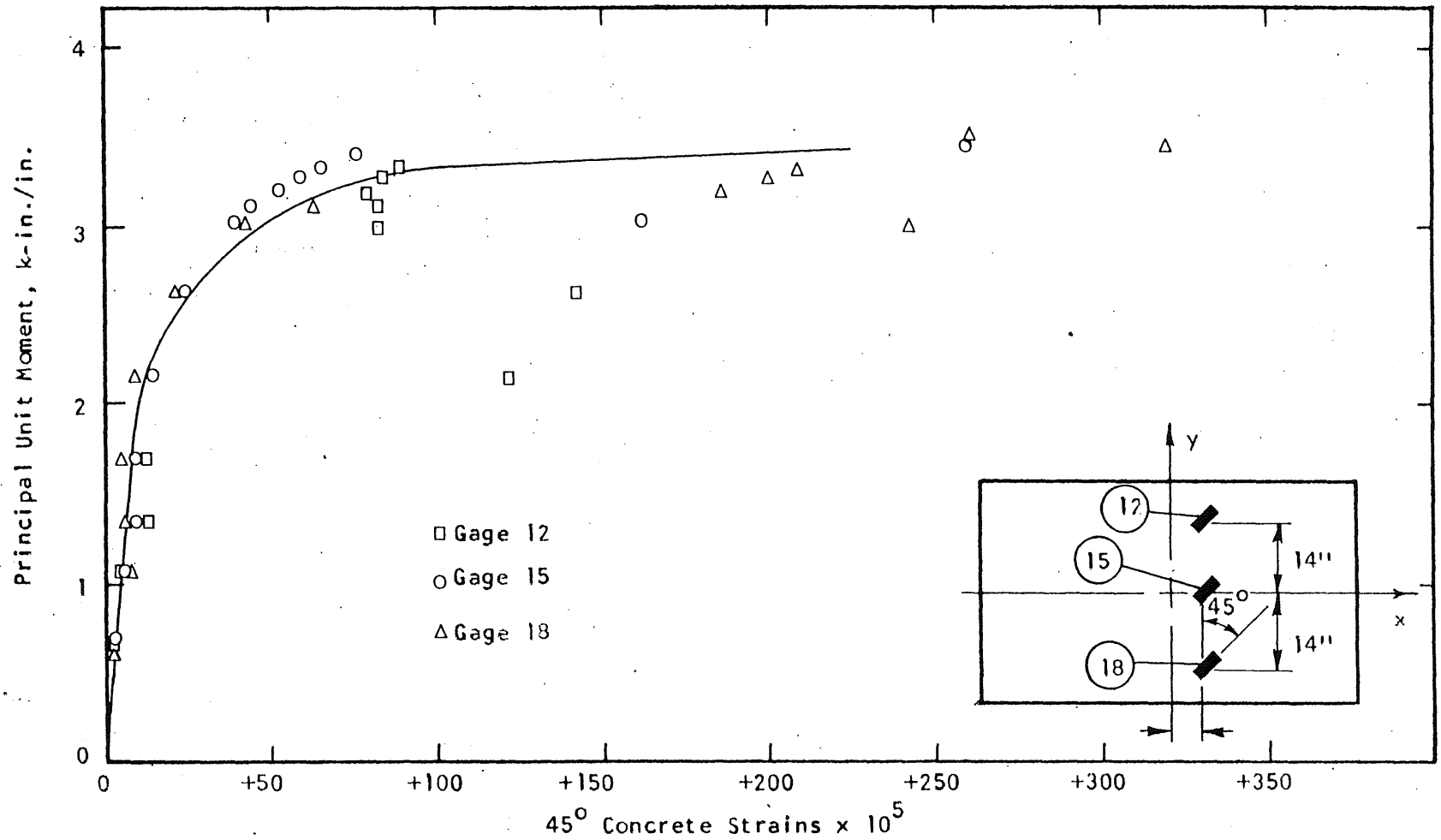

FIG. A.193 CONCRETE STRAIN PLOT, TOP SIDE OF SPECIMEN B19

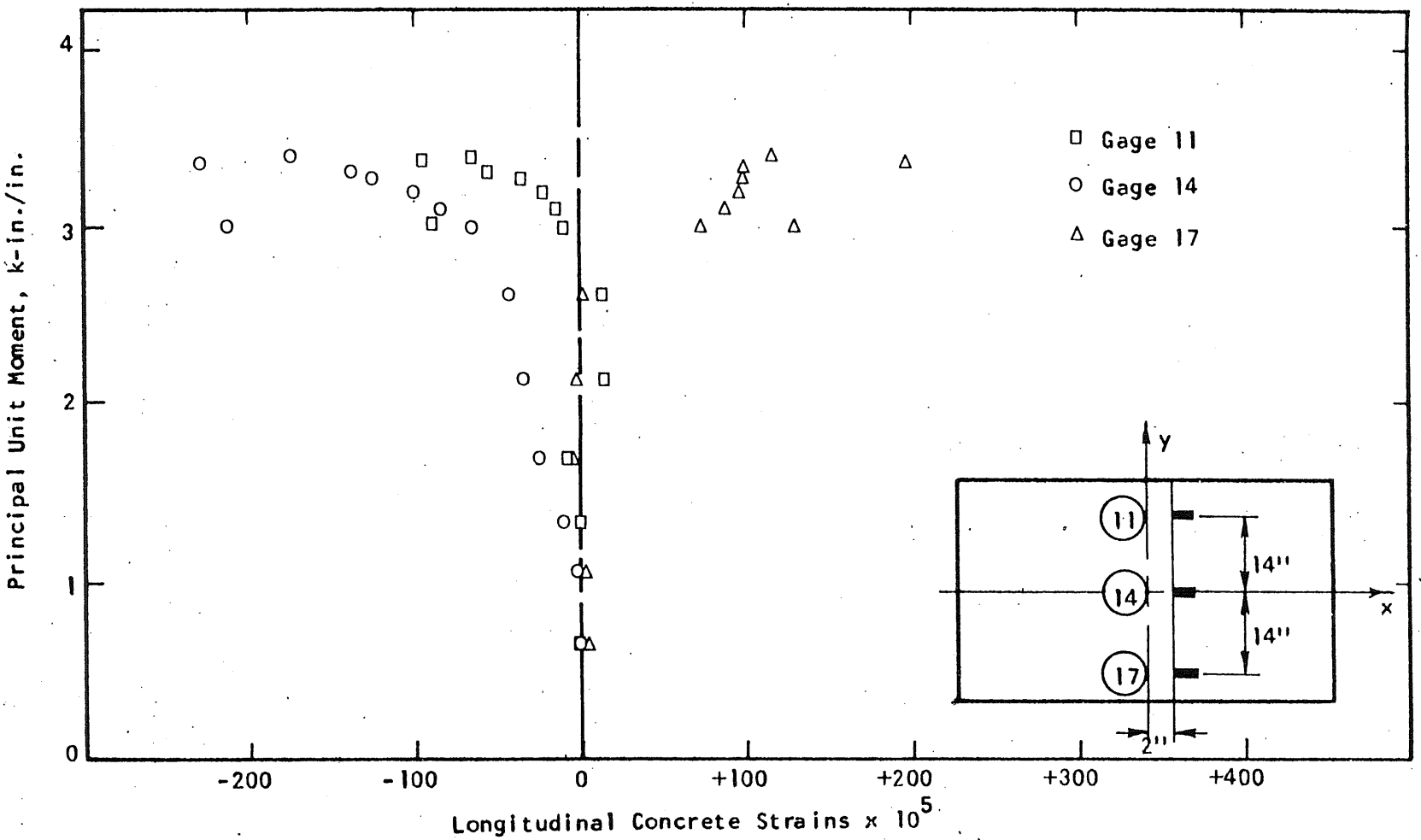

FIG. A.194 CONCRETE STRAIN PLOT, TOP SIDE OF SPECIMEN B19

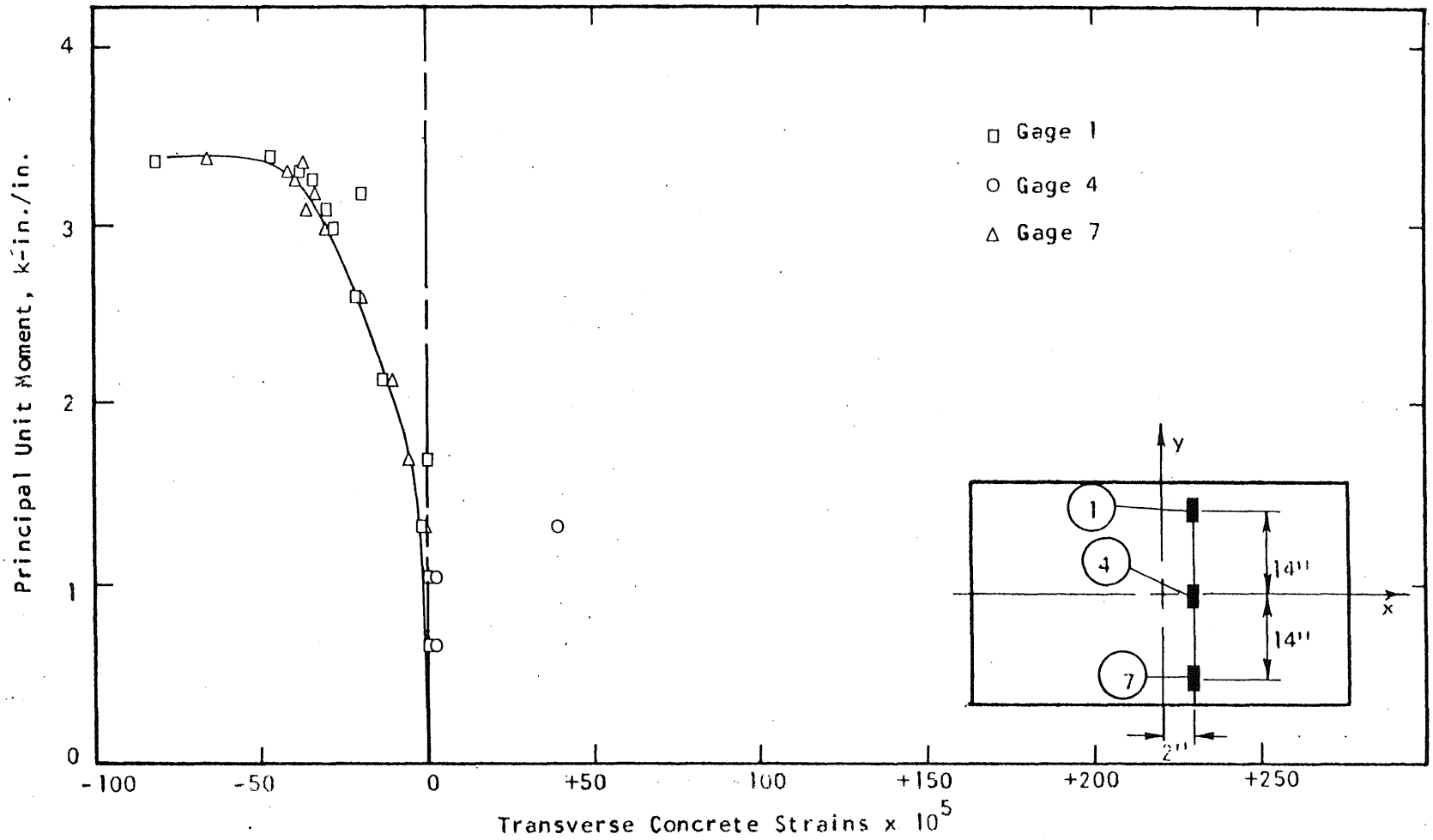

FIG. A.195 CONCRETE STRAIN PLOT, BOTTOM SIDE OF SPECIMEN B19

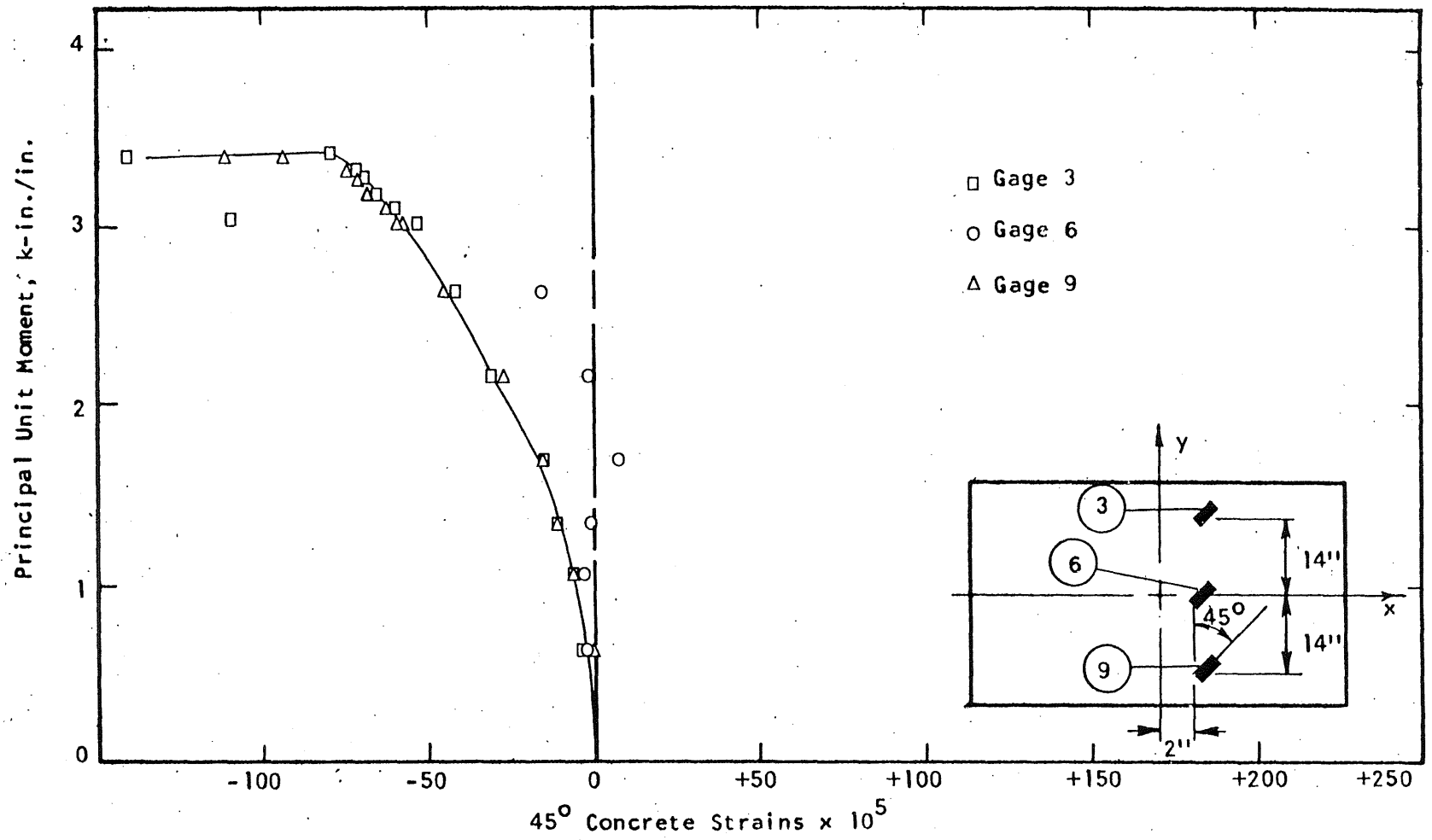

FIG. A.196 CONCRETE STRAIN PLOT, BOTTOM SIDE OF SPECIMEN B19

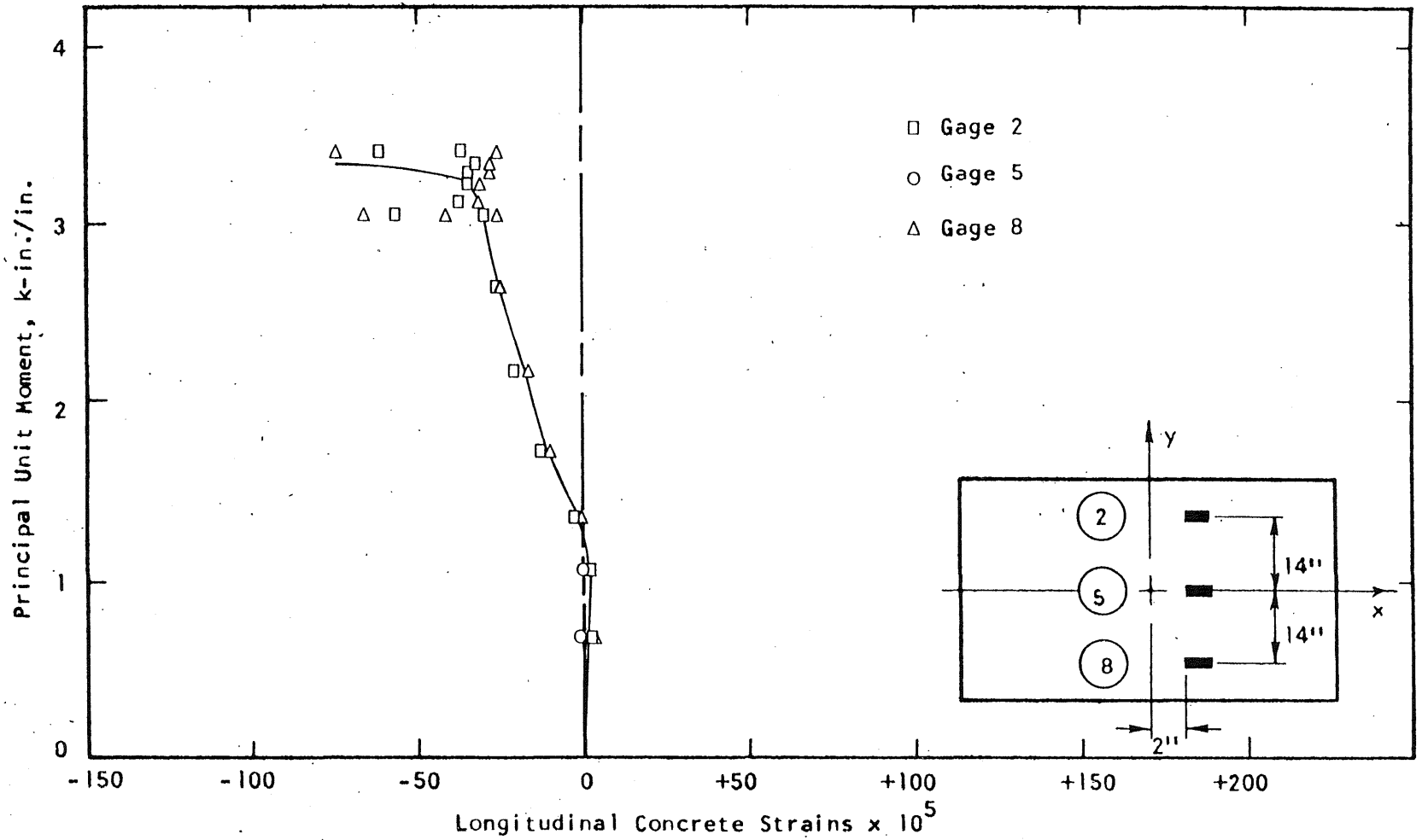

FIG. A.197 CONCRETE STRAIN PLOT, BOTTOM SIDE OF SPECIMEN B19

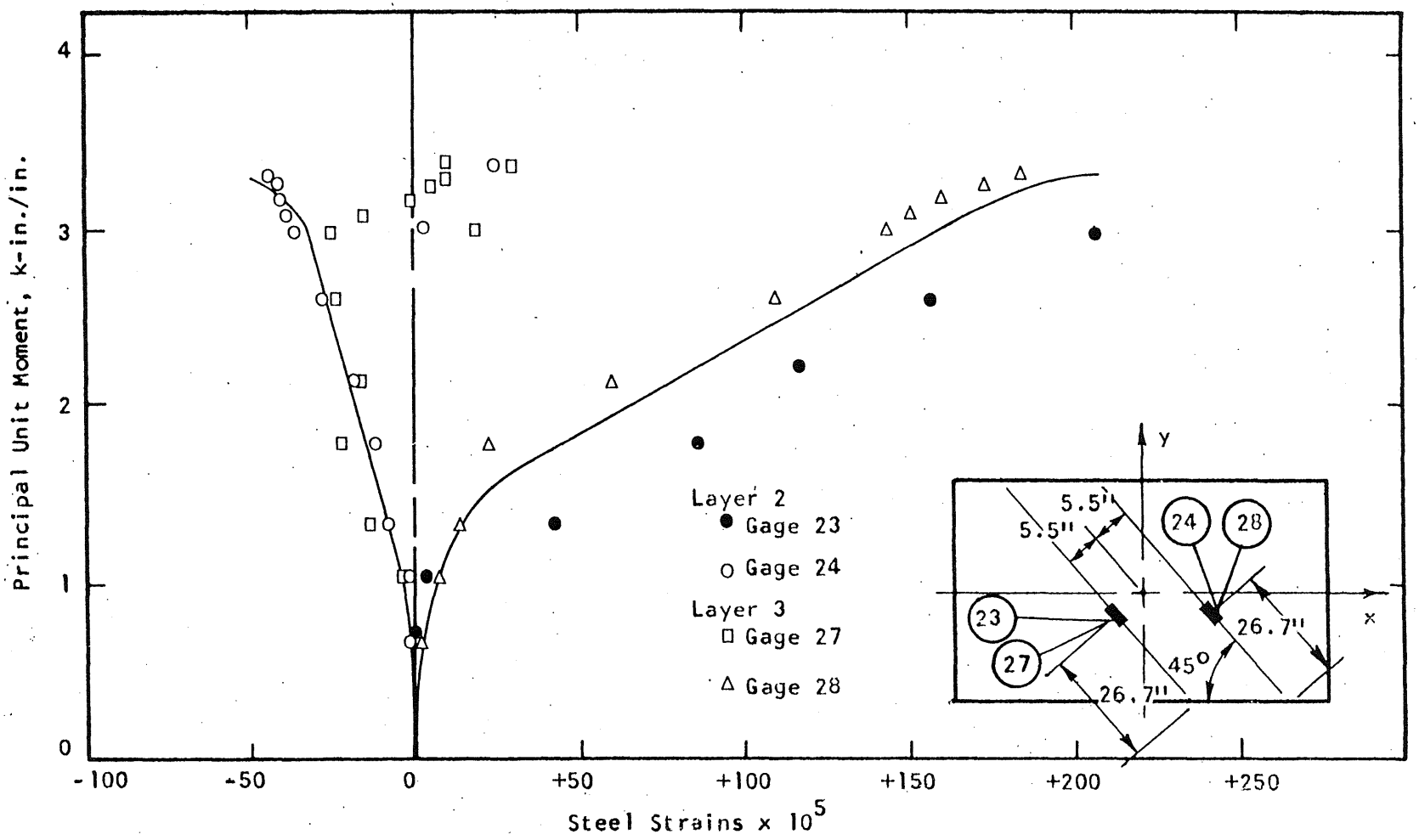

FIG. A.199 STEEL STRAIN PLOT, SPECIMEN B19

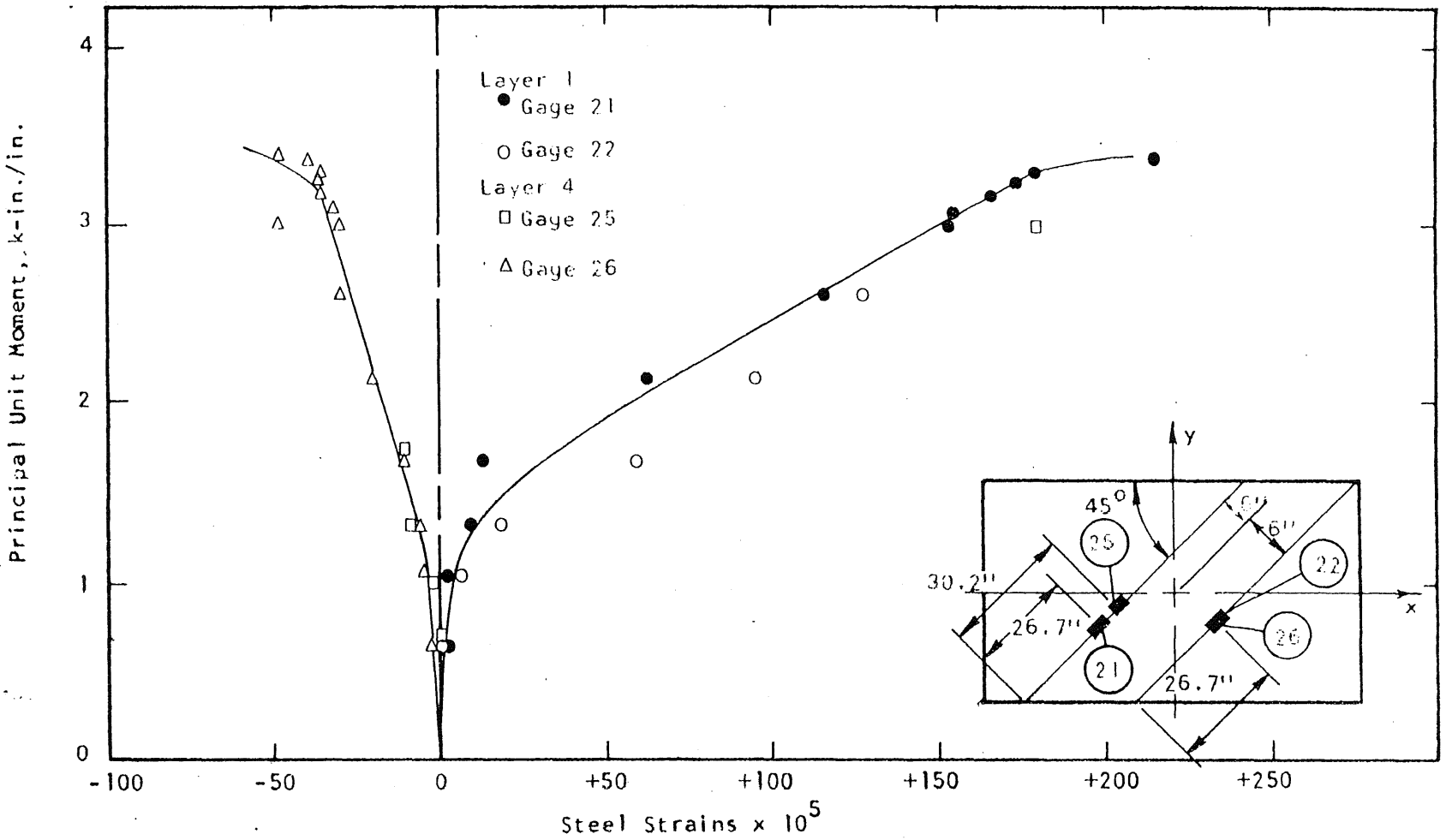

FIG. A 198 STEEL STRAIN PLOT, SPECIMEN B19

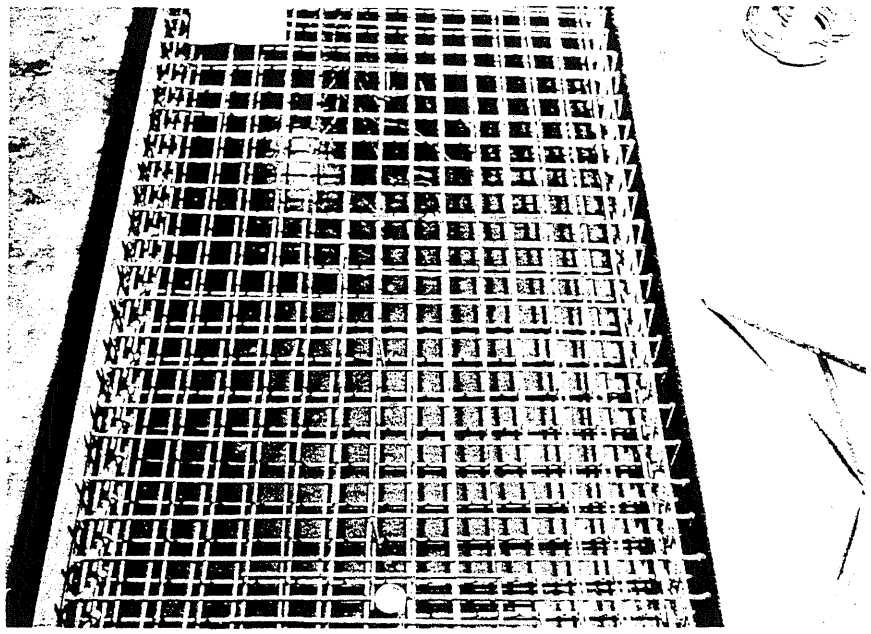

FIG. A.200 REINFORCEMENT IN SPECIMEN B20

FIG. A.201 CLOSE-UP END VIEW OF REINFORCEMENT IN B20

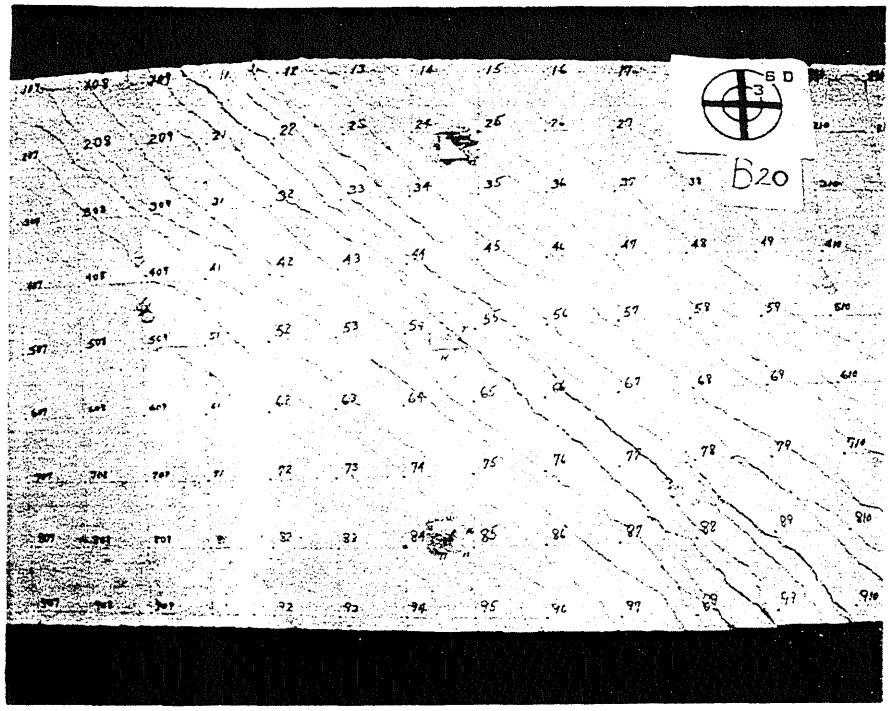

FIG. A.202 CRACK PATTERN IN TOP SURFACE OF B20

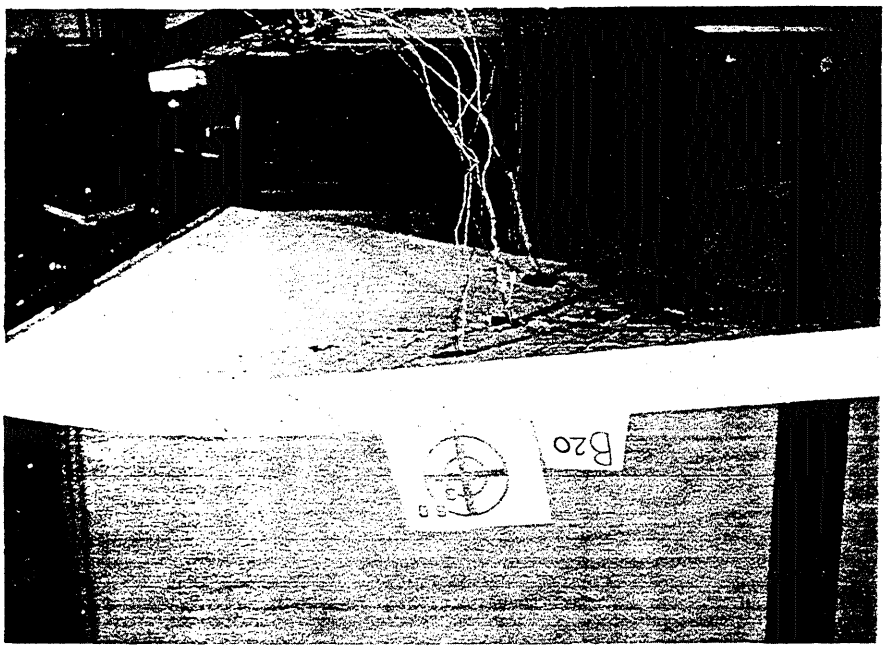

FIG. A.203 SIDE VIEW OF B20

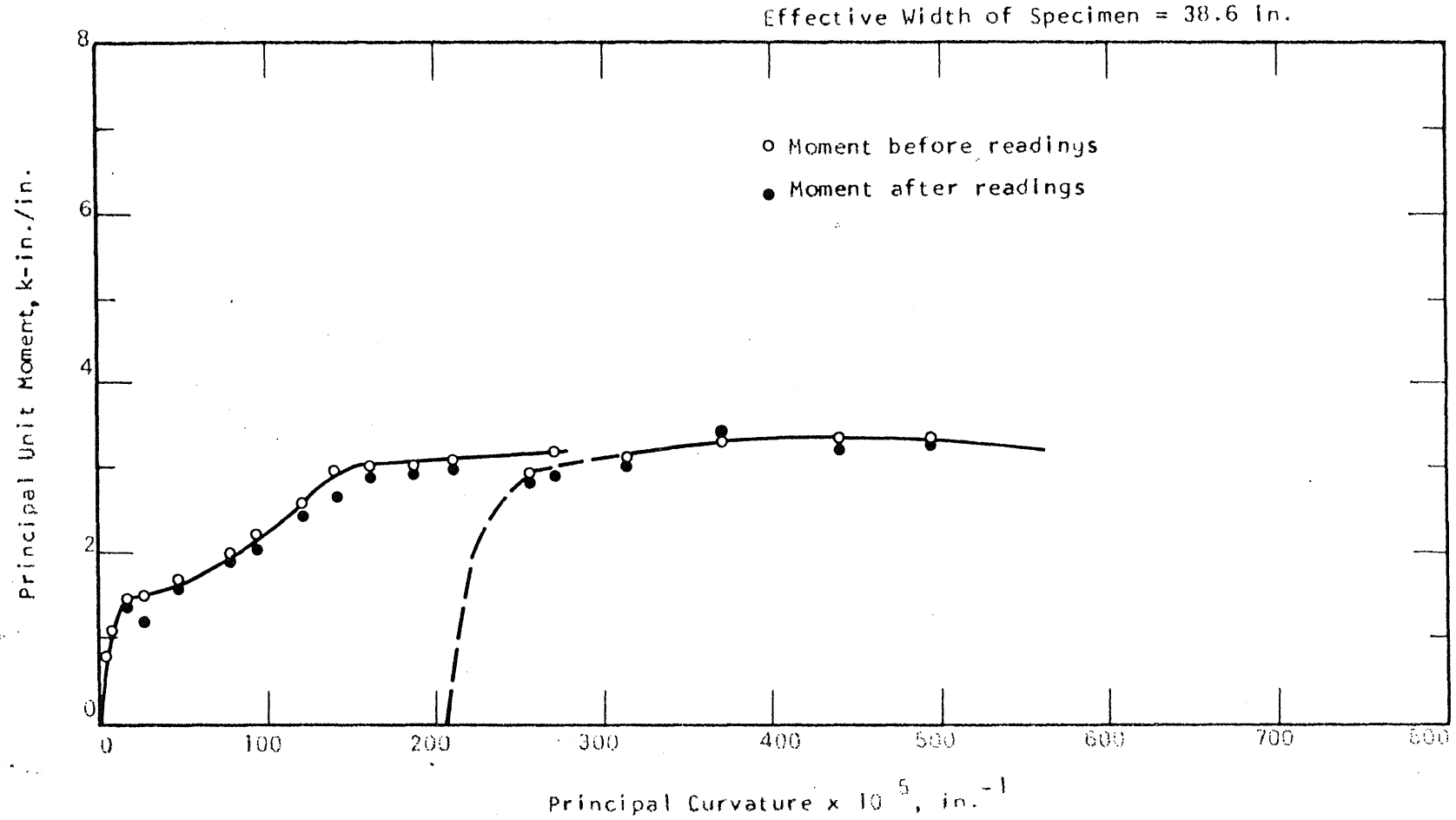

FIG. A.204 MOMENT-CURVATURE PLOT FOR SPECIMEN B20

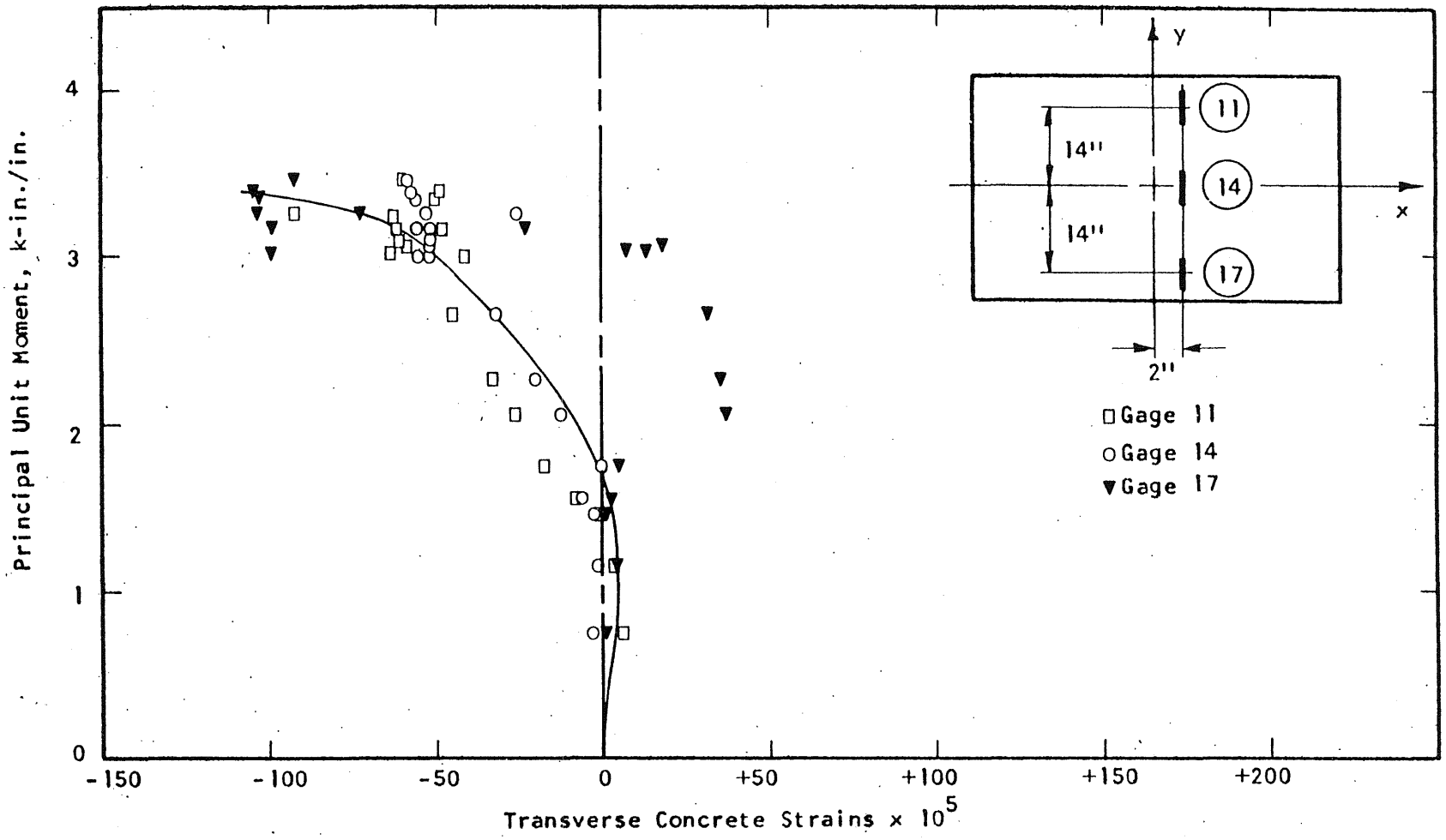

FIG. A.205 CONCRETE STRAIN PLOT, TOP SIDE OF SPECIMEN B20

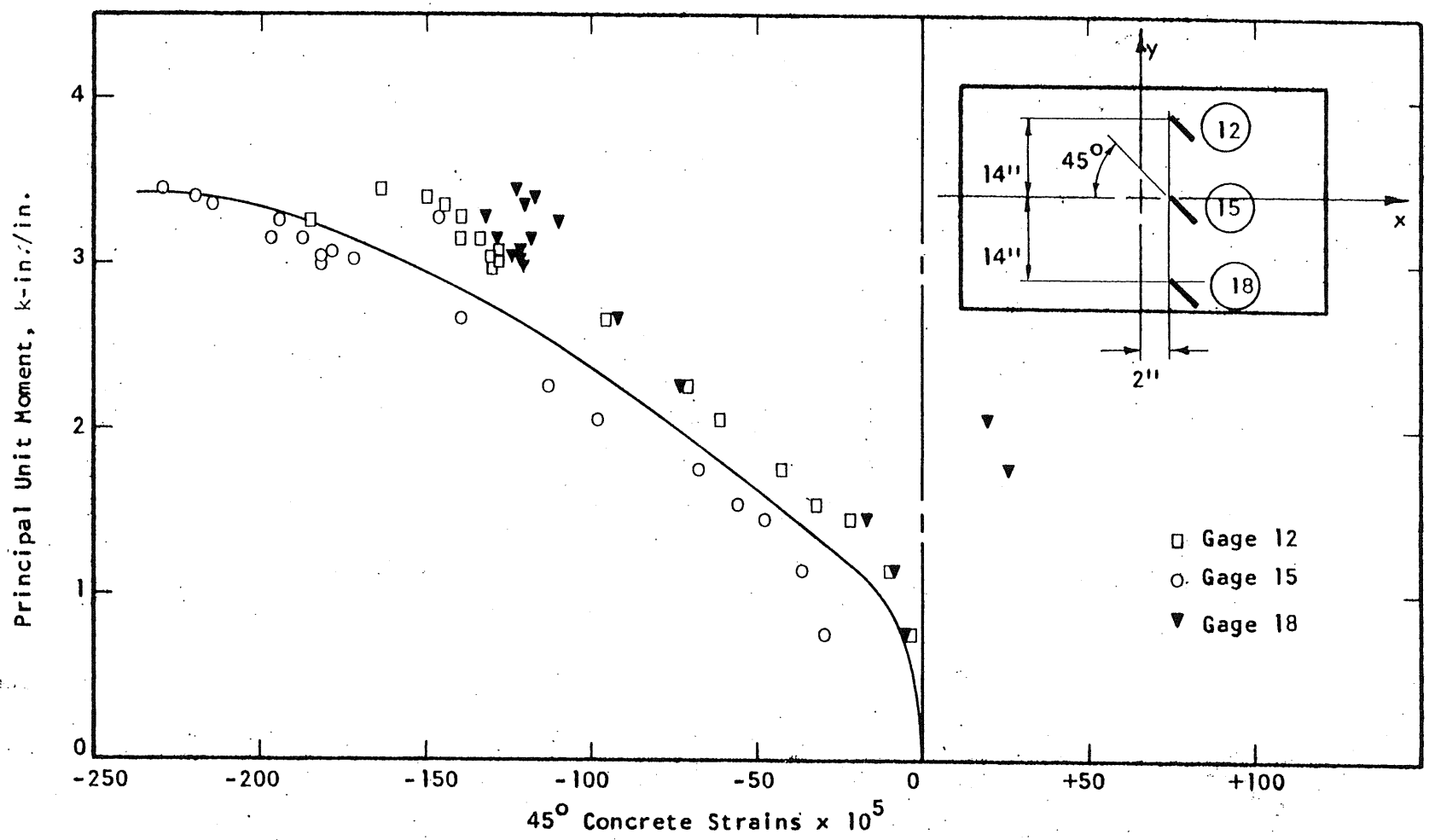

FIG. A.206 CONCRETE STRAIN PLOT, TOP SIDE OF SPECIMEN B20

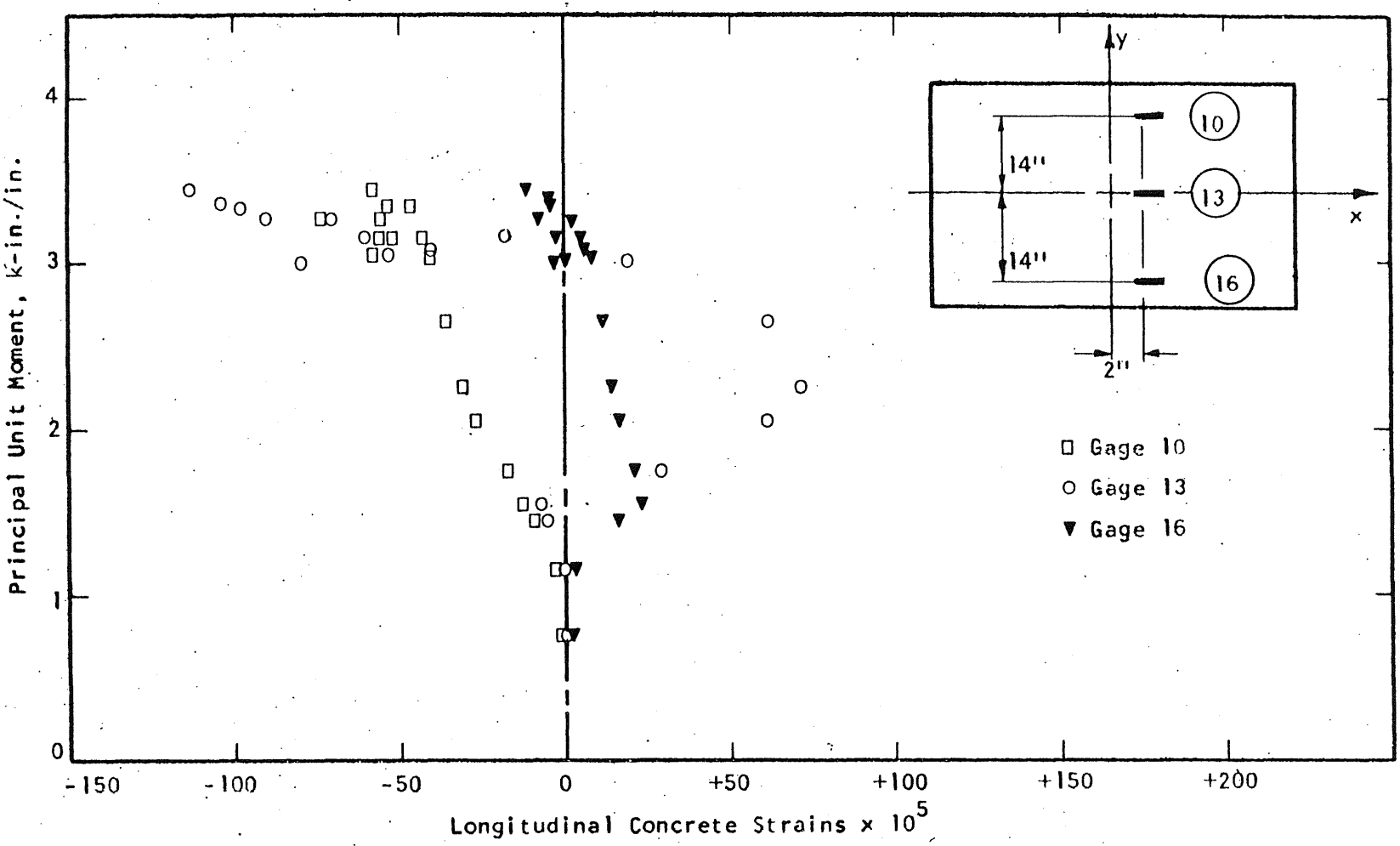

FIG. A.207 CONCRETE STRAIN PLOT, TOP SIDE OF SPECIMEN B20

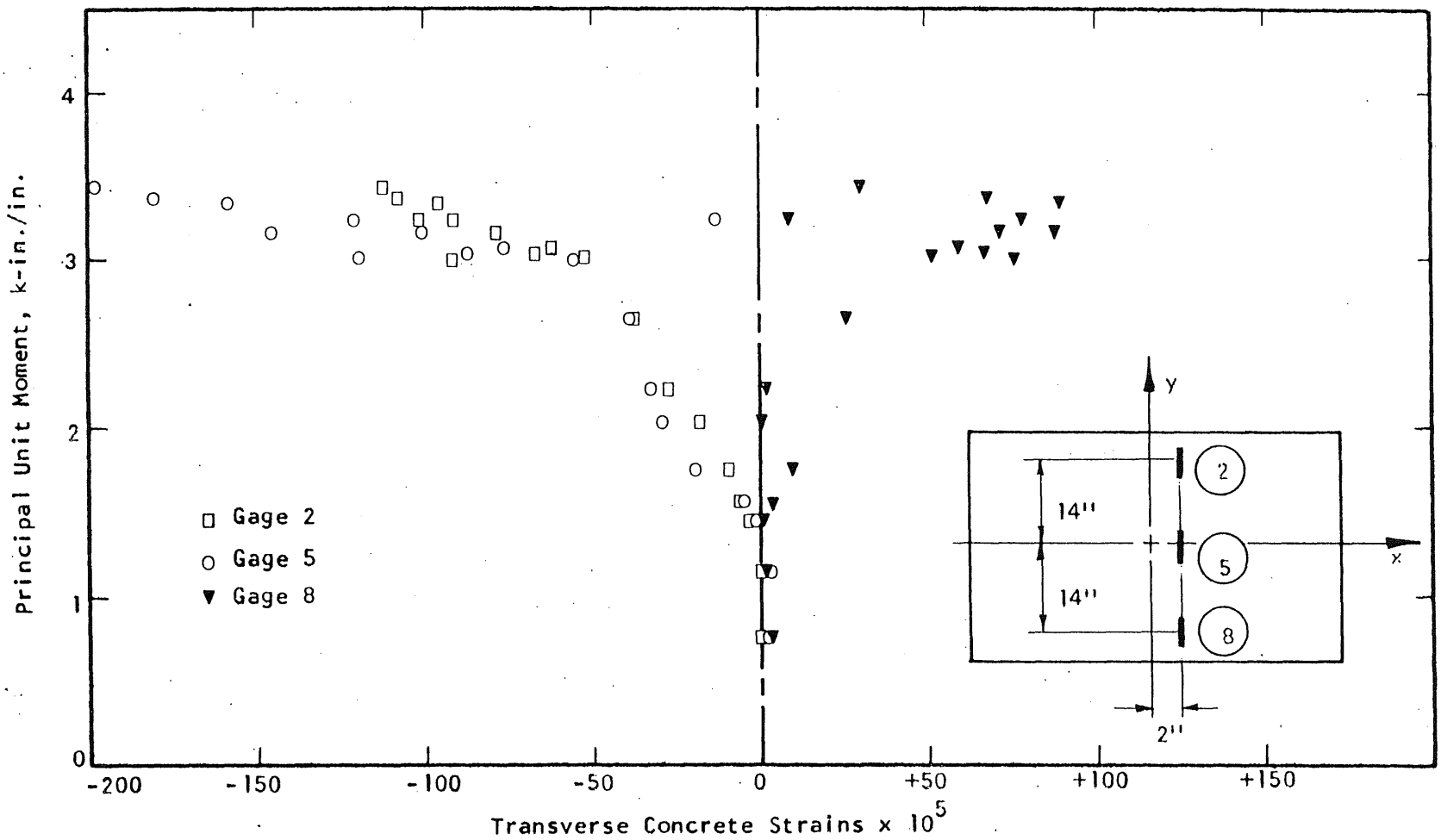

FIG. A.208 CONCRETE STRAIN PLOT, BOTTOM SURFACE OF B20

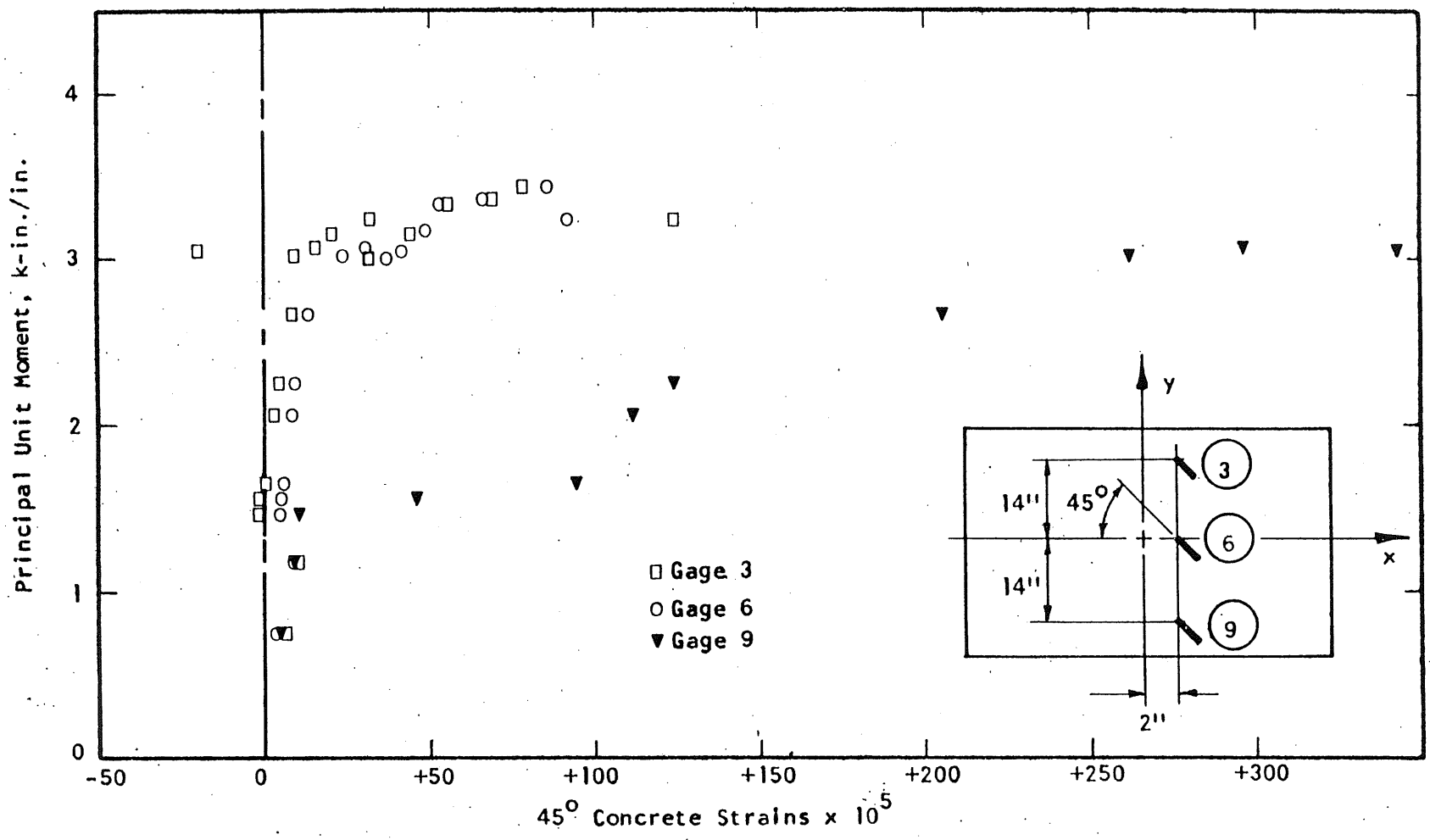

FIG. A.209 CONCRETE STRAIN PLOT, BOTTOM SIDE OF SPECIMEN B20

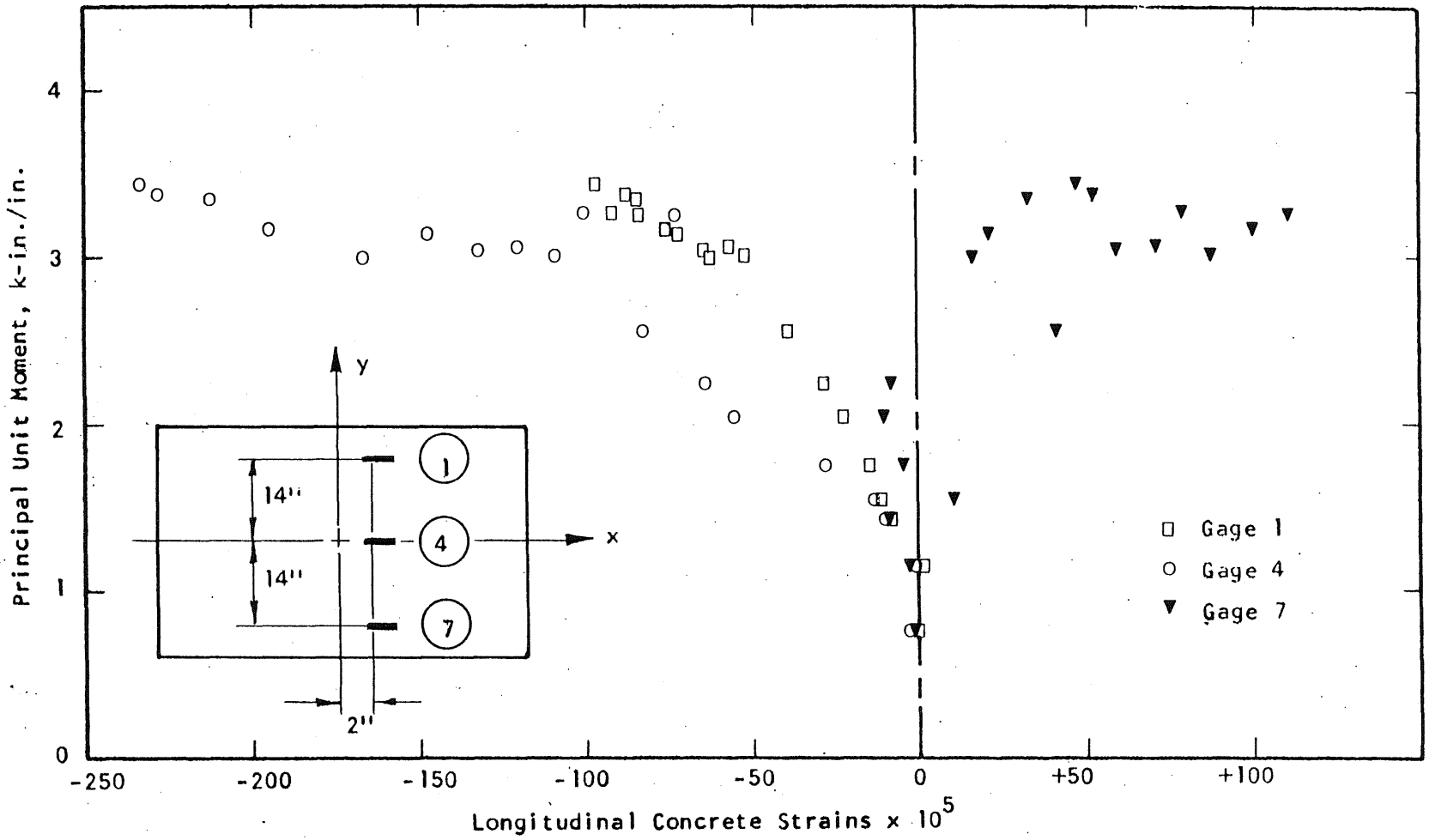

FIG. A.210 CONCRETE STRAIN PLOT, BOTTOM SIDE OF SPECIMEN B20

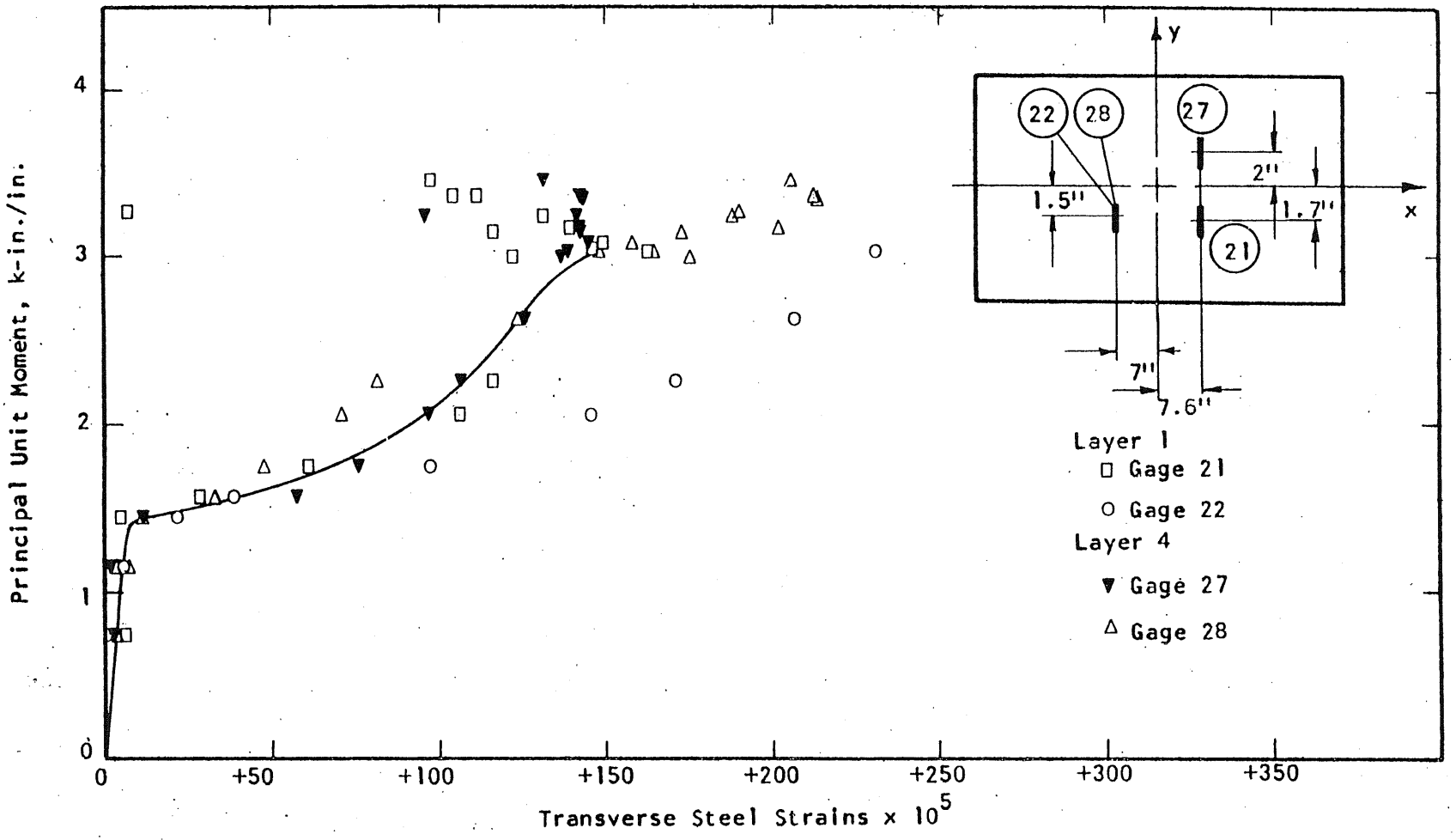

FIG. A.211 STEEL STRAIN PLOT, SPECIMEN B20

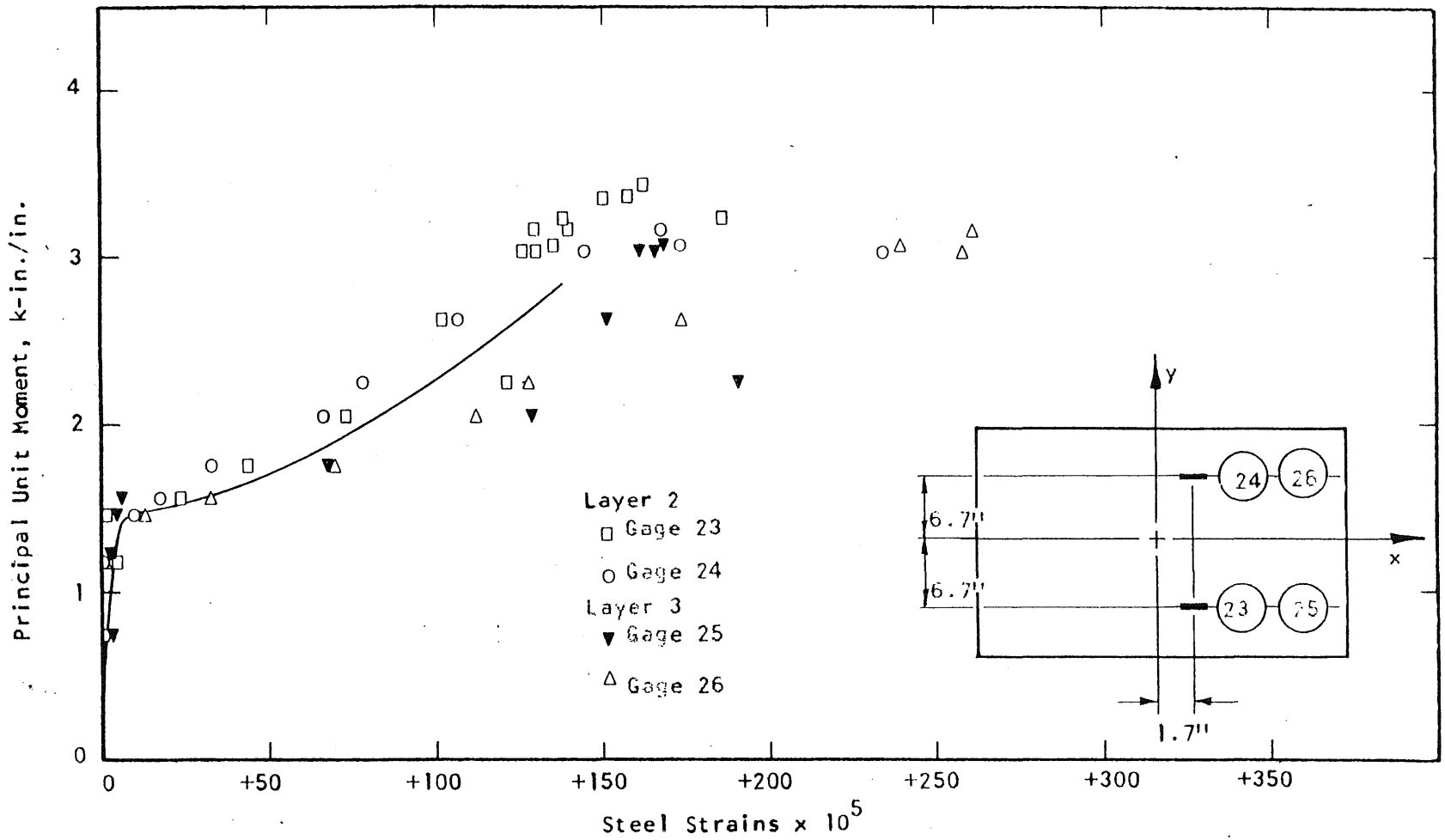

FIG. A.212 STEEL STRAIN PLOT, SPECIMEN B20

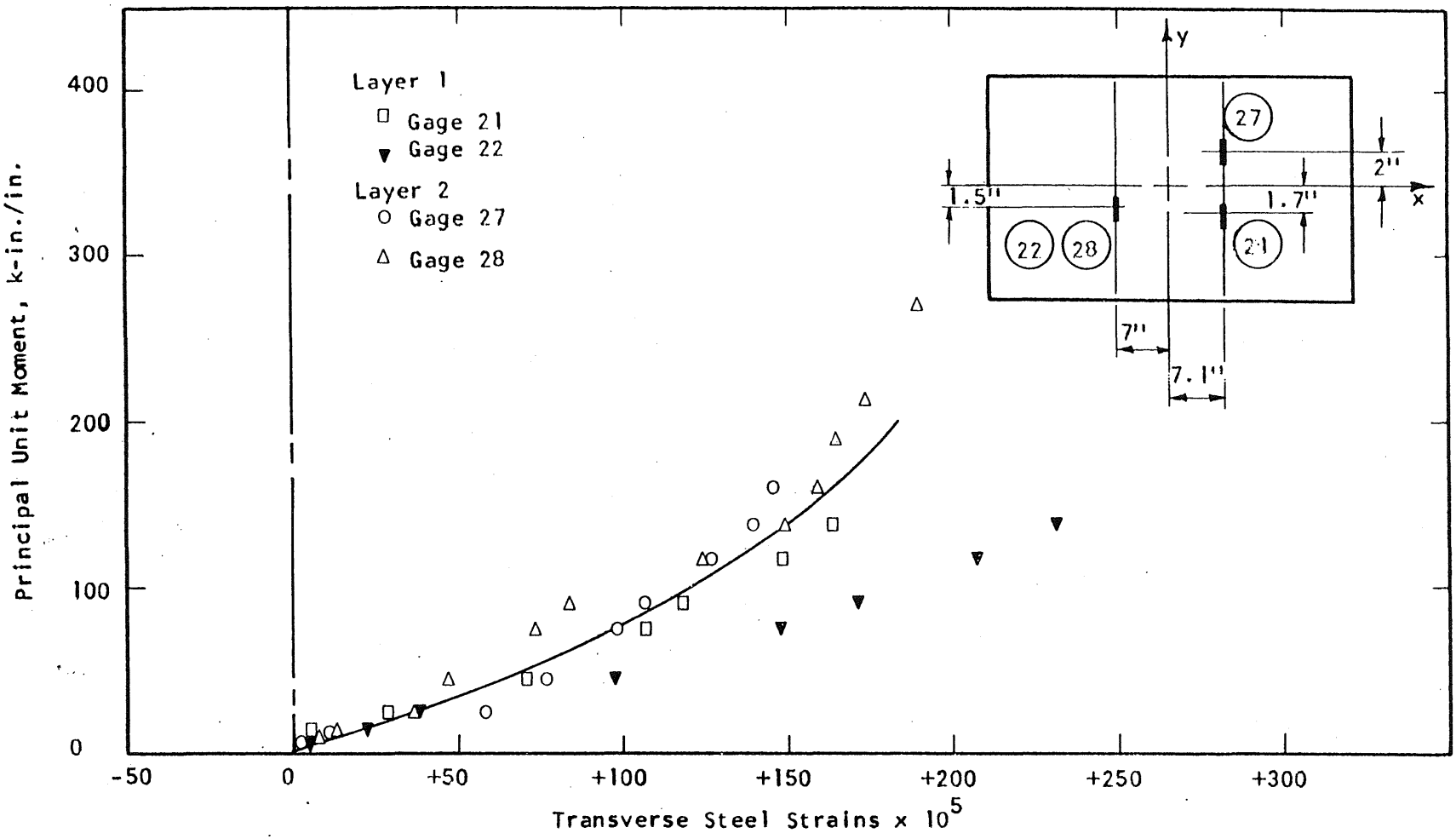

FIG. A.213 STEEL STRAIN PLOT, SPECIMEN B20

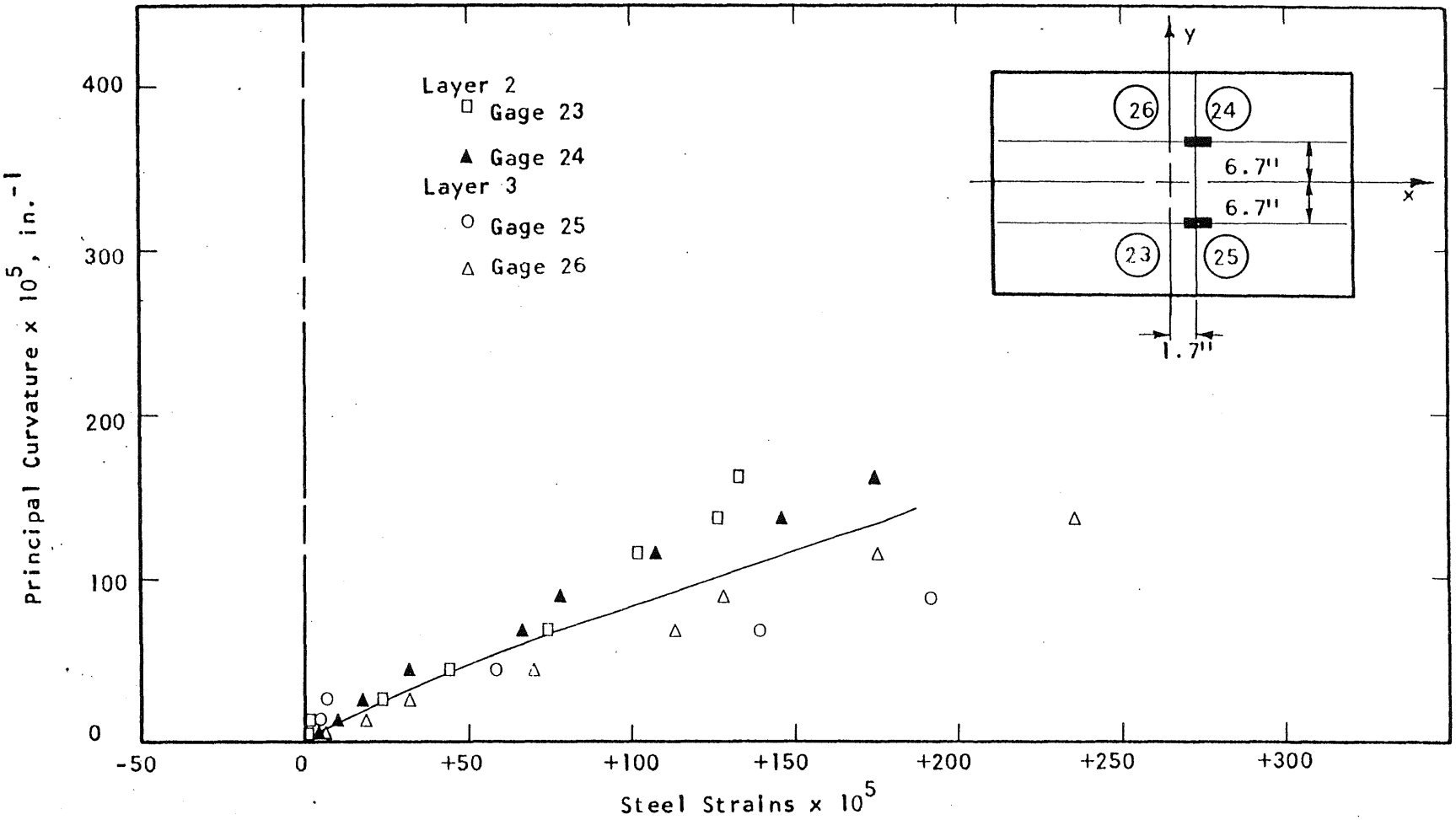

FIG. A.214 STEEL STRAIN PLOT, SPECIMEN B20

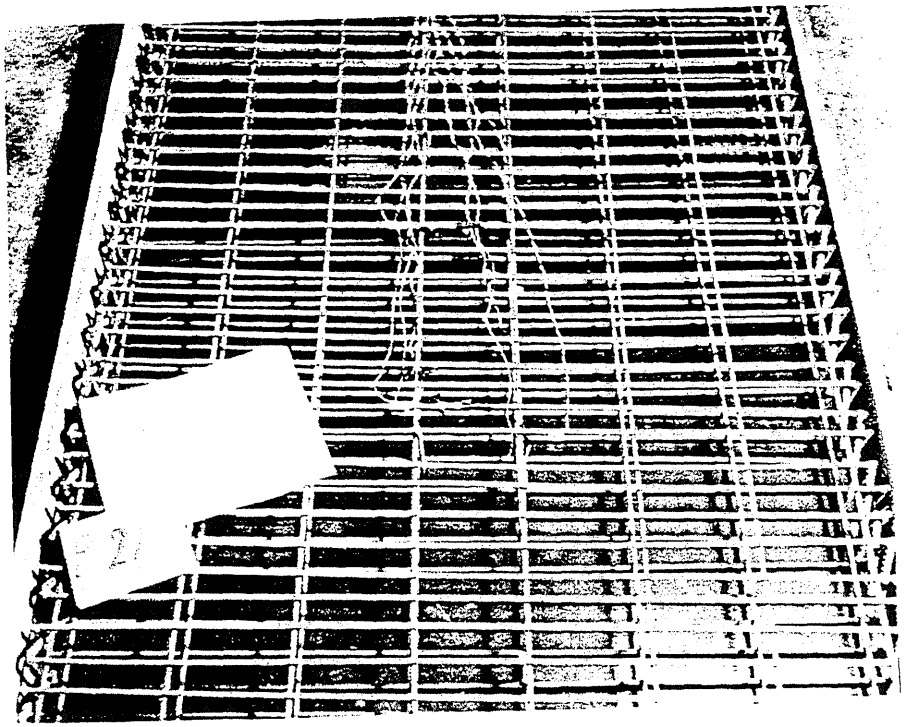

FIG. A.215 REINFORCEMENT IN SPECIMEN B21

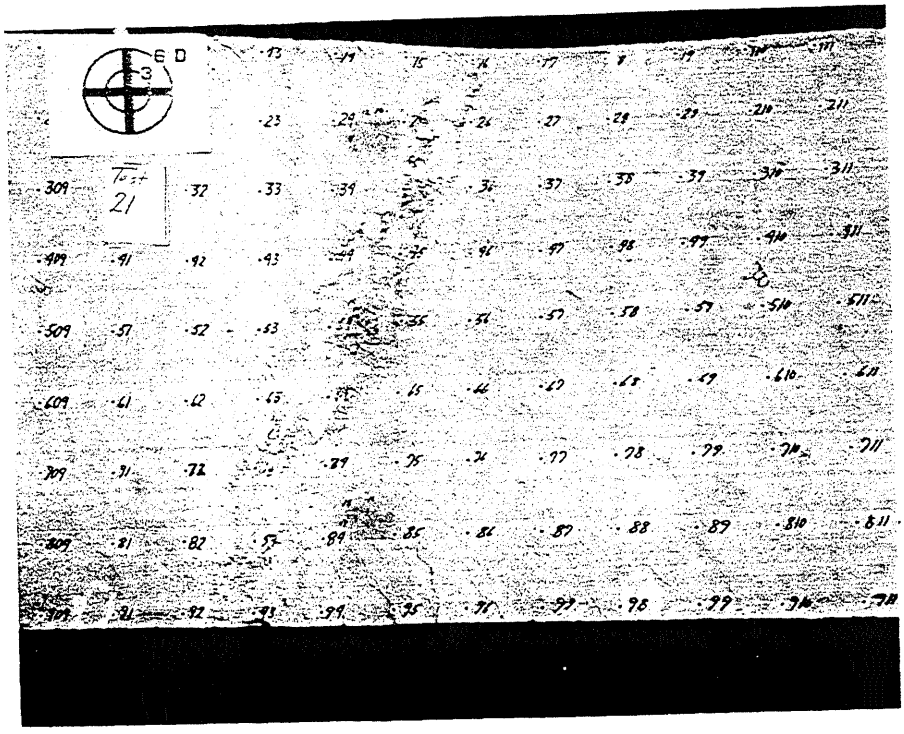

FIG. A.216 CRACK PATTERN IN TOP SURFACE OF B21

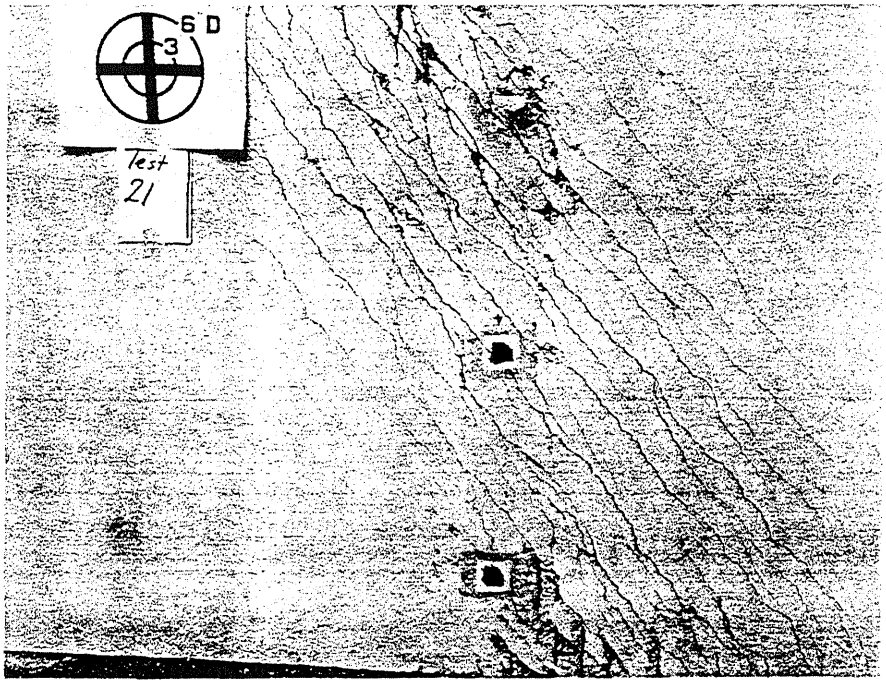

FIG. A.217 CRACK PATTERN IN BOTTOM SURFACE OF B21

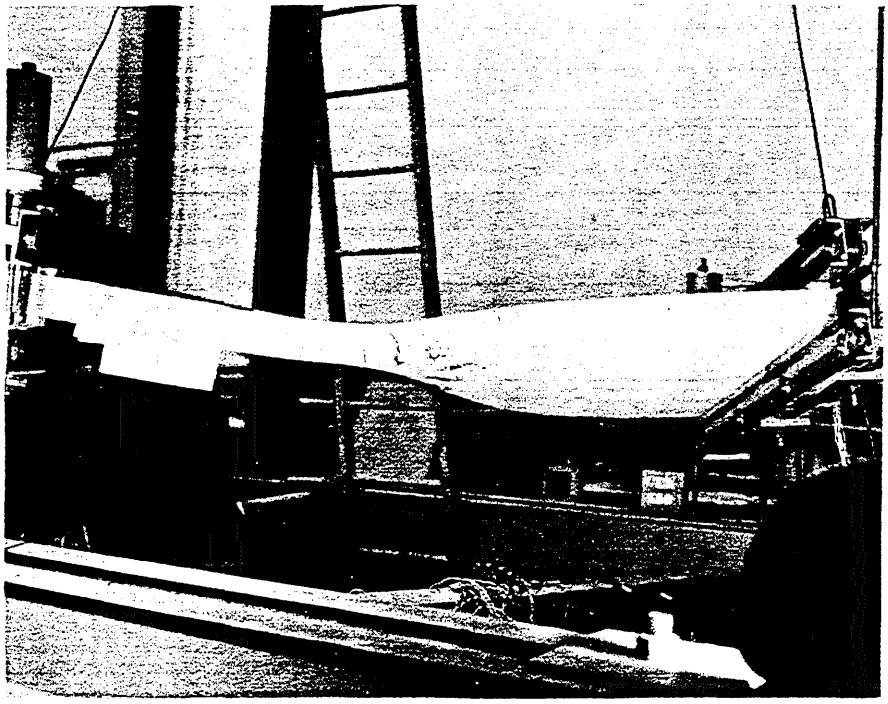

FIG. A.218 SIDE VIEW OF B21

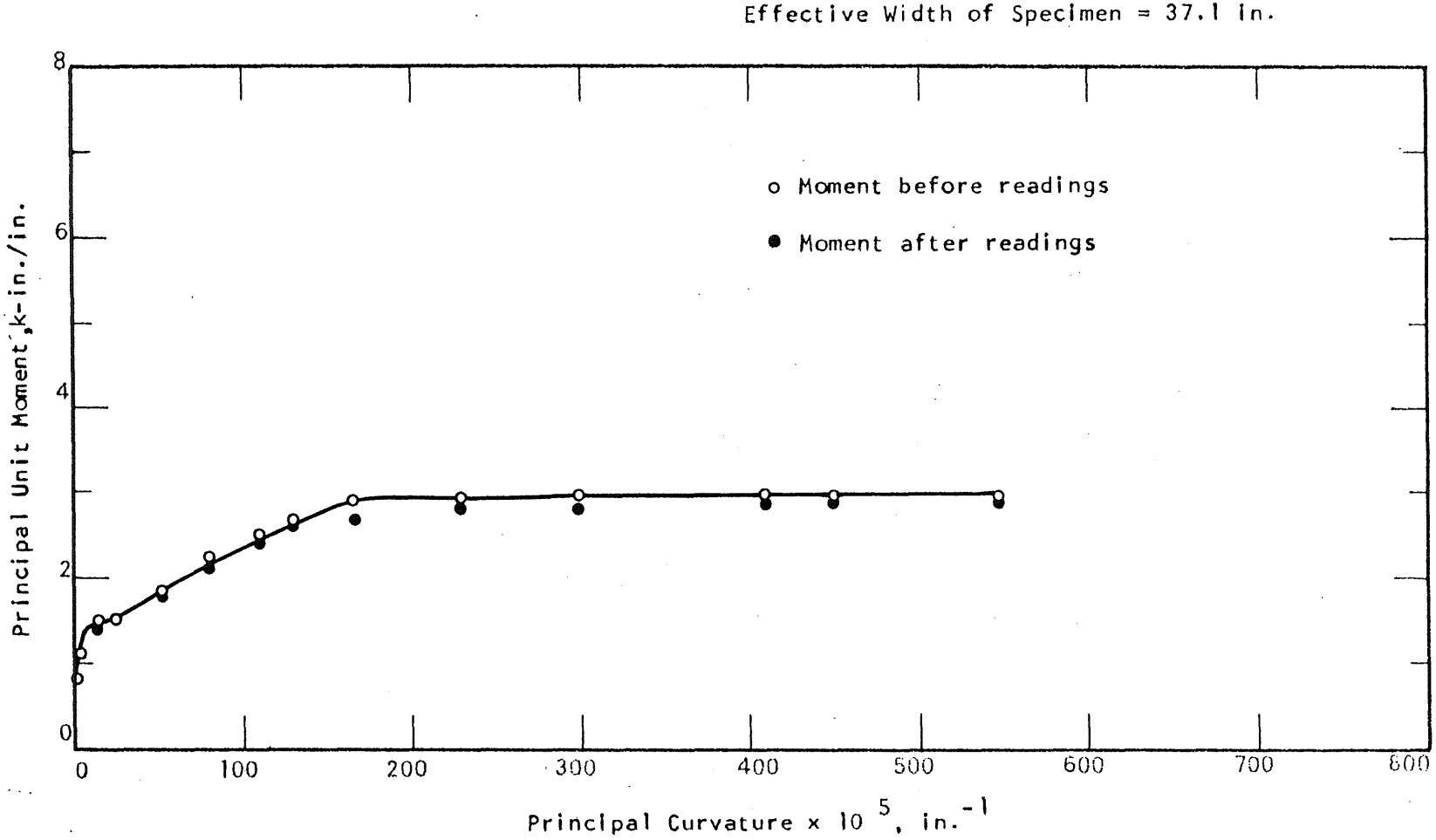

FIG. A.219 MOMENT-CURVATURE PLOT FOR SPECIMEN B21

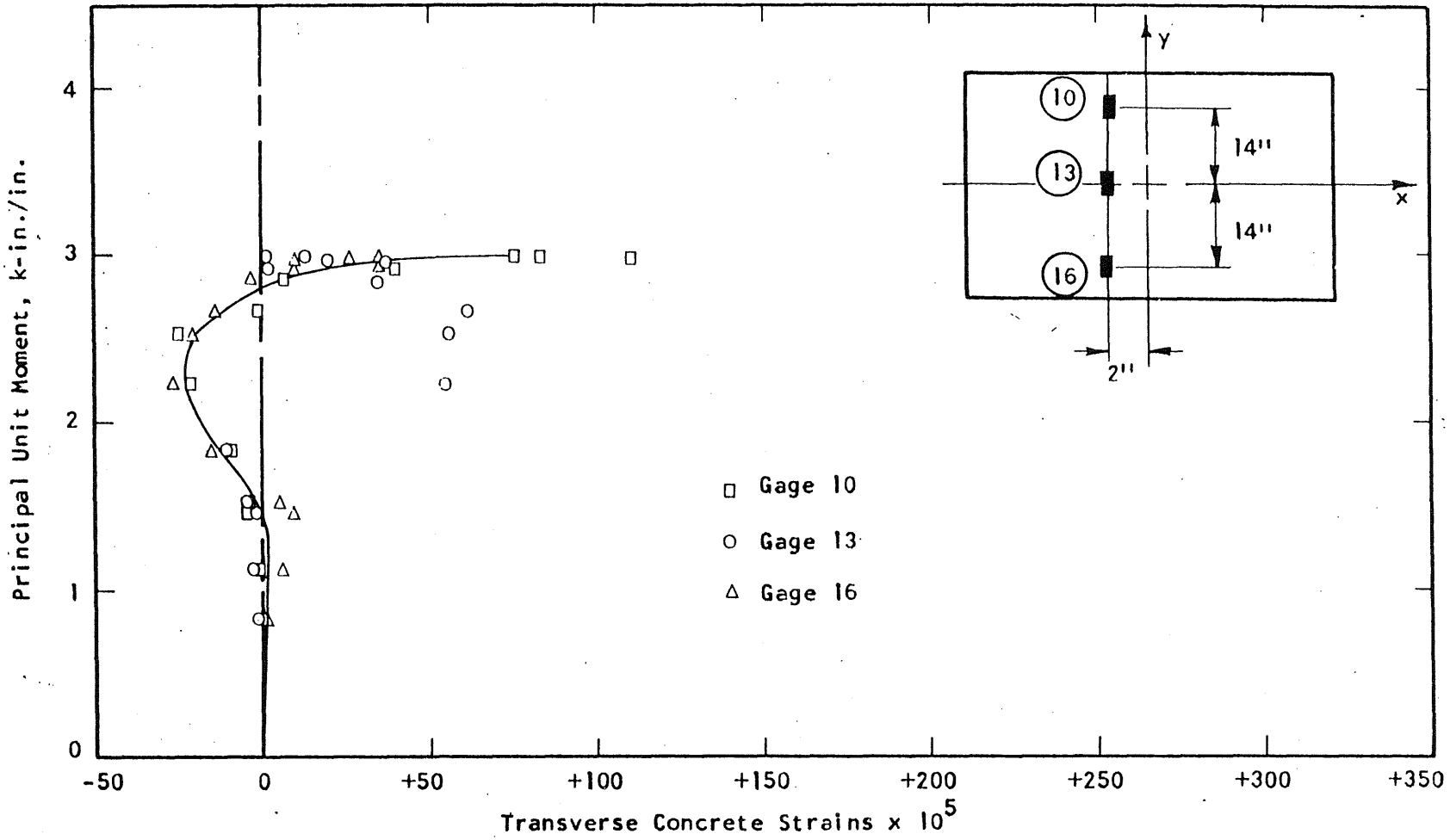

FIG. A.220 CONCRETE STRAIN PLOT, TOP SIDE OF SPECIMEN B21

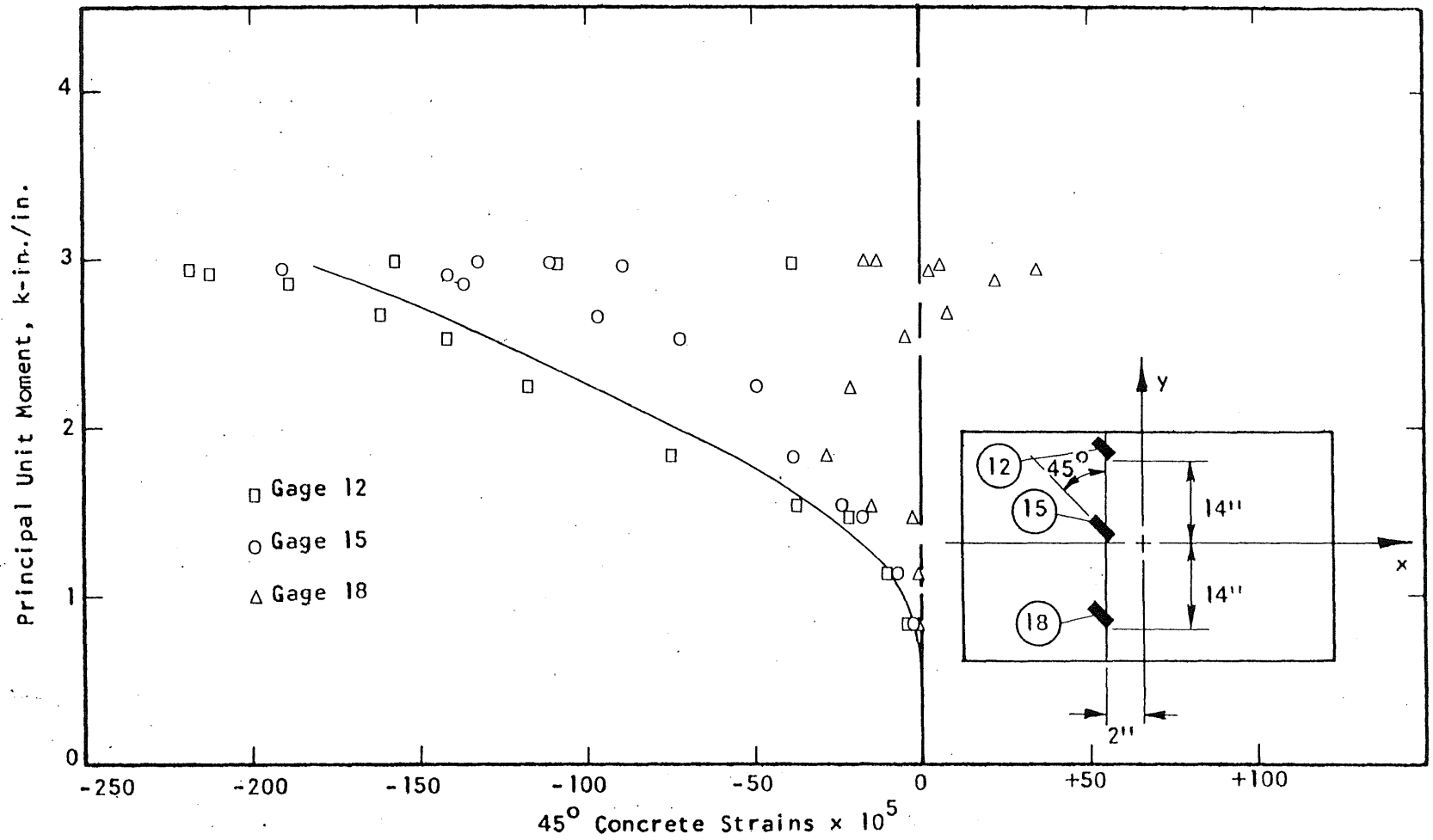

FIG. A.221 CONCRETE STRAIN PLOT, TOP SIDE OF SPECIMEN B21

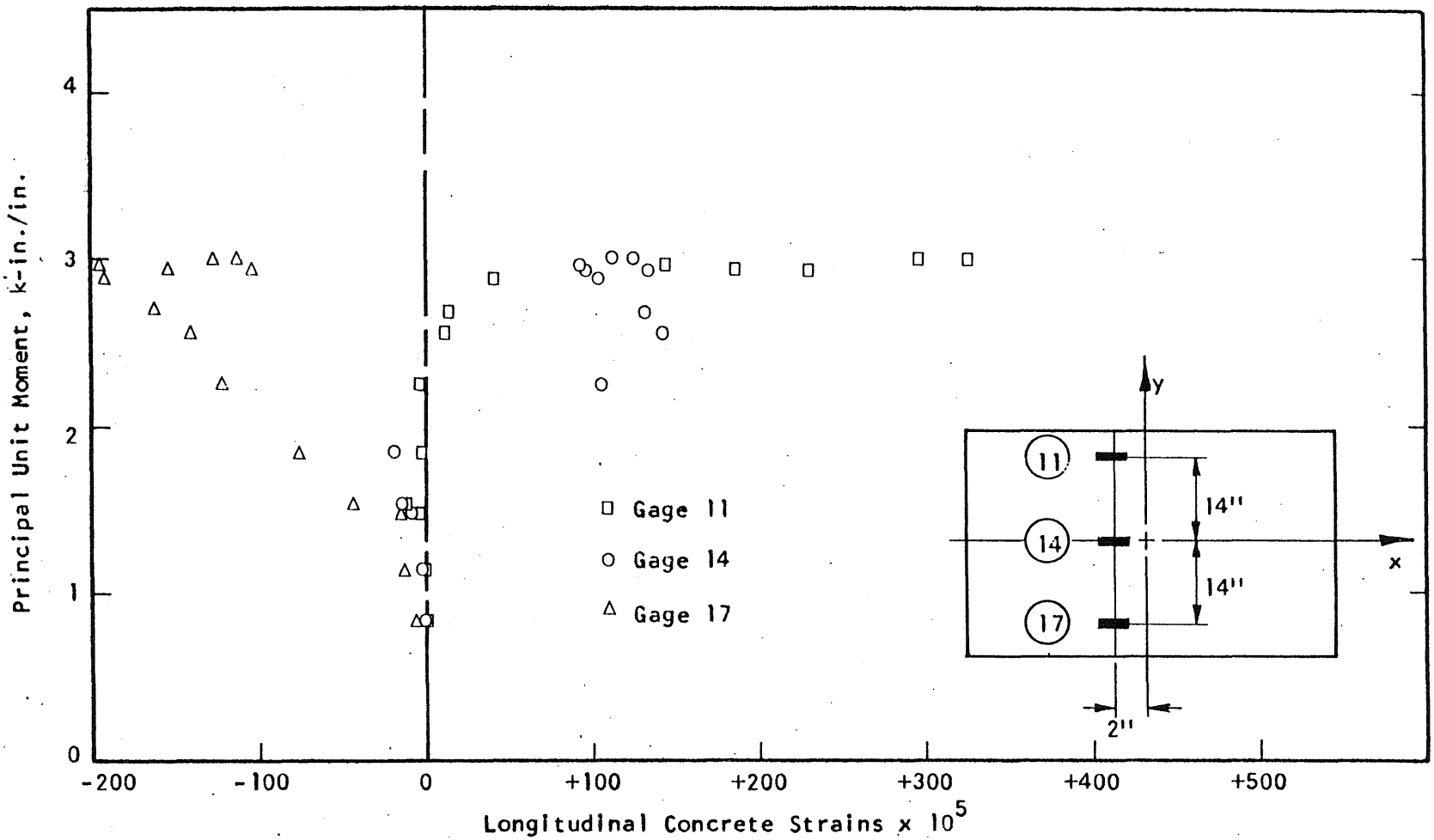

FIG. A.222 CONCRETE STRAIN PLOT, TOP SIDE OF SPECIMEN B21

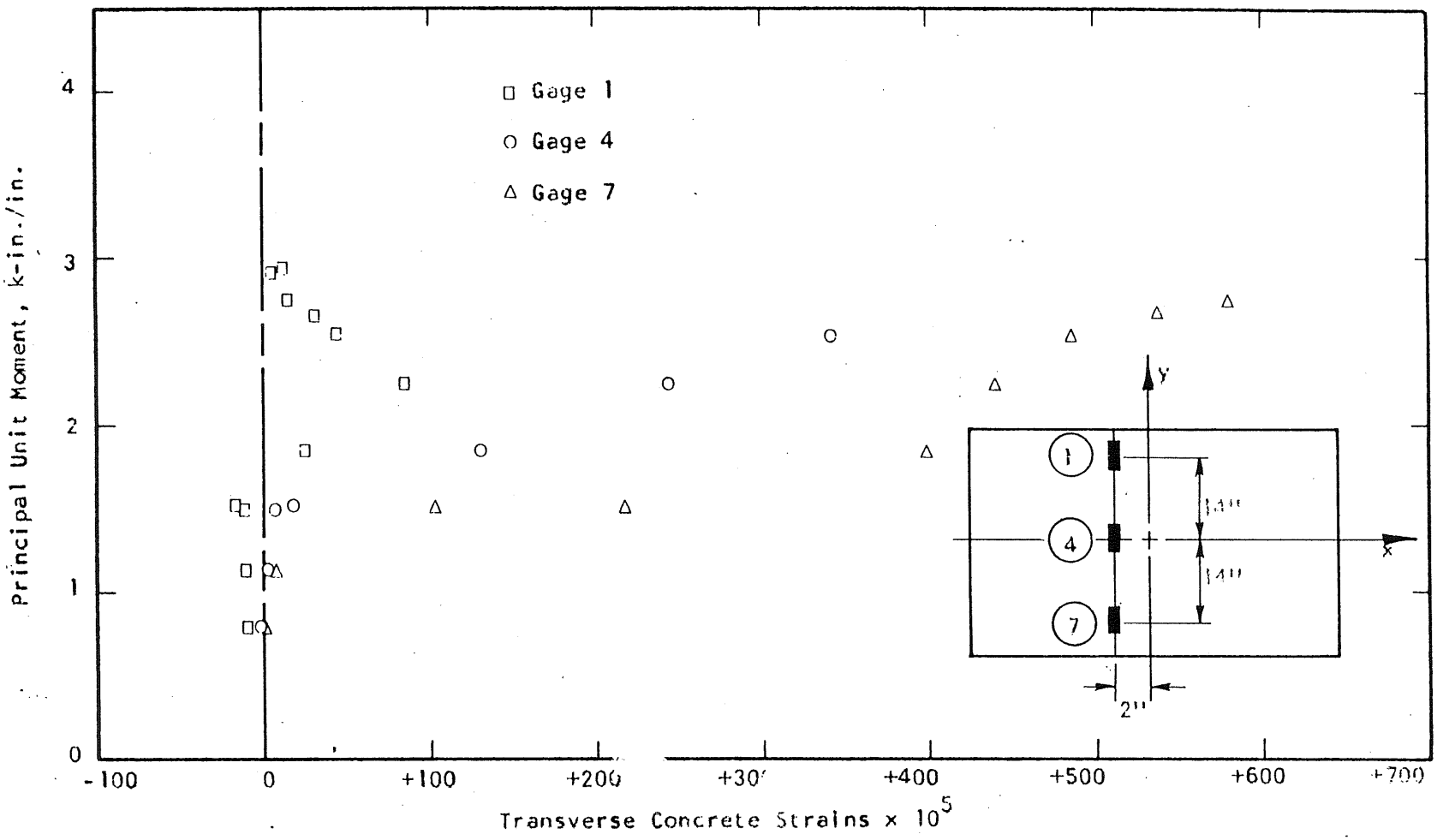

FIG. A.223 CONCRETE STRAIN PLOT, BOTTOM SIDE OF SPECIMEN B21

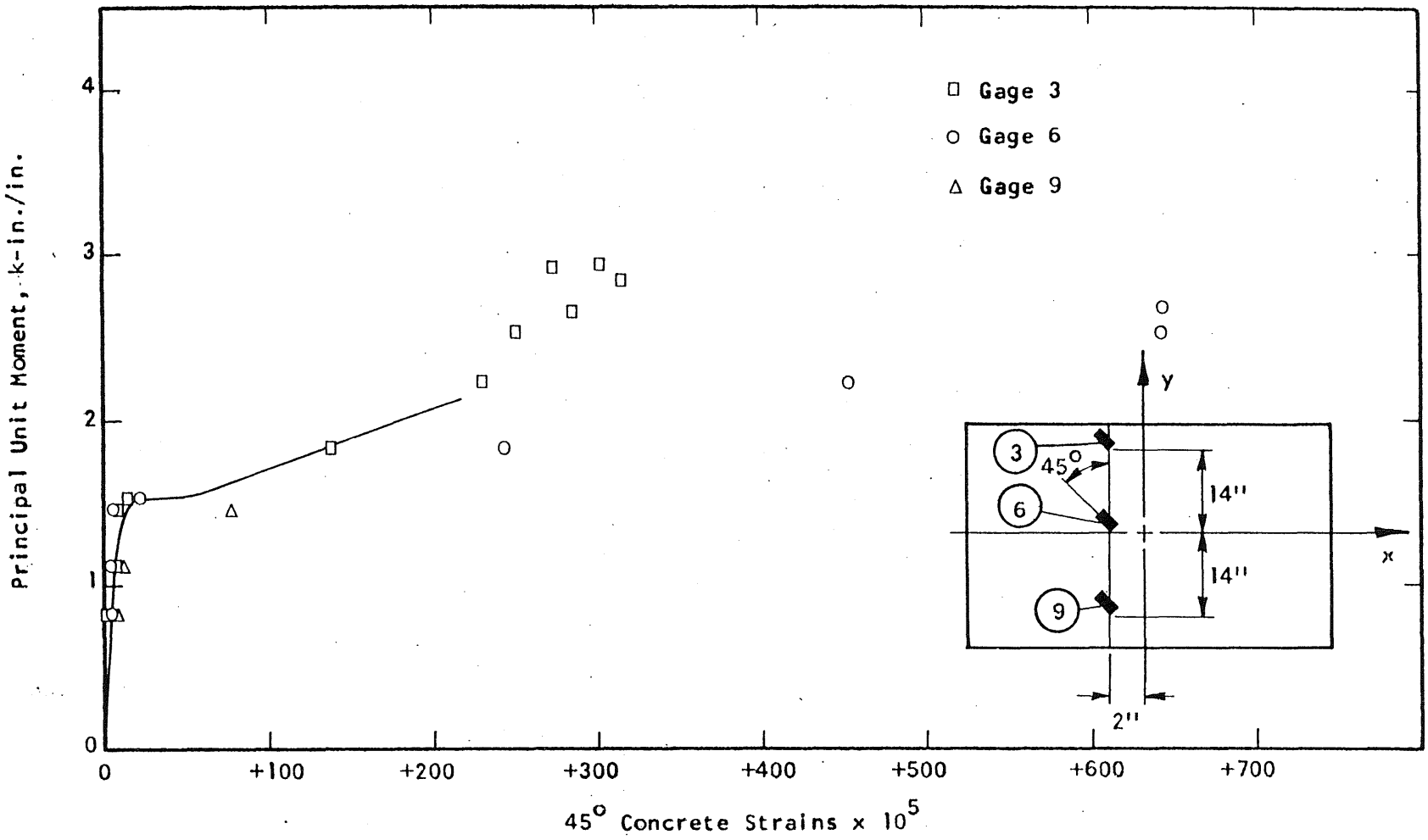

FIG. A.224 CONCRETE STRAIN PLOT, BOTTOM SIDE OF SPECIMEN B21

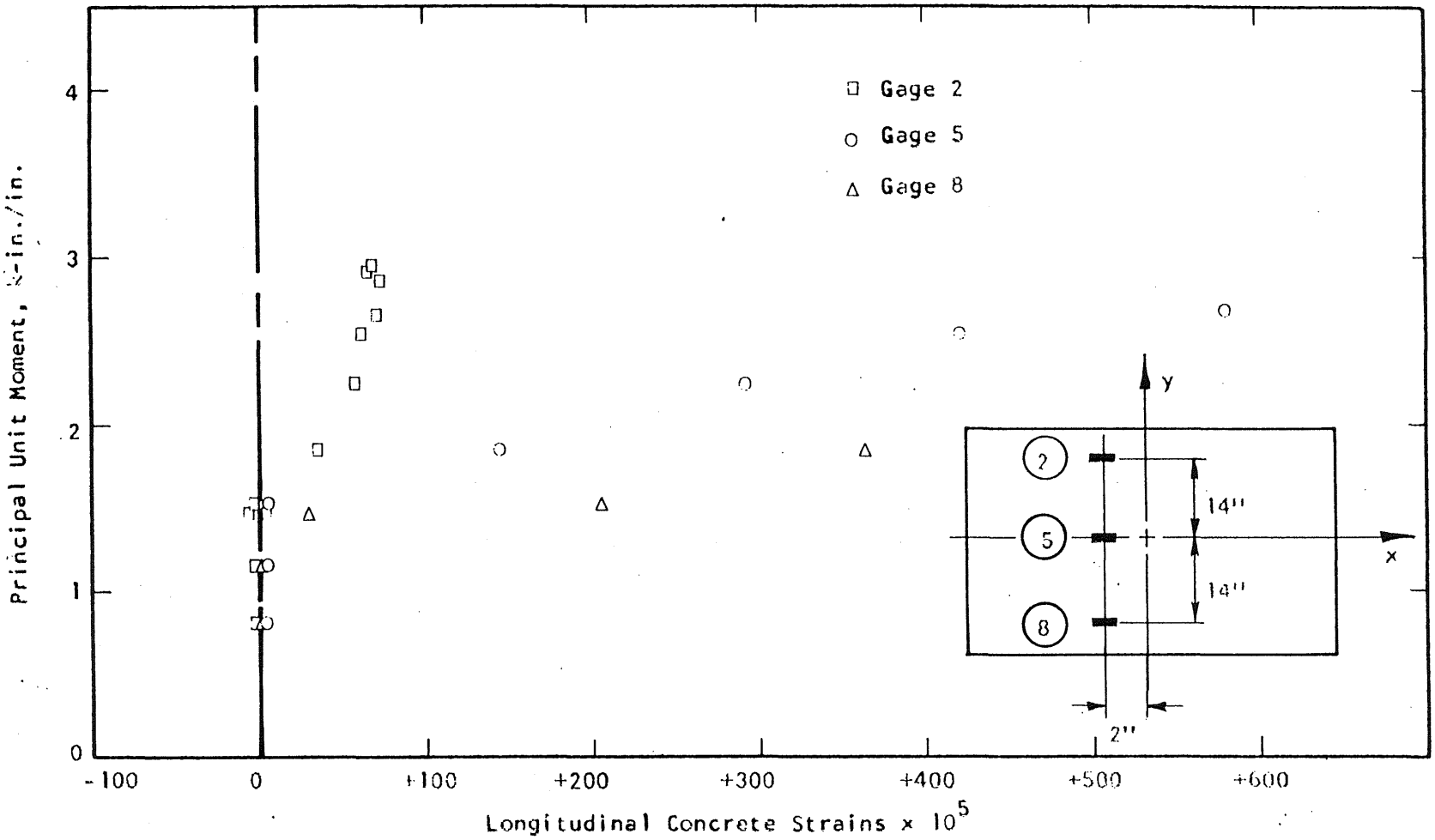

FIG. A.22S CONCRETE STRAIN PLOT, BOTTOM SIDE OF SPECIMEN B2I

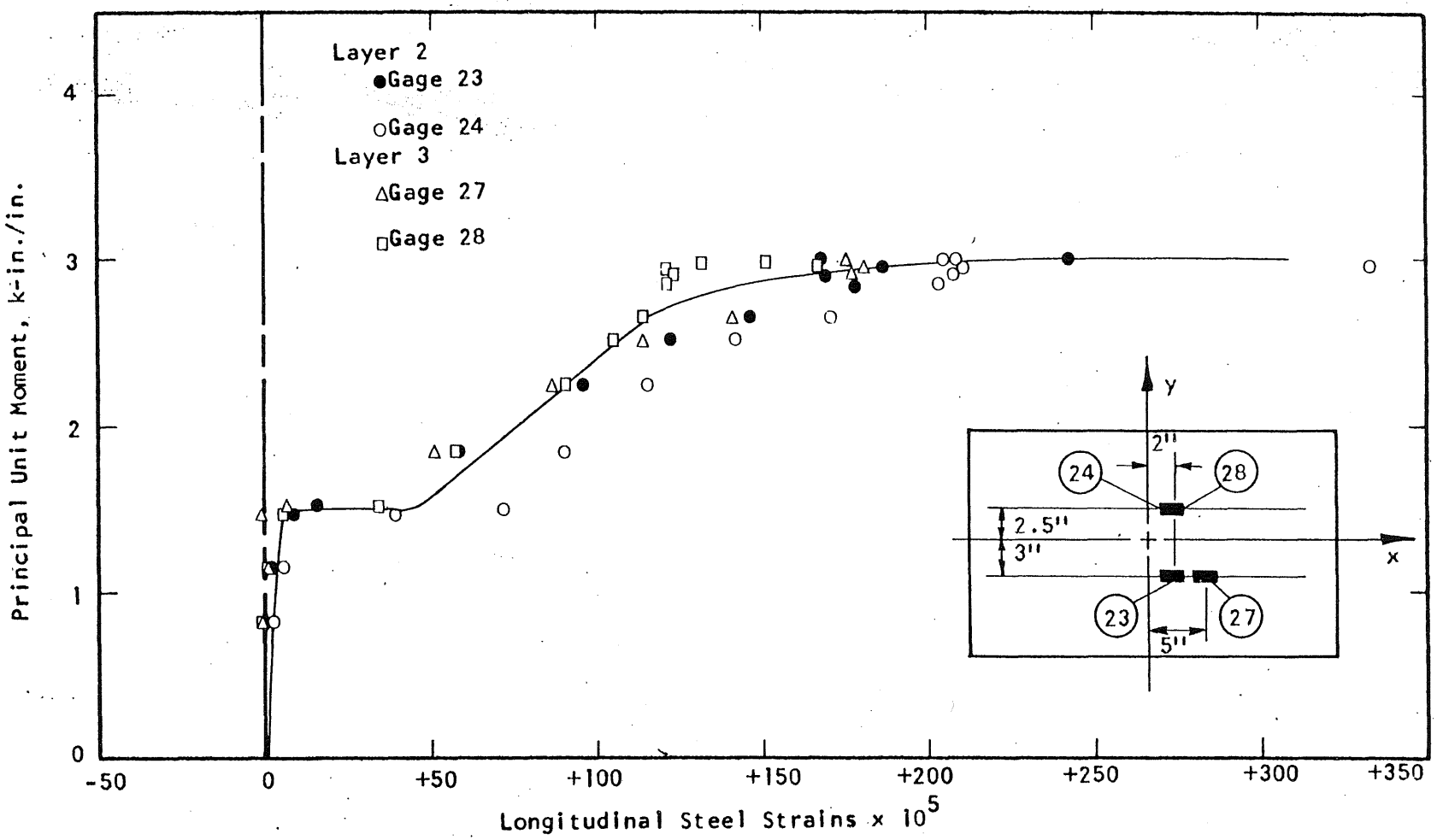

FIG. A.226 STEEL STRAIN PLOT, SPECIMEN B21

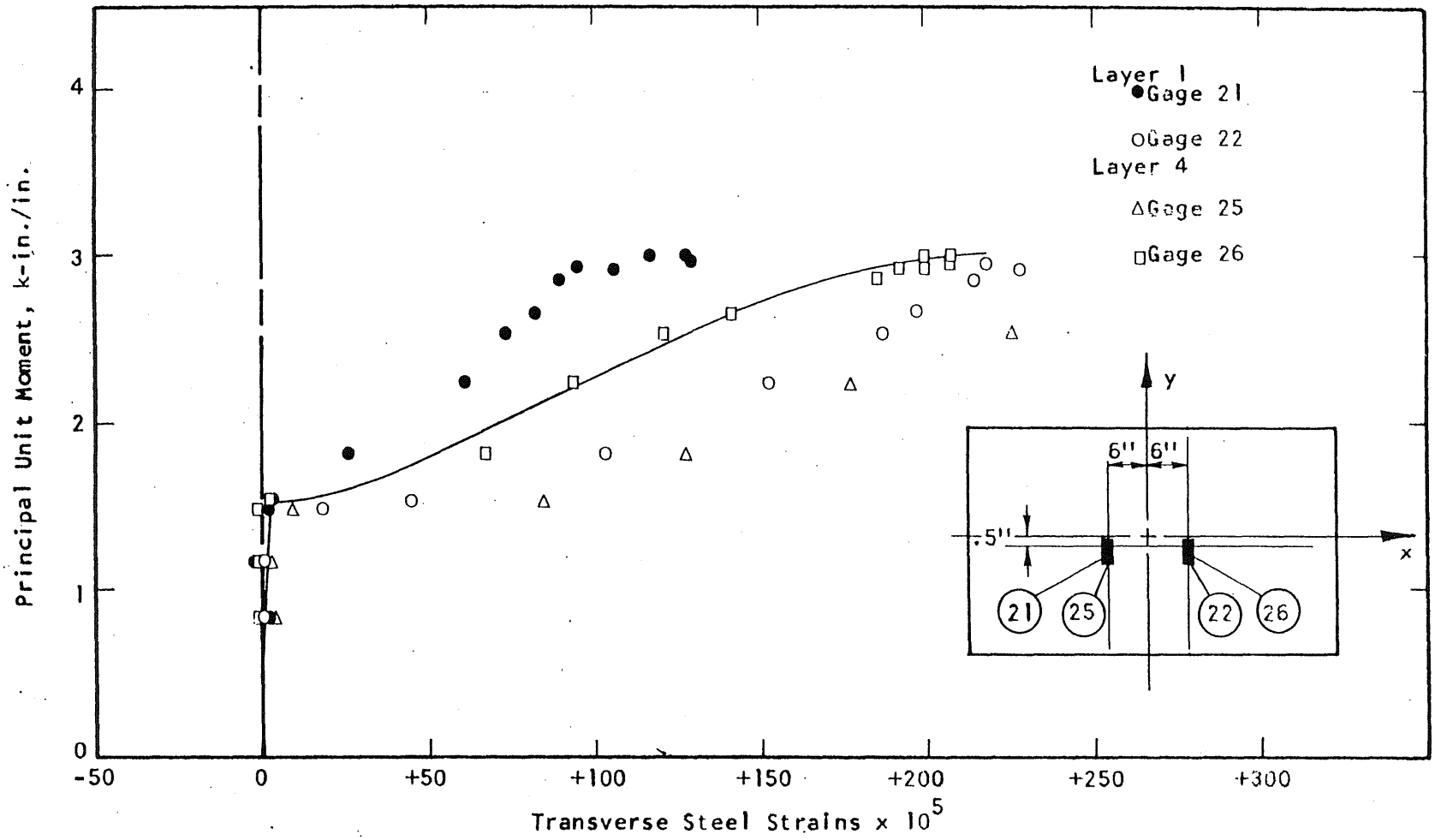

FIG. A.227 STEEL STRAIN PLOT, SPECIMEN B21

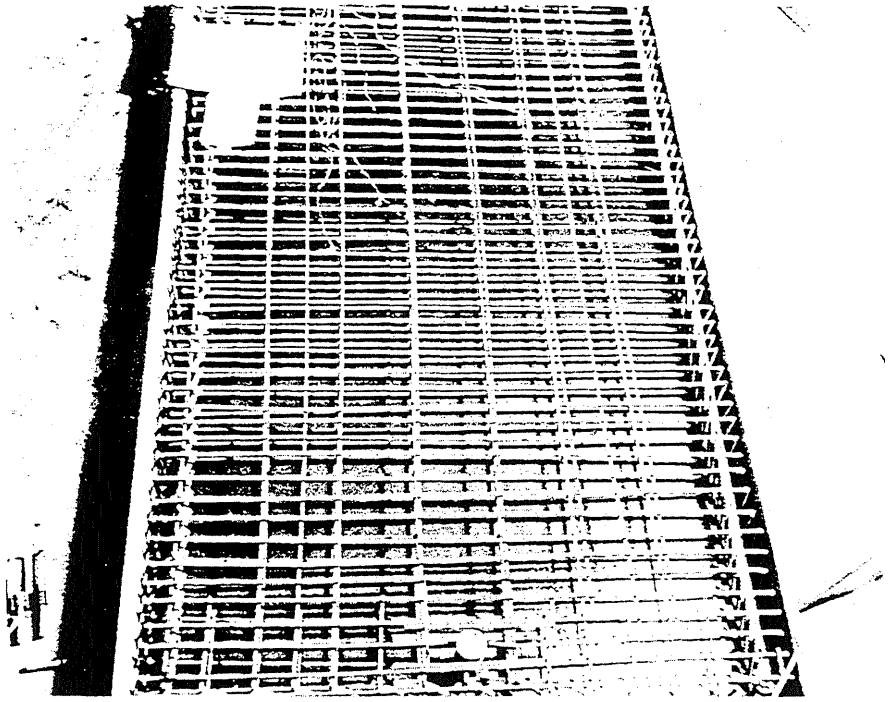

FIG. A.228 REINFORCEMENT IN SPECIMEN B22

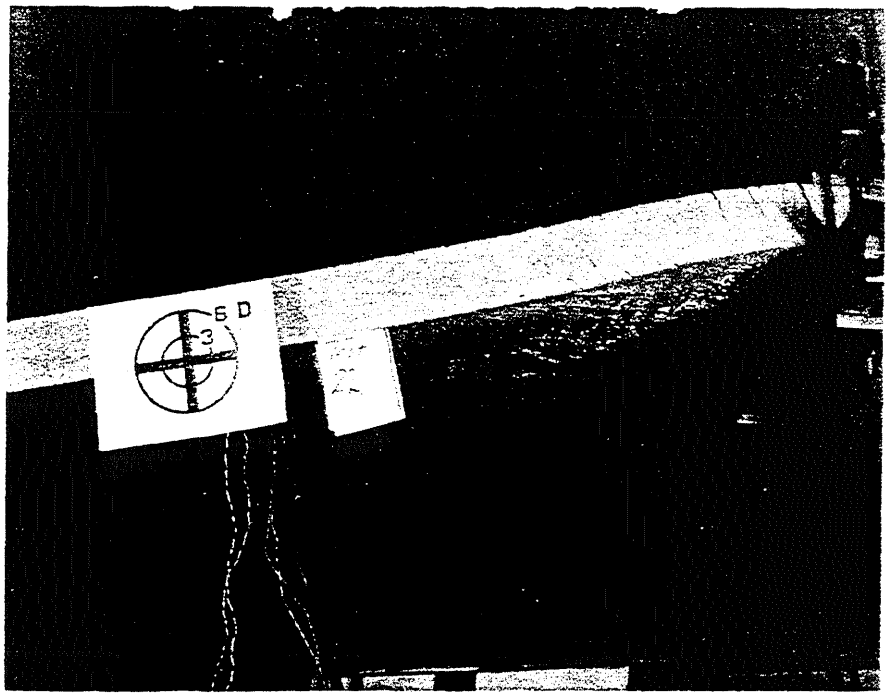

FIG. A.229 CLOSE-UP SIDE VIEW OF B22

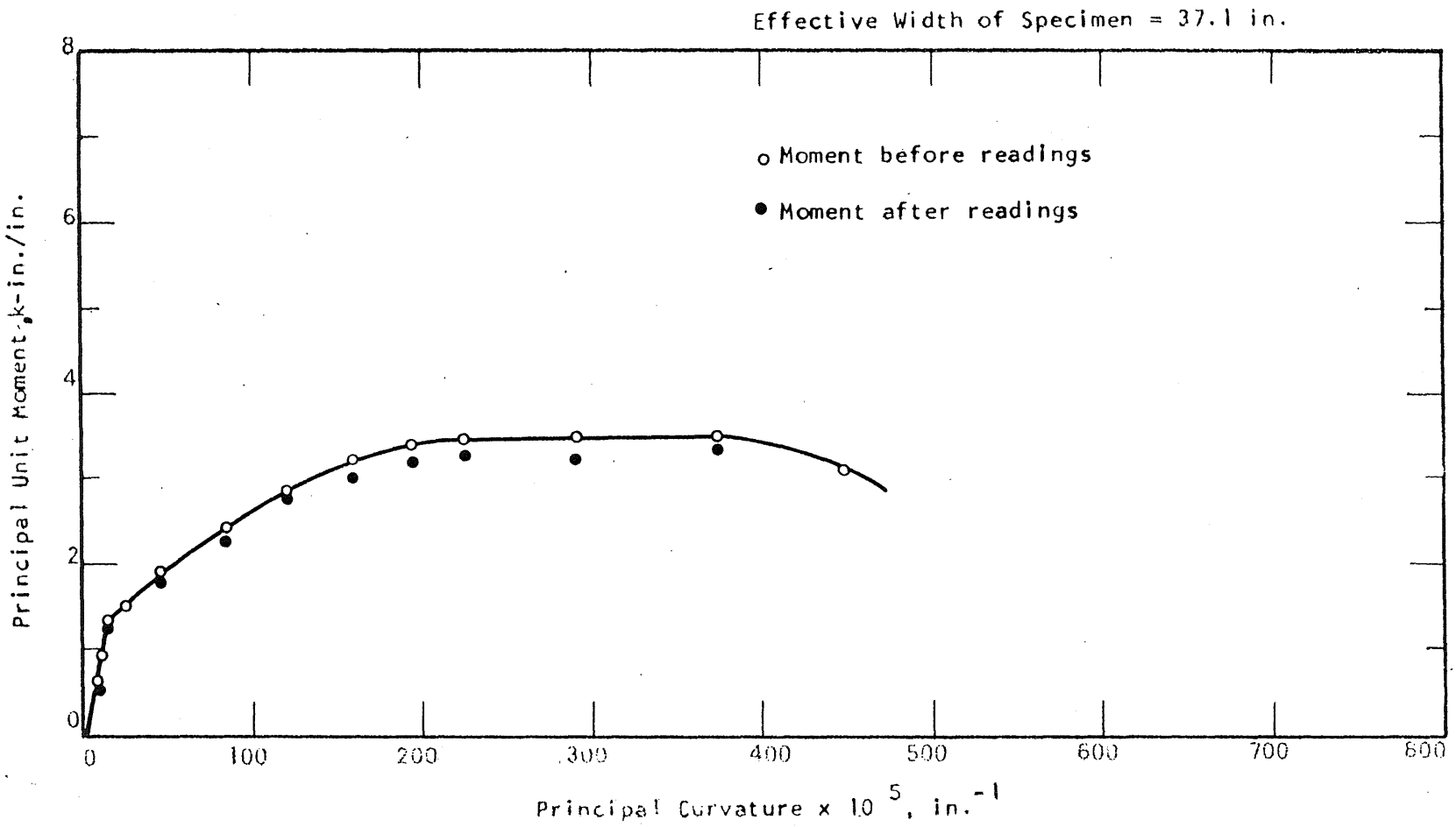

FIG. A.230 MOMENT-CURVATURE PLOT FOR SPECIMEN B22

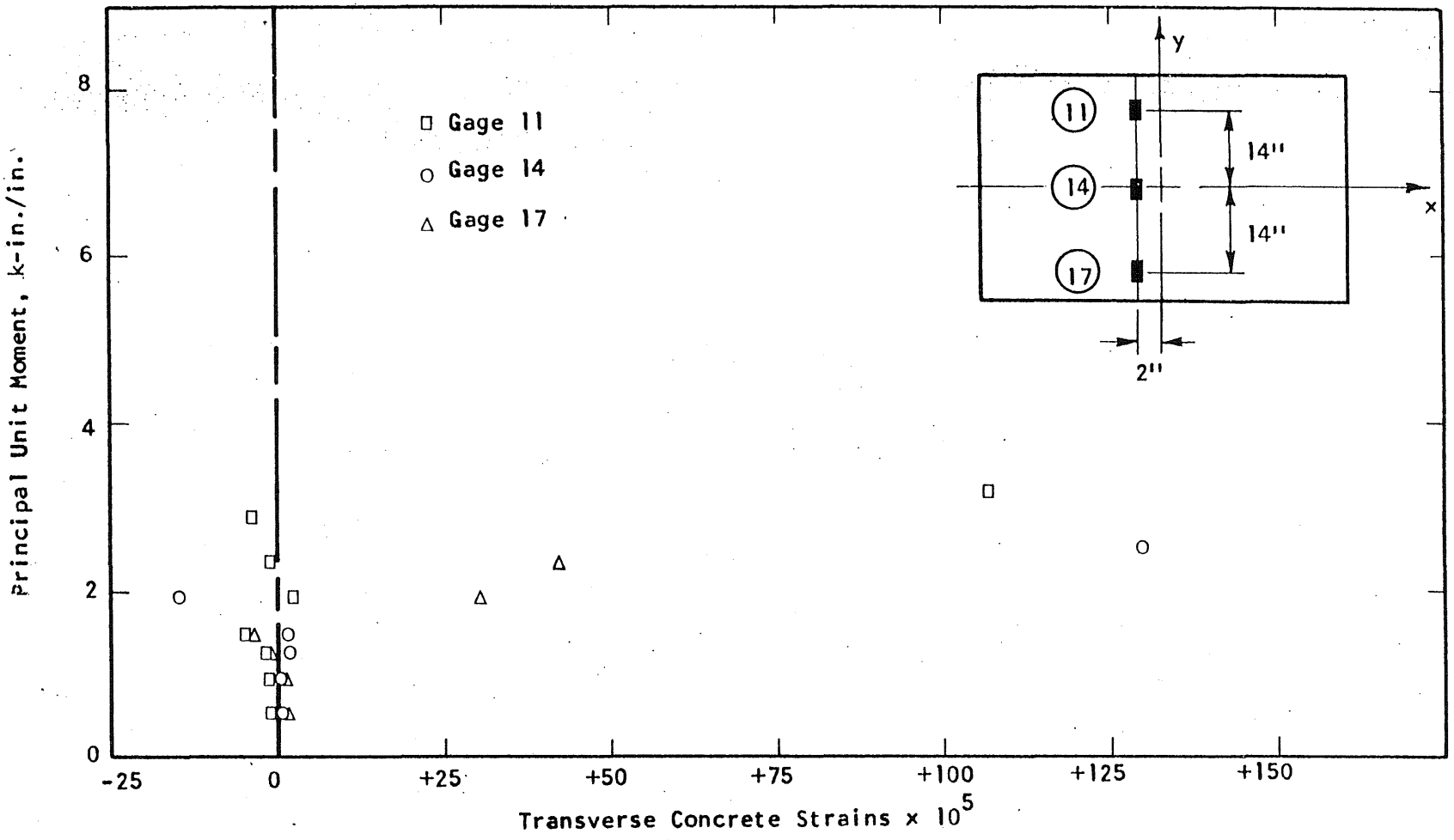

FIG. A.231 CONCRETE STRAIN PLOT, TOP SIDE OF SPECIMEN B22

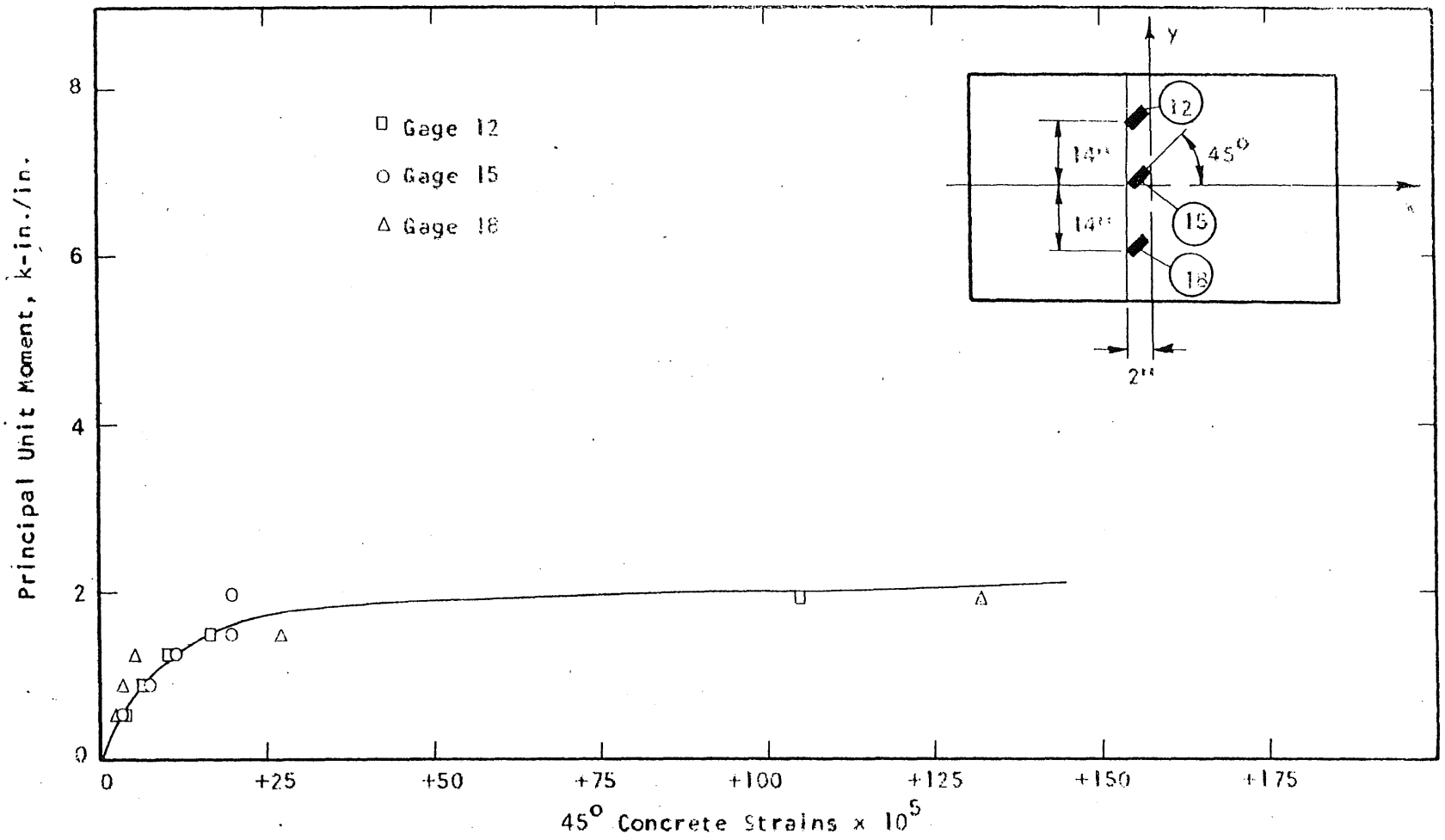

FIG. A.232 CONCRETE STRAIN PLOT, TOP SIDE OF SPECIMEN B2?

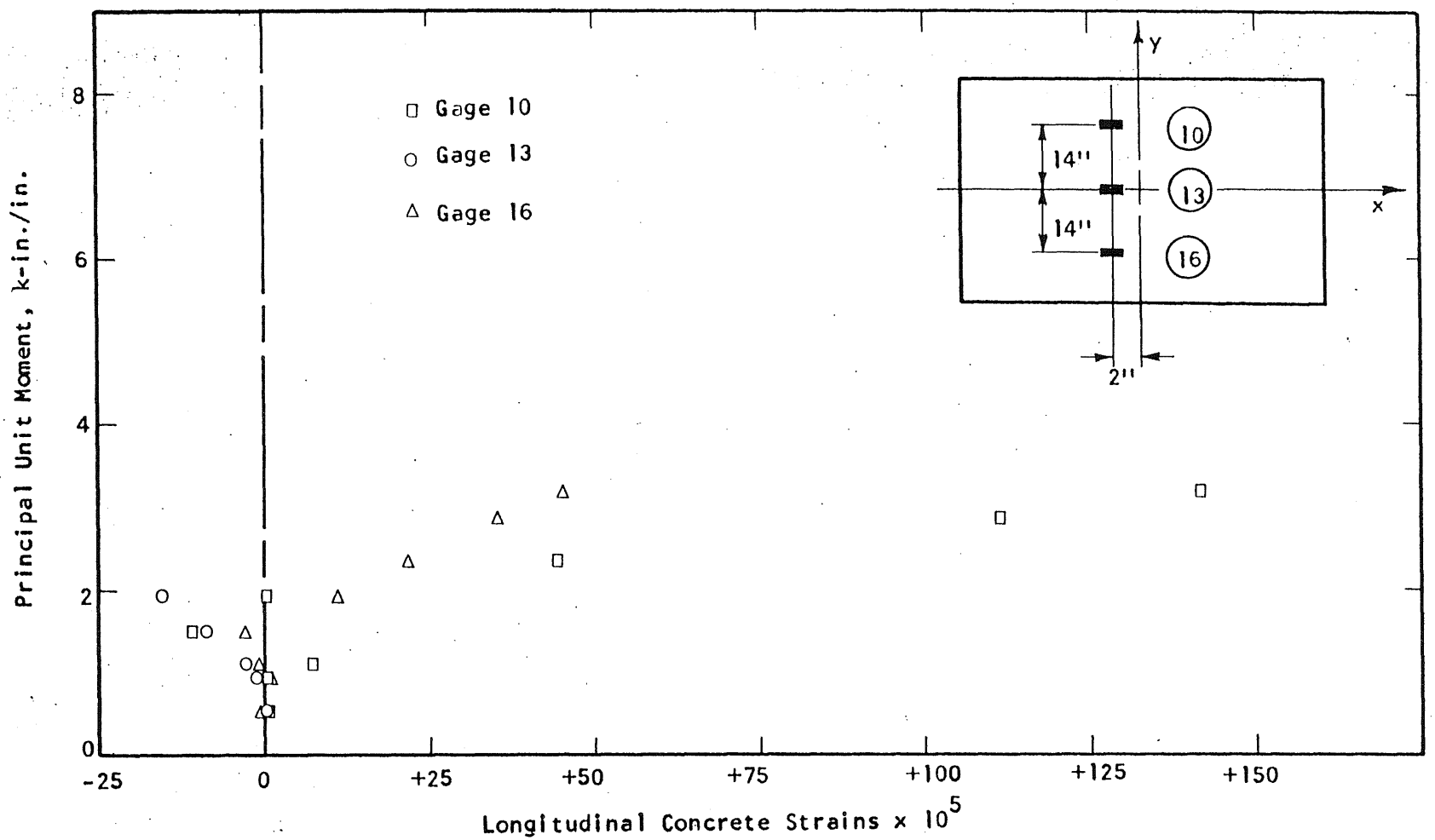

FIG. A.233 CONCRETE STRAIN PLOT, TOP SIDE OF SPECIMEN B22

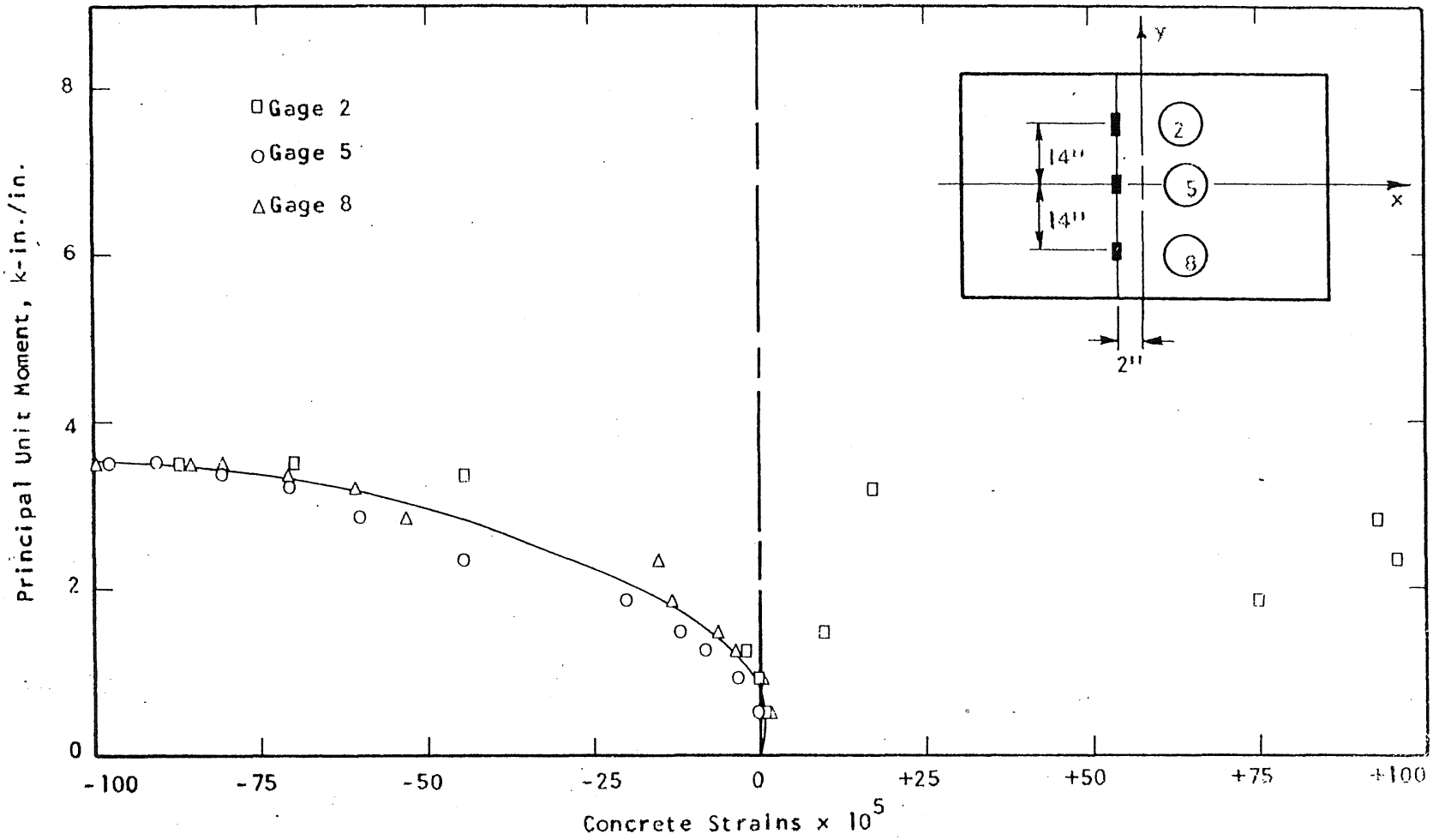

FIG. A.234 CONCRETE STRAIN PLOT, BOTTOM SIDE OF SPECIMEN B22

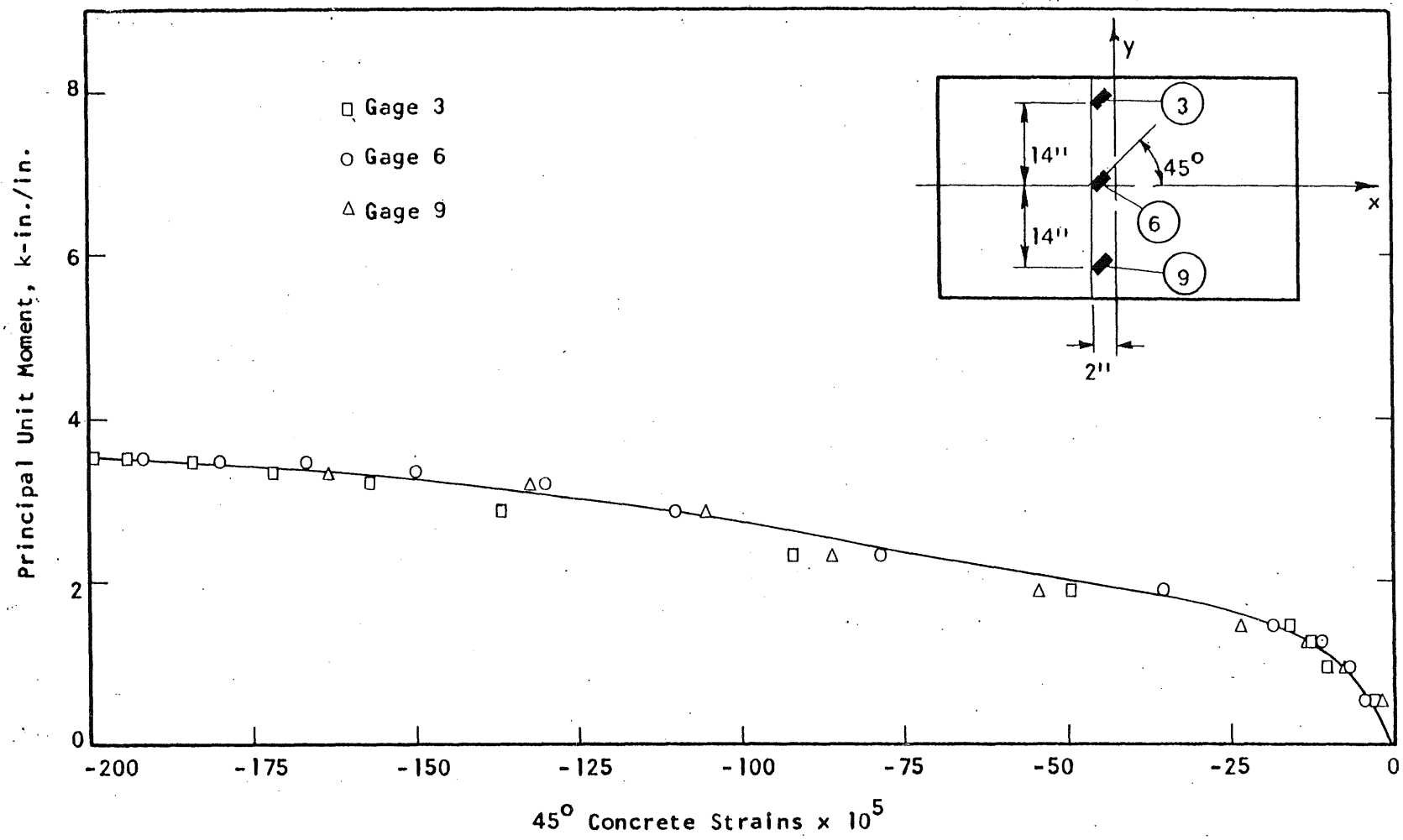

FIG. A.235 CONCRETE STRAIN PLOT, BOTTOM SIDE OF SPECIMEN B22

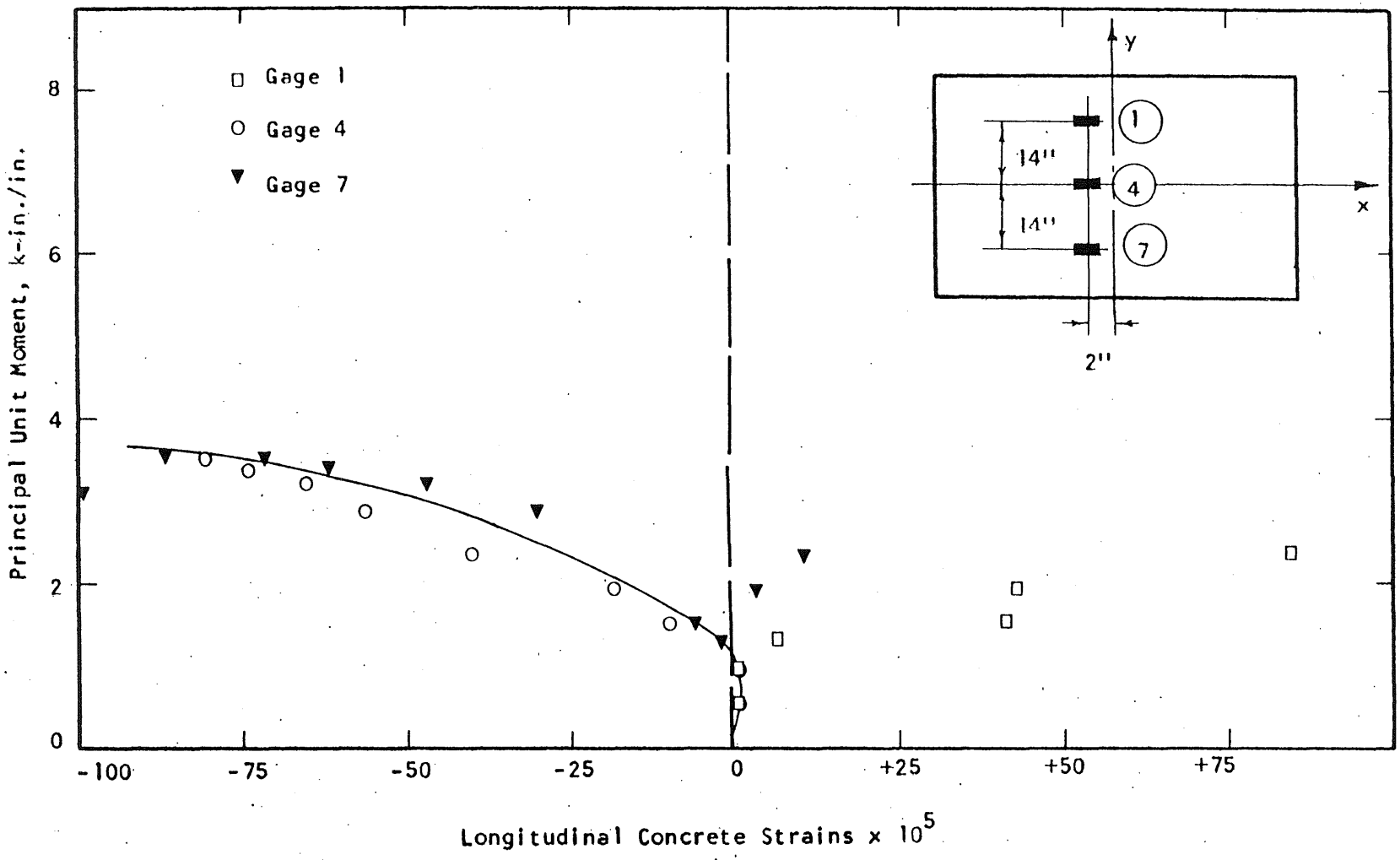

FIG. A.236 CONCRETE STRAIN PLOT, BOTTOM SIDE OF SPECIMEN B22

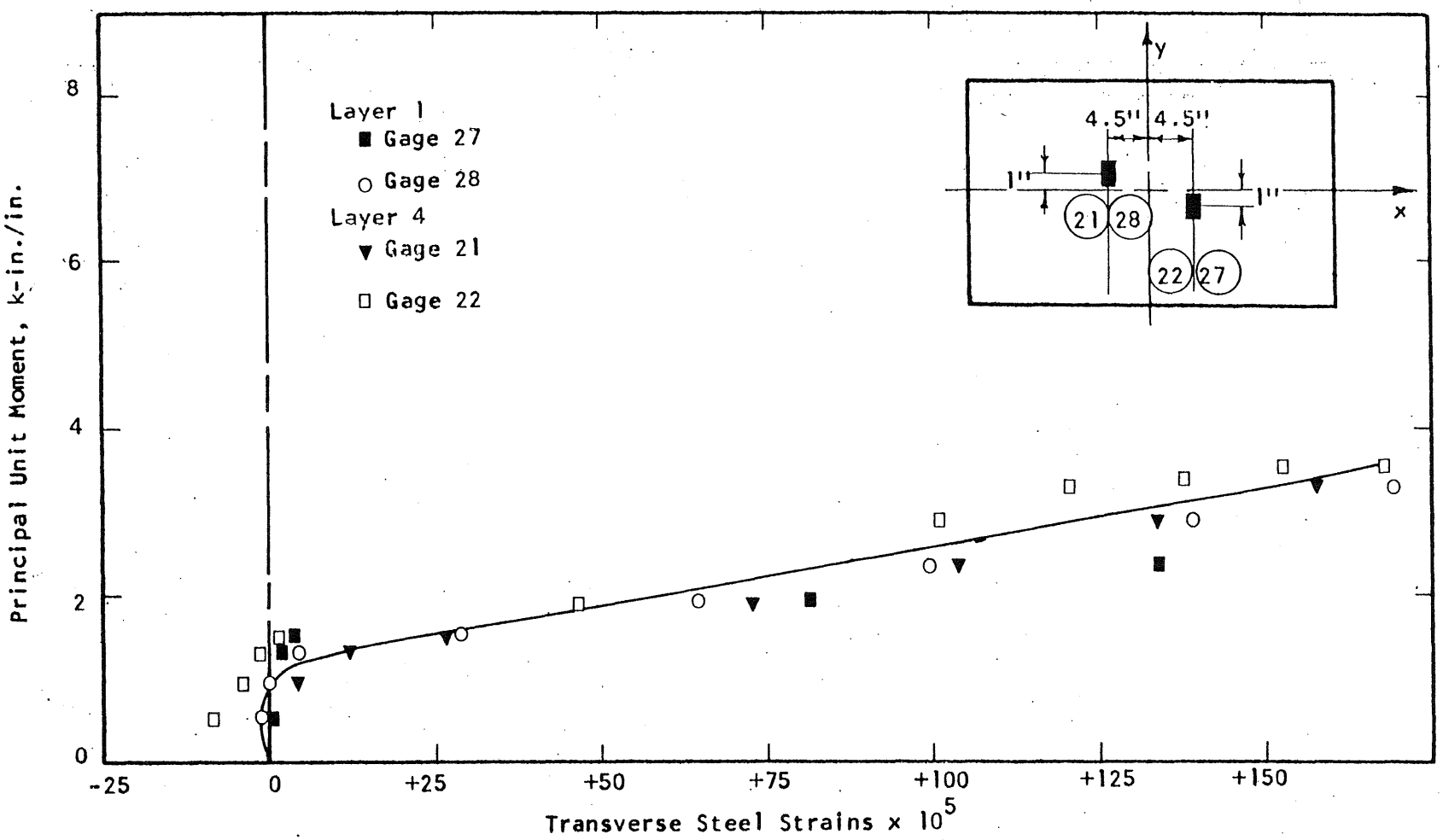

FIG. A.237 STEEL STRAIN PLOT, SPECIMEN B22

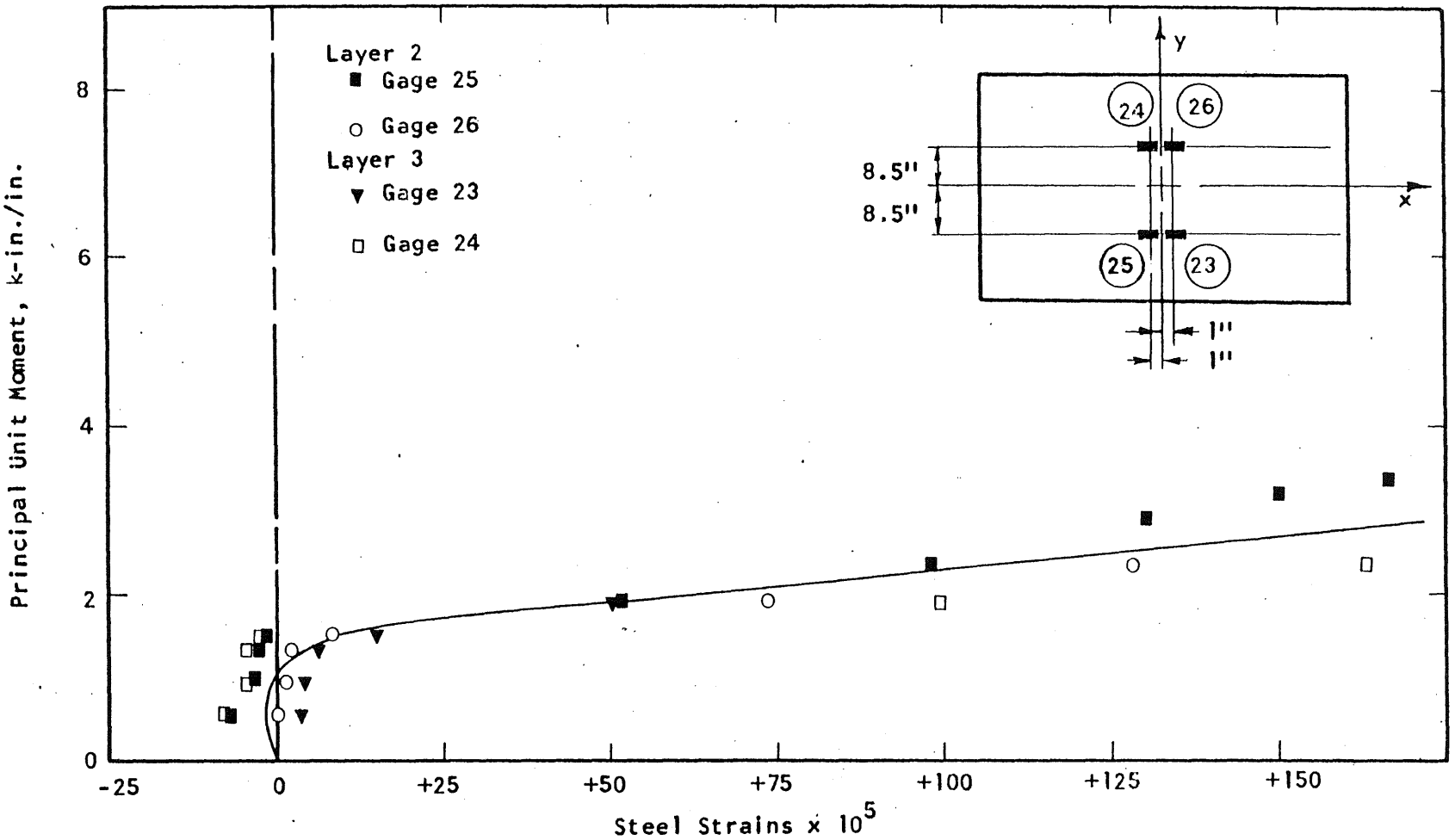

FIG. A.238 STEEL STRAIN PLOT, SPECIMEN B22

APPENDIX B

THE USE OF PHOTOGRAMMETRY IN THE EXPERIMENTAL INVESTIGATION

B.1 Introductory Remarks

During the planning stages of the investigation, it was deemed desirable to obtain a well defined record of the deflected shape of the slabs. The use of deflection dials for this purpose would be impractical. Consequently, two alternate methods were considered: electronic profile plotters and photogrammetry.

Preliminary trials with photogrammetry were interpreted by the staff of the surveying laboratory with the result that a standard deviation of 0.1 mm (0.004 in.) could be expected in the measurements. Since this was a tolerable error and since the measurement technique was simple, photogrammetry was chosen as the method of measurement. Subsequently, various direct checks were made of the accuracy of the photogrammetric method. The implementation and evaluation of the photogrammetric method for measuring deflections in the laboratory is discussed in this appendix.

The notation used in this appendix is independent of that used in the text (and Appendix C).

B.2 Method of Application

The surface of the slab facing the photogrammetric camera was provided with a grid. This grid consisted of squares 4 by 4-in. for the circular specimens and 5 by 5-in. for the rectangular specimens. The total dimensions of the grid were such that the testing area was completely covered. The grid was drawn using a pencil and a straight edge, and the intersection of the lines were marked with black ink. And a white

paper "reinforcement-ring" of about 5/8 in. external diameter and 1/4 in. internal diameter was placed on each point in order to make the intersections of the grid more distinct. Furthermore, each point on the grid was provided with an identification number. A matrix array was found to be the most suitable for this purpose.

The photogrammetric camera was set in place on top of a rigid steel beam (18 x 20-in.) which was part of the loading frame. The photogrammetric camera was secured to the steel beam by means of a wooden box which minimized any movement of the camera during its operation. The photogrammetric camera was placed so that its base axis was parallel to the plane of the slab and the camera directions were perpendicular to the slab.

B.3 Characteristics of the Photogrammetric Camera

The camera was a Wild Stereo camera with a base length of 120 cm. and a negative size of 6.5 by 9-cm. The lens had a constant or focal length of about 9 cm. The camera was ideally focused for 6 m. The depth of focus could be extended by use of a small aperture. The cameras were perpendicular to the base. On the back of the camera were mounted the adjustments for exposure time, the diaphragm opening and the device for winding the shutter. Both cameras were operated simultaneously. The diaphragms could be varied between 1:12 and 1:36. The exposure was performed simultaneously for both cameras by means of a cord release. In this investigation, the stereo camera was mounted on the tripod for use with the circular specimens and mounted on the loading frame for the rectangular specimens.

B.4 Geometry of the Solution

Photographs of the slab surface were taken at different stages of loading. These photographs were interpreted in sets of two in the Wild Stereocomparator (23) which was connected to a typewriter and an IBM key-punch machine to provide written and punched output.

The principles on which the interpretation of these pictures is based are the following:

X, Y, Z	system of axes whose origin is the left camera
x', y'	system of axes whose origin is the center of the left glass plate
x'', y''	system of axes whose origin is the center of the right glass plate
X', Y', Z'	system of axes whose origin is a point in the surface of the concrete slab
b	= distance between the cameras = 1200 mm
c	= distance from glass plate to lens = 91 mm
x'-x''	= horizontal parallax = p

Referring to triangles OBC and PO'O in Fig. B.1

$$Z = \frac{bc}{x'-x''} \tag{B.1}$$

or because $x'-x'' = p$

$$Z = \frac{bc}{p} \tag{B.2}$$

From triangles OAC and ORP

$$\frac{x'}{X} = \frac{c}{Z} \tag{B.3}$$

or

$$X = \frac{Zx'}{c} = \frac{bx'}{p} \tag{B.4}$$

From triangles OCD and OPQ

$$\frac{y'}{Y} = \frac{c}{Z} \tag{B.5}$$

$$Y = Z\,\frac{y'}{c} = \frac{by'}{p} = \frac{by''}{p} \tag{B.6}$$

The cartesian coordinates X, Y, Z of a general point P derived above are referred to the origin O which coincides with the location of the left camera.

However, any disturbance of the original position of the camera during its operation would introduce undesirable errors in the determination of the coordinates of each point on the slab. Furthermore, the motion of the slab does not allow for any fixed system or coordinates throughout the complete duration of the test.

This condition was solved by using a system of cartesian coordinates which would move together with the specimen being tested.

This was accomplished by transforming the coordinates measured with respect to the camera position to a new system whose origin is a point on the concrete slab and whose XY plane is a plane passing through three points on the concrete slab and its Z axis is always perpendicular to this plane. In this way any over-all motion of the concrete plate was taken care of.

B.5 Transformation of Coordinates

Let us take these particular points A, B and C on the slab surface and a general point P as shown in Fig. B.2.

The coordinates of a point P with respect to the original system of axes are X_p, Y_p, Z_p. The direction cosines of any line with respect to the original system of axes are ℓ_α, m_α, n_α. The coordinates of a point P with respect to the new system of axes are X'_p, Y'_p, Z'_p, and the direction cosines are L_α, M_α, N_α.

From the relations above, the following can be stated:

Line/Axis	X	Y	Z
1	ℓ_1	m_1	n_1
2	ℓ_2	m_2	n_2
3	ℓ_3	m_3	n_3

Direction cosines
Original System of Axes

Line/Axis	X'	Y'	Z'
1	1	0	0
2	L_2	M_2	0
3	L_3	M_3	N_3

Direction cosines
New System of Axes

The direction cosines of lines 1, 2, and 3 in Fig. B.2 can be computed without difficulty in the original system. In the new system they are evaluated using simple trigonometric relations

$$L_2 = \ell_1\ell_2 + m_1m_2 + n_1n_2 \tag{B.7}$$

$$M_2 = \pm\sqrt{1 - L_2^2} \tag{B.8}$$

The sign of M_2 is determined by considering the direction of the resultant cross product of unit vectors in the direction $\overline{AB}$ and $\overline{AC}$ in both systems

$$\text{sign of } M_2 = \frac{\overline{AB} \times \overline{AC}}{\overline{A'B'} \times \overline{A'C'}} \tag{B.9}$$

In a similar way we can evaluate

$$L_3 = \ell_1\ell_3 + m_1m_3 + n_1n_3 \tag{B.10}$$

$$M_3 = \frac{1}{M_2}\left(\ell_2\ell_3 + m_2m_3 + n_2n_3 - L_2L_3\right) \tag{B.11}$$

$$N_3 = \pm\sqrt{1 - L_3^2 - M_3^2} \tag{B.12}$$

Sign of N_3: The direction of the Z axis in the original system is given by the cross product of unit vectors in the directions of $\overline{AB}$ and $\overline{AC}$.

Call
$$\overline{C} = \overline{AB} \times \overline{AC} \tag{B.13}$$

The unit vector in the direction of P in the same system is

$$\overline{P} = i\ell_3 + jm_3 + k\,n_3 \tag{B.14}$$

If $\overline{C}.\overline{P}$ is positive, then $\overline{P}$ and the vector $\overline{C}$ go in the same direction. If $\overline{C}.\overline{P}$ is negative, then $\overline{C}$ and $\overline{P}$ go in opposite directions.

Therefore the sign of N_3 is given by the scalar product of unit vectors $\overline{C}.\overline{P}$.

The new coordinates X'_p, Y'_p and Z'_p are determined as

$$X'_p = DL_3 \quad Y'_p = DM_3 \quad Z'_p = DN_3 \tag{B.15}$$

Where L_3, M_3 and N_3 are determined by Eq. B.10 - B.12 and

$$D = \sqrt{(X_p - X_A)^2 + (Y_p - Y_A)^2 + (Z_p - Z_A)^2} \tag{B.16}$$

B.6 Evaluation of the Accuracy Involved

In order to have a good estimate of curvatures, the deflections obtained should be as accurate as possible. This means that the error in the Z coordinate should be maintained to a minimum.

From Eq. B.2

$$\log Z = \log b + \log c - \log p \tag{B.17}$$

$$\frac{dZ}{Z} = \frac{db}{b} + \frac{dc}{c} - \frac{dp}{p} \qquad (B.18)$$

which means that the error dZ in the deflection is the sum of the errors due to the error in the distance between cameras b, the camera constant c, and the horizontal parallax p.

The errors db and dc can be minimized because they depend on the accuracy of the dimensions of the photogrammetric camera. These dimensions are supplied by the manufacturers and can, for practical purposes, be neglected for this particular case. Hence, the error considered is introduced by the readings of the horizontal parallax p. Since this error can be positive or negative, its absolute value will be introduced in Eq. B.18

$$dZ = Z \frac{dp}{p} = Z^2 \frac{dp}{bc} \qquad (B.19)$$

The sensitivity of the stereo-comparator is .001 mm, however an over-all error in horizontal parallax of .01 mm is to be expected (23). The error in the measurement of the horizontal parallax p can be due to the following reasons:

(a) orientation of the glass plates on the stereo-comparator at the time that the readings are taken

(b) operational resolution

(c) observational errors

(d) deformation in the image material

(e) distortion errors due to the properties of the material of the glass plates

In the computer program written for the solution of this problem, provisions were made to reorientate the coordinate system in order to minimize error (a), and double precision calculations were used to minimize error (b).

Error (c) depends mainly on reading techniques, equipment used for the readings, quality of the pictures, sensitivity of the human eye, and experience of the observer.

Errors (d) and (e) depend on the photographic equipment and the type of material used in the negatives.

For these characteristics of the photogrammetric camera and its distance from the reinforced concrete slab, the error dZ can be calculated:

b = 1200 mm

c = 91 mm

dp = .01 mm

Z = 2900 mm (torsion and circular tests)

Z = 2700 mm (uniaxial bending)

Torsion and Circular Tests

$$dZ = (2900)^2 \frac{.01}{1200 \times 91} = 0.77 \text{ mm} \qquad \text{(B.20)}$$

Uniaxial Bending Tests

$$dZ = (2700)^2 \frac{.01}{1200 \times 91} = 0.67 \text{ mm} \qquad \text{(B.21)}$$

B.7 Direct Measurements on the Concrete Plate

The error in deflections was computed by evaluating the error in the distance between two points on the surface of the concrete plate.

Measurements were taken with a compass and a scale. The average error in this measurement was .34 mm. From simple geometry (Fig. B.3)

$$\frac{.34}{dZ} = \frac{1200}{Z} \tag{B.22}$$

For Z = 2900 mm (torsion and circular tests)

$$dZ = .34\ \frac{2900}{1200} = .82 \text{ mm} \tag{B.23}$$

For Z = 2700 mm

$$dZ = .34\ \frac{2700}{1200} = .76 \text{ mm} \tag{B.24}$$

The values of dZ in Eq. B.23 and B.24 agree within 10 percent with those in Eq. B.20 and B.21.

B.8 Influence of the Error dZ on the Curvature

Using finite differences the curvature can be expressed

$$\Phi = \frac{1}{h^2}\,(-Z_1 + 2Z_2 - Z_3) \tag{B.25}$$

where h = dimension of the grid used

Z_1, Z_2 and Z_3 = deflections of three consecutive points on the slab surface located h apart from each other.

Taking dZ as the relative error between points Z_2, Z_1 and Z_3, Eq. B.25 becomes

$$\Phi \text{ error} = \frac{1}{h^2}\,(2dZ) \tag{B.26}$$

for h = 5 in. and dZ = 0.8 mm (.0315 in.)

$$\Phi \text{ error} = \frac{1}{25}\ \ (2x.0315 \text{ in.}) = 252x10^{-5} \text{in.}^{-1} \tag{B.27}$$

The magnitude of the curvatures involved is approximately

$$\Phi \text{ yield} = 80 \times 10^{-5} \text{ in.}^{-1} \qquad \text{(B.28)}$$

From Eq. B.27 and B.28, we see that the error in curvature that we obtain due to the accuracy of the photogrammetric results is of the order of three times the curvature at yield.

B.9 Conclusion

It is obvious from these results that, for the obtained conditions of accuracy, the photogrammetry results were not suitable for determining curvatures or deflections in the test specimens. A similar analysis can show its nonsuitability for the determination of strains in the concrete slab surface. It should also be noted that, in this experiment, conditions of variations of the distance between the photogrammetric camera and the test specimen and possibilities of the camera itself inducing the errors have been held to a minimum.

However, it should be mentioned that better results could have been obtained with a setup having a greater distance between the two cameras placed at a smaller distance from the object.

It is also proposed, on the basis of the experience acquired, that tilting the cameras equally (approximately 45°) so that the measurement area occupies the whole field of vision for both cameras could lead to considerably better results.

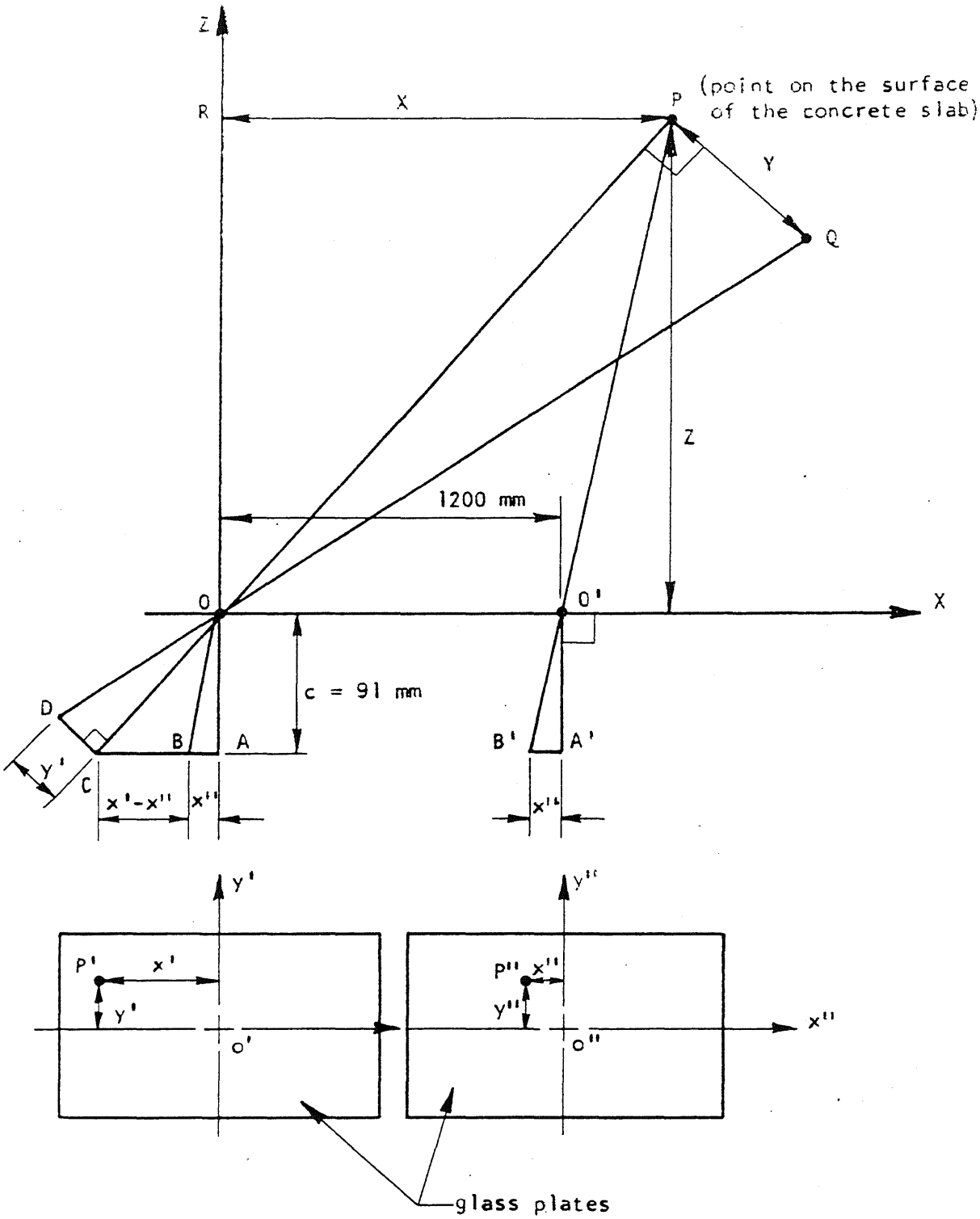

FIG. B.1 GEOMETRICAL INTERPRETATION OF THE METHOD

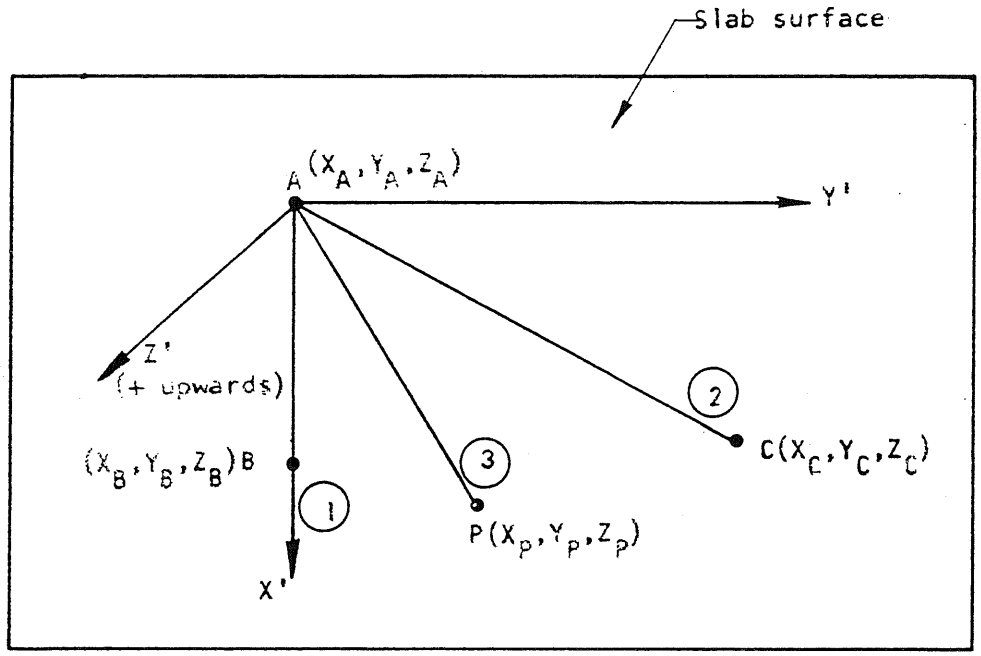

FIG. B.2 TRANSFORMATION OF COORDINATES

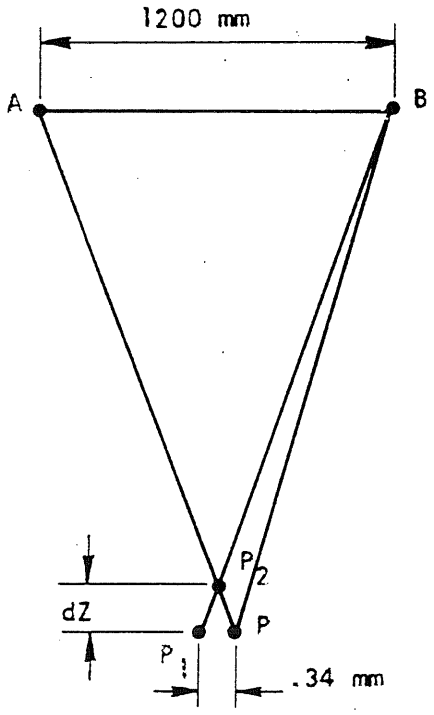

FIG. B.3 ERROR IN DEFLECTION DUE TO AN ERROR IN HORIZONTAL DISTANCE

APPENDIX C

DEFINITIONS AND NOTATIONS

C.1 Definitions

Isostatic moment denotes equal moment in all planar directions.

Layer of reinforcement or reinforcement layer consists of the reinforcing bars in one level in one direction.

Longitudinal direction denotes the direction of the longer axis of the rectangular test specimen.

C.2 Notations

Notations which are defined in the text may not be included in this list.

a_i = distance from the top surface of the section to the i^{th} resultant concrete force in the n-direction

a_n = strain at mid-height in the n-direction

a_t = strain at mid-height in the t-direction

a_{tn} = shear strain at mid-height

A = constant, defined when used

A_1 = constant to be determined

A_A = defined by Eq. 5.33

A_M = defined by Eq. 5.32

A_R = defined by Eq. 5.37

A_s = area of steel reinforcement per unit width in one layer

A_s^o = area of steel reinforcement per unit width in one layer at the top face

A_{seq} = equivalent amount of isotropic reinforcement to represent the effect of nonisotropic reinforcement

A_{sk} = amount of reinforcement per unit width in the heavier reinforcement layer.

A_{sx} = area of reinforcement per unit width in the x-direction

A_{sy} = area of reinforcement per unit width in the y-direction

A_T = defined by Eq. 5.36

b_i = distance from the top surface to the i^{th} resultant concrete force in the t-direction

b_n = curvature in the n-direction

b_t = curvature in the t-direction

b_{tn} = twisting in the n-t coordinate system

b_u = curvature in the u-direction

B = constant, defined when used

B_1 = constant to be determined

B_p = $E_s A_s \epsilon_c / (\sigma_{ca} h)$

B'_p = $2E_s A_s / (E_c h)$

B4, B5 etc. = designations of rectangular test specimens

c_n = distance from extreme compression fiber to neutral axis of a cross section perpendicular to the n-direction

c_t = distance from extreme compression fiber to neutral axis of a cross section perpendicular to the t-direction

C = constant to be determined

C_1 = constant to be determined

C1, C2, C3 = designations of circular test specimens

d = distance from extreme compression fiber to centroid of reinforcement

deg. = degrees

d_i = distance from top surface of the section to the i^{th} layer of reinforcement

d_{nb} = distance from the top face to the resultant force in the n-direction of the two reinforcement layers at the bottom

d_{ntb} = distance from the top face to the resultant shear force of the two reinforcement layers at the bottom

d_{ntu} = distance from the top face to the resultant shear force at the two reinforcement layers at the top

d_{nu} = distance from the top face to the resultant force in the n-direction of the two reinforcement layers at the top

d_{tb} = distance from the top face to the resultant force in the t-direction of the two reinforcement layers at the bottom

d_{tu} = distance from the top face to the resultant force in the t-direction of the two reinforcement layers at the top

D = diameter; or constant to be determined

e_1, e_2 = defined by Eq. 5.34

E_c = modulus of elasticity of concrete

E_s = modulus of elasticity of steel

f'_c = compressive cylinder strength of concrete (6 by 12-in. cylinder)

f'_t = split-cylinder strength of concrete (6 by 6-in. cylinder)

f_y = yield stress of reinforcement

F_{ni} = force per unit width in the n-direction in the i^{th} concrete compression zone

F_s = force in the reinforcing bar

F_{ti} = force per unit width in the t-direction in the i^{th} compression zone

F_x = component of the force in the reinforcing bar in the x-direction

g_1, g_2 = defined by Eq. 5.34

h = height of a cross section

i = 1, 2, 3, ---

j = distance from the center of the tension reinforcement to the resultant compressive force

k = "spring" constant

k_1 = distance from the extreme fiber of the compressive concrete to its resultant force

K = $(d_2 - c_n)/(d_1 - c_n)$

L = length

L_p = length of constant pressure

M = unit moment

M_1 = external principal unit moment in u-direction

M_2 = external principal unit moment in v-direction

M_α = unit yield moment across yield line

M_n = unit moment in the n-direction

M_{nt} = unit twisting moment at the cross section perpendicular to the n-direction

M_t = unit moment in the t-direction

M_{tn} = unit twisting moment at the cross section perpendicular to the t-direction

M_v = moment in the v-direction

M_x = unit resisting moment in the x-direction

M_{xy} = unit resisting twisting moment in the x-y coordinate system

M_y = unit resisting moment in the y-direction

ME_n = component of M_1 and M_2 in the n-direction

ME_{nt} = twisting moment along the n or t-direction caused by M_1 and M_2

ME_t = component of M_1 and M_2 in the t-direction

n = direction; variable (or number of bars in Silverj's test series)

N_n = force per unit width in the n-direction in the reinforcement

N_n^o = for per unit width in the n-direction in the reinforcement at the top face

N_{na} = allowable force per unit width for the reinforcement perpendicular to the cracks (n-direction)

N_{nf} = allowable force per unit width in the n-direction for the reinforcement making an angle α with the n-direction

N_{ni} = steel force per unit width in the n-direction in the i^{th} layer

N_{nt} = shear force per unit width in a cross section perpendicular to the n-direction

N_t = force per unit width in the t-direction in the reinforcement

N_t^o = force per unit width in the t-direction at the top face

N_{ti} = steel force per unit width in the t-direction in the i^{th} layer of reinforcement

N_x = force per unit width in the x-direction in the reinforcement

N_y = force per unit width in the y-direction in the reinforcement

P = location of the yield point in moment-curvature plot

q = load or pressure per unit length

r_1 = defined by Eq. 4.40

r_2 = defined by Eq. 4.62

r_3 = defined by Eq. 4.72

R_{21} = ratio of deformations at second and first yield

s_1 = spacing (center-center) of reinforcement, layer 1

s_2 = spacing (center-center) of reinforcement, layer 2

t = direction of yield line; or metric ton = 1000kg

u = direction of principal moment

v = direction of principal moment

w = crack width

x = variable; or direction of reinforcing bars

y = variable; or direction of reinforcing bars

y_o = value of y at the edge of the crack

y_o' = slope of reinforcing bar at the edge of the crack

z = variable, defined when used

z_n = distance from mid-height to the reinforcement in the z-direction

z_n^o = distance from the mid-height to the level of the top reinforcement in a section perpendicular to the n-direction

z_t^o = distance from the mid-height to the level of the top reinforcement in a section perpendicular to the t-direction

α = angle, inclination of the reinforcing bar with respect to the perpendicular to the crack; or when stated in the text, deviation from the span direction

α^o = angle, inclination of the reinforcing bar at the top face with respect to the perpendicular to the crack

α_1 and α_2 = angle of reinforcement, layer 1 and 2, with respect to the longitudinal direction. (For Houbolt's square specimens: with respect to the span direction)

β = angle between the direction of the principal moment M_1 (the u-direction) and the x-direction

γ = angle between the directions of the perpendicular to the considered principal moment and the direction of the respective yield line

γ_{nt} = "shear strain"

ϵ_{ax} = strain in the x-direction

ϵ_{ay} = strain in the y-direction

ϵ_c = maximum compressive strain in concrete

ϵ_{cn} = maximum compressive strain in concrete in n-direction

ϵ_{ct} = maximum compressive strain in concrete in t-direction

ϵ_{mt} = strain in the t-direction at mid-height of section

ϵ_{n} = strain in the n-direction

ϵ_{n}^{o} = strain in the n-direction at the top face

ϵ_{n}' = given by Eq. 4.37a

ϵ_{no} = strain in the direction of the load with the reinforcement in the same direction

ϵ_{sa} = unit average elongation of a reinforcing bar

ϵ_{sax} = strain in the reinforcement in the x-direction

ϵ_{say} = strain in the reinforcement in the y-direction

ϵ_{sx} = strain in the reinforcement placed in the x-direction and at the bottom of the section

ϵ_{sx}^{o} = strain in the reinforcement placed in the x-direction and at the top of the section

ϵ_{sy} = strain in the reinforcement placed in the y-direction and at the bottom of the section

ϵ_{sy}^{o} = strain in the reinforcement placed in the y-direction and at the top of the section

ϵ_{t} = strain in the t-direction

ϵ_{t}' = defined by Eq. 4.14a

ϵ_{t}'' = defined by Eq. 4.14

θ = angle between the direction of the principal curvature and the perpendicular to the yield line (Fig. 4.16)

κ $= \frac{\sigma_{sa}}{\sigma_s}$

κ' $= \frac{\sigma'_{sa}}{\sigma'_{su}}$

λ_i = distance from top surface of the section to the i^{th} resultant shear force in the t-direction

λ'_i = distance from top surface of the section to the i^{th} resultant shear force in the n-direction

μ = ratio between reinforcement in the two perpendicular directions. Magnitude can be assumed to be < 1.0 if not specifically stated otherwise.

μ^o = same as for μ, but related to reinforcement at the top surface

σ_c = maximum compressive stress in concrete which is assumed to be linearly elastic

σ_{ca} = average compressive concrete stress

σ_{ct} = average tensile concrete stress over the cross section

σ_s = stress in steel

σ'_s = stress in steel in the direction with μA_s amount of steel

σ_{sa} = average stress in steel bar

σ'_{sa} = average stress in steel in the direction with μA_s amount of steel

σ_{sc} = stress in reinforcement at the crack

σ_x = stress in the x-direction

σ_y = stress in the y-direction

τ_{xy} = shearing stress in x-y coordinate system

ν = M_y/M_x

φ = reorientation of a reinforcing bar (Chapter 3)

φ_o = reorientation of a bar at the crack (Chapter 3)

Φ_p = curvature at yield

Φ_n = curvature in the n-direction

Φ_t = curvature in the t-direction

ω = M_2/M_1

APPENDIX D

DERIVATION OF EQUATIONS 6.16 AND 6.17

$$M_{nt}ME_n + ME_{nt}M_n = 0 \tag{6.13}$$

$$M_n = M_y\cos^2(\beta + \gamma) + M_x\sin^2(\beta + \gamma) \tag{6.1}$$

$$M_y = \nu M_x \tag{6.11}$$

From Eq. 6.1 and Eq. 6.11

$$M_n = M_x\left[\nu\cos^2(\beta + \gamma) + \sin^2(\beta + \gamma)\right]$$

Expand $\cos^2(\beta + \gamma)$ and $\sin^2(\beta + \gamma)$

$$M_n = M_x\left[\nu(\cos\gamma\cos\beta - \sin\gamma\sin\beta)^2 + (\sin\beta\cos\gamma + \sin\gamma\cos\beta)^2\right]$$

Multiply out the squared terms

$$M_n = M_x\left[\nu(\cos^2\gamma\cos^2\beta - 2\cos\gamma\sin\gamma\cos\beta\sin\beta + \sin^2\gamma\sin^2\beta) + \cos^2\gamma\sin^2\beta + 2\cos\gamma\sin\gamma\cos\beta\sin\beta + \sin^2\gamma\cos^2\beta\right]$$

Substitute in the following trigonometric identities

$$\cos^2\gamma = 1/(1 + \tan^2\gamma) = 1/(1 + z^2)$$

$$\sin^2\gamma = \tan^2\gamma/(1 + \tan^2\gamma) = z^2/(1 + z^2) \tag{D.1}$$

$$\sin\gamma\cos\gamma = \tan\gamma/(1 + \tan^2\gamma) = z/(1 \times z^2)$$

where $z = \tan\gamma$

to get the following

$$(1 + z^2)M_n = M_x\left[\nu\cos^2\beta + 2(1 - \nu)\sin\beta\cos\beta + z^2\nu\sin^2\beta + \sin^2\beta + z^2\cos^2\beta\right] \qquad (D.2)$$

Operate on Eq. 6.3 similarly to that done on Eq. 6.1

$$M_{nt} = (M_x - M_y)\sin(\beta + \gamma)\cos(\beta + \gamma) \qquad (6.3)$$

$$M_{nt} = M_x(1 - \nu)\left[(\sin\beta\cos\gamma + \sin\gamma\cos\beta)(\cos\gamma\cos\beta - \sin\gamma\sin\beta)\right]$$

$$M_{nt} = M_x(1 - \nu)\left[\cos^2\gamma\sin\beta\cos\beta - \sin\gamma\cos\gamma\sin^2\beta + \sin\gamma\cos\gamma\cos^2\beta - \sin^2\gamma\sin\beta\cos\beta\right]$$

$$(1 + z^2)M_n = M_x(1 - \nu)\left[\sin\beta\cos\beta - z(\sin^2\beta - \cos^2\beta) - z^2\sin\beta\cos\beta\right] \qquad (D.3)$$

$$ME_n = M_2\cos^2\gamma + M_1\sin^2\gamma \qquad (6.4)$$

$$\omega M_1 = M_2 \qquad (6.11)$$

From Eq. 6.4 and Eq. 6.11

$$ME_n = M_1(\omega\cos^2\gamma + \sin^2\gamma)$$

Use Eq. D.1 to get

$$ME_n = M_1(\omega + z^2)/(1 + z^2) \qquad (D.4)$$

Similarly, from Eq. 6.6

$$ME_{nt} = (M_2 - M_1)\sin\gamma\cos\gamma \qquad (6.6)$$

$$ME_{nt} = M_1 z(\omega - 1)/(1 + z^2) \qquad (D.5)$$

Substitute Eq. D.4 and Eq. D.5 into Eq. 6.13 and multiply by $(1 + z^2)$

$$M_{nt}M_1(\omega + z^2) + M_n z(\omega - 1) = 0 \qquad (D.6)$$

Introduce Eq. D.2 and D.3 into Eq. D.6 and divide by $(1 + z^2)M_x$

$$(1 - \nu)(\omega + z^2)\left[\sin\beta\cos\beta - z(\sin^2\beta - \cos^2\beta) - z^2\sin\beta\cos\beta\right]$$

$$+z(\omega - 1)\left[\nu\cos^2\beta + 2z(1 - \nu)\sin\beta\cos\beta + z^2\nu\sin^2\beta + \sin^2\beta + z^2\cos^2\beta\right] = 0$$

Multiply through the terms containing z and factor

$$(1 - \nu)\left[\omega\sin\beta\cos\beta + z(\omega\cos^2\beta - \omega\sin^2\beta) + z^2(\sin\beta\cos\beta - \omega\sin\beta\cos\beta) + z^3(\cos^2\beta - \sin^2\beta) - z^4\sin\beta\cos\beta\right]$$

$$+(\omega - 1)\left[z(\nu\cos^2\beta + \sin^2\beta) + 2z^2(1 - \nu)\sin\beta\cos\beta + z^3(\nu\sin^2\beta + \cos^2\beta)\right] = 0$$

Collect terms

$$-z^4(1 - \nu)\sin\beta\cos\beta$$

$$+z^3\left[(1 - \nu)(\cos^2\beta - \sin^2\beta) + (\omega - 1)(\nu\sin^2\beta - \cos^2\beta)\right]$$

$$+z^2\left[(1 - \nu)(\sin\beta\cos\beta - \omega\sin\beta\cos\beta) + 2(\omega - 1)(1 - \nu)\sin\beta\cos\beta\right]$$

$$+z\left[(1 - \nu)(\omega\cos^2\beta - \omega\sin^2\beta) + (\omega - 1)(\nu\cos^2\beta + \sin^2\beta)\right]$$

$$+(1 - \nu)(\omega\sin\beta\cos\beta) = 0$$

Divide by $\sin^2\beta$ and express in terms of cotanβ

$$-z^4(1-\nu)\cot\beta$$

$$+z^3\left[(1-\nu)(\cot^2\beta - 1) + (\omega - 1)(\nu + \cot^2\beta)\right]$$

$$+z^2\left[-(1-\nu)(\omega - 1)\cot\beta + 2(\omega - 1)(1-\nu)\cot\beta\right]$$

$$+z\left[(1-\nu)(\omega\cot^2\beta - \omega) + (\omega - 1)(\nu\cot^2\beta + 1)\right]$$

$$+(1-\nu)\omega\cot\beta = 0$$

Expand terms containing z^3 and z

$$-z^4(1-\nu)\cot\beta$$

$$+z^3\left[\cot^2\beta - 1 - \nu\cot^2\beta + \nu + \omega\nu + \omega\cot^2\beta - \nu - \cot^2\beta\right]$$

$$+z\left[\omega\cot^2\beta - \omega - \nu\omega\cot^2\beta + \omega\nu + \omega\nu\cot^2\beta + \omega - \nu\cot^2\beta - 1\right]$$

$$+z^2(\omega - 1)(1-\nu)\cot\beta$$

$$+(1-\nu)\omega\cot\beta = 0$$

Collect terms

$$-z^4(1-\nu)\cot\beta$$

$$+z^3\left[-(\nu - \omega)\cot^2\beta + \omega\nu - 1\right]$$

$$+z\left[-(\nu - \omega)\cot^2\beta + \omega\nu - 1\right]$$

$$+z^2(\omega - 1)(1-\nu)\cot\beta \qquad (D.7)$$

$$+(1-\nu)\omega\cot\beta = 0$$

Let $(1 - \nu)\text{cotan}\beta = A$ (D.8)

$$-(\nu - \omega)\text{cotan}^2\beta + \omega\nu - 1 = -B$$

Using Eq. D.8, rewrite Eq. D.7 as

$$-z^4A + z^2\omega A - z^2A - z^3B - zB + A = 0$$

$$-z^2A(z^2 + 1) + \omega A(z^2 + 1) - zB(z^2 + 1) = 0$$

Divide by $(z^2 + 1)A$

$$-z^2 - zB/A + \omega = 0$$

Replace z with tanγ and let $B/A = \omega C_1$

$$-\tan^2\gamma - \omega C_1 \tan\gamma + \omega = 0 \qquad (6.16)$$

Substitute Eq. D.8 into $\omega C_1 = B/A$

$$\omega C_1 = \frac{(\nu - \omega)\text{cotan}^2\beta + 1 - \omega\nu}{(1 - \nu)\text{cotan}\beta} \qquad (6.17)$$